EMERGING INFECTIOUS DISEASES®

Emerging Pathogens

February 2023

***Jack in the Box* (circa 1890), Father Tucks Tiny Tots' Series.** Illustrated children's book. Raphael Tuck & Sons, Ltd., London; Paris; New York. Public domain image contributed by University of California Libraries.

EMERGING INFECTIOUS DISEASES®

Emerging Infectious Diseases is published monthly by the Centers for Disease Control and Prevention, 1600 Clifton Rd NE, Mailstop H16-2, Atlanta, GA 30329-4027, USA. Telephone 404-639-1960; email, eideditor@cdc.gov

EMERGING INFECTIOUS DISEASES®

Emerging Pathogens **February 2023**

On the Cover

Jack in the Box **(circa 1890), Father Tuck's Tiny Tots' Series. I**llustrated children's book. Raphael Tuck & Sons, Ltd., London; Paris; New York. Public domain image contributed by University of California Libraries.

About the Cover p. 462

Synopses

Research

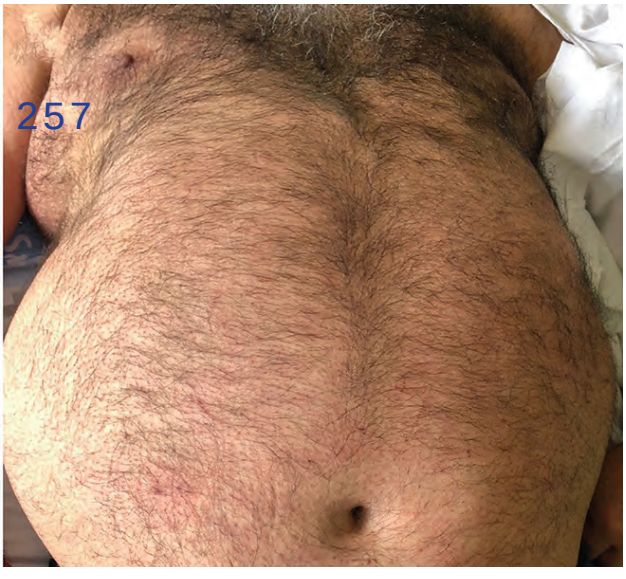

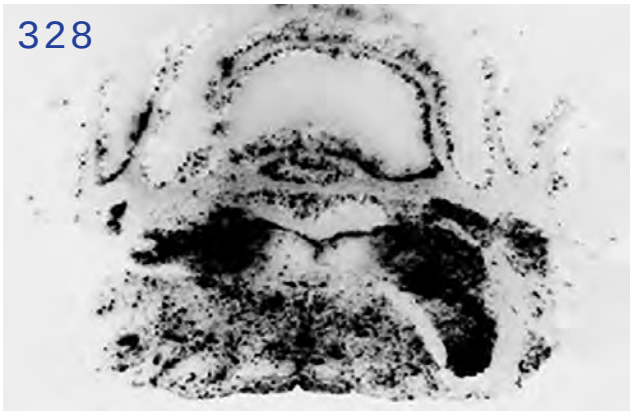

EMERGING INFECTIOUS DISEASES®
February 2023

Dispatches

Commentary

Research Letters

EMERGING INFECTIOUS DISEASES®
February 2023

Comment Letters

About the Cover

DAVID J. SENCER CDC MUSEUM

History·Legacy·Innovation

Dr. David J. Sencer, Mrs. Mountin and Jim Collins celebrate CDC's 25th anniversary, 1961.

CDC at 75

January 9, 2023–July 28, 2023

TEMPORARY EXHIBITIONS GALLERY

Opening January 9, *CDC at 75* is a commemorative exhibition that tells unique stories about the work of this fabled agency and provides a glimpse into the breadth and depth of CDC's history and vast accomplishments. It features rarely seen objects, documents, and media taken from the CDC Museum's rich collections and archives.

Hours

Monday–Wednesday: 9 a.m.–5 p.m.
Thursday: 9 a.m.–7 p.m.
Friday: 9 a.m.–5 p.m.
Closed weekends and federal holidays

Location

1600 Clifton Road, NE
Atlanta, GA
30329-4021
Phone (404) 639-0830

Admission and parking free • Vehicle inspection required
Government-issued photo ID required for adults over the age of 18
Passport required for non-U.S. citizens

Infant Botulism, Israel, 2007–2021

Bar Goldberg, Dana Danino, Yoel Levinsky, Itzhak Levy, Rachel Straussberg, Halima Dabaja-Younis, Alex Guri, Yotam Almagor, Diana Tasher, Daniel Elad, Zina Baider, Shlomo Blum, Oded Scheuerman

In support of improving patient care, this activity has been planned and implemented by Medscape, LLC and Emerging Infectious Diseases. Medscape, LLC is jointly accredited with commendation by the Accreditation Council for Continuing Medical Education (ACCME), the Accreditation Council for Pharmacy Education (ACPE), and the American Nurses Credentialing Center (ANCC), to provide continuing education for the healthcare team.

Medscape, LLC designates this Journal-based CME activity for a maximum of 1.00 ***AMA PRA Category 1 Credit(s)™***. Physicians should claim only the credit commensurate with the extent of their participation in the activity.

Successful completion of this CME activity, which includes participation in the evaluation component, enables the participant to earn up to 1.0 MOC points in the American Board of Internal Medicine's (ABIM) Maintenance of Certification (MOC) program. Participants will earn MOC points equivalent to the amount of CME credits claimed for the activity. It is the CME activity provider's responsibility to submit participant completion information to ACCME for the purpose of granting ABIM MOC credit.

All other clinicians completing this activity will be issued a certificate of participation. To participate in this journal CME activity: (1) review the learning objectives and author disclosures; (2) study the education content; (3) take the post-test with a 75% minimum passing score and complete the evaluation at http://www.medscape.org/journal/eid; and (4) view/print certificate. For CME questions, see page 465.

Release date: January 20, 2023; Expiration date: January 20, 2024

Learning Objectives

Upon completion of this activity, participants will be able to:

- Analyze the epidemiology and prognosis of infant botulism
- Assess characteristics of children with infant botulism in the current study
- Evaluate risk factors for infant botulism in the current study
- Assess outcomes of infant botulism in the current study

CME Editor

Jude Rutledge, BA, Technical Writer/Editor, Emerging Infectious Diseases. *Disclosure: Jude Rutledge has no relevant financial relationships.*

CME Author

Charles P. Vega, MD, Health Sciences Clinical Professor of Family Medicine, University of California, Irvine School of Medicine, Irvine, California. *Disclosure: Charles P. Vega, MD, has the following relevant financial relationships: consultant or advisor for GlaxoSmithKline; Johnson & Johnson Pharmaceutical Research & Development, L.L.C.*

Authors

Bar Goldberg, MD; Dana Danino, MD; Yoel Levinsky, MD; Itzhak Levy, MD; Rachel Straussberg, MD; Halima Dabaja-Younis, MD, MPH; Alex Guri, MD; Yotam Almagor, MD; Diana Tasher, MD; Daniel Elad, DVM, PhD; Zina Baider, DVM; Shlomo Blum, DVM, PhD; and ***Oded Scheuerman, MD.***

Author affiliations: Schneider Children's Medical Center, Petach Tikva, Israel (B. Goldberg, Y. Levinsky, I. Levy, R. Straussberg, O. Scheuerman); Sackler Faculty of Medicine, Tel Aviv University, Tel Aviv, Israel (B. Goldberg, I. Levy, R. Straussberg, D. Tasher, O. Scheuerman); Soroka Medical Center, Beer Sheva, Israel (D. Danino); Faculty of Health Sciences, Ben-Gurion University, Beer Sheva (D. Danino); Rambam Medical Center, Haifa, Israel (H. Dabaja-Younis); The Ruth and Bruce Rappaport Faculty of Medicine, Technion, Haifa, Israel (H. Dabaja-Younis); Kaplan Medical Center, Rehovot, Israel (A. Guri); Hadassah Faculty of Medicine, The Hebrew University of Jerusalem, Jerusalem (A. Guri); Meuhedet Healthcare, Jerusalem, Israel (Y. Almagor); Wolfson Medical Center, Holon, Israel (D. Tasher); National Reference Laboratory for Botulism, Kimron Veterinary Institute, Bet Dagan, Israel (D. Elad, Z. Baider, S. Blum)

DOI: https://doi.org/10.3201/eid2902.220991

Infant botulism (IB) is an intestinal toxemia that manifests as descending paralysis, constipation, and, in some cases, respiratory failure. Laboratory-confirmed IB cases are rare, and recent data in Israel are lacking. We conducted a national multicenter retrospective study of laboratory-confirmed IB cases reported in Israel during 2007–2021. A total of 8 cases were reported during the study period. During 2019–2021, incidence may have increased because of a cluster of 5 cases. Infant median age for diagnosis was 6.5 months, older than previously reported (3 months). Most cases occurred during March–July. Honey consumption was reported in 1 case, and possible environmental risk factors (living nearby rural or construction areas, dust exposure, and having a father who works as a farmer) were reported in 6 cases. Although IB is rare, its incidence in Israel may have increased over recent years, and its epidemiology and risk factors differ from cases reported previously in Israel.

Clostridium botulinum is a gram-positive, rod-shaped, spore-forming, obligate anaerobic bacterium. It is ubiquitous in the environment, such as soil and marine sediment, and can be easily isolated from the surfaces of vegetables, fruits, and seafood. Botulinum neurotoxins (BoNTs) secreted by *C. botulinum* bacteria are among the most potent toxins in nature. BoNTs target motor neurons, and block the cholinergic neuromuscular innervation of striated and smooth muscles in multiple tissues. BoNTs are classified into 7 antigenic serotypes (A to G). Types A, B, and, rarely, E and F, are linked to infant botulism (IB). IB can occur when an infant ingests *C. botulinum* spores because of exposure to contaminated soil or agricultural products, notably honey, when the bacteria develop and release BoNTs into the intestine (*1*,*2*).

IB is a rare disease with a peak incidence among infants 2–8 months of age. IB is classically described as a flaccid descending symmetric paralysis, and recovery can take several weeks (*3*). The disease manifests in a wide clinical spectrum, from mild symptoms to life-threatening conditions (*3*–*8*), and often leads to a late diagnosis (*9*,*10*). The standard and the most sensitive and specific in vivo method used to confirm IB is by mouse lethality bioassay (MLB) (*7*). Treatment includes monitoring, supportive management, and administration of antitoxin (*11*–*13*). In the United States, the mortality rate among hospitalized infants is ≈1% (*14*).

Since 1976, at least 3,350 cases of IB have been reported worldwide, 90% of them in the United States, the highest reported incidence in California. Many cases probably are unrecognized or unreported (*15*–*18*). The average incidence in the United States is 2.1 cases/100,000 live births (*15*), corresponding to ≈75–100 cases yearly (*7*).

Israel is a developed country with a high-quality and universally available healthcare system, and botulism diagnosis is conducted in a single centralized reference laboratory. Recent data on IB in Israel are lacking. The main goals of our study were to evaluate the current incidence of infant botulism in Israel and examine national epidemiologic and clinical data from the past 2 decades. The study was approved by the Institutional Review Board at the Rabin Medical Center (approval no. RMC 20–0972).

Methods

We conducted a retrospective multicenter national cohort study in Israel. Included in this study were all infants 1 week to 1 year of age who had IB diagnosed during 2007–2021 by the National Reference Laboratory for Botulism's Department of Bacteriology at Kimron Veterinary Institute (Bet Dagan, Israel). In addition, we verified with all pediatric infectious disease specialists in Israel that no other patients had IB diagnosed during the study period. Confirmed case-patients in the study were infants (<1 year of age) with clinical signs and symptoms suggesting IB and confirmed by MLB or mass spectrometric–based endopeptidase (EndoPep-MS) assay for detecting and differentiating BoTN serotypes.

We performed laboratory testing for IB by using standard MLB procedures under Kimron Veterinary Institute institutional approval for ethical use of laboratory animals. In parallel, we injected 0.5 mL of serum intraperitoneally into 2 mice and tested the presence of toxigenic *C. botulinum* bacteria in stool. We inspected mice for symptoms consistent with botulism. When both mice died within 96 hours of inoculation, or showed clear signs consistent with botulism in nonheated samples only, we conducted a neutralization test. We diluted culture supernatant (from stool samples) with A, B, or E antitoxins (provided by the US Centers for Disease Control and Prevention) and injected mice intraperitoneally with 0.5 mL of 1 of the following: native untreated supernatant; supernatant with A, B, or E antitoxin; or native supernatant heated at 80°C for 20 min. Finally, we confirmed botulinum by BoNT typing on the basis of survival and lack of symptoms in mice challenged with 1 of the neutralized samples and the heated samples, and deaths in mice challenged with the remaining native samples.

We used other diagnostic tools, such as an electromyographic test that showed characteristic findings for botulism (e.g., a repetitive stimulation leading to an

incremental response), stool PCR, and EndoPep-MS assay (*19*,*20*). The EndoPep-MS assay was conducted by the Israeli Institute for Biologic Research (Ness Ziona, Israel), as described by Rosen et al. (*21*).

We retrieved clinical information about the patients from medical records in 6 hospitals. To evaluate the number of IB cases per live births in Israel, we used data from the Israel Central Bureau of Statistics on live births during the study period (https://www.cbs.gov.il/en/subjects/Pages/Live-Births.aspx). For each case, we collected the following information: demographic data (age, sex, place of residence, hospital where the patient was treated; clinical data (perinatal information, underlying conditions, and breast feeding vs. formula); information on environmental exposures (agricultural occupation of parents or living nearby construction areas), positive toxin test results or clostridial spore presence (as determined by culture or MLB) in honey, formula, soil, and dust from habitant samples; and clinical manifestations. Laboratory results included the toxin type found (A, B, or E), electromyographic features, and blood and cerebrospinal fluid test results. We also collected information on treatment protocols (e.g., use of antibiotics, supportive care only, and administration of antitoxin) and prognosis.

Results

We identified 8 IB patients reported in Israel during 2007–2021; of those, 5 were boys and 3 girls. Three stool samples were positive for BoNT A– and 5 for BoNT B–producing *C. botulinum*. Seven patients were born at term and healthy with no underlying conditions. One patient was born at late preterm and had previous known hypotonia but was included in the study because of acute clinical deterioration, a positive BoNT B result, and improvement during sequential neurologic follow-ups.

The incidence of IB in Israel during 2007–2021 was 0.3 cases/100,000 live births (8 cases). A possible increase in IB incidence of IB occurred during 2019–2021 (0.9 cases/100,000 live births [5 cases]), compared with incidence during 1996–2018 (0.14 cases/100,000 live births [5 cases]) (Figure).

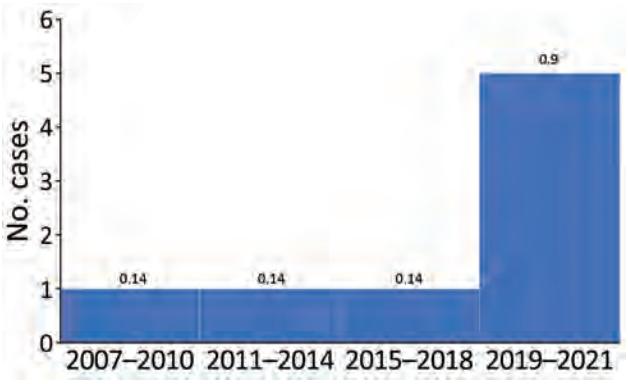

Figure. Cases of infant botulism by 3-year period, Israel, 2007–2021. Numbers above bars indicate incidence for that period (no. cases/100,000 population).

The median age for diagnosis in our study was 6.5 months (range 2.5–8 months). The median time to diagnosis (from symptom onset to suspected diagnosis) was 9.5 days (range 4–35 days). In 1 case, which was detected by the Endopep-MS (when MLB results were negative), time to diagnosis was 3 days from symptom onset.

The demographic and geographic data indicated that no geographic cluster occurred and that the cases were evenly distributed across Israel (Table 1). Similarly, ethnicity and socioeconomic characteristics of IB patients were diverse. Two of the case-patients resided in a rural area (1 in a temporary shed, 1 in a private house). The others resided in urban areas.

Potential Risk Factors

We found several potential risk factors and hazardous exposures. Most (7/8) cases occurred during March–July (spring and summer), and the last case was in a patient from the Negev Desert, characterized by a hot and dry climate year-round. Three infants lived near construction areas and had a history of traveling outside near the construction sites a few days before symptoms began. Two case-patients had a history of being given a homeopathic or plant-based traditional medicine (yannsoon [anise leaves], a common traditional medicine for infantile colic among Bedouin

Table 1. Demographic and clinical characteristics of infant botulism patients, Israel, 2007–2021

Patient no.	Age, mo/sex	Ethnicity	Term or preterm	Birthweight, kg	No. siblings	Region	Location type	Form of housing
1	2.5/F	Bedouin	Term	3.1	3	Negev (South)	Rural	Temporary shed
2	4/M	Jewish	Term	3.1	3	Negev (South)	Urban	Apartment building
3	6/M	Jewish	Term	3.3	1	Center	Urban	Apartment building
4	8/F	Jewish	Late preterm	1.9	1	Center	Rural	Private house
5	7/M	Jewish	Term	3.2	1	Center	Urban	Private house
6	8/M	Jewish	Term	2.9	0	Galil (North)	Urban	Apartment building
7	5/F	Jewish	Term	2.8	1	Center	Urban	Apartment building
8	7/M	Jewish	Term	3.6	4	Center	Urban	Apartment building

populations, and a nonrecognized mixture). Two patients were breastfed only. One infant was exposed to the contents of a vacuum cleaner. The father of 1 patient was an agriculturist and was therefore exposed to soilborne pathogens. In 1 case, a sample taken from a honey cake that the infant had eaten tested positive by culture and MLB (raw honey was poured over the topping of the cake after baking). No potential risk factors were found for 1 of the patients.

Clinical Features, Diagnosis, and Prognosis

The most common clinical signs and symptoms were hypotonia, poor feeding, and weak cry (Table 2). The classical descending paralysis was observed in 6/8 infants. Other symptoms, such as mydriasis, facial nerve palsy, hoarseness, and drooling, were less common.

Five patients were treated with antibiotics at admission: 4 with ceftriaxone (alone or in combination with ampicillin or vancomycin) because of general deterioration and to cover for a possible differential diagnosis of meningitis or epiglottitis (given the drooling observed in the patient) and 1 with azithromycin because the patient's sister had pertussis. The median length of hospitalization was 13 days for those who were treated with antibiotics versus 16 days for those who were not.

Antitoxin (equine-derived) treatment was given to 4 patients, 3 with trivalent antitoxin and 1 with heptavalent. No adverse reactions were observed. The median length of hospitalization for those who were treated with antitoxin was 17 days versus 13.5 days for those were not.

Only 2 infants were intubated, the youngest (2.5 and 4 months of age) among our study group, and both tested positive for BoNT B. Five of the 8 infants were fed by nasogastric tube for an average duration of 11 days.

Table 2. Clinical features, diagnosis, and course of infant botulism patients, Israel, 2007–2021*

Category	Value
Clinical feature, no. positive/no. tested	
Respiratory distress	3/8
Ptosis	6/8
Facialis	1/8
Poor feeding	7/8
Descending paralysis	6/8
Depressed tendon reflexes	4/6
Hypotonia	8/8
Constipation	7/8
Hoarseness	3/8
Aspiration or decreased gag reflex	4/8
Weak cry	7/8
Lack of smile	4/8
Drooling	1/8
Mydriasis	2/8
Diagnostic tool used, no. positive/no. tested	
Electromyographic test	3/4
Toxin A	3/8
Toxin B	5/8
Stool PCR	2/2
EndoPep-MS	2/2
Mouse lethality bioassay	7/8
Course of illness, d, median (range)	
Time to resolution	75 (16–180)
Duration of nasogastric tube support†	11 (10–27)
Duration of intubation‡	11.5 (2–21)
Duration of ICU stay§	10.5 (11–30)
Duration of hospitalization	16 (11–30)
Time to diagnosis	9.5 (4–35)

*EndoPep-MS, mass spectrometric–based endopeptidase assay for detecting and differentiating botulinum neurotoxin serotypes; ICU, intensive care unit.
†5/8 patients were supported by feeding tube.
‡2/8 patients were intubated.
§4/8 patients were admitted to ICU.

Long-term Prognosis

The long-term prognosis was good: 1 infant with previous hypotonia (before IB diagnosis) had made progress and showed improvement at neurologic follow-ups. One child still had mild fine motor delay at 6 months after diagnosis but recovered completely afterwards. One child had a relative relapse of the symptoms 3 months after initial diagnosis, but no new laboratory evidence indicated presence of spores or toxins, and the child had a complete recovery. No neurologic or other sequelae were found among the other patients, and no deaths were recorded.

Discussion

In this study, we describe cases of IB in Israel during 2007–2021. We found a possible increase in incidence in the last 3 years of the study period, especially in 2020, compared to the previous 2 decades. We also noted older ages of the infant patients at illness onset compared with those described previously (*4*). Honey consumption was reported in only 1 infant, whereas we observed an apparently stronger link to environmental factors as source of infection.

The age of diagnosis in our study (6.5 months) is much older than that found in other studies. Previous studies found that age at illness onset in 90% of IB cases was 1–6 months (*4*), with a median age of 91 days (*22*,*23*). A reasonable assumption is that around this age, the infant undergoes a sharp transition from breastfeeding-only or formula-fed only to exposure to different foods. All those changes can cause a sharp shift of the bowel microbiome and optimize conditions for colonization and proliferation of *C. botulinum* (*24*). In addition, around this age, the infant is exposed to other external factors, such as daycare environments, solid foods, and other environmental factors, that may expose them to *C. botulinum*.

Previous research has shown that the connection between honey consumption and IB in the United States is considerable; honey consumption accounts for ≈15%–20% of all IB cases, and up to 25% of honey products were found to be positive for *C. botulinum* spores (*3*,*25*,*26*). In Europe, 59% of the IB cases are related to exposure to honey before symptom onset (*18*). In our study, honey consumption was reported in only 1 case (a honey-cake that was later found to be *C. botulinum* contaminated). This modest link is notable, given that people in Israel are known to be avid consumers of both local honey and honey imported from Europe and the United States; further, honey consumption increases during some of the Jewish holidays, around September–October. In fact, we found no cases of IB during those months. Many case series show that IB cases linked to honey consumption were in patients who were positive for BoNT B (*25*). In our study, the infant who consumed honey was also positive for BoNT B. A possible explanation might be an early and mandatory parental education program in outpatient infant clinics in Israel that forbids honey products until the infant is 1 year of age.

We observed a possible link to certain environmental factors, including dust (vacuum cleaner content), having a father who works as a farmer, crowded living spaces, and living near construction sites, all already known as potential risk factors (*8*,*10*,*20*,*25*,*27*). Those cases might indicate that environmental factors are major risk factors and should be investigated thoroughly and carefully.

A possible seasonal relationship emerged from our findings. Most (7/8) of the cases occurred during spring and summer in the Northern Hemisphere (March–July). One case originated from the Negev Desert area, characterized by a year-round hot and dry climate. These findings suggest a possible influence of temperature on IB outbreaks. Supporting evidence of this distinct seasonal incidence was also shown in a study conducted in the US state of Utah, where all cases of IB occurred during March–October and no cases occurred during the winter months (*12*,*22*,*27*). Another possible explanation might be that those are the most convenient months for outdoor activities and traveling, and therefore more exposure to soil and other environmental factors occurs.

Our study demonstrates a possible rise in IB incidence throughout Israel. During 1996–2006 (a 10-year period), only 2 cases of IB were diagnosed (*15*,*28*–*30*), whereas in our study, 8 cases were diagnosed during 2007–2021 (a 15-year period). A possible explanation might be the rapidly increasing number of construction projects, higher population density, and increasing awareness of IB among pediatricians. Still, the national incidence of IB in Israel is relatively low (only ≈0.3 cases/100,000 live births, compared with 1.9–2.1 cases/100,000 live births in the United States [*4*,*15*] and 2.2 cases/100,000 live births in Argentina [*31*]) and is more similar to low-incidence countries such as England (*32*) or Germany (*15*).

We identified a notable cluster of 5 cases during 2019–2021 (0.9 cases/100,000 live births). This possible surge in incidence raises an interesting question about a possible link to the COVID-19 pandemic. Is the increase in IB incidence observed in Israel during 2020 also observed worldwide? No up-to-date data are available to answer this question. This possible surge in Israel might also be attributed to the plausibility of random variations in the occurrence of a rare disease.

Most of the cases in our study were caused by BoNT B (5/8) and the rest by BoNT A (3/8). A similar ratio exists in the United States (62% BoNT and 37% BoNT A), but the ratio is different in the rest of the world, where BoTN A is the more prevalent type (*15*).

The number of infants who required intubation and invasive ventilation in our study was notably lower (2/8) than that reported in other case-series reviews, such as one conducted in California, USA (60%–82%) (*20*,*33*,*35*). The 2 infants who were intubated were both positive for BoNT B, which is related to a higher incidence of respiratory failure (*33*). The older age of patients at onset observed in our study led to a milder clinical course and lower intubation rate.

Half of the infants in our study were treated with antitoxin, whereas the rest showed clinical improvement or recovered without antitoxin treatment. Previous reports showed that antitoxin treatment shortened the length of hospitalization from 23 to 13 days (*20*,*33*–*35*). In our study, infants who were treated with antitoxin were hospitalized for 17 days, and those who were not treated were hospitalized for 13.5 days. A possible explanation might be that the infants who received antitoxins had a more severe clinical picture, which necessitated the use of antitoxin but also led to a more complex and prolonged hospitalization. Another possible explanation might be the fact that in Israel the equine-derived botulism antitoxin is still used, whereas in the United States, the common antitoxin administered in recent years is the human botulism immune globulin.

The main strength of our study is its national reach. Because only 1 national laboratory for diagnosis of IB exists, we were able to access all the diagnosed case-patients' medical records. The main limitation of our study, which derives from the rarity of IB, is the

small sample size of only 8 cases. Another limitation is the retrospective nature of our study, which means some details are unrecorded or unknown.

In summary, although IB is still a rare disease, IB incidence may have increased in Israel during our study period, 2007–2021, and especially during the past 3 years of that period. We also found that honey consumption is less prominent as a risk factor compared with environmental exposures. Clinicians should be aware of the possible changing epidemiology and risk factors of this rare but serious disease in Israel.

Acknowledgments

We thank Debby Mir for editing the manuscript.

About the Author

Dr. Goldberg is a resident in pediatrics at Schneider Children's Medical Center of Israel, Petach Tikva, Israel. Her primary research interests include infectious diseases, immunology, and rheumatology.

References

1. Lindström M, Korkeala H. Laboratory diagnostics of botulism. Clin Microbiol Rev. 2006;19:298–314. https://doi.org/10.1128/CMR.19.2.298-314.2006
2. Rao AK, Sobel J, Chatham-Stephens K, Luquez C. Clinical guidelines for diagnosis and treatment of botulism, 2021. MMWR Recomm Rep. 2021;70:1–30. https://doi.org/10.15585/mmwr.rr7002a1
3. Cox N, Hinkle R. Infant botulism. Am Fam Physician. 2002;65:1388–92.
4. Centers for Disease Control and Prevention. Botulism in the United States, 1899–1996. Handbook for epidemiologists, clinicians, and laboratory workers. 1998 [cited 2022 Mar 24]. https://stacks.cdc.gov/view/cdc/6673
5. Cagan E, Peker E, Dogan M, Caksen H. Infant botulism. Eurasian J Med. 2010;42:92–4. https://doi.org/10.5152/eajm.2010.25
6. Midura TF. Update: infant botulism. Clin Microbiol Rev. 1996;9:119–25. https://doi.org/10.1128/CMR.9.2.119
7. Botulism SJ. Clin Infect Dis. 2005;41:1167–73. https://doi.org/10.1086/444507
8. Domingo RM, Haller JS, Gruenthal M. Infant botulism: two recent cases and literature review. J Child Neurol. 2008;23:1336–46. https://doi.org/10.1177/0883073808318200
9. Centers for Disease Control and Prevention. Investigational heptavalent botulinum antitoxin (HBAT) to replace licensed botulinum antitoxin AB and investigational botulinum antitoxin E. MMWR Morb Mortal Wkly Rep. 2010;59:299.
10. Francisco AM, Arnon SS. Clinical mimics of infant botulism. Pediatrics. 2007;119:826–8. https://doi.org/10.1542/peds.2006-0645
11. Nevas M, Lindström M, Virtanen A, Hielm S, Kuusi M, Arnon SS, et al. Infant botulism acquired from household dust presenting as sudden infant death syndrome. J Clin Microbiol. 2005;43:511–3. https://doi.org/10.1128/JCM.43.1.511-513.2005
12. Thompson JA, Filloux FM, Van Orman CB, Swoboda K, Peterson P, Firth SD, et al. Infant botulism in the age of botulism immune globulin. Neurology. 2005;64:2029–32. https://doi.org/10.1212/01.WNL.0000166950.35189.5E
13. Arnon SS, Schechter R, Maslanka SE, Jewell NP, Hatheway CL. Human botulism immune globulin for the treatment of infant botulism. N Engl J Med. 2006;354:462–71. https://doi.org/10.1056/NEJMoa051926
14. Jackson KA, Mahon BE, Copeland J, Fagan RP. Botulism mortality in the USA, 1975–2009. Botulinum J. 2015;3:6–17. https://doi.org/10.1504/TBJ.2015.078132
15. Koepke R, Sobel J, Arnon SS. Global occurrence of infant botulism, 1976–2006. Pediatrics. 2008;122:e73–82. https://doi.org/10.1542/peds.2007-1827
16. Pickett J, Berg B, Chaplin E, Brunstetter-Shafer MA. Syndrome of botulism in infancy: clinical and electrophysiologic study. N Engl J Med. 1976;295:770–2. https://doi.org/10.1056/NEJM197609302951407
17. Fox CK, Keet CA, Strober JB. Recent advances in infant botulism. Pediatr Neurol. 2005;32:149–54. https://doi.org/10.1016/j.pediatrneurol.2004.10.001
18. Aureli P, Franciosa G, Fenicia L. Infant botulism and honey in Europe: a commentary. Pediatr Infect Dis J. 2002;21:866–8. https://doi.org/10.1097/00006454-200209000-00016
19. Rosen O, Feldberg L, Yamin TS, Dor E, Barnea A, Weissberg A, et al. Development of a multiplex Endopep-MS assay for simultaneous detection of botulinum toxins A, B and E. Sci Rep. 2017;7:14859. https://doi.org/10.1038/s41598-017-14911-x
20. Fach P, Micheau P, Mazuet C, Perelle S, Popoff M. Development of real-time PCR tests for detecting botulinum neurotoxins A, B, E, F producing *Clostridium botulinum*, *Clostridium baratii* and *Clostridium butyricum*. J Appl Microbiol. 2009;107:465–73. https://doi.org/10.1111/j.1365-2672.2009.04215.x
21. Rosen O, Feldberg L, Gura S, Brosh-Nissimov T, Guri A, Zimhony O, et al. Early, real-time medical diagnosis of botulism by endopeptidase-mass spectrometry. Clin Infect Dis. 2015;61:e58–61. https://doi.org/10.1093/cid/civ861
22. Thompson JA, Glasgow LA, Warpinski JR, Olson C. Infant botulism: clinical spectrum and epidemiology. Pediatrics. 1980;66:936–42. https://doi.org/10.1542/peds.66.6.936
23. Payne JR, Khouri JM, Jewell NP, Arnon SS. Efficacy of human botulism immune globulin for the treatment of infant botulism: the first 12 years post licensure. J Pediatr. 2018;193:172–7. https://doi.org/10.1016/j.jpeds.2017.10.035
24. Shirey TB, Dykes JK, Lúquez C, Maslanka SE, Raphael BH. Characterizing the fecal microbiota of infants with botulism. Microbiome. 2015;3:54. https://doi.org/10.1186/s40168-015-0119-0
25. Arnon SS, Midura TF, Damus K, Thompson B, Wood RM, Chin J. Honey and other environmental risk factors for infant botulism. J Pediatr. 1979;94:331–6. https://doi.org/10.1016/S0022-3476(79)80863-X
26. Spika JS, Shaffer N, Hargrett-Bean N, Collin S, MacDonald KL, Blake PA. Risk factors for infant botulism in the United States. Am J Dis Child. 1989;143:828–32.
27. Espelund M, Klaveness D. Botulism outbreaks in natural environments—an update. Front Microbiol. 2014;5:287. https://doi.org/10.3389/fmicb.2014.00287
28. Yanay O, Lerman-Sagie T, Gilad E, Nissenkorn A, Jaferi J, Watemberg N, et al. Infant botulism in Israel: knowledge enables prompt diagnosis. Isr Med Assoc J. 2004;6:249–50.
29. Falk A, Afriat A, Hubary Y, Herzog L, Eisenkraft A. Infant botulism [in Hebrew]. Harefuah. 2014;153:180–3, 238.
30. Baron J, Greenberg D, Shorer Z, Hershkovitz E, Melamed R, Lifshitz M. Infant botulism: be aware of this rare disease. Isr Med Assoc J. 2007;9:682–3.

31. Lúquez C, Bianco MI, Sagua MD, Barzola CP, de Jong LIT, Degarbo SM, et al. Relationship between the incidence of infant botulism and the presence of botulinum-toxin producing clostridia in the soil of Argentina from 1982–2005. J Pediatr Neurol. 2007;5:279–86. https://doi.org/10.1055/s-0035-1557408
32. Grant KA, Nwarfor I, Mpamugo O, Mithani V, Lister P, Dixon G, et al. Report of two unlinked cases of infant botulism in the UK in October 2007. J Med Microbiol. 2009;58:1601–6. https://doi.org/10.1099/jmm.0.011510-0
33. Tseng-Ong L, Mitchell WG. Infant botulism: 20 years' experience at a single institution. J Child Neurol. 2007;22:1333–7. https://doi.org/10.1177/0883073807308707
34. Schreiner MS, Field E, Ruddy R. Infant botulism: a review of 12 years' experience at the Children's Hospital of Philadelphia. Pediatrics. 1991;87:159–65. https://doi.org/10.1542/peds.87.2.159
35. Underwood K, Rubin S, Deakers T, Newth C. Infant botulism: a 30-year experience spanning the introduction of botulism immune globulin intravenous in the intensive care unit at Children's Hospital Los Angeles. Pediatrics. 2007;120:e1380–5. https://doi.org/10.1542/peds.2006-3276

Address for correspondence: Oded Scheuerman, Department of Pediatrics B and Pediatric Infectious Diseases Unit, Schneider Children's Medical Center of Israel, Petach Tikva 4920235, Israel; email: odedshv@clalit.org.il

Sentinel Surveillance System Implementation and Evaluation for SARS-CoV-2 Genomic Data, Washington, USA, 2020–2021

Hanna N. Oltean, Krisandra J. Allen, Lauren Frisbie, Stephanie M. Lunn, Laura Marcela Torres, Lillian Manahan, Ian Painter, Denny Russell, Avi Singh, JohnAric MoonDance Peterson, Kristin Grant, Cara Peter, Rebecca Cao, Katelynn Garcia, Drew Mackellar, Lisa Jones, Holly Halstead, Hannah Gray, Geoff Melly, Deborah Nickerson, Lea Starita, Chris Frazar, Alexander L. Greninger, Pavitra Roychoudhury, Patrick C. Mathias, Michael H. Kalnoski, Chao-Nan Ting, Marisa Lykken, Tana Rice, Daniel Gonzalez-Robles, David Bina, Kelly Johnson, Carmen L. Wiley, Shaun C. Magnuson, Christopher M. Parsons, Eugene D. Chapman, C. Alexander Valencia, Ryan R. Fortna, Gregory Wolgamot, James P. Hughes, Janet G. Baseman, Trevor Bedford, Scott Lindquist

Genomic data provides useful information for public health practice, particularly when combined with epidemiologic data. However, sampling bias is a concern because inferences from nonrandom data can be misleading. In March 2021, the Washington State Department of Health, USA, partnered with submitting and sequencing laboratories to establish sentinel surveillance for SARS-CoV-2 genomic data. We analyzed available genomic and epidemiologic data during presentinel and sentinel periods to assess representativeness and timeliness of availability. Genomic data during the presentinel period was largely unrepresentative of all COVID-19 cases. Data available during the sentinel period improved representativeness for age, death from COVID-19, outbreak association, long-term care facility–affiliated status, and geographic coverage; timeliness of data availability and captured viral diversity also improved. Hospitalized cases were underrepresented, indicating a need to increase inpatient sampling. Our analysis emphasizes the need to understand and quantify sampling bias in phylogenetic studies and continue evaluation and improvement of public health surveillance systems.

Virus genome data can provide useful information for public health practice, particularly when combined with epidemiologic data in real time. Goals of genomic surveillance can include monitoring circulating and emerging variants, detecting and characterizing outbreaks, describing spatiotemporal patterns of virus transmission, supporting epidemiologic and genomic characterization of variants, and pinpointing introduction sources that might be risk factors (*1*). Information from a paired genomic and epidemiologic surveillance system can then be translated into public health interventions to prevent disease, control spread, and mitigate outbreaks. Interventions could include planning preparedness according to emerging variant characteristics, changing therapeutic and nonpharmaceutical interventions, and recommending control strategies on the basis of outbreak characteristics. To ensure generalizability and equity when using paired genomic and epidemiologic data for public health purposes, the methods for capturing those data must ensure a representative sample from the population of interest (*2*,*3*).

Author affiliations: Washington State Department of Health, Shoreline, Washington, USA (H.N. Oltean, K.J. Allen, L. Frisbie, S.M. Lunn, L.M. Torres, L. Manahan, I. Painter, D. Russell, A. Singh, J.M. Peterson, K. Grant, C. Peter, R. Cao, K. Garcia, D. Mackellar, L. Jones, H. Halstead, H. Gray, G. Melly, S. Lindquist); University of Washington, Seattle, Washington (H.N. Oltean, D. Nickerson, L. Starita, C. Frazar, A.L. Greninger, P. Roychoudhury, P.C. Mathias, J.P. Hughes, J.G. Baseman); Northwest Genome Center, Seattle (D. Nickerson, L. Starita, C. Frazar); Atlas Genomics, Seattle (M.H. Kalnoski, C.-N. Ting); Confluence Health, Wenatchee, Washington (M. Lykken, T. Rice, D. Gonzalez-Robles); Incyte Diagnostics, Spokane Valley, Washington (D. Bina, K. Johnson, C.L. Wiley); Interpath Laboratory, Boise, Idaho, USA (S.C. Magnuson, C.M. Parsons, E.D. Chapman, A. Valencia); Northwest Laboratory, Bellingham, Washington (R.R. Fortna, G. Wolgamot); Fred Hutchinson Cancer Research Center, Seattle (T. Bedford)

DOI: https://doi.org/10.3201/eid2902.221482

Ongoing global circulation of SARS-CoV-2 and repeated emergence of new variants indicate the need for robust genomic surveillance to inform public health responses (*4*). In Washington, USA, surveillance of SARS-CoV-2 is passive and, therefore, focused on cases of COVID-19 in persons seeking testing. In addition, methods for conducting next-generation sequencing introduce limitations on sampling; specimens must contain adequate quantities of viral RNA for sequencing efforts to be successful. Therefore, persons who had mild illness, delayed testing, reinfection, or other characteristics that might lower viral loads are less likely to be represented in sequencing data. Knowing those limitations, the Washington State Department of Health sought to establish a genomic sentinel surveillance system for SARS-CoV-2 in March 2021.

Before sentinel surveillance was initiated, large amounts of genomic data were produced by academic and clinical laboratories in Washington and shared publicly via the GISAID EpiCoV database (*5*–*7*). Studies using those data to rapidly produce critical viral transmission and evolution information were published early during the pandemic; however, the populations captured in those data remain unknown (*8*–*12*). Sampling bias or systematic differences in sample characteristics between COVID-19 cases with sequenced specimens and total COVID-19 cases is a concern. Using large datasets from a limited number of geographically sparse institutions might produce inaccurate phylogenetic representations of virus distribution and migration within the population (*13*,*14*). Specifically, discrete trait analysis is a type of phylogeographic analysis that treats lineage migration between locations as if the location was a discrete trait; models relying on this analysis type assume that sample sizes across subpopulations are proportional to their relative size and random sampling occurs (*15*). If 1 population is oversampled, large biases are expected in model output (*15*). This concern extends beyond state or country borders because representative sampling is often assumed for contextual data, which provides the backdrop upon which phylogenetic inference is based.

We describe implementing a sentinel surveillance system that enables pairing of genomic and epidemiologic data. In addition, we assessed representativeness and timeliness of genomic data availability before and after system implementation. By performing this evaluation, we provide information regarding populations of sampled cases and limitations on inference affecting genomic data use. To support planning efforts to obtain more equitable and representative sampling, we identified subpopulations that might be systematically excluded from sequencing surveillance. More broadly, we raise awareness regarding sampling bias in convenience-based genomic surveillance systems and support development of robust genomic surveillance systems in additional jurisdictions.

Methods

Sentinel Surveillance System Design

In March 2021, the Washington State Department of Health partnered with multiple laboratories to establish a sentinel surveillance program to monitor genomic epidemiology of SARS-CoV-2 within the state. Partner laboratories were selected to maximize geographic coverage and specimen numbers. The initial proportion of randomly selected positive specimens submitted for sequencing was designed to balance geographic coverage regionally and match available sequencing capacity; statewide case coverage varied from 8% to 25% during the study period (*16*). In addition to the Washington State Public Health Laboratories, the 6 sentinel laboratories are Atlas Genomics, Confluence Health/Central Washington Hospital, Interpath Laboratories, Incyte Diagnostics Spokane, Northwest Laboratories, and University of Washington Virology Division. PCR cycle threshold (Ct) is capped at 30 for this surveillance system. The surveillance program is supplemented by a national surveillance effort supported by the Centers for Disease Control and Prevention (CDC), which includes multiple commercial laboratories sequencing randomly selected specimens (*2*). Methods for next-generation sequencing vary across laboratories, but >90% sequences are generated by using an Illumina platform (https://www/illumina.com); assembly methods also vary.

Study Population Evaluation

We included all confirmed COVID-19 cases (SARS-CoV-2 RNA detected by molecular amplification) reported in the Washington Disease Reporting System from January 21, 2020, through December 31, 2021. Using laboratory accession numbers or patient demographics, we linked those cases to sequences uploaded to the GISAID EpiCoV database (*5*–*7*) from January 21, 2020, through January 31, 2022, that indicated the state of Washington in the geographic tag. We classified cases as presentinel surveillance if specimens were sequenced before March 1, 2021. We classified cases as sentinel surveillance if specimens were sequenced on or after March 1, 2021, and submitted

through the Washington State Department of Health sentinel surveillance program, or if the sequencing laboratory indicated that specimens were randomly selected. Specimens specifically selected for targeted sequencing as part of outbreak investigations because of travel history, known vaccine breakthrough status, or spike gene target failures were not considered sentinel surveillance if sampled outside the random selection process. Washington state and University of Washington Institutional Review Boards determined this project to be a surveillance activity and exempt from review.

Data Analysis

We assessed representativeness of data before and after implementing sentinel surveillance by comparing COVID-19 cases with sequenced specimens to all COVID-19 cases during the same period according to sex, age, race, ethnicity, language, long-term care facility (LTCF) association, occupation, county of residence, outbreak association, travel history, hospitalization, or death. All epidemiologic data analyses were performed using R version 4.0.3 (*17*). We compared categorical data by using Pearson χ^2 test or the formula $\Sigma(|E\text{-}O|)/E$, where E was expected and O observed counts. Expected counts were calculated by standardization to overall reported cases during the same period. We visualized geographic comparisons by mapping standardized ratios of observed versus expected cases at the county level. We graphed the percentage of cases with sequenced specimens by county and month to visualize spatiotemporal sampling. We evaluated areas with high presentinel sequencing coverage and high or low sentinel sequencing coverage to determine representativeness because data from those areas enabled robust phylogeographic studies.

To determine variability of genomic data, we constructed phylogenetic trees for 4 scenarios using the Nextstrain (*18*) pipeline for SARS-CoV-2. The scenarios were presentinel surveillance with high coverage, low representativeness; presentinel surveillance with high coverage, high representativeness; sentinel surveillance with high coverage, high representativeness; and sentinel surveillance with low coverage, low representativeness. We performed rarefaction analysis to examine how sampling affected the diversity of sequences captured in each of those 4 scenarios. For each value from 1 to n, where n is the total number of available sequences for a location/timeframe of interest, we generated 10 subsampled datasets (sampling without replacement). We counted and plotted the number of unique haplotypes as a function of the number of sampled sequences.

We assessed timeliness of data by comparing the interval between initial specimen collection and genomic data upload to the GISAID database. We assessed median timeliness by month and compared categorical data uploaded within <14 days, 14–27 days, and ≥28 days after specimen collection.

Results

During the presentinel surveillance period, 10,653 (3.3%) COVID-19 cases had sequencing information available, compared with 56,106 (12.1%) cases sampled during sentinel surveillance. For all categorical comparisons using Pearson χ^2 tests, we observed statistically significant differences between presentinel and sentinel cases that had sequencing data. To avoid having a single large discrepancy dominate the representativeness measurement, we used the formula $\Sigma(|E\text{-}O|)/E$ instead of Pearson χ^2 test to directly compare representativeness between populations (Table).

Both presentinel and sentinel cases with sequencing data were generally representative of all COVID-19 cases for sex at birth. During the presentinel surveillance period, older age groups and hospitalized persons with sequenced specimens were overrepresented. Persons who died of COVID-19 were overrepresented by ≈3-fold among presentinel cases with sequencing data compared with cases that had no sequencing data. Sentinel surveillance implementation resolved overrepresentation of decedents, but persons with COVID-19 who were hospitalized or ≥65 years of age were underrepresented.

Early during the pandemic, specimens from known outbreak-associated COVID-19 cases were more commonly sequenced, likely reflecting preferential sample selection of those cases for studies. Similarly, sequencing of specimens from LTCF-associated COVID-19 cases was enriched by 2.5-fold. Sentinel surveillance implementation decreased but did not completely resolve enrichment of outbreak-associated cases, whereas LTCF-associated case enrichment was substantially resolved.

Presentinel COVID-19 cases with sequenced specimens had more complete symptom information when compared with all COVID-19 cases. Both presentinel and sentinel cases with sequenced specimens had symptom information reported more frequently compared with all cases.

Persons self-reporting as a racial or ethnic minority were generally overrepresented among presentinel COVID-19 cases with sequenced specimens; race/ethnicity

data were less likely to be missing among those cases than among total COVID-19 cases. After sentinel surveillance implementation, persons reporting Hispanic ethnicity or Spanish language preference were overrepresented among COVID-19 cases with sequenced specimens. Differences in missing race data were resolved after sentinel surveillance implementation.

Industry information was missing for most cases. According to the available industry information, agriculture, forestry, fishing and hunting, and healthcare and social assistance were overrepresented among cases with sequenced specimens. Industry information was missing for >90% of cases during the sentinel surveillance period; therefore, industry representation was not assessed in this study.

More persons with sequenced specimens during the presentinel period traveled outside the United States than expected, indicating likely enrichment for international travelers. Travel information was missing for >95% of cases during the sentinel surveillance period; therefore, traveler representation was not assessed in this study.

Table. Comparison of demographic characteristics between COVID-19 cases with sequenced specimens and all confirmed COVID-19 cases in study of presentinel and sentinel surveillance system implementation and evaluation for SARS-CoV-2 genomic data, Washington, USA, 2020–2021*

	Presentinel period†				Sentinel period‡			
Variable	Overall	Sequenced	O/E	Σ(|E-O|)/E§	Overall	Sequenced	O/E	Σ(|E-O|)/E§
Total no.	326,850	10,653			463,639	56,106		
Sex				0.73				0.55
F	159,460 (48.8)	5,326 (50.0)	1.02		230,524 (49.7)	27,163 (48.4)	0.97	
M	157,133 (48.1)	4,932 (46.3)	0.96		223,711 (48.3)	27,916 (49.8)	1.03	
Other	287 (0.1)	NA¶	0.53		331 (0.1)	55 (0.1)	1.37	
Missing	9,970 (3.1)	390 (3.7)	1.20		9,073 (2.0)	972 (1.7)	0.89	
Age group, y				2.36				1.58
0–4	7,802 (2.4)	211 (2.0)	0.83		18,499 (4.0)	2,188 (3.9)	0.98	
5–17	32,121 (9.8)	932 (8.7)	0.89		77,782 (16.8)	9,815 (17.5)	1.04	
18–44	165,920 (50.8)	5,128 (48.1)	0.95		224,380 (48.4)	28,909 (51.5)	1.06	
45–64	83,046 (25.4)	2,628 (24.7)	0.97		102,215 (22.0)	11,309 (20.2)	0.91	
65–79	26,724 (8.2)	1,073 (10.1)	1.23		32,000 (6.9)	3,052 (5.4)	0.79	
≥80	10,998 (3.4)	680 (6.4)	1.90		8,591 (1.9)	832 (1.5)	0.80	
Unknown	239 (0.1)	NA¶	0.13		172 (0.0)	NA¶	0.05	
COVID-19 deaths	5,134 (1.6)	448 (4.2)	2.68	1.68	4,568 (1.0)	452 (0.8)	0.82	0.18
Hospitalized for COVID-19	18,992 (5.8)	891 (8.4)	1.44	0.44	25,060 (5.4)	1,721 (3.1)	0.57	0.43
Outbreak-associated	49,165 (15.0)	2,350 (22.1)	1.47	0.47	25,902 (5.6)	4,281 (7.6)	1.37	0.37
LTCF-associated	19,899 (6.1)	1,614 (15.2)	2.49	1.49	7,317 (1.6)	1,105 (2.0)	1.25	0.25
Symptoms				0.61				0.80
Yes	172,070 (52.6)	6,860 (64.4)	1.22		173,363 (37.4)	27,140 (48.4)	1.29	
No	24,182 (7.4)	701 (6.6)	0.89		44,731 (9.6)	3,430 (6.1)	0.63	
Unknown	130,598 (40.0)	3,092 (29.0)	0.73		245,545 (53.0)	25,536 (45.5)	0.86	
Race/Ethnicity				1.95				1.35
Hispanic	70,020 (21.4)	2,671 (25.1)	1.17		53,221 (11.5)	9,285 (16.5)	1.44	
Non-Hispanic, American Indian, or Alaska Native	3,953 (1.2)	161 (1.5)	1.25		5,455 (1.2)	685 (1.2)	1.04	
Non-Hispanic Asian	16,321 (5.0)	755 (7.1)	1.42		21,787 (4.7)	3,261 (5.8)	1.24	
Non-Hispanic Black	14,863 (4.5)	548 (5.1)	1.13		19,812 (4.3)	2,429 (4.3)	1.01	
Non-Hispanic multiracial	5,575 (1.7)	217 (2.0)	1.19		7,707 (1.7)	1,173 (2.1)	1.26	
Non-Hispanic Native Hawaiian or other Pacific Islander	5,338 (1.6)	203 (1.9)	1.17		6,432 (1.4)	704 (1.3)	0.90	
Non-Hispanic White	133,224 (40.8)	4,174 (39.2)	0.96		229,100 (49.4)	24,039 (42.8)	0.87	
Non-Hispanic, other race	3,211 (1.0)	138 (1.3)	1.32		3,271 (0.7)	345 (0.6)	0.87	
Unknown	74,345 (22.7)	1,786 (16.8)	0.74		116,854 (25.2)	14,185 (25.3)	1.00	
Language				0.94				2.15
English	104,984 (32.1)	3,357 (31.5)	0.98		138,437 (29.9)	18,484 (32.9)	1.10	
Spanish	23,408 (7.2)	884 (8.3)	1.16		9,849 (2.1)	2,474 (4.4)	2.08	
Other	5,137 (1.6)	239 (2.2)	1.43		1,745 (0.4)	337 (0.6)	1.60	
Unknown	12,519 (3.8)	273 (2.6)	0.67		9,261 (2.0)	1,434 (2.6)	1.28	
Missing	180,802 (55.3)	5,900 (55.4)	1.00		304,347 (65.6)	33,377 (59.5)	0.91	

*Values are no. or no. (%). We included all confirmed COVID-19 cases (SARS-CoV-2 RNA detected by molecular amplification) reported among Washington residents from January 21, 2020, through December 31, 2021, in the Washington Disease Reporting System. E, expected counts; LTCF, long-term care facility; NA, not applicable; O, observed counts.
†Cases were classified as presentinel if specimens were sequenced before March 1, 2021.
‡Cases were classified as sentinel if specimens were sequenced on or after March 1, 2021, through the sentinel surveillance program.
§Formula used to directly compare representativeness between populations.
¶Counts <10 are censored.

Reinfection data were captured starting on September 1, 2021; therefore, case-level data were not available for most of the study period. From September through December 2021, reinfection cases were underrepresented in the sequencing data, which might reflect a higher average Ct in this population.

Before sentinel surveillance implementation, geographic sequencing coverage was variable and focused on western Washington (Figure 1); King, San Juan, Pacific, and Yakima Counties had high coverage. Some areas of the state had little or no data available. After sentinel surveillance implementation, geographic coverage equalized regionally across the state; variable coverage because of sentinel laboratory service areas occurred as expected (Figure 1).

We investigated representativeness further in areas with high presentinel sequencing coverage and high cases numbers (Appendix Figure 1, https://wwwnc.cdc.gov/EID/article/29/2/22-1482-App1.pdf). During March–June 2020, Yakima County had 19%–30% sequencing coverage for all COVID-19 cases; high-quality genomic data were available for 1,696 cases. High coverage was partially driven by sequencing specimens from LTCF-associated cases. A total of 25% of cases with sequenced specimens were affiliated with LTCFs, compared with 11% of all COVID-19 cases during that period. Persons with sequenced specimens were more commonly ≥65 years of age and less commonly of Hispanic descent or with Spanish language preference.

We performed phylogenetic analysis of all sequenced specimens from Yakima County cases with COVID-19 onset dates during March–June 2020 (Appendix Figure 2, panel A**).** During this period, most (63%) sequences were classified as Nextstrain clade 20B (Pango lineage B.1.1), 23% were clade 19B (Pango lineage A), 9% were clade 20A (Pango lineage B.1) and 5% were clade 20C. Comparatively, within the entire state of Washington, clades 20C and 19B (Pango lineage A) were most prevalent during the same period.

Sequencing coverage was also high in Yakima County in February 2021. Sequencing coverage was 26% across all COVID-19 cases, and high-quality genomic data were available for 271 cases. During this period, we observed smaller differences between cases with sequenced specimens and all cases for ethnicity and outbreak-association; otherwise, cases with sequenced specimens were largely representative of all cases during this time. We performed phylogenetic analysis of Yakima cases during February 2021 (Appendix Figure 2, panel B). The most common lineage identified was 21C (Pango lineage B.1.427/429 or Epsilon), representing 33% of sequences, then 20G (Pango lineage B.1.2) at 29%, 20A at 13%, 20B at 9%, and 20C at 15%. In Washington, 30% of sequences in GISAID were Epsilon in February 2021.

After sentinel surveillance implementation, variability in geographic coverage was diminished regionally but persisted at the county level. We investigated counties with high and low sentinel sequencing coverage to determine effects of variable sentinel specimen sampling. We specifically compared Whatcom County, a county with high coverage from a sentinel laboratory, and Clark County, a county with low coverage. During the sentinel surveillance period, cases with sequenced specimens from Whatcom County were representative of all COVID-19 cases from the county for age, sex, race, death from COVID-19, and LTCF-association. Persons hospitalized for COVID-19 were underrepresented among sentinel surveillance cases, reflecting statewide findings. Outbreak-associated cases and symptomatic persons were slightly overrepresented among sentinel surveillance cases. We performed phylogenetic analysis of cases from Whatcom County during the sentinel surveillance period (Appendix Figure 2, panel C) and showed a transition from clade 20I (Alpha) to 21A/21I/21J (Delta) dominance, similar to what was observed in Washington overall.

Clark County had very low sequencing coverage over the sentinel surveillance period, ranging from 0.8% of cases in April 2021 to 4.9% of cases in June 2021. Persons <45 years of age and outbreak-associated cases were overrepresented among cases with sequenced specimens, and hospitalized persons were underrepresented. We performed phylogenetic analysis of cases from Clark County during the sentinel surveillance period (Appendix Figure 2, panel D). Despite limited coverage, we observed a variant profile similar to that of Whatcom County and Washington overall. We performed rarefaction analysis and found sentinel sampling from Clark and Whatcom counties displayed higher viral diversity than Yakima County at 2 presentinel timepoints (Figure 2). Additional sampling will be required in all scenarios to fully capture circulating viral diversity.

Timeliness of available genomic data in the GISAID database varied over the study period (Figure 3). During the presentinel period, median timeliness ranged from 23 days in February to 98 days in October of 2020; ≥50% of sequences were uploaded to GISAID >28 days after specimen collection for most months. During the sentinel period, median timeliness was 26 days in August and 15 days in December of 2021; most sequences were uploaded to GISAID

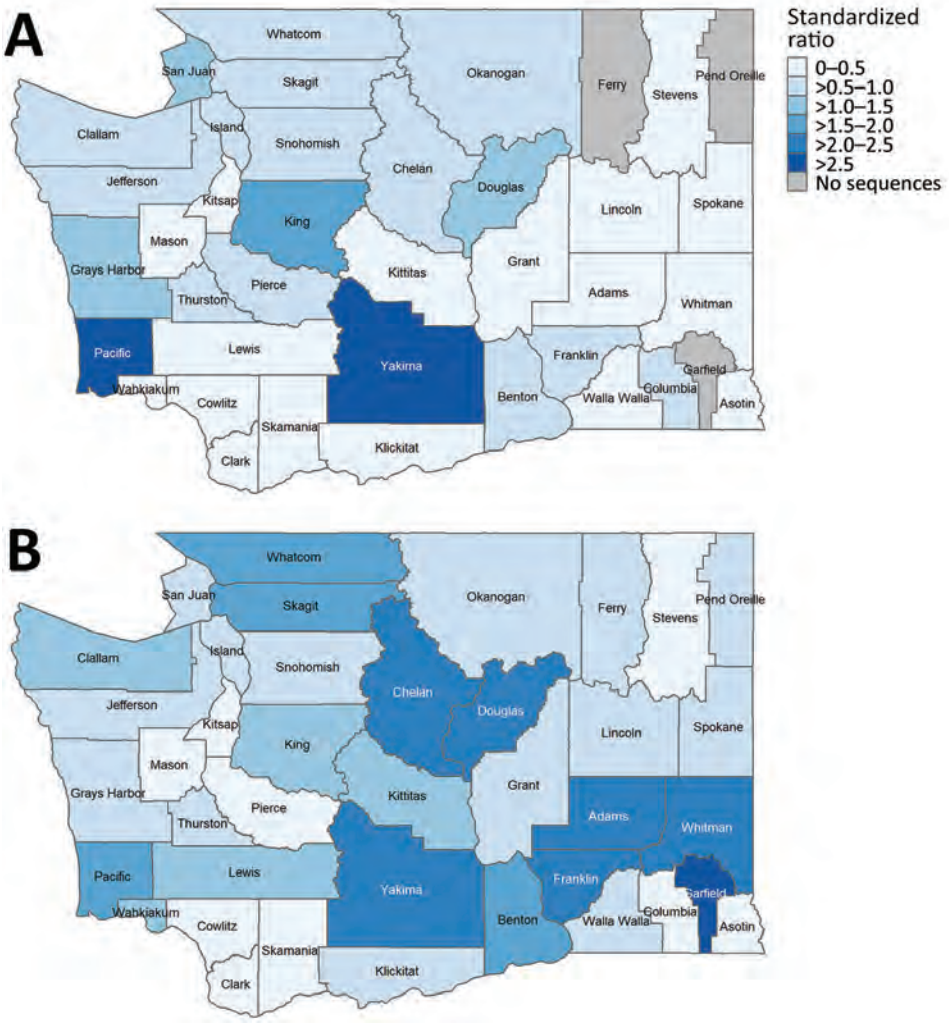

Figure 1. Geographic extent of sequencing data available for COVID-19 cases in study of sentinel surveillance system implementation and evaluation for SARS-CoV-2 genomic data, Washington, USA, 2020–2021. A) Presentinel surveillance (specimens sequenced before March 1, 2021). B) Sentinel surveillance (specimens sequenced on or after March 1, 2021, through the sentinel surveillance program). Standardized ratios (observed/expected counts) of cases with sequenced specimens are indicated by county. No sequence data were available for 3 counties during the presentinel period.

<28 days after specimen collection in all months after sentinel surveillance implementation.

Discussion

After a sentinel surveillance system for sequencing SARS-CoV-2 specimens was implemented in Washington, the available data were more epidemiologically and genomically representative of all COVID-19 cases and timelier than data before sentinel surveillance began. Specifically, representativeness of age, death from COVID-19, outbreak-association status, LTCF-affiliated status, and geographic coverage improved; increased viral diversity was also noted. Before sentinel surveillance began, we were unable to identify a county or period with representative sampling, except for Yakima County during February 2021. After implementation, representativeness improved across multiple areas. Increased representativeness is a critical achievement because genomic data are routinely available to public health leaders and decision-makers; ensuring equitable sampling coverage has substantial implications for response planning and interventions. Measuring effects of genomic surveillance on public health responses in Washington was not included in this study; however, methods for measuring and evaluating effectiveness should be explored.

Overrepresentation of older persons in presentinel genomic data was partly driven by selection of LTCF-associated COVID-19 cases and COVID-19 cases resulting in hospitalization or death. After sentinel surveillance began, the decrease in representation of persons ≥65 years of age improved overall representativeness but actually resulted in undersampling this age group, possibly indicating poor sequencing coverage by facilities where this population seeks care. Indeed, the sentinel surveillance system underrepresents hospitalized cases; further consideration is needed to improve data capture of both inpatient and outpatient COVID-19

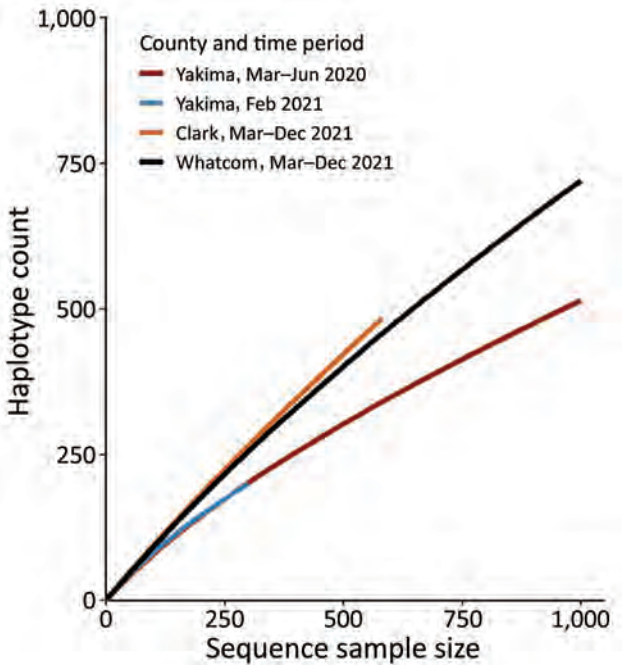

Figure 2. Rarefaction analysis of virus haplotype diversity in Yakima, Clark, and Whatcom Counties in study of sentinel surveillance system implementation and evaluation for SARS-CoV-2 genomic data, Washington, USA, 2020–2021. Presentinel COVID-19 cases (sequenced before March 1, 2021) with sequenced specimens from Yakima County (2 timepoints) were compared with sentinel COVID-19 cases (sequenced on or after March 1, 2021, through the sentinel surveillance program) with sequenced specimens in Clark and Whatcom Counties. Haplotype count indicates virus diversity.

cases. Before sentinel surveillance, outbreak-associated and symptomatic COVID-19 cases were oversampled. After implementation, overrepresentation of those cases decreased but was not resolved. At least 3 possible explanations exist for those findings: specimens from symptomatic SARS-CoV-2–infected persons are more likely to be sequenced because of higher average viral loads, which improves sequencing success; asymptomatic persons might be detected through screening programs not associated with sentinel laboratories; and outbreak-associated specimens might be sent to sentinel laboratories to ensure sequencing for investigative purposes. Random sampling among specimens received at sentinel laboratories could, thereby, still lead to biased samples.

Minority race and ethnicity were more commonly reported among presentinel cases with sequenced specimens; data were also more complete among those cases. Whether true overrepresentation occurred or race data were differentially missing among all cases is unclear. After sentinel surveillance implementation, persons reporting Hispanic ethnicity and Spanish language preference were overrepresented compared with overall cases statewide, which likely reflects the catchment areas of sentinel laboratories. Geographic coverage variability was identified during both presentinel and sentinel surveillance periods. Presentinel coverage focused on western Washington, where laboratories were connected to sequencing capacity. Sentinel surveillance enabled access to sequencing for additional laboratories and ensured greater equitable regional coverage, although variability at the county and subcounty levels remains. Variable coverage and representativeness at the substatewide level should be considered when using genomic data for specific analyses. Increasing geographic coverage will require additional sentinel laboratories that contribute specimens from areas of low coverage.

Other epidemiologic information was of interest in assessing representativeness, including industry and occupation, travel history, and reinfection status. However, data for those variables was incomplete, limiting their usefulness. As public health systems pivot away from capturing data through individual case interviews, datasets available for assessing sampling of specimens for sequencing should be considered. The full potential of genomic epidemiologic surveillance for improving public health requires pairing epidemiologic metadata with genomic data.

Viral diversity has been and continues to be dynamic over the course of the COVID-19 pandemic. Measuring true viral diversity requires random or complete sampling. Actual circulating viral diversity likely differed across locations and timepoints included in our study; if circulating diversity generally increased over time, our conclusions would be biased toward assumption of improved capture because of surveillance.

Other states and countries have used various practices to select SARS-CoV-2 specimens for sequencing. Methods that rely on convenience samples, such as our presentinel system, likely have sampling biases that affect phylogenetic inference. In those settings, weighting cases for inclusion in estimates by using selection probabilities might help to correct bias. Alternatively, approaches to correct for nonrepresentative sampling during analysis, such as inverse probability weighting, should be considered. Even after sentinel surveillance system is put in place, some biases remain, such as undersampling of hospitalized cases, that should be corrected by diversifying sources of specimens. Ongoing evaluation and improvement of systems is necessary, especially in the context of performing epidemiologic studies. Many epidemiologic

studies of COVID-19 have availability of genomic data as an inclusion criterion; if sampling biases are not clarified, biased conclusions might be drawn. Co-development of genomic epidemiology programs alongside bioinformatics programs is needed in public health departments because epidemiologic and phylogenetic analyses are best performed after sampling methods and data limitations are considered.

Although representativeness and timeliness were the focus of this study, other features should be considered in the design of surveillance systems, such as simplicity, flexibility, sensitivity, and stability (*4*). Sentinel surveillance systems are complicated and require ongoing coordination with laboratory partners; stability requires public health resources. Alternative systems to enable representativeness and timeliness while increasing simplicity and stability could include requirements for specimen submission, such as those commonly used for foodborne pathogens and other notifiable conditions. Sensitivity is essential for the surveillance system goals of rare variant detection and timely surveillance of circulating virus variants. Right-size sampling, such as that performed for influenza surveillance, should be considered (*19*; S. Wohl et al., unpub. data, https://www.medrxiv.org/content/10.1101/2021.12.30.21268453v1).

Even after careful consideration of surveillance system design for pathogen sequencing and pairing with epidemiologic data, limitations remain because of specimen requirements for sequencing. Studies using surveillance sequencing data should report the following limitations: application of laboratory-based diagnostic testing might depend on many factors that are difficult to assess and increasingly complex because of availability of improved at-home testing, and, among positive test results, those with a low PCR Ct are more likely to be sequenced. Therefore, representativeness of sequencing data is inherently limited.

Assessment of representativeness during presentinel and sentinel surveillance is limited in the causal inferences that can be drawn. Other concurrent factors might have affected representativeness and timeliness during this study period. For example, CDC surveillance efforts were also increased during this timeframe; samples sequenced under CDC surveillance were coded as sentinel and were analyzed as part of the sentinel surveillance system in Washington.

In conclusion, implementing a sentinel surveillance system for sequencing SARS-CoV-2 specimens was associated with improved genomic and epidemiologic representativeness and timeliness of available sequence data in Washington. Ongoing evaluation and improvements will be necessary to ensure representative capture of inpatient settings. As public health leaders discuss changes to COVID-19 surveillance systems nationally, datasets required to

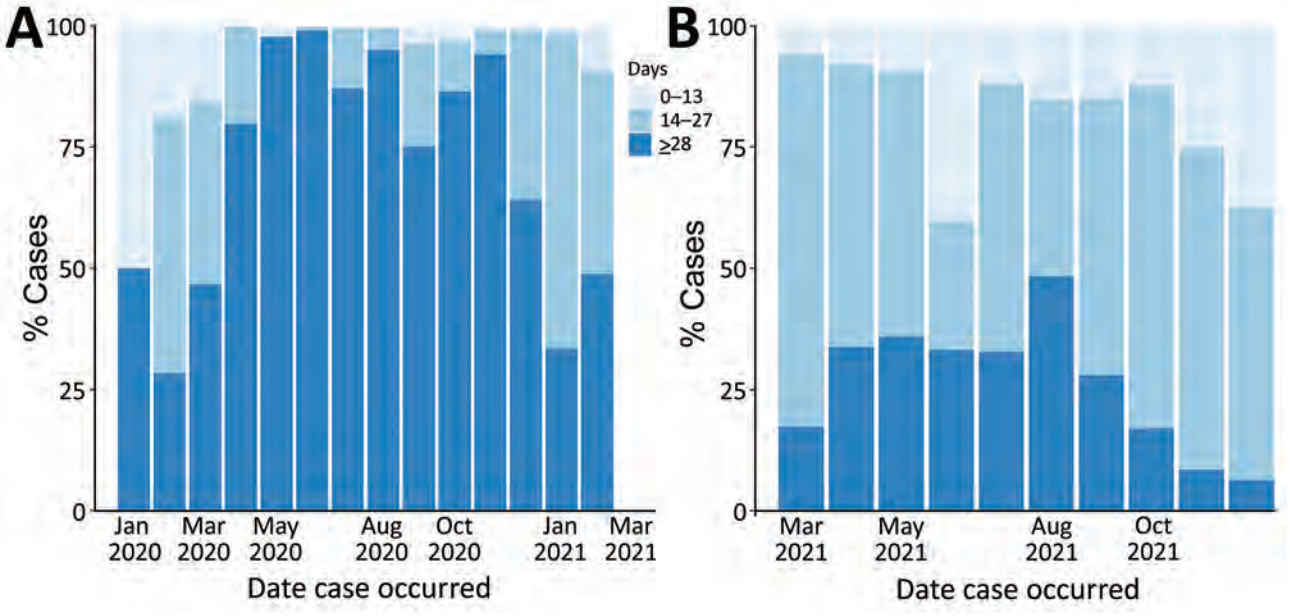

Figure 3. Timeliness of sequence data availability in study of sentinel surveillance system implementation and evaluation for SARS-CoV-2 genomic data, Washington, USA, 2020–2021. Graph shows percentages of COVID-19 cases with sequenced data uploaded to the GISAID database (https://www.gisaid.org) within 0–13, 14–27, and ≥28 days after specimen collection. A) Presentinel surveillance (specimens sequenced before March 1, 2021). B) Sentinel surveillance (specimens sequenced on or after March 1, 2021, through the sentinel surveillance program).

assess representativeness of sampling for sequencing should be considered. Cross-jurisdictional sampling bias is a concern when validating phylogeographic methods applications; attention to sampling will improve the usefulness of those datasets for public health practice.

Acknowledgments

We thank Peter Gibson, Cory Yun, Emily Nebergall, Allison Thibodeau, and Frank Aragona for data linkage and maintenance; Rebecca Thomure for data maintenance; Chris Destro, Renee Takara, Velma Xu, Kelly Thornton, Kelly Burchardt, Guadalupe Munoz-Vargas, Jade Hayes, Bri Spencer, Michelle McCartha, Alexandra Putzier, Micaela Pribic, Sarah Giadone, Linda Peart, Kimberly Dowdle, Katrina Sullivan, Kas Miller, Gillian Conkling, Sarah Haines, Joshua McNamara, Sarah Hulbert, Ashley Romana, Mikelle Quale, Rowan Day, Katelyn Fritz, Edwin Enciso, Helen Dolejsi, Emily Baril, Connor Nels, Kevin Nelson, and Michael Harvey for performing laboratory diagnostic tests and supporting sentinel laboratory specimen selection; Hong Xie, Isabel Arnould, Nathan Breit, Sean Ellis, and Saraswathi Sathees for performing sequencing; Eric Oltean for Python code review and revisions; the originating laboratories Aegis Sciences Corporation, Atlas Genomics, Centers for Disease Control and Prevention, Curative Labs, Fulgent Genetics, Gravity Diagnostics, LLC, Helix, Incyte Diagnostics, Interpath Laboratory, Laboratory Corporation of America, Northwest Laboratory, Overlake Hospital, Quest Diagnostics Incorporated, Seattle Flu Study, University of Washington Virology, Washington State Department of Health Public Health Laboratories for providing specimens for whole-genome sequencing; and the submitting laboratories Altius Institute for Biomedical Research, Centers for Disease Control and Prevention, Curative Labs, Gravity Diagnostics, LLC, Seattle Flu Study, University of Washington Virology, Washington State Department of Health Public Health Laboratories for providing sequence data to GISAID.

Dr. Nickerson is deceased.

This work was supported by the Epidemiology and Laboratory Capacity cooperative agreement from the US Centers for Disease Control and Prevention.

About the Author

Ms. Oltean is a senior epidemiologist at the Washington State Department of Health and a PhD candidate at the University of Washington School of Public Health. Her interests focus on genomic epidemiology and communicable disease surveillance systems design, implementation, and evaluation.

References

1. Ferdinand AS, Kelaher M, Lane CR, da Silva AG, Sherry NL, Ballard SA, et al. An implementation science approach to evaluating pathogen whole genome sequencing in public health. Genome Med. 2021;13:121. https://doi.org/10.1186/s13073-021-00934-7
2. Centers for Disease Control (CDC). Guidelines for evaluating surveillance systems. MMWR Suppl. 1988;37:1–18.
3. German RR, Lee LM, Horan JM, Milstein RL, Pertowski CA, Waller MN; Guidelines Working Group Centers for Disease Control and Prevention (CDC). Updated guidelines for evaluating public health surveillance systems: recommendations from the Guidelines Working Group. MMWR Recomm Rep. 2001;50:1–35. PubMed
4. Paul P, France AM, Aoki Y, Batra D, Biggerstaff M, Dugan V, et al. Genomic surveillance for SARS-CoV-2 variants circulating in the United States, December 2020–May 2021. MMWR Morb Mortal Wkly Rep. 2021;70:846–50. https://doi.org/10.15585/mmwr.mm7023a3
5. Shu Y, McCauley J. GISAID: global initiative on sharing all influenza data—from vision to reality. Euro Surveill. 2017;22:30494. https://doi.org/10.2807/1560-7917.ES.2017.22.13.30494
6. Elbe S, Buckland-Merrett G. Data, disease and diplomacy: GISAID's innovative contribution to global health. Glob Chall. 2017;1:33–46. https://doi.org/10.1002/gch2.1018
7. Khare S, Gurry C, Freitas L, Schultz MB, Bach G, Diallo A, et al. GISAID's role in pandemic response. China CDC Wkly. 2021;3:1049–51. https://doi.org/10.46234/ccdcw2021.255
8. Bedford T, Greninger AL, Roychoudhury P, Starita LM, Famulare M, Huang ML, et al.; Seattle Flu Study Investigators. Cryptic transmission of SARS-CoV-2 in Washington state. Science. 2020;370:571–5. https://doi.org/10.1126/science.abc0523
9. Jorden MA, Rudman SL, Villarino E, Hoferka S, Patel MT, Bemis K, et al.; CDC COVID-19 Response Team. Evidence for limited early spread of COVID-19 within the United States, January–February 2020. MMWR Morb Mortal Wkly Rep. 2020;69:680–4. https://doi.org/10.15585/mmwr.mm6922e1
10. Fauver JR, Petrone ME, Hodcroft EB, Shioda K, Ehrlich HY, Watts AG, et al. Coast-to-coast spread of SARS-CoV-2 during the early epidemic in the United States. Cell. 2020;181:990–996.e5. https://doi.org/10.1016/j.cell.2020.04.021
11. Tordoff DM, Greninger AL, Roychoudhury P, Shrestha L, Xie H, Jerome KR, et al. Phylogenetic estimates of SARS-CoV-2 introductions into Washington state. Lancet Reg Health Am. 2021;1:100018. https://doi.org/10.1016/j.lana.2021.100018
12. Müller NF, Wagner C, Frazar CD, Roychoudhury P, Lee J, Moncla LH, et al. Viral genomes reveal patterns of the SARS-CoV-2 outbreak in Washington state. Sci Transl Med. 2021;13:eabf0202. https://doi.org/10.1126/scitranslmed.abf0202
13. Magee D, Scotch M. The effects of random taxa sampling schemes in Bayesian virus phylogeography. Infect Genet Evol. 2018;64:225–30. https://doi.org/10.1016/j.meegid.2018.07.003
14. Lemey P, Rambaut A, Bedford T, Faria N, Bielejec F, Baele G, et al. Unifying viral genetics and human transportation data to predict the global transmission dynamics of human influenza H3N2. PLoS Pathog. 2014;10:e1003932. https://doi.org/10.1371/journal.ppat.1003932
15. De Maio N, Wu CH, O'Reilly KM, Wilson D. New routes to phylogeography: a Bayesian structured coalescent approximation. PLoS Genet. 2015;11:e1005421. https://doi.org/10.1371/journal.pgen.1005421

16 Washington State Department of Health. SARS-CoV-2 sequencing and variants in Washington state. 2022 [cited 2022 Jun 21]. https://doh.wa.gov/sites/default/files/2022-02/420-316-SequencingAndVariantsReport.pdf
17. R Core Team. R: a language and environment for statistical computing. R Foundation for Statistical Computing, Vienna. 2020 [cited 2022 Sep 19]. https://www.r-project.org
18. Hadfield J, Megill C, Bell SM, Huddleston J, Potter B, Callender C, et al. Nextstrain: real-time tracking of pathogen evolution. Bioinformatics. 2018;34:4121–3. https://doi.org/10.1093/bioinformatics/bty407
19. Association of Public Health Laboratories. Influenza virologic surveillance right size roadmap [cited 2022 Mar 21]. https://www.aphl.org/programs/infectious_disease/influenza/Influenza-Virologic-Surveillance-Right-Size-Roadmap/Pages/default.aspx

Address for correspondence: Hanna Oltean, Washington State Department of Health, 1610 NE 150th St, Shoreline, WA 98155, USA; email: hanna.oltean@doh.wa.gov

Crimean-Congo Hemorrhagic Fever, Spain, 2013–2021

Helena Miriam Lorenzo Juanes,[1] Cristina Carbonell,[1] Begoña Febrer Sendra, Amparo López-Bernus, Alberto Bahamonde, Alberto Orfao, Carmen Vieira Lista, María Sánchez Ledesma, Ana Isabel Negredo, Beatriz Rodríguez-Alonso, Beatriz Rey Bua, María Paz Sánchez-Seco, Juan Luis Muñoz Bellido, Antonio Muro, Moncef Belhassen-García

In support of improving patient care, this activity has been planned and implemented by Medscape, LLC and Emerging Infectious Diseases. Medscape, LLC is jointly accredited with commendation by the Accreditation Council for Continuing Medical Education (ACCME), the Accreditation Council for Pharmacy Education (ACPE), and the American Nurses Credentialing Center (ANCC), to provide continuing education for the healthcare team.

Medscape, LLC designates this Journal-based CME activity for a maximum of 1.00 ***AMA PRA Category 1 Credit(s)™***. Physicians should claim only the credit commensurate with the extent of their participation in the activity.

Successful completion of this CME activity, which includes participation in the evaluation component, enables the participant to earn up to 1.0 MOC points in the American Board of Internal Medicine's (ABIM) Maintenance of Certification (MOC) program. Participants will earn MOC points equivalent to the amount of CME credits claimed for the activity. It is the CME activity provider's responsibility to submit participant completion information to ACCME for the purpose of granting ABIM MOC credit.

All other clinicians completing this activity will be issued a certificate of participation. To participate in this journal CME activity: (1) review the learning objectives and author disclosures; (2) study the education content; (3) take the post-test with a 75% minimum passing score and complete the evaluation at http://www.medscape.org/journal/eid; and (4) view/print certificate. For CME questions, see page 466.

Release date: January 23, 2023; Expiration date: January 23, 2024

Learning Objectives

Upon completion of this activity, participants will be able to:

- Analyze the disease condition of Crimean-Congo hemorrhagic fever
- Assess the epidemiology of Crimean-Congo hemorrhagic fever in the current study
- Assess the clinical presentation of Crimean-Congo hemorrhagic fever in the current study
- Distinguish the most common genotype of Crimean-Congo hemorrhagic fever in the current study

CME Editor

Dana C. Dolan, BS, Technical Writer/Editor, Emerging Infectious Diseases. *Disclosure: Dana C. Dolan, BS, has disclosed no relevant financial relationships.*

CME Author

Charles P. Vega, MD, Health Sciences Clinical Professor of Family Medicine, University of California, Irvine School of Medicine, Irvine, California. *Disclosure: Charles P. Vega, MD, has the following relevant financial relationships: consultant or advisor for GlaxoSmithKline; Johnson & Johnson Pharmaceutical Research & Development, L.L.C.*

Authors

Helena Miriam Lorenzo Juanes, PharmD, PhD Student; Cristina Carbonell, MD, PhD; Begoña Febrer Sendra, BSc, PhD Student; Amparo López-Bernus, MD, PhD; Alberto Bahamonde, MD, PhD; Alberto Orfao, MD, PhD; Carmen Viera Lista, BSc, PhD Student; María Sánchez Ledesma, MD, PhD; Ana Isabel Negredo, PhD; Beatriz Rodríguez Alonso, MD, PhD; Beatriz Rey Bua, MD; María Paz Sánchez Seco, PhD; Juan Luis Muñoz Bellido, MD, PhD; Antonio Muro, MD, PhD; Moncef Belhassen-García, MD, PhD.

[1]These authors contributed equally to this article.

Crimean-Congo hemorrhagic fever (CCHF) is a viral infectious disease for which distribution of the main vector, *Hyalomma* spp. ticks, is expanding. We analyzed all 10 cases of CCHF diagnosed in Spain during 2013–2021; case-patient median age was 56.5 years, and 7 were men. We identified CCHF virus genotypes III and V. Six case-patients acquired the infection in urban areas. Sixty percent of patients were infected in summer and 40% in spring. Two patients met criteria for hemophagocytic syndrome. Seven patients survived. The epidemiologic pattern of CCHF in Spain is based on occasional cases with an elevated mortality rate. Genotype III and, to a less extent also genotype V, CCHF circulates in humans in a common geographic area in Spain. Those data suggest that the expansion pathways are complex and may change over time. Physicians should remain alert to the possibility of new CCHF cases.

Crimean-Congo hemorrhagic fever (CCHF) is a tickborne viral disease caused by the CCHF virus (CCHFV), a negative single-stranded RNA virus of the genus *Orthonairovirus* in the Nairoviridae family (*1*). CCHF is considered an emerging infectious disease because of the expanding distribution of its main vector, ticks of the genus *Hyalomma*. Consequently, CCHF is listed by the World Health Organization as one of the top-priority diseases for research and development in public health emergency contexts (https://www.who.int/activities/prioritizingdiseases-for-research-and-development-in-emergency-contexts) (*2*).

The spectrum of clinical manifestations of CCHF ranges from subclinical illness (including fever, headache, malaise, myalgia, sore throat, dizziness, abdominal pain, nausea, vomiting, conjunctivitis, and photophobia) (*3*) to acute infection with hemorrhage, multiorgan failure, and death (*4*). Laboratory findings are frequently remarkable, including leukopenia, thrombocytopenia, and elevated liver transaminases in serum (*5*). Some studies have suggested the relevance of the innate immune system in limiting the spread of the virus, but the specific mechanisms leading to asymptomatic versus severe disease remain unknown.

In recent years, the epidemiology of CCHFV has changed; climate change has been identified as one of the factors driving the circulation of the virus. CCHFV has been identified in Africa, Asia, and Europe, in territories located south of the 50th North parallel, the area inhabited by its main vector (*6*–*8*). CCHFV has caused major outbreaks in eastern Europe (*9*). In turn, CCHF is considered endemic in areas of southwestern Europe.

Our group identified the first human cases in western Spain in summer 2013 (*10*–*13*). In Spain, the CCHFV genotype identified from patients in 2016 and 2018 belonged to the African genotype III, the European genotype V, and the Asian genotype IV where the group Africa 4 is placed (*10*,*12*,*13*). A strong clinical suspicion is required to obtain fast and accurate diagnosis, initiate supportive treatment if needed, and activate biosafety measures to prevent nosocomial transmission (*10*). Herein, we report on the clinical and epidemiologic pattern and the genotype of the virus identified in all patients with CCHF investigated in Spain from 2013 through May 2022.

The Clinical Research Ethics Committee of Investigation with Drugs of the Hospital Universitario de Salamanca (Salamanca, Spain) approved the study protocol (CEIMC PI 91 09/2017). All procedures described were carried out in accordance with the ethical standards described in the Revised Declaration of Helsinki of 2013. All clinical and epidemiologic data were anonymized.

Methods

Study Type and Sample Collection

We retrospectively analyzed records of all patients that had been diagnosed of CCHF in Spain during 2013–2022. Five cases were identified after searching PubMed for literature published during 2016–May 2022. Four cases were identified at Hospital Universitario de Salamanca (Salamanca, Spain) in 2020–2021.

Author affiliations: Universidad de Salamanca, Salamanca, Spain (H. Lorenzo-Juanes, C. Carbonell, B. Febrer-Sendra, A. López-Bernus, A. Orfao, C. Viera Lista, M. Sánchez Ledesma, B. Rodriguez Alonso, B. Rey Bua, J.L. Muñoz Bellido, A. Muro, M. Belhassen-Garcia); Instituto de Investigación Biomédica de Salamanca, Salamanca (H.M. Lorenzo Juanes, C. Carbonell, B. Febrer Sendra, A. López-Bernus, C. Vieira Lista, B. Rodriguez-Alonso, B. Rey Bua, M.P. Sánchez-Seco, A. Muro, M. Belhassen-Garcia); Hospital Universitario de Salamanca, Salamanca (H.M. Lorenzo Juanes, C. Carbonell, M. Sánchez Ledesma, B. Rodríguez-Alonso, B. Rey Bua); Hospital El Bierzo, Ponferrada, Spain (A. Bahamonde); Centro de Investigación del Cáncer, Salamanca (A. Orfao); Centro de Investigación Biomédica en Red de Cáncer, Madrid, Spain (A. Orfao); Centro Nacional de Microbiologiia, Majadahonda, Spain (A.I. Negredo, M.P. Sánchez-Seco); Red de Investigación Colaborativa en Enfermedades Tropicales, Madrid (A.I. Negredo, M.P. Sánchez-Seco, J.L. Muñoz Bellido) Centro de Investigación Biomédica en Red en Enfermedades Infecciosas, Madrid (A.I. Negredo, M.P. Sánchez-Seco)

DOI: https://doi.org/10.3201/eid2902.220677

Another case was identified at Hospital del Bierzo (Ponferrada, Spain) in June 2021. All epidemiologic, clinical, and analytical parameters were recorded according to a predefined clinical protocol. For all cases, diagnosis of CCHF was confirmed at the National Microbiology Center of the Instituto de Salud Carlos III (Madrid, Spain).

Phylogenetic Analysis

We aligned CCHFV sequences using ClustalW software (https://www.genome.jp/tools-bin/clustalw). We constructed the phylogenetic tree using a Tamura 3-parameter model based on sequences of the CCHFV small segment. We used the neighbor-joining method in MEGA X software version 10.2.5 (https://www.megasoftware.net) and based bootstrap confidence limits on 1,000 replicates.

Statistical Analyses

We used the SPSS Statistics 25.0 (https://www.ibm.com/spss) for all statistical analyses. We calculated median (range) and mean values and their SDs for continuous variables; we used frequencies for categorical variables.

Results

We extracted data for patients 1, 2, 3, 4, and 8 from published papers (*10*–*13*). In turn, we conducted retrospective analysis on the medical records of all other patients with CCHF identified from Hospital Universitario de Salamanca and Hospital del Bierzo; we recorded demographic patient data, case history, symptoms, clinical signs, laboratory results, and outcomes for each patient (Table 1). Patient median age was 56.5 years (range 30–74 years); 7 were men and 3 women. Six patients had been infected in urban areas. The distribution of cases during the year was as follows: 1 case in April, 1 in May, 2 in June, 2 in July, and 4 in August (Figure 1).

Eight of the 10 patients reported tick bites (Table 2). The mean ±SD time from the bite to the onset of symptoms was 5.1 ± 3.4 days (range 2–12 days). The median duration between the onset of symptoms and hospital admission was 5.1 ± 3.1 days (range 2–12 days). All case-patients had sought care for fever and exanthema with a mean duration of 5.2 ± 1.64 days (Figure 2). Eight patients had muscle soreness; 4 patients had diarrhea, and 4 had vomiting, nausea, or both. Three case-patients (5, 6, and 9) underwent bone marrow biopsy; 2 of them, patients 5 and 9, had hemophagocytosis, which fulfilled the criteria for hemophagocytic syndrome (Figure 3). Ferritin serum level was elevated in 7 patients.

All patients received antimicrobial treatment with doxycycline while hospitalized. In addition, 5 patients received supportive treatment, 4 patients had taken treatment for bleeding, and 3 patients received ribavirin. None of those receiving antiviral treatment died; however, the sample size was small.

The mean ±SD score on the Bakir prognostic scale (*16*) was 5.0 ± 2.3. Seven patients survived with full recovery, whereas the other 3 died. Those 3 patients who died had the highest scores on the Bakir scale (1 patient scored 8 and the other 2 scored 7).

In most cases (patients 1, 2, 5, 6, and 7), disease was caused by CCHFV genotype III (Africa 3). Patient 3 had a new lineage, Africa 4 (Figure 1) within genotype IV. Isolates from patients 4 and 9 belonged to genotype V (Europe 1). We did not identify the genotype for patients 8 and 10. Of note, genotypes III and V were found to circulate in the same geographic area. We deposited the sequences into GenBank under accession nos. KY492290 (patient 1), KY492289 (patient 2), MN689739 (patient 3), ON227355 (patient 4), OP776634 (patient 5), OP776632 (patient 6), OP776631 (patient 7), and OP776633 (patient 9).

Table 1. Main epidemiologic data of patients with Crimean-Congo hemorrhagic fever, Spain, 2013–2021*

Characteristic	Patient no. and source									
	1 (*10*)	2 (*10*)	3 (*12*)	4 (*13*)	5	6	7	8 (*11*)	9	10
Age, y	62	50	74	53	70	54	69	32	59	30
Sex	M	F	M	M	M	M	M	F	M	F
Rural location	No	No	No	Yes	Yes	Yes	Yes	No	Yes	No
Date	2016 Aug	2016 Aug	2018 Jul	2018 Aug	2020 Jun	2020 Jul	2020 Aug	2013 May	2021 Apr	2021 Jun
Risk factors†	Leisure	Nurse	Hunting	Ag	Ag	Ag	Leisure	Leisure	Ag	Leisure
Comorbidities	HTN, OSA	None	None	Hepatic steatosis, active drinker	Tongue cancer	TB, brucellosis, active drinker	HTN	None	Diabetes mellitus, dyslipemia	Diabetes mellitus
Bakir scale at admission	7	0	7	6	6	4	8	5	2	5
Outcome	Died	Good	Died	Good	Good	Good	Died	Good	Good	Good

*Source is indicated if other than this study. Ag, agriculture; HTN, hypertension; OSA, obstructive sleep apnea.
†Risk factors include high-risk occupations; agriculture includes shepherding activities.

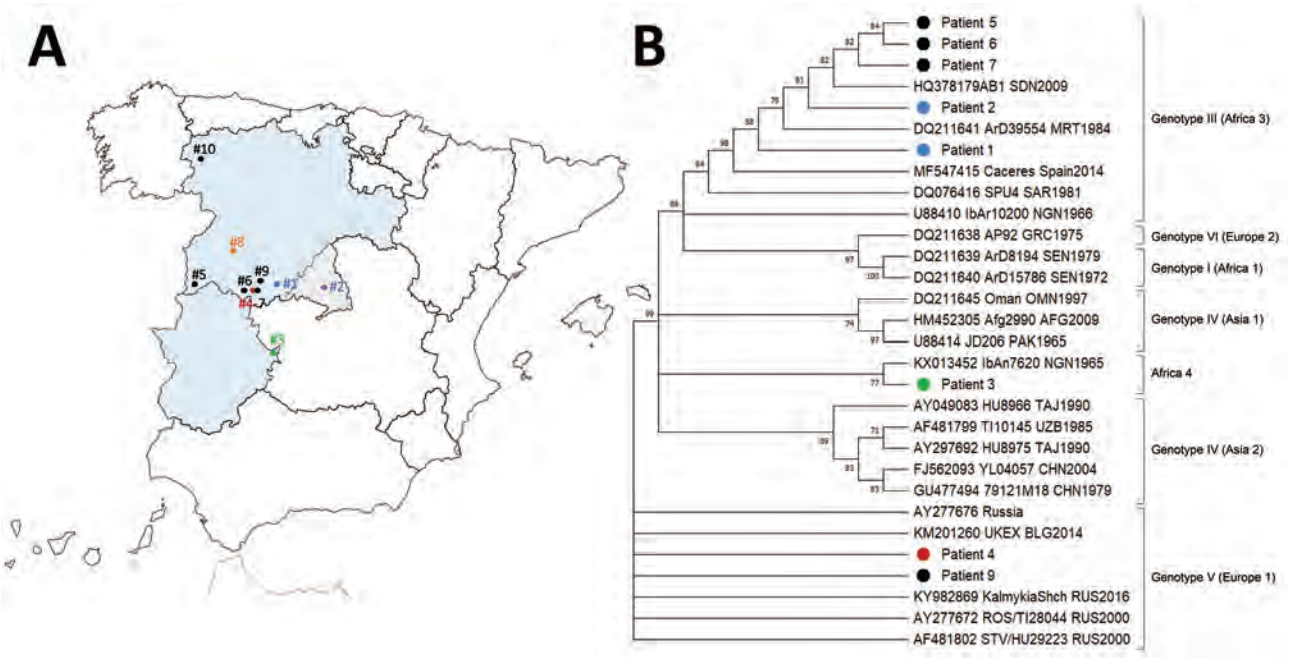

Figure 1. Locations of CCHF cases (A) and phylogenetic tree of CCHFV (B) in Spain, 2013–2021. Dots on the map indicate patients with a CCHF diagnosis in Spain: black dots indicate cases from this study, and colored dots indicate cases previously described. Two cases (patients 8 and 10) were not sequenced. The phylogenetic tree was constructed by the neighbor-joining method based on sequences of the small segment of the virus. The numbers on the right indicate bootstrap values for the groups; values <75 are not shown. Other sequences are listed by GenBank accession number, strain, geographic origin, and sampling year. Genotypes are indicated by Roman numerals according to Carrol et al. (*29*) with the equivalent clade nomenclature according to Chamberlain et al. (*30*) in brackets; I, West Africa (Africa 1); III, South and West Africa (Africa 3); IV, Middle East/Asia, divided into 2 groups (Asia 1/Asia 2); V, Europe/Turkey (Europe 1); VI, Greece (Europe 2). New lineage, Africa 4 described by Negredo et al. (*12*). CCHF, Crimean-Congo hemorrhagic fever; CCHFV, CCHF virus.

Discussion

We describe the demographic, epidemiologic, clinical, and laboratory features of all 10 cases of CCHFV reported in Spain since 2013, when the causative agent was first discovered in this country (*11*). Our findings have updated the knowledge of CCHFV in Spain to show the pattern during the period 2013–2021 in southern Europe. Half (5/10) of the cases we described in this article were treated at Hospital Universitario de Salamanca *(10–13*). CCHFV was found in western Spain in 2010 in ticks (*Hyalomma lusitanicum*) feeding on wild animals in the province of Caceres (*17*).

Studies carried out in the same period and the same geographic areas in Spain in healthy donors (*18*) showed a serologic prevalence of past infection of ≈1.16% and in patients who sought emergency care for febrile syndrome (*13*) of ≈2.22%. Altogether, these results suggest that CCHF is underdiagnosed in this region. However, the high frequency of asymptomatic patients, which exceeds 88% in some studies, might also account for such differences (*3,4*).

Spain's geographic proximity to Africa is a risk factor for continuous entry of CCHFV. Its favorable climate, the wide presence of the vector involved in transmission, the variety of vertebrate animals that can act as amplifying hosts, and its location along the path of transit for migratory birds from CCHFV-endemic areas all increase the risk for spread of the virus.

Most infections in this study occurred in spring and summer in rural areas of central-western Spain. Of the cases that occurred in the southern part of the autonomous community of Castile and León, likely causes are specific climatic features (e.g., temperature, humidity), geographic conditions, flora and wildlife, the animal husbandry sector, and increased contact with animals and ticks. In this regard, field studies have confirmed that these areas are at risk for CCHF because of the abundance of *H. lusitanicum* ticks, the presence of CCHFV in the specimens collected, together with the high prevalence observed in wild and domestic animals in these and other areas of the country (*17,19–22*).

The epidemiologic pattern we report for Spain resembles that of countries such as Greece and Kosovo (*23,24*), with few and occasional cases, and clearly

differs from the epidemiologic evolution of countries such as Turkey (*25*), which has a marked and progressive increase in cases since its earliest recorded case in 2002. Those distinct epidemiologic evolution profiles might be related to differences in farming and sheep-herding activities, as well as the specific climate conditions; in Turkey, a notable and specific risk factor is living at altitudes >836.5 m (*26*). We noted the possibility of secondary transmission of CCHF to healthcare workers, particularly during accidental contact such as resuscitation of severely ill patients, and the need for strict rules and protocol for handling potential secondary cases (*10*).

Clinical findings in the patients we reviewed revealed that the most common symptoms were fever, exanthema, and myalgia. However, we also noted findings of bleeding (7/10 cases) at higher frequencies than those reported previously (*25*). Two patients with CCHFV experienced hemophagocytic syndrome with hemophagocytosis in the bone marrow. Hemophagocytic syndrome is a rare and severe disease characterized by fever; hepatosplenomegaly; cytopenia; elevated ferritin, lactate dehydrogenase and triglyceride levels; and hemophagocytosis in the bone marrow. Clinical and biologic symptoms of hemophagocytic syndrome are caused by cytokines secreted by T-lymphocytes and macrophages. A main challenge in patients with hemophagocytic syndrome is its diagnosis, which must meet well-established criteria (*27*). The relationship between CCHFV and hemophagocytic syndrome has been previously described (*28*), but unlike in those studies, the patients in our

Table 2. Main clinical and laboratory data of patients with Crimean-Congo hemorrhagic fever, Spain, 2013–2021*

Characteristic	Patient no. and source									
	1 (*10*)	2 (*10*)	3 (*12*)	4 (*13*)	5	6	7	8 (*11*)	9	10
Main clinical data										
Tick bite	Y	N	Y	N	Y	Y	Y	Y	Y	Y
First symptom	Fever	Fever	Fever	Fever	Fever	Fever	Fever	Fever	Fever	Fever
Fever duration, d	4	5	6	6	9	5	4	4	4	5
Days from first symptom to admission	3	2	4	5	9	7	3	2	4	12
Digestive symptoms	Y	Y	Y	N	Y	N	Y	Y	Y	Y
Any bleeding	Y	Y	Y	N	Y	N	Y	Y	N	Y
Laboratory data†										
Hemoglobin, g/dL	13.4	13.9	13.5	14.1	14.6	15.5	13.4	14.4	17	17
Leukocytes, $\times 10^3$ cells/mm^3	13.9	6.2	10.7	3.1	2.4	2.3	5.5	1.5	2.8	11.1
Neutrophils, %	85.5	83	90	62	33	66.4	69	63	68.5	90
Lymphocytes, %	7.9	10.2	5	27	38	26.1	25	31	24.4	4
Platelets, $\times 10^3$/mm^3	30	174	229	41	44	32	7	44	76	159
Glucose, mg/d	80	102	83	135	110	134	280	106	116	491
Creatinine, mg/dL	1.69	1.24	0.83	1.33	0.92	0.75	4.8	0.67	0.85	1.1
CRP, mg/L	87.6	2.9	ND	15.2	0.3	0.65	3.72	0.6	0.55	52
AST, U/L	203	24	20	347	273	273	1,305	494	107	72
ALT, U/L	88	37	9	161	281	135	347	171	141	70
Ferritin, ng/mL	ND	ND	>40,000‡	15,718	34,044	28,393	60,000	ND	7,878	1,147
Bilirubin, mg/dL	0.9	0.5	0.5	0.7	0.43	0.35	1.4	0.29	0.58	ND
GGT, U/L	ND	ND	ND	425	272	132	1,420	77	136	ND
ALP, U/L	ND	ND	ND	103	84	59	239	58	72	91
LDH, U/L	ND	ND	172	721	358	589	2,311	1,085	341	272
Triglycerides, mg/dL	ND	ND	ND	ND	ND	407‡	ND	ND	164‡	ND
Prothrombin time, s	18.1	15.6	10.7	10.2	10	12	13	12	11	ND
Prothrombin activity, %	52.8	62	104	106	123	99	86	81	102	84
Partial thromboplastin time, s	18.1	48.7	26.2	43.8	30.2	52.7	61.4	128	ND	29
Functional fibrinogen, mg/dL	ND	265.9	320	605	281	304	156	141	272	325
D-dimer, ng/mL	ND	35,200	ND	ND	ND	1.3	5.5	3.48	ND	ND
Genotype	III	III	IV	V	III	III	III	ND	V	ND
Treatment	DOX; support	DOX; ribavirin orally for 9 d	DOX; support	DOX	DOX; ribavirin orally for 10 d§	DOX; ribavirin orally for 10 d§	DOX support	DOX; support	DOX	DOX; support
Length of stay, d	9	23	8	6	22	9	2	17	9	8

*Source is indicated if other than this study. ALP, alkaline phosphatase; ALT, alanine aminotransferase; AST, aspartate aminotransferase; CRP, C-reactive protein; DOX, doxycycline; GGT, gamma-glutamyl transferase; LDH, lactate dehydrogenase; ND, no data.
†Analysis upon admission or during the first 24 hours.
‡Analysis performed during hospital admission.
§In accordance with World Health Organization guidelines.

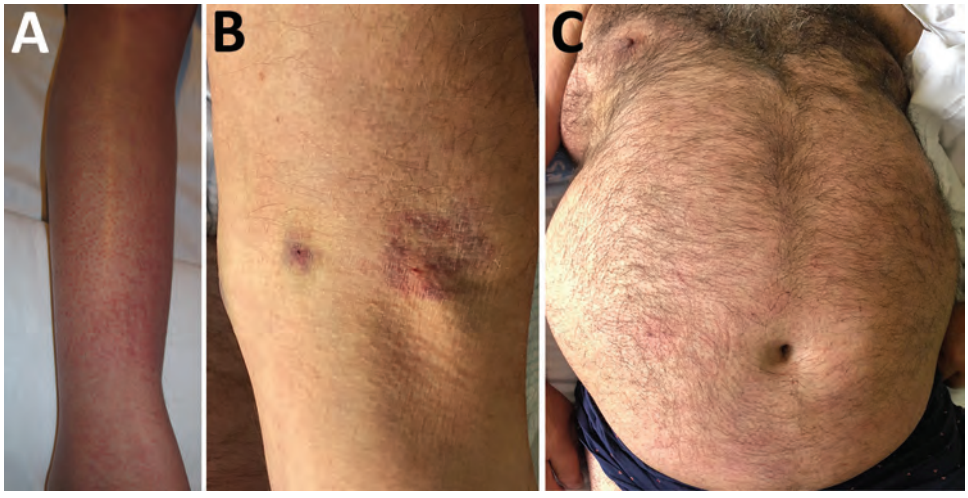

Figure 2. Images of patients in study of Crimean-Congo hemorrhagic fever, Spain, 2013–2021. A) Details of a slightly purpuric rash on the leg of patient 8. B) Ecchymosis on the arm of patient 5. C) Mild rash on the chest of patient 9.

review did not experience serious bleeding episodes. However, high levels of serum ferritin in patients who underwent analytical determination suggest a higher prevalence of hemophagocytic syndrome than previously described; further research is needed to elucidate the specific mechanisms involved.

All patients received doxycycline accompanied by other antimicrobial drugs, possibly because of initial suspicion of rickettsiosis. Five patients required intensive care treatment; 3 of them died. Ribavirin was prescribed to 3 patients, who all recovered and survived. Despite the potential benefit of ribavirin, the small number of patients makes it difficult to draw conclusions regarding its effectiveness for treating CCHF patients. Furthermore, a recent Cochrane meta-analysis was unable to confirm the potential benefit of ribavirin in CCHFV-infected patients (*29*).

In Spain, where most CCHF patients have been diagnosed since 2018, the fatality rate of CCHF was as high as 30%. Of note, those 3/10 patients who died showed the highest Bakir-scale scores (>7) at admission. Previous studies have shown that in this viral infection transmitted by ticks, regional differences in mortality rates may be related to factors including the availability of advanced medical care facilities, faster diagnosis because of a better surveillance system that enables early detection of cases with mild to moderate clinical findings, the routes of acquisition of the infection, and the genotype of the virus. In Turkey, which has a CCHF mortality rate of ≈5%, the most common strain is homologous to the strain detected in Russia and Kosovo, whereas in Spain, the most common strain is the Africa III. Two of our cases infected with strain V have had good outcomes described; cases of genotypes III and V have been detected in the same area.

Previous studies indicated that birds are involved in the transmission of the Africa genotype III virus (*30*). Domestic animals such as pigs have been imported from countries in eastern Europe, indicating a possible relationship with the CCHF epidemiology of European strains, particularly those of genotype V. Of interest, a strain of CCHFV was detected in ticks in Spain (*21*). From a clinical point of view, genotypes III and IV have been associated with more deaths than genotype V in our cases, although the number of patients still remains very limited.

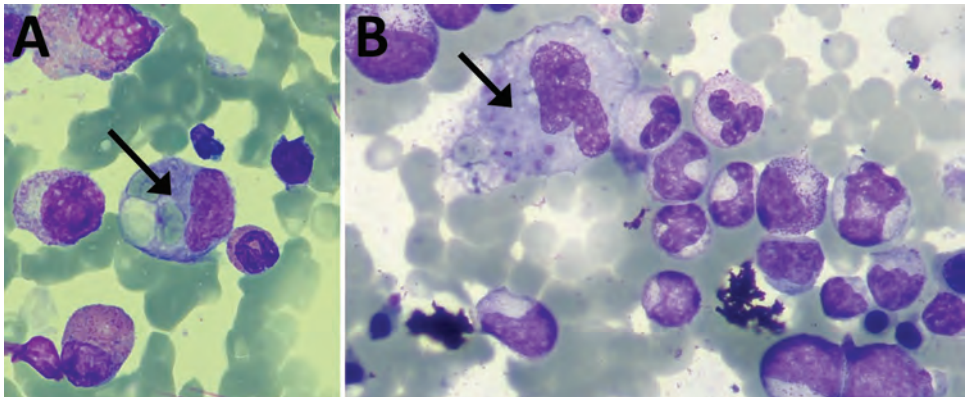

Figure 3. Bone marrow biopsy findings from patient 5 (A) and patient 9 (B) in study of Crimean-Congo hemorrhagic fever, Spain, 2013–2021. Arrows indicate macrophages with hemophagocytosis phenomena of red blood cells and platelets.

In Spain, circulation in wild animals of 3 different genotypes (III, IV, and V) of CCHFV has been demonstrated, even in the same geographic area; genotype III was the most prevalent. Those data suggest that the expansion pathways of the different CCHFV genotypes in Spain are complex and coincide over time; further studies are needed to clarify the dissemination of CCHFV in southern Europe. In addition, our results revealed a complex epidemiologic pattern in Spain in which uncommon CCHF cases were associated with high mortality rates. Thus, although the risk is considered low, hospital doctors and general practitioners should be alert to the possibility of new CCHF cases, given the high pathogenicity of CCHFV. A detailed medical history of the patient, including travel history and possible risk factors, is critical for fast diagnosis and appropriate adoption of therapeutic measures for timely control of the infection.

Acknowledgments

We thank all the staff of the Hospitals of Castilla y Leon, Spain, for their extraordinary dedication and contribution to the care of patients with CCHF.

Funding was provided by Consejería de Sanidad, Junta de Castilla y León; Institute of Health Carlos III, Spain; and Red de Investigación Cooperativa en Enfermedades Tropicales (grant nos. RD16/0027/0018 and RD16CIII/0003/0003). European Union co-financing was through Fondo Europeo de Desarrollo Regional ("Una manera de hacer Europa" funding and grant no. IPI16/01784).

About the Author

Ms. Lorenzo Jaunes is a clinical microbiologist at Hospital Universitario de Salamanca, Salamanca, Spain, pursuing her PhD at the time of this study. Her primary research interests include zoonotic diseases and arthropod-borne and emerging diseases.

References

1. Ballinger MJ, Medeiros AS, Qin J, Taylor DJ. Unexpected differences in the population genetics of phasmavirids (*Bunyavirales*) from subarctic ponds. Virus Evol. 2017;3:vex015. https://doi.org/10.1093/ve/vex015
2. Dai S, Deng F, Wang H, Ning Y. Crimean-Congo hemorrhagic fever virus: current advances and future prospects of antiviral strategies. Viruses. 2021;13:1195. https://doi.org/10.3390/v13071195
3. Çevik MA, Erbay A, Bodur H, Gülderen E, Baştuğ A, Kubar A, et al. Clinical and laboratory features of Crimean-Congo hemorrhagic fever: predictors of fatality. Int J Infect Dis. 2008;12:374–9. https://doi.org/10.1016/j.ijid.2007.09.010
4. Bodur H, Akinci E, Ascioglu S, Öngürü P, Uyar Y. Subclinical infections with Crimean-Congo hemorrhagic fever virus, Turkey. Emerg Infect Dis. 2012;18:640–2. https://doi.org/10.3201/eid1804.111374
5. Mostafavi E, Pourhossein B, Chinikar S. Clinical symptoms and laboratory findings supporting early diagnosis of Crimean-Congo hemorrhagic fever in Iran. J Med Virol. 2014;86:1188–92. https://doi.org/10.1002/jmv.23922
6. Bente DA, Forrester NL, Watts DM, McAuley AJ, Whitehouse CA, Bray M. Crimean-Congo hemorrhagic fever: history, epidemiology, pathogenesis, clinical syndrome and genetic diversity. Antiviral Res. 2013;100:159–89. https://doi.org/10.1016/j.antiviral.2013.07.006
7. Spengler JR, Bente DA. Crimean-Congo hemorrhagic fever in Spain—new arrival or silent resident? N Engl J Med. 2017;377:106–8. https://doi.org/10.1056/NEJMp1707436
8. Estrada-Peña A, de la Fuente J. The ecology of ticks and epidemiology of tick-borne viral diseases. Antiviral Res. 2014;108:104–28. https://doi.org/10.1016/j.antiviral.2014.05.016
9. Monsalve-Arteaga L, Alonso-Sardón M, Muñoz Bellido JL, Vicente Santiago MB, Vieira Lista MC, López Abán J, et al. Seroprevalence of Crimean-Congo hemorrhagic fever in humans in the World Health Organization European region: a systematic review. PLoS Negl Trop Dis. 2020;14:e0008094. https://doi.org/10.1371/journal.pntd.0008094
10. Negredo A, de la Calle-Prieto F, Palencia-Herrejón E, Mora-Rillo M, Astray-Mochales J, Sánchez-Seco MP, et al.; Crimean Congo Hemorrhagic Fever@Madrid Working Group. Autochthonous Crimean-Congo hemorrhagic fever in Spain. N Engl J Med. 2017;377:154–61. https://doi.org/10.1056/NEJMoa1615162
11. Negredo A, Sánchez-Ledesma M, Llorente F, Pérez-Olmeda M, Belhassen-García M, González-Calle D, et al. Retrospective identification of early autochthonous case of Crimean-Congo hemorrhagic fever, Spain, 2013. Emerg Infect Dis. 2021;27:1754–6. https://doi.org/10.3201/eid2706.204643
12. Negredo A, Sánchez-Arroyo R, Díez-Fuertes F, de Ory F, Budiño MA, Vázquez A, et al. Fatal case of Crimean-Congo hemorrhagic fever caused by reassortant virus, Spain, 2018. Emerg Infect Dis. 2021;27:1211–5. https://doi.org/10.3201/eid2704.203462
13. Monsalve Arteaga L, Muñoz Bellido JL, Negredo AI, García Criado J, Vieira Lista MC, Sánchez Serrano JÁ, et al. New circulation of genotype V of Crimean-Congo haemorrhagic fever virus in humans from Spain. PLoS Negl Trop Dis. 2021;15:e0009197. https://doi.org/10.1371/journal.pntd.0009197
14. Carroll SA, Bird BH, Rollin PE, Nichol ST. Ancient common ancestry of Crimean-Congo hemorrhagic fever virus. Mol Phylogenet Evol. 2010;55:1103–10. https://doi.org/10.1016/j.ympev.2010.01.006
15. Chamberlain J, Cook N, Lloyd G, Mioulet V, Tolley H, Hewson R. Co-evolutionary patterns of variation in small and large RNA segments of Crimean-Congo hemorrhagic fever virus. J Gen Virol. 2005;86:3337–41. https://doi.org/10.1099/vir.0.81213-0
16. Bakır M, Gözel MG, Köksal I, Aşık Z, Günal Ö, Yılmaz H, et al. Validation of a severity grading score (SGS) system for predicting the course of disease and mortality in patients with Crimean-Congo hemorrhagic fever (CCHF). Eur J Clin Microbiol Infect Dis. 2015;34:325–30. https://doi.org/10.1007/s10096-014-2238-0
17. Estrada-Peña A, Palomar AM, Santibáñez P, Sánchez N, Habela MA, Portillo A, et al. Crimean-Congo hemorrhagic fever virus in ticks, southwestern Europe, 2010. Emerg Infect Dis. 2012;18:179–80. https://doi.org/10.3201/eid1801.111040

18. Monsalve Arteaga L, Muñoz Bellido JL, Vieira Lista MC, Vicente Santiago MB, Fernández Soto P, Bas I, et al. Crimean-Congo haemorrhagic fever (CCHF) virus-specific antibody detection in blood donors, Castile-León, Spain, summer 2017 and 2018. Euro Surveill. 2020;25:1900507. https://doi.org/10.2807/1560-7917.ES.2020.25.10.1900507
19. Moraga-Fernández A, Ruiz-Fons F, Habela MA, Royo-Hernández L, Calero-Bernal R, Gortazar C, et al. Detection of new Crimean-Congo haemorrhagic fever virus genotypes in ticks feeding on deer and wild boar, Spain. Transbound Emerg Dis. 2021;68:993–1000. https://doi.org/10.1111/tbed.13756
20. Espunyes J, Cabezón O, Pailler-García L, Dias-Alves A, Lobato-Bailón L, Marco I, et al. Hotspot of Crimean-Congo hemorrhagic fever virus seropositivity in wildlife, northeastern Spain. Emerg Infect Dis. 2021;27:2480–4. https://doi.org/10.3201/eid2709.211105
21. Sánchez-Seco MP, Sierra MJ, Estrada-Peña A, Valcárcel F, Molina R, de Arellano ER, et al.; Group for CCHFv Research. Widespread detection of multiple strains of Crimean-Congo hemorrhagic fever virus in ticks, Spain. Emerg Infect Dis. 2021;28:394–402. https://doi.org/10.3201/eid2802.211308
22. Negredo A, Habela MÁ, Ramírez de Arellano E, Diez F, Lasala F, López P, et al. Survey of Crimean-Congo hemorrhagic fever enzootic focus, Spain, 2011–2015. Emerg Infect Dis. 2019;25:1177–84. https://doi.org/10.3201/eid2506.180877
23. Papa A, Sidira P, Larichev V, Gavrilova L, Kuzmina K, Mousavi-Jazi M, et al. Crimean-Congo hemorrhagic fever virus, Greece. Emerg Infect Dis. 2014;20:288–90. https://doi.org/10.3201/eid2002.130690
24. Ahmeti S, Berisha L, Halili B, Ahmeti F, von Possel R, Thomé-Bolduan C, et al. Crimean-Congo hemorrhagic fever, Kosovo, 2013–2016. Emerg Infect Dis. 2019;25:321–4. https://doi.org/10.3201/eid2502.171999
25. Yilmaz GR, Buzgan T, Irmak H, Safran A, Uzun R, Cevik MA, et al. The epidemiology of Crimean-Congo hemorrhagic fever in Turkey, 2002–2007. Int J Infect Dis. 2009;13:380–6. https://doi.org/10.1016/j.ijid.2008.07.021
26. Aker S, Akıncı H, Kılıçoğlu C, Leblebicioglu H. The geographic distribution of cases of Crimean-Congo hemorrhagic fever: Kastamonu, Turkey. Ticks Tick Borne Dis. 2015;6:730–6. https://doi.org/10.1016/ j.ttbdis.2015.06.008
27. Henter JI, Horne A, Aricó M, Egeler RM, Filipovich AH, Imashuku S, et al. HLH-2004: Diagnostic and therapeutic guidelines for hemophagocytic lymphohistiocytosis. Pediatr Blood Cancer. 2007;48:124–31. https://doi.org/10.1002/pbc.21039
28. Tasdelen Fisgin N, Fisgin T, Tanyel E, Doganci L, Tulek N, Guler N, et al. Crimean-Congo hemorrhagic fever: five patients with hemophagocytic syndrome. Am J Hematol. 2008;83:73–6. https://doi.org/10.1002/ajh.20969
29. Johnson S, Henschke N, Maayan N, Mills I, Buckley BS, Kakourou A, et al. Ribavirin for treating Crimean Congo haemorrhagic fever. Cochrane Database Syst Rev. 2018;6:CD012713. https://doi.org/10.1002/14651858.CD012713.pub2
30. Palomar AM, Portillo A, Santibáñez P, Mazuelas D, Arizaga J, Crespo A, et al. Crimean-Congo hemorrhagic fever virus in ticks from migratory birds, Morocco. Emerg Infect Dis. 2013;19:260–3. https://doi.org/10.3201/eid1902.121193

Address for correspondence: Moncef Belhassen-García, Servicio de Medicina Interna, Unidad de Infecciosas. Universidad de Salamanca, Paseo San Vicente 58 Salamanca, Salamanca 37007, Spain; email: belhassen@usal.es

Streptococcus dysgalactiae Bloodstream Infections, Norway, 1999–2021

Oddvar Oppegaard, Marte Glambek, Dag Harald Skutlaberg, Steinar Skrede, Audun Sivertsen, Bård Reiakvam Kittang

Streptococcus dysgalactiae increasingly is recognized as a pathogen of concern for human health. However, longitudinal surveillance data describing temporal trends of *S. dysgalactiae* are scarce. We retrospectively identified all β-hemolytic streptococcal bloodstream infections reported in Bergen, in western Norway, during 1999–2021. To explore *S. dysgalactiae* disease burden in a broader context, we mapped the incidence of all microbial species causing bloodstream infections during 2012–2021. We found *S. dysgalactiae* incidence rates substantially increased during the study period; by 2021, *S. dysgalactiae* was the fifth most common pathogen causing bloodstream infections in our region. We noted genotypic shifts and found that the rising trend was related in part to the introduction and expansion of the *stG62647 emm*-type. *S. dysgalactiae* is among the most common causes of bloodstream infections in western Norway, and increased surveillance and unambiguous species identification are needed to monitor the disease burden attributable to this pathogen.

Streptococcus dysgalactiae is a potent pathogen that has similar disease manifestations as *S. pyogenes*, including cellulitis, necrotizing soft tissue infections, and streptococcal toxic shock syndrome (*1*–*3*). Nevertheless, in contrast to the well-established surveillance networks for *S. pyogenes* and *S. agalactiae* infections in many countries, epidemiologic reports on *S. dysgalactiae* are scarce (*4*–*6*).

The *S. dysgalactiae* epithet and delineation of its 2 subspecies, *dysgalactiae* and *equisimilis*, was proposed as late as 1996, and until recently identification of this pathogen has relied predominantly on phenotypic β-hemolysis and a Lancefield agglutination reaction (*7*). However, the promiscuous repertoire of Lancefield antigens potentially displayed by *S. dysgalactiae* (mostly C or G, occasionally A or L) has caused considerable taxonomic confusion (*8*). In addition, *S. equi* harbors the C antigen and *S. canis* harbors the G antigen, which adds further ambiguity to speciation. Although *S. equi* and *S. canis* rarely cause human disease, their added ambiguity further illustrates that the Lancefield classification lacks taxonomic resolution to the species level for the group C and G *Streptococcus* (GCGS).

Clinical and epidemiologic features of *S. dysgalactiae* have often been fragmented and concealed in separate scientific reports on group C and group G *Streptococcus*, a practice that continues to some extent (*9*–*12*). This practice has likely underestimated *S. dysgalactiae* incidence rates and clouded its clinical significance. Moreover, most recent publications involving precise identification of *S. dysgalactiae* comprise insufficient sample sizes or observation periods to evaluate temporal trends (*3*,*13*–*15*).

Drawing power from the enhanced taxonomic precision of sequencing technology and mass spectrometry, we revisited *S. dysgalactiae* bloodstream infection epidemiology in a health region in western Norway during the past 23 years. Moreover, to explore *S. dysgalactiae* disease burden in a broader context, we compared *S. dysgalactiae* incidence against all other pathogens that cause bloodstream infections.

Methods

Study Setting and Definitions

Health Region Bergen (Bergen, Norway) had a catchment area of ≈460,000 inhabitants in 2021 and encompasses the tertiary care institution Haukeland

Author affiliations: Haukeland University Hospital, Bergen Norway (O. Oppegaard, M. Glambek, D.H. Skutlaberg, S. Skrede, A. Sivertsen); University of Bergen, Bergen (O. Oppegaard, S. Skrede, B.R. Kittang); Haraldsplass Deaconess Hospital, Bergen (B.R. Kittang)

DOI: https://doi.org/10.3201/eid2902.221218

University Hospital and 2 local hospitals, Haraldsplass Deaconess Hospital and Voss Hospital. The region is served by a single microbiology laboratory located at Haukeland University Hospital.

We reviewed the electronic records of the microbiology laboratory and retrospectively identified all bloodstream infections caused by *S. pyogenes*, *S. agalactiae*, and *S. dysgalactiae* in Health Region Bergen during 1999–2021. We also extracted information on specimen type, sample date and species identification, as well as patient age, sex, and residential postal code.

We defined bloodstream infection as microbial growth in blood cultures collected from patients in a hospital setting. We considered cases from which repeated cultures were positive for the same identified organism within 30 days of initial isolation as a single bloodstream infection. To avoid referral bias, we excluded patients with a residential postal code outside the catchment areas of the 3 hospitals at the time of specimen sampling.

To explore the incidence of *S. dysgalactiae* bloodstream infections in a wider context, we also retrospectively identified bloodstream infections caused by other pathogens during 2012–2021 in our region. We confined the study period to a decade that had relatively stable standards and protocols for pathogen identification in the routine microbiology laboratory. The main tool for species identification during this era was matrix-assisted laser desorption/ionization time-of-flight (MALDI-TOF) mass spectrometry and the MALDI Biotyper database (Bruker Daltonik, https://www.bruker.com), which received annual or biannual updates from the manufacturer.

Bacterial Identification of β-hemolytic Streptococci

Primary identification in the routine microbiology laboratory was based on β-hemolytic reaction on 5% sheep-blood agar, colony size of ≥0.5 mm after 24 h incubation, and Lancefield serogroup specificity (Oxoid, http://www.oxoid.com). Identification of β-hemolytic streptococci was supplemented with MALDI-TOF mass spectrometry beginning in 2012. For this study, we retrieved all β-hemolytic streptococcal isolates identified in bloodstream infections during 1999–2021 from the freezer and confirmed species identity by MALDI-TOF mass spectrometry. Moreover, we taxonomically verified all strains identified as *S. dysgalactiae*, *S. canis*, *S. equi*, or *S. pyogenes* by using either *emm* typing (*16*) or whole genome sequencing (*17*), as previously described. A subset of these strains had already been characterized by *emm* typing in previous studies (*1*,*17*).

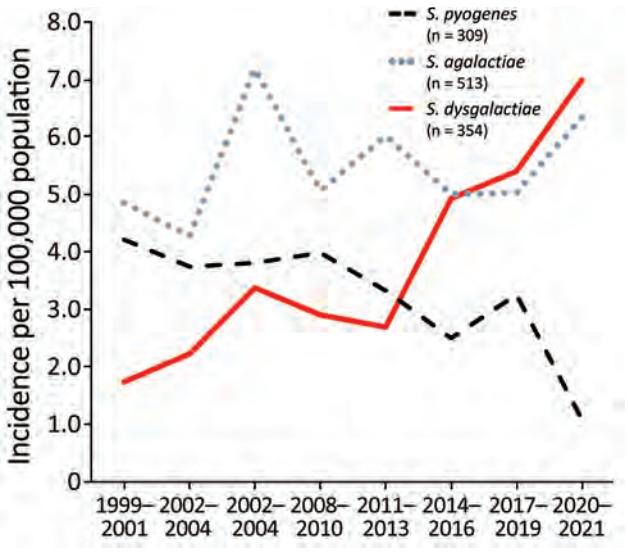

Figure 1. β-hemolytic streptococcal bloodstream infections caused by *Streptococcus pyogenes*, *S. agalactiae*, and *S. dysgalactiae*, western Norway, 1999–2021. We calculated incidence rates for β-hemolytic streptococcal bloodstream infections in Health Region Bergen, Bergen, Norway, in 3-year periods, except 2020–2021. We calculated incidence rates as the total number of cases during each time period, divided by the number of years in the period.

Statistical Analyses

We calculated incidence rates by using contemporary population data extracted from Statistics Norway (https://www.ssb.no). We tested temporal trends for statistical significance by using negative binomial regression analysis and evaluated nonparametric data by using the Mann Whitney U-test. We considered a 2-sided p value ≤0.05 statistically significant. We used SPSS Statistics 26.0 (IBM, https://www.ibm.com/products) for statistical analyses, Excel 2016 (Microsoft, https://www.crosoft.com) to create graphs, and R version 4.1.2 (The R Foundation for Statistical Computing, https://www.r-project.org) to construct violin plots. Regional Ethics Committee West, Norway, conducted institutional ethics review and approved this study (approval no. 2021/350196).

Results

A total of 1,179 cases of β-hemolytic streptococcal bloodstream infections were detected during 1999–2021, comprising 309 cases of *S. pyogenes*, 513 cases of *S. agalactiae*, and 354 cases of *S. dysgalactiae*. We excluded 3 Lancefield group C isolates identified as *S. equi* from the analysis. No cases of *S. canis* bloodstream infection were detected. Whole-genome sequencing identified one *S. dysgalactiae* isolate as *S. dysgalactiae* subspecies

dysgalactiae (*18*), whereas the remaining 353 isolates belonged to the subspecies *equisimilis*.

We plotted temporal trends for β-hemolytic streptococcal bloodstream infections (Figure 1). The incidence rate of *S. dysgalactiae* increased significantly from 1.4 to 7.6 (incidence rate ratio [IRR] 1.064, 95% CI 1.045–1.083; p<0.0001) per 100,000 inhabitants, during 1999–2021; by the end of the study period *S. dysgalactiae* had become the leading cause of β-hemolytic streptococcal bloodstream infections. Conversely, *S. pyogenes* displayed decreasing incidence rates (IRR 0.969, 95% CI 0.949–0.988; p = 0.002), whereas we detected no significant temporal change for *S. agalactiae* bloodstream infections (IRR 1.006, 95% CI 0.989–1.024; p = 0.46).

Reviewing all bloodstream infections in Health Region Bergen during 2012–2021, we identified 12,346 cases caused by 292 different bacterial species (Appendix Table 1, https://wwwnc.cdc.gov/EID/article/29/2/22-1218-App1.xlsx). We excluded 1,678 cases of coagulase-negative staphylococci from our study because we considered these species to be likely skin contaminants. Thus, we included 10,668 cases of bloodstream infection for further analysis. We ranked the most frequent pathogens detected per year and calculated the relative proportion of each pathogen (Figure 2).

The proportion of bloodstream infections caused by *S. dysgalactiae* gradually expanded from 1.3% to 2.9% during the study period, and *S. dysgalactiae* climbed from being the 16th most frequent common in 2012 to the 5th most common in 2021. We noted significantly increasing incidence rates for 3 pathogens: *S. dysgalactiae* (IRR 1.086, 95% CI 1.037–1.137; p<0.0001), *Escherichia coli* (IRR 1.038, 95% CI 1.018–1.058; p = 0.0002), and *Staphylococcus aureus* (IRR 1.031, 95% CI 1.011–1.052; p = 0.002). We found that rates of *S. pneumoniae* bloodstream infections decreased significantly during 2012–2021 (IRR 0.915, 95% CI 0.878–0.953; p<0.0001).

Rank	2012	2013	2014	2015	2016	2017	2018	2019	2020	2021
1	*E. coli* (29.0)	*E. coli* (29.1)	*E. coli* (32.0)	*E. coli* (33.8)	*E. coli* (30.8)	*E. coli* (35.3)	*E. coli* (37.6)	*E. coli* (34.4)	*E. coli* (32.6)	*E. coli* (31.9)
2	*S. aure* (11.2)	*S. aure* (12.2)	*S. aure* (11.3)	*S. aure* (10.8)	*S. aure* (10.6)	*S. aure* (10.9)	*S. aure* (11.2)	*S. aure* (11.1)	*S. aure* (11.3)	*S. aure* (13.3)
3	*K. pneu* (7.9)	*K. pneu* (7.4)	*K. pneu* (6.9)	*K. pneu* (8.4)	*K. pneu* (8.7)	*K. pneu* (6.8)	*K. pneu* (6.3)	*K. pneu* (6.3)	*K. pneu* (6.3)	*E. faeca* (5.5)
4	*S. pneu* (6.5)	*S. pneu* (5.3)	*E. faeca* (5.7)	*S. pneu* (3.4)	*E. faeca* (6.6)	*E. faeca* (3.5)	*E. faeca* (3.9)	*E. faeca* (3.8)	*E. faeca* (4.9)	*K. pneu* (5.3)
5	*E. faeca* (5.0)	*E. faeca* (4.4)	*S. pneu* (3.4)	*E. faeca* (3.0)	*S. pneu* (4.2)	*S. pneu* (3.1)	*S. pneu* (3.0)	*S. pneu* (3.2)	*P. aeru* (2.9)	*SD* (2.9)
6	*B. frag* (2.5)	*S. agal* (3.9)	*P. aeru* (2.6)	*SD* (2.9)	*K. oxyt* (2.4)	*E. cloa* (2.2)	*S. agal* (2.2)	*P. aeru* (2.7)	*S. agal* (2.5)	*K. oxyt* (2.8)
7	*S. agal* (2.5)	*E. faeci* (3.1)	*S. mitis* (2.4)	*E. cloa* (2.6)	*S. agal* (2.3)	*SD* (2.1)	*SD* (2.2)	*E. faeci* (2.3)	*SD* (2.5)	*P. aeru* (2.4)
8	*E. cloa* (2.3)	*P. aeru* (2.0)	*E. faeci* (2.1)	*S. agal* (2.4)	*E. faeci* (2.1)	*E. faeci* (1.9)	*E. cloa* (1.8)	*K. oxyt* (2.1)	*P. mira* (2.2)	*S. agal* (2.4)
9	*C. albi* (2.1)	*K. oxyt* (1.9)	*K. oxyt* (1.9)	*P. aeru* (2.2)	*S. mitis* (2.1)	*S. mitis* (1.8)	*B. frag* (1.8)	*SD* (2.1)	*B. frag* (2.1)	*E. cloa* (2.3)
10	*P. aeru* (2.1)	*S. mitis* (1.8)	*P. mira* (1.8)	*K. oxyt* (2.0)	*P. mira* (1.7)	*S. agal* (1.8)	*P. aeru* (1.8)	*P. mira* (2.0)	*S. mitis* (2.1)	*S. pneu* (2.3)
11	*S. mitis* (1.9)	*P. mira* (1.8)	*E. cloa* (1.8)	*E. faeci* (1.7)	*SD* (1.7)	*P. mira* (1.7)	*S. mitis* (1.8)	*S. mitis* (2.0)	*E. cloa* (1.9)	*P. mira* (2.1)
12	*K. oxyt* (1.8)	*S. pyog* (1.8)	*S. agal* (1.8)	*B. frag* (1.5)	*P. aeru* (1.6)	*S. pyog* (1.6)	*P. mira* (1.7)	*K. vari* (2.0)	*K. oxyt* (1.8)	*S. mitis* (1.8)
13	*P. mira* (1.7)	*B. frag* (1.6)	*SD* (1.8)	*S. angi* (1.3)	*E. cloa* (1.6)	*P. aeru* (1.5)	*S. pyog* (1.4)	*S. agal* (1.9)	*K. vari* (1.7)	*K. vari* (1.7)
14	*E. faeci* (1.6)	*SD* (1.6)	*S. sali* (1.5)	*S. pyog* (1.2)	*S. pyog* (1.2)	*B. frag* (1.4)	*K. oxyt* (1.2)	*E. cloa* (1.5)	*S. pneu* (1.7)	*E. faeci* (1.7)
15	*S. pyog* (1.3)	*E. cloa* (1.1)	*C. albi* (1.2)	*S. mitis* (1.2)	*B. frag* (1.1)	*K. vari* (1.4)	*S. angi* (1.2)	*B. frag* (1.5)	*E. faeci* (1.5)	*B. frag* (1.6)
16	*SD* (1.3)	*S. sali* (0.9)	*B. frag* (1.2)	*P. mira* (1.2)	*S. angi* (1.0)	*S. angi* (1.0)	*E. faeci* (1.0)	*E. lenta* (1.4)	*S. angi* (1.1)	*S. angi* (1.3)
Other pathogens	19.3%	20.1%	20.6%	20.4%	20.3%	22.0%	19.9%	19.7%	20.9%	18.7%
Total isolates	894	937	1,008	984	1,058	1,154	1,125	1,162	1,146	1,200

Figure 2. Leading causes of bloodstream infections, western Norway, 2012–2021. We investigated bloodstream infections in Health Region Bergen, Bergen, Norway, and ranked the most common pathogens detected in each year by frequency. Red shading indicates *Streptococcus dysgalactiae* (abbreviated as *SD*). Numbers in parentheses represent the percentage of all identified cases of bloodstream infections for each pathogen. Percentages of other pathogens detected and the total number of bloodstream infections per year are shown across the bottom. *B. frag*, *Bacteroides fragilis*; *C. albi*, *Candida albicans*; *E. cloa*, *Enterobacter cloacae*; *E.coli*, *Escherichia coli*; *E. faeca*, *Enterococcus faecalis*; *E. faeci*, *Enterococcus faecium*; *E. lenta*, *Eggerthella lenta*; *K. oxyt*, *Klebsiella oxytoca*; *K. pneu*, *Klebsiella pneumoniae*; *K. vari*, *Klebsiella variicola*; *P. aeru*, *Pseudomonas aeruginosa*; *P. mira*, *Proteus mirabilis*; *S. agal*, *Streptococcus agalactiae*; *S. angi*, *Streptococcus anginosus*; *S. aure*, *Staphylococcus aureus*; *S. mitis*, *Streptococcus mitis*; *S. pneu*, *Streptococcus pneumoniae*; *S. pyog*, *Streptococcus pyogenes*; *S. sali*, *Streptococcus salivarius*.

The 3 β-hemolytic streptococcal species were associated with different profiles of age distribution (Figure 3). *S. dysgalactiae* was intimately linked to higher age (median 75 years, range 4–100 years), and only 2 patients with *S. dysgalactiae* bloodstream infections were <18 years of age. The *S. dysgalactiae* cases were among much older patients than were *S. pyogenes* (median age 53 years, range 1–95 years; p<0.0001) and *S. agalactiae* (median age 64 years, range 0–99 years; p<0.0001) cases. In fact, the median age in the *S. dysgalactiae* group was significantly higher than that for any other major streptococcal pathogen (p<0.0001), including *S. pneumoniae* (median age 67 years), *S. mitis/oralis* (median age 65 years), *S. anginosus* (median age 62 years), *S. salivarius* (median age 61 years), and *S. sanguinis* (median age 71 years) (Figure 4).

We also assessed *emm*-type distribution among the *S. dysgalactiae* bloodstream infection isolates (Appendix Table 2). We detected high genotypic diversity, comprising 30 different *emm*-types. Genotypic shifts during the study period were evident, and *emm*-type *stG62647* gradually became dominant beginning in 2014 (Figure 5). Inversely, 1 major *emm*-type from early in the study, *stG643*, was infrequently detected after 2015. The remaining *emm*-types displayed annual fluctuations, but we observed no temporal trend. Two isolates were not available for *emm* sequencing.

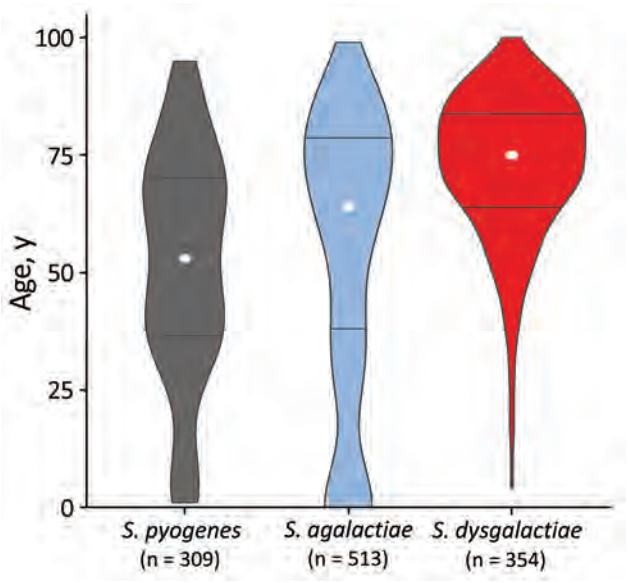

Figure 3. Age distribution for patients with β-hemolytic streptococcal bloodstream infections, western Norway, 1999–2021. The violin plot is based on 1,176 cases of β-hemolytic streptococcal bloodstream infection in Health Region Bergen, Bergen, Norway. The total number of cases is indicated for each species. The width of each figure corresponds to the proportion of patients in that age group. White circles represent the median age and horizontal bars indicate interquartile range.

Discussion

In this large epidemiologic study of invasive *S. dysgalactiae* bloodstream infections in western Norway, we found that *S. dysgalactiae* is rapidly emerging as a potent pathogen and currently is the fifth most common cause of bloodstream infections in the Bergen health region. *S. dysgalactiae* also appears to have surpassed *S. pyogenes* and *S. agalactiae* as the leading cause of invasive β-hemolytic streptococcal disease in Japan and Finland (*2*,*3*). Moreover, studies from several geographic regions, including Canada, Hungary, Denmark, and Australia, have noted substantial increases in incidence rates for invasive GCGS infections during the past decade (*19*–*22*).

Unfortunately, many larger epidemiologic studies on β-hemolytic streptococcal infections have been hampered by taxonomic imprecision. Several studies report separate incidence curves for group C and group G *Streptococcus*, and some have even exclusively included group G *Streptococcus* (*10*,*11*,*23*,*24*). The lack of species identification is also reflected in the scarce published national surveillance data.

National surveillance on antimicrobial resistance in Norway reports combined annual incidence rates of GCGS bloodstream infections (*25*). In line with our findings, GCGS has been the leading β-hemolytic streptococcal pathogen in Norway since 2017 (Figure 6, panel A). Although not necessarily equivalent to *S. dysgalactiae*, GCGS is a fair estimate of incidence, as demonstrated by the data retrieved from our health region in this study. Nevertheless, the GCGS epithet represents an aggregate of several bacterial species and might easily shroud the magnitude of *S. dysgalactiae* infections from clinicians.

The United Kingdom has monitored β-hemolytic streptococcal bloodstream infections for several decades but tracks group C and group G *Streptococcus* infections by separate incidence curves (Figure 6, panel B) (*12*). However, that practice can make group C and group G *Streptococcus* appear to be relatively uncommon causes of bloodstream infections. Combining those incidence curves could reveal a completely different picture.

In Finland, the annual incidence rates of invasive *S. pyogenes* and *S. agalactiae* disease are reported separately, whereas *S. dysgalactiae* infections are included in the other β-hemolytic streptococci category (*6*). Of note, the category of other β-hemolytic streptococci greatly expanded during 2008–2017 to become the 4th most common cause of bloodstream infections in Finland (Figure 6, panel C).

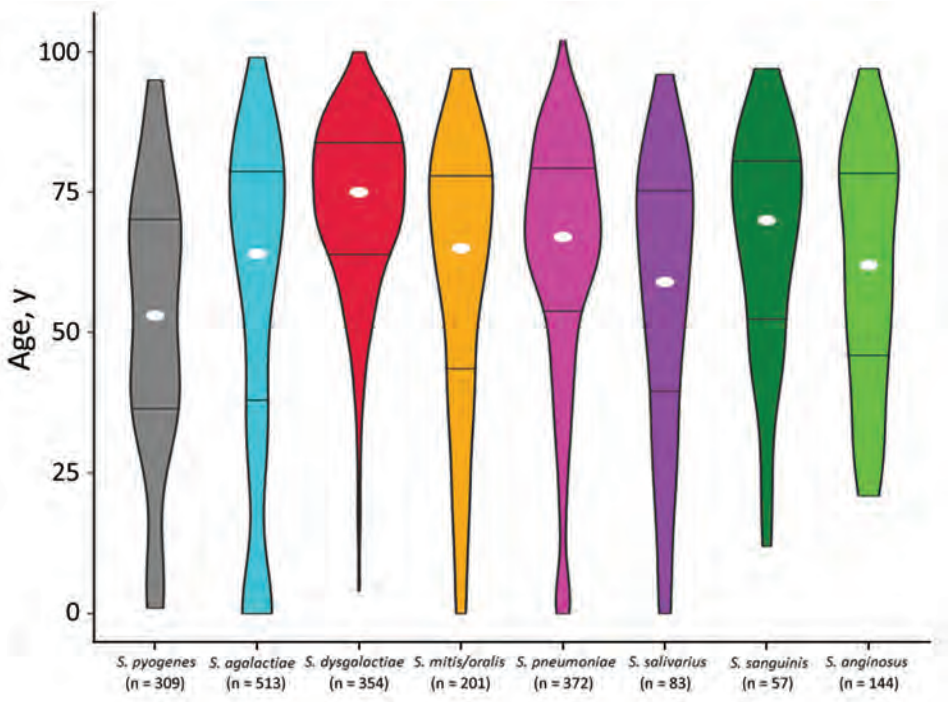

Figure 4. Age distribution for patients with streptococcal bloodstream infections, western Norway, 1999–2021. The violin plot is based on 2,033 cases of bloodstream infection caused by the 8 most common streptococcal species in Health Region Bergen, Bergen, Norway. The total number of cases is indicated for each species. The width of each figure corresponds to the proportion of patients in that age group. White circles indicate the median age and horizontal bars indicate interquartile range.

Such taxonomic imprecision is detrimental to the surveillance of *S. dysgalactiae* infections. The Lancefield agglutination reaction is a cheap and pragmatic method for sorting β-hemolytic streptococcal isolates but lacks sufficient phylogenetic resolution. To report reliable and comprehensible epidemiologic data, identification to the species level is necessary. MALDI-TOF mass spectrometry is a relatively cheap and efficient alternative, but concerns have been raised about its ability to discern *S. dysgalactiae* from *S. canis* and *S. pyogenes* (*28*). However, modifications and updates to the MALDI-TOF database has largely resolved this issue (*29*). Thus, we propose that future epidemiologic surveillance and publications report the identity of *S. dysgalactiae* to the species level.

The increasing burden of *S. dysgalactiae* disease is likely multifactorial. In line with findings from previous reports, our results showed this pathogen exhibited a predilection for older persons (*3*,*22*). This preference could be a consequence of immunosenescence but likely also reflects the burden of underlying conditions. Some reports have identified predisposing factors in >90% of the invasive *S. dysgalactiae* cases (*13*,*30*). One report explored risk factors for invasive β-hemolytic streptococcal disease and found the highest average Charlson Comorbidity Index score among patients with GCGS bloodstream infections, including a strong association with diabetes (*22*). In Norway, the estimated life expectancy increased by >5 years during the study period (https://www.ssb.no),

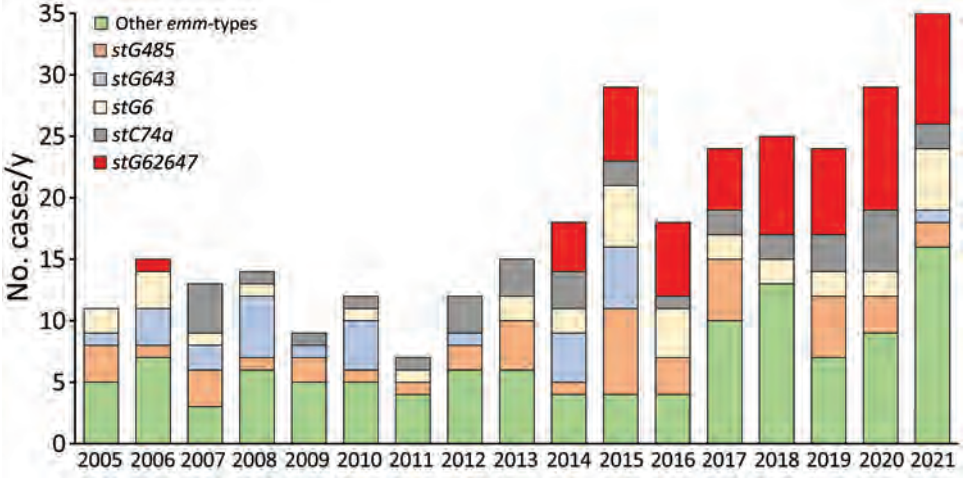

Figure 5. Distribution of the most common *emm*-types among *Streptococcus dysgalactiae* bloodstream infections, western Norway, 2005–2021. We identified most common *emm*-types among 351 *S. dysgalactiae* bloodstream infections in Health Region Bergen, Bergen, Norway. Two isolates were not available for typing, and the *S. dysgalactiae* subspecies *dysgalactiae* isolate could not be typed.

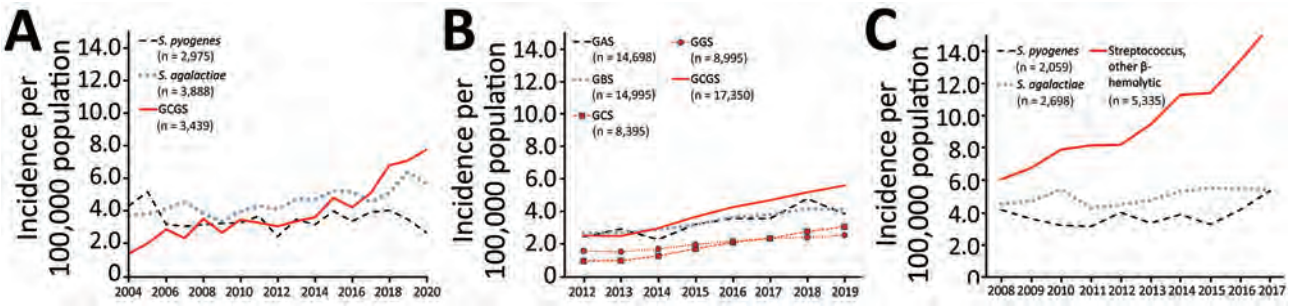

Figure 6. National surveillance data for β-hemolytic streptococcal bloodstream infections in 3 countries: A) Norway, 2004–2020; B) United Kingdom, 2012–2019; C) Finland, 2008–2017. We compiled data from annual surveillance reports published during the given time periods (*6*,*25*–*27*). The 3 countries use different surveillance methods. UK surveillance is based on voluntary reporting from the microbiology laboratories, whereas in Norway and Finland, surveillance data are collected electronically from the laboratories' information systems. We calculated incidence rates by acquiring contemporary population data from Norway (https://www.ssb.no), the United Kingdom (https://www.ons.gov.uk), and Finland (https://www.stat.fi). We used taxonomic labels that appeared in the original publications, except GCGS, which we constructed for the purpose of this study by combining incidence data for GCS and GGS. GAS, group A *Streptococcus*; GBS, group B *Streptococcus*; GCS, group C *Streptococcus*; GGS, group G *Streptococcus*; GCGS, group C and G *Streptococcus*.

and the prevalence of diabetes in the population of Norway has doubled in the past decade (https://www.fhi.no). These developments are projected to continue; thus, the epidemiologic trend for invasive *S. dysgalactiae* disease is unlikely to revert.

Shorter term abrupt changes in incidence rates could be related in part to epidemiologic shifts in circulating *emm*-types. We previously documented the introduction of the *stG62647 emm*-type into our health region in 2013 (*17*). This *emm*-type appears to have continued to expand and constituted a major contribution to the increasing rates of *S. dysgalactiae* bloodstream infections.

In line with our findings, the *stG62647* genotype appears to have gained a strong foothold in several geographic regions, accounting for 47% of the *S. dysgalactiae* isolates in Germany during 2012–2016 (*15*), 31% in Canada during 2012–2014 (*13*), and 26% in Switzerland during 2006–2015 (*14*). The rapid expansion of this genotype could be related to a lack of herd immunity in the population, but the emergence of a clone with enhanced virulence potential cannot be ruled out. We previously documented a disruption of the streptococcal invasive locus in this genotype, a feature previously associated with increased virulence (*17*,*31*). However, the exact pathogenetic implications of this genetic event have yet to be experimentally elucidated.

Historically, *S. dysgalactiae* has been considered an opportunistic microbe with low pathogenicity, but its potential for severe disease manifestations should not be disregarded. In a large, prospective, multicenter study (*32*), *S. dysgalactiae* was the second most common cause of monomicrobial necrotizing soft tissue infections, and mortality rates for *S. dysgalactiae* cases were even higher than for *S. pyogenes* cases. Moreover, >40% of case-patients experienced septic shock. Recent data from the Swedish Registry of Infective Endocarditis indicated that *S. dysgalactiae* endocarditis was associated with an aggressive clinical course, and rates of embolic events and surgical intervention comparable to endocarditis caused by *Staphylococcus aureus* (*33*). Of note, the *stG62647* genotype was reported as the predominant *emm*-type in both these studies.

Our study is limited by a retrospective design, increasing the risk for taxonomic misclassification. We cannot rule out the possibility that improved taxonomic resolution during the study period could account for some of the increase in the *S. dysgalactiae* disease burden. However, during a thorough review and reconfirmation of all registered cases of β-hemolytic streptococcal infections, including *S. canis* and *S. equi*, we did not identify evidence for such misclassification of the streptococcal isolates.

Prevention measures taken against the SARS-CoV-2 pandemic had a substantial effect on incidence rates of bacterial diseases, particularly for those caused by airway pathogens (*34*). In line with those effects, epidemiology of bloodstream infections observed in our study might have been influenced to some extent by restrictions during the early pandemic phases, for instance, the rapid decline of *S. pneumoniae* bloodstream infections observed in 2020. Nevertheless, the rising trend of *S. dysgalactiae* predates the pandemic on both a national and international level; this pathogen became the 6th most common cause of bloodstream infections in our region by 2015.

In conclusion, our findings indicate that *S. dysgalactiae* is a potent and common pathogen that should not be overlooked. Enhanced taxonomic precision of this streptococcal species is needed to ensure that epidemiologic data are unambiguous and comprehensible. Moreover, increased attention to *S. dysgalactiae* disease is warranted, and *S. dysgalactiae* should be included in national surveillance programs on equal terms with *S. pyogenes* and *S. agalactiae*.

Acknowledgments

We thank the staff at the microbiological department at Haukeland University Hospital for excellent technical assistance and for providing access to their laboratory facilities. We particularly acknowledge Haima Mylvaganam for her significant contribution to streptococcal research at Haukeland University Hospital during the past 2 decades and for inspiration to continued scientific exploration.

This study received financial contributions from the Western Norway Regional Health Authority (grant no. 912231).

O.O., B.K.R., and S.S. conceived the study; O.O., D.H.S., and A.S. extracted and analyzed the data; O.O. and M.G. performed laboratory work. All authors contributed to drafting the manuscript and have read and approved the final version.

About the Author

Dr. Oppegaard is an infectious disease specialist at the Department of Infectious Diseases, Haukeland University Hospital, Bergen, Norway. He is also an associate professor at the University of Bergen, Norway. His research interests focuses on beta-hemolytic streptococcal infections, spanning from clinical features and epidemiology to dissection of microbial genetics and host responses.

References

1. Oppegaard O, Mylvaganam H, Kittang BR. Beta-haemolytic group A, C and G streptococcal infections in Western Norway: a 15-year retrospective survey. Clin Microbiol Infect. 2015;21:171–8. https://doi.org/10.1016/j.cmi.2014.08.019
2. Rantala S, Vuopio-Varkila J, Vuento R, Huhtala H, Syrjänen J. Clinical presentations and epidemiology of β-haemolytic streptococcal bacteraemia: a population-based study. Clin Microbiol Infect. 2009;15:286–8. https://doi.org/10.1111/j.1469-0691.2008.02672.x
3. Wajima T, Morozumi M, Hanada S, Sunaoshi K, Chiba N, Iwata S, et al. Molecular characterization of invasive *Streptococcus dysgalactiae* subsp. *equisimilis*, Japan. Emerg Infect Dis. 2016;22:247–54. https://doi.org/10.3201/eid2202.141732
4. US Centers for Disease Control and Prevention. Active bacterial core surveillance [cited 2022 Nov 16]. www.cdc.gov/abcs/reports-findings/surv-reports.html
5. Australian Government, Department of Health and Aged Care. Australian national notifiable diseases case definition [cited 2022 Nov 16]. https://www.health.gov.au/resources/publications/invasive-group-a-streptococcal-disease-igas-surveillance-case-definition
6. Finnish Institute for Health and Welfare. Infectious diseases in Finland 2017. Helsinki: The Institute; 2017.
7. Vandamme P, Pot B, Falsen E, Kersters K, Devriese LA. Taxonomic study of Lancefield streptococcal groups C, G, and L (*Streptococcus dysgalactiae*) and proposal of *S. dysgalactiae* subsp. *equisimilis* subsp. nov. Int J Syst Bacteriol. 1996;46:774–81. https://doi.org/10.1099/00207713-46-3-774
8. Facklam R. What happened to the streptococci: overview of taxonomic and nomenclature changes. Clin Microbiol Rev. 2002;15:613–30. https://doi.org/10.1128/CMR.15.4.613-630.2002
9. Bradley SF, Gordon JJ, Baumgartner DD, Marasco WA, Kauffman CA. Group C streptococcal bacteremia: analysis of 88 cases. Rev Infect Dis. 1991;13:270–80. https://doi.org/10.1093/clinids/13.2.270
10. Leitner E, Zollner-Schwetz I, Zarfel G, Masoud-Landgraf L, Gehrer M, Wagner-Eibel U, et al. Prevalence of *emm* types and antimicrobial susceptibility of *Streptococcus dysgalactiae* subsp. *equisimilis* in Austria. Int J Med Microbiol. 2015;305:918–24. https://doi.org/10.1016/j.ijmm.2015.10.001
11. Lo HH, Cheng WS. Distribution of virulence factors and association with *emm* polymorphism or isolation site among beta-hemolytic group G *Streptococcus dysgalactiae* subspecies equisimilis. APMIS. 2015;123:45–52. https://doi.org/10.1111/apm.12305
12. UK Health Security Agency. Laboratory surveillance of pyogenic and non-pyogenic streptococcal bacteraemia in England: 2020 update. Health Protection Report, vol. 15, no. 19. London: The Agency; 2021.
13. Lother SA, Demczuk W, Martin I, Mulvey M, Dufault B, Lagacé-Wiens P, et al. Clonal clusters and virulence factors of group C and G *Streptococcus* causing severe infections, Manitoba, Canada, 2012–2014. Emerg Infect Dis. 2017;23:1079–88. https://doi.org/10.3201/eid2307.161259
14. Ruppen C, Rasmussen M, Casanova C, Sendi P. A 10-year observational study of *Streptococcus dysgalactiae* bacteraemia in adults: frequent occurrence among female intravenous drug users. Swiss Med Wkly. 2017;147:w14469.
15. Rößler S, Berner R, Jacobs E, Toepfner N. Prevalence and molecular diversity of invasive *Streptococcus dysgalactiae* and *Streptococcus pyogenes* in a German tertiary care medical centre. Eur J Clin Microbiol Infect Dis. 2018;37:1325–32. https://doi.org/10.1007/s10096-018-3254-2
16. Kittang BR, Langeland N, Mylvaganam H. Distribution of *emm* types and subtypes among noninvasive group A, C and G streptococcal isolates in western Norway. APMIS. 2008;116:457–64. https://doi.org/10.1111/j.1600-0463.2008.00976.x
17. Oppegaard O, Mylvaganam H, Skrede S, Lindemann PC, Kittang BR. Emergence of a *Streptococcus dysgalactiae* subspecies *equisimilis stG62647*-lineage associated with severe clinical manifestations. Sci Rep. 2017;7:7589. https://doi.org/10.1038/s41598-017-08162-z
18. Jordal S, Glambek M, Oppegaard O, Kittang BR. New tricks from an old cow: infective endocarditis caused by *Streptococcus dysgalactiae* subsp. *dysgalactiae*. J Clin Microbiol. 2015;53:731–4. https://doi.org/10.1128/JCM.02437-14
19. Gajdács M, Ábrók M, Lázár A, Burián K. Beta-haemolytic group A, C and G streptococcal infections in Southern Hungary: a 10-year population-based retrospective survey (2008–2017) and a review of the literature. Infect Drug Resist. 2020;13:4739–49. https://doi.org/10.2147/IDR.S279157

20. Lambertsen LM, Ingels H, Schønheyder HC, Hoffmann S; Danish Streptococcal Surveillance Collaboration Group 2011. Nationwide laboratory-based surveillance of invasive beta-haemolytic streptococci in Denmark from 2005 to 2011. Clin Microbiol Infect. 2014;20:O216–23. https://doi.org/10.1111/1469-0691.12378
21. Harris P, Siew DA, Proud M, Buettner P, Norton R. Bacteraemia caused by beta-haemolytic streptococci in North Queensland: changing trends over a 14-year period. Clin Microbiol Infect. 2011;17:1216–22. https://doi.org/10.1111/j.1469-0691.2010.03427.x
22. Couture-Cossette A, Carignan A, Mercier A, Desruisseaux C, Valiquette L, Pépin J. Secular trends in incidence of invasive beta-hemolytic streptococci and efficacy of adjunctive therapy in Quebec, Canada, 1996–2016. PLoS One. 2018;13:e0206289. https://doi.org/10.1371/journal.pone.0206289
23. Trell K, Nilson B, Rasmussen M. Species and *emm*-type distribution of group C and G streptococci from different sites of isolation. Diagn Microbiol Infect Dis. 2016;86:467–9. https://doi.org/10.1016/j.diagmicrobio.2016.09.008
24. Schwartz IS, Keynan Y, Gilmour MW, Dufault B, Lagacé-Wiens P. Changing trends in β-hemolytic streptococcal bacteremia in Manitoba, Canada: 2007–2012. Int J Infect Dis. 2014;28:211–3. https://doi.org/10.1016/j.ijid.2014.03.1376
25. NORM and NORM-VET. Usage of antimicrobial agents and occurrence of antimicrobial resistance in Norway, 2004–2020 [cited 2022 Nov 16]. https://unn.no/fag-og-forskning/norm-norsk-overvakingssystem-for-antibiotikaresistens-hos-mikrober#rapporter
26. Public Health England. Laboratory surveillance of pyogenic and non-pyogenic streptococcal bacteraemia in England: 2019 update. Health protection report; vol. 14, no. 24. London: The Agency; 2020.
27. Public Health England. Voluntary surveillance of pyogenic and non-pyogenic streptococcal bacteraemia 2016: appendix data for England only. Health protection report; vol. 11, no. 41. London: The Agency; 2017.
28. Jensen CS, Dam-Nielsen C, Arpi M. Matrix-assisted laser desorption/ionization-time of flight mass spectrometry identification of large colony beta-hemolytic streptococci containing Lancefield groups A, C, and G. Infect Dis (Lond). 2015;47:575–9. https://doi.org/10.3109/23744235.2015.1043940
29. Nybakken EJ, Oppegaard O, Gilhuus M, Jensen CS, Mylvaganam H. Identification of *Streptococcus dysgalactiae* using matrix-assisted laser desorption/ionization-time of flight mass spectrometry; refining the database for improved identification. Diagn Microbiol Infect Dis. 2021;99:115207. https://doi.org/10.1016/j.diagmicrobio.2020.115207
30. Oppegaard O, Skrede S, Mylvaganam H, Kittang BR. Temporal trends of β-haemolytic streptococcal osteoarticular infections in western Norway. BMC Infect Dis. 2016;16:535. https://doi.org/10.1186/s12879-016-1874-7
31. Michael-Gayego A, Dan-Goor M, Jaffe J, Hidalgo-Grass C, Moses AE. Characterization of *sil* in invasive group A and G streptococci: antibodies against bacterial pheromone peptide SilCR result in severe infection. Infect Immun. 2013;81:4121–7. https://doi.org/10.1128/IAI.00359-13
32. Bruun T, Rath E, Madsen MB, Oppegaard O, Nekludov M, Arnell P, et al.; INFECT Study Group. Risk factors and predictors of mortality in streptococcal necrotizing soft-tissue infections: a multicenter prospective study. Clin Infect Dis. 2021;72:293–300. https://doi.org/10.1093/cid/ciaa027
33. Bläckberg A, Nilson B, Özenci V, Olaison L, Rasmussen M. Infective endocarditis due to *Streptococcus dysgalactiae*: clinical presentation and microbiological features. Eur J Clin Microbiol Infect Dis. 2018;37:2261–72. https://doi.org/10.1007/s10096-018-3367-7
34. Steens A, Knol MJ, Freudenburg-de Graaf W, de Melker HE, van der Ende A, van Sorge NM. Pathogen- and type-specific changes in invasive bacterial disease epidemiology during the first year of the COVID-19 pandemic in the Netherlands. Microorganisms. 2022;10:972. https://doi.org/10.3390/microorganisms10050972

Address for correspondence: Oddvar Oppegaard, Department of Medicine, Haukeland University Hospital, Jonas Lies vei 1, 5021 Bergen, Norway; email: oddvar.oppegaard@helse-bergen.no

Changing Disease Course of Crimean-Congo Hemorrhagic Fever in Children, Turkey

Pembe Derin Oygar,[1] Sibel Laçinel Gürlevik, Erdal Sağ, Sare İlbay, Tekin Aksu, Osman Oğuz Demir, Yasemin Coşgun, Selin Aytaç Eyüpoğlu, Jale Karakaya, Şule Ünal Cangül, Ali Bülent Cengiz, Yasemin Özsürekci

Crimean-Congo hemorrhagic fever (CCHF), endemic in certain regions of the world, is listed as a priority disease with pandemic potential. Since CCHF was first identified in Turkey, children have been known to experience milder disease than adults. However, during the COVID-19 pandemic, we observed an unusually severe disease course, including hemophagocytic lymphohistiocytosis (HLH). We examined cytokine/chemokine profiles of 9/12 case-patients compared with healthy controls at 3 time intervals. Interferon pathway–related cytokines/chemokines, including interleukin (IL) 18, macrophage inflammatory protein 3α, and IL-33, were elevated, but tumor necrosis factor-α, IL-6, CXCL8 (formerly IL-8), and cytokines acting through C-C chemokine receptor 2 and CCR5 were lower among case-patients than controls. Interferon pathway activation and cytokines/chemokines acting through CCR2 and CCR5 improved health results among children with severe CCHF. Children can experience severe CCHF, including HLH, and HLH secondary to CCHF can be successfully treated with intravenous immunoglobulin and steroid therapy.

Crimean-Congo hemorrhagic fever (CCHF) is a tickborne viral disease widely distributed throughout the world (*1*). CCHF virus (order *Bunyavirales*, family *Nairoviridae*, genus *Orthonairovirus*) causes disease only in humans, but its natural cycle includes wild mammals, livestock, birds, and ticks. The virus has been detected in ≥35 tick species; *Hyalomma* genus ticks are recognized vectors, and *H. marginatum* ticks are the most efficient vectors (*2*). Transmission by direct contact with infected human or animal secretions, fluids, or tissues, and nosocomial outbreaks, including transmission related to aerosol generation, have also been reported (*3*–*9*).

The course of CCHF ranges from asymptomatic to severe (*3*) and even fatal in 3%–40% of cases (*4*). Hemorrhagic complications and hemophagocytic lymphohistiocytosis (HLH) are usually responsible for deaths among adults; CCHF is usually mild in children for reasons that remain unclear. Severe disease and fatalities in adults have been attributed to high viral loads and excessive cytokine release (*10*,*11*). Previous studies have reported varying results in which proinflammatory cytokines are responsible for severe and fatal CCHF. One study (*10*) reported interferon-γ (IFN-γ), interleukin (IL) 10 (IL-10), and tumor necrosis factor-α (TNF-α) to be associated with high viral load and disease severity. Another reported that IL-10, C-X-C motif chemokine ligand 10 (CXCL-10, formerly IFN-γ inducible protein 10) and CC chemokine ligand 2 (CCL2, formerly monocyte chemoattractant protein 1) levels were higher in patients with high viral loads (*12*), but patients with severe disease had higher levels of CXCL10 and CCL2 than did patients with less-severe cases. IL-6 and CXCL-8 (formerly IL-8) were proposed as the main cytokines predicting fatality in 1 study (*13*); another study reported that TNF-α and IL-6 levels were higher in fatal cases (*14*). Another study comparing cytokine levels between adults and children revealed that IL-2, IL-5, IL-9, IL-12p70, and IL-13 were higher in fatal cases among adults.

Author affiliations: Hacettepe University, Ankara, Turkey (P.D. Oygar, S.L. Gürlevik, E. Sağ, T. Aksu, O.O. Demir, S.A. Eyüpoğlu, J. Karakaya, Ş.Ü. Cangül, A.B. Cengiz, Y. Özsürekci); İhsan Doğramacı Children's Hospital, Ankara (P.D. Oygar, S.L. Gürlevik, T. Aksu, O.O. Demir, S.A. Eyüpoğlu, Ş.Ü. Cangül, A.B. Cengiz, Y. Özsürekci); Ankara Training and Research Hospital, Ankara (E. Sağ); Hacettepe University Rheumatology Translational Medicine Laboratories, Ankara (S. İlbay); General Directorate of Public Health, Ministry of Health, Microbiology Reference and Biological Materials Laboratory, Ankara (Y. Coşgun)

DOI: https://doi.org/10.3201/eid2902.220976

[1]Current affiliation: Nicosia State Hospital, Burhan Nalbantoglu General Hospital, Nicosia, Cyprus.

Although some pediatric patients have died, their cytokine profiles did not differ from those for adults or other children on the basis of disease severity (*15*).

Since 2015, CCHF has been considered one of the emerging infectious diseases most likely to cause major epidemics; at present, it is listed by the World Health Organization as a priority disease with pandemic potential (*16*). During the COVID-19 pandemic, we observed an increased number of pediatric CCHF cases in Turkey associated with unexpectedly severe disease, including certain cases referred to or misdiagnosed as multisystem inflammatory syndrome in children (MIS-C) (*17*). In this study, we aimed to explain the reasons for variations in disease severity among children by determining cytokine/chemokine profiles over time, as well as evaluating clinical and laboratory parameters of patients.

Materials and Methods

Study Design and Patients

We conducted a retrospective study of 12 patients with PCR-confirmed CCHF and 11 healthy volunteers as a control population during April 22, 2020–August 31, 2021, at Hacettepe University İhsan Doğramacı Children's Hospital in Ankara, Turkey. We obtained demographic information, self-reported times of tick bites and onset of symptoms, and results from physical examinations and diagnostic tests from patient medical records. We performed quantitative reverse transcription PCR (qRT-PCR) targeting CCHF virus for all patients at the Turkey Public Health Reference Laboratory (PHRL).

All 12 patients seeking treatment were diagnosed with HLH on the basis of criteria from the Histiocyte Society HLH-2004 study (*18*). We tested all CCHF patients for SARS-CoV-2 at admission by using qRT-PCR targeting SARS-CoV-2 with primers supplied by PHRL. The volunteer controls had no history, signs or symptoms, or physical findings of disease and no underlying conditions. Because the study was performed during the pandemic, we also tested controls for SARS-CoV-2 to eliminate the possibility of asymptomatic COVID-19. We obtained informed written consent from guardians of all patients and controls. Our study was approved by the Hacettepe University Ethics Committee (GO21/413).

Serum Collection and Laboratory Tests

For each CCHF patient, we measured complete blood count with differentials, C-reactive protein (CRP), erythrocyte sedimentation rate (ESR), aspartate aminotransferase (AST), alanine aminotransferase (ALT), creatine kinase (CK), lactate dehydrogenase (LDH), ferritin, prothrombin time, activated partial thromboplastin time (aPTT), international normalized ratio (INR), fibrinogen, D-dimer, triglycerides, sodium, potassium, blood urea nitrogen, albumin, and glucose at admission and every 8–12 h until laboratory findings were at safe levels, then daily. At 8–12, 48–60, and 96–120 h after admission, we collected an additional 3 sets of serum samples in addition to the HLH marker samples, centrifuged them at 4,000 rpm for 10 min at room temperature, and stored them at −80°C until used for cytokine/chemokine profiling. We obtained blood samples from controls once and stored them at −80°C until used as group measures for cytokine/chemokine profiling.

Cytokine/Chemokine Profiling

We studied serum cytokine/chemokine levels from the serum samples collected 8–12, 48–60, and 96–120 h after admission using cytometric bead-based multiplex assay panels according to manufacturer instructions. Then, we analyzed them using the Agilent Novocyte 3005 flow cytometer (https://www.agilent.com). We used Biolegend LEGENDplex Human Inflammation [13-plex] panel 1 (https://www.biolegend.com) for panel 1 for IL-1β, IFN-α2, IFN-γ, TNF-α, CCL2, IL-6, CXCL8, IL-10, IL-12p70, IL-17A, IL-18, IL-23, and IL-33. We used Biolegend LEGENDplex HU proinflammatory chemokine panel 1 [13-plex] for panel 2 for CCL2, CCL5 (formerly regulated on activation, normal T-cell expressed and secreted [RANTES]), CXCL10, CCL11 (formerly Eotaxin), CCL17 (formerly thymus- and activation-regulated chemokine [TARC]), CCL3 (formerly macrophage inflammatory proteins-1α [MIP-1α]), CCL4 (formerly MIP-1β) CXCL9 (formerly monokine-induced γ interferon [MIG]), CCL20 (formerly MIP-3α), CXCL5 (formerly epithelial neutrophil-activating-78 [ENA-78]), CXCL1 (formerly growth related protein α [GRO-α]), CXCL11 (formerly interferon-inducible T-cell alpha chemoattractant [I-TAC]), and CXCL8. For 9 CCHF patients, we adjusted time intervals for cytokine/chemokine measurements on the basis of first day of self- or parent-reported symptoms, rather than day of hospital admission. We then studied cytokine/chemokine levels at 3 subsequent adjusted time intervals: first (68–72 h after baseline), second (120–132 h), and third (156–180 h).

Statistical Analysis

We used IBM SPSS Statistics 26 (https://www.ibm.com) for all statistical analyses. We expressed categorical variables as frequencies and percentages and

continuous variables as medians with interquartile ranges (IQRs). To compare cytokine/chemokine levels between patient and control groups, we used the Mann-Whitney U test and set $p < 0.05$ as statistically significant. We performed Friedman 2-way analysis of variance of ranks to determine the changes in cytokine/chemokine and laboratory parameter levels over the 3 time intervals. We calculated the time interval contributing to change using Pearson pairwise comparison with Bonferroni correction. Finally, we determined correlation between laboratory tests and cytokine/chemokine levels with Pearson correlation analysis. We used GraphPad Prism version 9.2.0 (https://www.graphpad.com) for figure configurations.

Results

Demographics and Clinical Findings for Patients and Controls

We included 23 children, 12 with diagnosed CCHF (3 girls, 9 boys; median age 12.5 [IQR 6–15] years) and 11 controls (6 boys, 5 girls; median age 7 [IQR 2–16] years) in the study. We recorded age, initial symptoms, major pathologic physical examination findings, treatments, and outcomes for all 12 CCHF patients (Table 1). All 12 had a history of tick bites and came from endemic regions; 9 (75%) had close contact with livestock. None had underlying conditions. All patients had fever when initially seeking treatment; the second most common complaint was headache (n = 6, 50%), followed by nausea (n = 4, 33.3%) and malaise (n = 4, 33.3%). Two patients (16.7%) had vomiting and diarrhea. The 2 patients (16.7%) with longest times, 8 and 12 days, from tick bite until hospital admission had myalgia. Median duration of symptoms was 2.5 (IQR 2–5) days; median time between tick bite and baseline was 5.5 (IQR 3–12) days. All patients had conjunctival injection, facial hyperemia, and hepatosplenomegaly at presentation. Seven (58%) patients had petechia at hospital admission, 4 (30%) had findings consistent with central nervous system involvement, 3 (25%) exhibited confusion, and 1 (0.8%) had somnolence; none of the patients had gross bleeding. Median duration of fever after hospital admission was 4 (IQR 3–6) days; median hospital stay was 10 (IQR 5–10) days.

Laboratory Findings

All patients had leukopenia, lymphopenia, neutropenia, and thrombocytopenia when initially seeking treatment; 10/12 (83%) had normal hemoglobin levels. Other laboratory findings varied at admission and each time interval (Table 2). We observed that all patients deteriorated clinically over the course of the first time interval, consistent with their worsening laboratory tests. Except for triglycerides, fibrinogen, ESR, ALT, and AST, all laboratory parameters were at their worst levels during the first time interval; ALT and AST levels were at their highest during the second time interval, and ESR, fibrinogen, and triglycerides reached their maximum levels during the third interval. Increases were not statistically significant for

Table 1. Demographic and clinical characteristics, management, and outcomes of 12 pediatric case-patients with Crimean-Congo hemorrhagic fever, Turkey*

Case no.	Age, y/sex	Initial signs and symptoms	Physical findings	FFPT/PT	Ribavirin duration, d	IVIG duration, d	Steroids duration, d	Complications
1	15/M	Fever, myalgia, headache	HSM, petechia	+/+	9	5	8	Transient bradycardia
2	7/F	Fever, malaise, nausea	HSM, petechia, somnolence	+/+	10	5	10	Transient adrenal insufficiency
3	12/M	Fever, headache, myalgia	HSM	+/−	7	1	3	None
4	8/M	Fever, malaise, nausea	HSM, petechia, confusion	+/+	2	4	10	Transient bradycardia
5	10/F	Fever, headache	HSM	+/−	5	1	10	None
6	13/M	Fever, headache	HSM, petechia	+/−	5	1	9	Transient bradycardia
7	15/M	Fever	HSM	+/−	5	1	5	Transient bradycardia
8	15/M	Fever, somnolence	HSM, petechia, confusion	+/−	4	1	8	Transient bradycardia
9	11/M	Fever, malaise	HSM, petechia	+/−	5	5	10	Transient bradycardia, transient adrenal insufficiency
10	15.5/M	Fever, headache, vomiting, diarrhea	HSM	+/−	5	1	5	Transient bradycardia
11	14/M	Fever, vomiting, diarrhea	HSM, petechia	+/−	5	1	5	Transient bradycardia
12	7/F	Fever, malaise	HSM, petechia	+/+	5	1	5	None

*All 12 case-patients survived. IVIG, intravenous immunoglobulin; FFPT, fresh frozen plasma transfusion; PT, platelet transfusion; HSM, hepatosplenomegaly; +, transfusion administered; –, transfusion not administered.

Table 2. Laboratory parameters for 12 pediatric case-patients with Crimean-Congo hemorrhagic fever at hospital admission and for 3 subsequent time intervals, Turkey*

Parameters, units	Reference range	Admission, median ±SD (min–max)	1st interval, median ±SD (min–max)	2nd interval, median ±SD (min–max)	3rd interval, median ±SD (min–max)
Hemoglobin, g/dL	11.1–14	13.95 ±1.57 (11.30–16.60)	13.90 ±1.74 (10.70–16.20)	12.80 ±1.57 (9.40–15.30)	12.70 ±2.07 (8.50–15.80)
Leukocytes, × 10^3 cells/μL	5–13	2.25 ±1.01 (1.10–4.70)	1.85 ±0.42 (1.30–2.70)	2.00 ±1.30 (1.10–4.10)	3.60 ±1.97 (2.60–7.60)
Neutrophils, × 10^3 cells/μL	5–13	1.66 ±1.08 (0.25–3.89)	1.28 ±0.59 (0.20–1.87)	1.00 ±0.83 (0.33–2.96)	2.04 ±1.36 (0.58–4.29)
Lymphocytes, × 10^3 cells/μL	1–5	0.46 ±0.26 (0.23–1.11)	0.46 ±0.25 (0.21–1.00)	0.64 ±0.50 (0.24 ±1.80)	0.83 ±0.49 (0.38–1.93)
Platelets, × 10^3 μL	159–388	55.00 ±36.38 (13.00–144.00)	40.50 ±39.34 (11.00–127.00)	58.50 ±33.01 (22.00–116.00)	91.00 ±52.18 (33.00–219.00)
aPTT, s	22.5–32	34.70 ±7.28 (14.80–44.90)	33.10 ±6.92 (25.90–46.10)	25.55 ±3.33 (20.20–29.50)	21.90 ±4.90 (19.90–32.20)
INR	0.8–1.2	1.30 ±0.23 (0.96–1.70)	1.30 ±0.27 (0.96–1.89)	0.92 ±0.14 (0.85–1.37)	0.92 ±0.05 (0.72–1.00)
Fibrinogen, mg/dL	180–350	209.81 ±48.47 (153.68–323.81)	198.33 ±48.97 (140.84–303.00)	231.28 ±6,848.78 (170.91–22,691.00)	213.40 ±41.43 (153.29–286.21)
D-dimer, mg/dL	0–0.55	7.16 ±27.89 (1.48–67.15)	5.71 ±26.28 (1.89–78.48)	1.91 ±1.03 (0.79–4.45)	2.21 ±3.35 (0.56–10.68)
ALT, U/L	<39	65.00 ±159.188 (18.00–580.00)	58.50 ±174.94 (19.00–635.00)	129.00 ±86.74 (32.00–354.00)	143.00 ±79.78 (29.00–253.00)
AST, U/L	<51	162.50 ±443.42 (45.00–1648.00)	159.50 ±500.83 (47.00–1,818.00)	187.50 ±131.10 (72.00–519.00)	140.00 ±90.54 (52.00–359.00)
CK, U/L	<145	205.00 ±2,237.28 (69.00–7,297.00)	266.50 ±2,136.11 (54.00–6,292.00)	130.50 ±116.01 (60.00–364.00)	96.00 ±99.61 (42.00–301.00)
Triglyceride, mg/dL	<150	93.50 ±53.29 (43.00–192.00)	118.00 ±35.28 (46.00–142.00)	190.00 ±56.69 (130.00–304.00)	220.50 ±92.75 (91.00–378.00)
LDH, U/L	110–295	577 ±528.32 (288.00–2,091.00)	651.00 ±49.69 (295.00–1,757.00)	525.00 ±214.18 (313.00–1,089.00)	428.00 ±206.11 (212.00–848.00)
C-reactive protein, mg/dL	0–0.5	1.24 ±2.08 (0.10–6.95)	0.54 ±0.56 (0.12–1.85)	0.17 ±0.10 (0.03–0.39)	0.14 ±0.10 (0.02–0.4)
ESR, mm/h	0–20	3.00 ±5.54 (2.00–21.00)	8.00 ±7.79 (2.00–23.00)	22.00 ±12.74 (12.00–49.00)	36.00 ±15.40 (7.00–56.00)
Ferritin, μL	11–307	2,816.00 ±5,779.20 (309.00–21,690.00)	4,257.00 ±12,330.80 (648–40,455)	2,762.50 ±5,423.00 (558.00–18,772.00)	1,619.50 ±2,822.24 (404.00–9,981.00)

*First time interval, 68–72 h after baseline; second, 120–132 h; third, 156–180 h. aPTT, activated partial thromboplastin time; INR, international normalized ratio; ESR, erythrocyte sedimentation rate; AST, aspartate aminotransferase; ALT, alanine aminotransferase; CK, creatine kinase; LDH, lactate dehydrogenase.

ALT (p = 0.76), AST (p = 0.138), or fibrinogen (p = 0.07) but were for both ESR (p = 0.016) and triglycerides (p = 0.001). Over the third time interval, neutrophil (p = 0.134) and lymphocyte (p = 0.105) counts did not differ significantly, but both platelet (p = 0.045) and erythrocytes (p = 0.05) counts increased significantly. All patients had a significant decline in hemoglobin levels during the third time interval (p = 0.001).

By the third time interval, INR was within normal range for all patients and aPTT levels for 91.7% (11/12), but only 8.3% (1/12) of patients had normal D-dimer levels. Declines in all 3 coagulation parameters over time were significant (p = 0.005 for INR, p = 0.002 for aPTT, and p = 0.001 for D-dimer). Median CRP levels were within normal limits for all 3 intervals, but change over time was significant (p = 0.001). Serum ferritin, CK, and LDH levels peaked during the first time interval and declined significantly over time (p = 0.035 for ferritin, p = 0.01 for CK, and p = 0.005 for LDH). Although nearly half (5/12) of patients had normal CK values at the third time interval, LDH and ferritin levels were above normal in all patients. We performed bone marrow aspiration on 10/12 (83%) patients, all of whom exhibited hemophagocytosis within 24–48 hours after admission.

Treatment

We administered 2 g/kg body weight intravenous immunoglobulin to all patients within 12 hours of admission, either as a 48-hour infusion or 400–500 mg/kg/day over 4–5 days. As part of HLH treatment for all patients, we administered dexamethasone to 8 patients and methylprednisolone to 4. Initial doses were 10 mg/m^2 body surface area for dexamethasone and 2 mg/kg/day for methylprednisolone. Median ±SD initiation time for corticosteroid treatment was 25 ±3.86 hours (range 24–36 hours) and median duration of treatment was 8 ±2.57 days (range 3–10 days). We administered antiviral treatment (ribavirin) to all patients for a median of 5 ±2.54 days (range 2–10

days). We gave fresh frozen plasma and vitamin K to all patients; 3 (25%) required platelet transfusions. Nine (75%) patients experienced transient bradycardia during the treatment, and 2 (16.7%) had transient adrenal suppression. All 12 patients survived.

Serum Cytokine/Chemokine Levels

Cytokine/chemokine values varied both over time and between patient and control groups (Table 3). CCL5 levels were not evaluated further after they measured above upper limits indicated by the manufacturer in 6/11 control patients.

First Time Interval, 68–72 Hours

From beginning to end of the first time interval, 11/23 cytokine/chemokine levels differed significantly. Significantly elevated cytokines/chemokines were those associated with innate and adaptive T-helper 1 immune response: IFN-α ($p<0.001$), IFN-γ ($p = 0.001$), CXCL10 ($p<0.001$), and CXCL11 ($p<0.001$); IL-18 ($p = 0.001$) and CCL20 (formerly MIP-3α; $p = 0.031$), which regulate monocyte migration and the activation of macrophages and natural killer cells; CCL2 ($p = 0.013$), which acts through T-helper 2 cells; and antiinflammatory cytokine IL-10 ($p = 0.0005$). Patient CXCL1 ($p = 0.025$), CXCL5 ($p <0.001$), and CCL17 ($p<0.001$) were significantly lower than those for controls (Table 3; Figure).

Second Time Interval, 120–132 Hours

From beginning to end of the second time interval, 12/23 cytokines/chemokines differed significantly. IL-1β ($p = 0.001$) and IL-33 ($p = 0.025$), which activate T-helper 2 response, were elevated. In addition, IFN-α ($p = 0.003$), IFN-γ ($p = 0.009$), CXCL10 ($p <0.001$), CXCL11 ($p <0.001$), IL-18 ($p = 0.001$), and IL-10 ($p <0.001$) remained significantly elevated. CCL11, which is chemotactic for eosinophils, together with CXCL5 ($p = 0.031$), CCL17 ($p <0.001$), and CXCL1, were significantly lower compared with the controls (Table 3; Figure).

Third Time Interval, 156–180 Hours

From beginning to end of the third time interval, except for IL-1β ($p = 0.502$) and CCL11 ($p = 0.095$), the same cytokines/chemokines were elevated as in the second time interval: IFN-α ($p = 0.006$), IFN-γ ($p = 0.020$), CXCL10 ($p <0.001$), CXCL11 ($p <0.001$), IL-18 ($p = 0.038$), IL-10 ($p <0.001$) and IL-33 ($p = 0.006$). Moreover, the same cytokines/chemokines remained lower than among the control group as in the second time interval: CXCL5 ($p <0.001$), CCL17 ($p <0.001$), and CXCL1 ($p = 0.002$) (Table 3; Figure).

Serum Cytokine/Chemokine Differences Based on Time Intervals

Five cytokines/chemokines, IFN-α ($p = 0.016$), CXCL10 ($p = 0.016$), CXCL11 ($p = 0.016$), CCL11 ($p = 0.016$), and CCL2 ($p = 0.003$), differed significantly depending on the time interval in which they were measured. IFN-α, CXCL10, and CXCL11, were significantly high throughout all 3 intervals, although highest during the first time interval. In contrast, CCL2 was significantly elevated only during the first time interval (Table 3).

Serum Cytokine/Chemokine Correlation with Laboratory Parameters

Some cytokines/chemokines were correlated with CCHF patient laboratory parameters depending on time interval (Table 4, https://wwwnc.cdc.gov/EID/article/29/2/22-0976-T4.htm). Fibrinogen correlated with IL-18 during the first time interval, also with INF-α, IFN-γ, and IL-33 during the second interval. IL-18 and IL-33 were the only cytokines that correlated with ALT. Platelets correlated with CCL17 during the first and second time intervals, whereas they correlated with IL-10 during the third. CCL17 was the only chemokine that correlated with AST. Triglycerides correlated with INF-α, IFN-γ, IL-33, IL-1β, CXCL10, and CXCL11. LDH correlated with CCL3, IL-1β, CXCL11, CCL17, and CCL11. Finally, neutrophils correlated with CCL3 and IL-18, and ferritin with CCL3, IFN-γ, and CCL11. CXCL5 was the only chemokine that correlated with hemoglobin and ESR levels.

Discussion

Since CCHF was first identified in Turkey, children have been observed to have milder disease (*19*,*20*). During the past 2 decades, studies have shown that the course and outcome of CCHF depend on viral load, host genetic factors, and host immune response, together with the level of release of cytokines/chemokines (*10*,*12*,*14*,*21*). Furthermore, the association of hemorrhagic fevers with HLH suggests the involvement of cytokines/chemokines in the pathogenesis of the disease (*22*–*25*). One study reported HLH in 50% of adult CCHF patients (*26*); however, a case report describing an adult CCHF patient with HLH reported HLH as a rare condition (*27*). HLH is rarely reported among pediatric patients (*28*).

After the official announcement of the COVID-19 pandemic in Turkey on March 11, 2020, we began to observe certain changes in pediatric CCHF cases. The first noticeable change was admission

of patients earlier in the year. Although ticks are known to emerge as early as March, the CCHF season in Turkey runs May–September, with June and July as the peak months (*26*,*29*–*31*). During the study period, the first 2 cases were admitted in April, earlier than expected, probably because the patients had relocated to endemic rural valley districts as a result of restrictions and early school closures because of COVID-19.

A second change was observed in clinical manifestations. All 12 CCHF case-patients in the study manifested ≥1 severe disease sign fulfilling the criteria for HLH: all had fever and hepatosplenomegaly, headache was the next most common

Table 3. Median cytokine/chemokine levels of 9 pediatric case-patients with Crimean-Congo hemorrhagic fever and 11 healthy controls, Turkey*

Cytokine/ chemokine	1st time interval, pg/mL (range)	p value†	2nd time interval, pg/mL (range)	p value†	3rd time interval, pg/mL (range)	p value†	Controls, pg/mL (range)
IL-1β	31.19 (0–246.51)	0.94	76.97 (0–259.83)	**0.0014**	50.10 (7.99–300.16)	0.5019	49.13 (0–743.64)
INF-α	105.88 (22.68–239.73)	**<0.0001**	26.03 (8.95–94.97)	**0.0031**	20.26 (99.08–26.45)	**0.0057**	6.98 (2.43–25.41)
INF-γ	36.03 (16.94–106.43)	**0.0097**	44.07 (9.59–157.74)	**0.0097**	32.99 (13.91–286.60)	**0.0200**	8.33 (1.89–39.78)
TNF-α	7.10 (0–29.84)	0.1747	31.51 (5.77–105.14)	0.6556	30.90 (14.22–290.76)	0.1519	10.74 (0–200.89)
MCCL2	1,947.00 (638.74–3,342.00)	**0.0125**	487.64 (247.30–4,974.00)	0.2947	396.94 (212.85–1,477.00)	0.0674	893.33 (477.73–1,101.00)
IL-6	115.30 (13.58–808.78)	0.0674	51.08 (13.19–717.75)	0.1308	39.87 (14.27–266.12)	0.1754	21.99 (2.92–1,297.00)
CXCL8	372.79 (35.34–4,712.00)	0.3312	130.62 (30.35–3,265.00)	0.6556	11.60 (61.16–3,619.00)	0.8238	116.79 (0–26,173.00)
IL-10	144.98 (16.73–1,194)	**0.0005**	223.72 (161.65–1,355.00)	**<0.0001**	146.44 (68.54–545.34)	**<0.0001**	14.46 (0–40.00)
IL-12p70	5.74 (0–20.37)	0.8662	9.46 (3.59–86.07)	0.2299	11.42 (5.38–70.99)	0.1119	5.72 (0–18.11)
IL-17α	0.41 (0–4.59)	0.6406	2.05 (0.19–7.97)	0.4893	1.36 (0.16–395.36)	0.4893	0.67 (0–6.16)
IL-18	2,862 (857.42–4,179.00)	**0.0012**	1,208 (55.17–3,818.00)	**0.0012**	1,124.00 (623.86–6,374.00)	**0.0381**	66.79 (299.29–1,779.00)
IL-23	10.66 (2.63–38.06)	0.5508	31.85 (6.05–43.74)	0.1302	23.51 (6.59–171.03)	0.1513	7.02 (0–54.01)
IL-33	33.06 (0–273.62)	0.6550	75.26 (29.76–496.32)	**0.0251**	147.45 (36.87–500.62)	**0.0057**	19.41 (0–161.00)
CXCL10	3,495.00 (1,677.00–5,475.00)	**<0.0001**	1,674.00 (1,336.00–3,975.00)	**<0.0001**	1,798.00 (972.37–2,620.00)	**<0.0001**	215.35 (123.96–396.45)
CCL11	244.95 (81.83–352.51)	>0.9999	142.16 (90.23–237.45)	**0.0310**	182.57 (72.10–260.51)	0.0952	219.07 (100.08–452.04)
CCL17	99.34 (62.75–175.50)	**<0.0001**	101.56 (54.95–209.21)	**<0.0001**	112.09 (26.97–258.12)	**<0.0001**	766.77 (321.96–1,897.00)
RANTES	3,727.00 (2,357.00–4,642.00)	0.3455	2,849.00 (1,674.00–4,642.00)	**0.0139**	2,045.00 (709.44–4,642.00)	**0.0048**	161.00 (161.00)
MIP-1	95.90 (0–236.97)	0.7609	44.72 (0–2,605.00)	0.3269	124.29 (0–1,638.00)	0.1718	15.05 (0–2,112.00)
MIG	471.00 (296.89–791.29)	0.6027	369.51 (214.11–759.69)	0.7664	660.36 (292.87–851.42)	0.1119	382.81 (249.06–3,035.00)
CXCL5	203.91 (59.04–471.44)	**<0.0001**	119.60 (35.72–441.08)	**<0.0001**	103.63 (19.16–591.52)	**<0.0001**	1,209.00 (467.16–1,875.00)
MIP-3α	130.05 (2.55–231.59)	**0.0310**	80.30 (18.10–396.55)	0.2014	46.17 (14.45–329.60)	0.2947	41.81 (4.87–156.68)
GRO-α	218.75 (53.5–481.01)	**0.0251**	131.41 (65.77–437.74)	**0.0008**	145.73 (65.98–441.94)	**0.0016**	370.46 (260.79–805.93)
CXCL11	1,332.00 (506.05–6,571.00)	**<0.0001**	338.10 (127.82–926.57)	**<0.0001**	315.48 (178.08–515.34)	**<0.0001**	50.29 (24.06–124.47)
MIP-1β	50.36 (26.79–272.66)	0.7103	28.82 (13.30–300.44)	0.2610	26.87 (9.81–405.40)	0.2610	44.54 (13.26–406.35)

*First time interval, 68–72 h after baseline; second, 120–132 h; third, 156–180 h. Bold indicates significance. CCL, CC chemokine ligand; CXCL, C-X-C motif chemokine ligand; IL, interleukin; INF, interferon; TNF, tumor necrosis factor; MCP, monocyte chemoattractant protein; IP, IFN-γ-inducible protein; TARC, hymus- and activation-regulated chemokine; RANTES, regulated upon activation, normal t cell expressed and presumably secreted; MIP, macrophage inflammatory proteins; MIG, monokine-induced γ interferon; ENA, epithelial neutrophil-activating; GRO, growth related protein; I-TAC, interferon-inducible T-cell alpha chemoattractant.

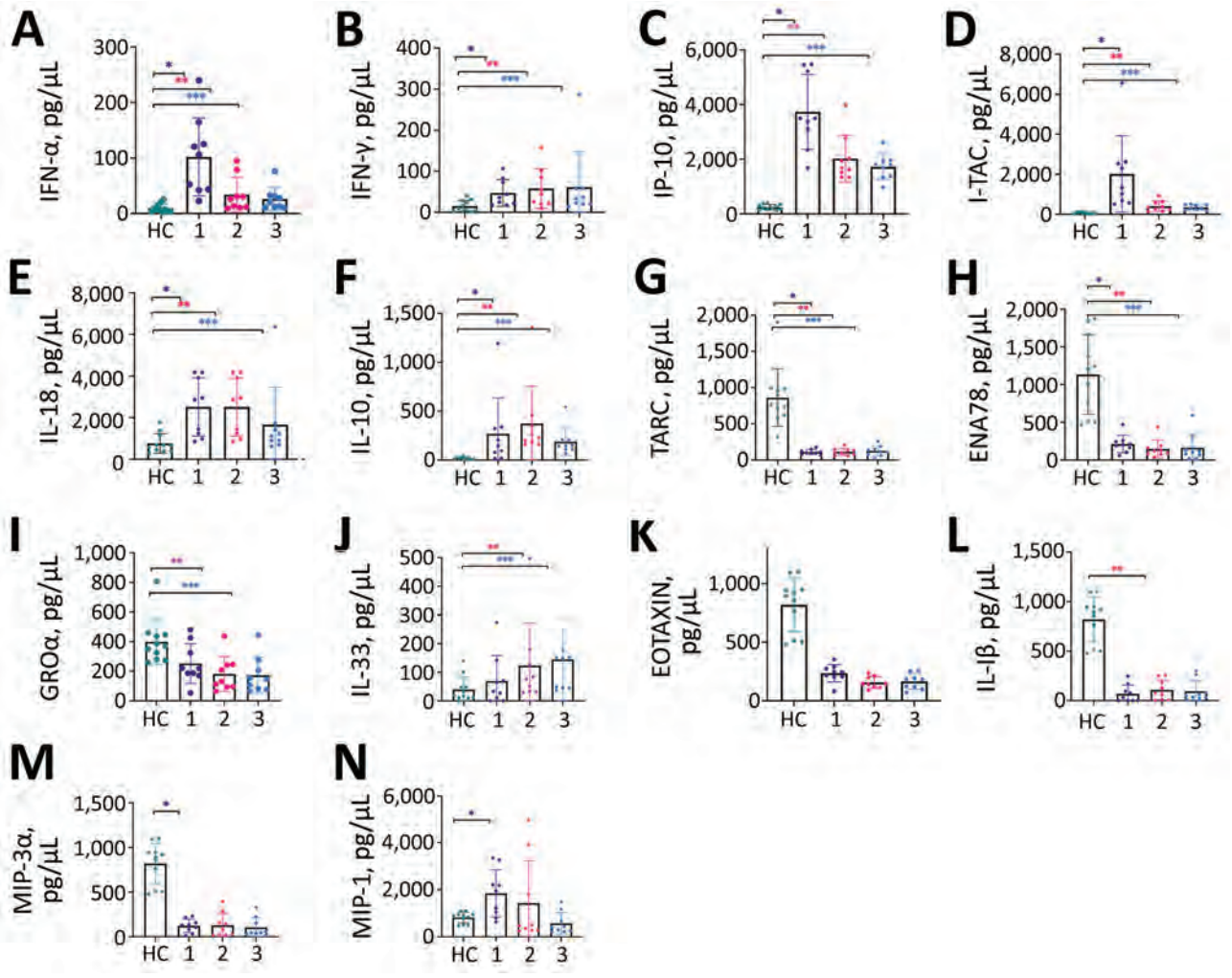

Figure. Quantitative levels of cytokines/chemokines among 12 case-patients with CCHF for 3 time intervals compared with results for controls, Turkey. 1, 1st time interval, 68–72 hours after admission (black); 2, 2nd time interval, 120–132 hours after admission (red); 3, 3rd time interval, 156–180 hours after admission (blue). Controls are shown in green. Time intervals contributing to significant changes designated by number of asterisks (*). *1st time interval; **2nd time interval; ***3rd time interval. CCL, CC chemokine ligand; CXCL, C-X-C motif chemokine ligand; ENA, epithelial neutrophil-activating; HC, healthy controls; IL, interleukin; IFN, interferon; IP, IFN-γ-inducible protein; I-TAC, interferon-inducible T-cell alpha chemoattractant; RANTES, regulated upon activation, normal t cell expressed and presumably secreted; MIP, macrophage inflammatory proteins; NA, not applicable; TARC, hymus- and activation-regulated chemokine.

complaint, most patients had petechiae, and 3 had neurologic findings at admission; none had tonsillopharyngitis. In previously published research on pediatric CCHF, the most common symptoms reported were fever and nausea, and tonsillopharyngitis was observed in a substantial percentage of patients, but hepatomegaly and splenomegaly were rarely reported (*20*,*32*).

Cytokines/chemokines play substantial roles in the pathogeny of viral hemorrhagic fevers, and previous work has proposed that CCHF cytokine profiles are similar to cytokine profiles of other hemorrhagic fevers (*13*,*33*). Studies on the cytokine and chemokine profiles of CCHF patients have mainly been conducted in adults, and the levels of the inflammatory cytokines IL-6 and CXCL8 have been proposed as correlated with severe and fatal CCHF (*13*). Contrary to those findings, in our study, neither IL-6 nor CXCL8 was elevated in any patient during any time interval. Our finding that IL-6 and TNF-α levels were not elevated was consistent with a previous pediatric study (*15*). However, the finding on IL-6 levels differed from another pediatric study in which pediatric CCHF patients were reported to have elevated levels of IL-6 and IL-10 compared with control groups (*34*). The difference might have been because of timing and a single measurement of cytokines/chemokines. In

our study, IFN-α, IFN-γ, CXCL10, and CXCL11 were elevated during all 3 time intervals, indicating the consequential role of the T-helper 1–dependent pathway in pediatric CCHF cases.

Certain strains of CCHF virus have been shown in vitro to delay IFN production (*35*) by suppressing IFN-β-promoter–mediated gene expression, hampering the interferon type 1 response (*36*). However, that pattern seems not to have been the case with the pediatric CCHF patients in our study, among whom the IFN-γ pathway was consistently active. IFN-γ induces production of CXCL10 and CXCL11, structurally associated chemokines that attract C-X-C chemokine receptor type 3^+ ($CXCR3^+$) lymphocytes expressed by T-helper 1 cells (*37*). Our findings suggest that CXCL10 and CXCL11 also modulate T-helper 1–adaptive immunity for the progression of CCHF. IL-18, a proinflammatory cytokine that was elevated during all 3 time intervals, induced IFN-γ production by CD4 and CD8 T-cells and natural killer cells. IL-33, another inducer of IFN-γ production, was elevated in the second and third time intervals. IL-17, which acts in concert with TNF-α and IL-1β and is inhibited by INF-γ, was not elevated in any time interval. The levels of CXCL5, a chemokine inhibited by INF-γ, were significantly low in all time intervals, further supporting INF-γ upregulation.

CCL2, which is expressed by macrophages in response to INF-γ, IL-6, TNF-α, IL-1β, and lipopolysaccharides, is another chemokine reported to correlate with the severity of CCHF (*12,13*). One study proposed that the course of disease in fatal cases was responsible for significantly high chemokines, mainly CCL2 in adult patients but not in pediatric patients, including patients with severe disease (*38*). This finding differs from our observation that all patients had high CCL2 levels during the first time interval; however, we did not observe elevated CCL2 levels in the subsequent intervals. MCP-1 binds to CCR2 and CCR5 receptors. Downregulation of CCR5 is known to be protective against HIV (*39*) and dengue virus (*40*); it has been reported that the lower the expression of CCR5, the better the outcome. Furthermore, proinflammatory cytokine CXCL1 acting through CCR2 levels was lower among patients than controls, suggesting that CCR2 receptors are downregulated in pediatric CCHF patients.

Correlations between cytokine/chemokine levels and laboratory parameters varied. Although all patients fulfilled the HLH criteria, triglyceride levels were invariably low during the first time interval. In that period, triglyceride levels negatively correlated with CXCL10 and CXCL11, both chemokines known to cause hypertriglyceridemia. Another notable laboratory parameter was CRP, which did not correlate with any cytokines/chemokines. A recent report described CCHF patients misdiagnosed with MIS-C during the pandemic (*17*). Indeed, 3 case-patients in our study were referred with a preliminary diagnosis of MIS-C. However, CRP levels differed uniquely between CCHF and MIS-C cases. CRP levels of almost all the CCHF cases were within reference limits throughout all time intervals, but median CRP levels in MIS-C cases were low, at 18.7 mg/dL in 1 study (*41*) and 19.6 mg/dL in another (*42*). Meanwhile, the CRP levels of the MIS-C cases associated with HLH were 7.5–21.9 mg/dL (*43*). Combined with a tick-bite history, low CRP levels should raise suspicion of CCHF in pediatric patients with HLH in endemic regions.

Among limitations of our study, the small number of CCHF patients, all of whom had severe disease, did not allow us to generalize findings to all CCHF patients. However, we believe that serial measurement of cytokines/chemokines in our study represents a notable advantage over studies that used a single measurement. Another limitation was that, although all patients had a cycle threshold value <20, it was not possible to have viral loads measured or CCHF virus strains sequenced because of increased laboratory workload during the COVID-19 pandemic.

In conclusion, our results show that children can have severe CCHF that manifests with HLH-like signs and symptoms. We observed strong IFN pathway activation and a T-helper 1–biased immune response. Downregulation of cytokines acting through CCR2 and CCR5 had a favorable effect among case-patients despite severe disease. In the future, larger controlled studies including CCHF pediatric patients with various disease severity should be conducted to verify the actual roles of different cytokine/chemokine profiles among children. Clinicians should be aware that children can manifest severe CCHF and that, in the context of the ongoing COVID-19 pandemic, those cases might be initially considered to be MIS-C. Our results further suggest that HLH secondary to CCHF can be successfully treated with intravenous immunoglobulin and steroid therapy.

Acknowledgments

We thank Hacettepe University İhsan Doğramacı Children's Hospital, Ankara, Turkey, where the study was conducted.

About the Author

Dr. Oygar is a pediatric infectious diseases specialist at İhsan Doğramacı Children's Hospital.

References

1. World Health Organization (WHO). Roadmap for research and product development against Crimean-Congo haemorrhagic fever (CCHF) [cited 2022 Mar 24]. https://www.who.int/publications/m/item/crimean-congo-haemorrhagic-fever-(cchf)-research-and-development-(r-d)-roadmap
2. Gargili A, Estrada-Peña A, Spengler JR, Lukashev A, Nuttall PA, Bente DA. The role of ticks in the maintenance and transmission of Crimean-Congo hemorrhagic fever virus: a review of published field and laboratory studies. Antiviral Res. 2017;144:93–119. https://doi.org/10.1016/j.antiviral.2017.05.010
3. Sidira P, Maltezou HC, Haidich AB, Papa A. Seroepidemiological study of Crimean-Congo haemorrhagic fever in Greece, 2009–2010. Clin Microbiol Infect. 2012;18:E16–9. https://doi.org/10.1111/j.1469-0691.2011.03718.x
4. Bente DA, Forrester NL, Watts DM, McAuley AJ, Whitehouse CA, Bray M. Crimean-Congo hemorrhagic fever: history, epidemiology, pathogenesis, clinical syndrome and genetic diversity. Antivir Res. 2013;100:159–89.
5. Ergönül O. Clinical and pathologic features of Crimean-Congo hemorrhagic fever. In: Ergonul, O, Whitehouse CA, editors. Crimean-Congo hemorrhagic fever: a global perspective. Dordrecht (the Netherlands): Springer; 2007. https://doi.org/10.1007/978-1-4020-6106-6_16
6. Whitehouse CA. Crimean-Congo hemorrhagic fever. Antiviral Res. 2004;64:145–60. https://doi.org/10.1016/j.antiviral.2004.08.001
7. Gunes T, Engin A, Poyraz O, Elaldi N, Kaya S, Dokmetas I, et al. Crimean-Congo hemorrhagic fever virus in high-risk population, Turkey. Emerg Infect Dis. 2009;15:461–4. https://doi.org/10.3201/eid1503.080687
8. Tsergouli K, Karampatakis T, Haidich AB, Metallidis S, Papa A. Nosocomial infections caused by Crimean-Congo haemorrhagic fever virus. J Hosp Infect. 2020;105:43–52. https://doi.org/10.1016/j.jhin.2019.12.001
9. Pshenichnaya NY, Nenadskaya SA. Probable Crimean-Congo hemorrhagic fever virus transmission occurred after aerosol-generating medical procedures in Russia: nosocomial cluster. Int J Infect Dis. 2015;33:120–2. https://doi.org/10.1016/j.ijid.2014.12.047
10. Saksida A, Duh D, Wraber B, Dedushaj I, Ahmeti S, Avsic-Zupanc T. Interacting roles of immune mechanisms and viral load in the pathogenesis of Crimean-Congo hemorrhagic fever. Clin Vaccine Immunol. 2010;17:1086–93. https://doi.org/10.1128/CVI.00530-09
11. Papa A, Drosten C, Bino S, Papadimitriou E, Panning M, Velo E, et al. Viral load and Crimean-Congo hemorrhagic fever. Emerg Infect Dis. 2007;13:805–6. https://doi.org/10.3201/eid1305.061588
12. Papa A, Tsergouli K, Çağlayık DY, Bino S, Como N, Uyar Y, et al. Cytokines as biomarkers of Crimean-Congo hemorrhagic fever. J Med Virol. 2016;88:21–7. https://doi.org/10.1002/jmv.24312
13. Ergönül Ö, Şeref C, Eren Ş, Çelikbaş A, Baykam N, Dokuzoğuz B, et al. Cytokine response in Crimean-Congo hemorrhagic fever virus infection. J Med Virol. 2017;89:1707–13. https://doi.org/10.1002/jmv.24864
14. Kaya S, Elaldi N, Kubar A, Gursoy N, Yilmaz M, Karakus G, et al. Sequential determination of serum viral titers, virus-specific IgG antibodies, and TNF-α, IL-6, IL-10, and IFN-γ levels in patients with Crimean-Congo hemorrhagic fever. BMC Infect Dis. 2014;14:416. https://doi.org/10.1186/1471-2334-14-416
15. Ozsurekci Y, Arasli M, Karadag Oncel E, Caglayik DY, Kaya A, Icagasioglu FD, et al. Can the mild clinical course of Crimean-Congo hemorrhagic fever in children be explained by cytokine responses? J Med Virol. 2013;85:1955–9. https://doi.org/10.1002/jmv.23697
16. World Health Organization. Prioritizing diseases for research and development in emergency contexts [cited 2022 Mar 24]. https://www.who.int/activities/prioritizing-diseases-for-research-and-development-in-emergency-contexts
17. Yalçinkaya R, Polat M, Gümüşer Cinni R, Öz FN, Tanir G, Uysal Yazici M. Crimean-Congo hemorrhagic fever mimicking multisystem inflammatory syndrome in children associated with COVID-19: a diagnostic challenge. Pediatr Infect Dis J. 2021;40:e524–5. https://doi.org/10.1097/INF.0000000000003269
18. Henter JI, Horne A, Aricó M, Egeler RM, Filipovich AH, Imashuku S, et al. HLH-2004: diagnostic and therapeutic guidelines for hemophagocytic lymphohistiocytosis. Pediatr Blood Cancer. 2007;48:124–31. https://doi.org/10.1002/pbc.21039
19. Dilber E, Cakir M, Acar EA, Orhan F, Yaris N, Bahat E, et al. Crimean-Congo haemorrhagic fever among children in north-eastern Turkey. Ann Trop Paediatr. 2009;29:23–8. https://doi.org/10.1179/146532809X401999
20. Tezer H, Sucakli IA, Sayli TR, Celikel E, Yakut I, Kara A, et al. Crimean-Congo hemorrhagic fever in children. J Clin Virol. 2010;48:184–6. https://doi.org/10.1016/j.jcv.2010.04.001
21. Papa A, Bino S, Velo E, Harxhi A, Kota M, Antoniadis A. Cytokine levels in Crimean-Congo hemorrhagic fever. J Clin Virol. 2006;36:272–6. https://doi.org/10.1016/j.jcv.2006.04.007
22. McElroy AK, Shrivastava-Ranjan P, Harmon JR, Martines RB, Silva-Flannery L, Flietstra TD, et al. Macrophage activation marker soluble CD163 associated with fatal and severe Ebola virus disease in humans. Emerg Infect Dis. 2019;25:290–8. https://doi.org/10.3201/eid2502.181326
23. Wan Jamaludin WF, Periyasamy P, Wan Mat WR, Abdul Wahid SF. Dengue infection associated hemophagocytic syndrome: therapeutic interventions and outcome. J Clin Virol. 2015;69:91–5. https://doi.org/10.1016/j.jcv.2015.06.004
24. Kan FK, Tan CC, Von Bahr Greenwood T, Khalid KE, Supramaniam P, Hed Myrberg I, et al. Dengue infection complicated by hemophagocytic lymphohistiocytosis: experiences from 180 patients with severe dengue. Clin Infect Dis. 2020;70:2247–55. https://doi.org/10.1093/cid/ciz499
25. Usmani GN, Woda BA, Newburger PE. Advances in understanding the pathogenesis of HLH. Br J Haematol. 2013;161:609–22. https://doi.org/10.1111/bjh.12293
26. Karti SS, Odabasi Z, Korten V, Yilmaz M, Sonmez M, Caylan R, et al. Crimean-Congo hemorrhagic fever in Turkey. Emerg Infect Dis. 2004;10:1379–84. https://doi.org/10.3201/eid1008.030928
27. Cagatay A, Kapmaz M, Karadeniz A, Basaran S, Yenerel M, Yavuz S, et al. Haemophagocytosis in a patient with Crimean Congo haemorrhagic fever. J Med Microbiol. 2007;56(Pt 8):1126–8. https://doi.org/10.1099/jmm.0.46910-0
28. Gayretli Aydin ZG, Yesilbas O, Reis GP, Guven B. The first pediatric case of hemophagocytic lymphohistiocytosis secondary to Crimean-Congo haemorrhagic fever successfully treated with therapeutic plasma exchange ac-

companying ribavirin and intravenous immunoglobulin. J Clin Apher. 2021;36:780–4. https://doi.org/10.1002/jca.21915
29. Ozdarendeli A, Aydin K, Tonbak S, Aktas M, Altay K, Koksal I, et al. Genetic analysis of the M RNA segment of Crimean-Congo hemorrhagic fever virus strains in Turkey. Arch Virol. 2008;153:37–44. https://doi.org/10.1007/s00705-007-1056-4
30. Ergönül O, Zeller H, Kiliç S, Kutlu S, Kutlu M, Cavusoglu S, et al. Zoonotic infections among veterinarians in Turkey: Crimean-Congo hemorrhagic fever and beyond. Int J Infect Dis. 2006;10:465–9. https://doi.org/10.1016/j.ijid.2006.06.005
31. Ozkurt Z, Kiki I, Erol S, Erdem F, Yilmaz N, Parlak M, et al. Crimean-Congo hemorrhagic fever in eastern Turkey: clinical features, risk factors and efficacy of ribavirin therapy. J Infect. 2006;52:207–15. https://doi.org/10.1016/j.jinf.2005.05.003
32. Kızılgun M, Ozkaya-Parlakay A, Tezer H, Gulhan B, Kanik-Yüksek S, Celikel E, et al. Evaluation of Crimean-Congo hemorrhagic fever virus infection in children. Vector Borne Zoonotic Dis. 2013;13:804–6. https://doi.org/10.1089/vbz.2013.1297
33. Korva M, Rus KR, Pavletič M, Saksida A, Knap N, Jelovšek M, et al. Characterization of biomarker levels in Crimean-Congo hemorrhagic fever and hantavirus fever with renal syndrome. Viruses. 2019;11:686. https://doi.org/10.3390/v11080686
34. Tezer H, Ozkaya-Parlakay A, Kizilgün M, Kaya A, Gulhan B, Kanik Yüksek S, et al. Cytokine concentrations in pediatric patients with Crimean-Congo hemorrhagic fever. Pediatr Infect Dis J. 2014;33:1185–7. https://doi.org/10.1097/INF.0000000000000398
35. Andersson I. Karlberg H, Mousavi-Jazi M, Martínez-Sobrido L, Weber F, Mirazimi A. Crimean-Congo hemorrhagic fever virus delays activation of the innate immune response. J Med Virol. 2008;80:1397–404. https://doi.org/10.1002/jmv.21222
36. Fajs L, Resman K, Avšič-Županc T. Crimean-Congo hemorrhagic fever virus nucleoprotein suppresses IFN-beta-promoter-mediated gene expression. Arch Virol. 2014;159:345–8. https://doi.org/10.1007/s00705-013-1816-2
37. Singh UP, Singh S, Iqbal N, Weaver CT, McGhee JR, Lillard JW Jr. IFN-γ-inducible chemokines enhance adaptive immunity and colitis. J Interferon Cytokine Res. 2003;23:591–600. https://doi.org/10.1089/107999003322485099
38. Arasli M, Ozsurekci Y, Elaldi N, McAuley AJ, Karadag Oncel E, Tekin IO, et al. Elevated chemokine levels during adult but not pediatric Crimean-Congo hemorrhagic fever. J Clin Virol. 2015;66:76–82. https://doi.org/10.1016/j.jcv.2015.03.010
39. Claireaux M, Robinot R, Kervevan J, Patgaonkar M, Staropoli I, Brelot A, et al. Low CCR5 expression protects HIV-specific CD4+ T cells of elite controllers from viral entry. Nat Commun. 2022;13:521. https://doi.org/10.1038/s41467-022-28130-0
40. Islam M, Kalita T, Saikia AK, Begum A, Baruah V, Singh N, et al. Significance of RANTES-CCR5 axis and linked downstream immunomodulation in dengue pathogenesis: a study from Guwahati, India. J Med Virol. 2019;91:2066–73. https://doi.org/10.1002/jmv.25561
41. Gurlevik SL, Ozsurekci Y, Sağ E, Derin Oygar P, Kesici S, Akca ÜK, et al. The difference of the inflammatory milieu in MIS-C and severe COVID-19. Pediatr Res. 2022:1–10. https://doi.org/10.1038/s41390-022-02029-4
42. Ozsurekci Y, Gürlevik S, Kesici S, Akca UK, Oygar PD, Aykac K, et al. Multisystem inflammatory syndrome in children during the COVID-19 pandemic in Turkey: first report from the Eastern Mediterranean. Clin Rheumatol. 2021;40:3227–37. [Erratum in Clin Rheumatol. 2021;40:2523]. https://doi.org/10.1007/s10067-021-05631-9
43. Lacinel Gurlevik S, Aksu T, Ozen S, Kesici S, Gumruk F, Ozsurekci Y. Hemophagocytosis in bone marrow aspirates in multisystem inflammatory syndrome in children. Pediatr Blood Cancer. 2021;68:e28931. https://doi.org/10.1002/pbc.28931

Address for correspondence: Yasemin Özsürekci, Hacettepe University, İhsan Doğramacı Children's Hospital, 06100 Sıhhıye, Ankara, Turkey; email: yas.oguz99@yahoo.com

Relationship between Telework Experience and Presenteeism during COVID-19 Pandemic, United States, March–November 2020

Livvy Shafer, Faruque Ahmed, Sara Kim, Karen J. Wernli, Michael L. Jackson, Mary Patricia Nowalk, Todd Bear, Richard K. Zimmerman, Emily T. Martin, Arnold S. Monto, Manjusha Gaglani, Michael Reis, Jessie R. Chung, Brendan Flannery, Amra Uzicanin

Persons with COVID-19–like illnesses are advised to stay home to reduce the spread of SARS-CoV-2. We assessed relationships between telework experience and COVID-19 illness with work attendance when ill. Adults experiencing fever, cough, or loss of taste or smell who sought healthcare or COVID-19 testing in the United States during March–November 2020 were enrolled. Adults with telework experience before illness were more likely to work at all (onsite or remotely) during illness (87.8%) than those with no telework experience (49.9%) (adjusted odds ratio 5.48, 95% CI 3.40–8.83). COVID-19 case-patients were less likely to work onsite (22.1%) than were persons with other acute respiratory illnesses (37.3%) (adjusted odds ratio 0.36, 95% CI 0.24–0.53). Among COVID-19 case-patients with telework experience, only 6.5% worked onsite during illness. Telework experience before illness gave mildly ill workers the option to work and improved compliance with public health recommendations to stay home during illness.

In response to the then-evolving COVID-19 pandemic, a public health emergency was declared in the United States on January 31, 2020, and several closure and containment policies were subsequently put in place. Those policies included restrictions on international and domestic travel, cancellation of public events, restrictions on gathering size, closure of schools and nonessential workplaces, and stay-at-home requirements (*1*). The prevalence of the closure and containment policies was greatest in April 2020 (*2*). The availability of COVID-19 testing was limited early in the pandemic but increased over time (*3*,*4*).

SARS-CoV-2 is spread through respiratory droplets produced by sneezing and coughing, as well as short-range and long-range aerosols (*5*). Shared workspaces, such as open office floor plans, shared offices, and break rooms, encourage the spread of SARS-CoV-2, thus making workplace transmission a concern. Employers in the United States were advised to implement a variety of measures to prevent and reduce transmission within the workplace, including symptom and temperature screening, mask wearing, physical distancing, increasing remote work where feasible, providing flexible paid sick leave, and actively encouraging sick employees to stay home (*6*). To support workers and businesses during the COVID-19 shutdown and reduce workplace spread of COVID-19, beginning April 1, 2020, the federal government provided direct financial support to workers and businesses and required covered employers to provide paid sick leave or expanded family and medical leave if an employee was unable to work because of COVID 19 illness (*7*). Nonetheless, outbreaks of COVID-19 in workplaces have been reported, in part attributed

Author affiliations: Oak Ridge Institute for Science and Education, Oak Ridge, Tennessee, USA (L. Shafer); Centers for Disease Control and Prevention, Atlanta, Georgia, USA (L. Shafer, F. Ahmed, S. Kim, J.R. Chung, B. Flannery, A. Uzicanin); Kaiser Permanente Washington Health Research Institute, Seattle, Washington, USA (K.J. Wernli, M.L. Jackson); University of Pittsburgh, Pittsburgh, Pennsylvania, USA (M.P. Nowalk, T. Bear, R.K. Zimmerman); University of Michigan, Ann Arbor, Michigan, USA (E.T. Martin, A.S. Monto); Baylor Scott and White Health, Temple, Texas, USA (M. Gaglani, M. Reis); Texas A&M University College of Medicine, Temple (M. Gaglani, M. Reis)

DOI: https://doi.org/10.3201/eid2902.221014

to presenteeism (*8*–*10*). Workplace presenteeism has been described as "the phenomenon of people, despite complaints and ill health that should prompt rest and absence from work, still turning up at their jobs" (*11*).

In a study of employed adults with influenza and other acute respiratory illnesses (ARIs) before the COVID-19 pandemic, Ahmed et al. (*12*) found that experience with telework before illness enabled workers to work more days overall during the first 3 days of illness than employees without telework experience. This experience enabled workers to maintain some level of workflow where they might otherwise have needed to use a sick day (*12*). Our study, conducted during the first year of the COVID-19 pandemic in the United States, examined whether telework experience before illness onset affected work attendance during illness.

Methods

Study Population

We enrolled adults 18–69 years of age seeking testing at COVID-19 testing sites or ambulatory medical care (i.e., telehealth, primary care, urgent care, or emergency department) for ARI (<10 days' duration) manifesting as fever, cough, or loss of taste or smell. The sites were located in Michigan (Ann Arbor and Detroit), Pennsylvania (Pittsburgh), Texas (Temple and surrounding areas in Central Texas), and Washington (Puget Sound region) and were affiliated with the US Influenza Vaccine Effectiveness Network. Research staff screened persons for eligibility by telephone at 3 sites and by telephone or online survey at 1 site (Pennsylvania). The study methods have been published previously (*13*). This study was approved by institutional review boards at the Centers for Disease Control and Prevention and all participating sites. Study participants provided informed consent and were compensated $15–$20 for enrolling in the study.

Data Collection

We collected data for this study during March 2020–November 2020, a period during which COVID-19 vaccines were not available in the United States. Participants completed an enrollment survey to provide information on their age, sex, race and ethnicity, education, occupation, general health status before illness, cigarette smoking or vaping, date of illness onset, and symptoms during illness. Persons who reported that they were healthcare workers might or might not have had close contact with patients. We tested respiratory specimens from midturbinate nasal swabs for SARS-CoV-2 by using reverse transcription PCR and recorded specimen collection and testing dates. Data on when participants received their COVID-19 test results were not available.

We asked participants to complete a follow-up survey 1–2 weeks after enrollment (Appendix Table 1). The follow-up survey included questions about employment status, hours expected to work in a typical week, hours usually worked from home (i.e., telework, telecommute, or remote work), and work status during illness (worked onsite, worked from home, did not work). We also asked participants about recovery from illness.

Inclusion and Exclusion Criteria for Analysis

If an adult enrolled in the study >1 time because of multiple episodes of ARI, only the first enrollment was included. We excluded participants if they were unemployed, self-employed, owned their own business, worked solely from home before illness, or were employed for <20 hours per week. To minimize recall bias, we also excluded those who completed the follow-up survey >28 days after onset of illness.

Definitions

We classified adults who reported that they regularly worked ≥1 hour from home in a typical week before their illness as having experience with telework (*12*). We computed duration of illness from the date of illness onset to the date of having fully or mostly recovered from illness. We categorized persons who reported working onsite for ≥1 day during their illness, regardless of whether they also teleworked during their illness, as having worked onsite during their illness. Among the remaining persons, we categorized those who reported teleworking for ≥1 day during their illness as having teleworked during illness (i.e., solely teleworked). We classified participants who did not fall into these 2 categories as not having worked during their illness. We computed days worked during illness by summing the days worked onsite and the days teleworked during illness. We defined laboratory-confirmed COVID-19 as a positive result from a PCR test.

Statistical Analysis

We determined the associations between telework experience before illness and laboratory-confirmed COVID-19 with working onsite during illness to assess the potential to infect coworkers. We also assessed associations with working at all (onsite or solely telework) to assess maintenance of workflow.

We used Student *t*-test to determine differences between means and χ^2 test to assess differences between the observed frequencies and the expected frequencies if the null hypothesis was true. Wilcoxon's rank-sum test was used to compare differences in spread and medians (*14*). We used PROC GLIMMIX in SAS version 9.4 (SAS Institute Inc., https://www.sas.com) to conduct multilevel logistic regressions to account for the clustering of participants within study sites. We determined covariables for inclusion in the models by using a backward selection process, assessing model fit using change in −2 log likelihood. Age, sex, health status, and smoking or vaping status were ultimately eliminated.

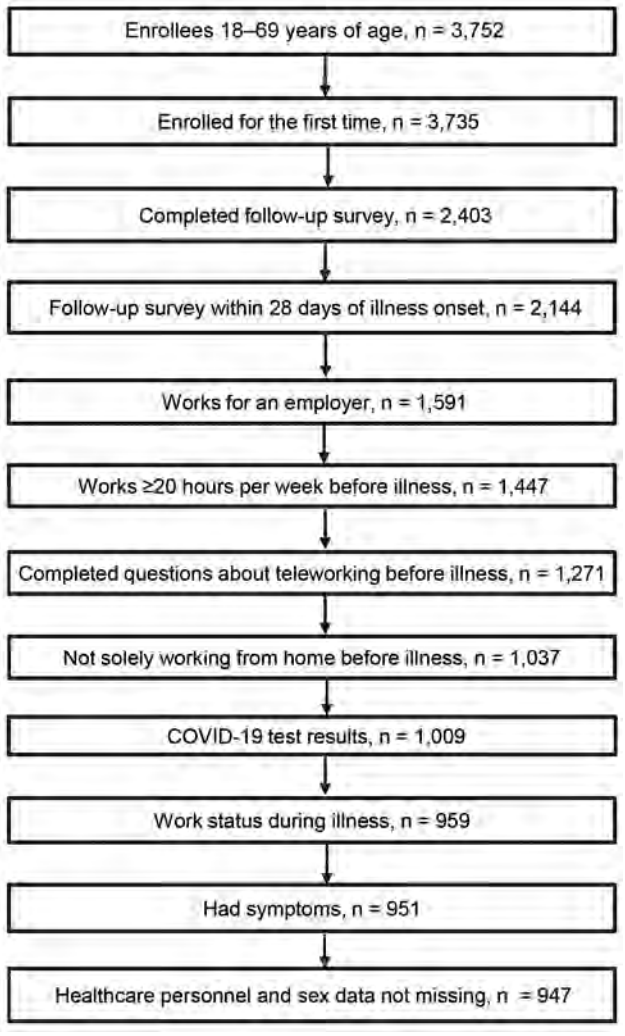

Figure. Enrollment flow diagram for adults seeking ambulatory medical care or testing at COVID-19 testing sites in study of relationship between telework experience and presenteeism during COVID-19 pandemic, United States, March–November 2020. Enrollment sites were in Michigan (Ann Arbor and Detroit), Pennsylvania (Pittsburgh), Texas (Temple and surrounding area in Central Texas), and Washington (Puget Sound region).

Results

A total of 3,752 adults were enrolled across the study sites. Among 3,735 persons enrolled for the first time, 2,144 (57%) completed the follow-up survey within 28 days of illness onset. Survey completion rates were 22% (Michigan), 47% (Texas), 60% (Washington), and 80% (Pennsylvania). In total, 1,447 adults worked for an employer for ≥20 hours per week. After excluding persons who worked solely from home before illness, had missing information on telework experience before illness or work status during illness, had indeterminate or missing COVID-19 test results, had no symptoms, or had missing information for sex and healthcare personnel status, 947 persons were eligible (Figure).

The median number of days from illness onset to specimen collection was 3 (interquartile range [IQR] 2–5) days, from illness onset to COVID-19 testing was 5 (IQR 3–8) days, from onset to enrollment was 6 (IQR 4–9) days, and from onset to follow-up was 15 (IQR 12–19) days. Enrollment occurred on the same day the specimen was collected in 28% of participants. Among the 947 participants, 231 (24.4%) persons had COVID-19 and 716 (75.6%) persons had non–COVID-19 ARIs. Compared with persons who did not have experience with telework before illness, those with telework experience were more likely to have illness onset during the fall than the spring (46.8% vs. 34.8%; p<0.01), more likely to have higher education levels (p<0.001), less likely to be a healthcare worker (36.6% vs. 52.7%; p<0.001), and less likely to have COVID-19 (15.1% vs. 27.0%; p<0.001) (Table 1).

Persons with telework experience before illness were less likely to work onsite during their illness (21.5%) than those without telework experience (36.9%) (adjusted odds ratio [aOR] 0.45, 95% CI 0.30–0.68) (Table 2). COVID-19 case-patients were less likely to report working onsite during their illness (22.1%) than persons with non–COVID-19 ARIs (37.3%) (aOR 0.36, 95% CI 0.24–0.53) (Table 2). Among persons with telework experience before illness, only 6.5% of COVID-19 case-patients worked onsite (Table 2).

Persons with telework experience before illness were more likely to work at all (onsite or telework) during their illness (87.8%) than those with no telework experience (49.9%) (aOR 5.48, 95% CI 3.40–8.83) (Table 3). Among persons who worked, the median days worked was greater for those with telework experience than for those with no telework experience (≥5 days vs. 3 days; p<0.001). Persons with COVID-19 were less likely to work at all during their illness (41.6%) than persons with non–COVID-19 ARIs (63.4%) (aOR 0.40, 95% CI 0.28–0.58) (Table 3).

About 16% (75/467) of healthcare workers had telework experience before illness compared with 27% (130/481) of nonhealthcare personnel. The findings for working at all or onsite were similar in healthcare personnel and nonhealthcare personnel (Appendix Tables 2, 3). Findings for persons with illness onset during the spring were similar to those with illness onset during the fall (Appendix Tables 4, 5). Findings for the sites with higher survey completion rates (Pennsylvania and Washington) were similar to those for sites with lower survey completion rates (Michigan and Texas) (Appendix Tables 6, 7).

Discussion

Our findings show that, during the early part of the COVID-19 pandemic, employed adults who had telework experience before becoming ill were less likely to work onsite but more likely to work at all (onsite or telework) during illness than those without telework experience, thus enabling them to maintain a greater level of productivity without risk of workplace-related onward spread of infection. Persons with COVID-19 were less likely to work at all, remotely or onsite, during illness than were persons with other ARIs. Among COVID-19

Table 1. Characteristics of employed adults seeking ambulatory medical care or testing at COVID-19 testing sites, United States, March–November 2020*

Characteristic	Experience with telework before illness		p value
	Yes, n = 205	No, n = 742	
Site			<0.05†
Michigan	18 (8.8)	42 (5.7)	
Pennsylvania	101 (49.3)	437 (58.9)	
Texas	49 (23.9)	169 (22.8)	
Washington	37 (18.1)	94 (12.7)	
Illness onset period			<0.01†
Spring 2020, March–June	109 (53.2)	484 (65.2)	
Fall 2020, July–November	96 (46.8)	258 (34.8)	
Mean age, y (SD)	42.4 (11.1)	39.4 (11.6)	<0.001‡
Sex			<0.05†
M	69 (33.7)	188 (25.3)	
F	136 (66.3)	554 (74.7)	
Race/ethnicity			
White, non-Hispanic	169 (82.8)	590 (79.8)	
Black, non-Hispanic	6 (2.9)	60 (8.1)	
Other, non-Hispanic	14 (6.9)	39 (5.3)	
Hispanic, any race	15 (7.4)	50 (6.8)	
Education			<0.001†
Less than high school, high school diploma, or GED	5 (2.4)	92 (12.4)	
Some college, including vocational and associate's degree	32 (15.6)	285 (38.5)	
Bachelor's degree	68 (33.2)	214 (28.9)	
Advanced degree	100 (48.8)	149 (20.2)	
Healthcare personnel			<0.001†
No	130 (63.4)	351 (47.3)	
Yes	75 (36.6)	391 (52.7)	
Self-rated general health status			
Excellent	40 (19.5)	100 (13.5)	
Very good	89 (43.4)	308 (41.6)	
Good	61 (29.8)	270 (36.4)	
Fair/poor	15 (7.3)	63 (8.5)	
Smokes or vapes			
No	173 (84.4)	617 (83.2)	
Yes	32 (15.6)	125 (16.9)	
Median hours worked in a typical week before illness (10th, 90th percentile)	40 (36, 60)	40 (32, 48)	<0.001§
Fully or mostly recovered from illness at follow-up¶			<0.05†
No	22 (11.2)	124 (17.7)	
Yes	175 (88.8)	577 (82.3)	
Among persons fully or mostly recovered from illness, median duration of illness, d (10th, 90th percentile)	10 (4, 17)	10 (4, 17)	
COVID-19 case			<0.001†
Yes	31 (15.1)	200 (27.0)	
No	174 (84.9)	542 (73.1)	

*Values are no. (%) except as indicated.
†By χ^2 test.
‡By Student t test.
§By Wilcoxon rank-sum test.
¶Data not available for 49 persons.

Table 2. Associations between telework experience before illness and COVID-19 status with working onsite during illness, United States, March–November 2020

Characteristic	Worked onsite during illness*		Adjusted odds ratio (95% CI)†
	Yes, n = 318	No, n = 629	
Telework experience before illness			
Yes	44 (21.5)	161 (78.5)	0.45 (0.30–0.68)
No	274 (36.9)	468 (63.1)	Referent
COVID-19 case			
Yes	51 (22.1)	180 (77.9)	0.36 (0.24–0.53)
No	267 (37.3)	449 (62.7)	Referent
Telework experience before illness: Yes			
COVID-19 case			
Yes	2 (6.5)	29 (93.6)	0.16 (0.03–0.82)
No	42 (24.1)	132 (75.9)	Referent
Telework experience before illness: No			
COVID-19 case			
Yes	49 (24.5)	151 (75.5)	0.38 (0.26–0.57)
No	225 (41.5)	317 (58.5)	Referent

*Among 318 persons categorized as having worked onsite during illness, 58 persons worked both onsite and remotely. Persons categorized as not having worked onsite during illness consisted of persons who did not work or solely teleworked.
†Dependent variable in the multi-level logistic regression model is worked onsite during illness (0 = No, 1 = Yes). Independent variables are telework experience before illness (0 = No, 1 = Yes), COVID-19 case (0 = No, 1 = Yes), race/ethnicity, education, healthcare personnel status, hours typically worked per week before illness, illness onset period, and study site.

case-patients with telework experience before illness, few worked onsite when ill.

Persons with no telework experience might have been more likely to be in occupations that are less amenable to telework, and so they might not have had the option to work remotely instead of working onsite or using a sick day. For example, we found that healthcare personnel were less likely to telework than were nonhealthcare personnel. Previous studies reported that jobs in hospitality and leisure, transportation, utilities, production, agriculture, and construction are less likely to be amenable to telework than jobs in finance, law, computers, information, business and professional services, and many science fields (*15*,*16*).

Persons with COVID-19 might have been more likely to refrain from working during illness than those with non–COVID-19 ARIs for several reasons, including more, or more severe symptoms, such as fever, muscle aches, and a loss of smell or taste associated with COVID-19 illness (*13*); being advised to isolate by case investigators; and employers discouraging or prohibiting sick persons from entering the worksite. Our study found that 22% of persons with COVID-19 worked onsite, but that proportion was lower among persons with telework experience before illness. Some persons with COVID-19 might have worked onsite before they received a positive test result. Among persons with COVID-19

Table 3. Associations between telework experience before illness and COVID-19 status with working at all during illness, United States, March–November 2020

Characteristic	Worked onsite or solely teleworked during illness*		Adjusted odds ratio (95% CI)†
	Yes, n = 550	No, n = 397	
Telework experience before illness‡			
Yes	180 (87.8)	25 (12.2)	5.48 (3.40–8.83)
No§	370 (49.9)	372 (50.1)	Referent
COVID-19 case			
Yes	96 (41.6)	135 (58.4)	0.40 (0.28–0.58)
No	454 (63.4)	262 (36.6)	Referent
Telework experience before illness: Yes			
COVID-19 case			
Yes	27 (87.1)	4 (12.9)	0.75 (0.22–2.61)
No	153 (87.9)	21 (12.1)	Referent
Telework experience before illness: No			
COVID-19 case			
Yes	69 (34.5)	131 (65.5)	0.39 (0.26–0.56)
No	301 (55.5)	241 (44.5)	Referent

*Persons categorized as having worked onsite includes persons who worked both onsite and teleworked.
†Dependent variable in the multilevel logistic regression model is worked onsite or teleworked exclusively during illness (0 = No, 1 = Yes). Independent variables are telework experience before illness (0 = No, 1 = Yes), COVID-19 case (0 = No, 1 = Yes), race/ethnicity, education, healthcare personnel status, hours typically worked per week before illness, illness onset period, and study site.
‡Among the 550 persons who worked, the median days worked was ≥5 days for those with telework experience compared to 3 days for those with no telework experience ($p<0.001$).
§Among 742 persons with no telework experience before illness, 117 (16%) teleworked during illness.

who had no telework experience, about one quarter worked onsite during illness, which is concerning because persons with COVID-19 are contagious for a prolonged period (*17*). Lockdown-style closures and containment measures were more prevalent in the spring of 2020 and COVID-19 testing was more available in the fall, but our findings were similar for these 2 periods (*3*,*4*).

A study in London found that approximately one third of persons with COVID-19 worked onsite while sick but did not assess the effect of experience with telework before illness (*18*). A study conducted before the COVID-19 pandemic during the 2017–18 influenza season found that persons with ARI or influenza who had telework experience before illness worked more days overall during illness than those without telework experience, although the number of days worked onsite was similar between the 2 groups (*12*). That study assessed work status during the first 3 days of illness, whereas our study assessed work status during illness over a longer period. In addition, 15% of participants had experience with telework before illness in the Ahmed et al. study, compared with 22% in our study. The proportion of persons who were excluded because of working solely from home was also lower in the Ahmed et al. study than in our study, which likely reflects the increased use of telework during the pandemic (*19*). Another study found that workers in Washington were significantly less likely to work while sick after the state passed a paid sick leave law (*20*), indicating a paid sick leave policy in combination with other nonpharmaceutical interventions could help reduce the spread of illness in the workplace.

A strength of our study was that participants were asked about frequency of telework before illness onset and during illness, enabling us to examine how telework experience before illness affected working onsite while sick. Another strength is the laboratory confirmation of COVID-19, which enabled us to distinguish those who had COVID-19 from those with other ARIs. Collecting sociodemographic data enabled us to control for variables such as race, ethnicity, and education.

The first limitation of our study is that a substantial number of persons did not complete follow up. It could be argued that nonrespondents were more likely to work onsite while sick. However, findings were similar for sites with higher follow-up rates (Pennsylvania and Washington) and those with lower follow-up rates (Michigan and Texas). Second, participants could have underreported working onsite because of the potential stigma around doing so in light of intensive public health messaging to stay home when ill. The comparisons between groups, however, would be valid if the underreporting was nondifferential. Third, we did not collect data on workplace policies, culture, and norms, and thus we are unable to assess how these factors affected our findings. Fourth, we do not know when participants learned the results of COVID-19 testing, so we could not assess what proportion of COVID-19 case-patients worked onsite before they were aware that they were SARS-CoV-2–positive. Fifth, we do not know when persons worked onsite during their illness. Persons who worked onsite later in the course of their illness might have been less infectious or even noninfectious. Finally, our findings might not be generalizable to asymptomatic persons, persons with milder symptoms who might not have sought medical care, or those with severe illness who were hospitalized for a prolonged period.

A systematic review published in 2019 found that the rate of persons going to work or school with an infectious illness ranged widely, from 35% to 97% (*21*). Presenteeism rates were generally higher in healthcare and social care workers (*21*). Reasons for presenteeism include lack of paid sick leave, a culture of presenteeism, potential disciplinary action, lack of coverage for work responsibilities, professionalism, job demands, concerns about being a burden on colleagues, colleagues' perceptions, the threshold for absence because of sickness (i.e., illness was not severe and the person was well enough to work), and financial concerns. Future research should assess how workplace policies, culture, and occupations affect presenteeism in persons with COVID-19. Research should be done to quantify productivity in those who work during illness, as well as to assess the potential cost of infecting coworkers with illness if persons work onsite.

Our research demonstrates that telework experience before illness gave workers who were well enough the option to work during illness and improved compliance with the public health recommendation to stay home when ill. For jobs that are amenable to remote work, strategies should be developed to enable teleworking to become the norm for persons with ARIs.

Acknowledgments

We gratefully thank the following persons for their contributions: Rachael Burganowski, Erika Kiniry, Kathryn A. Moser, Matt Nguyen, Suzie Park, Hallie Phillips, Stacie Wellwood, Brianna Wickersham, G.K. Balasubramani, Erin Bowser, Karen Clarke, Lloyd G. Clarke, Klancie Dauer, Chris Deluca, Blair Dierks, Linda Haynes, Robert Hickey,

Monika Johnson, Leah McKown, Alanna Peterson, Theresa M. Sax, Miles Stiegler, Michael Susick, Joe Suyama, Louise Taylor, Sara Walters, Alexandra Weissman, John V. Williams, Sarah Bauer, Kim Beney, Caroline K. Cheng, Nahla Faraj, Amy Getz, Michelle Grissom, Michelle Groesbeck, Samantha Harrison, Kristen Henson, Kim Jermanus, Emileigh Johnson, Anne Kaniclides, Armanda Kimberly, Lois E. Lamerato, Adam Lauring, Regina Lehmann-Wandell, E. J. McSpadden, Louis Nabors, Rachel Truscon, Michael Smith, Spencer Rose, Kayan Dunnigan, Kempapura Murthy, Eric Hoffman, Martha Zayed, Marcus Volz, Kimberly Walker, Natalie Settele, Jason Ettlinger, Elisa Priest, Jennifer Thomas, Arundhati Rao, Manohar Mutnal, Madhava Beeram, and Alexander Arroliga.

This work was supported through cooperative agreements funded by the US Centers for Disease Control and Prevention and by infrastructure funding from the National Institutes of Health (UL1 TR001857) at the University of Pittsburgh. It was supported in part by an appointment to the Research Participation Program at the Centers for Disease Control and Prevention and administered by the Oak Ridge Institute for Science and Education through an interagency agreement between the US Department of Energy and the Centers for Disease Control and Prevention.

About the Author

Ms. Shafer is an ORISE Fellow in the Community Interventions for Infection Control Unit in the Division of Global Migration and Quarantine, National Center for Emerging and Zoonotic Infectious Diseases, Centers for Disease Control and Prevention. Her research interests include nonpharmaceutical interventions for COVID-19 and influenza prevention.

References

1. Hale T, Angrist N, Goldszmidt R, Kira B, Petherick A, Phillips T, et al. A global panel database of pandemic policies (Oxford COVID-19 Government Response Tracker). Nat Hum Behav. 2021;5:529–38. https://doi.org/10.1038/s41562-021-01079-8
2. Hallas L, Hatibie A, Koch R, Majumdar S, Pyarali M, Wood A, et al. Variation in US states' COVID-19 policy responses. Blavatnik School of Government Working Paper Series. 2021; version 3.0 [cited 2022 Jun 1]. https://www.bsg.ox.ac.uk/sites/default/files/2021-05/BSG-WP-2020-034-v3.pdf
3. Davis K. Better late than never: COVID-19 testing across the United States. 2020 [cited 2022 Sep 28]. https://sitn.hms.harvard.edu/flash/2020/covid-19-testing
4. Our World in Data. Total COVID-19 tests [cited 2022 Sep 20]. https://ourworldindata.org/grapher/full-list-total-tests-for-covid-19
5. World Health Organization. Coronavirus disease (COVID-19): How is it transmitted? 2021 [cited 2022 Jun 1]. https://www.who.int/news-room/q-a-detail/coronavirus-disease-covid-19-how-is-it-transmitted
6. Centers for Disease Control and Prevention. Guidance for businesses and employers responding to Coronavirus Disease 2019 (COVID-19). 2021 [cited 2021 Sep 21]. https://www.cdc.gov/coronavirus/2019-ncov/community/guidance-business-response.html
7. U.S. Department of Labor. Families First Coronavirus Response Act: Employee paid leave rights. 2020 [cited 2022 Feb 14]. https://www.dol.gov/agencies/whd/pandemic/ffcra-employee-paid-leave
8. Bonwitt J, Deya RW, Currie DW, Lipton B, Huntington-Frazier M, Sanford SJ, et al.; Public Health—Seattle & King County COVID-19 Community Investigation Team; Public Health—Seattle & King County Analytics and Informatics Team. COVID-19 surveillance and investigations in workplaces—Seattle & King County, Washington, June 15–November 15, 2020. MMWR Morb Mortal Wkly Rep. 2021;70:916–21. https://doi.org/10.15585/mmwr.mm7025a3
9. Murti M, Achonu C, Smith BT, Brown KA, Kim JH, Johnson J, et al. COVID-19 Workplace outbreaks by industry sector and their associated household transmission, Ontario, Canada, January to June, 2020. J Occup Environ Med. 2021;63:574–80. https://doi.org/10.1097/JOM.0000000000002201
10. Waltenburg MA, Victoroff T, Rose CE, Butterfield M, Jervis RH, Fedak KM, et al.; COVID-19 Response Team. Update: COVID-19 among workers in meat and poultry processing facilities—United States, April–May 2020. MMWR Morb Mortal Wkly Rep. 2020;69:887–92. https://doi.org/10.15585/mmwr.mm6927e2
11. Aronsson G, Gustafsson K, Dallner M. Sick but yet at work. An empirical study of sickness presenteeism. J Epidemiol Community Health. 2000;54:502–9. https://doi.org/10.1136/jech.54.7.502
12. Ahmed F, Kim S, Nowalk MP, King JP, VanWormer JJ, Gaglani M, et al. Paid leave and access to telework as work attendance determinants during acute respiratory illness, United States, 2017–2018. Emerg Infect Dis. 2020;26:26–33. https://doi.org/10.3201/eid2601.190743
13. Chung JR, Kim SS, Jackson ML, Jackson LA, Belongia EA, King JP, et al. Clinical symptoms among ambulatory patients tested for SARS-CoV-2. Open Forum Infect Dis. 2020;8:ofaa576.
14. Hart A. Mann-Whitney test is not just a test of medians: differences in spread can be important. BMJ. 2001;323:391–3. https://doi.org/10.1136/bmj.323.7309.391
15. Dingel JI, Neiman B. How many jobs can be done at home? J Public Econ. 2020;189:104235. https://doi.org/10.1016/j.jpubeco.2020.104235
16. Hensvik L, Barbanchon TL, Rathelot R. Which jobs are done from home? Evidence from the American Time Use Survey. IZA Institute of Labor Economics [cited 2021 Dec 14]. https://www.iza.org/publications/dp/13138/which-jobs-are-done-from-home-evidence-from-the-american-time-use-survey
17. Singanayagam A, Patel M, Charlett A, Lopez Bernal J, Saliba V, Ellis J, et al. Duration of infectiousness and correlation with RT-PCR cycle threshold values in cases of COVID-19, England, January to May 2020 [Erratum in: Euro Surveill. 2020;25]. Euro Surveill. 2020;25:2001483. https://doi.org/10.2807/1560-7917.ES.2020.25.32.2001483
18. Jain V, Waghorn M, Thorn-Heathcock R, Lamb P, Bell A, Addiman S. Attendance at London workplaces after symptom onset: a retrospective cohort study of staff

members with confirmed COVID-19. J Public Health (Oxf). 2021;43:236–42. https://doi.org/10.1093/pubmed/fdaa239
19. Brynjolfsson E, Horton JJ, Ozimek A, Rock D, Sharma G. TuYe H. COVID-19 and remote work: An early look at US data. National Bureau of Economic Research Working Paper 27344. 2020 [cited 2022 Feb 10]. https://www.nber.org/papers/w27344
20. Schneider D. Paid sick leave in Washington State: evidence on employee outcomes, 2016–2018. Am J Public Health. 2020;110:499–504. https://doi.org/10.2105/AJPH.2019.305481
21. Webster RK, Liu R, Karimullina K, Hall I, Amlôt R, Rubin GJ. A systematic review of infectious illness presenteeism: prevalence, reasons and risk factors. BMC Public Health. 2019;19:799. https://doi.org/10.1186/s12889-019-7138-x

Address for correspondence: Faruque Ahmed, Centers for Disease Control and Prevention, 1600 Clifton Rd NE, Mailstop V18-2, Atlanta, GA 30329-4027, USA; email: fahmed@cdc.gov

Circovirus Hepatitis Infection in Heart-Lung Transplant Patient, France

Philippe Pérot,[1] Jacques Fourgeaud,[1] Claire Rouzaud,[1] Béatrice Regnault, Nicolas Da Rocha, Hélène Fontaine, Jérôme Le Pavec, Samuel Dolidon, Margaux Garzaro, Delphine Chrétien, Guillaume Morcrette, Thierry Jo Molina, Agnès Ferroni, Marianne Leruez-Ville, Olivier Lortholary, [2] Anne Jamet,[2] Marc Eloit[2]

In March 2022, a 61-year-old woman in France who had received a heart-lung transplant sought treatment with chronic hepatitis mainly characterized by increased liver enzymes. After ruling out common etiologies, we used metagenomic next-generation sequencing to analyze a liver biopsy sample and identified an unknown species of circovirus, tentatively named human circovirus 1 (HCirV-1). We found no other viral or bacterial sequences. HCirV-1 shared 70% amino acid identity with the closest known viral sequences. The viral genome was undetectable in blood samples from 2017–2019, then became detectable at low levels in September 2020 and peaked at very high titers (10^{10} genome copies/mL) in January 2022. In March 2022, we found >10^{8} genome copies/g or mL in the liver and blood, concomitant with hepatic cytolysis. We detected HCirV-1 transcripts in 2% of hepatocytes, demonstrating viral replication and supporting the role of HCirV-1 in liver damage.

Solid organ transplant recipients are highly susceptible to infections that sometimes have uncommon clinical manifestations (*1*–*3*). Etiologic diagnosis of hepatitis is even more problematic in organ transplant recipients because a wide range of possible drug toxicities induced by immunosuppressive therapies must be considered (*4*). Diagnosing unexplained hepatitis remains a challenge, as exemplified by 74 cases of acute hepatitis of unknown etiology reported in children in the United Kingdom, 3 cases in Spain, and up to 5 possible cases in Ireland (*5*). Among transplant recipients, it is especially critical to detect infection, often viral, to prevent unnecessary interruption of treatment. Cases of direct viral transmission from the graft itself have been reported (*6*,*7*). Agnostic metagenomic analysis of clinical samples based on next-generation sequencing (NGS) combined with specifically designed PCRs constitute promising tools for diagnosing infection with unforeseen or novel microorganisms (*8*). We report identifying a novel circovirus infecting humans, tentatively named human circovirus type 1 (HCirV-1), and its role in causing liver damage in a solid organ transplant recipient.

Case Report

A woman, 61 years of age, sought treatment in France with cytolytic hepatitis of unknown etiology. The patient had received a heart-lung transplant 17 years earlier because of Eisenmenger syndrome related to

Author affiliations: Institut Pasteur Pathogen Discovery Laboratory, Paris, France (P. Pérot, B. Regnault, N. Da Rocha, D. Chrétien, M. Eloit); The OIE Collaborating Center for the Detection and Identification in Humans of Emerging Animal Pathogens, Paris (P. Pérot, B. Regnault, N. Da Rocha, D. Chrétien, M. Eloit); Institut Imagine, Paris (J. Fourgeaud, M. Leruez-Ville); Université Paris Cité, Paris (J. Fourgeaud, A. Jamet); Necker-Enfants Malades Hospital, Paris (J. Fourgeaud, G. Morcrette, T.J. Molina, A. Ferroni, M. Leruez-Ville, A. Jamet); Hôpital Necker Enfants-Malades Centre d'Infectiologie Necker-Pasteur, Paris (C. Rouzaud, M. Garzaro, O. Lortholary); Groupe Hospitalier Paris Saint Joseph-Marie Lannelongue, Équipe Mobile de Microbiologie Clinique, Paris (C. Rouzaud); Hôpital Cochin Département d'Hépatologie-Addictologie, Paris (H. Fontaine); Université Paris–Sud, Paris (J. Le Pavec); Hôpital Marie Lannelongue Service de Pneumologie et Transplantation Pulmonaire, Le Plessis-Robinson, France (J. Le Pavec, S. Dolidon); Institut Necker Enfants Malades, Paris (A. Jamet); Ecole Nationale Vétérinaire d'Alfort, Maisons-Alfort, France (M. Eloit)

DOI: https://doi.org/10.3201/eid2902.221468

[1]These authors contributed equally to this article.

[2]These senior authors contributed equally to this article.

ventricular septal defect. Her maintenance immunosuppressive regimen included tacrolimus, mycophenolate mofetil, and prednisone. She had received pulse steroids 16 months before the hepatitis occurred to treat acute lung allograft dysfunction. The patient had had a localized left upper lobe pulmonary adenocarcinoma treated by surgery 2.5 years before this episode. She also had a history of chronic renal failure from calcineurin inhibitor (Cockcroft-Gault up to 23 mL/min), *Aspergillus* spp. and *Scedosporium* spp. bronchopulmonary infections, and parvovirus B19 and COVID-19 infections. In November 2021, 14 months after receiving pulsed corticosteroid therapy, the patient was hospitalized for cytomegalovirus (CMV) colitis with ganciclovir-resistant virus requiring treatment with foscavir, then maribavir, followed by letermovir for long-term maintenance therapy. At that time ultrasound examination detected cytolysis without symptoms or liver abnormalities (Figure 1).

Four months after that hospitalization, hepatitis worsened; transaminase serum levels increased to up to 40 times the normal upper limit (Figure 1), leading to hospital readmission. The patient was asymptomatic except for recent weight loss but without biological severity because the prothrombin time level was normal. We ruled out common infections, including hepatitis A, B, C, and E, as well as HIV, CMV, herpes simplex virus, varicella zoster virus (VZV), human herpes virus 6 (HHV6), adenovirus, enterovirus in blood and feces, parvovirus B19, toxoplasmosis, syphilis, and leptospirosis. Only Epstein-Barr virus (EBV) PCR was positive ($10^{4.4}$ genome copies/mL of blood). There was no evidence for a timeline relationship between levels of liver enzymes and use of various medications by the patient.

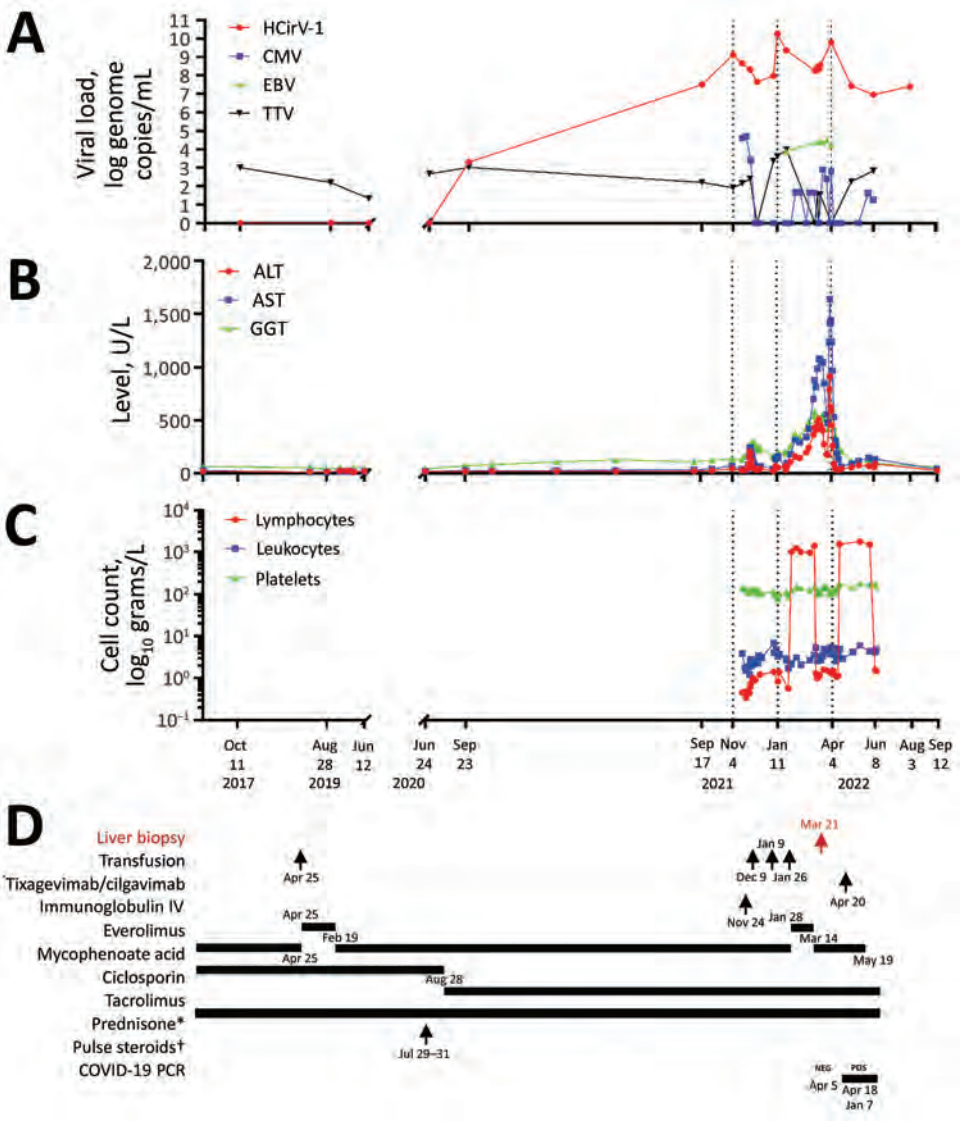

Figure 1. Clinical and laboratory data over time for a heart-lung transplant patient in France who had cytolytic hepatitis caused by HCirV-1 develop. A–C) Monitoring of patient over time: A) viral loads; B) liver cytolysis markers; C) blood cell counts. D) Patient's treatment history; red indicates timing of liver biopsy (March 21, 2022). Average values are depicted for HCirV-1 and TTV viral loads in plasma and blood on June 8 and August 3, 2022. *Dose 5 mg/day; †, solumedrol, dose 500 mg/day. ALT, alanine transaminase; AST, aspartate aminotransferase; CMV, cytomegalovirus; EBV, Epstein-Barr virus; GGT, gamma-glutamyl transferase; HCirV-1, human circovirus type 1; IV, intravenous; TTV, Torque teno virus.

She reported no use of paracetamol (acetaminophen), alcohol, illicit drugs, or phytotherapy (use of herbal/plant supplements). A cardiac ultrasound did not show cardiac failure. We found no cardiac arrhythmia or vascular or biliary abnormalities from liver ultrasound and Doppler examinations, computerized tomography scan, or biliary magnetic resonance imaging results. Test results for autoimmune abnormalities were negative. Finally, aceruleoplasminemia test results were normal.

Pathological examination of a liver biopsy showed lobular hepatitis, slightly inflammatory, without epithelioid granuloma, substantial portal inflammation and fibrosis, or lymphoproliferation (Figure 2). Results of Ziehl, EBV, CMV, and adenovirus stains and bacteriological examinations of the biopsy sample, including mycobacterial cultures and PCR, broad-range 16S ribosomal RNA gene PCR, were negative. Herpes simplex virus 1 and 2, CMV, adenovirus, and enterovirus PCR results were negative; EBV PCR was positive (135 genome copies/µg DNA, cycle threshold = 35) but not ascribed to acute hepatitis. Overall, the lymphocytic pattern of inflammation in contrast to the lack of eosinophil infiltration, vascular or biliary injuries, and autoimmune liver disease (no plasmocytes), strongly suggested viral hepatitis. We considered the extent of both centrilobular necrosis and resorption by macrophages, which suggested recent liver cytolysis. After these first-line negative results from the liver biopsy, we conducted metagenomic NGS (mNGS), which revealed presence of the novel circovirus, HCirV-1. We further explored and quantified HCirV-1 using quantitative PCR (qPCR) on liver tissue, historical blood samples, feces, bronchoalveolar lavage, urine, and saliva samples from the patient (Table).

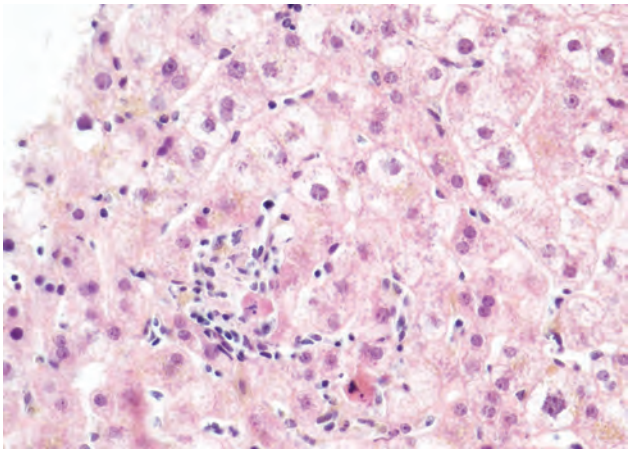

Figure 2. Lobular hepatitis in a heart-lung transplant patient in France. Apoptotic bodies, hepatocyte swelling and ballooning were present surrounded by a slight inflammatory infiltrate made of lymphocytes and histiocytes. Hematoxylin and eosin stain; original magnification ×40.

In November 2022, the patient's clinical condition was stable, and we noted complete recovery from cytolysis. In the context of her recent infectious diseases, we minimized the patient's immunosuppressive treatment, discontinuing mycophenolate mofetil (Figure 1). When we tried to ascertain possible sources of her HCirV-1 infection, the patient reported contact with 2 cats, both of which had contact with birds and rodents. HCirV-1 PCR was negative in the feces of the cats 2 months after her diagnosis. The patient reported no international travel. She did report receiving a blood transfusion 17 months before HCirV-1 was first detected (Figure 1).

Methods

Description of Controls

We performed retrospective HCirV-1 qPCRs on feces and blood samples from immunocompromised or immunocompetent control patients with or without hepatitis (Appendix Table 1, https://wwwnc.cdc.gov/EID/article/29/2/22-1468-App1.pdf). We also reviewed the results of mNGS routinely performed since 2019 on all liver biopsies in our laboratory to detect pathogens (Appendix Table 2).

Nucleic Acid Extraction

We extracted nucleic acids from the patient's liver biopsy using the geneLEAD VIII instrument (Diagenode, https://www.diagenode.com). We extracted nucleic acids from 200 µL of plasma, serum, whole blood, bronchoalveolar lavage (BAL), and feces using the bioMérieux Emag instrument (https://www.biomerieux.com).

mNGS

We generated complementary DNA from a biopsy from the patient's liver using the Invitrogen SuperScript IV First-Strand Synthesis System kit (ThermoFisher Scientific, https://www.thermofisher.com) and used MALBAC amplification (Yikon Genomics, https://en.yikongenomics.com) as described elsewhere (*9*) to use as input for Illumina DNAPrep (https://www.illumina.com). We sequenced the library in 1 × 151 bp on an Illumina NextSeq500 instrument generating ≈80 million raw reads. We processed raw reads with Microseek (*10*) using the RVDB-prot reference viral database (*11*).

qPCR HCirV-1

We designed PCR primers HCirV1-Fw1, 5′-ACCTGGATGGACCCTGGAAT-3′, and HCirV1-Rv1, 5′-AGAGTTCCACCAGGTTCTGC-3′ (194 bp), in the capsid

gene of HCirV-1. We performed qPCRs in SYBR green format with 45 cycles of amplification at an annealing temperature of 58°C and purified positive amplicons after 45 cycles on gel, confirmed them by Sanger sequencing, and used them for serial-dilutions to generate standard curves for the calculation of viral loads.

Acquisition of Complete Genome

After preamplification with the QIAGEN whole transcriptome analysis ϕ29 polymerase (https://www.qiagen.com), we obtained the full genome of HCirV-1 by sequencing plasma from the patient, sampled on January 12, 2022, which harbored 10^{10} viral copies/mL. We applied an iterative mapping approach using Geneious Prime 2022.1.1 (https://www.geneious.com) to perform the final assembly and deposited the complete genome sequence at GenBank (accession no. ON677309).

Phylogeny

We performed phylogenetic reconstructions on the capsid protein sequence (Figure 3), on the replicase (Rep) protein sequence (Appendix Figure 1), and on the complete nucleotide sequence of HCirV-1 (Appendix Figure 2). We aligned complete open reading frames of the capsid and Rep genes along with other representative sequences of circoviruses using Multiple Alignment using Fast Fourier Transform (https://www.ebi.ac.uk/Tools/msa/mafft) under the L-INS-i parameter. We performed maximum-likelihood phylogenetic reconstruction with PhyML implemented through the NGPhylogeny portal (*12*) and evaluated nodal support using the approximate Bayes branch supports.

TTV and EBV qPCR

We performed TTV (Torque teno virus) DNA load using the TTV R-GENE kit (bioMérieux, https://www.biomerieux.com) as described elsewhere (*13*) and EBV DNA load using the bioMérieux EBV R-GENE kit. We performed real-time PCR amplification on an Applied Biosystems AB7500 platform (ThermoFisher).

In Situ Hybridization

We used a ThermoFisher 2-plex ViewRNA ISH Tissue Assay Kit for in situ hybridization (ISH) to detect RNA sequences of HCirV-1 as a marker of virus replication. We designed a cocktail of 12 custom-branched DNA probes to target HCirV-1 capsid genes and 20 probes to target Rep genes, which were revealed by a red signal (probe type 1 in the assay kit); a blue signal (probe type 6 in the kit) revealed a mix of control probes targeting human housekeeping transcripts. We applied 20-min heat pretreatment and 15-min protease digestion to tissue sections after deparaffinization using xylene to unmask RNA targets and used Harris hematoxylin for counterstaining. We used negative controls for ISH that included a no-probe negative control from the patient infected with HCiV-1, as recommended by the manufacturer, and a negative control biopsy sample from a different patient that tested negative for HCirV-1 with mNGS.

We obtained informed consent for publication of our findings from the patient. The samples we analyzed were from control patients in a retrospective noninterventional study with no additional standard care procedures. Our study was performed in accordance with ethical guidelines for medical research and approved by the institutional review boards of Necker Hospital.

Table. Samples tested by qPCR to detect and quantify human circovirus type 1 infection in a heart-lung transplant patient in France*

Sample type	Sampling date	Ct values	Virus copies†
Serum	2017 Oct 11	Negative	Negative
Serum	2019 Aug 28	Negative	Negative
Serum	2020 Jun 12	Negative	Negative
Serum	2020 Jul 24	Negative	Negative
Plasma	2020 Sep 17	17.9	3.24×10^7
Serum	2020 Sep 23	32.4	2.00×10^3
Serum	2021 Nov 05	12.4	1.25×10^9
Serum	2021 Nov 18	13.9	4.38×10^8
Feces	2021 Nov 19	23.5	3.12×10^5
Serum	2021 Nov 30	15.1	2.07×10^8
Serum	2021 Dec 10	17.4	4.49×10^7
Serum	2022 Jan 05	16.3	9.19×10^7
BAL	2022 Jan 06	24.8	3.24×10^5
Serum	2022 Jan 12	8.4	1.72×10^{10}
Serum	2022 Jan 25	11.5	2.19×10^9
Feces	2022 Jan 27	25.5	7.98×10^4
Plasma	2022 Mar 10	15.3	1.77×10^8
Serum	2022 Mar 14	14.6	2.77×10^8
Plasma	2022 Mar 16	15.1	2.08×10^8
Serum	2022 Mar 18	14.3	3.52×10^8
Liver biopsy	2022 Mar 21	16.4	3.57×10^8
Feces	2022 Apr 01	23.7	2.68×10^5
Blood	2022 Apr 04	10.0	5.81×10^9
Serum	2022 May 05	18.1	2.73×10^7
Serum	2022 May 05	17.2	4.92×10^7
Feces	2022 May 11	28.6	1.06×10^4
Urine	2022 Jun 08	26.4	1.13×10^5
Saliva	2022 Jun 08	26.0	1.45×10^5
Plasma	2022 Jun 08	19.2	1.36×10^7
Blood	2022 Jun 08	20.3	6.36×10^6
Feces	2022 Jun 09	27.2	2.60×10^4
Blood	2022 Aug 03	18.8	1.70×10^7
Plasma	2022 Aug 03	17.5	4.01×10^7

*Virus copies are per gram for liver biopsy and feces samples, per milliliter for all other samples. BAL, bronchoalveolar lavage; qPCR, quantitative PCR; Ct, cycle threshold.

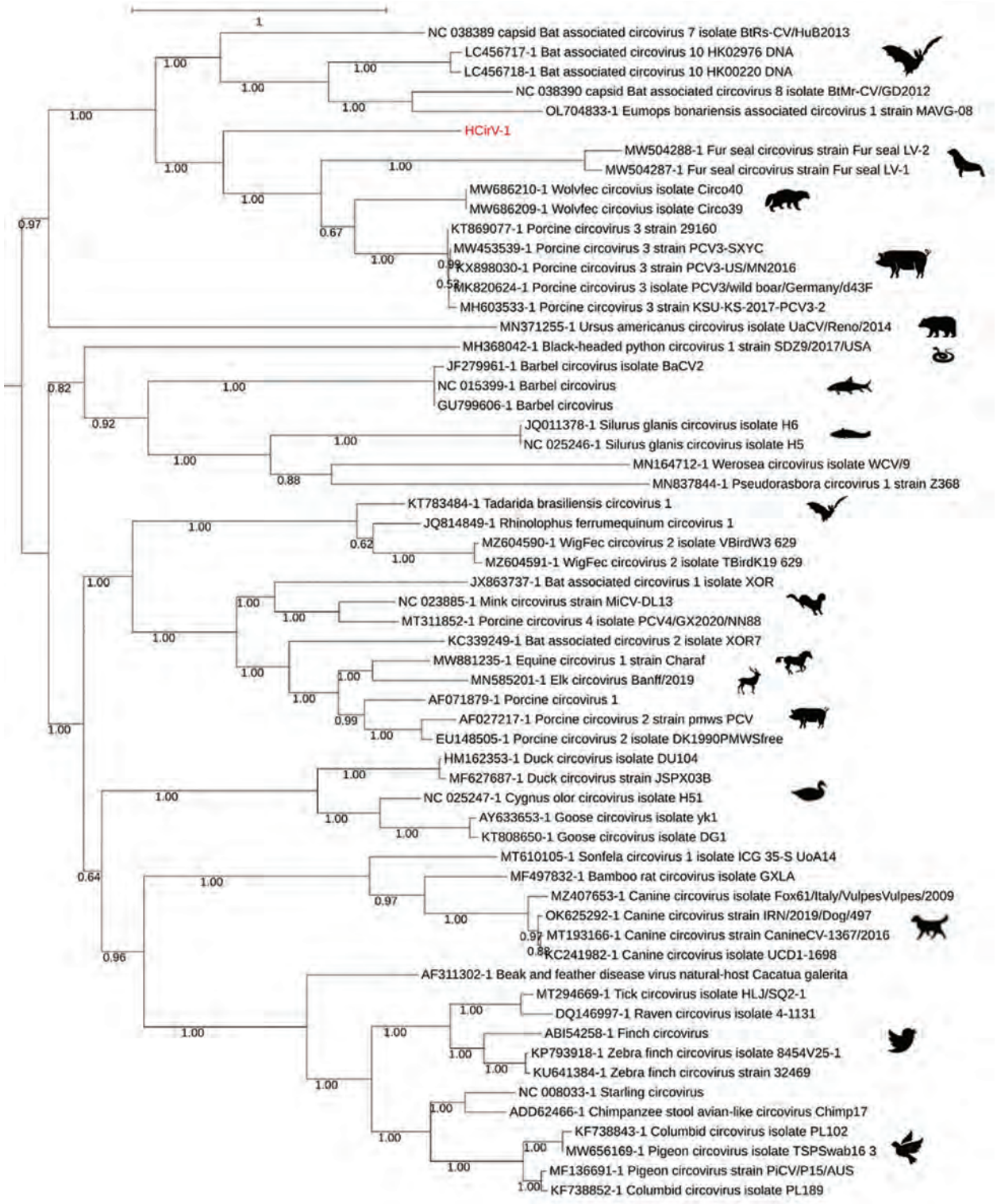

Figure 3. Phylogenetic analysis of capsid protein sequences of human circovirus type 1 (HCirV-1) from a heart-lung transplant patient in France (red) and representative circovirus strains. Sequences were aligned with Multiple Alignment using Fast Fourier Transform (https://www.ebi.ac.uk/Tools/msa/mafft) under the L-INS-I parameter, and maximum-likelihood phylogenetic reconstruction was performed with PhyML implemented through the NGPhylogeny portal (https://ngphylogeny.fr). GenBank accession numbers for reference sequences are indicated, along with graphic representations of the animal of origin. Scale bar indicates the number of amino acid substitutions per site.

Results

Identifying Distant Circovirus Sequences by Liver Biopsy

Using NGS to analyze viral sequences from the liver biopsy specimen, we identified 1,011 sequences corresponding to the capsid and Rep genes from the *Circoviridae* family. From a plasma sample taken at the peak of viremia, we derived a consensus full-genomic sequence (2,021 nt) of the HCirV-1 virus (Genbank accession no. ON677309) and confirmed that the sequence was identical to partial sequences of the capsid gene found in the liver. We conducted phylogenetic analyses on the 2 HCirV-1 viral proteins, capsid and Rep, and on representative animal circoviruses; congruent analyses showed that HCirV-1 defines a new clade at a basal position relative to its closest viral species, Wolvfec circovirus (host: *Gulo gulo*) and porcine circovirus 3.

Kinetics of Infection

We designed an assay and conducted qPCR to assess changes in the viral load in plasma and other biologic samples taken from the case-patient since 2017. We also evaluated the viral load for TTV, a commensal virus whose level of viremia is well correlated with the immune status of graft recipients (*14*). TTV DNA load varied (0–3.99 log copies/mL), indicating a low level of immune suppression (*15*); peaks in TTV viremia and cytolysis were not temporally correlated. In contrast, HCirV-1 was first detected in patient blood samples ($10^{3.3}$ genome copies/mL) in September 2020, 2 months after steroids pulse therapy, but a July 2020 sample tested negative. However, it is noteworthy that the finding of a low level of HCirV-1 in the September 2020 sample was questionable because the tubes were opened at the same time as others harboring up to $10^{9.1}$ genome copies/mL, possibly resulting in cross-contamination. The next available sample, taken in September 2021, was strongly positive ($10^{7.5}$ genome copies/mL); thereafter, loads varied ($10^{8.3}$–$10^{10.2}$ genome copies/mL). HCirV-1 loads were high only during the period of pronounced cytolysis.

Assessing HCirV-1 Presence in Controls

We tested 36 blood and 20 feces samples from 56 control patients using the same specific qPCR primers for assessing HCirV-1 presence, but none tested positive (Appendix Table 1). Among those patients, 19 (34%) were primitively immunocompromised, 17 (30%) immunocompetent, 13 (23%) solid organ transplant recipients, 5 (9%) hematopoietic stem cell transplant recipients or receiving immunosuppressive treatment, and 2 (4%) HIV positive. Among 16 patients with hepatic cytolysis (Appendix Table 1), 8 cases were of unknown etiology. Control biopsies routinely screened by mNGS since 2019 did not show HCirV-1 sequences among 57 patients with hepatitis of suspected infectious origin, among whom 25 (44%) were primitively immunocompromised, 20 (35%) hematopoietic stem cell transplant recipients or receiving immunosuppressive treatment, 5 (9%) immunocompetent, 5 (9%) solid organ transplant recipients, and 2 (4%) HIV positive (Appendix Table 2).

ISH

ISH of the liver biopsy specimen showed 2% infected hepatocytes (Figure 4); red labeling was strong in the nuclei and mild in the cytoplasm. Some hepatocytes were also poorly labeled in the nuclei, and, in this case, labeling was negative in the cytoplasm. Endothelial cells and lymphocytes were not infected. No red signal was recorded in the ISH-negative controls.

Discussion

Our findings show a temporal association between hepatitis and a high load of a novel virus, HCirV-1, in the liver and blood of a 61 year-old female heart-lung transplant recipient. The patient received standard immunosuppressive therapy of tacrolimus, mycophenolate mofetil, and corticosteroids, but CMV colitis developed a year after pulsed corticosteroid therapy, suggesting a contemporary drug-induced high level of immunosuppression. Our results should be evaluated with Hill's criteria for causality (*16*).

We demonstrated the specificity of association using agnostic mNGS in the liver biopsy sample, showing absence of any additional virus except PCR-detected EBV. Given the low concentration of EBV in the liver biopsy, the concomitant higher replication in the blood ($10^{4.4}$ genome copies/mL), and the negative result from staining on liver biopsy, we did not consider EBV to be responsible for the cytolysis. In total, we did not detect HCirV-1 in 113 control participants: 40 tested by qPCR without hepatitis, 16 with hepatitis of known (50%) or unknown (50%) etiology (Appendix Table 1), and 57 mNGS-tested case-patients with hepatitis of unknown etiology (unpub. data, Appendix Table 2).

Circoviruses are DNA viruses. Of note, transcripts were detected in the nucleus of 2% of liver cells by HCirV-1–specific ISH, therefore consistent with viral expression and probably with virus replication. Given the lytic cycle of circoviruses, the results strongly support the role of HCirV-1 as the

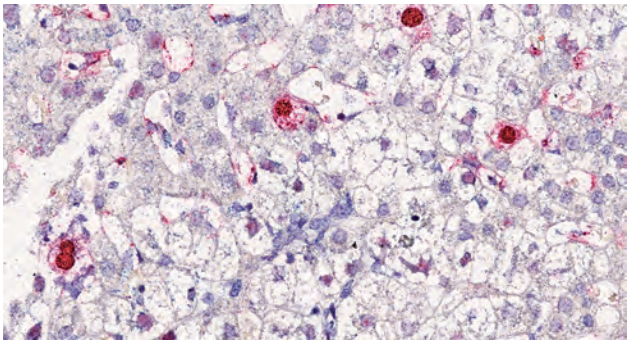

Figure 4. In situ hybridization in liver section from a heart-lung transplant patient in France. Chromogenic in situ hybridization detected human circovirus type 1 mRNA (red staining) in hepatocytes nuclei and cytoplasm. Nuclei were counterstained with Harris hematoxylin and eosin stain; original magnification ×40.

causative agent of hepatitis by targeting and lysing hepatocytes and also likely as a trigger of immune cytotoxic responses.

Animal circoviruses, such as porcine circoviruses (PCV) 1–4, have been responsible for reproductive failure, dermatitis, nephropathy, and respiratory diseases in animals (*17*,*18*), manifestations not found in the case we report. However, PCV2 associated with cases of jaundice in pigs (*19*–*21*) and hepatitis in a horse have been demonstrated (*22*). After PCV3 is inoculated into piglets, viremia progressively increases up to $10^{8.9}$ copies/mL, reflective of findings in our study, but generally peaks around 21 days after infection, contrary to the more delayed peak we identified. Pathological lesions and PCV3 antigens have been detected in the liver, including white-gray nodules and necrosis with PCV3 antigen detected in liver lobular stroma, the hepatic sinus antral wall, and the cytoplasm in the sinus (*23*) and in other organs (lung, heart, kidney, lymph nodes, spleen, and small intestine) (*24*). PCV3 viremia could still be observed 140 days after infection (*25*), which is indicative of the ability of circoviruses to sustain long-term infection, as described in our patient. PCV3 was also able to infect nonhuman primate recipients of porcine cardiac xenografts (*26*,*27*).

Supporting the plausibility of HCirV-1 as disease agent, we found no temporal link for drug etiology or pathological evidence as alternative explanations. We ruled out common hepatitis virus infections, including hepatitis E virus. EBV test results were positive, but we ruled out a pathogenic role because EBV viral load remained stable around 10^4 genome copies/mL (Figure 1) and Epstein-Barr encoding region (EBER) staining was negative.

We first detected HCirV-1 before the liver pathology testing. Viral loads peaked 3 times, before the first and second cytolysis peaks and a third time concurrently with cytolysis peak (Figure 1). The high viral load of HCirV-1 (10^{10} genome copies/mL) also favors interpretation of its causative role in hepatitis. Indeed, a strong relationship between high virus load and disease severity has been described for hepatitis A (*23*) and B (*28*) viruses and adenovirus in hematopoietic stem cell transplant recipients (*29*), further illustrating that viral load often influences organ pathology (*30*).

As of November 2022, we had not identified the source of infection for this patient; specifically, we were unable to determine whether it was because of spillover of an animal virus or if it might be a previously unknown human virus. Although phylogenetic analysis placed this virus closest to known viruses hosted by a wild exotic animal that was not a possible source for our patient, we speculate that that HCirV-1 could be of animal origin, possibly from a dietary source in a similar manner as hepatitis E virus. Developing a specific antibody test will be instrumental in deciphering the ecology of the virus and better understanding its mechanisms of transmission. HCirV-1 was shed in saliva, urine, and feces (Table); whether the virus can possibly be transmitted between persons remains to be investigated.

In conclusion, detection of HCirV-1 expression in liver cells by ISH, the exclusion of other hepatitis etiologies, and the temporal association of severe cytolysis with very high HCirV-1 loads in the liver and blood strongly suggest a causal link. Furthermore, our experience using mNGS in immunocompromised patients, including transplant recipients, as well as the specific qPCR we performed on a representative cohort of these patients prove that, unlike TTV, HCirV-1 is not part of the commensal viral flora. Agnostic NGS was key to elucidate the etiology of this hepatitis case. HCirV-1 could now be tested for in hepatitis cases of unknown origin in solid organ transplant recipients.

Acknowledgments

We thank the Biomics platform of Institut Pasteur for providing access to the sequencers. We thank the histology embryology cytogenetic department of Necker Hospital for providing access to the in situ hybridization platform.

This work was supported by Institut Pasteur and the Necker-Enfants malades University Hospital.

About the Author

Dr. Pérot works at Institut Pasteur, Virology Department, Paris. His research focuses on pathogen discovery, clinical metagenomics, molecular virology, and bioinformatics.

References

1. Lease ED, Budev MM. Infectious complications in lung transplant recipients. Thorac Surg Clin. 2022;32:211–20. https://doi.org/10.1016/j.thorsurg.2021.12.002
2. Kunnathu Puthanveedu NDK, Lum J. Central nervous system infections after solid organ transplantation. Curr Opin Infect Dis. 2021;34:207–16. https://doi.org/10.1097/QCO.0000000000000722
3. Ivana T, Robert P, Pavel S, Lenka T, Irena K. Cytomegalovirus and other herpesviruses after hematopoietic cell and solid organ transplantation: from antiviral drugs to virus-specific T cells. Transpl Immunol. 2022;71:101539. https://doi.org/10.1016/j.trim.2022.101539
4. Hirschi S, Biondini D, Ohana M, Solis M, D'Urso A, Rosner V, et al. Herpes simplex virus 2 hepatitis in a lung transplant recipient: a diagnostic challenge. Transpl Infect Dis. 2015;17:904–8. https://doi.org/10.1111/tid.12459
5. World Health Organization. Acute hepatitis of unknown aetiology—the United Kingdom of Great Britain and Northern Ireland [cited 2022 Dec 15]. https://www.who.int/emergencies/disease-outbreak-news/item/2022-DON368
6. Mrzljak A, Novak R, Pandak N, Tabain I, Franusic L, Barbic L, et al. Emerging and neglected zoonoses in transplant population. World J Transplant. 2020;10:47–63. https://doi.org/10.5500/wjt.v10.i3.47
7. Soto RA, McDonald E, Annambhotla P, Velez JO, Laven J, Panella AJ, et al. West Nile virus transmission by solid organ transplantation and considerations for organ donor screening practices, United States. Emerg Infect Dis. 2022;28:403–6. https://doi.org/10.3201/eid2802.211697
8. Casto AM, Fredricks DN, Hill JA. Diagnosis of infectious diseases in immunocompromised hosts using metagenomic next generation sequencing-based diagnostics. Blood Rev. 2022;53:100906. https://doi.org/10.1016/j.blre.2021.100906
9. Regnault B, Bigot T, Ma L, Pérot P, Temmam S, Eloit M. Deep impact of random amplification and library construction methods on viral metagenomics results. Viruses. 2021;13:253. https://doi.org/10.3390/v13020253
10. Pérot P, Bigot T, Temmam S, Regnault B, Eloit M. Microseek: a protein-based metagenomic pipeline for virus diagnostic and discovery. Viruses. 2022;14:1990. https://doi.org/10.3390/v14091990
11. Bigot T, Temmam S, Pérot P, Eloit M. RVDB-prot, a reference viral protein database and its HMM profiles. F1000 Res. 2019;8:530. https://doi.org/10.12688/f1000research.18776.1
12. Lemoine F, Correia D, Lefort V, Doppelt-Azeroual O, Mareuil F, Cohen-Boulakia S, et al. NGPhylogeny.fr: new generation phylogenetic services for non-specialists. Nucleic Acids Res. 2019;47(W1):W260–5. https://doi.org/10.1093/nar/gkz303
13. Kulifaj D, Durgueil-Lariviere B, Meynier F, Munteanu E, Pichon N, Dubé M, et al. Development of a standardized real time PCR for Torque teno viruses (TTV) viral load detection and quantification: A new tool for immune monitoring. J Clin Virol. 2018;105:118–27. https://doi.org/10.1016/j.jcv.2018.06.010
14. Jaksch P, Görzer I, Puchhammer-Stöckl E, Bond G. Integrated immunologic monitoring in solid organ transplantation: the road toward Torque teno virus-guided immunosuppression. Transplantation. 2022;106:1940–51. https://doi.org/10.1097/TP.0000000000004153
15. Redondo N, Navarro D, Aguado JM, Fernández-Ruiz M. Viruses, friends, and foes: The case of Torque Teno Virus and the net state of immunosuppression. Transpl Infect Dis. 2022;24:e13778. https://doi.org/10.1111/tid.13778
16. Hill AB. The environment and disease: association or causation? Proc R Soc Med. 1965;58:295–300. https://doi.org/10.1177/003591576505800503
17. Sirisereewan C, Thanawongnuwech R, Kedkovid R. Current understanding of the pathogenesis of porcine circovirus 3. Pathogens. 2022;11:64. https://doi.org/10.3390/pathogens11010064
18. Wang D, Mai J, Yang Y, Xiao CT, Wang N. Current knowledge on epidemiology and evolution of novel porcine circovirus 4. Vet Res (Faisalabad). 2022;53:38. https://doi.org/10.1186/s13567-022-01053-w
19. Gillespie J, Opriessnig T, Meng XJ, Pelzer K, Buechner-Maxwell V. Porcine circovirus type 2 and porcine circovirus-associated disease. J Vet Intern Med. 2009;23:1151–63. https://doi.org/10.1111/j.1939-1676.2009.0389.x
20. Staebler S, Buergi E, Litzenberger B, McCullough K, McNair I, McNeilly F, et al. Porcine circovirus as a possible cause of postweaning wasting in pigs in Switzerland. Schweiz Arch Tierheilkd. 2004;146:461–8, discussion 469. https://doi.org/10.1024/0036-7281.146.10.461
21. Harding JCS. Postweaning multisystemic wasting syndrome: epidemiology and clinical presentation. J Swine Health Prod. 1998;6:249–54.
22. Hui A, Altan E, Slovis N, Fletcher C, Deng X, Delwart E. Circovirus in blood of a febrile horse with hepatitis. Viruses. 2021;13:944. https://doi.org/10.3390/v13050944
23. Fujiwara K, Kojima H, Yasui S, Okitsu K, Yonemitsu Y, Omata M, et al. Hepatitis A viral load in relation to severity of the infection. J Med Virol. 2011;83:201–7. https://doi.org/10.1002/jmv.21958
24. Jiang H, Wang D, Wang J, Zhu S, She R, Ren X, et al. Induction of porcine dermatitis and nephropathy syndrome in piglets by infection with porcine circovirus type 3. J Virol. 2019;93:e02045–18. https://doi.org/10.1128/JVI.02045-18
25. Opriessnig T, Prickett JR, Madson DM, Shen HG, Juhan NM, Pogranichniy RR, et al. Porcine circovirus type 2 (PCV2)-infection and re-inoculation with homologous or heterologous strains: virological, serological, pathological and clinical effects in growing pigs. Vet Res. 2010;41:31. https://doi.org/10.1051/vetres/2010003
26. Denner J, Mankertz A. Porcine circoviruses and xenotransplantation. Viruses. 2017;9:83. https://doi.org/10.3390/v9040083
27. Krüger L, Längin M, Reichart B, Fiebig U, Kristiansen Y, Prinz C, et al. Transmission of porcine circovirus 3 (PCV3) by xenotransplantation of pig hearts into baboons. Viruses. 2019;11:650. https://doi.org/10.3390/v11070650
28. Yu SJ, Kim YJ. Hepatitis B viral load affects prognosis of hepatocellular carcinoma. World J Gastroenterol. 2014;20:12039–44. https://doi.org/10.3748/wjg.v20.i34.12039
29. Lion T, Baumgartinger R, Watzinger F, Matthes-Martin S, Suda M, Preuner S, et al. Molecular monitoring of adenovirus in peripheral blood after allogeneic bone marrow transplantation permits early diagnosis of disseminated disease. Blood. 2003;102:1114–20. https://doi.org/10.1182/blood-2002-07-2152
30. Funk GA, Gosert R, Hirsch HH. Viral dynamics in transplant patients: implications for disease. Lancet Infect Dis. 2007;7:460–72. https://doi.org/10.1016/S1473-3099(07)70159-7

Address for correspondence: Marc Eloit, Institut Pasteur, Pathogen Discovery Laboratory, 25-28 rue du Dr. Roux, 75015, Paris, France; email: marc.eloit@pasteur.fr

Incidence and Transmission Dynamics of *Bordetella pertussis* Infection in Rural and Urban Communities, South Africa, 2016–2018

Fahima Moosa, Stefano Tempia, Jackie Kleynhans, Meredith McMorrow, Jocelyn Moyes, Mignon du Plessis, Maimuna Carrim, Florette K. Treurnicht, Orienka Helfersee, Thulisa Mkhencele, Azwifarwi Mathunjwa, Neil A. Martinson, Kathleen Kahn, Limakatso Lebina, Floidy Wafawanaka, Cheryl Cohen, Anne von Gottberg, Nicole Wolter, for the PHIRST Group

We conducted 3 prospective cohort studies (2016–2018), enrolling persons from 2 communities in South Africa. Nasopharyngeal swab specimens were collected twice a week from participants. Factors associated with *Bordetella pertussis* incidence, episode duration, and household transmission were determined by using Poisson regression, Weibull accelerated time-failure, and logistic regression hierarchical models, respectively. Among 1,684 participants, 118 episodes of infection were detected in 107 participants (incidence 0.21, 95% CI 0.17–0.25 infections/100 person-weeks). Children <5 years of age who had incomplete vaccination were more likely to have pertussis infection. Episode duration was longer for participants who had higher bacterial loads. Transmission was more likely to occur from male index case-patients and persons who had ≥7 days infection duration. In both communities, there was high incidence of *B. pertussis* infection and most cases were colonized.

Despite high vaccine coverage with either the whole-cell or acellular vaccine in many countries, the incidence of pertussis has increased globally during the past 20 years (*1*–*4*). Disease increase has been attributed to several factors, including increased awareness by clinicians, more sensitive molecular diagnostic techniques (*2*,*4*), serologic markers for identification of infection in adolescents and adults who are commonly asymptomatic carriers of *Bordetella pertussis* (*1*), pathogen adaptation, or waning immunity (*3*,*5*).

Infection indicates that bacteria are in or on the body and make a person sick. Colonization indicates that bacteria are on the body but do not make a person sick.

In South Africa, pertussis is a notifiable medical condition (*6*). The whole-cell pertussis vaccine was introduced in South Africa in 1950 and was replaced by the acellular pertussis vaccine in April 2009. The vaccine is given to infants at 6, 10, and 14 weeks of age, and a booster dose is given at 18 months of age. In 2019, according to the World Health Organization/United Nations Children's Fund, coverage for the first dose of the acellular vaccine in South Africa was 84%, and coverage for the third dose was 77% (*7*).

Data on pertussis epidemiology in low- and middle-income countries, particularly in Africa, are lacking; as a result, the epidemiology of the disease is poorly understood (*8*). In South Africa during

Author affiliations: University of the Witwatersrand, Johannesburg, South Africa (F. Moosa, S. Tempia, J. Moyes, M. du Plessis, M. Carrim, O. Hellferscee, C. Cohen, A. von Gottberg, N. Wolter); National Institute for Communicable Diseases of the National Health Laboratory Service, Johannesburg (F. Moosa, J. Kleynhans, J. Moyes, M. du Plessis, M. Carrim, F.K. Treurnicht, O. Hellferscee, T. Mkhencele, A. Mathunjwa, C. Cohen, A. von Gottberg, N. Wolter); Centers for Disease Control and Prevention, Atlanta, Georgia, USA (S. Tempia, M.L McMorrow); Johns Hopkins University, Baltimore, Maryland, USA (N.A. Martinson); National Research Foundation, Pretoria, South Africa (N.A. Martinson); South African Medical Research Council, Cape Town, South Africa (N.A. Martinson, K. Kahn, L. Lebina, K. Mothlaoleng, F. Wafawanaka, A. Mathee); North-West University, Potchefstroom, South Africa (S. Piketh)

DOI: https://doi.org/10.3201/eid2902.221125

2013–2018, among persons hospitalized because of pneumonia, annual *B. pertussis* incidence was 17 cases/100,000 population, and the highest incidence of disease and most deaths were in children <1 year of age (*9*). In 2018, clusters of pertussis were observed in several provinces in South Africa, and 54% of cases were detected in infants <3 months of age (*10*). Infants <1 year of age were at highest risk for severe pertussis and death. It is essential to understand infection in older children and adults because these age groups are likely sources of transmission to infants (*3*,*5*). This study reports the incidence, factors associated with infection, duration of infection, and transmission dynamics in persons of all ages in an urban community and a rural community in South Africa.

Materials and Methods

Study Population

During 2016–2018 (May–October 2016, January–October 2017, and January–October 2018), we conducted a community cohort study in 2 communities in South Africa: 1 rural (Agincourt, Mpumalanga Province) and 1 urban (Klerksdorp, North West Province). We enrolled consenting members of randomly selected households each year. During the household enrollment process, at least 80% of the household members within each household had to consent to be included in the study for a household to be enrolled. A detailed account of the study methods and the cohort profile has been previously reported (*11*,*12*).

Household Visits

Demographic and baseline health status (including HIV) were collected for all participants at enrollment. Participants were considered HIV infected if they had 1 of the following during the follow-up period: 2 positive rapid HIV test results, evidence of a positive HIV laboratory result, or evidence of receiving antiretroviral treatment. Vaccination status was obtained for children <5 years of age from Road-to-Health Cards, which serve as a child's formal health record in South Africa. Households were visited twice a week for nasopharyngeal specimen collection and symptom determination by using a structured questionnaire. Symptom data included fever (self-reported or measured tympanic temperature ≥38°C), cough, difficulty breathing, sore throat, nasal congestion, chest pain, muscle aches, headache, vomiting, or diarrhea. In addition, during 2018, persons who tested PCR positive for *B. pertussis* were retrospectively interviewed (interviews were conducted immediately after a positive PCR result) to confirm if the persons experienced any pertussis-specific symptoms (cough, inspiratory whoop, post-tussive vomiting, or apnea) during the infection.

Specimen Collection and Testing

At each visit, a nasopharyngeal swab specimen was collected and placed in PrimeStore Molecular Transport Medium (Longhorn Vaccines & Diagnostics, https://lhnvd.com) and transported to the laboratory within 48–72 hours for testing. Specimens were received in the laboratory in real-time and then batched for further processing. Total nucleic acids were extracted by using the Roche MagNA Pure 96 Instrument (Roche Diagnostics, https://www.roche.com) and the MP96 DNA and Viral NA SV Kits (Roche Diagnostics). Extracts were tested by using an internally validated IS*481* and human ribonuclease P (RNaseP) duplex real-time PCR. Any specimen that tested positive for IS*481* with a cycle threshold (Ct) value ≤45 was repeated (from extraction using a fresh aliquot) and retested (2 replicates) by using a second, multitarget real-time PCR targeting *B. pertussis*, *B. parapertussis*, and *B. holmesii* (*13*). A specimen was considered positive for *B. pertussis* if IS*481* or *ptxS1* targets was detected with Ct values ≤45 in at least 2/3 replicates and negative for hIS*1001* (*B. holmesii*) and pIS*1001* (*B. parapertussis*).

Study Definitions and Data Analysis

We defined an episode of *B. pertussis* infection as ≥1 consecutive visits in which *B. pertussis* was detected. A new episode was one that began after a period of at least 12 consecutive visits (i.e., 6 weeks) in which *B. pertussis* was not detected. We determined the incidence of *B. pertussis* infection by dividing the number of PCR-positive episodes by the person-time under observation, expressed as 100 person-weeks. We assessed factors associated with incidence by using Poisson regression accounting for the person-time under observation. For analysis of incidence, we considered all identified episodes of infections, including multiple episodes in the same person.

We estimated the duration of a *B. pertussis* infection as the date of the last positive specimen minus the date of the first positive specimen (within the same episode of infection) plus 2.5 days to account for gaps between visits; values are expressed as mean ±SD. We performed analysis of factors associated with the duration of infection (time-to-event outcome) by using accelerated time failure Weibull regression and analysis of *B. pertussis* bacterial loads by using IS*481* Ct as a proxy for bacterial load. We characterized IS*481* bacterial load as follows: Ct ≤34,

higher bacterial load; Ct 34–39, intermediate bacterial load; Ct 40–44, lower bacterial load.

We defined an episode of symptomatic *B. pertussis* infection as illness in a person who had ≥1 symptoms reported from 1 visit before to 1 visit after the *B. pertussis* episode. Signs and symptoms included fever, cough, difficulty breathing, sore throat, nasal congestion, chest pain, muscle aches, headache, vomiting, and diarrhea. In 2018, we used the pertussis-specific symptom data collected to determine if positive cases could be classified as pertussis by using the South Africa notifiable medical condition pertussis case definition (cough lasting ≥14 days, or cough of any duration for children <1 year of age, along with ≥1 of the following symptoms: paroxysms of coughing, inspiratory whoop, posttussive vomiting, and apnea [with or without cyanosis; only for infants <1 year of age]).

A cluster of cases included all *B. pertussis* infections in a single household that occurred within an interval of <7 days. The index case was the first person testing positive within a cluster. We estimated cluster duration as the time from the first day of positivity of the first person in a cluster to the last day of positivity of the last person. We defined household cumulative infection risk (HCIR) as the proportion of subsequent infections within a household after the first PCR-positive case and evaluated HCIR among all households in which ≥1 household member had *B. pertussis* infection. The formula for HCIR was the number of infected persons within a household (excluding the index case) divided by number of enrolled persons living within the household. We excluded households that had coprimary cases from the HCIR analysis. We defined crowding as >2 persons sharing a sleeping room within the household.

We used logistic regression to analyze factors associated with symptomatic fraction and HCIR. Pertussis vaccine status was based on number of vaccine doses received by age. For all analyses, we accounted for clustering by study site and households within site by using hierarchical mixed effect models. For the multivariable models, we assessed all variables that were significant at $p<0.2$ by univariate analysis and removed nonsignificant factors ($p\geq0.05$) by using manual backward elimination. We set statistical significance at $p<0.05$ and performed all statistical analyses in Stata version 14.1 (StataCorp LP, https://www.stata.com).

Ethics

Ethics approval for the Prospective Household cohort study of Influenza, Respiratory Syncytial virus, and other respiratory pathogens community burden and Transmission dynamics in South Africa (PHIRST) was obtained from the University of the Witwatersrand Human Research Ethics Committee, South Africa (protocol no. 150808, C.C.). Written informed consent was obtained from all enrolled persons, or parents/guardians in the case of minors. A separate ethics application for the pertussis component of the PHIRST was obtained from the University of the Witwatersrand Human Research Ethics Committee, South Africa (protocol no. M210676, F.M.).

Results

Study Population

During 2016–2018, a total of 1,684 persons from 327 households were enrolled: 542 persons in 2016, 577 in 2017, and 565 in 2018 (Table 1), as described (*12*). Overall, 16.6% (279/1,684) of the participants were <5 years of age, of whom 97.3% (214/220) were fully vaccinated for age with the acellular *B. pertussis* vaccine. HIV prevalence for the cohort was 15.3% (249/1,628).

Specimen-Level Data

There were 122,133 possible individual follow-up visits, from which 105,687 (86.5%) nasopharyngeal swab specimens were collected and tested for *Bordetella* species (Appendix Figures 1–3, https://wwwnc.cdc.gov/EID/article/29/2/22-1125-App1.pdf). Of the specimens tested, 276 (0.3%) were PCR positive for *B. pertussis* and 413 (0.4%) were PCR positive for *B. holmesii*. *B. parapertussis* was not detected. Of the specimens positive for *B. pertussis*, 20.3% (56/276) were positive for both IS*481* and ptx*S1*, and 79.7% (220/276) were positive for IS*481* only.

Individual-Level Data

Incidence and Factors Associated with Incidence

Among 1,684 study participants, 118 episodes of *B. pertussis* infection were detected in 107 participants; 11 persons had 2 episodes of *B. pertussis* infection. There were no demographic/clinical differences observed between persons who had 1 or 2 episodes of infection. The incidence of *B. pertussis* infection was 0.21 (95% CI 0.17–0.25)/100 person-weeks (Table 2). The highest incidence of *B. pertussis* infection was observed in persons 5–14 years of age (0.27 [95% CI 0.20–0.35]/100 person-weeks). Children <5 years of age who had incomplete vaccination for age were more likely to be infected with *B. pertussis* than were vaccinated children (adjusted incidence rate ratio 4.48, 95% CI 1.38–14.59). Among the 36

enrolled infants, 5 *B. pertussis* infections were identified in those 9–11 months of age. Of those infants, 4 were fully vaccinated for age; 1 infant (incomplete vaccination) had symptoms (runny nose) during the *B. pertussis* infection.

Duration of PCR-Positive B. pertussis Infection

The mean ± SD duration of *B. pertussis* infection was 12.0 ±19.1 days. The duration of *B. pertussis* infection was longer when ≥2 symptoms were reported (adjusted hazard ratio 0.26, 95% CI 0.18–0.67) (Table 3) when compared with colonized persons. Duration of infection was longer for participants who had higher and intermediate bacterial loads (Ct values ≤34 and 35–39) when compared with persons who had lower bacterial loads (Ct values 40–44; adjusted hazard ratio for Ct ≤34, was 0.16 [95% CI 0.06–0.44] and for wCt 35–39 was 0.41 [95% CI 0.22–0.74]).

Factors Associated with Symptomatic B. pertussis Infection

Of the 107 persons positive for *B. pertussis*, 34 (31.8%) reported symptoms during any given episode of infection (Table 4). Common respiratory signs and symptoms reported during an episode of *B. pertussis* infection were runny nose (55.9%, 19/34), cough (82.4%, 28/34), fever (29.4%, 10/34), and sore throat (14.7%, 5/34). Other, less commonly reported, symptoms were muscle aches, difficulty breathing, chest pain, and vomiting. In 2018, a total of 47.1% (24/51) of persons testing positive for *B. pertussis* were retrospectively interviewed (Appendix Table). A total of 83% (20/24) of these persons reported ≥1 symptom consistent with pertussis (cough, inspiratory whoop, posttussive vomiting, or apnea) and 60.0% (12/20) of symptomatic persons met the pertussis clinical case definition. Among the symptomatic *B. pertussis*–positive persons <5 years of age, 67.0% (4/6) were fully vaccinated for age. Persons positive for *B. pertussis*

Table 1. Characteristics for 1,684 persons enrolled in the PHIRST, South Africa, 2016–2018*

Characteristic	No. positive/no. tested (%)		
	Overall	Rural	Urban
Year			
2016	542/1,684 (32.2)	280/849 (32.9)	262/835 (31.4)
2017	577/1,684 (34.3)	289/849 (34.0)	288/835 (34.5)
2018	565/1,684 (33.6)	280/849 (32.9)	285/835 (34.1)
Sex			
M	675/1,684 (40.1)	316/849 (37.2)	359/835 (42.9)
F	1,009/1,684 (59.9)	533/849 (62.8)	479/835 (57.1)
Age group, y			
<1	36/1,684 (2.1)	15/849 (1.8)	21/835 (2.5)
1–4	243/1,684 (14.4)	156/849 (18.4)	87/835 (10.4)
5–14	547/1,684 (32.5)	309/849 (36.4)	238/835 (28.5)
15–24	273/1,684 (16.2)	124/849 (14.6)	149/835 (17.8)
25–44	317/1,684 (18.8)	141/849 (16.6)	176/835 (21.1)
45–64	195/1,684 (11.6)	74/849 (8.7)	121/835 (14.5)
≥65	73/1,684 (4.3)	30/849 (3.5)	43/835 (5.2)
HIV status			
Negative	1,379/1,628 (84.7)	715/832 (85.9)	664/796 (83.4)
Positive	249/1,628 (15.3)	117/832 (14.1)	132/796 (16.6)
Nutritional status†			
Underweight	131/1,676 (7.8)	55/849 (6.5)	76/827 (9.2)
Normal	993/1,676 (59.3)	552/849 (65.0)	441/827 (53.3)
Overweight	265/1,676 (15·8)	123/849 (14.5)	142/827 (17.2)
Obese	287/1,676 (17.1)	119/849 (14.0)	168/827 (20.3)
Underlying illness‡			
No	1,634/1,684 (97.0)	844/849 (99.4)	790/835 (94.6)
Yes	50/1,684 (3.0)	5/849 (0.6)	45/835 (5.4)
Pertussis vaccination§			
Incomplete	6/220 (2.7)	3/128 (2.3)	3/92 (3.3)
Fully vaccinated	214/220 (97.3)	125/128 (97.7)	89/92 (96.7)
Crowding¶			
No	738/1,684 (43.8)	361/849 (42.5)	377/835 (45.2)
Yes	946/1,684 (56.2)	488/849 (57.5)	458/835 (54.9)

*PHIRST, Prospective Household cohort study of Influenza, Respiratory Syncytial virus, and other respiratory pathogens community burden and Transmission dynamics in South Africa.
†Nutritional status is based on a person's body mass index (BMI). We defined BMI categories as follows: underweight, age <18 y weight for age or BMI <–2 SDs of World Health Organization (WHO) Child Growth Standards; age ≥18 y BMI <18.5 kg/m^2; overweight, age <18 y BMI >+1 and ≤+2 SD of the WHO growth standards, age ≥18 y BMI ≥25 and <30kg/m^2; obese, age <18 y BMI >+2 SD of WHO growth standards, age ≥18 y BMI ≥30 kg/m^2.
‡Defined as self-reported history of asthma, lung disease, heart disease, stroke, spinal cord injury, epilepsy, organ transplant, immunosuppressive therapy, organ transplantation, cancer, liver disease, renal disease, or diabetes.
§Collected only for children <5 y of age.
¶More than 2 persons in a household sleeping in the same room.

Table 2. Incidence rate and factors associated with *Bordetella pertussis* incidence for 1,684 participants in the PHIRST study of respiratory infections, South Africa, 2016–2018*

Characteristic	*B. pertussis* incidence (95% CI)	Univariate analysis		Multivariable analysis	
		Incidence rate ratio (95% CI)	p value	Adjusted incidence rate ratio (95% CI)	p value
Overall	0.2 (0.17–0.25)	NA	NA	NA	NA
Year					
2016	0.25 (0.17–0.35)	Referent		NA	NA
2017	0.13 (0.09–0.19)	0.53 (0.17–1.63)	0.27	NA	NA
2018	0.26 (0.20–0.33)	1.04 (0.44–2.49)	0.92	NA	NA
Site					
Rural	0.17 (0.13–0.22)	Referent		NA	NA
Urban	0.24 (0.19–0.31)	1.5 (0.77–2.96)	0.23	NA	NA
Sex					
M	0.23 (0.17–0.30)	Referent		NA	NA
F	0.19 (0.15–0.24)	0.83 (0.58–1.19)	0.31	NA	NA
Age group, y					
<5	0.21 (0.14–0.33)	1.41 (0.69–2.90)	0.37	1.62 (0.56–4.65)	0.37
5–14	0.27 (0.20–0.35)	1.76 (0.96–3.21)	0.09	1.73 (0.91–3.31)	0.09
15–44	0.17 (0.12–0.24)	1.12 (0.62–2.04)	0.78	1.09 (0.59–2.00)	0.78
≥45	0.15 (0.09–0.25)	Referent		Referent	
HIV status					
Uninfected	0.22 (0.18–0.27)	Referent		NA	NA
Infected	0.14 (0.08–0.25)	0.64 (0.36–1.11)	0.11	NA	NA
Nutritional status†					
Underweight	0·20 (0.10–0.38)	0.68 (0.28–1.66)	0.39	NA	NA
Normal	0.23 (0.18–0.28)	Referent		NA	NA
Overweight/obese	0.30 (0.21–0.43)	0.76 (0.52–1.13)	0.18	NA	NA
Underlying illness‡					
No	0.20 (0.17–0.24)	Referent		NA	NA
Yes	0.36 (0.16–0.80)	1.78 (0.68–4.70)	0.24	NA	NA
Pertussis vaccination§					
Incomplete	0.91 (0.23–3.64)	4.89 (1.47–16.02)	0.01	**4.48 (1.38–14.59)**	**0.01**
Fully vaccinated	0.19 (0.11–0.32)	Referent		Referent	
Unknown	0.20 (0.17–0.25)	1.08 (0.61–1.91)	0.78	1.32 (0.42–4.13)	0.64
Crowding¶					
No	0.15 (0.11–0.21)	Referent		Referent	
Yes	0.25 (0.20–0.31)	1.63 (0.86–3.08)	0.13	1.53 (0.78–2.97)	0.21

*Bold indicates statistical significance. Variables adjusted for in final model were age group, pertussis vaccination, and crowding. NA, not applicable; PHIRST, Prospective Household cohort study of Influenza, Respiratory Syncytial virus, and other respiratory pathogens community burden and Transmission dynamics in South Africa.
†Nutritional status is based on a person's body mass index (BMI). We defined BMI categories as follows: underweight, age <18 y weight for age or BMI <–2 SDs of World Health Organization (WHO) Child Growth Standards; age ≥18 y BMI <18.5 kg/m^2; overweight, age <18 y BMI >+1 and ≤+2 SD of the WHO growth standards, age ≥18 y BMI ≥25 and <30 kg/m^2; obese, age <18 y BMI >+2 SD of WHO growth standards, age ≥18 y BMI ≥30 kg/m^2.
‡Defined as self-reported history of asthma, lung disease, heart disease, stroke, spinal cord injury, epilepsy, organ transplant, immunosuppressive therapy, organ transplantation, cancer, liver disease, renal disease, or diabetes.
§Collected only for children <5 y of age· Vaccine status calculate based on number of doses of vaccine received by age.
¶More than 2 persons in a household sleeping in the same room.

were 4 times more likely to have symptoms if they were infected for ≥7 days than persons infected for <7 days (adjusted odds ratio [aOR] 4.12, 95% CI 1.70–9.98) (Table 4).

Household Cumulative Infection Risk

The overall household cumulative infection risk was 14.4% (43/298 susceptible exposed persons). Transmission was more likely to occur from male index case-patients than female index case-patients (aOR 12.20, 95% CI 1.57–94.96) and persons who had ≥7 days episode duration than <7 days (aOR 24.79, 95% CI 2.74–224.30) (Table 5). Within households with confirmed *B. pertussis* transmission, 38.8% (14/36) of index case-patients transmitting to household contacts were colonized.

Discussion

In this study population, we found a high incidence of *B. pertussis* and most infected persons were colonized. We detected 118 episodes of *B. pertussis* infection in 107 participants, of which 11 persons had 2 episodes. The overall HCIR was 14%, and 39% of index cases in the household were colonized with *B. pertussis*. The mean duration of PCR-positive *B. pertussis* infection was 12 days. Persons positive for *B. pertussis* were more likely to report symptoms if they were infected for ≥7 days. Transmission was more likely to occur from male index case-patients and persons who had longer episode duration.

In this community cohort study of healthy persons in South Africa, the incidence of *B. pertussis* was 0.21 cases/100 person-weeks. Incidence in this study

was higher than the mean annual incidence risk of 17 cases/100,000 population previously reported in South Africa for persons hospitalized because of pneumonia during 2013–2018 (*9*). This difference was probably caused by the fact that the study conducted by Wolter et al. (*9*) was a cross-sectional study enrolling hospitalized patients who had respiratory illness, whereas our study was a community cohort study enrolling healthy persons. It is difficult to compare our incidence with those of other studies that report incidence data because our study was a community cohort study, whereas other studies focus on populations with *B. pertussis* disease or populations that had outbreaks of *B. pertussis*. Thus, more data describing the incidence of *B. pertussis* among healthy persons over time, and additional longitudinal community data are required for meaningful comparisons to be made. Assessing factors associated with *B. pertussis* incidence, children <5 years of age who did not receive the full schedule of pertussis vaccine for age were more likely to be infected with *B. pertussis* than were vaccinated children. Similarly, other studies in South Africa showed that risk for pertussis and risk for hospitalization caused by pertussis decreased when persons were vaccinated (*9*,*14*).

Data on duration of PCR-positive *B. pertussis* infection among persons are limited. In our study, the average duration of naturally acquired *B. pertussis* infection was 12 days and episode duration was longer for participants with higher bacterial loads, similar to findings for influenza virus infection in the same cohort (*11*). A human challenge study that induced *B. pertussis* colonization in healthy adults showed that *B. pertussis* persisted within the nasopharynx for up to 16 days postinoculation in some of the study participants (*15*). However, it should be noted that in the

Table 3. Factors associated with PCR-positive *Bordetella pertussis* infection duration for 118 persons participants in the PHIRST study of respiratory infections, South Africa, 2016–2018*

Characteristic	*B. pertussis* mean ± SD infection duration, d	Univariate analysis Hazard ratio (95% CI)	p value	Multivariable analysis Adjusted hazard ratio (95% CI)	p value
Sex					
M	11.9 ± 21.1	Referent		NA	NA
F	14.1 ± 18.8	0.77 (0.45–1.31)	0.34	NA	NA
Age group, y					
<5	6.3 ± 6·2	1.87 (0.84–4.20)	0.13	2.20 (0.87–5.58)	0.09
5–14	12.3 ± 14.5	1.09 (0.59–2.02)	0.78	1.16 (0.58–2.33)	0.67
15–44	15.4 ± 20.8	1.16 (0.50–2.67)	0.73	2.07 (0.81–5.27)	0.13
≥45	22.4 ± 38.8	Referent		Referent	
HIV status					
Uninfected	13.8 ± 20.7	Referent		NA	NA
Infected	9.3 ± 10.2	1.06 (0.50–2.26)	0.88	NA	NA
Nutritional status†					
Underweight	4.4 ± 2.7	2.78 (0.98–8.00)	0.06	NA	NA
Normal	13.0 ± 18.7	Referent		NA	NA
Overweight/obese	16.2 ± 25.3	0.44 (0.71–2.17)	0.44	NA	NA
Underlying illness‡					
No	12.4 ± 18.7	Referent		NA	NA
Yes	28.2 ± 34.9	0.80 (0.27–2.33)	0.68	NA	NA
Pertussis vaccination§					
Incomplete	3.0 ± 0.0	2.44 (0.33–17.82)	0.38	NA	NA
Fully vaccinated	6.7 ± 6.6	Referent		NA	NA
Unknown	14.4 ± 21.1	0.63 (0.29–1.36)	0.24	NA	NA
Symptoms					
None	9.3 ± 14.1	Referent		Referent	
1	22.2 ± 20.3	0.62 (0.19–2.04)	0.44	0.39 (0.18–1.62)	0.19
≥2	11.1 ± 10.2	0.38 (0.16–0.93)	0.03	**0.26 (0.8–0.67)**	**0.006**
IS*481* Ct category¶					
<34	17.0 ± 11.6	0.17 (0.06–0.45)	<0.001	**0.16 (0.06–0.44)**	**0.0001**
35–39	13.5 ± 20.7	0.43 (0.24–0.76)	0.004	**0.41 (0.22–0.74)**	**0.003**
40–44	11.1 ± 20.7	Referent		Referent	

*Bold indicates statistical significance. Variables adjusted for in final model: age group, presence/absence of symptoms, and IS*481* Ct category. Ct, cycle threshold; IS, insertion sequence; NA, not applicable; PHIRST, Prospective Household cohort study of Influenza, Respiratory Syncytial virus, and other respiratory pathogens community burden and Transmission dynamics in South Africa.
†Nutritional status is based on a person's body mass index (BMI). We defined BMI categories as follows: underweight, age <18 y weight for age or BMI <–2 SDs World Health Organization (WHO) Child Growth Standards; age ≥18 y BMI <18.5 kg/m^2; overweight, age <18 y BMI >+1 and ≤+2 SD of the WHO growth standards, age ≥18 y BMI ≥25 and <30kg/m^2; obese, age <18 y BMI >+2 SD of WHO growth standards, age ≥18 y BMI ≥30 kg/m^2.
‡Defined as self-reported history of asthma, lung disease, heart disease, stroke, spinal cord injury, epilepsy, organ transplant, immunosuppressive therapy, organ transplantation, cancer, liver disease, renal disease, or diabetes.
§Collected only for children <5 y of age· Vaccine status calculate based on number of doses of vaccine received by age.
¶Used as a proxy for bacterial load.

Table 4. Factors associated with symptomatic *Bordetella pertussis* infection for 107 persons participants in the PHIRST study of respiratory infections, South Africa, 2016–2018*

Characteristic	*B. pertussis* symptomatic, no. positive/no. tested (%)	Univariate analysis		Multivariable analysis	
		Odds ratio (95% CI)	p value	Adjusted odds ratio (95% CI)	p value
Year					
2016	6/33 (18.2)	Referent		NA	NA
2017	2/29 (31.0)	2.03 (0.62–6.62)	0.24	NA	NA
2018	19/56 (33.9)	2.31 (0.81–6.56)	0.12	NA	NA
Site					
Rural	13/48 (27.1)	Referent		NA	NA
Urban	21/70 (30.0)	1.15 (0.51–2.61)	0.73	NA	NA
Sex					
M	10/52 (19.2)	Referent		NA	NA
F	24/66 (36.4)	2.40 (1.02–5.63)	0.04	NA	NA
Age group, y					
<5	4/20 (20.0)	0.25 (0.05–1.14)	0.07	0.33 (0.06–1.69)	0.18
5–14	15/56 (26.8)	0.37 (0.11–1.22)	0.10	0.41 (0.11–1.54)	0.19
15–44	8/28 (28.6)	0.40 (0.11–1.51)	0.18	0.28 (0.06–1.22)	0.09
≥45	7/14 (50.0)	Referent		Referent	
HIV status					
Uninfected	28/104 (26.9)	Referent		Referent	
Infected	6/12 (50.0)	2.71 (0.81–9.11)	0.11	3.37 (0.77–14.56)	0.10
Nutritional status†					
Underweight	0/9 (0.0)	0.15 (0.01–2.65)	0.19	NA	NA
Normal	20/77 (25.9)	Referent		NA	NA
Overweight/obese	13/28 (46.4)	2.44 (1.00–5.93)	0.05	NA	NA
Underlying illness‡					
No	31/112 (27.7)	Referent		NA	NA
Yes	3/6 (50.0)	2.61 (0.50–13.65)	0.26	NA	NA
Pertussis vaccination§					
Incomplete	0/2 (0.0)	0.47 (0.02–11.81)	0.64	NA	NA
Fully vaccinated	4/14 (28.6)	Referent		NA	NA
Unknown	30/102 (29.4)	0.98 (0.30–3.20)	0.98	NA	NA
IS*481* Ct category¶					
≤34	6/15 (40.0)	3.05 (0.82–11.38)	0.09	NA	NA
35–39	21/64 (32.8)	2.23 (0.85–5.89)	0.11	NA	NA
40–44	7/39 (17.9)	Referent		NA	NA
Episode duration, d					
<7	14/75 (18.7)	Referent		Referent	
≥7	20/43 (46.5)	3.79 (1.64–8.73)	0.002	**4.12 (1.70–9.98)**	**0.002**
Smoking, ≥15 y of age					
No	14/37 (37.8)	Referent		NA	NA
Yes	5/16 (31.3)	0.75 (0.21–2.60)	0.65	NA	NA

*Bold indicates statistical significance. Variables adjusted for in final model: age group, HIV status, and episode duration. Ct, cycle threshold; IS, insertion sequence; NA, not applicable; PHIRST, Prospective Household cohort study of Influenza, Respiratory Syncytial virus, and other respiratory pathogens community burden and Transmission dynamics in South Africa.
†Nutritional status is based on a person's body mass index (BMI). We defined BMI categories as follows: underweight, age <18 y weight for age or BMI <–2 SDs World Health Organization (WHO) Child Growth Standards; age ≥18 y BMI <18.5 kg/m^2; overweight, age <18 y BMI >+1 and ≤+2 SD of the WHO growth standards, age ≥18 y BMI ≥25 and <30kg/m^2; obese, age <18 y BMI >+2 SD of WHO growth standards, age ≥18 y BMI ≥30 kg/m^2.
‡Defined as self-reported history of asthma, lung disease, heart disease, stroke, spinal cord injury, epilepsy, organ transplant, immunosuppressive therapy, organ transplantation, cancer, liver disease, renal disease, or diabetes.
§Collected only for children <5 y of age. Vaccine status calculate based on number of doses of vaccine received by age.
¶Used as a proxy for bacterial load.

human challenge study, adults had received vaccination within the previous 5 years and were treated for colonization from day 14. In our study, data on vaccination of persons ≥5 years of age and treatment were missing, and that information could have potentially affected the duration of *B. pertussis* within the nasopharynx of study participants.

Symptoms associated with *B. pertussis* PCR-positive cases vary from mild, nonspecific respiratory symptoms to pertussis-specific symptoms. In this study, symptomatic *B. pertussis*–infected persons reported nonspecific respiratory symptoms, such as runny nose, cough, fever, or sore throat. For the 2018 subset of symptomatic persons who were investigated for *B. pertussis*–specific symptoms, 60% met the notifiable medical condition pertussis case definition. A study in Spain determining factors influencing the spread of *B. pertussis* in households found that participants of all ages experienced *B. pertussis*–specific signs and symptoms, such as cough lasting >2 weeks, paroxysmal cough, posttussive vomiting, inspiratory stridor, apnea, and fever (*16*). In South Africa,

common signs and symptoms reported in children hospitalized with laboratory pertussis were nonspecific cough and fever (*17*).

Evidence suggests that colonization is a major trait of the *B. pertussis* pathogen. In our study, two thirds of persons infected with *B. pertussis* did not report any symptoms. *B. pertussis* incidence data from the United States and the United Kingdom provided evidence of colonization of *B. pertussis* (*18*). de Graaf et al. showed that colonization could be induced by the intranasal inoculation of *B. pertussis* in a human challenge model (*15*). Warfel et al. found that persons previously vaccinated with the acellular pertussis vaccine can become colonized with *B. pertussis* (*19*). There is evidence in the literature supporting colonization of *B. pertussis* in the nasopharynx of persons, which was also observed in our study. In addition to colonization, we found a high proportion of index case-patients transmitting *B. pertussis* to other household contacts. However, it is difficult to draw any

Table 5. Factors associated with household cumulative infection risk for 118 persons, PHIRST, South Africa, 2016–2018*

Characteristic	*B. pertussis* HCIR, no. positive/no. tested (%)	Univariate analysis		Multivariable analysis	
		Odds ratio (95% CI)	p value	Odds ratio (95% CI)	p value
Characteristics of index case-patient					
Sex					
M	30/143 (20.9)	16.81 (1.43–197.69)	0.025	**12.20 (1.57–94.96)**	**0.02**
F	6/150 (4.0)	Referent		Referent	
Age group, y					
<5	2/43 (4.7)	0.05 (0.0003–7.40)	0.24	NA	NA
5–14	27/182 (14.8)	0.38 (0.02–7.59)	0.53	NA	NA
15–44	1/42 (2.4)	0.03 (0.0001–14.52)	0.27	NA	NA
>45	6/22 (27.3)	Referent		NA	NA
IS*481* Ct category†					
≤34	16/57 (28.1)	Referent		NA	NA
35–39	11/138 (7.9)	0.35 (0.02–6.17)	0.47	NA	NA
40–44	9/98 (9.2)	0.43 (0.02–8.87)	0.59	NA	NA
Episode duration, d					
<7	12/216 (5.7)	Referent		Referent	
≥7	24/77 (31.2)	40.84 (3.37–495.19)	0.004	**24.79 (2.74–224.30)**	**0.004**
Characteristics of household contacts					
Sex					
M	15/110 (13.6)	Referent		NA	NA
F	21/183 (11.5)	0.65 (0.22–1.93)	0.44	NA	NA
Age group, y					
<5	8/50 (16.0)	6.60 (1.22–35.64)	0.03	NA	NA
5–14	11/88 (12.5)	2.10 (0.51–8.73)	0.31	NA	NA
15–44	13/106 (12.3)	2.32 (0.30–17.76)	0.42	NA	NA
≥45	4/49 (8.20)	Referent		NA	NA
HIV status					
Negative	31/243 (12.8)	Referent		NA	NA
Positive	5/44 (11.4)	1.27 (0.32–5.14)	0.73	NA	NA
Unknown	0/6 (0.0)	Referent	NA	NA	NA
Nutritional status‡					
Underweight	3/23 (13.0)	0.76 (0.08–6.95)	0.80	NA	NA
Normal weight	21/160 (13.1)	Referent		NA	NA
Overweight	11/107 (10.2)	0.76 (0.23–2.47)	0.65	NA	NA
Underlying illness§					
No	34/285 (11.9)	Referent		NA	NA
Yes	2/8 (25.0)	16.93 (0.61–471.04)	0.09	NA	NA
Crowding¶					
No	8/100 (8.0)	Referent		NA	NA
Yes	28/193 (14.5)	1.84 (0.21–16.42)	0.59	NA	NA
Sleep in same room as index case-patient					
No	24/158 (15.2)	Referent		NA	NA
Yes	12/134 (8.9)	0.71 (0.22–2.26)	0.56	NA	NA

*Bold indicates statistical significance. Variables adjusted for in final model: sex and episode duration. Ct, cycle threshold; HCIR, household cumulative infection risk; IS, insertion sequence; NA, not applicable; PHIRST, Prospective Household cohort study of Influenza, Respiratory Syncytial virus, and other respiratory pathogens community burden and Transmission dynamics in South Africa.
†Used as a proxy for bacterial load.
‡Nutritional status is based on a person's body mass index (BMI). We defined BMI categories as follows: underweight, age <18 y weight for age or BMI <–2 SDs World Health Organization (WHO) Child Growth Standards; age ≥18 y BMI <18.5 kg/m^2; overweight, age <18 y BMI >+1 and ≤+2 SD of the WHO growth standards, age ≥18 y BMI ≥25 and <30kg/m^2; obese, age <18 y BMI >+2 SD of WHO growth standards, age ≥18 y BMI ≥30 kg/m^2.
§Defined as self-reported history of asthma, lung disease, heart disease, stroke, spinal cord injury, epilepsy, organ transplant, immunosuppressive therapy, organ transplantation, cancer, liver disease, renal disease, or diabetes.
¶More than 2 persons in a household sleeping in the same room.

conclusions from that result because additional longitudinal community data are required for meaningful comparisons to be made.

The transmission dynamics of *B. pertussis* within households is poorly understood and requires additional research. Within the PHIRST, the overall HCIR was 14%. In 2001, a pertussis outbreak in New South Wales in Australia showed a 22.3% secondary household attack rate (*20*) and increased risk for household transmission when the index case-patient began antimicrobial drug treatment >7 days after onset of symptoms (*20*). Transmission in our study was associated with male sex, and the index case-patient had a long episode duration (≥7 days). The association between prolonged episode duration and increased transmission is biologically plausible and has been demonstrated for other pathogens, such as influenza virus (*11*). Previous studies have not documented a difference in transmission between male and female patients (*15*,*20*), so this finding should be further explored.

The first limitation of our study is that it was conducted at only 2 sites in South Africa, and results might not be generalizable to other areas and communities within this country. Over the study period, specimens were collected from each person twice a week for a period of 6–10 months. Because we did not collect samples for a full year and therefore could not accurately estimate the incidence over the period of a year, we presented incidence as per 100 person-weeks. Vaccination status was confirmed only for children <5 years of age, so we could conduct analyses regarding vaccination only for this age group. Symptom data collection was poor for 2016 but improved in 2017 and 2018; therefore, the symptom data presented could be an underestimate. The number of *B. pertussis* cases detected in this study is small, so some statistical analyses were underpowered.

The PHIRST was unique in that it was a community cohort study investigating *B. pertussis* infection among healthy persons. A major strength of the study was the repeated, longitudinal sampling of persons over time according to a specified schedule, irrespective of symptoms. This study method ensured that the data collected over time were robust against sampling bias and enabled us to identify the large proportion of persons who were colonized with *B. pertussis*.

In conclusion, in 2 disparate communities in South Africa, we found a high incidence of *B. pertussis*, and two thirds of cases were colonizations. We have demonstrated that persons who are colonized with *B. pertussis* can transmit this bacteria to other household members and thus represent a source of transmission to susceptible age groups.

Acknowledgments

We thank all persons who kindly agreed to participate in this study.

The South African Medical Research Council and University of the Witwatersrand Rural Public Health and Health Transitions Research Unit and Agincourt Health and Socio-Demographic Surveillance System, a node of the South African Population Research Infrastructure Network, is supported by the Department of Science and Innovation, University of the Witwatersrand, Johannesburg, South Africa; and the South African Medical Research Council, Johannesburg, South Africa, and previously the Wellcome Trust, London, UK (grants 058893/Z/99/A, 069683/Z/02/Z, 085477/Z/08/Z, and 085477/B/08/Z). This study was supported by the US Centers for Disease Control and Prevention (grant 5U51IP000155), Sanofi Pasteur (grant PER00059], and in part by a Fogarty International Center Global Infectious Disease research training grant, National Institutes of Health, to the University of Pittsburgh and National Institute for Communicable Diseases (grant D43TW011255).

About the Author

Ms. Moosa is a senior medical scientist in the Centre for Respiratory Diseases and Meningitis, National Institute for Communicable Diseases, Johannesburg, South Africa. Her primary research interests include obtaining epidemiology and molecular data on respiratory pathogens, *B. pertussis*, influenza virus, respiratory syncytial virus, and SARS-CoV-2.

References

1. Dalby T, Harboe ZB, Krogfelt KA, Dalby T, Harboe ZB, Krogfelt KA. Seroprevalence of pertussis among Danish patients with cough of unknown etiology. Clin Vaccine Immunol. 2010;17:2016–23. https://doi.org/10.1128/CVI.00270-10
2. Fisman DN, Tang P, Hauck T, Richardson S, Drews SJ, Low DE, et al. Pertussis resurgence in Toronto, Canada: a population-based study including test-incidence feedback modeling. BMC Public Health. 2011;11:694. https://doi.org/10.1186/1471-2458-11-694
3. Witt MA, Katz PH, Witt DJ. Unexpectedly limited durability of immunity following acellular pertussis vaccination in preadolescents in a North American outbreak. Clin Infect Dis. 2012;54:1730–5. https://doi.org/10.1093/cid/cis287
4. Zouari A, Smaoui H, Brun D, Njamkepo E, Sghaier S, Zouari E, et al. Prevalence of *Bordetella pertussis* and *Bordetella parapertussis* infections in Tunisian hospitalized infants: results of a 4-year prospective study. Diagn Microbiol Infect Dis. 2012;72:303–17. https://doi.org/10.1016/j.diagmicrobio.2012.01.002
5. Baxter R, Bartlett J, Rowhani-Rahbar A, Fireman B, Klein NP. Effectiveness of pertussis vaccines for adolescents and adults: case-control study. BMJ. 2013;347:f4249. https://doi.org/10.1136/bmj.f4249

6. The National Institute for Communicable Diseases. Category 1 notifiable medical conditions [cited 2022 Jan 30]. https://www.nicd.ac.za
7. World Health Organization. WHO and UNICEF estimates of immunization coverage: 2019 revision, 2020 [cited 2022 Apr 24]. https://www.who.int/immunization/monitoring surveillance/data/zaf.pdf
8. Soofie N, Nunes MC, Kgagudi P, van Niekerk N, Makgobo T, Agosti Y, et al. The burden of pertussis hospitalization in HIV-exposed and HIV-unexposed South African infants. Clin Infect Dis. 2016;63(suppl 4):S165–73. https://doi.org/10.1093/cid/ciw545
9. Wolter N, Cohen C, Tempia S, Walaza S, Moosa F, du Plessis M, et al. Epidemiology of pertussis in individuals of all Ages hospitalized with respiratory illness in South Africa, January 2013–December 2018. Clin Infect Dis. 2021;73:e745–53. https://doi.org/10.1093/cid/ciab089
10. National Health Laboratory Service. Increase in pertussis cases in South Africa [cited 2021 Apr 24]. https://www.nhls.ac.za/increase-in-pertussis-cases-in-south-africa
11. Cohen C, Kleynhans J, Moyes J, McMorrow ML, Treurnicht FK, Hellferscee O, et al.; PHIRST group. Asymptomatic transmission and high community burden of seasonal influenza in an urban and a rural community in South Africa, 2017–18 (PHIRST): a population cohort study. Lancet Glob Health. 2021;9:e863–74. https://doi.org/10.1016/S2214-109X(21)00141-8
12. Cohen C, McMorrow ML, Martinson NA, Kahn K, Treurnicht FK, Moyes J, et al.; PHIRST group. Cohort profile: a prospective household cohort study of influenza, respiratory syncytial virus and other respiratory pathogens community burden and transmission dynamics in South Africa, 2016–2018. Influenza Other Respir Viruses. 2021;15:789–803. https://doi.org/10.1111/irv.12881
13. Moosa F, du Plessis M, Wolter N, Carrim M, Cohen C, von Mollendorf C, et al. Challenges and clinical relevance of molecular detection of *Bordetella pertussis* in South Africa. BMC Infect Dis. 2019;19:276. https://doi.org/10.1186/s12879-019-3869-7
14. Muloiwa R, Dube FS, Nicol MP, Hussey GD, Zar HJ. Risk factors for *Bordetella pertussis* disease in hospitalized children. PLoS One. 2020;15:e0240717. https://doi.org/10.1371/journal.pone.0240717
15. de Graaf H, Ibrahim M, Hill AR, Gbesemete D, Vaughan AT, Gorringe A, et al. Controlled human infection with *Bordetella pertussis* induces asymptomatic, immunizing colonization. Clin Infect Dis. 2020;71:403–11. https://doi.org/10.1093/cid/ciz840
16. Godoy P, García-Cenoz M, Toledo D, Carmona G, Caylà JA, Alsedà M, et al.; Transmission of Pertussis in Households Working Group. Factors influencing the spread of pertussis in households: a prospective study, Catalonia and Navarre, Spain, 2012 to 2013. Euro Surveill. 2016;21:1–10. https://doi.org/10.2807/1560-7917.ES.2016.21.45.30393
17. Muloiwa R, Dube FS, Nicol MP, Zar HJ, Hussey GD. Incidence and diagnosis of pertussis in South African children hospitalized with lower respiratory tract infection. Pediatr Infect Dis J. 2016;35:611–6. https://doi.org/10.1097/INF.0000000000001132
18. Althouse BM, Scarpino SV. Asymptomatic transmission and the resurgence of *Bordetella pertussis*. BMC Med. 2015;13:146. https://doi.org/10.1186/s12916-015-0382-8
19. Warfel JM, Zimmerman LI, Merkel TJ. Acellular pertussis vaccines protect against disease but fail to prevent infection and transmission in a nonhuman primate model. Proc Natl Acad Sci U S A. 2014;111:787–92. https://doi.org/10.1073/pnas.1314688110
20. Terry JB, Flatley CJ, van den Berg DJ, Morgan GG, Trent M, Turahui JA, et al. A field study of household attack rates and the effectiveness of macrolide antibiotics in reducing household transmission of pertussis. Commun Dis Intell Q Rep. 2015;39:E27–33.

Address for correspondence: Fahima Moosa, Centre for Respiratory Diseases and Meningitis, National Institute for Communicable Diseases of the National Health Laboratory Service, Johannesburg 2193, South Africa; email: fahimam@nicd.ac.za

Influence of Landscape Patterns on Exposure to Lassa Fever Virus, Guinea

Stephanie Longet,[1] Cristina Leggio,[1] Joseph Akoi Bore,[1] Stephanie Key, Tom Tipton, Yper Hall, Fara Raymond Koundouno, Hilary Bower, Tapan Bhattacharyya, N'Faly Magassouba, Stephan Günther, Ana-Maria Henao-Restrapo, Jeremy S. Rossman, Mandy Kader Konde, Kimberly Fornace,[2] Miles W. Carroll[2]

Lassa fever virus (LASV) is the causative agent of Lassa fever, a disease endemic in West Africa. Exploring the relationships between environmental factors and LASV transmission across ecologically diverse regions can provide crucial information for the design of appropriate interventions and disease monitoring. We investigated LASV exposure in 2 ecologically diverse regions of Guinea. Our results showed that exposure to LASV was heterogenous between and within sites. LASV IgG seropositivity was 11.9% (95% CI 9.7%–14.5%) in a coastal study site in Basse-Guinée, but it was 59.6% (95% CI 55.5%–63.5%) in a forested study site located in Guinée Forestière. Seropositivity increased with age in the coastal site. We also found significant associations between exposure risk for LASV and landscape fragmentation in coastal and forested regions. Our study highlights the potential link between environmental change and LASV emergence and the urgent need for research on land management practices that reduce disease risks.

Author affiliations: Pandemic Sciences Institute, Oxford, UK (S. Longet, J.A. Bore, T. Tipton, M.W. Carroll); UK Health Security Agency, Porton Down–Salisbury, UK (C. Leggio, Y. Hall, M.W. Carroll); London School of Hygiene and Tropical Medicine, London, UK (C. Leggio, S. Key, H. Bower, T. Bhattacharyya, K. Fornace); Ministry of Health, Conakry, Guinea (J.A. Bore, F.R. Koundouno); Center of Excellence for Training, Research on Malaria & Priority Diseases in Guinea, Conakry (J.A. Bore, M.K. Konde); University of Kent School of Biosciences, Canterbury, UK (J.A. Bore, J.S. Rossman); Projet Laboratoire Fièvres Hémorragiques, Conakry (N. Magassouba); Bernhard Nocht Institute for Tropical Medicine, Hamburg, Germany (S. Günther); German Center for Infection Research, Hamburg–Lübeck–Borstel–Riems, Germany (S. Günther); World Health Organization, Geneva, Switzerland (A.-M. Henao-Restrapo); Research-Aid Networks, Chicago, Illinois, USA (J.S. Rossman); University of Glasgow, Glasgow, Scotland, UK (K. Fornace)

DOI: https://doi.org/10.3201/eid2902.212525

Lassa virus (LASV), the cause of Lassa fever in humans, is an enveloped and negative-sense, single-stranded RNA virus belonging to the *Arenaviridae* family (*1*). Initial clinical manifestations, such as fever, weakness, headache, respiratory and gastrointestinal symptoms, and conjunctivitis, are often nonspecific and could indicate several other febrile illnesses (*2*). The mortality rate is unclear because of inconsistent reporting practices and lack of diagnostic services in most endemic areas but is estimated to be 5%–20% in hospitalized patients (*2*,*3*).

The Natal multimammate rat (*Mastomys natalensis*) is considered the main natural reservoir of LASV. It is a commensal rodent and agricultural pest that aggregates in human dwellings and surrounding fields (*4*). Both zoonotic and nonzoonotic transmission mechanisms have been described (*5*). Human LASV infections most commonly occur through infected rodent excreta, contaminated food, and inhalation of aerosols from rodent urine or droppings (*6*,*7*). Person-to-person transmission may also occur through exposure to contaminated bodily fluids (*5*,*8*).

The distribution of the Natal multimammate rat is a major risk factor for LASV exposure. The presence of the rat increases in houses during the dry season because of restricted food supply, which enhances the risk for humans encountering rodents or being in contact with excreta (*9*). Climatic variability leading to changes in human agriculture, food storage practices, and land cover can affect rodent population dynamics (*10*). Recent studies have also identified additional rodent reservoirs (e.g., African wood mouse and Guinea multimammate mouse), indicating the potential for a wider ecologic niche for the virus (*11*,*12*).

LASV is endemic in West Africa, particularly in Nigeria, Sierra Leone, Liberia, and Guinea (*13*,*14*).

[1]These first authors contributed equally to this article.

[2]These senior authors contributed equally to this article.

Estimates on annual human cases of LASV infections in West Africa range from 100,000 to 300,000, with 5,000–10,000 estimated deaths per year and 80% asymptomatic infections. Further epidemiologic studies are needed because these figures have been extrapolated from 1 longitudinal study conducted in Sierra Leone in 1987 (*15*). Characterizing the distribution and transmission intensity of LASV in endemic areas is essential for designing effective surveillance and disease prevention and control programs.

Exposure to LASV may lead to IgG seroconversion (*16*). Analysis of age-stratified serologic responses is a powerful tool to estimate exposure to LASV and to reconstruct historical patterns of transmission and distribution of previously unreported cases (*17*–*19*). Measurement of LASV antibodies has been used to detect circulation of LASV across Guinea in previous studies conducted in the 1990s and early 2000s (*6*,*20*,*21*). However, the current incidence and distribution of LASV in Guinea is largely unknown.

Our study aimed to characterize LASV exposure in human populations in 2 ecologically diverse regions of Guinea: the Basse-Guinée (coastal site); and the Guinée Forestière region, which includes the town of Guéckédou and Macenta Prefecture (forested site). We describe LASV-specific IgG levels within these populations, estimate transmission intensity by using age-stratified antibody responses, and explore associations with demographic and environmental risk factors, including fragmentation (the breaking apart of an organism's preferred habitat into smaller patches).

Materials and Methods

Ethics Considerations

The part of the study conducted in Basse-Guinée (coastal site) was approved by the London School of Hygiene and Tropical Medicine Ethics Committee (reference no. 17429) and the Guinean Ministry of Health. For the part conducted in the town of Guéckédou and Macenta Prefecture (forested site), ethics approval for research projects on human volunteers was obtained from the Republic of Guinea's National Ethics Committee for Health Research on March 16 (approval no. 012/CNERS/17).

Study Sites

Guinea is administratively classified into regions on the basis of broad ecologic characteristics, including the Basse-Guinée and Guinée Forestière regions (*22*). The samples used in this study were collected during 3 separate studies in 2 geographically diverse regions of Guinea: Basse-Guinée (coastal site); and Guinée Forestière, including Macenta Prefecture and the town of Guéckédou (forested site) (*22*). Basse-Guinée (population 2,749,909, area 60,059 km^2) is the coastal region of Guinea, extending for 30–40 miles inland from the Atlantic Ocean to the coastal plains. Basse-Guinée is mainly covered by mangroves and cultivated areas. The rainy season lasts 3 months per year in this region (Figure 1, panel A). Macenta Prefecture (population 297,779, area 8,600 km^2) and the town of Guéckédou (population 346,908) are located to the southeast of the country, close to the border with Liberia and Sierra Leone, within Guinée Forestière. In addition to primary and secondary forests (umbrella and palm trees), which mainly cover this area, mountains and savannah can also be found. The rainy season lasts 9 months per year in this region (*23*–*25*) (Figure 1, panel A).

Study Participants

We obtained written informed consent from participants. Consent forms stated that blood samples would be tested for antibodies specific to Ebola virus and other pathogens, including LASV.

Samples from Basse-Guinée were collected in 2016 as part of a clinical trial evaluating the safety and immunogenicity of the vesicular stomatitis virus–based Ebola virus vaccine in contacts of Ebola survivors. That trial was performed in partnership with Guinea's Ministry of Health, the World Health Organization, and Public Health England. For this study site, we randomly selected 702 samples taken before vaccination and tested them for the presence of LASV-specific IgG. Data recorded included the person's age, sex, and village of residence at the time of vaccination. The selected samples originated from 7 prefectures in Basse-Guinée, encompassing 24 subprefectures and 29 villages or neighborhoods.

We collected samples from Macenta Prefecture during February–December 2017 as part of a seroepidemiologic study on Ebola virus that included both affected and nonaffected villages during the 2013–2016 Ebola virus disease (EVD) outbreak (*26*). In total, 517 participants living in 7 subprefectures encompassing 44 villages were enrolled. Volunteers were recruited upon agreement. The volunteers were from the general population of the village, including bush meat hunters, their family members, local healthcare workers. Volunteers <16 years of age, pregnant persons, travelers or visitors, and persons with chronic disease were excluded

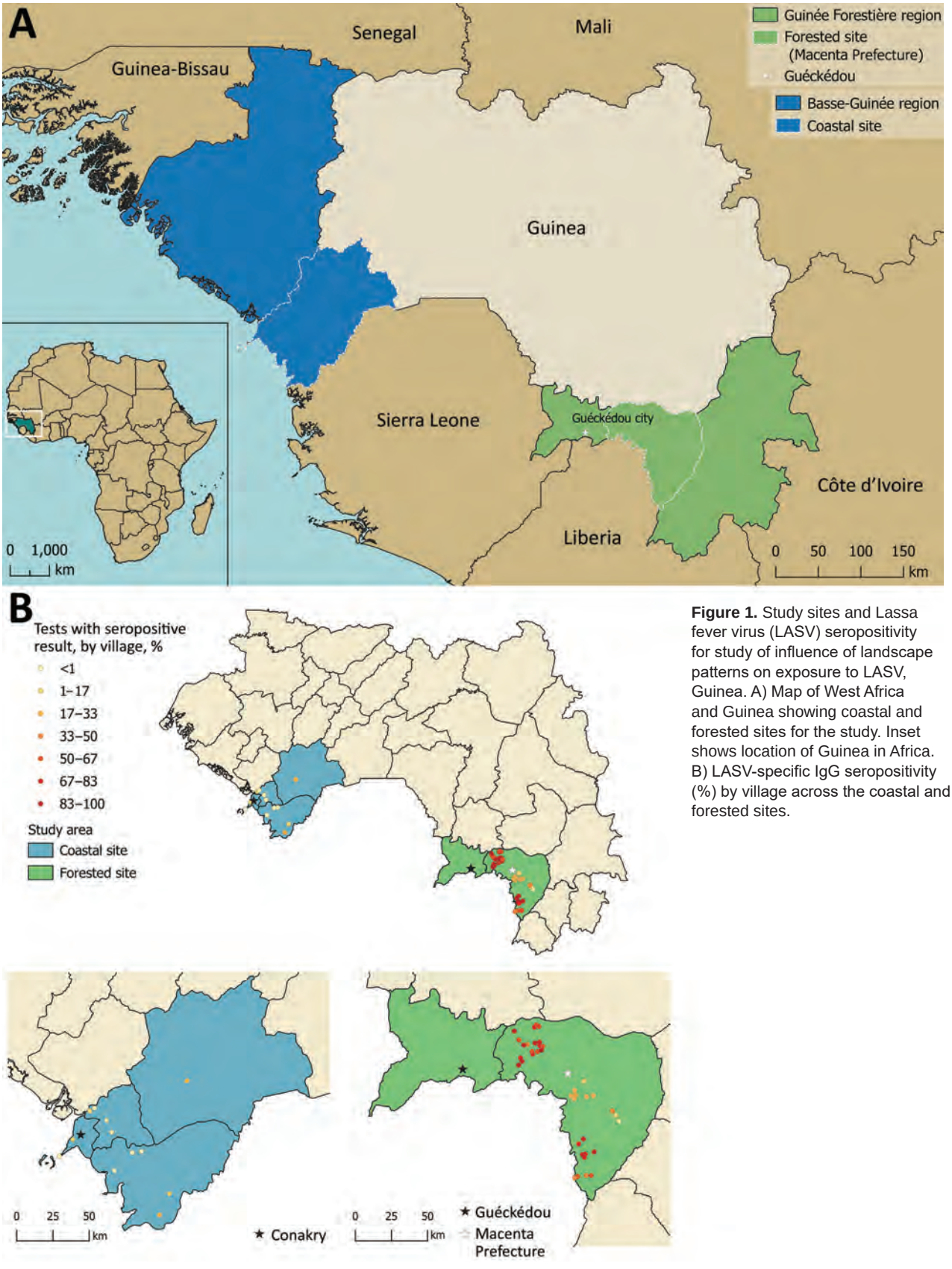

Figure 1. Study sites and Lassa fever virus (LASV) seropositivity for study of influence of landscape patterns on exposure to LASV, Guinea. A) Map of West Africa and Guinea showing coastal and forested sites for the study. Inset shows location of Guinea in Africa. B) LASV-specific IgG seropositivity (%) by village across the coastal and forested sites.

from the original study. In total, we tested 516 samples from the Macenta Prefecture cohort for the presence of LASV-specific IgG. One sample was not analyzed because not enough serum remained to run the assay. For our analysis, we included 68 samples from Guéckédou, collected in 2018 in the context of a longitudinal study of EVD survivors in the Macenta Prefecture population because both Guéckédou and Macenta Prefecture are located within Guinée Forestière.

Blood Sample Collection and Processing

We collected samples (5–20 mL) of human peripheral blood into nonanticoagulant Vacutainer blood collection tubes (Becton, Dickinson and Company, https://www.bd.com). Blood clotted within 2 hours, and we transported samples to the laboratory at 4°C. We centrifuged samples at 2,000 × *g* for 10 min at room temperature and aliquoted serum into 2-mL microtube tubes (Starsted, https://www.sarstedt.com) in an air-purifying class II microbiologic safety cabinet (Envair, https://envairtechnology.com). We shipped aliquots of serum samples at –20°C; we processed and stored samples at –80°C at Public Health England's Porton Down laboratories.

Samples Analysis by LASV-Specific ELISA

LASV exposure, which is defined as the contact with the virus, can be assessed by the presence of LASV-specific antibodies in the blood (*27*). We used the Blackbox LASV IgG Kit from Bernhard Nocht Institute for Tropical Medicine in Germany (https://www.bnitm.de) for qualitative serologic detection of acute or past LASV infection (*28*,*29*). We used the kit according to the manufacturer's instructions; all reagents were provided, including positive and negative controls. We ran each sample as single replicate. After washing them with a saline solution, we transferred 25 μL of diluted biotinylated recombinant LASV nucleoprotein onto the ELISA plate and added 25 μL of diluted sample before plate incubation for 24 h at 4°C. After a wash step, we added 50 μL of diluted streptavidin horseradish peroxidase and incubated the plate for 1 h at 4°C. Finally, we developed the plate by using 100 μL/well of 3,3′,5,5′-tetramethylbenzidine peroxidase substrate and stopped the chemical reaction by using 100 μL/well of 1 mol/L H_2SO_4. We obtained optical density (OD) readings at wavelengths 450–620 nm ($OD_{450–620}$) by using SpectraMax plate reader with SoftMaxPro 9 software (Molecular Devices, https://www.moleculardevices.com). OD is a term used to describe the propagation of the light induced by the reaction. We interpreted results as valid if the following criteria were met: $OD_{450–620}$ of negative control <0.10 and $OD_{450–620}$ of positive control >1.00. We used average absolute $OD_{450–620}$ absorbance value for negative control samples $OD_{Neg,AV}$ to calculate the assay cutoff OD_{CO} according to the formula $OD_{Neg,AV}$ + 0.150 = OD_{CO}. Index values (IVs) are values comparing the ODs of the sample and the cutoff. We calculated IV for the tested samples (IV_{sample}) by using the formula $IV_{sample} = OD_{450–620}$ (sample)/OD_{CO}. Results classification for IV was carried out as follows: $IV_{sample} \geq 1.00$ = positive; $0.90 < IV_{sample} < 1.00$ = equivocal; $IV_{sample} \leq 0.90$ = negative.

Environmental and Spatial Covariates

To assess the effect of land cover and other environmental covariates on LASV exposure, we assembled a dataset of remote sensing–derived land cover maps from 2017 at 100 m resolution (*30*). We reclassified land cover into the following standardized categories, which are mutually exclusive: closed forest (canopy cover >70% of surface area), open forest (canopy cover 15%–70% of surface area), shrubs (woody perennial plants with persistent stems <5 m), vegetation (plants without persistent stems and canopy cover <10% of surface area), and urban or built up areas.

Village populations had been recorded during field surveys. Because villages were only geolocated to centroids, we extracted environmental data within buffer radii of 500 m, 1 km, 2 km, 5 km, and 10 km from the village centroid to represent the possible distributions of the village and lands used (*31*). For all buffer radii, we extracted the proportions of different land cover types and the mean canopy cover. To evaluate the importance of landscape configuration (spatial arrangement of different elements of the landscape) (*32*), we also extracted class-level metrics, including perimeter area ratio, shape index (patch perimeter divided by the minimum possible patch perimeter), and fractal dimension index (an index of shape complexity) (*33*). Those indices are commonly used as measures of landscape fragmentation, with higher values indicating greater levels of fragmentation (*34*,*35*).

Models and Statistical Analyses

Because assays were not validated for quantitative antibody responses, we fit all models by using classified values of seropositivity. To characterize transmission intensity in both sites, we integrated data on age-specific frequency of seropositivity. We fit reversible catalytic models to age-specific seroprevalence

Table. Characteristics of Lassa fever study participants from coastal and forested sites, Guinea

Characteristic	Coastal site	Forested site
No. participants	702	584*
Sex, no. (%)		
M	459 (65.4)	322 (51.1)
F	243 (34.6)	262 (44.9)
Mean age (range), y	32.3 (6–99)	38.8 (17–90)
Sampling dates	2016	2017–2018

*516 in Macenta Prefecture and 68 in the town of Guéckédou.

data by using maximum-likelihood methods (*17*). Those models generate age-specific seroprevalence curves, enabling the calculation of a seroconversion rate (SCR), which representing the force of infection for the community, a measure of transmission intensity (number of infections per person per year). SCR is the rate at which seronegative persons become seropositive; although it is a measure of transmission intensity, SCR is not incidence because it does not capture seropositive persons who are repeatedly exposed. Those models are widely used to characterize transmission of endemic diseases such as malaria (*36*). We used profile likelihood plots to explore possible historical changes in transmission intensity represented by the SCR and selected final models by using likelihood ratio tests (*37*).

We additionally assessed whether fine-scale patterns of seroconversion were associated with landscape characteristics. Because environmental variables can be associated with risk at different spatial scales, we used a data-driven approach to identify environmental risk factors (*38*). Because our environmental dataset was high-dimensional and highly correlated, we first performed mixed-effects logistic regression models for each environmental variable at each spatial scale (126 in total). We excluded from subsequent analysis any environmental variables with p values >0.2. We used Pearson correlation to identify highly correlated variables (Pearson correlation coefficient >0.75). For these highly correlated variables (e.g., environmental factors at different spatial scales), we identified a single variable for inclusion based on the Akaike information criteria. Because sampling frames were different between sites, we ran models separately for both sites, using the primary outcome as the binary classification for person-level seropositivity. We fitted models with village as a random effect to account for observations within villages lacking independence. We first assessed associations with key demographic factors, including sex, continuous age, and age category. For the forested site model, we included only environmental predictors because demographic factors (age and sex) were not associated with exposure risks. For the coastal site, we included age category in all models in addition to environmental predictors. When assessing for inclusion in the multivariate analysis, we considered univariate results to be statistically significant at p<0.2 to avoid exclusion of variables that alone lack significance but contribute in the presence of other variables. We conducted final multivariate model selection by using the dredge function in the MuMIn package (*39*), selecting the best model according to the Akaike information criteria and using model averaging approaches to obtain average regression coefficients for the best fitting models. The code for environmental data extraction and model fitting is available online (https://github.com/kfornace/LFV_environmental).

Results

In this study, we assessed LASV IgG seropositivity in 1,286 persons by using serum samples collected in 2 sites in Guinea during 2016–2018. In the coastal site, we analyzed 702 samples (Table; Figure 1, panel A; Appendix Table 1, https://wwwnc.cdc.gov/EID/article/29/2/21-2525-App1.pdf). In the forested site, we analyzed 516 samples from Macenta Prefecture and 68 from the town of Guéckédou (Table; Figure 1, panel A; Appendix Table 2).

We observed that exposure to LASV was highly heterogenous both between and within each study site (Figure 1, panel B). The LASV IgG seropositivity was 11.9% (95% CI 9.7%–14.5%) in the coastal site (Figure 1, panel B; Appendix Table 1), whereas it was 59.6% (95% CI 55.5%–63.5%) in the forested site (Figure 1, panel B; Appendix Table 2).

Demographic characteristics of exposed persons varied by study site. In the coastal site, seropositivity in women was 9.0% (95% CI 5.8%–13.1%) and in men was 13.5% (95% CI 11.0%–17.0%). For the forested site, seropositivity in women was 61.8% (95% CI 56.0%–67.7%) and in men was 58.0% (95% CI 52.5%–63.3%). Sex was not significantly associated with seropositivity in either site (coastal site, odds ratio 1.25 [95% CI 0.69–2.27], p = 0.46; forested site, odds ratio 0.90 [95% CI 0.61–1.33], p = 0.59).

Age patterns of seropositivity differed markedly between sites. In the coastal site, exposure was strongly associated with age, and seropositivity increased with age (Figure 2, panel A). In that population, reversible catalytic models estimated the force of infection (SCR) as 0.0041 (95% CI 0.0033–0.0050). We observed no changes in historical transmission intensity (p = 0.328). In contrast, in the forested site, we identified no clear age patterns, and neither continuous nor categorical age were associated with person-level seropositivity (Figure 2, panel B).

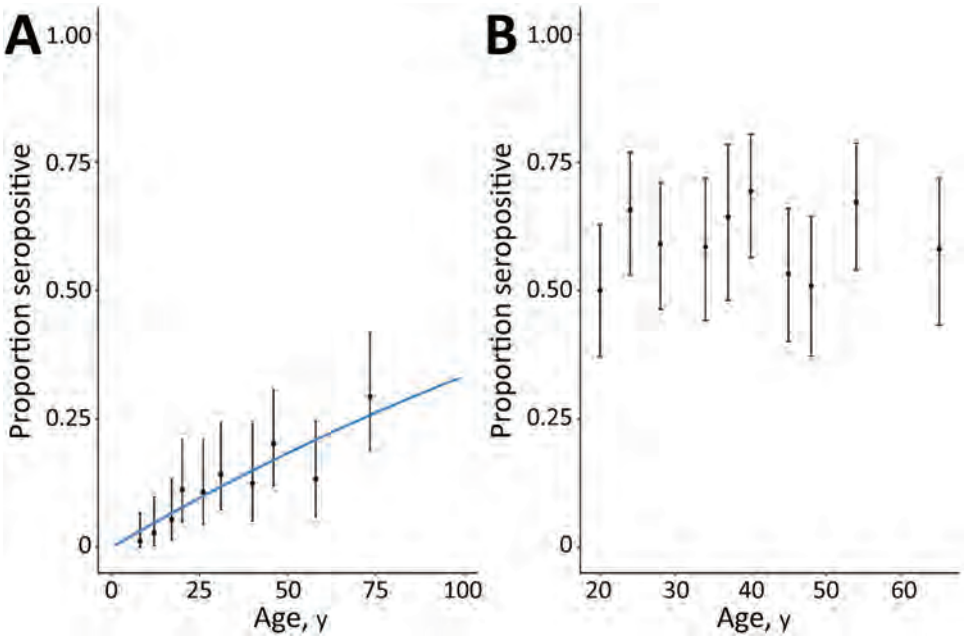

Figure 2. Lassa fever virus (LASV) seropositivity by age for study of influence of landscape patterns on exposure to LASV, by study site, Guinea. Dots show the proportion of LASV seropositive persons (no. positive/total no.) by age decile for the coastal site (A) and the forested site (B). Blue line indicates modeled seroconversion rate curve. Error bars indicate 95% CIs.

Although age ranges for included persons were different between both sites (Table), we detected substantial differences in exposure risks in similar age groups between sites. For example, persons 17–20 years of age had an estimated seropositivity of 5.4% (95% CI 1.5%–13.3%) in the coastal site, compared with 50.0% in the forested site j(95% CI 37.2%–62.8%). The high proportions of seropositivity in the youngest age groups and lack of association with age precluded fitting reversible catalytic models for the forested region.

Despite clear differences in seropositivity between sites, we identified strong associations between exposure and environmental factors for both sites (Figure 3). As characterized by perimeter area ratios, fragmentation was strongly positively associated with exposure risk for both sites (Figure 4; Appendix Tables 3, 4). In the coastal site, odds of exposure increased with the perimeter area ratio of built-up areas but were lower where the proportion of vegetation in the landscape was higher. The fractal dimension index measuring fragmentation of shrubland was not

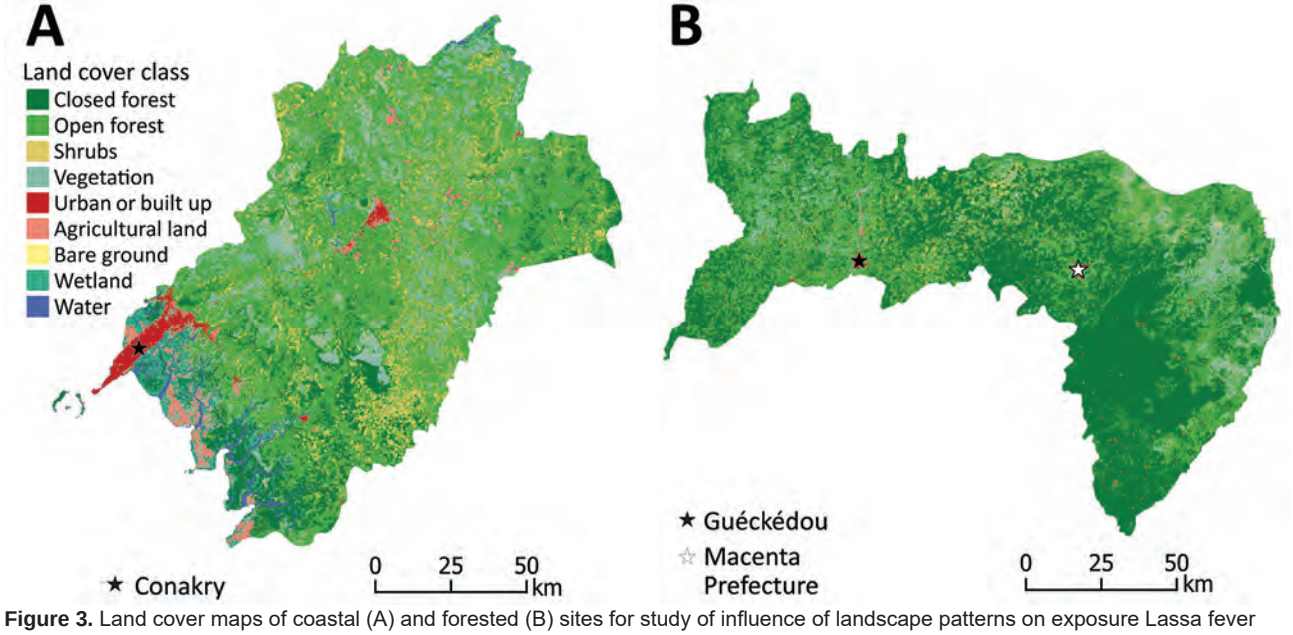

Figure 3. Land cover maps of coastal (A) and forested (B) sites for study of influence of landscape patterns on exposure Lassa fever virus, Guinea.

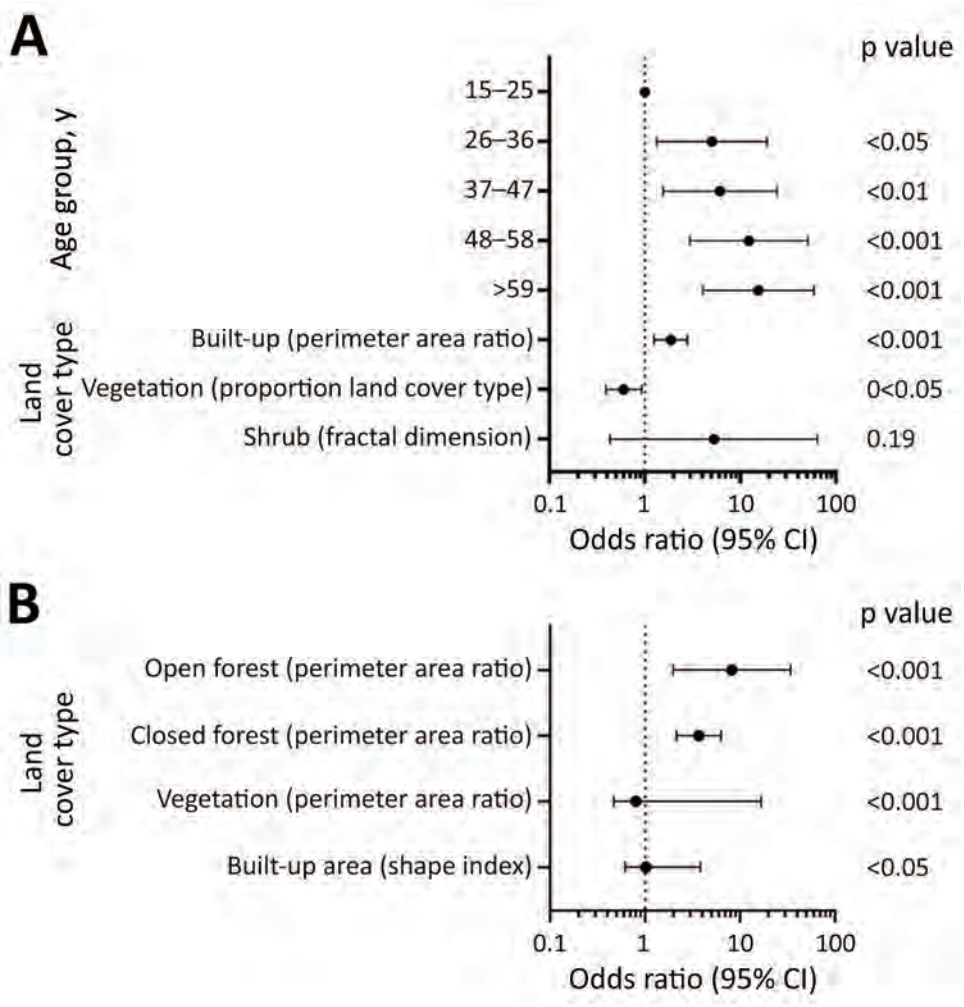

Figure 4. Associations between Lassa fever virus exposure risk and environmental factors by study site for study of influence of landscape patterns on exposure Lassa fever virus, Guinea. A) Coastal site. B) Forested site

significantly associated with exposure risk but improved overall model fit (Figure 4, panel A; Appendix Table 3). In the forested site, higher perimeter area ratios of both open and closed forests and the shape index of built areas, all indicating higher fragmentation levels, were positively associated with risk, whereas for vegetation a high perimeter area ratio was protective (Figure 4, panel B; Appendix Table 4). Across both sites, significant variables were identified at different spatial scales.

Discussion

This study aimed to estimate LASV transmission intensity from serologic data in Guinea and analyze environmental risk factors. We found that LASV seropositivity was significantly greater in the forested site than in the coastal site. In 1993, Lukashevich et al. (*20*) also found high LASV nucleoprotein–specific IgG positivity among inhabitants of tropical forest (Guéckédou, Yomou, and Lola prefectures) and Guinea savannah (Faranah and Kindia prefectures) (25%–55%) and a lower positivity among inhabitants of mountainous areas (Pita, Labe, and Mali prefectures) and coastal areas (Boffa and Boké prefectures) (4%–7%).

We found that sex was not significantly associated with seropositivity in either site. This result was consistent with previous studies conducted in Guinea and Sierra Leone (*15*,*20*).

Our findings showed a significant increase in LASV IgG seropositivity with age in the coastal site but not in the forested site. Because no persons <16 years of age were included in our study, additional serologic studies of children would be needed to assess the age of exposure and how this is affected by environment. Although previous studies did not detect any correlation between antibody prevalence and age in these regions (*20*), differences in age patterns of seropositivity between regions were observed in other studies in West Africa. A study conducted in a forested region in 2000 found that children <10 and adults 20–29 years of age had the highest LASV IgG prevalence (*6*). A study conducted in

Sierra Leone found that antibody prevalence increased with age, reaching a peak at 20–50 years of age and decreasing thereafter (*15*). A similar trend was reported in a 2015 study conducted in Nigeria (*40*). Age, often associated with differences in occupation or daily activities, may play a role in exposure (e.g., bushmeat hunters are mainly young to middle-age men and may have more contact with rodents). However, our results in the forested site suggest that in some areas, age-independent factors such as environmental features may have a greater effect on exposure risk.

All models showed an association between landscape patterns and exposure risk for both study sites (Appendix Tables 3–6). Associations between landscape fragmentation and exposure risk to zoonotic diseases also have been observed for malaria (*41*,*42*) and Ebola virus (*43*). Fragmentation may affect disease transmission by increasing spatial overlap between humans and wildlife populations at habitat edges (*41*). In our study, the fragmentation and the proportion of forests appear to affect exposure risk but their exact role in the complex dynamics of LASV circulation remains to be determined. Because the distribution of Natal multimammate rats is the leading LASV risk factor (*9*), the link between landscape patterns and the distribution of rodent reservoirs should be further explored. Of interest, one study found that the proportion of LASV-infected Natal multimammate rats was higher in forested regions than in coastal regions (*13*).

One limitation of our study is that, although the Blackbox IgG ELISA was shown to be sensitive (90%) and very specific (99%) (*28*), it was not tested against other arenaviruses because of a lack of suitable serum panels. We cannot fully exclude the potential circulation of related or yet undescribed arenaviruses in specific regions (*44*) and a partial cross-reactivity of antibodies against other arenaviruses. In addition, because the samples were collected as part of a vaccine evaluation and a seroepidemiologic study on Ebola virus, the sampling procedure was not standardized between the studies. Because the sampling approaches were not designed to be representative of the wider populations across Guinea, the estimates cannot be used to generalize about population-level disease risks.

In addition, behavioral exposure risks (e.g., occupation, medical history, hunting or foraging habits, location of previous residence, methods for food storage, and rodent trapping around the house) could not be evaluated because we did not collect person-level questionnaire data. Future studies could assess the number of persons in the household, the quality of the building, and proximity to rodent burrows. This study measured only IgG in serum samples collected at a single timepoint. As such, our data do not enable us to capture the potential effect of changes in seasonal rodent activity, vegetation patterns surrounding the villages, or the fluctuation of LASV persistence in rodents linked to climate variation. Because persons tend to move frequently across wide regions, either to find work during harvest season or to hunt (*45*) or in response to EVD hotspots, they may have been exposed to LASV in a different location from their current residence.

Because samples were not collected uniformly from younger age groups and a high proportion of persons from the forested region were exposed by 18 years of age, transmission intensity could not be directly compared between sites using reversible catalytic models. Although population-based epidemiologic studies are required to characterize wider LASV exposure and risk factors, the differences between these populations surveyed highlight the potential heterogeneity of LASV transmission intensity in Guinea.

In conclusion, LASV dynamics result from complex interactions between several human and environmental factors. Our study compared the LASV-specific IgG seropositivity in coastal and forested regions in Guinea and described associations between exposure to LASV and landscape patterns. Enhanced knowledge of regions with a potentially increased risk for LASV exposure can help improve epidemiologic surveillance; devise a global approach to optimize the health of humans, animals, and the environment; and highlight potential trial sites to assess new LASV vaccines and therapeutics.

This work was funded by the US Food and Drug Administration (grant no. HHSF223201510104C) and the CGIAR Research Program on Agriculture for Nutrition and Health (grant no. A4NH). S.G. was supported by grants from the German Research Foundation (grant nos. GU883/5-1 and GU883/5-2). K.F. is supported by a Sir Henry Dale Fellowship jointly funded by the Wellcome Trust and the Royal Society (grant no. 221963/Z/20/Z).

About the Author

Dr. Longet is a postdoctoral researcher in immunology at the University of Oxford. She specializes in infectious diseases and vaccines.

References

1. Hensley LE, Smith MA, Geisbert JB, Fritz EA, Daddario-DiCaprio KM, Larsen T, et al. Pathogenesis of Lassa fever in cynomolgus macaques. Virol J. 2011;8:205. https://doi.org/10.1186/1743-422X-8-205
2. Richmond JK, Baglole DJ. Lassa fever: epidemiology, clinical features, and social consequences. BMJ. 2003;327:1271–5. https://doi.org/10.1136/bmj.327.7426.1271

3. McCormick JB, Walker DH, King IJ, Webb PA, Elliott LH, Whitfield SG, et al. Lassa virus hepatitis: a study of fatal Lassa fever in humans. Am J Trop Med Hyg. 1986;35:401–7. https://doi.org/10.4269/ajtmh.1986.35.401
4. Monath TP, Newhouse VF, Kemp GE, Setzer HW, Cacciapuoti A. Lassa virus isolation from *Mastomys natalensis* rodents during an epidemic in Sierra Leone. Science. 1974;185:263–5. https://doi.org/10.1126/science.185.4147.263
5. Fisher-Hoch SP, Tomori O, Nasidi A, Perez-Oronoz GI, Fakile Y, Hutwagner L, et al. Review of cases of nosocomial Lassa fever in Nigeria: the high price of poor medical practice. BMJ. 1995;311:857–9. https://doi.org/10.1136/bmj.311.7009.857
6. Kernéis S, Koivogui L, Magassouba N, Koulemou K, Lewis R, Aplogan A, et al. Prevalence and risk factors of Lassa seropositivity in inhabitants of the forest region of Guinea: a cross-sectional study. PLoS Negl Trop Dis. 2009;3:e548. https://doi.org/10.1371/journal.pntd.0000548
7. Stephenson EH, Larson EW, Dominik JW. Effect of environmental factors on aerosol-induced Lassa virus infection. J Med Virol. 1984;14:295–303. https://doi.org/10.1002/jmv.1890140402
8. Ajayi NA, Nwigwe CG, Azuogu BN, Onyire BN, Nwonwu EU, Ogbonnaya LU, et al. Containing a Lassa fever epidemic in a resource-limited setting: outbreak description and lessons learned from Abakaliki, Nigeria (January–March 2012). Int J Infect Dis. 2013;17:e1011–6. https://doi.org/10.1016/j.ijid.2013.05.015
9. Fichet-Calvet E, Lecompte E, Koivogui L, Soropogui B, Doré A, Kourouma F, et al. Fluctuation of abundance and Lassa virus prevalence in *Mastomys natalensis* in Guinea, West Africa. Vector Borne Zoonotic Dis. 2007;7:119–28. https://doi.org/10.1089/vbz.2006.0520
10. Redding DW, Gibb R, Dan-Nwafor CC, Ilori EA, Yashe RU, Oladele SH, et al. Geographical drivers and climate-linked dynamics of Lassa fever in Nigeria. Nat Commun. 2021;12:5759. https://doi.org/10.1038/s41467-021-25910-y
11. Olayemi A, Oyeyiola A, Obadare A, Igbokwe J, Adesina AS, Onwe F, et al. Widespread arenavirus occurrence and seroprevalence in small mammals, Nigeria. Parasit Vectors. 2018;11:416. https://doi.org/10.1186/s13071-018-2991-5
12. Olayemi A, Cadar D, Magassouba N, Obadare A, Kourouma F, Oyeyiola A, et al. New hosts of the Lassa virus. Sci Rep. 2016;6:25280. https://doi.org/10.1038/srep25280
13. Lecompte E, Fichet-Calvet E, Daffis S, Koulémou K, Sylla O, Kourouma F, et al. *Mastomys natalensis* and Lassa fever, West Africa. Emerg Infect Dis. 2006;12:1971–4. https://doi.org/10.3201/eid1212.060812
14. Ogbu O, Ajuluchukwu E, Uneke CJ. Lassa fever in West African sub-region: an overview. J Vector Borne Dis. 2007;44:1–11.
15. McCormick JB, Webb PA, Krebs JW, Johnson KM, Smith ES. A prospective study of the epidemiology and ecology of Lassa fever. J Infect Dis. 1987;155:437–44. https://doi.org/10.1093/infdis/155.3.437
16. Bond N, Schieffelin JS, Moses LM, Bennett AJ, Bausch DG. A historical look at the first reported cases of Lassa fever: IgG antibodies 40 years after acute infection. Am J Trop Med Hyg. 2013;88:241–4. https://doi.org/10.4269/ajtmh.12-0466
17. Drakeley CJ, Corran PH, Coleman PG, Tongren JE, McDonald SL, Carneiro I, et al. Estimating medium- and long-term trends in malaria transmission by using serological markers of malaria exposure. Proc Natl Acad Sci U S A. 2005;102:5108–13. https://doi.org/10.1073/pnas.0408725102
18. Greenhouse B, Daily J, Guinovart C, Goncalves B, Beeson J, Bell D, et al.; Malaria Serology Convening. Priority use cases for antibody-detecting assays of recent malaria exposure as tools to achieve and sustain malaria elimination. Gates Open Res. 2019;3:131. https://doi.org/10.12688/gatesopenres.12897.1
19. Arnold BF, Scobie HM, Priest JW, Lammie PJ. Integrated serologic surveillance of population immunity and disease transmission. Emerg Infect Dis. 2018;24:1188–94. https://doi.org/10.3201/eid2407.171928
20. Lukashevich IS, Clegg JC, Sidibe K. Lassa virus activity in Guinea: distribution of human antiviral antibody defined using enzyme-linked immunosorbent assay with recombinant antigen. J Med Virol. 1993;40:210–7. https://doi.org/10.1002/jmv.1890400308
21. Bausch DG, Demby AH, Coulibaly M, Kanu J, Goba A, Bah A, et al.; Epidemiology of Human Disease and Clinical Observations. Lassa fever in Guinea: I. Epidemiology of human disease and clinical observations. Vector Borne Zoonotic Dis. 2001;1:269–81. https://doi.org/10.1089/15303660160025903
22. L'Institut Guinéen d'Études et de Sondages. Histoire politique de la Guinée [cited 2022 Oct 18]. https://www.iges-guinee.com/histoire-politique-de-la-guinee
23. République de Guinée. Institut National de la Statistique [cited 2022 Oct 18]. https://www.stat-guinee.org
24. Wey J, Guillaume J, Kolie D, Souma Y, Cisse S, Traoré S. Guinée Forestière: de l'etude de systemes de productions a base riz pluvial à la conception de systemes d'agriculture durable. 2001 [cited 2022 Oct 18]. https://agritrop.cirad.fr/485415/1/document_485415.pdf
25. Diallo MB. Présentation générale du pays et méthodologie de l'enquête: caractéristiques de la Guinée [cited 2022 Oct 18]. https://dhsprogram.com/pubs/pdf/FR109/01Chapitre01.pdf
26. Thom R, Tipton T, Strecker T, Hall Y, Akoi Bore J, Maes P, et al. Longitudinal antibody and T cell responses in Ebola virus disease survivors and contacts: an observational cohort study. Lancet Infect Dis. 2021;21:507–16. https://doi.org/10.1016/S1473-3099(20)30736-2
27. Ogunro BN, Olugasa BO, Kayode A, Ishola OO, Kolawole ON, Odigie EA, et al. Detection of antibody and antigen for Lassa virus nucleoprotein in monkeys from southern Nigeria. J Epidemiol Glob Health. 2019;9:125–7. https://doi.org/10.2991/jegh.k.190421.001
28. Gabriel M, Adomeh DI, Ehimuan J, Oyakhilome J, Omomoh EO, Ighodalo Y, et al. Development and evaluation of antibody-capture immunoassays for detection of Lassa virus nucleoprotein-specific immunoglobulin M and G. PLoS Negl Trop Dis. 2018;12:e0006361. https://doi.org/10.1371/journal.pntd.0006361
29. Schmitz H, Gabriel M, Emmerich P. Specific detection of antibodies to different flaviviruses using a new immune complex ELISA. Med Microbiol Immunol (Berl). 2011;200:233–9. https://doi.org/10.1007/s00430-011-0195-0
30. Buchhorn M, Smets B, Bertels L, De Roo B, Lesiv M, Tsendbazar N-E, et al. Copernicus Global Land Service: land cover 100m: collection 3: epoch 2019: globe. 2020 Sep 8 [cited 2022 May 27]. https://zenodo.org/record/3939050
31. Brock PM, Fornace KM, Grigg MJ, Anstey NM, William T, Cox J, et al. Predictive analysis across spatial scales links zoonotic malaria to deforestation. Proc Biol Sci. 2019;286:20182351.
32. Thierry H, Rose E, Rogers H. Landscape configuration and frugivore identity affect seed rain during restoration. Oikos. 2021 Oct 1 [cited 2022 May 27]. https://onlinelibrary.wiley.com/doi/full/10.1111/oik.08323

33. McGarigal K, Cushman S, Catherine Neel M.E.E. Spatial pattern analysis program for categorical maps. 2002 [cited 2022 May 27]. https://github.com/kmcgarigal/Fragstats
34. Flowers B, Huang K-T, Aldana G. Analysis of the habitat fragmentation of ecosystems in Belize using landscape metrics. Sustainability. 2020;12:3024. https://doi.org/10.3390/su12073024
35. Liu Z, He C, Wu J. The relationship between habitat loss and fragmentation during urbanization: an empirical evaluation from 16 world cities. PLoS One. 2016;11:e0154613. https://doi.org/10.1371/journal.pone.0154613
36. Cook J, Reid H, Iavro J, Kuwahata M, Taleo G, Clements A, et al. Using serological measures to monitor changes in malaria transmission in Vanuatu. Malar J. 2010;9:169. https://doi.org/10.1186/1475-2875-9-169
37. Stewart L, Gosling R, Griffin J, Gesase S, Campo J, Hashim R, et al. Rapid assessment of malaria transmission using age-specific sero-conversion rates. PLoS One. 2009;4:e6083. https://doi.org/10.1371/journal.pone.0006083
38. Fornace KM, Brock PM, Abidin TR, Grignard L, Herman LS, Chua TH, et al. Environmental risk factors and exposure to the zoonotic malaria parasite *Plasmodium knowlesi* across northern Sabah, Malaysia: a population-based cross-sectional survey. Lancet Planet Health. 2019;3:e179–86. https://doi.org/10.1016/S2542-5196(19)30045-2
39. Bartoń K. Package "MuMIn". 2022 Oct 12 [cited 2022 Oct 18]. https://cran.r-project.org/web/packages/MuMIn/MuMIn.pdf
40. Tobin E, Asogun D, Akpede N, Adomeh D, Odia I, Gunther S. Lassa fever in Nigeria: insights into seroprevalence and risk factors in rural Edo State: a pilot study. J Med Trop. 2015;17:51–5. https://doi.org/10.4103/2276-7096.162258
41. Fornace KM, Abidin TR, Alexander N, Brock P, Grigg MJ, Murphy A, et al. Association between landscape factors and spatial patterns of *Plasmodium knowlesi* infections in Sabah, Malaysia. Emerg Infect Dis. 2016;22:201–8. https://doi.org/10.3201/eid2202.150656
42. Stefani A, Dusfour I, Corrêa AP, Cruz MC, Dessay N, Galardo AK, et al. Land cover, land use and malaria in the Amazon: a systematic literature review of studies using remotely sensed data. Malar J. 2013;12:192. https://doi.org/10.1186/1475-2875-12-192
43. Olivero J, Fa JE, Real R, Márquez AL, Farfán MA, Vargas JM, et al. Recent loss of closed forests is associated with Ebola virus disease outbreaks. Sci Rep. 2017;7:14291. https://doi.org/10.1038/s41598-017-14727-9
44. Coulibaly-N'Golo D, Allali B, Kouassi SK, Fichet-Calvet E, Becker-Ziaja B, Rieger T, et al. Novel arenavirus sequences in *Hylomyscus* sp. and *Mus* (*Nannomys*) *setulosus* from Côte d'Ivoire: implications for evolution of arenaviruses in Africa. PLoS One. 2011;6:e20893. https://doi.org/10.1371/journal.pone.0020893
45. Mari Saez A, Cherif Haidara M, Camara A, Kourouma F, Sage M, Magassouba N, et al. Rodent control to fight Lassa fever: evaluation and lessons learned from a 4-year study in Upper Guinea. PLoS Negl Trop Dis. 2018;12:e0006829. https://doi.org/10.1371/journal.pntd.0006829

Address for correspondence: Miles W. Carroll and Stephanie Longet, Pandemic Sciences Institute, Nuffield Department of Medicine University of Oxford, Oxford, OX3 7BN, UK; email: miles.carroll@ndm.ox.ac.uk and stephanie.longet@well.ox.ac.uk

Increased Multidrug-Resistant *Salmonella enterica* I Serotype 4,[5],12:i:- Infections Associated with Pork, United States, 2009–2018

Ian D. Plumb, Allison C. Brown, Erin K. Stokes, Jessica C. Chen, Heather Carleton, Beth Tolar, Preethi Sundararaman, Amy Saupe, Daniel C. Payne, Hazel J. Shah, Jason P. Folster, Cindy R. Friedman

Reports of *Salmonella enterica* I serotype 4,[5],12:i:- infections resistant to ampicillin, streptomycin, sulphamethoxazole, and tetracycline (ASSuT) have been increasing. We analyzed data from 5 national surveillance systems to describe the epidemiology, resistance traits, and genetics of infections with this *Salmonella* strain in the United States. We found ASSuT-resistant *Salmonella* 4,[5],12:i:- increased from 1.1% of *Salmonella* infections during 2009–2013 to 2.6% during 2014–2018; the proportion of *Salmonella* 4,[5],12:i:- isolates without this resistance pattern declined from 3.1% to 2.4% during the same timeframe. Among isolates sequenced during 2015–2018, a total of 69% were in the same phylogenetic clade. Within that clade, 77% of isolates had genetic determinants of ASSuT resistance, and 16% had genetic determinants of decreased susceptibility to ciprofloxacin, ceftriaxone, or azithromycin. Among outbreaks related to the multidrug-resistant clade, 63% were associated with pork consumption or contact with swine. Preventing *Salmonella* 4,[5],12:i:- carriage in swine would likely prevent human infections with this strain.

Nontyphoidal *Salmonella* infection is the leading cause of global foodborne illnesses (*1*,*2*) and is estimated to cause 1.35 million illnesses annually in the United States (*3*). *Salmonella enterica* I serotype 4,[5],12:i:- (hereafter 4,[5],12:i:-), is a monophasic variant of *Salmonella enterica* serotype Typhimurium lacking expression of the second phase flagellar antigen, which is encoded by the *fljB* gene (*4*,*5*). In the United States, 4,[5],12:i:- is the fifth most commonly reported *Salmonella* serotype causing human illness (*5*).

Infections caused by 4,[5],12:i:- have been increasingly reported since the 1990s (*4*,*6*). In recent years, a multidrug-resistant (MDR) strain of 4,[5],12:i:- has been described in Europe (*7*,*8*), Canada (*9*), Australia (*10*), and the United States (*11*). This MDR strain is characterized by resistance to ampicillin, streptomycin, sulphamethoxazole, and tetracycline (ASSuT). The ASSuT resistance pattern in this strain is encoded by a genomic region containing the antimicrobial drug resistance determinants $bla_{\text{TEM-1B}}$, *strA-strB*, *sul2*, and *tet(B)*, in the usual location of an absent *fljB* gene (*11*,*12*). A separate genomic island (SGI-4) contains genes conferring tolerance to heavy metals (*8*,*11*).

Limited reports are available about the epidemiology of 4,[5],12:i:- in the United States. We used data from 5 national surveillance systems to describe the epidemiology, antimicrobial resistance, and molecular genetics of infections with 4,[5],12:i:- strains that were associated with ASSuT resistance.

Methods

Sources and Analysis of Surveillance Data

Laboratory-based Enteric Disease Surveillance System

The Laboratory-based Enteric Disease Surveillance (LEDS) system of the Centers for Disease Control and Prevention (CDC) collects information on *Salmonella* isolates collected from persons with infections and submitted to state and territorial public health laboratories in the United States (*5*). We summarized the incidence

Author affiliations: Centers for Disease Control and Prevention, Atlanta, Georgia, USA (I.D. Plumb, A.C. Brown, E.K. Stokes, J.C. Chen, H. Carleton, B. Tolar, P. Sundararaman, D.C. Payne, H.J. Shah, J.P. Folster, C.R. Friedman); Minnesota Department of Health, St. Paul, Minnesota, USA (A. Saupe)

DOI: https://doi.org/10.3201/eid2902.220950

of 4,[5],12:i:- during 2009–2018 by using population estimates from the US Census (https://www.census.gov) as denominators and summarized the proportion of nontyphoidal *Salmonella* isolates that were 4,[5],12:i:. Throughout this article, we use the term *Salmonella* to refer to nontyphoidal *Salmonella*; that is, excluding serotypes Typhi and Paratyphi A, C, and tartrate-negative B, which represent <2% of serotyped isolates (*5*).

PulseNet

PulseNet, the national molecular subtyping network for US foodborne disease surveillance, monitors strains of *Salmonella* and other enteric bacteria for potential outbreaks. During 1996–2019, participating laboratories performed molecular subtyping by pulsed-field gel electrophoresis (PFGE) on *Salmonella* isolates by using standard methods (*13*). Since 2015, these laboratories have increasingly performed whole-genome sequencing (WGS). After sequencing isolates using established protocols, participating laboratories analyze sequence data using BioNumerics Software (Applied Maths, http://www.applied-maths.com) (*14*,*15*). When sequences meet PulseNet quality metrics, participating laboratories upload sequence information to the CDC *Salmonella* PulseNet national database with other isolate data and upload a subset of this information to the National Center for Biotechnology Information (https://www.ncbi.nlm.nih.gov). We analyzed PulseNet data for sequenced 4,[5],12:i:- isolates collected during 2015–2018 that were concordant between genotypic serotyping by using SeqSero (http://www.denglab.info/SeqSero) and phenotypic serotyping. We used core genome multilocus sequence typing (cgMLST) to identify phylogenetic clustering of isolates within the PulseNet database. We then used the National Center for Biotechnology Information pathogen detection portal to determine the relationship of clustered isolates to sequences reported in other studies on the basis of single-nucleotide polymorphism analysis (*8*,*11*,*16*,*17*). For a subset of isolates, we determined whether SGI-4 or the *hin* or *iroB* genes were present, because these genetic markers can distinguish 4,[5],12:i:- from some previously reported strains (*11*). We identified antimicrobial resistance determinants (ARDs) and plasmid replicons among sequenced isolates by using previously described protocols (*18*) and assigned predicted antimicrobial resistance using ResFinder and PointFinder drug keys in the National Antimicrobial Resistance Monitoring System (NARMS; https://github.com/StaPH-B/resistanceDetectionCDC). For isolates collected during 2015–2018, we identified PFGE patterns that were specific for membership of a cgMLST clade associated with ASSuT resistance (the MDR clade). We then used these PFGE patterns as a marker of clade expansion during 2009–2018, including a period before WGS data were routinely available.

NARMS

NARMS is a collaboration between CDC, the US Food and Drug Administration (FDA), US Department of Agriculture (USDA), and state and local health departments that monitors antimicrobial resistance of enteric bacteria isolated from ill persons, retail meats, and food animals (*19*). As part of CDC NARMS, public health laboratories submit every 20th nontyphoidal *Salmonella* isolate. CDC performs antimicrobial susceptibility testing by broth microdilution for a standard panel of 14 antimicrobial drug agents and interprets results using Clinical and Laboratory Standards Institute criteria, when available. Testing for decreased susceptibility to azithromycin started in 2011 and is defined as an MIC of ≥0.12 μg/mL (*20*,*21*). We described antimicrobial resistance and changes in resistance patterns among 4,[5],12:i:- isolates collected as part of NARMS surveillance during 2009–2018.

Foodborne Diseases Active Surveillance Network

The Foodborne Diseases Active Surveillance Network (FoodNet) conducts population-based active surveillance for laboratory-confirmed enteric infections, including *Salmonella* (*22*). FoodNet is a collaboration of CDC, 10 state health departments, USDA Food Safety and Inspection Service, and FDA. For each reported *Salmonella* infection, FoodNet collects data on patient demographics, hospitalizations, international travel in the 7 days before illness onset, and whether the infection was associated with a recognized outbreak. Since 2014, FoodNet has also collected data on consumption of pork, chicken, turkey, and beef during the 7 days before illness onset. We compared characteristics of 4,[5],12:i:- infections to other *Salmonella* serotype infections during 2009–2018. After linking FoodNet data with PulseNet data, we compared characteristics of 4,[5],12:i:- infections with PFGE patterns in the MDR clade to 4,[5],12:i:- infections with other PFGE patterns.

National Outbreak Reporting System

The National Outbreak Reporting System (NORS) collects information about outbreaks transmitted by food, water, environmental sources, infected persons or animals, or unknown modes of transmission (*23*). State, local, and territorial public health agencies submit reports to CDC that document outbreak characteristics, food and animal sources, and the pathogens that caused each outbreak. We analyzed NORS data collected during 2009–2018, and obtained PFGE data by linking

with PulseNet. We compared the characteristics of outbreaks from 4,[5],12:i:- with outbreaks from other *Salmonella* serotypes. Among 4,[5],12:i:- outbreaks, we compared outbreaks by whether the PFGE pattern was found in the MDR clade identified in PulseNet.

Statistical Methods

We used a 2-sample test of proportions to compare characteristics of 4,[5],12:i:- infections between 2009–2013 and 2014–2018. We used logistic regression to compare characteristics of *Salmonella* infections and outbreaks by 4,[5],12:i:- serotype and association with the cgMLST clade; we adjusted multivariable logistic regression models for age, sex, race, and ethnicity. We conducted statistical analyses by using SAS version 9.3 (SAS Institute Inc., https://www.sas.com) and Stata 15.0 (StataCorp LLC, https://www.stata.com).

Results

Incidence of Reported Infections

Among *Salmonella* isolates reported to LEDS during 2009–2018, a total of 19,212 (4.3%) were 4,[5],12:i:, and 4,[5],12:i:- was reported from all 50 states. This total represented an average annualized incidence of 0.60 isolates per 100,000 persons. From 2009–2013 to 2014–2018, the frequency of 4,[5],12:i:- increased from 3.7% (7,828 isolates) to 4.9% (11,384 isolates) of reported *Salmonella* (p<0.001); thus, the annualized incidence increased from 0.50 to 0.71 reported infections per 100,000 persons (Appendix 1 Figure 1, https://wwwnc.cdc.gov/EID/article/29/1/22-0950-App1.pdf).

Genotype Characteristics

For the 2015–2018 timeframe, we included 3,036 sequenced 4,[5],12:i:- isolates from the PulseNet database in the analysis (Appendix 2, https://wwwnc.cdc.gov/EID/article/29/1/22-0950-App2.xlsx). Of those, 73% (2,215 isolates) had genetic resistance determinants, and 13% (404 isolates) had predicted resistance to antimicrobial drugs recommended as empiric treatment (first-line agents) for invasive *Salmonella* infections: 11% (320 isolates) were resistant to ciprofloxacin, 4.4% (135 isolates) to ceftriaxone, and 0.5% (14 isolates) to azithromycin (Appendix 1 Table 1). Ciprofloxacin resistance was conferred by the *qnr*B1 gene in 69% (222/320) of isolates; ceftriaxone resistance was conferred most frequently by $bla_{\text{CMY-2}}$ (44%; 60/135 isolates) or $bla_{\text{SHV-12}}$ (34%; 46/135 isolates). Decreased susceptibility to azithromycin was conferred most frequently by *mph*(*A*) (64%; 9/14 isolates). Genes conferring ASSuT resistance were detected in 54% (1,645) of isolates, of which 96% (1,579) carried *aph(3'')-Ib*, *aph(3')-Ia*, *aph(6)-Id*, $bla_{\text{TEM-1B}}$, *sul2*, and *tet*(*B*). Five isolates had determinants of resistance to colistin: 3 isolates had *mcr*-1, 1 had *mcr*-3, and 1 had *pmrB* (Appendix 1 Table 1).

Overall, 69% (2,087/3,036) of 4,[5],12:i:- isolates were part of the MDR clade (median 18 alleles between isolates, range 0–108) (Appendix 1 Figure 2). Within this clade, 77% (1,612/2,087) of isolates had genetic determinants of ASSuT resistance, and 75% (1,561/2,087) had the same combination of *aph(3'')-Ib*, *aph(3')-Ia*, *aph(6)-Id*, $bla_{\text{TEM-1B}}$, *sul2*, and *tet*(*B*); this set of genes was found in only 1.9% (18/949) of isolates outside the MDR clade. Among 4,[5],12:i:- isolates in the clade, 16% (333/2,087) had resistance determinants against first-line antimicrobial agents (ciprofloxacin, ceftriaxone, or azithromycin), compared with 7.5% (71/945) outside the clade (p<0.001). Isolates of 4,[5],12:i:- in the MDR clade were more likely to contain determinants conferring resistance to ciprofloxacin (13% vs. 5.2%; p<0.001) or ceftriaxone (5.4% vs. 2.3%; p<0.001), compared with isolates outside the clade (Appendix 1 Table 2).

Among isolates in the MDR clade, 2,008 (96%) belonged to the same single-nucleotide polymorphism cluster (PDS000076482.92) as previously reported ASSuT-resistant strains (*8*,*11*,*16*). Among a subset of 102 (5.1%) 4,[5],12:i:- isolates in the MDR clade, SGI-4 was detected in all isolates, *iroB* was detected in 99%, and *hin* was absent in 99%.

For isolates with both PFGE and WGS information, 275 PFGE patterns were identified in isolates within the MDR clade. MDR-associated PFGE patterns were detected in only 0.8% (7/937) of isolates outside the MDR clade. During 2009–2018, the proportion of 4,[5],12:i- isolates with MDR-associated PFGE patterns increased from 29% (2,424/8,455) during 2009–2013 to 60% (6,900/11,546) during 2014–2018 (p<0.001) (Figure).

Antimicrobial Susceptibility Testing

During 2009–2018, 4.7% (1,079/23,175) of *Salmonella* isolates included in NARMS surveillance were 4,[5],12:i:-, of which 57% (613 isolates) had decreased susceptibility to antimicrobial drugs, 41% (440 isolates) had a resistance pattern that included ASSuT, and 35% (373 isolates) had only ASSuT resistance. From 2009–2013 to 2014–2018, the percentage of *Salmonella* isolates that were 4,[5],12:i:- increased from 4.3% (476/11,139) to 5.0% (603/12,036; p = 0.009), and the percentage that were 4,[5],12:i:- with ASSuT resistance increased from 1.1% (126/11,139) to 2.6% (p<0.001); meanwhile, the proportion that were 4,[5],12:i:- without ASSuT resistance declined from 3.1% (350/11,139) to 2.4% (289/12,036; p<0.001). Similarly, the percentage of

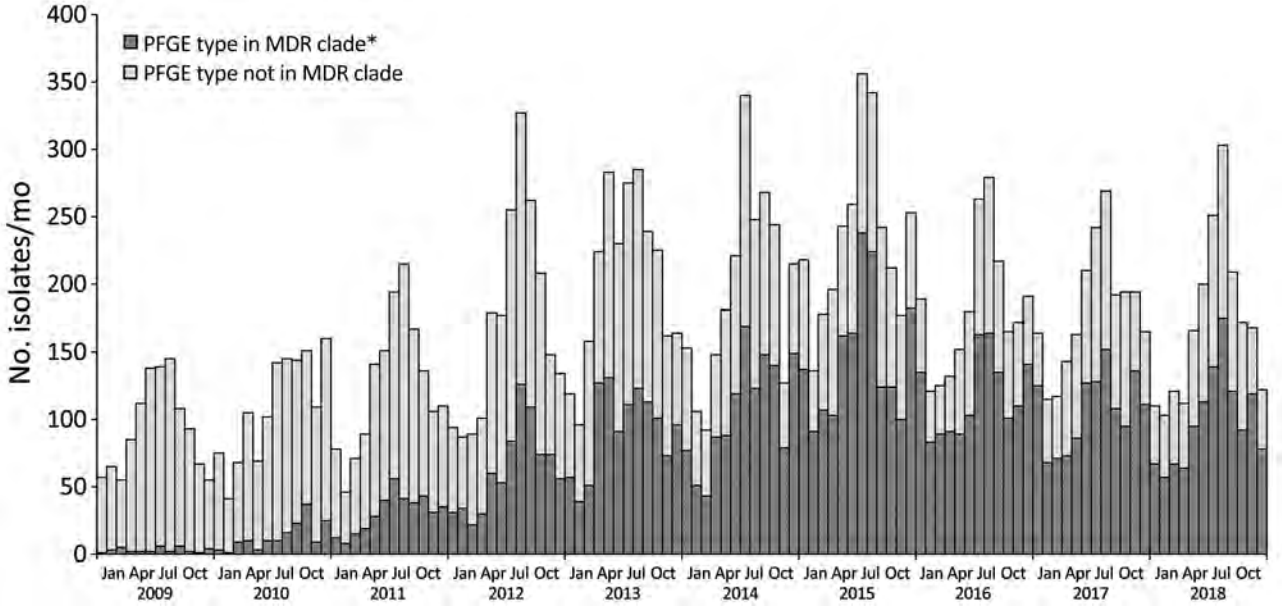

Figure. Clinical multidrug-resistant *Salmonella enterica* I serotype 4,[5],12:i:- in a study of infections associated with pork, United States, 2009–2018. Isolates were identified by whether PFGE pattern was linked to the multidrug resistant cgMLST clade. Among 3,007 sequenced clinical PulseNet isolates during 2015–2018 that had PFGE information, 69% (n = 2,070) belonged to a cgMLST clade associated with multidrug resistance containing 275 PFGE patterns; those patterns also were noted in 0.8% (7/937) of isolates outside the clade. cgMLST, core genome multilocus sequence type; PFGE, pulse-field gel electrophoresis.

Salmonella isolates that were 4,[5],12:i:- with PFGE patterns in the MDR clade increased, whereas the percentage that were 4,[5],12:i:- without those PFGE patterns declined (Appendix 1 Table 3, Figures 3, 4).

Overall, 8.4% (91/1,079) of 4,[5],12:i:- isolates had decreased susceptibility to first-line antimicrobial drugs: ciprofloxacin (6.1%, 66 isolates), ceftriaxone (2.9%, 31 isolates), or azithromycin (0.3%, 3 isolates). The percentage of 4,[5],12:i:- isolates that had decreased susceptibility to these drugs increased from 3.4% (16/476) during 2009–2013 to 12% (75/603) during 2014–2018 ($p<0.001$), including an increase in ciprofloxacin resistance from 1.1% (5 isolates) to 10% (66 isolates; $p<0.001$). Ciprofloxacin resistance increased between these periods, both among 4,[5],12:i:- isolates with PFGE patterns found in the MDR clade (1.0% to 7.4%; $p<0.001$), and among 4,[5],12:i:- isolates without MDR-associated PFGE patterns (1.8% to 12%; $p = 0.001$) (Appendix 1 Tables 3, 4).

Case Characteristics

During 2009–2018, FoodNet sites reported 3,772 infections caused by 4,[5],12:i:-. Among infections with specified patient information, 29% (1,053/3,666) were in patients admitted to a hospital overnight, 4.1% (154/3772) of patients had bacteremia, and 0.5% (17/3,669) of patients died. Compared with other *Salmonella* infections, 4,[5],12:i:- infection was less frequently associated with international travel (adjusted odds ratio [aOR] 0.72, CI 0.62–0.83) (Table 1). Infection with 4,[5],12:i:- was more likely in the 1–18 year age group (aOR 1.83, 95% CI 1.58–2.12; referent age group <1 year of age), and for persons whose race and ethnicity was Black, non-Hispanic (aOR 1.29, 95% CI 1.17–1.42), other non-White/non-Hispanic (aOR 1.44, 95% CI 1.27–1.63), or Hispanic (aOR 1.28, 95% CI 1.15–1.42) (Table 1).

Of 3,160 (84%) 4,[5],12:i:- infections with PFGE information, 1,427 (45%) had PFGE patterns found in the MDR clade. Among 4,[5],12:i:- infections, those linked to the MDR clade were associated with the 18–64 years of age group (aOR 1.42, 95% CI 1.02–1.97). Infections linked to the MDR clade also were associated with being Black and non-Hispanic (aOR 1.66, 95% CI 1.34–2.06), other non-White race with non-Hispanic ethnicity (aOR 2.46, 95% CI 1.88–3.23), having Hispanic ethnicity (aOR 2.26, 95% CI 1.80–2.83), and international travel (aOR 1.62, CI 1.17–2.24) (Table 2).

Pork consumption was more frequently associated with serotype 4,[5],12:i:- compared with other *Salmonella* infections (aOR 1.39, CI 1.18–1.65), and among 4,[5],12:i:- infections, consumption of pork was associated with PFGE patterns found in the MDR clade (aOR 1.86, CI 1.29–2.67). Those associations persisted after we excluded the 222 (5.9%) cases linked to recognized outbreaks (Appendix 1 Table 5).

Table 1. Characteristics of multidrug-resistant *Salmonella enterica* 4,[5],12:i:- and other nontyphoidal *Salmonella* infections, United States, 2009–2018*

Characteristic	*Salmonella* 4,[5],12:i:-, n = 3,772	Other nontyphoidal *Salmonella*, n = 65,518	Odds ratio (95% CI)	Adjusted odds ratio (95% CI)†
Age group, y	N = 3,772	N = 65,509		
<1	258 (6.8)	6,157 (9.4)	Referent	Referent
1–17	1,440 (38.2)	18,614 (28.4)	1.85 (1.61–2.11)	1.83 (1.58–2.12)
18–64	1,618 (42.9)	31,493 (48.1)	1.23 (1.07–1.40)	1.25 (1.08–1.45)
≥65	456 (12.1)	9,245 (14.1)	1.18 (1.01–1.38)	1.27 (1.07–1.50)
Sex	N = 3,771	N = 65,424		
M	1,887 (50)	30,825 (47.1)	Referent	Referent
F	1,884 (50)	34,599 (52.9)	0.89 (0.83–0.95)	0.93 (0.86–0.99)
Race and ethnicity	N = 3,728	N = 54,505		
White, non-Hispanic	1,916 (58.5)	36,240 (66.5)	Referent	Referent
Black, non-Hispanic	559 (17.1)	7,769 (14.3)	1.36 (1.23–1.50)	1.29 (1.17–1.42)
Hispanic	485 (14.8)	6,634 (12.2)	1.38 (1.25–1.53)	1.28 (1.15–1.42)
Other, non-Hispanic	318 (9.7)	3,862 (7.1)	1.56 (1.38–1.76)	1.44 (1.27–1.63)
International travel	220 (6.7), n = 3,275	4,848 (9.4), n = 51,516	0.69 (0.6–0.8)	0.72 (0.62–0.83)
Clinical outcome	N = 3,669	N = 63,696		
Hospitalized	1,053 (28.7)	18,219 (28.7)	1.00 (0.93–1.08)	1.03 (0.95–1.12)
Died	17 (0.5)	260 (0.4)	1.14 (0.69–1.86)	1.15 (0.67–1.99)

*Values are no. (%) except as indicated.
†Adjusted for age, sex, race, and ethnicity.

Outbreaks

During 2009–2018, 123 outbreaks caused by 4,[5],12:i:- were reported from 37 states, comprising 2,004 reported outbreak-associated illnesses, 295 hospitalizations, and 3 deaths. The percentage of *Salmonella* outbreaks attributed to 4,[5],12:i:- increased from 4.5% (42/926) during 2009–2013 to 7.9% (81/1,026) during 2014–2018 (OR 1.80, CI 1.23–2.65) (Appendix 1 Figure 5). Among the 123 outbreaks of 4,[5],12:i:- infections, 61% (75 outbreaks) were linked to food, 15% (18 outbreaks) to animal contact, and 5.7% (7 outbreaks) to transmission from other humans; 19% (23 outbreaks) had an unknown transmission mode (Table 3).

Of 114 4,[5],12:i:- outbreaks with PFGE information, 62.2% (74 outbreaks) had PFGE patterns found in the MDR clade. Among these 114 outbreaks, 22 were linked to a single food source, of which 12 were linked to pork; among those 12, 11 had PFGE patterns found in the MDR clade. Among 12 outbreaks linked to contact with a single animal, 5 were linked to contact with swine; all 5 had PFGE patterns found in the MDR clade. Foodborne outbreaks of 4,[5],12:i:- infections with PFGE patterns in the MDR clade were also linked to consumption of chicken, turkey, and a dairy product. Additional outbreaks were linked to contact with live poultry and cattle. Compared with 4,[5],12:i:- outbreaks showing other PFGE patterns,

Table 2. Characteristics of multidrug-resistant *Salmonella enterica* 4,[5],12:i:- infections, United States, 2009–2018*

Characteristics	PFGE link to MDR clade		Odds ratio (95% CI)	Adjusted odds ratio (95% CI)†
	Linked, n = 1,427	Not linked, n = 1,733		
Age group, y				
<1	90 (6.3)	119 (6.9)	Referent	Referent
1–17	529 (37.1)	661 (38.1)	1.06 (0.79–1.42)	1.06 (0.76–1.47)
18–64	641 (44.9)	738 (42.6)	1.15 (0.86–1.54)	1.42 (1.02–1.97)
≥65	167 (11.7)	215 (12.4)	1.03 (0.73–1.44)	1.28 (0.88–1.86)
Sex				
M	704 (49.3)	874 (50.4)	Referent	Referent
F	723 (50.7)	859 (49.6)	1.04 (0.91–1.20)	1.02 (0.88–1.19)
Race and ethnicity	N = 1,259	N = 1,494		
White, non-Hispanic	643 (51.1)	995 (66.6)	Referent	Referent
Black, non-Hispanic	225 (17.9)	219 (14.7)	1.59 (1.29–1.96)	1.66 (1.34–2.06)
Hispanic	235 (18.7)	174 (11.6)	2.09 (1.68–2.60)	2.26 (1.8–2.83)
Other, non-Hispanic	156 (12.4)	106 (7.1)	2.28 (1.75–2.97)	2.46 (1.88–3.23)
International travel	107 (8.4), n = 1,277	78 (5.2), n = 1,499	1.67 (1.23–2.25)	1.62 (1.17–2.24)
Clinical outcome				
Hospitalized	389 (27.8), n = 1,401	488 (29), n = 1,680	0.94 (0.80–1.10)	0.87 (0.73–1.04)
Died	7 (0.5), n = 1,392	7 (0.4), n = 1,685	1.21 (0.42–3.46)	1.40 (0.43–4.54)

*Values are no. (%) except as indicated. Values exclude 612 isolates without PFGE information. Among sequenced clinical PulseNet isolates collected during 2015–2018 that also had PFGE information, 2,070/3,007 (69%) belonged to a clade associated with ASSuT resistance that contained 275 PFGE patterns; these patterns were identified in 7/937 (0.8%) isolates outside the clade. ASSuT, ampicillin, streptomycin, sulphamethoxazole, and tetracycline; MDR, multidrug resistant; PFGE, pulsed-field gel electrophoresis.
†Adjusted for age, sex, race, and ethnicity.

Table 3. Characteristics of outbreaks caused by multidrug-resistant *Salmonella enterica* 4,[5],12:i:- compared with other nontyphoidal *Salmonella*, United States, 2009–2018*

Outbreak type and transmission mode	*Salmonella* 4,[5],12:i:-, n = 123	Other *Salmonella*, n = 1,829	PFGE link to MDR clade	
			Linked, n = 4	Not linked, n = 45
Multistate outbreak	13 (10.6)	284 (15.5)	3 (4.1)	10 (22.2)
Mode of transmission				
Foodborne, no single food category†	52 (42.3)	792 (43.3)	25 (33.8)	26 (57.8)
Foodborne, single food category	23 (18.7)	414 (22.6)	17 (23)	5 (11.1)
Animal contact, no single animal type	6 (4.9)	15 (0.8)	4 (5.4)	2 (4.4)
Animal contact, single animal type	12 (9.8)	138 (7.5)	8 (10.8)	4 (8.9)
Person-to-person	7 (5.7)	126 (6.9)	6 (8.1)	1 (2.2)
Environmental	0	15 (0.8)	0	0
Waterborne	0	2 (0.1)	0	0
Unknown transmission	23 (18.7)	327 (17.9)	14 (18.9)	7 (15.6)
Food source, single food category	N = 23	N = 406	N = 17	N = 5
Chicken	4 (17.4)	77 (19)	3 (17.6)	1 (20)
Pork	13 (56.5)	47 (11.6)	11 (64.7)	1 (20)
Turkey	2 (8.7)	27 (6.7)	2 (11.8)	0
Other food category	4 (17.4)‡	255 (62.8), n = 406	1 (5.9), n = 17	3 (60)
Animal contact, single animal type	N = 12	N = 138	N = 8	N = 4
Live poultry	3 (25.0)§	77 (55.8)	2 (25.0)	1 (25)
Swine	5 (41.7)	0	5 (62.5)	0
Other animal	4 (33.3)¶	61 (44.2)	1 (12.5)	3 (75)

*Values are no. (%) except as indicated. PFGE used as a marker for the MDR clade as defined by core genome multilocus sequence typing in PulseNet. Among sequenced clinical PulseNet isolates collected during 2015–2018 that also had PFGE information, 2,070/3,007 (69%) belonged to a clade associated with ASSuT resistance that contained 275 PFGE patterns; these patterns were identified in 7/937 (0.8%) isolates outside the clade. Excludes 4 outbreaks without PFGE information. ASSuT, ampicillin, streptomycin, sulphamethoxazole, and tetracycline; MDR, multidrug resistant; PFGE, pulsed-field gel electrophoresis.
†Includes confirmed 4,[5],12:i:- outbreaks classified as foodborne transmission for which no specific food was reported.
‡Includes dairy (n = 1), nuts or seeds (n = 1), seeded vegetables (n = 1), and sprouts (n = 1).
§Linked to contact with chicken (n = 1), turkey (n = 1), or baby chick or duckling (n = 1).
¶Linked to contact with rodents (n = 2), turtles (n = 1), or cattle (n = 1).

4,[5],12:i:- outbreaks with PFGE patterns found in the MDR clade were more likely to be linked to consumption of pork or contact with swine (64% [16/25] vs. 11% [1/9]; p = 0.007) (Table 3).

Discussion

In the United States, nearly 20,000 reported infections were caused by 4,[5],12:i:- during 2009–2018, and >100 outbreaks were reported across 37 states. An overall increase in 4,[5],12:i:- infections was driven by expansion of a phylogenetic clade associated with ASSuT resistance (the MDR clade). By 2015–2018, a total of 69% of 4,[5],12:i:- isolates belonged to the MDR clade. That clade also contained a substantial proportion of isolates that might not respond to antimicrobial drugs recommended as empiric treatment for invasive *Salmonella* infections (*24*,*25*).

Isolates in the MDR clade in this study were closely related to isolates previously reported in Europe (*7*,*8*,*12*,*26*), the United States (*11*), Canada (*9*), Australia (*10*), and Japan (*27*) and had the same genes conferring ASSuT resistance (*11*,*12*,*16*) and the same genomic island conferring tolerance to heavy metals (*8*,*11*,*16*). Using PFGE data as a proxy for clade membership before the introduction of routine WGS, we found evidence that infections caused by this clade have been increasing in the United States since 2010. This finding is consistent with recent phylogenetic evidence that the strain was likely transmitted from Europe to the United States multiple times during 2000–2006 (*11*,*28*).

Infections in the MDR clade were more likely than other 4,[5],12:i:- isolates to have genetic determinants of resistance to ciprofloxacin or ceftriaxone. During 2015–2018, a total of 16% of sequenced isolates had predicted decreased susceptibility to ciprofloxacin, ceftriaxone, or azithromycin; beyond those antimicrobial drugs, few alternative agents are available to treat invasive *Salmonella* infections (*24*,*25*). Moreover, some isolates in the clade contained extended-spectrum β-lactamase genes conferring resistance to ceftriaxone or *mcr* genes conferring colistin resistance, consistent with reports from other countries (*10*,*11*,*29*,*30*).

Infections related to the MDR clade were more likely to occur among persons from ethnic and racial minority groups. The reasons for this association are unknown but might reflect differences in consumption of contaminated food, food preparation, or animal contact and warrants further investigation. The low proportion of infected persons with a history of international travel suggests that the main source of infections from the MDR clade was within the United States.

Our analysis indicates that infections from the MDR clade resulted from consumption of contaminated pork or contact with swine. Pork was the food most often implicated in 4,[5],12:i:- outbreaks and was

more likely to be implicated compared with other *Salmonella* outbreaks. Among outbreaks of 4,[5],12:i:- infections linked to pork consumption or contact with swine, 89% were caused by strains with PFGE types that were characteristic of the MDR clade. Among outbreaks caused by these strains, 62% of those linked to a single food or animal were linked to pork or contact with swine; other outbreaks were linked to contact with poultry or cattle. In FoodNet sites, 4,[5],12:i:- infections with PFGE patterns that were characteristic of the MDR clade were more likely to be reported in patients who ate pork within 7 days before their illness onset than were other 4,[5],12:i:- or *Salmonella* infections. Collectively, our findings are consistent with previous reports indicating that swine is the predominant source of ASSuT-resistant 4,[5],12:i:- infections (*8*,*11*,*26*,*31*,*32*). Those studies also identified poultry and cattle as sources of ASSuT-resistant 4,[5],12:i:-, suggesting movement of this clade between animal reservoirs (*8*,*11*,*26*,*33*).

ASSuT-resistant strains can persist in swine herds (*34*), survive in swine feces (*35*), contaminate animal environments, including animal feed (*36*), and form biofilms (*36*). The 4,[5],12:i:- MDR clade might have a selective advantage in swine because of use of antimicrobial drugs or heavy metals. Use of tetracycline in swine production can select for tetracycline-resistant enteric bacteria (*37*), and ≈2 million cubic kilograms of tetracycline were sold for use in swine in the United States in 2019 (*38*). In this study, ciprofloxacin resistance was mainly encoded by *qnr*B19, a plasmid-mediated gene that confers resistance to enrofloxacin (*39*), a quinolone approved for use in US swine since 2008 (*40*). Resistance to enrofloxacin increased among *Salmonella* in swine during 2006–2015 (*41*), and similar ASSuT-resistant 4,[5],12:i:- isolates in swine have been reported that also contain *qnr*B19 (*42*). This gene might be acquired from other bacteria during swine production cycles (*39*). Another defining characteristic of this strain is the presence of SGI-4, which confers heavy metal tolerance (*8*,*11*,*43*). The reported frequent use of metals, such as copper and zinc, for disease prevention and growth promotion, might also provide a selective advantage (*40*,*44*,*45*).

One limitation of our study is that some of the reported increase in 4,[5],12:i:- infections might have resulted from improved serotyping, which can be difficult to perform (*46*). To address this concern, we limited our analysis to a recent period when serotyping was more reliable. In addition, misclassifying 4,[5],12:i:- as Typhimurium, or vice versa, would not explain the selective increase in isolates related to the MDR clade. Another limitation is that we were not able to verify the presence of the clade directly in several surveillance systems. Instead, we relied on PFGE patterns as a proxy for likely membership of the MDR clade in the outbreak and FoodNet surveillance systems and for isolates in the PulseNet database collected before 2015. We were not able to explain associations of the MDR clade with race, ethnicity, or other characteristics. The analyses depended implicitly on submission of isolates and data to national surveillance systems.

Our findings indicate that 4,[5],12:i:- infections have increased in the United States because of an MDR clade that has expanded since 2010. Illness is likely to have resulted from transmission from swine that carry it. The potential health threat from carriage among swine is highlighted by the recent identification of a 4,[5],12:i:- isolate from a retail pork specimen that contained extensive antimicrobial resistance genes (*47*). Further selection for this strain in swine might be prevented by limiting unnecessary agricultural use of classes of antibiotics to which the strain has resistance and by limiting unnecessary use of heavy metals in feed. Human illness from 4,[5],12:i:- also might be prevented by strategies to reduce carriage of 4,[5],12:i:- in swine, such as through the development and use of vaccines targeting 4,[5],12:i:- (*39*,*40*), and by improved husbandry and biosecurity measures (*48*). After an outbreak of the MDR clade that was attributed to contaminated whole hogs, a second outbreak occurred despite changes in practices at the slaughter facility, and inability to conduct on-farm investigations was cited as a major limitation (*49*). Prevention of human illness from this strain is likely to depend on addressing gaps in understanding at the preharvest stage.

A substantial proportion of 4,[5],12:i:- isolates have resistance to antimicrobial agents recommended as empiric treatment for invasive *Salmonella* infections. Consumers can minimize the risk for infection from contaminated products by safe food preparation and by avoiding consumption of undercooked pork. Clinicians caring for patients with suspected invasive salmonellosis or risk factors for invasive disease can confirm the diagnosis using stool culture and request antimicrobial susceptibility testing to guide therapy. Public health professionals can enact measures to identify clinically relevant resistance determinants that might emerge within this growing subgroup of 4,[5],12:i:- infections (*50*).

Acknowledgments

We thank Patricia Griffin, Beau Bruce, Gayle Langley, and Matthew Wise for helpful feedback in drafting this manuscript.

About the Author

Dr. Plumb trained as an infectious diseases physician and conducted this analysis in the Division of Foodborne, Waterborne and Environmental Diseases, National Center for Emerging and Zoonotic Infectious Diseases, Centers for Disease Control and Prevention, Atlanta, Georgia, USA. His research interests include infectious disease surveillance and *Salmonella* infections, with a focus on antibiotic resistance.

References

1. Kirk MD, Pires SM, Black RE, Caipo M, Crump JA, Devleesschauwer B, et al. World Health Organization estimates of the global and regional disease burden of 22 foodborne bacterial, protozoal, and viral diseases, 2010: a data synthesis. PLoS Med. 2015;12:e1001921. https://doi.org/10.1371/journal.pmed.1001921
2. Batz M, Hoffmann S, Morris JG Jr. Disease-outcome trees, EQ-5D scores, and estimated annual losses of quality-adjusted life years (QALYs) for 14 foodborne pathogens in the United States. Foodborne Pathog Dis. 2014;11:395–402. https://doi.org/10.1089/fpd.2013.1658
3 Collier SA, Deng L, Adam EA, Benedict KM, Beshearse EM, Blackstock AJ, et al. Estimate of burden and direct healthcare cost of infectious waterborne disease in the United States. Emerg Infect Dis. 2021;27:140–9. https://doi.org/10.3201/eid2701.190676
4. Moreno Switt AI, Soyer Y, Warnick LD, Wiedmann M. Emergence, distribution, and molecular and phenotypic characteristics of Salmonella enterica serotype 4,5,12:i:-. Foodborne Pathog Dis. 2009;6:407–15. https://doi.org/10.1089/fpd.2008.0213
5. Centers for Disease Control and Prevention. National enteric disease surveillance: *Salmonella* annual report, 2016. Atlanta: The Centers; 2018.
6. Centers for Disease Control and Prevention. National Antimicrobial Resistance Monitoring System: enteric bacteria (NARMS): 2013 human isolates final report. Atlanta: The Centers; 2015.
7. Hopkins K, Kirchner M, Guerra B, Granier S, Lucarelli C, Porrero M, et al. Multiresistant Salmonella enterica serovar 4,[5],12:i:- in Europe: a new pandemic strain? Euro Surveill. 2010;15:19580.
8. Petrovska L, Mather AE, AbuOun M, Branchu P, Harris SR, Connor T, et al. Microevolution of monophasic *Salmonella* Typhimurium during epidemic, United Kingdom, 2005–2010. Emerg Infect Dis. 2016;22:617–24. https://doi.org/10.3201/eid2204.150531
9. Mulvey MR, Finley R, Allen V, Ang L, Bekal S, El Bailey S, et al. Emergence of multidrug-resistant *Salmonella enterica* serotype 4,[5],12:i:- involving human cases in Canada: results from the Canadian Integrated Program on Antimicrobial Resistance Surveillance (CIPARS), 2003–10. J Antimicrob Chemother. 2013;68:1982–6. https://doi.org/10.1093/jac/dkt149
10. Arnott A, Wang Q, Bachmann N, Sadsad R, Biswas C, Sotomayor C, et al. Multidrug-resistant *Salmonella enterica* 4,[5],12:i:- sequence type 34, New South Wales, Australia, 2016–2017. Emerg Infect Dis. 2018;24:751–3. https://doi.org/10.3201/eid2404.171619
11. Elnekave E, Hong S, Mather AE, Boxrud D, Taylor AJ, Lappi V, et al. *Salmonella enterica* serotype 4,[5], 12: i:-in swine in the United States Midwest: an emerging multidrug resistant clone. Clin Infect Dis. 2018;66:877–85. https://doi.org/10.1093/cid/cix909
12. García P, Malorny B, Rodicio MR, Stephan R, Hächler H, Guerra B, et al. Horizontal acquisition of a multidrug-resistance module (R-type ASSuT) is responsible for the monophasic phenotype in a widespread clone of *Salmonella* serovar 4,[5],12:i. Front Microbiol. 2016;7:680. https://doi.org/10.3389/fmicb.2016.00680
13. Swaminathan B, Barrett TJ, Hunter SB, Tauxe RV, Force CPT; CDC PulseNet Task Force. PulseNet: the molecular subtyping network for foodborne bacterial disease surveillance, United States. Emerg Infect Dis. 2001;7:382–9. https://doi.org/10.3201/eid0703.017303
14. Tolar B, Joseph LA, Schroeder MN, Stroika S, Ribot EM, Hise KB, et al. An overview of PulseNet USA databases. Foodborne Pathog Dis. 2019;16:457–62. https://doi.org/10.1089/fpd.2019.2637
15. US Centers for Disease Control and Prevention. Whole genome sequencing (WGS) PulseNet methods [cited 2022 Aug 8]. https://www.cdc.gov/pulsenet/pathogens/wgs.html
16. Bearson BL, Trachsel JM, Holman DB, Brunelle BW, Sivasankaran SK, Simmons M, et al. Complete genome sequence of multidrug-resistant *Salmonella enterica* serovar I 4,[5],12:i:- 2015 U.S. pork outbreak isolate USDA15WA-1. Microbiol Resour Announc. 2019;8:e00791-19. https://doi.org/10.1128/MRA.00791-19
17. US National Library of Medicine. Isolates browser [cited 2021 Mar 17]. https://www.ncbi.nlm.nih.gov/pathogens/isolates
18. Tagg KA, Amir A, Ikram A, Chen JC, Kim JY, Meservey E, et al. Sequencing and Characterization of five extensively drug-resistant *Salmonella enterica* serotype Typhi isolates implicated in human infections from Punjab, Pakistan. Microbiol Resour Announc. 2020;9:e01466-19. https://doi.org/10.1128/MRA.01466-19
19. Karp BE, Tate H, Plumblee JR, Dessai U, Whichard JM, Thacker EL, et al. National Antimicrobial Resistance Monitoring System: two decades of advancing public health through integrated surveillance of antimicrobial resistance. Foodborne Pathog Dis. 2017;14:545–57. https://doi.org/10.1089/fpd.2017.2283
20. US Centers for Disease Control and Prevention. National Antimicrobial Monitoring System NARMS 2015 human isolates surveillance report. Atlanta: US Department of Health and Human Services; 2018.
21. Clinical and Laboratory Standards Institute (CLSI). Performance standards for antimicrobial susceptibility testing, 30th edition. CLSI supplement M100. Wayne (PA): The Institute; 2020.
22. US Centers for Disease Control and Prevention. Foodborne Diseases Active Surveillance Network (FoodNet) [cited 2022 May 14]. https://www.cdc.gov/foodnet/about.html
23. Wikswo ME, Roberts V, Marsh Z, Manikonda K, Gleason B, Kambhampati A, et al. Enteric illness outbreaks reported through the National Outbreak Reporting System—United States, 2009–2019. Clin Infect Dis. 2022;74:1906–13. https://doi.org/10.1093/cid/ciab771
24. Kimberlin DW. Salmonella infections. In: Kimberlin DW, Brady MT, Jackson MA, Long SS, editors. Red book (2018): 2018–2021 report of the committee on infectious diseases (31st edition). Itasca (IL): American Academy of Pediatrics; 2018. p. 711–18. https://doi.org/10.1542/9781610021470-part03-salmonella_infections
25. Pegues DA, Miller SI. *Salmonella* species. In: Bennett JE, Dolin R, Blaser MJ, editors. Mandell, Douglas, and Bennett's principles and practice of infectious diseases. Amsterdam: Elsevier Saunders; 2020. p. 2725–36.

26. Gymoese P, Sørensen G, Litrup E, Olsen JE, Nielsen EM, Torpdahl M. Investigation of outbreaks of *Salmonella enterica* serovar Typhimurium and its monophasic variants using whole-genome sequencing, Denmark. Emerg Infect Dis. 2017;23:1631–9. https://doi.org/10.3201/eid2310.161248
27. Arai N, Sekizuka T, Tamamura Y, Tanaka K, Barco L, Izumiya H, et al. Phylogenetic characterization of *Salmonella enterica* serovar Typhimurium and its monophasic variant isolated from food animals in Japan revealed replacement of major epidemic clones in the last 4 decades. J Clin Microbiol. 2018;56:e01758-17. https://doi.org/10.1128/JCM.01758-17
28. Elnekave E, Hong SL, Lim S, Boxrud D, Rovira A, Mather AE, et al. Transmission of multidrug-resistant *Salmonella enterica* subspecies *enterica* 4,[5],12:i:- sequence type 34 between Europe and the United States. Emerg Infect Dis. 2020;26:3034–8. https://doi.org/10.3201/eid2612.200336
29. Biswas S, Li Y, Elbediwi M, Yue M. Emergence and dissemination of mcr-carrying clinically relevant Salmonella Typhimurium monophasic clone ST34. Microorganisms. 2019;7:298. https://doi.org/10.3390/microorganisms7090298
30. Carnevali C, Morganti M, Scaltriti E, Bolzoni L, Pongolini S, Casadei G. Occurrence of *mcr*-1 in colistin-resistant *Salmonella enterica* isolates recovered from humans and animals in Italy, 2012 to 2015. Antimicrob Agents Chemother. 2016;60:7532–4. https://doi.org/10.1128/AAC.01803-16
31. Hauser E, Tietze E, Helmuth R, Junker E, Blank K, Prager R, et al. Pork contaminated with *Salmonella enterica* serovar 4,[5],12:i:-, an emerging health risk for humans. Appl Environ Microbiol. 2010;76:4601–10. https://doi.org/10.1128/AEM.02991-09
32. Mossong J, Marques P, Ragimbeau C, Huberty-Krau P, Losch S, Meyer G, et al. Outbreaks of monophasic *Salmonella enterica* serovar 4,[5],12:i:- in Luxembourg, 2006. Euro Surveill. 2007;12:E11-2. https://doi.org/10.2807/esm.12.06.00719-en
33. Mody RK, Meyer S, Trees E, White PL, Nguyen T, Sowadsky R, et al. Outbreak of *Salmonella enterica* serotype I 4,5,12:i:- infections: the challenges of hypothesis generation and microwave cooking. Epidemiol Infect. 2014;142:1050–60. https://doi.org/10.1017/S0950268813001787
34. Weaver T, Valcanis M, Mercoulia K, Sait M, Tuke J, Kiermeier A, et al. Longitudinal study of *Salmonella* 1,4,[5],12:i:- shedding in five Australian pig herds. Prev Vet Med. 2017;136:19–28. https://doi.org/10.1016/j.prevetmed.2016.11.010
35. Naberhaus SA, Krull AC, Arruda BL, Arruda P, Sahin O, Schwartz KJ, et al. Pathogenicity and competitive fitness of *Salmonella enterica* serovar 4,[5], 12: i:-compared to *Salmonella typhimurium* and *Salmonella* Derby in swine. Front Vet Sci. 2020;6:502. https://doi.org/10.3389/fvets.2019.00502
36. Tassinari E, Duffy G, Bawn M, Burgess CM, McCabe EM, Lawlor PG, et al. Microevolution of antimicrobial resistance and biofilm formation of *Salmonella* Typhimurium during persistence on pig farms. Sci Rep. 2019;9:8832. https://doi.org/10.1038/s41598-019-45216-w
37. Delsol A, Anjum M, Woodward MJ, Sunderland J, Roe JM. The effect of chlortetracycline treatment and its subsequent withdrawal on multi–resistant *Salmonella enterica* serovar Typhimurium DT104 and commensal *Escherichia coli* in the pig. J Appl Microbiol. 2003;95:1226–34. https://doi.org/10.1046/j.1365-2672.2003.02088.x
38. US Food and Drug Administration. 2019 summary report on antimicrobials sold or distributed for use in food-producing animals. Washington (DC): The Administration; 2020.
39. Elnekave E, Hong SL, Lim S, Hayer SS, Boxrud D, Taylor AJ, et al. Circulation of plasmids harboring resistance genes to quinolones and/or extended-spectrum cephalosporins in multiple *Salmonella enterica* serotypes from swine in the United States. Antimicrob Agents Chemother. 2019;63:e02602-18. https://doi.org/10.1128/AAC.02602-18
40. US Food and Drug Administration. Animal drugs @ FDA. FDA approved animal drug products. NADA 141-068. [cited 2020 Dec 1]. https://animaldrugsatfda.fda.gov/adafda/views/#/home/previewsearch/141-068
41. Hong S, Rovira A, Davies P, Ahlstrom C, Muellner P, Rendahl A, et al. Serotypes and antimicrobial resistance in *Salmonella enterica* recovered from clinical samples from cattle and swine in Minnesota, 2006 to 2015. PLoS One. 2016;11:e0168016. https://doi.org/10.1371/journal.pone.0168016
42. Gonzalez S, Harvey RB, Scott HM, Lawhon SD, Vinasco J, Mariño-Ramírez L, et al. Whole-genome sequences of *Salmonella enterica* serovar I 4,[5],12:i:- isolates from swine. Microbiol Resour Announc. 2019;8:e00223-19. https://doi.org/10.1128/MRA.00223-19
43. Bearson BL, Trachsel JM, Shippy DC, Sivasankaran SK, Kerr BJ, Loving CL, et al. The role of *Salmonella* genomic island 4 in metal tolerance of *Salmonella enterica* serovar I 4,[5],12:i:- pork outbreak isolate USDA15WA-1. Genes (Basel). 2020;11:1291. https://doi.org/10.3390/genes11111291
44. Holman DB, Chénier MR. Antimicrobial use in swine production and its effect on the swine gut microbiota and antimicrobial resistance. Can J Microbiol. 2015;61:785–98. https://doi.org/10.1139/cjm-2015-0239
45. Flohr JR, DeRouchey JM, Woodworth JC, Tokach MD, Goodband RD, Dritz SS. A survey of current feeding regimens for vitamins and trace minerals in the US swine industry. J Swine Health Prod. 2016;24:290–303.
46. Barco L, Lettini AA, Ramon E, Longo A, Saccardin C, Pozza MCD, et al. A rapid and sensitive method to identify and differentiate Salmonella enterica serotype Typhimurium and Salmonella enterica serotype 4,[5],12:i:- by combining traditional serotyping and multiplex polymerase chain reaction. Foodborne Pathog Dis. 2011;8:741–3. https://doi.org/10.1089/fpd.2010.0776
47. US Food and Drug Administration. NARMS retail meat testing interim data update: multidrug-resistant (MDR) *Salmonella* I 4,[5],12:i:-. [cited 2022 May 15]. https://www.fda.gov/animal-veterinary/national-antimicrobial-resistance-monitoring-system/narms-interim-data-updates
48. Dickson J, Hurd H, Rostagno MH. Salmonella in the pork production chain. Pork information gateway factsheet 2006 [cited 2018 May 25]. https://porkgateway.org/resource/salmonella-in-the-pork-production-chain
49. Kawakami V, Bottichio L, Lloyd J, Carleton H, Leeper M, Olson G, et al. Multidrug-resistant *Salmonella* I 4,[5],12:i:- and *Salmonella infantis* infections linked to whole roasted pigs from a single slaughter and processing facility. J Food Prot. 2019;82:1615–24. https://doi.org/10.4315/0362-028X.JFP-19-048
50. Baker S, Thomson N, Weill F-X, Holt KE. Genomic insights into the emergence and spread of antimicrobial-resistant bacterial pathogens. Science. 2018;360:733–8. https://doi.org/10.1126/science.aar3777

Address for correspondence: Ian Plumb, Centers for Disease Control and Prevention, 1600 Clifton Rd NE, Atlanta, GA 30329-4027, USA; email: iplumb@cdc.gov

Novel Prion Strain as Cause of Chronic Wasting Disease in a Moose, Finland

Julianna L. Sun, Sehun Kim, Jenna Crowell, Bailey K. Webster, Emma K. Raisley, Diana C. Lowe, Jifeng Bian, Sirkka-Liisa Korpenfelt, Sylvie L. Benestad, Glenn C. Telling

Our previous studies using gene-targeted mouse models of chronic wasting disease (CWD) demonstrated that Norway and North America cervids are infected with distinct prion strains that respond differently to naturally occurring amino acid variation at residue 226 of the prion protein. Here we performed transmissions in gene-targeted mice to investigate the properties of prions causing newly emergent CWD in moose in Finland. Although CWD prions from Finland and Norway moose had comparable responses to primary structural differences at residue 226, other distinctive criteria, including transmission kinetics, patterns of neuronal degeneration, and conformational features of prions generated in the brains of diseased mice, demonstrated that the strain properties of Finland moose CWD prions are different from those previously characterized in Norway CWD. Our findings add to a growing body of evidence for a diverse portfolio of emergent strains in Nordic countries that are etiologically distinct from the comparatively consistent strain profile of North America CWD.

Prions are infectious proteins that cause fatal, incurable neurodegenerative diseases of humans and animals, which include Creutzfeldt-Jakob disease (CJD), sheep scrapie, bovine spongiform encephalopathy, and chronic wasting disease (CWD) of cervids. The extraordinary biology and transmissibility of these disorders stems from the protean conformational properties of the prion protein (PrP). Although the secondary structure of host-encoded cellular PrP (PrP^{C}) is predominantly α-helical, during disease its relatively underglycosylated infectious counterpart (PrP^{Sc}) assembles into amyloid fibrils with parallel, in-register, intermolecular β-sheets (*1*–*7*). The replicative properties of prions stem from the capacity of PrP^{Sc} to template its conformation on PrP^{C} in a cyclical process resulting in exponential accumulation of prion infectivity (*8*–*11*).

Although they lack nucleic acids, prions exhibit heritable strain properties that influence disease outcomes, including the time between infection and disease onset (incubation period), clinical signs, patterns of neuronal degeneration and PrP^{Sc} deposition in the central nervous system (CNS), and the ability to replicate in non-CNS tissues such as the lymphoreticular system and musculature (*12*). Strain properties also influence the capacity of prions from one species to cause disease in a different species (*13*). Heritable strain information appears to be enciphered by distinct PrP^{Sc} conformations that are faithfully propagated during prion replication (*14*,*15*).

The food-chain transmission of bovine spongiform encephalopathy prions that resulted in a variant form of CJD illustrates the unpredictable potential of emergent strains for zoonotic transmission (*13*). Although novel prion diseases and strain variants continue to arise in increasing numbers of animal species, CWD elicits particular concern (*16*). After its initial description in a captive deer facility (*17*), uncontrolled contagious transmission has resulted in growing numbers of CWD-affected cervids in at least 30 US states and 3 Canada provinces (*18*). Inadvertent importation of subclinically diseased animals from North America led to the establishment of CWD in South Korea (*19*–*21*). CWD was also diagnosed in free-ranging Norwegian reindeer in 2016 (*22*), and additional cases were subsequently identified in growing numbers of moose, red deer, and reindeer from Norway, Sweden, and Finland (*23*).

The development and application of genetically modified, CWD-susceptible mice expressing cervid PrP^{C} ($CerPrP^{C}$) has provided insights into multiple

Author affiliations: Colorado State University, Fort Collins, Colorado, USA (J.L. Sun, S. Kim, J. Crowell, B.K. Webster, E.K. Raisley, D.C. Lowe, J. Bian, G.C. Telling); Finnish Food Authority, Helsinki, Finland (S.-L. Korpenfelt); Norwegian Veterinary Institute, Ås, Norway (S.L. Benestad)

DOI: https://doi.org/10.3201/eid2902.220882

aspects of pathogenesis, including the impact of naturally occurring *PRNP* coding sequence variations (*16*). Whereas North America deer and moose encode glutamine (Q) at codon 226 (CerPrP-Q226), North America elk encode glutamate (E) at this position (CerPrP-E226). Early studies in transgenic (Tg) mice suggested a role for this variation in the selection and propagation of CWD strains (*24*–*26*). To precisely assess the effects of this primary structural difference, we created CWD-susceptible gene-targeted (Gt) mice in which the PrP coding sequence was replaced with CerPrP-Q226 or CerPrP-E226 (*27*). Because the resulting mice, referred to as GtQ and GtE mice, express equivalent, physiologically controlled levels of $CerPrP^{C}$ and are otherwise syngeneic, we were able to ascribe distinct disease outcomes in each line to the effects of these amino acids (*27*). Furthermore, in contrast to previous CWD-susceptible Tg mice, Gt mice recapitulated the lymphotropic properties of CWD strains (*27*,*28*). By using Gt mice, we showed that emergent strains causing CWD in Norway reindeer and moose were unrelated to established North American forms of CWD and that they responded differently to variation at residue 226 (*28*). These findings underscored the utility of Gt mice for accurately defining the strain properties of emergent CWD prions (*28*). The goal of this study was to characterize a newly emergent form of CWD in Finland moose.

Materials and Methods

Ethics Statement

We performed all animal work in an Association for Assessment for Accreditation of Laboratory Animal Care–accredited facility in accordance with the Guide for the Care and Use of Laboratory Animals (https://www.ncbi.nlm.nih.gov/books/NBK54050). All procedures used in this study were performed in compliance with and were approved by the Colorado State University Institutional Animal Care and Use Committee.

Isolates

The Finland moose (M-F1) CWD isolate was from a free-ranging female moose identified to be sick and later found dead in 2018. The North America moose (M-US1) CWD isolate was from a captive moose orally inoculated with a pooled preparation of deer CWD. North America elk CWD isolate (E-US1), and Norway moose CWD isolates (M-NO1, M-NO2, and M-NO3) have been described previously (*28*).

Mouse Models and Incubation Time Assay

Development and characterization of Tg mice expressing cervid PrP with glutamine at residue 226 (TgQ), Tg mice expressing cervid PrP with glutamate at residue 226 (TgE), GtQ and GtE mice (expressing the same as the Tg mice), and the prion incubation time assay have been described previously (*24*,*27*–*29*). We used equal numbers of male and female mice in inoculation studies. We confirmed clinical diagnoses of prion disease by PrP^{Sc} detection in the CNS and neuropathologic assessments.

Analysis of PrP^{Sc} by Western Blotting

We performed analysis of PrP^{Sc} by western blotting as described previously (*27*,*28*). Equivalent amounts of protein were treated with 50 μg/mL of proteinase K (PK; Roche, https://www.roche.com) in the presence of 2% sarkosyl for 1 hour at 37°C. We performed sodium dodecyl sulfate–polyacrylamide gel electrophoresis by using precast 12% discontinuous Bis-Tris gels (Bio-Rad Laboratories, Inc., https://www.bio-rad.com). We detected proteins transferred to Immobilon-FL PVDF membranes (Millipore, https://www.emdmillipore.com) with monoclonal antibody (mAb) PRC5 at a dilution of 1:5,000 and mAb PRC1 at a dilution of 1:2,500 (*30*), followed by horseradish peroxidase–conjugated anti-mouse IgG secondary antibody. We developed membranes by using ECL 2 Western Blotting Substrate (ThermoFisher Scientific, https://www.thermofisher.com).

Conformational Stability Assay

We conducted a conformational stability assay as described previously (*27*,*28*). We detected PrP^{Sc} on membranes with mAb PRC5 (*30*) at a dilution of 1:5,000, followed by horseradish peroxidase–conjugated goat anti-mouse IgG secondary antibody. We developed membranes with ECL 2 Western Blotting Substrate and scanned them with an ImageQuant LAS 4000 digital camera system (GE Healthcare, https://www.gehealthcare.com) and analyzed signals with ImageQuant TL 7.0 software (GE Healthcare).

Histoblot Analysis

We performed histoblot analysis as described previously (*31*). We detected PrP^{Sc} on membranes by using mAb PRC5 at a dilution of 1:5,000, followed by alkaline phosphatase conjugated goat anti-mouse IgG (Southern Biotech, https://www.southernbiotech.com) at a dilution of 1:5,000. We developed membranes by using 5-bromo-4-chloro-3-indolyl phosphate/nitro blue tetrazolium (Sigma Aldrich, https://www.sigmaaldrich.com) and captured images with a Nikon SMZ1000 microscope (https://www.microscope.healthcare.nikon.com).

Neuropathologic and Immunohistochemical Analyses

We dissected brains rapidly after euthanizing the animal and immersion fixed tissues in 10% buffered formalin. We embedded tissues in paraffin and mounted 8 μm–thick coronal microtome sections onto positively charged glass slides. We performed immunohistochemical analyses of PrP in brain sections by using mAb D18 as described previously (*28*).

Neuropathologic Lesion Profiling

We sectioned paraffin-embedded mouse brains coronally to areas corresponding to 5 levels of the brain containing the 9 mouse brain regions of interest. We captured images of hematoxylin and eosin–stained sections by using a Photometrics CoolSNAP digital camera (https://www.photometrics.com) and an Olympus BX51 fluorescence microscope (https://www.olympus-lifescience.com) and analyzed them by using Olympus cellSens imaging software (standard version). We assessed the severity of vacuolar degeneration in cerebral gray matter from 9 regions, as described previously (*32*), by using a team of 4 investigators, who scored the images on scale of 0 to 4, with 4 corresponding to severe vacuolation.

Statistical Analyses

We performed statistical analyses by using GraphPad Prism 8.0 software (https://www.graphpad.com). We assessed statistical significance between survival curves of inoculated groups by comparing median times of survival of various inoculated groups using the log-rank (Mantel-Cox) test. We assessed statistical significance between denaturation curves of PrP^{Sc} by comparing log half maximal effective concentration values.

Results

We registered disease after ≈260 days in all but 1 of 11 GtQ mice inoculated with a homogenate of CNS from the index case of Finland CWD, M-F1 (Table 1; Figure 1, panel A). Brain homogenates from 2 diseased GtQ mice, referred to as GtQ (M-F1) brain 1 and brain 2 (Figure 1, panel A), produced disease after ≈225 days following intracerebral inoculation of additional GtQ mice (Table 2; Figure 1, panel D, E). By contrast, all GtE mice inoculated with M-F1 brain homogenate remained free of disease for up to 545 days (Table 1; Figure 1, panel A), and GtQ (M-F1) brain 1 produced disease in only 4 of 7 inoculated GtE mice after ≈470 days (Table 2; Figure 1, panel D), whereas GtQ (MF-1) brain 2 failed to produced disease in GtE mice after >510 days (Table 2; Figure 1, panel E). We conclude that M-F1 prion replication is supported when Q is encoded at residue 226 of host-encoded PrP ($CerPrP^{C}$-Q226) and relatively restricted when E is present at that position. In support of this conclusion, whereas CNS overexpression of $CerPrP^{C}$-Q226 produced faster times to disease in TgQ compared with GtQ mice, only a single inoculated TgE mouse had disease after ≈390 days (Appendix Table 1, Figure 1, panel A, https://wwwnc.cdc.gov/EID/article/29/2/22-0882-App1.pdf).

We confirmed clinical diagnoses of prion disease by using western blotting of PK-resistant $CerPrP^{Sc}$ in brain homogenates (Figure 2, panels A, C), histoblotting of $CerPrP^{Sc}$ in coronal sections (Figure 3, panels A–C), and microscopic analyses of neuronal vacuolation (Figure 4; Appendix Figure 3, panel B) and $CerPrP^{Sc}$ deposition in the CNS (Figure 5, panels A, B). Although spleen homogenates of GtQ mice infected with North America CWD and Norway reindeer CWD prions contained $CerPrP^{Sc}$, there was no evidence of prion replication in the spleens of GtQ mice after primary or secondary passage of the M-F1 isolate, or, as observed previously (*28*), in the spleens of GtQ mice infected with Norway moose CWD isolate M-NO1 (Figure 2, panel E). We conclude that whereas North America and Norway reindeer CWD prions are lymphotropic, Finland and Norway moose CWD prions are nonlymphotropic. In support of this conclusion, neither Gt nor Tg mice had disease after intracerebral inoculation with lymphoid tissue homogenates from M-F1 (Figure 1, panel B; Appendix Figure 1, panel B).

We questioned whether the inefficient transmission of M-F1 prions in GtE and TgE mice could be overcome by adaptation in a CerPrP-E226 background. Serial passage of M-F1 prions from the diseased TgE mouse, referred to as TgE (M-F1) (Figure 2, panel A; Appendix Table 1, Figure 1, panel A), produced disease in GtQ mice after ≈230 days but failed to produce

Table 1. Susceptibility of gene-targeted mice to intracerebral challenges with CWD prions from Finland and Norwway moose*

Inoculum	GtQ	GtE
M-F1 CNS	259 ±19 (10/11)	>545 (0/9)
M-NO1	440 ±13 (13/13)	
M-NO2	486 ±34 (13/13)	
M-NO3	451 ±33 (4/4)	
M-F1 LRS	>545 (0/10)	>550 (0/6)

*Time to disease onset (incubation time) is expressed as the mean number of days after which inoculated mice first showed ultimately progressive signs of neurologic disease ± SD. Parentheses include the numbers of diseased mice/number of inoculated mice. Incubation times of Norway moose CWD prions have been described previously (*27*). GtE, CWD-susceptible gene-targeted mice in which the prion protein coding sequence was replaced with one encoding glutamate at codon 226; GtQ, CWD-susceptible gene-targeted mice in which the prion protein coding sequence was replaced with one encoding glutamine at codon 226; M-F1 CNS, Finland moose 1 (central nervous system); M-F1 LRS, Finland moose 1 (lymphoreticular system); M-NO1, Norway moose 1; M-NO2, Norway moose 2; M-NO3, Norway moose 3.

Table 2. Susceptibility of gene-targeted mice to intracerebral challenges with serial passages of Finnish and Norwegian moose CWD prions*

Inoculum	GtQ	GtE
GtQ (M-F1) brain 1	228 ±3 (10/10)	>469 ±17 (4/7)
GtQ (M-F1) brain 2	223 ±4 (9/9)	>507 (0/5)
GtQ (M-NO1)	281 ±24 (5/5)	
GtQ (M-NO2)	541 ± 5 (5/7)	

*Time to disease onset (incubation time) is expressed as the mean number of days after which inoculated mice first showed ultimately progressive signs of neurologic disease ±SD. Parentheses include the numbers of diseased mice/number of inoculated mice. Incubation times of Norway moose CWD prions have been described previously (*27*). CWD, chronic wasting disease; GtE, CWD-susceptible gene-targeted mice in which the prion protein coding sequence was replaced with one encoding glutamate at codon 226; GtQ, CWD-susceptible gene-targeted mice in which the prion protein coding sequence was replaced with one encoding glutamine at codon 226; M-F1, Finland moose 1; M-NO1, Norway moose 1; M-NO2, Norway moose 2.

disease in GtE mice after ≈500 days (Appendix Table 2, Figure 1, panel E). Because serial passage of M-F1 prions from diseased TgQ mice also produced disease in GtQ mice after ≈230 days and failed to produce disease in GtE mice after ≈500 days (Appendix Table 2, Figure 1, panel D), we conclude that the M-F1 strain favors conformational conversion of CerPrP^{C}-Q226 over CerPrP^{C}-E226 regardless of whether prions are composed of CerPrP^{Sc}-E226 or CerPrP^{Sc}-Q226.

Our previous studies showed that propagation of prions from 3 Norway moose CWD isolates, referred to as M-NO1, M-NO2, and M-NO3, was also supported by expression of CerPrP^{C}-Q226 and relatively restricted by CerPrP^{C}-E226 (*28*). Despite this shared feature, comparisons of primary transmissions to GtQ mice showed that the mean incubation time of M-F1 was faster than those of M-NO1, M-NO2, or M-NO3 ($p<0.0001$) (Table 1; Figure 1, panel C). Primary transmission of M-F1 was also faster than Norway moose CWD isolates in TgQ mice ($p>0.0001$) (Appendix Table 1, Figure 1, panel C). We also observed faster disease onsets when serial transmissions of GtQ (M-F1) brains 1 and 2 were compared with serially transmitted M-NO1 and M-NO2 in GtQ mice (Table 2; Figure 1, panel F) and when M-F1 and Norway moose CWD prions were serially propagated from TgQ to GtQ mice (Appendix Table 2, Figure 1, panel F). Those consistently different disease kinetics during primary and secondary transmissions are indicative of strain differences between Finland and Norway moose CWD prions.

To substantiate that conclusion, we assessed additional strain features in infected GtQ mice. Semiquantitative assessment by brain lesion profiling (*32*)

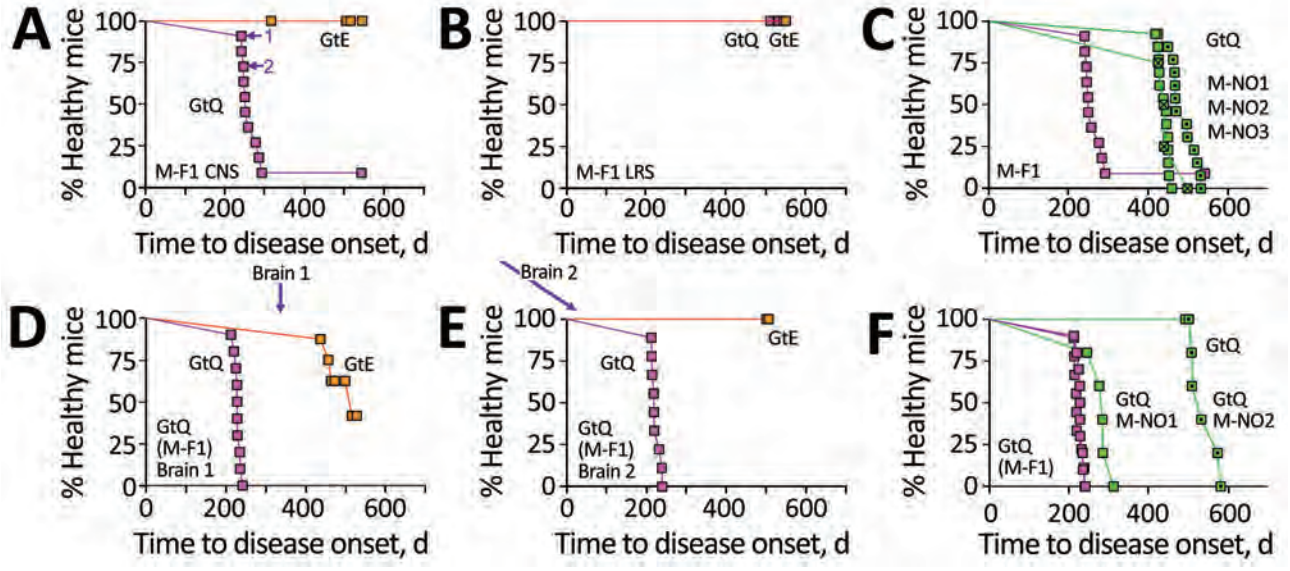

Figure 1. Transmission properties of Finland moose chronic wasting disease (CWD) prions in GtQ and GtE mice. Survival curves of intracerebrally inoculated GtQ and GtE mice are shown. A–C) Primary transmissions; D–F) secondary transmissions. A, B) Transmission to GtE mice (orange squares) and GtQ mice (magenta squares) of CNS homogenate from M-F1 (A) and LRS tissue homogenate from M-F1 (B). Arrows in GtQ mouse brains 1 and 2 (A) used for serial transmissions (D and E). C) Survival of GtQ mice infected with M-F1 from (A) (magenta squares) compared with Norway moose CWD isolates M-NO1 (green squares), M-NO2 (dotted green squares), and M-NO3 (crossed green squares). D) Serial passage of M-F1 prions from GtQ mouse brain 1 to GtE (orange squares) and GtQ (magenta squares). E) Serial passage of M-F1 prions from GtQ mouse brain 2 to GtE and GtQ mice. F) incubation times in GtQ mice of GtQ-passaged M-F1 (brains 1 and 2) from mice in panels D and E (magenta squares) compared with GtQ-passaged M-NO1 (green squares) and M-NO2 (dotted green squares). CNS, central nervous system; GtE, CWD-susceptible gene-targeted mice in which the prion protein coding sequence was replaced with one encoding glutamate at codon 226; GtQ, CWD-susceptible gene-targeted mice in which the prion protein coding sequence was replaced with one encoding glutamine at codon 226; LRS, lymphoreticular system; M-F1, Finland moose 1, M-NO1: Norway moose 1, M-NO2: Norway moose 2, M-NO3: Norway moose 3; p1, primary transmissions; p2, secondary transmissions.

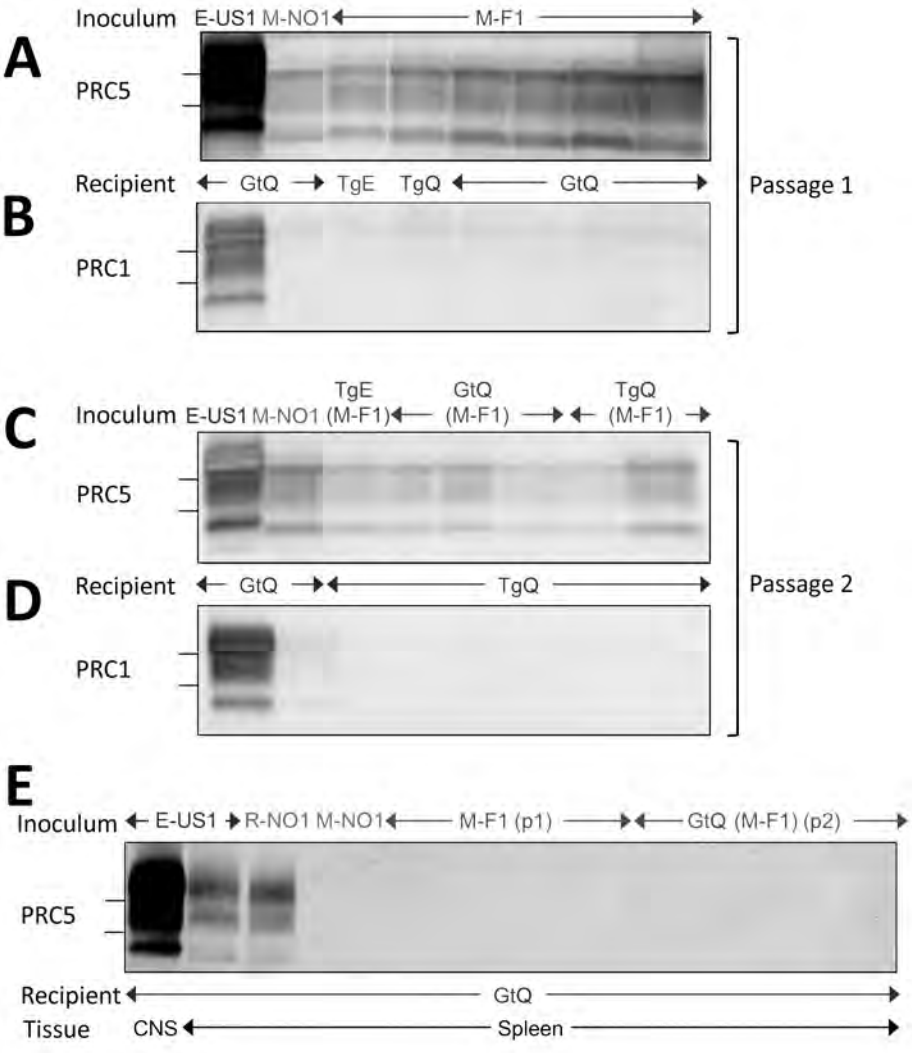

Figure 2. Western blot analyses of cervid prion protein (PrP) scrapie in mice infected with Finland, Norway, and North America chronic wasting disease (CWD) isolates. A, B) Western blots of CNS homogenates from GtQ, TgQ, and TgE mice after primary transmissions E-US1, Norway moose CWD (M-NO1), or Finland moose CWD (M-F1) probed with monoclonal antibody (mAb) PRC5 (A) or PRC1 (B). C–D) Western blots of CNS homogenates of GtQ and TgQ mice infected with E-US1 isolate, Norway isolate M-NO1, and M-F1 passaged through TgE, GtQ, or TgQ, referred to as TgE (M-F1), GtQ (M-F1), and TgQ (M-F1), respectively, probed with mAb PRC5 (C) or PRC1 (D). E) Lane 1, CNS homogenate of GtQ mice infected with E-US1 isolate. Remaining lanes are spleen homogenates from GtQ mice infected with E-US1 isolate, Norway reindeer isolate R-NO1, Norway moose isolate M-NO1, and spleens from infected GtQ mice during primary and secondary transmissions of M-F1. The positions of 25 and 20 kDa molecular weight markers are shown to the left of immunoblots. CNS, central nervous system; E-US1, US elk 1; GtQ, CWD-susceptible gene-targeted mice in which the prion protein coding sequence was replaced with one encoding glutamine at codon 226; M-F1, Finland moose 1; M-NO1, Norway moose 1; PRC1, mAb PCR1; PRC5, mAb PCR5; TgE, transgenic mice expressing cervid PrP with glutamate at residue 226; TgQ, transgenic mice expressing cervid PrP with glutamine at residue 226.

showed that the extent and regional distribution of spongiform degeneration varied depending on whether GtQ mice were infected with Finland or Norway moose CWD prions (Figure 4). Differences between GtQ mice infected with M-F1 and M-NO1 were particularly evident in the septum, retrosplenial and adjacent motor cortex, and cingulate and adjacent motor cortex. In these areas the intensity of spongiform degeneration was more pronounced in GtQ mice infected with M-F1 (Figure 4; Appendix Figure 3, panel A, B). The distinctive lesion profile of M-F1 was sustained after serial passage to additional GtQ mice (Figure 4).

We assessed the responses of $CerPrP^{Sc}$ produced in the brains of mice infected with Finland, Norway, and North America moose CWD prions to denaturation with increasing concentrations of guanidine hydrochloride (GdnHCl) (Figure 6). This measure of PrP^{Sc} stability is associated with conformational variation among prion strains (*33*). Denaturation profiles and concentrations of GdnHCl producing half-maximal denaturation indicated that the stability of $CerPrP^{Sc}$ in GtQ mice infected with M-F1 was equivalent to $CerPrP^{Sc}$ in the brains of GtQ mice infected with North America moose CWD and lower than that of $CerPrP^{Sc}$ in the brains of GtQ mice infected with M-NO1 ($p<0.0001$) (Figure 6, panel A). The conformational stability of $CerPrP^{Sc}$ produced on primary passage of M-F1 was maintained upon serial transmissions of GtQ (M-F1) brains 1 and 2 to GtQ mice (Figure 6, panel B). We also observed overlapping denaturation curves and comparable half-maximal denaturation values in the range of 2.59 to 2.95 upon infection of TgQ mice with M-F1 prions and M-F1 prions passaged in TgE or TgQ mice (Figure 6, panel C). We conclude that conformational properties of M-F1 prions are distinct from those of

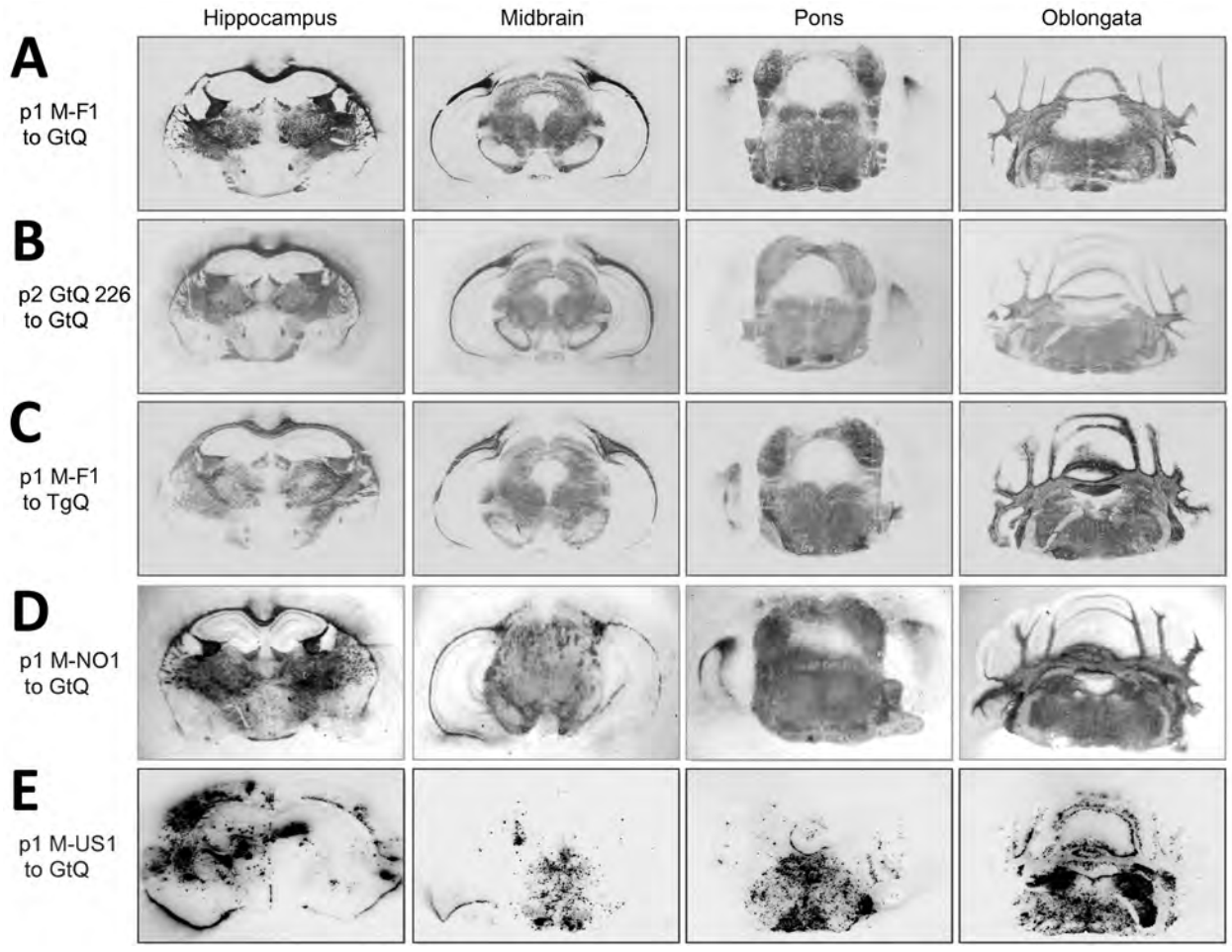

Figure 3. Global central nervous system distribution of cervid prion protein scrapie in Tg and Gt mice infected with Finland, Norway, and North America chronic wasting disease (CWD) cryostat coronal brain sections taken at the level of the hippocampus, midbrain, pons, and oblongata, transferred to slides and then to nitrocellulose. Sections were proteinase K–treated and immunoprobed with monoclonal antibody PRC5 after denaturation. A, B) Passage 1 and 2 of M-F1 in GtQ mice. C) TgQ mice infected with M-F1. D) GtQ mice infected with Norway M-NO1 CWD. E) GtQ mice infected with CWD isolate M-US1. Gt, gene-targeted; GtQ, CWD-susceptible gene-targeted mice in which the prion protein coding sequence was replaced with one encoding glutamine at codon 226; M-F1: Finland moose 1; M-NO1, Norway moose 1; M-US1, US moose 1; p1, primary transmissions; p2, secondary transmissions; Tg, transgenic; TgQ, transgenic mice expressing cervid PrP with glutamine at residue 226.

M-NO1 prions, they are stable during iterative passages, and they remain unchanged after passage in mice expressing CerPrP^{C}-E226.

Despite their different transmission properties, neuropathologic profiles, and conformations, Finland and Norway CWD prions shared certain features. Western blotting showed that levels of CerPrP^{Sc} in the brains of GtQ mice infected with M-F1 and M-NO1 were lower than the levels of CerPrP^{Sc} in the brains of GtQ mice infected with North America CWD (Figure 2). This finding is consistent with previous studies showing consistently reduced CerPrP^{Sc} accumulation after Norway moose CWD prion infection (*28*). The electrophoretic migration profiles of CerPrP^{Sc} resulting from infection of GtQ mice with M-F1 and M-NO1 were both more rapid than CerPrP^{Sc} produced by infection with North America CWD (Figure 2, panel A). This finding also is consistent with our previous descriptions of Norway moose CerPrP^{Sc} (*28*). Finally, also in accordance with previous findings (*28*), CerPrP^{Sc} in the brains of M-F1 and M-NO1 infected mice was relatively refractory to detection by mAb PRC1 compared with CerPrP^{Sc} generated by infection with North America CWD (Figure 2, panel B). The faster migration of CerPrP^{Sc} generated by infection with M-F1 and M-NO1 and its comparative resistance to detection by PRC1 results from PK cleavage downstream from the PRC1 epitope at residue 90 in both strains (Appendix Figure 2). Serial transmissions of M-F1, M-NO1, and North America CWD

prions produced CerPrP^{Sc} immunoblotting profiles consistent with primary passages (Figure 2, panel C, D). We speculate that the low levels of PRC1-reactive CerPrP^{Sc} in brain extracts of mice infected with M-F1 and M-NO1 CWD prions (Figure 2, panel B, D) correspond to minor strain components that remain obscured when probing with nondiscriminatory mAbs. Using discriminatory mAbs revealed similar coexistence of multiple PrP^{Sc} types in persons with CJD (*34*).

Analyses of PK-resistant CerPrP^{Sc} in histoblotted coronal brain sections revealed a diffuse, symmetric deposition pattern in GtQ mice infected with M-F1 (Figure 3, panel A) that was indistinguishable from the pattern in GtQ mice infected with M-NO1 CWD (Figure 3, panel D), and consistent with previous analyses of mice infected with Norway moose CWD (*28*). This pattern was recapitulated after iterative passage of GtQ (M-F1) prions to GtQ mice (Figure 3, panel B) and after infection of TgQ mice with M-F1 (Figure 3, panel C). This diffuse pattern differed from the disorganized, asymmetrically distributed amalgamations of CerPrP^{Sc} produced by infection of GtQ mice with North America CWD prions (Figure 3, panel E) (*28*). Microscopic analysis of immunohistochemically stained CNS sections from GtQ mice infected with M-F1 CWD revealed small punctate accumulations of disease-associated CerPrP set against a background of diffuse staining (Figure 5, panel A). We observed a similar pattern in brain sections of TgE mice infected with M-F1 (Figure 5, panel B). We also detected small punctate accumulations in GtQ mice infected with M-NO1 (Figure 5, panel C). By contrast, and consistent with previous findings (*27,28*), GtQ mice infected with North America CWD contained intensely staining, amorphous aggregates of disease-associated CerPrP (Figure 5, panel D).

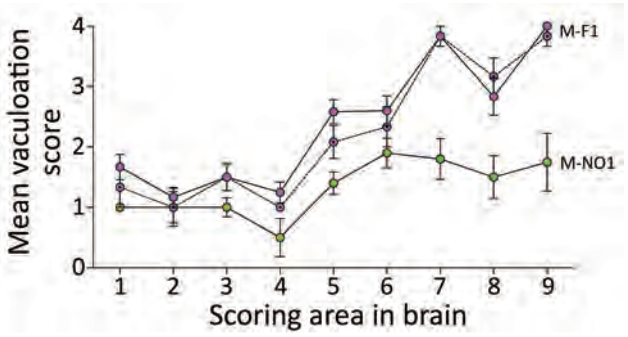

Figure 4. Lesion profiling in GtQ mice infected with Finland and Norway moose chronic wasting disease (CWD) isolates. Lesion profiles in groups of GtQ mice (CWD-susceptible gene-targeted mice in which the prion protein coding sequence was replaced with one encoding glutamine at codon 226) infected with M-F1 (magenta symbols) and Norway moose isolate M-NO1 (green symbols). For M-F1, open circles and solid lines depict primary passage; dotted circles and dashed lines depict second passage. Data points represent the mean ±SEM of ≥5 GtQ mice per group. Brain-scoring areas: medulla (1), cerebellum (2), superior colliculus (3), hypothalamus (4), thalamus (5), hippocampus (6), septum (7), retrosplenial and adjacent motor cortex (8), and cingulate and adjacent motor cortex (9). M-F1, Finland moose 1; M-NO1, Norway moose 1.

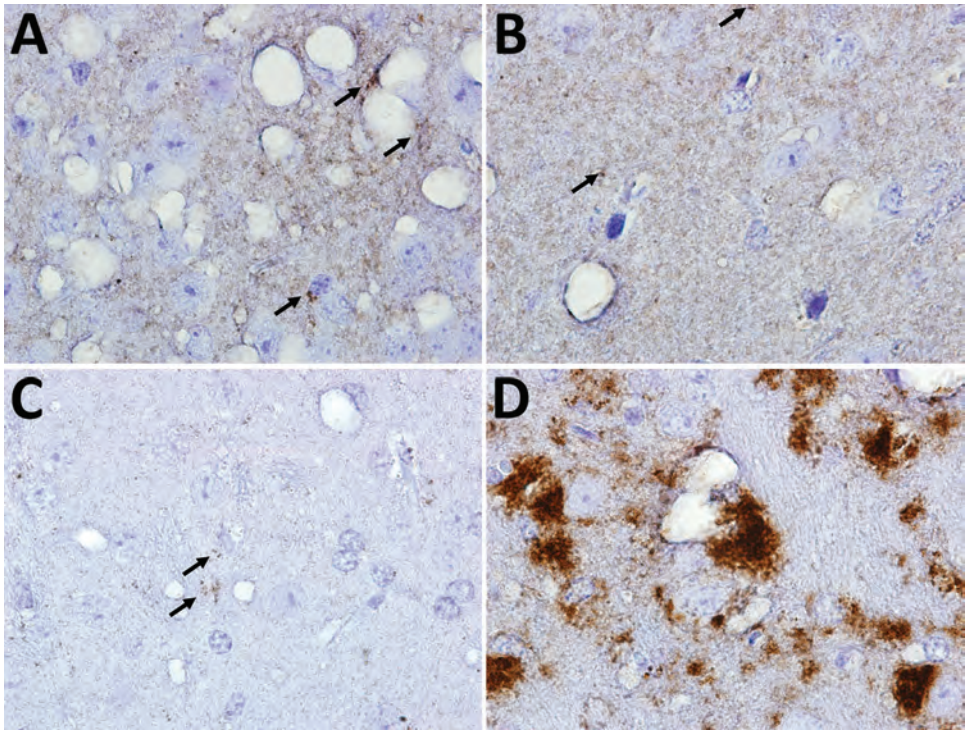

Figure 5. Immunohistochemical analyses of disease-associated prion protein (PrP) in the CNS of transgenic (Tg) and gene-targeted (Gt) mice infected with Finland, Norwway, and North America chronic wasting disease (CWD) isolates. A) GtQ mice (CWD-susceptible Gt mice in which the PrP coding sequence was replaced with one encoding glutamine at codon 226) infected with CWD isolate from Finland moose 1 (MF-1). B) TgE mice (Tg mice expressing cervid PrP with glutamate at residue 226) infected with M-F1. C) GtQ mice infected with CWD isolate from Norway moose 1 (M-NO1). D) GtQ mice infected with CWD isolate from US moose 1. Arrows in panels A, B, and C indicate small puncta of PrP. Immunohistochemistry sections were stained with fragment antigen binding D18. Original magnification ×10.

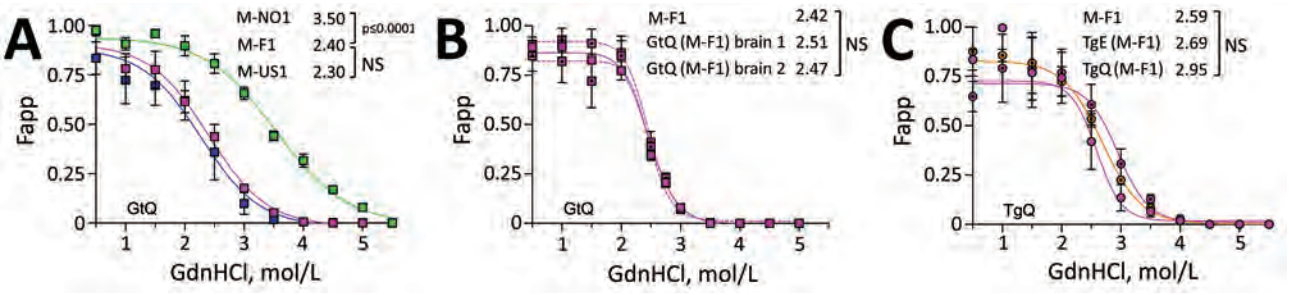

Figure 6. Responses of Finland, Norway, and North America moose chronic wasting disease (CWD) prions propagated in CWD-susceptible mice to increasing concentrations of GdnHCl. A) Responses of $CerPrP^{Sc}$ in central nervous system (CNS) of diseased GtQ mice to proteinase K treatment after denaturation with increasing concentrations of GdnHCl. Magenta symbols indicate M-F1 CWD, green symbols M-NO1 CWD, and blue symbols M-US1 CWD. B) Denaturation profiles of cervid PrP scrapie in CNS of GtQ mice infected with M-F1. Magenta squares and solid lines depict passage 1; dotted magenta squares and dashed lines depict GtQ (M-F1) brains 1 and 2 (passage 2). C) Denaturation profiles of cervid PrP scrapie in the CNS of TgQ mice infected with M-F1 (magenta circles), TgQ mice infected with M-F1 passaged through TgE mice [TgE (M-F1)] (orange circles), and TgQ mice infected with M-F1 passaged through TgQ mice [TgQ (M-F1)] (dotted magenta circles). Proteinase K–resistant PrP^{Sc} was quantified by densitometry of immunoprobed dot blots and plotted against GdnHCl concentration. Sigmoidal dose-response curves were plotted using a 4-parameter algorithm and nonlinear least-square fit. Error bars indicate ±SEM of data from analyses of ≥3 animals per group. $GdnHCl_{1/2}$ values (mol/L) for each infection are reported on the right-hand side of each graph. Significance calculated by pairwise analysis of $GdnHCl_{1/2}$ values from best fit curves. F_{app}, fraction of apparent PrP^{Sc} = (maximum signal-individual signal)/(maximum signal-minimum signal); GdnHCl, guanidine hydrochloride; $GdnHCl_{1/2}$, guanidine hydrochloride half-maximal denaturation; GtQ, CWD-susceptible gene-targeted mice in which the prion protein coding sequence was replaced with one encoding glutamine at codon 226; NS, not significant; PK, proteinase K; PrP, prion protein; TgE, transgenic mice expressing cervid PrP with glutamate at residue 226; TgQ, transgenic mice expressing cervid PrP with glutamine at residue 226.

Discussion

Our previous studies showed that although Gt and Tg mice expressing either $CerPrP^{C}$-E226 or $CerPrP^{C}$-Q226 were susceptible to North America CWD, times to disease onset were more rapid in mice expressing $CerPrP^{C}$-E226 (*24*,*26*–*28*). By comparison, although efficient transmission of Norway moose CWD prions was registered in Gt and Tg mice expressing $CerPrP^{C}$-Q226, their counterparts expressing $CerPrP^{C}$-E226 were resistant to infection or had prolonged incubation times and incomplete attack rates (*28*). Those studies also revealed strain variation among Norway moose CWD isolates, the properties of which were different from Norway reindeer CWD (*28*). The different properties of emergent Norway strains compared with North America CWD made it unlikely that they were causally related. Parallel experiments in bank voles supported this interpretation (*35*). Differences in the strain properties of M-F1 and North America CWD enable us to build on our previous conclusions (*28*,*35*) and to state more broadly that the etiology of Nordic CWD is distinct from North America CWD.

Our analyses reveal that certain characteristics of M-F1 CWD prions overlap with those of Norway moose CWD. M-F1 and Norway moose CWD both propagated more efficiently in mice expressing $CerPrP^{C}$-Q226. Western and histoblot profiles of M-F1 and M-NO1 $CerPrP^{Sc}$ are also indistinguishable. Our findings in this study show that M-F1 prions, like Norway moose CWD prions, are nonlymphotropic. Despite these broadly similar characteristics, other measures, including consistently different disease kinetics, distinct neuropathologic lesion profiles, and variable responses to GdnHCl denaturation, indicate that the strain properties of Finland and Norway moose CWD prions are different. This finding adds to an increasing body of evidence for a surprising variety of strains among Nordic cervids, which stands in contrast to the relatively consistent CWD strain profile among North America deer, elk, and moose. As yet, there appears to be no clear explanation for this diversity of Nordic CWD strains or insights into their origins. Although efficient prion dissemination to peripheral tissues of affected cervids has been cited as a reason for the contagious properties of North America CWD (*36*), the nonlymphotropic properties of Finland and Norway moose CWD strains suggests a decreased potential for contagious propagation. The emergence of increasing numbers of CWD strains in a confined geographic location during a short timeframe presents challenges when considering a sporadic etiology; however, our findings showing dissimilar CWD profiles in Nordic moose can be explained by divergent strains arising from unrelated, stochastic conversion events in different animals. CWD has also been diagnosed in moose in Sweden (*23*). Analyses of the strain properties of those additional emergent CWD cases will be of considerable interest.

Additional findings from this study build on our previous observations and warrant discussion.

Seminal studies indicating that related PrP^{Sc} and PrP^{C} primary structures supported optimal prion propagation laid the foundation for the development of Tg mice with susceptibility to human and animal prions (*37*–*39*). Because moose express $CerPrP^{C}$-Q226, we reasoned that the relatively inefficient transmission of M-F1 prions in GtE and TgE mice might be overcome by acclimatization in mice expressing $CerPrP^{C}$-E226, resulting in adapted M-F1 prions composed of $CerPrP^{Sc}$-E226. However, our findings showing comparable transmission profiles of TgE (M-F1) and TgQ (M-F1) prions indicate that M-F1 favors conformational conversion of $CerPrP^{C}$-Q226 over $CerPrP^{C}$-E226 regardless of whether prions are composed of $CerPrP^{Sc}$-E226 or $CerPrP^{Sc}$-Q226. Resistance of M-F1 prions to adapt to a host expressing a single amino acid difference is reminiscent of our description of nonadaptive prion amplification (NAPA) (*40*). Those studies showed that prions produced during particular interspecies transmissions are not adapted for sustained propagation in that new host. Instead, prions resulting from NAPA retain atavistic preferences for their species of origin (*40*). In this context, although M-F1 prions are capable of suboptimal propagation by NAPA using $CerPrP^{C}$-E226 as template for replication, the resulting TgE (M-F1) prions are not adapted for further propagation by $CerPrP^{C}$-E226 but instead retain a preference for conversion of $CerPrP^{C}$-Q226.

Acknowledgment

We thank Marja Isomursu for CWD surveillance and sample collection in Finland.

About the Author

Ms. Sun is a PhD candidate in the Cell and Molecular Biology Program at Colorado State University. Her primary research interests are focused on characterizing novel strains of chronic wasting disease and ascertaining the mechanism by which prions encipher strain properties.

References

1. Riek R, Hornemann S, Wider G, Billeter M, Glockshuber R, Wüthrich K. NMR structure of the mouse prion protein domain PrP(121-231). Nature. 1996;382:180–2. https://doi.org/10.1038/382180a0
2. Kraus A, Hoyt F, Schwartz CL, Hansen B, Artikis E, Hughson AG, et al. High-resolution structure and strain comparison of infectious mammalian prions. Mol Cell. 2021;81:4540–4551.e6. https://doi.org/10.1016/j.molcel.2021.08.011
3. Kang HE, Bian J, Kane SJ, Kim S, Selwyn V, Crowell J, et al. Incomplete glycosylation during prion infection unmasks a prion protein epitope that facilitates prion detection and strain discrimination. J Biol Chem. 2020;295:10420–33. https://doi.org/10.1074/jbc.RA120.012796
4. Basler K, Oesch B, Scott M, Westaway D, Wälchli M, Groth DF, et al. Scrapie and cellular PrP isoforms are encoded by the same chromosomal gene. Cell. 1986;46:417–28. https://doi.org/10.1016/0092-8674(86)90662-8
5. Hoyt F, Standke HG, Artikis E, Schwartz CL, Hansen B, Li K, et al. Cryo-EM structure of anchorless RML prion reveals variations in shared motifs between distinct strains. Nat Commun. 2022;13:4005. https://doi.org/10.1038/s41467-022-30458-6
6. Manka SW, Zhang W, Wenborn A, Betts J, Joiner S, Saibil HR, et al. 2.7 Å cryo-EM structure of ex vivo RML prion fibrils. Nat Commun. 2022;13:4004. https://doi.org/10.1038/s41467-022-30457-7
7. Telling GC. The shape of things to come: structural insights into how prion proteins encipher heritable information. Nat Commun. 2022;13:4003. https://doi.org/10.1038/s41467-022-31460-8
8. Prusiner SB. Novel proteinaceous infectious particles cause scrapie. Science. 1982;216:136–44. https://doi.org/10.1126/science.6801762
9. Büeler H, Aguzzi A, Sailer A, Greiner R-A, Autenried P, Aguet M, et al. Mice devoid of PrP are resistant to scrapie. Cell. 1993;73:1339–47. https://doi.org/10.1016/0092-8674(93)90360-3
10. Castilla J, Saá P, Hetz C, Soto C. In vitro generation of infectious scrapie prions. Cell. 2005;121:195–206. https://doi.org/10.1016/j.cell.2005.02.011
11. Legname G, Baskakov IV, Nguyen HO, Riesner D, Cohen FE, DeArmond SJ, et al. Synthetic mammalian prions. Science. 2004;305:673–6. https://doi.org/10.1126/science.1100195
12. Bartz JC. Prion strain diversity. Cold Spring Harb Perspect Med. 2016;6:a024349. https://doi.org/10.1101/cshperspect.a024349
13. Will RG, Cousens SN, Farrington CP, Smith PG, Knight RSG, Ironside JW. Deaths from variant Creutzfeldt-Jakob disease. Lancet. 1999;353:979. https://doi.org/10.1016/S0140-6736(99)01160-5
14. Telling GC, Parchi P, DeArmond SJ, Cortelli P, Montagna P, Gabizon R, et al. Evidence for the conformation of the pathologic isoform of the prion protein enciphering and propagating prion diversity. Science. 1996;274:2079–82. https://doi.org/10.1126/science.274.5295.2079
15. Bessen RA, Marsh RF. Distinct PrP properties suggest the molecular basis of strain variation in transmissible mink encephalopathy. J Virol. 1994;68:7859–68. https://doi.org/10.1128/jvi.68.12.7859-7868.1994
16. Benestad SL, Telling GC. Chronic wasting disease: an evolving prion disease of cervids. Handb Clin Neurol. 2018;153:135–51. https://doi.org/10.1016/B978-0-444-63945-5.00008-8
17. Williams ES, Young S. Chronic wasting disease of captive mule deer: a spongiform encephalopathy. J Wildl Dis. 1980;16:89–98. https://doi.org/10.7589/0090-3558-16.1.89
18. US Geological Survey. Expanding distribution of chronic wasting disease. 2022 Sep 26 [cited 2022 Dec 22]. https://www.usgs.gov/centers/nwhc/science/expanding-distribution-chronic-wasting-disease
19. Sohn HJ, Kim JH, Choi KS, Nah JJ, Joo YS, Jean YH, et al. A case of chronic wasting disease in an elk imported to Korea from Canada. J Vet Med Sci. 2002;64:855–8. https://doi.org/10.1292/jvms.64.855
20. Kim TY, Shon HJ, Joo YS, Mun UK, Kang KS, Lee YS. Additional cases of chronic wasting disease in imported deer in Korea. J Vet Med Sci. 2005;67:753–9. https://doi.org/10.1292/jvms.67.753

21. Lee YH, Sohn HJ, Kim MJ, Kim HJ, Park KJ, Lee WY, et al. Experimental chronic wasting disease in wild type VM mice. J Vet Med Sci. 2013;75:1107–10. https://doi.org/10.1292/jvms.13-0018
22. Benestad SL, Mitchell G, Simmons M, Ytrehus B, Vikøren T. First case of chronic wasting disease in Europe in a Norwegian free-ranging reindeer. Vet Res (Faisalabad). 2016;47:88. https://doi.org/10.1186/s13567-016-0375-4
23. Tranulis MA, Gavier-Widén D, Våge J, Nöremark M, Korpenfelt SL, Hautaniemi M, et al. Chronic wasting disease in Europe: new strains on the horizon. Acta Vet Scand. 2021;63:48. https://doi.org/10.1186/s13028-021-00606-x
24. Angers RC, Seward TS, Napier D, Green M, Hoover E, Spraker T, et al. Chronic wasting disease prions in elk antler velvet. Emerg Infect Dis. 2009;15:696–703. https://doi.org/10.3201/eid1505.081458
25. Angers RC, Kang HE, Napier D, Browning S, Seward T, Mathiason C, et al. Prion strain mutation determined by prion protein conformational compatibility and primary structure. Science. 2010;328:1154–8. https://doi.org/10.1126/science.1187107
26. Angers R, Christiansen J, Nalls AV, Kang HE, Hunter N, Hoover E, et al. Structural effects of PrP polymorphisms on intra- and interspecies prion transmission. Proc Natl Acad Sci U S A. 2014;111:11169–74. https://doi.org/10.1073/pnas.1404739111
27. Bian J, Christiansen JR, Moreno JA, Kane SJ, Khaychuk V, Gallegos J, et al. Primary structural differences at residue 226 of deer and elk PrP dictate selection of distinct CWD prion strains in gene-targeted mice. Proc Natl Acad Sci U S A. 2019;116:12478–87. https://doi.org/10.1073/pnas.1903947116
28. Bian J, Kim S, Kane SJ, Crowell J, Sun JL, Christiansen J, et al. Adaptive selection of a prion strain conformer corresponding to established North American CWD during propagation of novel emergent Norwegian strains in mice expressing elk or deer prion protein. PLoS Pathog. 2021;17:e1009748. https://doi.org/10.1371/journal.ppat.1009748
29. Browning SR, Mason GL, Seward T, Green M, Eliason GA, Mathiason C, et al. Transmission of prions from mule deer and elk with chronic wasting disease to transgenic mice expressing cervid PrP. J Virol. 2004;78:13345–50. https://doi.org/10.1128/JVI.78.23.13345-13350.2004
30. Kang HE, Weng CC, Saijo E, Saylor V, Bian J, Kim S, et al. Characterization of conformation-dependent prion protein epitopes. J Biol Chem. 2012;287:37219–32. https://doi.org/10.1074/jbc.M112.395921
31. Taraboulos A, Jendroska K, Serban D, Yang S-L, DeArmond SJ, Prusiner SB. Regional mapping of prion proteins in brain. Proc Natl Acad Sci U S A. 1992;89:7620–4. https://doi.org/10.1073/pnas.89.16.7620
32. Fraser H, Dickinson AG. The sequential development of the brain lesion of scrapie in three strains of mice. J Comp Pathol. 1968;78:301–11. https://doi.org/10.1016/0021-9975(68)90006-6
33. Peretz D, Williamson RA, Legname G, Matsunaga Y, Vergara J, Burton DR, et al. A change in the conformation of prions accompanies the emergence of a new prion strain. Neuron. 2002;34:921–32. https://doi.org/10.1016/S0896-6273(02)00726-2
34. Polymenidou M, Stoeck K, Glatzel M, Vey M, Bellon A, Aguzzi A. Coexistence of multiple PrPSc types in individuals with Creutzfeldt-Jakob disease. Lancet Neurol. 2005;4:
805–14. https://doi.org/10.1016/S1474-4422(05)70225-8
35. Nonno R, Di Bari MA, Pirisinu L, D'Agostino C, Vanni I, Chiappini B, et al. Studies in bank voles reveal strain differences between chronic wasting disease prions from Norway and North America. Proc Natl Acad Sci U S A. 2020;117:31417–26. https://doi.org/10.1073/pnas.2013237117
36. Davenport KA, Christiansen JR, Bian J, Young M, Gallegos J, Kim S, et al. Comparative analysis of prions in nervous and lymphoid tissues of chronic wasting disease-infected cervids. J Gen Virol. 2018;99:753–8. https://doi.org/10.1099/jgv.0.001053
37. Prusiner SB, Scott M, Foster D, Pan K-M, Groth D, Mirenda C, et al. Transgenetic studies implicate interactions between homologous PrP isoforms in scrapie prion replication. Cell. 1990;63:673–86. https://doi.org/10.1016/0092-8674(90)90134-Z
38. Scott M, Groth D, Foster D, Torchia M, Yang S-L, DeArmond SJ, et al. Propagation of prions with artificial properties in transgenic mice expressing chimeric PrP genes. Cell. 1993;73:979–88. https://doi.org/10.1016/0092-8674(93)90275-U
39. Telling GC, Scott M, Mastrianni J, Gabizon R, Torchia M, Cohen FE, et al. Prion propagation in mice expressing human and chimeric PrP transgenes implicates the interaction of cellular PrP with another protein. Cell. 1995; 83:79–90. https://doi.org/10.1016/0092-8674(95)90236-8
40. Bian J, Khaychuk V, Angers RC, Fernández-Borges N, Vidal E, Meyerett-Reid C, et al. Prion replication without host adaptation during interspecies transmissions. Proc Natl Acad Sci U S A. 2017;114:1141–6. https://doi.org/10.1073/pnas.1611891114

Address for correspondence: Glenn Telling, Colorado State University, 300 W Lake St, Fort Collins, CO 80523, USA; email: glenn.telling@colostate.edu

Novel Species of *Brucella* Causing Human Brucellosis, French Guiana

Frédégonde About, Theo Pastre, Mathilde Boutrou, Alex Yahiaoui Martinez, Alessia Melzani, Sandrine Peugny, Céline Michaud, Sami Zouaoui, Thierry Carage, Vincent Sainte Rose, Magalie Demar, Jean-Philippe Lavigne, Félix Djossou, David O'Callaghan, Loïc Epelboin, Anne Keriel

Human brucellosis is a zoonoses caused by bacteria of the genus *Brucella*. Infection results in subacute or chronic debilitating disease with nonspecific clinical manifestations and is often associated with consuming unpasteurized dairy products. We report 2 cases of brucellosis in male patients who were hospitalized in distinct towns of French Guiana, an overseas territory of France located on the northeastern shore of South America. Both men were citizens of Brazil working as clandestine goldminers in the deep Amazonian rainforest. Characterization of the 2 bacterial isolates revealed that they represent a potential new species of *Brucella*. Medical practitioners working in contact with wildlife in this region of the world should be aware of the existence of these pathogens and the potential for human infection.

Human brucellosis is a subacute or chronic debilitating disease with nonspecific clinical manifestations. Presenting classically as an influenza-like syndrome, this zoonosis remains endemic in most developing countries, mainly in areas with extensive farming, and transmission is commonly traced to consumption of unpasteurized dairy products (*1*). Direct exposure to diseased animals can also transmit infection, and cases have been reported in persons who had prior contact with wild animals (*2*,*3*).

Brucellosis is caused by gram-negative, facultative intracellular bacteria of the *Brucella* genus that can infect many organs and soft tissues. For ≈40 years, only 6 *Brucella* species were known, including the 3 species most predominant in livestock and humans: *B. melitensis* (goats), *B. abortus* (cows), and *B. suis* (swine, reindeer, and hares). The past decade, however, has seen a rapid expansion of both known members of the *Brucella* genus and the variety of associated animal hosts, which now range from mammals to amphibians and fish (*4*). Recently described *Brucella* species include *B. ceti* (cetaceans), *B. pinnipedialis* (pinnipeds), *B. inopinata* (humans), *B. microti* (voles), *B. papionis* (baboons), and *B. vulpis* (foxes). Several *Brucella* isolates, identified in rodents, frogs, reptiles, fish, and bats, still await formal taxonomic description.

Genomically, the *Brucella* genus is divided into classical species—*B. melitensis*, *B. abortus*, *B. suis*, *B. canis* (dog), *B. ovis* (sheep), *B. neotomae* (desert rats), *B. ceti*, *B. pinnipedialis*, *B. papionis,* and *B. microti*—and so-called atypical species. All *Brucella* are genetically closely related, showing genome similarities of >90% at the nucleotide level. However, *Brucella* species can be clearly separated from each other by highly discriminating molecular techniques, such as multiplex PCR, multilocus sequencing typing, or multiple loci variable-number tandem repeat analysis.

French Guiana is an overseas region of France that is on the northeastern coast of South America and covered largely (95%) by the Amazon rainforest. A recent report described human infection in French Guiana with *B. suis* bv1, which was likely contracted from domestic pigs (A. Melzani et al., unpub. data). We report 2 cases of human brucellosis in 2 patients hospitalized in distinct towns of French Guiana. Genome analysis revealed that 2 bacterial isolates represent a potential new species of *Brucella*.

Author affiliations: Centre Hospitalier de Cayenne Andrée Rosemon, Cayenne, French Guiana (F. About, M. Boutrou, A. Melzani, C. Michaud, V. Sainte Rose, M. Demar, F. Djossou, L. Epelboin); Centre Hospitalier de Kourou, Kourou, French Guiana (F. About, M. Boutrou, S. Zouaoui, T. Carage); Carémeau University Hospital de Nimes, Nimes, France (T. Pastre, A.Y. Martinez, J.-P. Lavigne, D. O'Callaghan, A. Keriel); Centre Hospitalier de l'Ouest Guyanais, Saint-Laurent du Maroni, French Guiana (S. Peugny); Université de Guyane, Cayenne (M. Demar, L. Epelboin); Université de Montpellier, Nimes (J.-P. Lavigne, D. O'Callaghan, A. Keriel); Institut National de la Santé et de la Recherche Médicale (INSERM), Nimes (D. O'Callaghan, A. Keriel); INSERM, Cayenne (L. Epelboin)

DOI: http://doi.org/10.3201/eid2902.220725

Material and Methods

Case Reports

Patient 1 was a 39-year-old man, originally from Belem, Brazil, who made his living as a clandestine goldminer. He had lived in Suriname for 10 years and had arrived in French Guiana 8 days before the onset of his symptoms in Maripasoula, a town of ≈10,000 inhabitants on the Maroni River (Figure 1). He sought care at Maripasoula Health Center in early September 2020 for fever, asthenia, and lower back pain. He did not have a relevant medical history. Clinical examination found hepatomegaly. Biological analyses showed hemoglobin of 10.2 g/dL (reference range 13–18 g/dL), mean corpuscular volume 78 µm3 (reference range 80–100 µm3), leukocytes 3.9 g/L (reference range 4.5–11 g/L), platelets 184 g/L (reference range 150–400 g/L), C-reactive protein 47.9 mg/L (reference range 3–10 mg/L), aspartate aminotransferase 201 IU/L (reference range <40 IU/L), and alanine aminotransferase 187 IU/L (reference range <35 IU/L). HIV serology results were was negative. The patient was transferred to Cayenne Hospital on day 3 of empirical treatment, with a treatment course of intravenous ceftriaxone (1 g/d). Because of ongoing fever, antimicrobial therapy was switched to piperacillin/tazobactam. Computed tomography of the chest, abdomen, and pelvis showed isolated hepatomegaly (19 cm) and splenomegaly (13 cm). Gram-negative bacilli were identified in blood cultures on day 9, after 68 hours of incubation. Mass spectrometry (MALDI Biotyper [Bruker, https://www.bruker.com/en.html];

Figure 1. Locations of main towns and care facilities in French Guiana.

Table. Results of gallery tests for *Brucella* isolates obtained from 2 patients with brucellosis, French Guiana, 2020

Incubation time	Test	BRSO-2020-213	BRSO-2021-230
24 h	Reduction of nitrates to nitrites or nitrogen	+	+
	Indole production	–	–
	Fermentation of glucose	–	–
	Arginine dihydrolase	–	–
	Urease	+	+
	Hydrolysis of esculin	–	–
	Hydrolysis of gelatin	–	–
	β-galactosidase production	–	–
48 h	Glucose assimilation	+	+
	Arabinose assimilation	+	+
	Mannose assimilation	+	+
	Mannitol assimilation	-	-
	N-acetyl-glucosamine assimilation	+	+
	Maltose assimilation	–	–
	Potassium gluconate assimilation	–	–
	Capric acid assimilation	–	–
	Adipic acid assimilation	–	–
	Malate assimilation	–	–
	Trisodium citrate assimilation	–	–
	Phenyl acetic acid assimilation	–	–
	Cytochrome oxidase	+	+

*API20NE gallery tests (bioMérieux, https://www.biomerieux.com) were performed according to the manufacturer's instructions. +, positive, –, negative.

security-relevant database; score 2.4) and VITEK 2GN ID card (bioMerieux, https://www.biomerieux.fr) (score 98%) identified the presence of *B. melitensis*. No serodiagnosis could be performed.

After establishing a diagnosis of brucellosis (September 15, 2020), we switched the patient's antibiotic regimen to a combination of rifampin (900 mg 1×/d) plus oral doxycycline (100 mg 2×/d) and a dose of gentamicin (250 mg). Blood cultures were positive for *Brucella* species through September 21. Transthoracic echocardiography showed no evidence of endocarditis. The patient denied being exposed to farm animals or consuming unpasteurized milk and cheese but admitted to consuming game hunted in the forest around the goldmine camp, including wild pork meat. He was discharged and returned home, continuing antibacterial therapy for a total of 6 weeks. At the last consultation (after 1 month of antibiotics), his progress was satisfactory, but the patient was unavailable for further follow-up.

Patient 2 was a 45-year-old man from Macapá, Brazil, who was working as a blacksmith at an illegal goldmine near Apatou (Figure 1). He had been living on both the French Guiana and Surinam sides of the Maroni River since approximatly 2002. In October 2020, the patient sought treatment at the Hospital of Saint-Laurent du Maroni for fever, lower back pain, weight loss of ≈8 kg in 10 months, and functional impairment of his left leg. He had no relevant medical history. Clinical examination found pain during active mobilization of the left psoas. Testing ruled out neurologic disorders. Laboratory tests showed hemoglobin of 11.1 g/dL, mean corpuscular volume 86 μm^3, leukocytes 5.4 g/L, platelets of 274 g/L, and C-reactive protein 126.5 mg/L. HIV serology results were negative. Computed tomography of the lumbar spine revealed advanced spondylodiscitis of the L4–L5 interline line, anterior prevertebral collection and destruction of adjacent vertebral bodies, and posterior disc filling narrowing the spinal canal. Collection extended to the left psoas. The paravertebral collections measured 49 × 51 × 19 mm and a left psoas collection measured 95 × 39 × 42 mm. Magnetic resonance imaging of the lumbar spine revealed epidural inflammation and compression of the terminal cone by the intra-anal collection. Transthoracic echocardiography revealed no valvular disease and infective endocarditis.

The patient was transferred to the orthopedic surgery unit of Kourou Hospital for psoas abscess sampling. He was treated empirically with antituberculosis drugs (rifampin 480 mg, isoniazid 200 mg, pyrazinamide 1,200 mg, and ethambutol 750 mg 1×/d) in combination with corticosteroids. *B. melitensis* was identified on culture, after 6 days of incubation, from a sample obtained from the psoas abscess. All blood culture results before administration of antibiotics were negative after 5 days of incubation. After a diagnosis of brucellosis, we changed the patient's treatment to doxycycline (100 mg 2×/d) and rifampin (600 mg 1×/d), in combination with gentamicin (250 mg/d for 6 d). The patient did not declare being exposed to farm animals, but he did eat meat hunted in the forest. His initial clinical outcome was favorable, with a decrease of fever. However, the patient left the hospital (on day 18 of treatment) and before completion of treatment and was not available for follow-up.

Molecular Typing of Bacteria

We extracted bacterial genomic DNA by using the DNeasy UltraClean Microbial Kit (QIAGEN, https://www.qiagen.com) according to the manufacturer's instructions and quantified genomic DNA with a Qubit fluorimeter (ThermoFisher Scientific, https://www.thermofisher.com). We performed Bruce-Ladder and Suis-Ladder multiplex PCRs as described (*5*,*6*).

Genome Sequencing and Analysis

We sequenced genomic DNA by using an Illumina MiSeq (Illumina, https://www.illumina.com) platform. We used a Nextera DNA Flex Kit (Illumina) for the library preparation, using 500 ng of DNA as input. We assessed library molarity and quality on the Qubit and the tape station using a DNA high-sensitivity chip (Agilent Technologies, https://www.agilent.com). We used the MiSeq Reagent Kit v2 (Illumina) to load libraries. Paired-end reads of 150 bp were generated de novo and assembled by using Shovill 1.1.0, a GALAXY webtool (*7*), and the contigs were assembled via the CONTIGuator web server, using the *B. ceti TE10759–12* genome (BioProject PRJNA224116) as a reference. We annotated consensus sequences by using the PATRIC genome annotation service (RASTtk) (*8*).

We deposited the genome sequences in GenBank under BioProject no. PRJNA728965 (accession nos. CP074683 for chromosome 1 and CP074684 for chromosome 2 of BRSO-2021–230 [BioSample SAMN19108195]; CP075601 for chromosome 1 and CP075602 for chromosome 2 of BRSO-2020–213 [BioSample SAMN19107925]).

Results

Microbiological Characterization

We shipped bacterial isolates from both patients to the French *Brucella* National Reference Center in Nimes, France, for confirmation of identification; they were named BRSO-2020–213 (Cayenne) and BRSO-2021–230 (Kourou). Analysis by matrix-assisted laser desorption/ionization time-of-flight mass spectrometry (Vitek MS with IVD database v3.2.0; bioMérieux) confirmed that both isolates belong to the *Brucella* genus. Slide agglutination using a polyclonal serum anti-*Brucella* (ANSES, https://www.anses.fr) also yielding positive results. Both isolates are gram-negative bacteria, forming nonhaemolytic, round, convex, smooth, greyish colonies with a diameter of ≈0.5mm after 48 hours of incubation on tryptic soy agar. Both isolates showed positive reactions for catalase (slide test), cytochrome-oxidase and urease (analytical profile index gallery tests) and a negative result for indole production (Table).

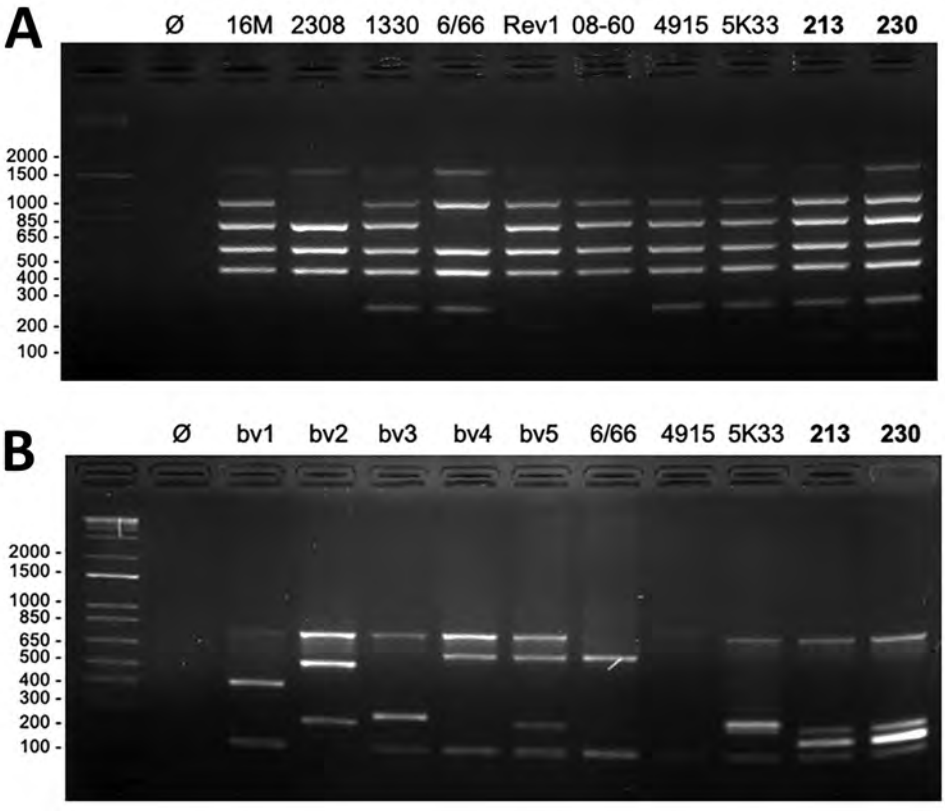

Figure 2. PCR typing of newly discovered *Brucella* isolates obtained from 2 patients in French Guiana, 2020**.** Genomic DNA from bacterial isolates BRSO-2020-213 and BRSO-2021-230 (numbers in bold) were used as a template for Bruce-Ladder (*5*) (A) or Suis-Ladder (*6*) (B) multiplex PCR. The profiles obtained after agarose gel electrophoresis were compared with the profile of type strains 16M (*Brucella melitensis*), 2308 (*B. abortus*), 1330 (*B. suis* bv1), Thomsen *(B. suis* bv2), 686 (*B. suis* bv3), 40 (*B. suis* bv4), 513 (*B. suis* bv5), RM6/66 (*B. canis*), Rev1 (*B. melitensis* vaccine strain), F8/08–60 (*B. papionis*), CCM 4915 (*B. microti*), or 5K33 (*B. neotomae*). Molecular-weight size markers in bp are shown at left. bv, biovar; Ø, negative control.

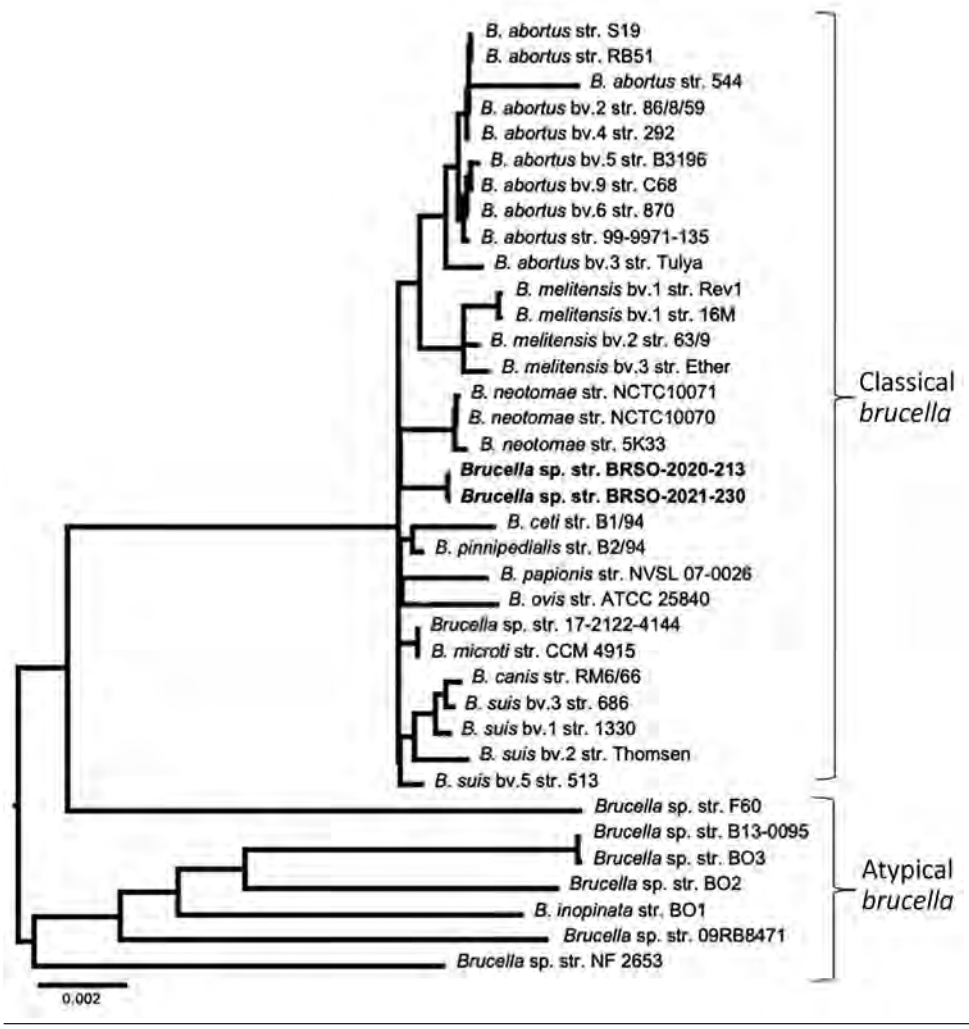

Figure 3. Phylogenetic placement of *Brucella* isolates BRSO-2020-213 and BRSO-2021-230 from 2 patients diagnosed with brucellosis in French Guiana, 2020. A genome-based tree was constructed by using a selection of reference *Brucella* genomes (Appendix Table, https://wwwnc.cdc.gov/EID/article/29/2/22-0725-App1.xlsx) on the PATRIC platform (BRC NIAID Bioinformatics Resource Centers, https://www.bv-brc.org). The number of compared genes was fixed at 1,000, and all other parameters were set by default. Scale bar indicates number of substitutions per site.

Analysis of Bacterial Genomes

We further characterized the isolates at the genomic level using the Bruce-Ladder multiplex PCR (*5*). The profiles obtained suggested that both could belong to the species *B. suis*, *B. microti*, or *B. neotomae* (Figure 2, panel A). However, profiles derived by using the Suis-Ladder PCR, a multiplex PCR designed to discriminate between different biovars of *B. suis*, were not similar to any reported *Brucella* species (Figure 2, panel B) (*6*). We then performed whole-genome sequencing, which revealed that both genomes contain 2 chromosomes (Chr) with a size and guanine-cytosine content similar to other *Brucella* species (BRSO-2020-213: Chr1 = 2,104,069 pb, Chr2 = 1,192,383 pb, 57.25% guanine-cytosine; BRSO-2021-230: Chr1 = 2,097,320 pb, Chr2 = 1,191,781 bp, 57.26% guanine-cytosine). No plasmid was detected. Annotation of genomes revealed the presence of several genetic features that are specific to *Brucella*: the bcsp31 gene on Chr1, the *virB* operon (*9*) on Chr2, and several copies of the IS711 insertion sequence (*10*).

Construction of a genome-based phylogenetic tree showed that BRSO-2020–213 and BRSO-2021-230 are very closely related and that both belong to the classical *Brucella* clade (Figure 3). Importantly, they did not cluster with any existing *Brucella* species. In silico multilocus sequencing typing, performed on GALAXY using CONTIGuator products as inputs (Florence Computation Biology Group, https://www.bio.unifi.it/p162.html), likewise showed that BRSO-2020-213 and BRSO-2021-230 do not belong to any known *Brucella* genotype. We performed alignments on 3 genes that are commonly used to discriminate *Brucella* species and reveal phylogenetic relationships among this genus: *recA*, 16S rRNA, and *omp2b* (*11*). We found the nucleotide sequences of *recA* to be 100% identical between BRSO-2020-213, BRSO-2021-230, and all other *Brucella* species (Figure 4), with the exception of *B. neotomae* and *B. microti*,

for a which a single-nucleotide polymorphism was already described (*12*). We noted the same results for the 16S rRNA gene, with the exception of *B. neotomae* and *B. papionis*. The *omp2b* gene provided the most discriminant findings, with only 88% identity between BRSO-2020–213 and BRSO-2021-230. Altogether, these analyses indicate that BRSO-2020-213 and BRSO-2021-230 are 2 distinct isolates, representing a new species of *Brucella*.

Discussion

Our report of 2 cases of human brucellosis in French Guiana follows a previous report of a single case of human brucellosis in this region, which described a 29-year-old man from Brazil who worked as a gold-miner and became infected with *B. suis* biovar 1, likely because of contamination in a pork farm in the state of Maranhão, Brazil (A. Melzani et al., unpub. data). In the cases we report here, both patients were also citizens of Brazil who were smuggled into French Guiana, most likely for clandestine goldmining. Characterization of bacteria from our patients, however, revealed 2 distinct isolates representing a new species of *Brucella*, for which we propose the name *Brucella amazoniensis* sp. nov.

French Guiana spreads over 84,000 km^2 and has a population of ≈300,000. The French territory

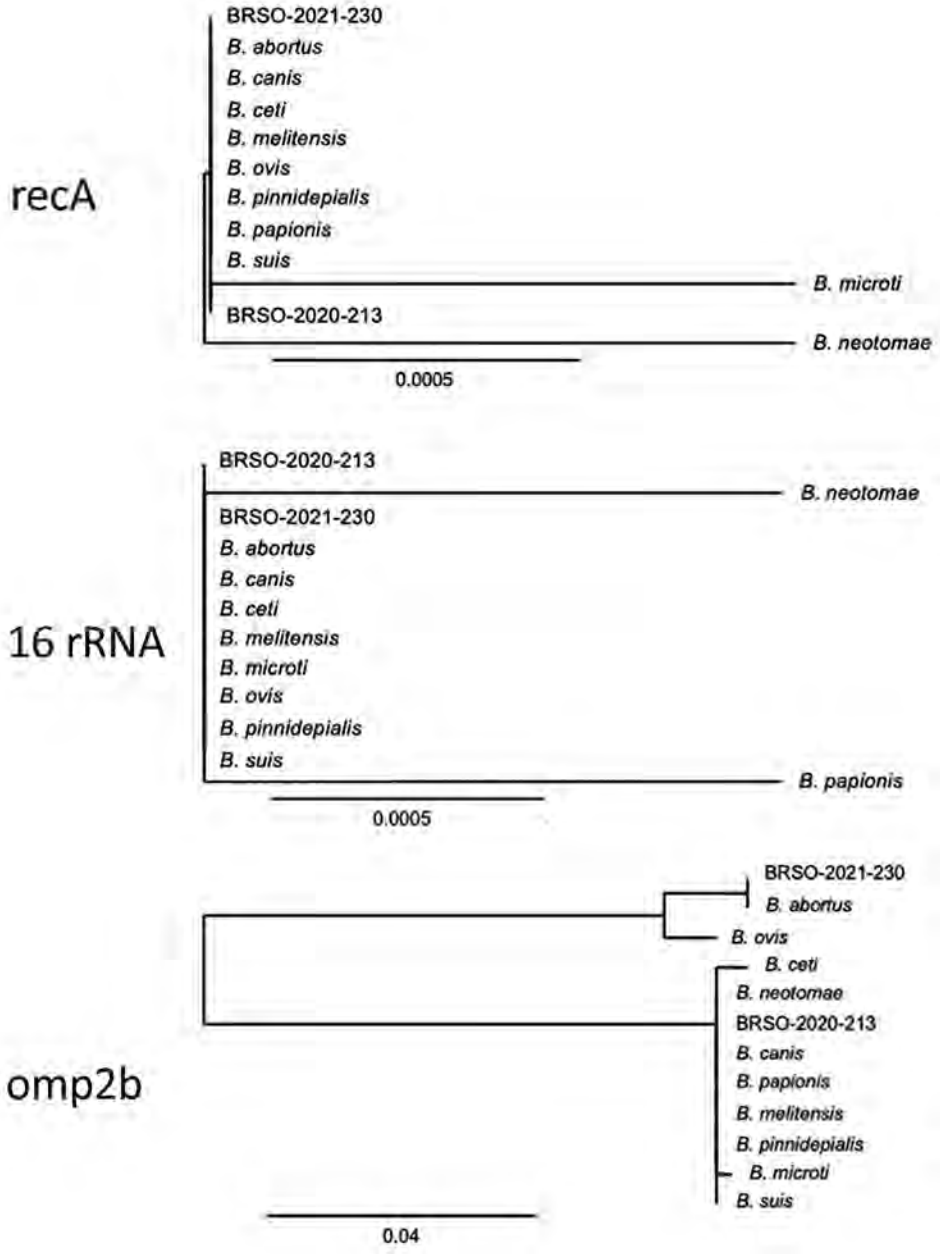

Figure 4. Phylogenetic placement of *Brucella* isolates BRSO-2020-213 and BRSO-2021-230 from 2 patients diagnosed with brucellosis in French Guiana, 2020, using alignments of *Brucella* genes. Sequences of the genes *recA*, 16S rRNA, and *omp2b* were aligned using the web tool Phylogeny (*17*) using the default parameters ("One Click" mode). Scale bar indicates number of substitutions per site.

is separated from Suriname by the Maroni River to the west and from Brazil by the Oyapock River to the east (Figure 1). Illegal gold mining is a growing practice in the territory, mainly in deep Amazon rainforest regions, and is carried out predominantly by clandestine immigrants from Brazil. Such clandestine goldminers represent a particularly vulnerable population who face precarious life conditions and high risks of exposure to wildlife and, thus, zoonotic pathogens (*13*–*15*).

We speculate a probable zoonotic transmission in the cases we report, most likely from a wild animal living in the Amazonian Forest. Both patients declared living "in the forest," hunting and consuming "bush meat," especially from swine. Although this new *Brucella* species seems genetically distinct from *B. suis*, it cannot be excluded that wild swine might be its animal reservoir. Two species of wild pigs live in this region and are commonly hunted: the collared peccary (*Pecari tajacu*) and white-lipped peccary (*Tayassu pecari*). We are conducting further research to determine if these suids, or other local wild Amazonian fauna, are the reservoir of this new *Brucella* species.

Medical practitioners should be aware of the existence of *Brucella* in this region of the world and that first-line laboratories perform simple *Brucella* serology tests (i.e., the Rose Bengal slide agglutination test or lateral flow assays) whenever symptoms or epidemiologic evaluations suggest possible brucellosis. When a gram-negative bacterium is isolated, positive reactions for urease, catalase, and oxidase is strongly indicative of *Brucella* spp., and suspect isolates should be manipulated using appropriate biosafety measures. Mass spectrometry can be used to confirm bacteriological identification (*16*) and should lead to further molecular characterization in specialized laboratories.

Acknowledgments

We thank the physicians that supported the patients and biologists that performed the blood tests. We are also grateful to Elise Martin for preparing the map of French Guiana (Figure 1).

This work was supported by the Institut National de la Sante et de la Recherche Medicale (INSERM), Universite de Montpellier, and Sante Publique France. Nimes University hospital provided structural, human, and financial support through the award obtained by our team during the internal call for tenders "Thematiques phares." J.P.L., D.O.C., and A.K. belong to the FHU InCh (Federation Hospitalo Universitaire Infections Chroniques, Aviesan).

The protection of human subjects afforded in this study were in accordance with the International Committee of Medical Journal Editors guidelines. The study was registered in the DPO processing of Cayenne Hospital Center, from which 3 coastal hospital centers (Saint Laurent du Maroni, Kourou, and Cayenne) and 2 health centers in the interior (Maripasoula and Apatou) are all administratively dependent. Because this study involved retrospective data collected in the context of routine care, this research is not considered to involve human subjects and therefore follows the "méthodologie de référence MR-004" of the French National Commission for Information Technology and Liberties. Every effort was made to contact the 2 patients to obtain their informed consent for the publication of these case reports, but this effort was unsuccessful. If the patients, at some time in the future, express their opposition, their data would be deleted from the database.

About the Author

Dr. About is chief resident in Infectious and Tropical Diseases at the Hospital Andrée Rosemon, Cayenne, French Guiana. Her doctoral studies focused on the human genetics of infectious diseases applied to conditions associated with Hepititis C virus infection.

References

1. Godfroid J, Al Dahouk S, Pappas G, Roth F, Matope G, Muma J, et al. A "One Health" surveillance and control of brucellosis in developing countries: moving away from improvisation. Comp Immunol Microbiol Infect Dis. 2013;36:241–8. https://doi.org/10.1016/j.cimid.2012.09.001
2. Moreno E. Retrospective and prospective perspectives on zoonotic brucellosis. Front Microbiol. 2014;5:213. https://doi.org/10.3389/fmicb.2014.00213
3. Fredriksson-Ahomaa M. Wild boar: a reservoir of foodborne zoonoses. Foodborne Pathog Dis. 2019;16:153–65. https://doi.org/10.1089/fpd.2018.2512
4. González-Espinoza G, Arce-Gorvel V, Mémet S, Gorvel JP. *Brucella*: reservoirs and niches in animals and humans. Pathogens. 2021;10:1–21. https://doi.org/10.3390/pathogens10020186
5. López-Goñi I, García-Yoldi D, Marín CM, de Miguel MJ, Muñoz PM, Blasco JM, et al. Evaluation of a multiplex PCR assay (Bruce-ladder) for molecular typing of all *Brucella* species, including the vaccine strains. J Clin Microbiol. 2008;46:3484–7. https://doi.org/10.1128/JCM.00837-08
6. López-Goñi I, García-Yoldi D, Marín CM, de Miguel MJ, Barquero-Calvo E, Guzmán-Verri C, et al. New Bruce-ladder multiplex PCR assay for the biovar typing of *Brucella* suis and the discrimination of *Brucella suis* and *Brucella canis*. Vet Microbiol. 2011;154:152–5. https://doi.org/10.1016/j.vetmic.2011.06.035
7. Afgan E, Baker D, Batut B, van den Beek M, Bouvier D, Cech M, et al. The GALAXY platform for accessible, reproducible and collaborative biomedical analyses: 2018 update. Nucleic Acids Res. 2018;46(W1):W537–44. https://doi.org/10.1093/nar/gky379

8. Brettin T, Davis JJ, Disz T, Edwards RA, Gerdes S, Olsen GJ, et al. RASTtk: a modular and extensible implementation of the RAST algorithm for building custom annotation pipelines and annotating batches of genomes. Sci Rep. 2015;5:8365. https://doi.org/10.1038/srep08365
9. Boschiroli ML, Ouahrani-Bettache S, Foulongne V, Michaux-Charachon S, Bourg G, Allardet-Servent A, et al. Type IV secretion and *Brucella* virulence. Vet Microbiol. 2002;90:341–8. https://doi.org/10.1016/S0378-1135(02)00219-5
10. Cloeckaert A, Bernardet N, Koylass MS, Whatmore AM, Zygmunt MS. Novel IS711 chromosomal location useful for identification of marine mammal *Brucella* genotype ST27, which is associated with zoonotic infection. J Clin Microbiol. 2011;49:3954–9. https://doi.org/10.1128/JCM.05238-11
11. Eisenberg T, Hamann HP, Kaim U, Schlez K, Seeger H, Schauerte N, et al. Isolation of potentially novel *Brucella* spp. from frogs. Appl Environ Microbiol. 2012;78:3753–5. https://doi.org/10.1128/AEM.07509-11
12. Al Dahouk S, Hofer E, Tomaso H, Vergnaud G, Le Flèche P, Cloeckaert A, et al. Intraspecies biodiversity of the genetically homologous species *Brucella microti.* Appl Environ Microbiol. 2012;78:1534–43. https://doi.org/10.1128/AEM.06351-11
13. Douine M, Mosnier E, Le Hingrat Q, Charpentier C, Corlin F, Hureau L, et al. Illegal gold miners in French Guiana: a neglected population with poor health. BMC Public Health. 2017;18:23. https://doi.org/10.1186/s12889-017-4557-4
14. Epelboin L, Eldin C, Thill P, de Santi VP, Abboud P, Walter G, et al. Human Q fever on the Guiana Shield and Brazil: recent findings and remaining questions. Curr Trop Med Rep. 2021;8:173–82. https://doi.org/10.1007/s40475-021-00243-4
15. Schwartz FW, Lee S, Darrah TH. A review of the scope of artisanal and small-scale mining worldwide, poverty, and the associated health impacts. Geohealth. 2021;5(1):e2020GH000325. https://doi.org/10.1029/2020GH000325
16. Mesureur J, Arend S, Cellière B, Courault P, Cotte-Pattat PJ, Totty H, et al. A MALDI-TOF MS database with broad genus coverage for species-level identification of *Brucella*. PLoS Negl Trop Dis. 2018;12(10):e0006874. https://doi.org/10.1371/journal.pntd.0006874
17. Dereeper A, Guignon V, Blanc G, Audic S, Buffet S, Chevenet F, et al. Phylogeny.fr: robust phylogenetic analysis for the non-specialist. Nucleic Acids Res. 2008;36:W465-9. https://doi.org/10.1093/nar/gkn180

Address for correspondence: Anne Keriel, VBIC, U1047, Faculté de Médecine, 186 chemin du Carreau de Lanes, 30908 Nimes CEDEX 2, France; email: anne.keriel@inserm.fr

etymologia revisited

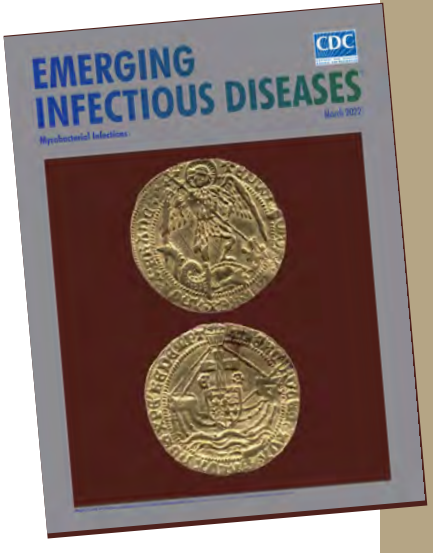

Originally published in March 2022

Schizophyllum commune

[skiz-of′-ĭ-ləm kom′-yoon]

Schizophyllum commune, or split-gill mushroom, is an environmental, wood-rotting basidiomycetous fungus. *Schizophyllum* is derived from "*Schíza*" meaning split because of the appearance of radial, centrally split, gill like folds; "*commune*" means common or shared ownership or ubiquitous. Swedish mycologist, Elias Magnus Fries (1794–1878), the Linnaeus of Mycology, assigned the scientific name in 1815. German mycologist Hans Kniep in 1930 discovered its sexual reproduction by consorting and recombining genomes with any one of numerous compatible mates (currently >2,800).

Sources

1. Chowdhary A, Kathuria S, Agarwal K, Meis JF. Recognizing filamentous basidiomycetes as agents of human disease: a review. Med Mycol. 2014;52:782–97. https://doi.org/10.1093/mmy/myu047
2. Cooke WB. The genus *Schizophyllum*. Mycologia. 1961;53:575–99. https://doi.org/10.1080/00275514.1961.12017987
3. Greer DL. Basidiomycetes as agents of human infections: a review. Mycopathologia. 1978;65:133–9. https://doi.org/10.1007/BF00447184
4. O'Reilly P. *Schizophyllum commune*, split gill fungus, 2016 [cited 2021 Aug 23]. https://www.first-nature.com/fungi/schizophyllum-commune.php
5. Raper CA, Fowler TJ. Why study *Schizophyllum*? Fungal Genet Rep. 2004;51:30–6. https://doi.org/10.4148/1941-4765.1142

https//wwwnc.cdc.gov/eid/article/28/3/et-2803_article

Penicillin and Cefotaxime Resistance of Quinolone-Resistant *Neisseria meningitidis* Clonal Complex 4821, Shanghai, China, 1965–2020

Mingliang Chen[1], Youxing Shao,[1] Jiayuan Luo, Lingyue Yuan, Minggui Wang, Min Chen, Qinglan Guo

Clonal complex 4821 (CC4821) *Neisseria meningitidis*, usually resistant to quinolones but susceptible to penicillin and third-generation cephalosporins, is increasing worldwide. To characterize the penicillin-nonsusceptible (Pen^{NS}) meningococci, we analyzed 491 meningococci and 724 commensal *Neisseria* isolates in Shanghai, China, during 1965–2020. The Pen^{NS} proportion increased from 0.3% in 1965–1985 to 7.0% in 2005–2014 and to 33.3% in 2015–2020. Of the 26 Pen^{NS} meningococci, 11 (42.3%) belonged to the CC4821 cluster; all possessed mutations in penicillin-binding protein 2, mostly from commensal *Neisseria*. Genetic analyses and transformation identified potential donors of 6 *penA* alleles. Three Pen^{NS} meningococci were resistant to cefotaxime, 2 within the CC4821 cluster. With 96% of the Pen^{NS} meningococci beyond the coverage of scheduled vaccination and the cefotaxime-resistant isolates all from toddlers, quinolone-resistant CC4821 has acquired penicillin and cefotaxime resistance closely related to the internationally disseminated ceftriaxone-resistant gonococcal FC428 clone, posing a greater threat especially to young children.

Neisseria meningitidis colonizes the pharynx of humans and is responsible for severe invasive meningococcal diseases (IMD), such as septicemia and meningitis; case-fatality rate for IMD is ≈11% (*1*).

Author affiliations: Shanghai Institutes of Preventive Medicine, Shanghai, China (Mingliang Chen); Shanghai Municipal Center for Disease Control and Prevention, Shanghai (Mingliang Chen, J. Luo, L. Yuan, Min Chen); Huashan Hospital, Fudan University, Shanghai (Y. Shao, M. Wang, Q. Guo); Key Laboratory of Clinical Pharmacology of Antibiotics, National Heath Commission of the People's Republic of China, Shanghai (Y.Shao, M.G. Wang, Q. Guo)

DOI: https://doi.org/10.3201/eid2902.221066

N. meningitidis can be divided into 12 serogroups, and evolutionary relationships among isolates from within and without serogroup can be described by clonal complex (CC), defined by multilocus sequence typing (MLST) (*2*). The distribution of serogroups and CCs varies by time and geographic location.

In the past 20 years in China, *N. meningitidis* serogroup C (NmC) CC4821 has replaced *N. meningitidis* serogroup A (NmA) CC5 as being predominant nationwide (*3*–*6*). This replacement was driven by national dissemination of a hyperinvasive and quinolone-resistant clone within CC4821, China$^{CC4821\text{-}R1\text{-}C/B}$, and led to the high frequency of resistance (≈70%) of meningococci in China against fluoroquinolones, which had been used as antimicrobial prophylaxis for close contacts of IMD patients since 2005 (*5*).

CC4821 is expanding worldwide and has been found in 19 countries outside of China (*7*); infections include urogenital and anorectal infections among men who have sex with men in Europe (*8*). Global CC4821 diverges into 4 sublineages, of which a high proportion (79.3%) of CC4821 isolates in Europe and in North and South America possess molecular markers of nonsusceptibility to penicillin (Pen^{NS}). In contrast, the proportion was much lower in China (10.5%) (*7*).

In several countries, the first-line therapeutic antimicrobial therapies for IMD have been penicillin and third-generation cephalosporins (3GCs), such as cefotaxime and ceftriaxone (*9*); long-term meningococcal chemoprophylaxis for patients using complement inhibitors includes penicillin (*10*). Because IMD can cause death within hours (*11*), the frequency of

[1]These authors contributed equally to this article.

infections with *N. meningitidis* resistant to penicillin and 3GCs is an issue of great concern worldwide.

N. meningitidis resistance to 3GCs is rare, and only 1 cefotaxime-resistant isolate has been reported in the United Kingdom (*12*). In recent years, Pen^{NS} meningococci have become more frequent worldwide (*13*,*14*), but data for meningococci from China with Pen^{NS} and 3GCs resistance remain poorly described. Two studies from the China Center for Disease Control and Prevention (China CDC) showed that the Pen^{NS} proportion was 4.9% during 2003–2012 and 15.2% during 2005–2019 nationwide and that 2.6% of isolates showed intermediate resistance to cefotaxime (without MIC values) during 2005–2019 (*15*,*16*). A provincial study from Zhejiang showed a Pen^{NS} proportion of 51.4% during 2011–2021 (*17*). However, information regarding the resistance mechanism and the genetic origin is unavailable. On the basis of *N. meningitidis* and commensal *Neisseria* isolates in Shanghai, China, since 1965, our aim with this study was to report the proportion and clonal relationship of Pen^{NS} isolates, demonstrate the origin and evolutionary changes of their *penA* genes, and evaluate the role of CC4821 in disseminating penicillin and 3GC resistance.

Materials and Methods

Isolate Collection

During 1965–2020, a total of 491 meningococcal and 724 commensal *Neisseria* isolates were collected in Shanghai. The meningococci were isolated from 171 IMD patients and 320 asymptomatic carriers during 1965–1985 and 2005–2020 (*5*), and the commensal *Neisseria* isolates were isolated from healthy persons during 2013 and 2019 (*18*).

Antimicrobial Susceptibility Testing

Using the agar-dilution method, we determined MICs of penicillin, azithromycin, cefotaxime, ceftriaxone, meropenem, chloramphenicol, ciprofloxacin, minocycline, rifampin, and trimethoprim/sulfamethoxazole. Using antibiotic gradient strip diffusion methods (Etest; bioMérieux, https://www.biomerieux.com), we determined the MICs for the Pen^{NS} isolates and cefotaxime-resistant isolates. We interpreted breakpoints according to the 2022 guidelines of the Clinical and Laboratory Standards Institute (*19*).

N. meningitidis Isolate Typing

We determined the serogroup of *N. meningitidis* isolates by using slide agglutination with monoclonal antiserum (Remel Europe Ltd., www.remel.com). All isolates were analyzed by MLST and typing for PorA and FetA according to previously described protocols (*3*). We analyzed whole-genome sequences of the Pen^{NS} meningococci by using the meningococcal core-genome MLST (cgMLST) schemes of *N. meningitidis* cgMLST version 1.0 for Pen^{NS} meningococci and the L44 cgMLST schemes for CC4821 isolates (*7*,*20*).

Analysis of Penicillin and 3GC Resistance–Associated Genes

Low-level penicillin resistance and 3GC resistance of *N. meningitidis* are mainly associated with mutations in the penicillin-binding protein (PBP) 2, which can be determined by sequencing its coding gene, *penA*, using the primers recommended by Taha et al. (*14*). On the basis of a 402-bp fragment (nucleotides 1321–1722) encoding transpeptidase domain (*14*), we determined the *penA* alleles according to the nomenclature in the *Neisseria* PubMLST database (*21*). We submitted novel *penA* alleles discovered in this study, and they were assigned new allele numbers in the database. The *ponA* gene encoding PBP1, in which the mutation L421P was reportedly associated with penicillin resistance in *N. gonorrhoeae*, was analyzed as previously described (*22*). We performed phylogenetic analyses via maximum-likelihood analysis with IQ-TREE version 2.2.0 (*23*), using the 402-bp *penA* sequences collected in this study and those in the *Neisseria* PubMLST database from different *Neisseria* species and different countries, deposited before December 25, 2021 (*21*).

Determination of Potential Donors and Recombination Crossover Points of Meningococcal *penA* Alleles

On the basis of previously described criteria, we considered a commensal *Neisseria* strain to be a potential donor for a recombinant *penA* allele in *N. meningitidis* (*18*). To identify the donors and the crossover points, we performed Illumina sequencing (https://www.illumina.com) on representative *N. meningitidis* and commensal *Neisseria* isolates that shared a candidate recombinant *penA* allele. We checked combination crossover points identified by visual inspection by using RDP software (Recombination Detection Program), version 4.97 (*24*).

Genetic Transformation

We performed the transformation of chromosomal DNA (500 ng) and *penA* fragment (100 ng) from *Neisseria* donor isolates into *N. meningitidis* as previously described (*18*). We selected 3 transformants of each pair of donor and recipient isolates for further study. We determined the penicillin MICs by using Etest and the genomes of the transformants by using Illumina sequencing. We submitted the genomes of *N. meningitidis*

and commensal *Neisseria* that were sequenced in this study to PubMLST *Neisseria* Database with PubMLST identification numbers (Appendix 1 Table 1, https://wwwnc.cdc.gov/EID/article/29/2/22-1066-App1.xlsx).

Results

Increased Penicillin Nonsusceptibility of Meningococcal Isolates

A total of 491 isolates were available from IMD patients and asymptomatic carriers in Shanghai during 1965–2020. The predominant serogroup of isolates causing IMD shifted from *N. meningitidis* serogroup A (NmA) (72.6%, 90/124) in 1965–1985 to *N. meningitidis* serogroup C (NmC) 42.6%, 20/47) and *N. meningitidis* serogroup B (NmB) (40.4%, 19/47) in 2005–2020. NmB sustained prevalence in carriage isolates in both periods, and NmA and NmC decreased markedly more in carriage isolates during 2005–2020 than 1965–1985 (Appendix 2 Figure 1, https://wwwnc.cdc.gov/EID/article/29/2/22-1066-App2.pdf).

Antimicrobial susceptibility tests showed that 26 (5.3%) isolates were Pen^{NS}, of which 3 isolates (Nm462, Nm463, and Nm507) were also resistant to cefotaxime (MIC range 0.25–0.50 μg/mL). The average proportion of penicillin nonsusceptibility was 3.5% (6/171) for IMD isolates and 6.3% (20/320) for carriage isolates, showing a total increase from 0.3% (1/303) in 1965–1985 to 7.0% (10/143) in 2005–2014 and to 33.3% (15/45) in 2015–2020 (Table). Correspondingly, the MIC at which 50% of tested isolates are inhibited (MIC_{50}) for the 3 periods increased from 0.03 μg/mL in 1965–1985 to 0.048 μg/mL in 2005–2014 and to 0.06 μg/mL in 2015–2020 (Figure 1). The average proportions of nonsusceptibility during 1965–2020 were 26.3% (129/491) for ciprofloxacin and 93.9% (461/491) for trimethoprim/sulfamethoxazole. All isolates were susceptible to azithromycin, ceftriaxone, meropenem, chloramphenicol, minocycline, and rifampin.

Epidemiologic and Molecular Characterizations of Pen^{NS} Isolates

Of the Pen^{NS} isolates, NmB was predominant (69.2%, 18/26; Appendix 1 Table 2). Except for 14 isolates unable to be assigned to any CCs (singletons), 8 isolates were assigned to CC4821 and another 4 each were assigned to a different CC. Nineteen (73.1%) Pen^{NS} isolates also showed quinolone resistance (MIC range 0.06–0.5 μg/mL), representing 13 *gyrA* alleles harboring GyrA mutations (T91I, n = 16; D95N, n = 3).

Genome analysis showed that 11 Pen^{NS} isolates were clustered together, of which 8 isolates belonged to CC4821 and 3 were singletons (2 ST-7962 and 1 ST-13502, each shared 4 loci with a CC4821 ST-5664) (Figure 2), so the cluster was designated as CC4821 cluster. We located the 11 Pen^{NS} CC4821 cluster isolates within the known 4 global CC4821 sublineages (*7*) and found that the L44.2 sublineage was predominant (n = 7), followed by L44.1 (n = 2), L44.3 (n = 1), and L44.4 (n = 1) (Appendix 2 Figure 2).

Characteristics of Cefotaxime-Resistant Isolates

The 3 Pen^{NS} and cefotaxime-resistant isolates, recovered during 2017 and 2019, displayed reduced susceptibility to ceftriaxone (0.064–0.125 μg/mL) compared with the wild-type strain NM040 (≤0.002 μg/mL). They all conferred resistance to ciprofloxacin, harboring the T91I mutation in GyrA. Two invasive isolates were assigned to the CC4821 cluster (L44.1 and L44.2; Figure 2) with different characterizations (Appendix 2 Table 1). Harboring different *penA* alleles (*penA777*, *penA795*, and *penA865*), they all possessed 5 penicillin-resistance-associated mutations (F504L, A510V, I515V, H541N, and I566V) and mutations associated with reduced cephalosporin susceptibility, including A311V, I312M, V316T, T483S, and G545S in the C-terminal or penicillin-binding domain of PBP2.

Evolution of Meningococcal *penA* Alleles

The *penA* alleles were obtained from all 491 *N. meningitidis* isolates. From the 465 penicillin-susceptible

Table. Frequency of identification of penicillin-nonsusceptible meningococcal isolates, Shanghai, China, 1965–2020*

Isolate source	Total	1965–1985	2005–2020		
			Total	2005–2014	2015–2020
Total	26/491 (5.3)	1/303 (0.3)	25/188 (13.3)	10/143 (7.0)	15/45 (33.3)
IMD, n = 171					
Average	6/17 (3.5)	0/124 (0)	6/47 (12.8)	1/38 (2.6)	5/9 (55.6)
Age <18 y	4/81 (4.9)	0/46 (0)	4/35 (11.4)	1/29 (3.4)	3/6 (50)
Age ≥18 y	2/90 (2.2)	0/78 (0)	2/12 (16.7)	0/9 (0)	2/3 (66.7)
Carriage, n = 320					
Average	20/320 (6.3)	1/179 (0.6)	19/141 (13.5)	9/105 (8.6)	10/36 (27.8)
Age <18 y	12/51 (23.5)	0/8 (0)	12/43 (27.9)	3/22 (13.6)	9/21 (42.9)
Age ≥18 y	8/269 (3.0)	1/171 (0.6)	7/98 (7.1)	6/83 (7.2)	1/15 (6.7)

*Values are no./no. nonsusceptible isolates (%). IMD, invasive meningococcal disease.

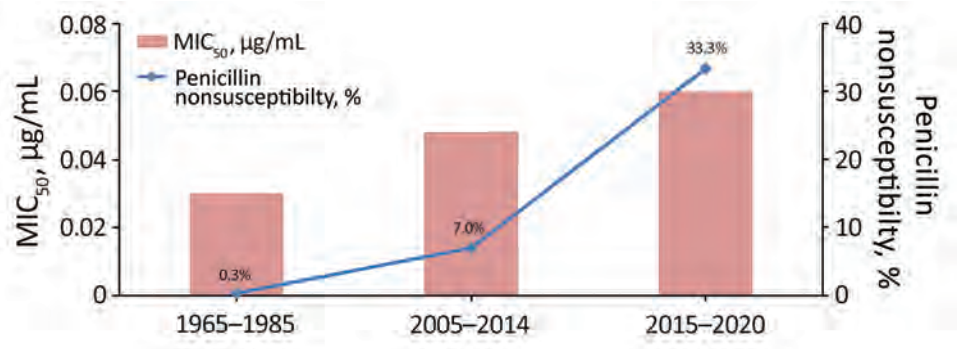

Figure 1. Percentage of meningococcal isolates with penicillin nonsusceptibility and MIC_{50} values, Shanghai, China, 1965–2020. MIC_{50}, minimum inhibitory concentrations at which 50% of the tested isolates are inhibited.

isolates, we identified 22 *penA* alleles; the most frequently isolated alleles were *penA1* (27.5%, 135/491), *penA4* (23.8%, 117/491), *penA3* (14.5%, 71/491), and *penA83* (10.2%, 50/491). Most of those isolates (95.7%, 445/465) harbored the *penA1* allele or an allele with a deduced amino acid sequence identical to the *penA*1 allele. The allele *penA83* was prevalent only during 1973–1985 and was almost always possessed by the NmA CC1 epidemic clone of that period (94%, 47/50). In contrast, both *penA4* and *penA1* were prevalent in the 3 periods; percentages were 52.6% (159/302) during 1965–1985, 59.4% (79/133) during 2005–2014, and 46.7% (14/30) during 2015–2020.

In the 26 Pen^{NS} isolates, we found 20 *penA* alleles, in which 18 alleles possessed the 5 common PBP2 mutations, 1 allele (*penA866*) possessed only 2 mutations (F504L and A510V), and another allele (*penA184*) harbored none of the 5 mutations but had an A549T mutation in the transpeptidase region (amino acid sites 441–574). Except for the alleles *penA405* (n = 3 isolates), *penA293* (n = 2), *penA552* (n = 2), *penA832* (n = 2), and *penA843* (n = 2), another 15 alleles were each possessed by only 1 isolate. Allele *penA405* was carried by 3 penicillin-intermediate CC4821 isolates of L44.2, and the other alleles were scattered in various CCs or singletons (Figure 2; Appendix 2 Figure 2). No isolates possessed mutations in the *ponA* gene of nucleotides 1219–1293 (75 bp).

Phylogenetic Analysis of *penA* Alleles of Pen^{NS} Meningococci

To track the genetic origin of *penA* alleles of the Pen^{NS} isolates, we also analyzed the *penA* nucleotides of 724 commensal *Neisseria* isolates collected during 2013–2019. We found 288 *penA* alleles, all with the 5 common amino acid mutations in PBP2. The allele *penA*795 was the most frequent (8.6%, 62/724), followed by *penA964* (4.7%, 34/724) and *penA808* (4.4%, 32/724).

For phylogenetic analysis, we used 580 *penA* alleles, including 250 *penA* alleles represented by 21,091 *N. meningitidis* and 8,218 commensal *Neisseria* genomes in the *Neisseria* PubMLST database, 20 alleles from Shanghai Pen^{NS} meningococci, 22 alleles from Shanghai penicillin-susceptible meningococci, and 288 alleles from Shanghai commensal *Neisseria* isolates. We found 5 clusters, corresponding to *N. meningitidis*, *N. lactamica*, *N. gonorrhoeae*, *N. mucosa*, and *N. subflava* (Figure 3).

Among the 20 *penA* alleles from the Shanghai Pen^{NS} meningococci, only *penA184* (A549T) was within the *N. meningitidis* cluster; the other 19 alleles (with ≥2 of the 5 mutations) scattered into the *N. lactamica* cluster (n = 7), the *N. subflava* cluster (n = 3), the *N. gonorrhoeae* cluster (n = 1), or outside the 5 clusters (n = 8). Those findings suggest that the PBP2 for the mutations was acquired by horizontal gene transfer (Figure 3).

Crossover Point of Recombination Events in *penA*

Among the 19 Pen^{NS} meningococcal *penA* alleles acquired by horizontal gene transfer, we found that 6 *penA* alleles (*penA110*, *penA405*, *penA552*, *penA795*, *penA832*, and *penA843*) were shared by *N. meningitidis* and commensal *Neisseria* isolates (Appendix 2 Table 2). We analyzed 47 *Neisseria* genomes harboring these 6 alleles and found all potential donors of the 6 *penA* alleles; the sizes of the recombination fragments were 805–2,491 bp (Appendix 2 Table 2).

We discovered that the *penA795* allele, an allele associated with dual resistance to penicillin and 3GCs, was also harbored in the internationally disseminated ceftriaxone-resistant *N. gonorrhoeae* FC428 clone (Appendix 2 Table 2) (*25*). It was difficult to judge the origin donor of *penA795* because it was outside all the phylogenetic clusters and shared by 6 species of *Neisseria* (Appendix 2 Table 2).

Genetic Transformation of *penA* Fragments with Mutations

Penicillin-susceptible *N. meningitidis* isolate Nm040 (B:P1.20,13-1:F5-2:ST-5798[CC4821]) was transformed

with the chromosomal DNA of 9 commensal *Neisseria* isolates, each of which was considered to be 1 potential donor of the 5 meningococcal *penA* alleles (*penA405*, *penA552*, *penA795*, *penA832*, and *penA843*) (Appendix 2 Table 2). Transformants each acquired a *penA* allele the same as that of the corresponding donor isolate, leading to increased penicillin MICs from 0.032 μg/mL to 0.125-0.38 μg/mL. The lengths of the recombinant fragments carrying the partial or entire *penA* gene ranged from 512 to 10,534 bp (Appendix 2 Table 3). All transformants with *penA795* also acquired additional mutations (A311V, T483S, and N512Y), showing resistance to cefotaxime (0.25 or 0.5 μg/mL) (Appendix 2 Table 3).

The *penA* fragments (nucleotides 1237–1751) from 2 penicillin-intermediate meningococcal isolates (MIC 0.125 μg/mL) with only 1 or 2 mutations in PBP2, Nm469 (A549T) and Nm465 (F504L and A510V), were also used for transformation. Two groups of transformants each acquired the same PBP2 mutation(s) as their corresponding donor strain, and the penicillin MIC increased to 0.125 μg/mL, without increased cefotaxime MIC (Appendix 2 Table 3).

Discussion

Pen^{NS} *N. meningitidis* strains (MICs 0.25–0.5 μg/mL) were recovered as early as 1985 in Spain (*26*). We discovered more Pen^{NS} isolates from carriers after 2007 and from patients after 2013 in Shanghai, although penicillin-intermediate meningococcus arose initially in 1967 (MIC 0.125 μg/mL; *penA379*; carrier; Appendix 1 Table 2). Our study presents the increasing trend of penicillin nonsusceptibility among *N. meningitidis* isolates in China during 1965–2020 (Figure

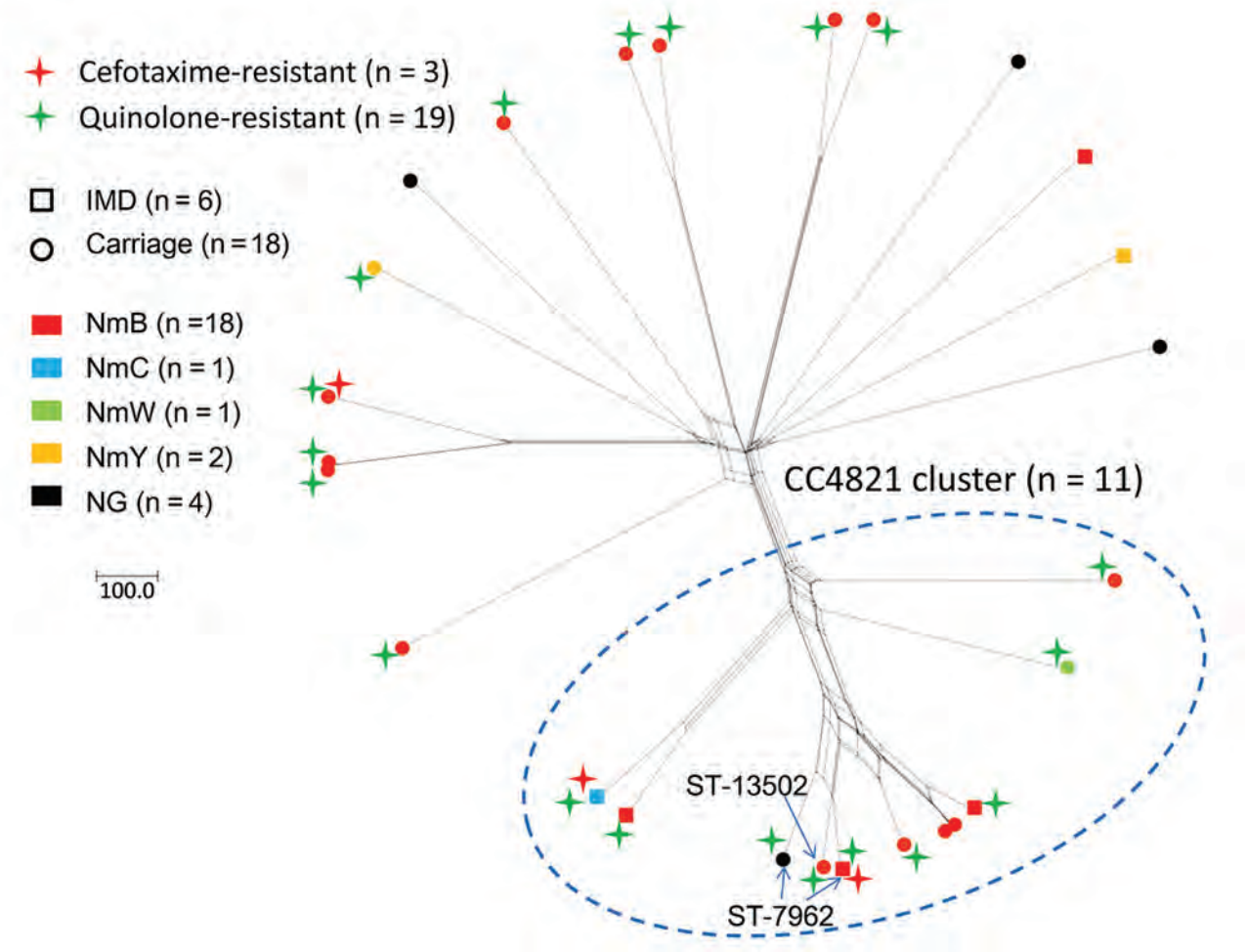

Figure 2. Allele-based clusters of penicillin-nonsusceptible meningococcal isolates identified by using *Neisseria meningitidis* core-genome multilocus sequence typing (MLST) v1.0 scheme, Shanghai, China, 1965–2020. Arrows indicated the 3 singleton isolates identified by 7-locus–based MLST but assigned to CC4821 cluster by core-genome MLST analysis. Scale bar indicates numbers of loci. CC, clonal complex; IMD, invasive meningococcal disease; NG, nongroupable; NmB, serogroup B; NmC, serogroup C; NmW, serogroup W; NmY, serogroup Y; ST, sequence type.

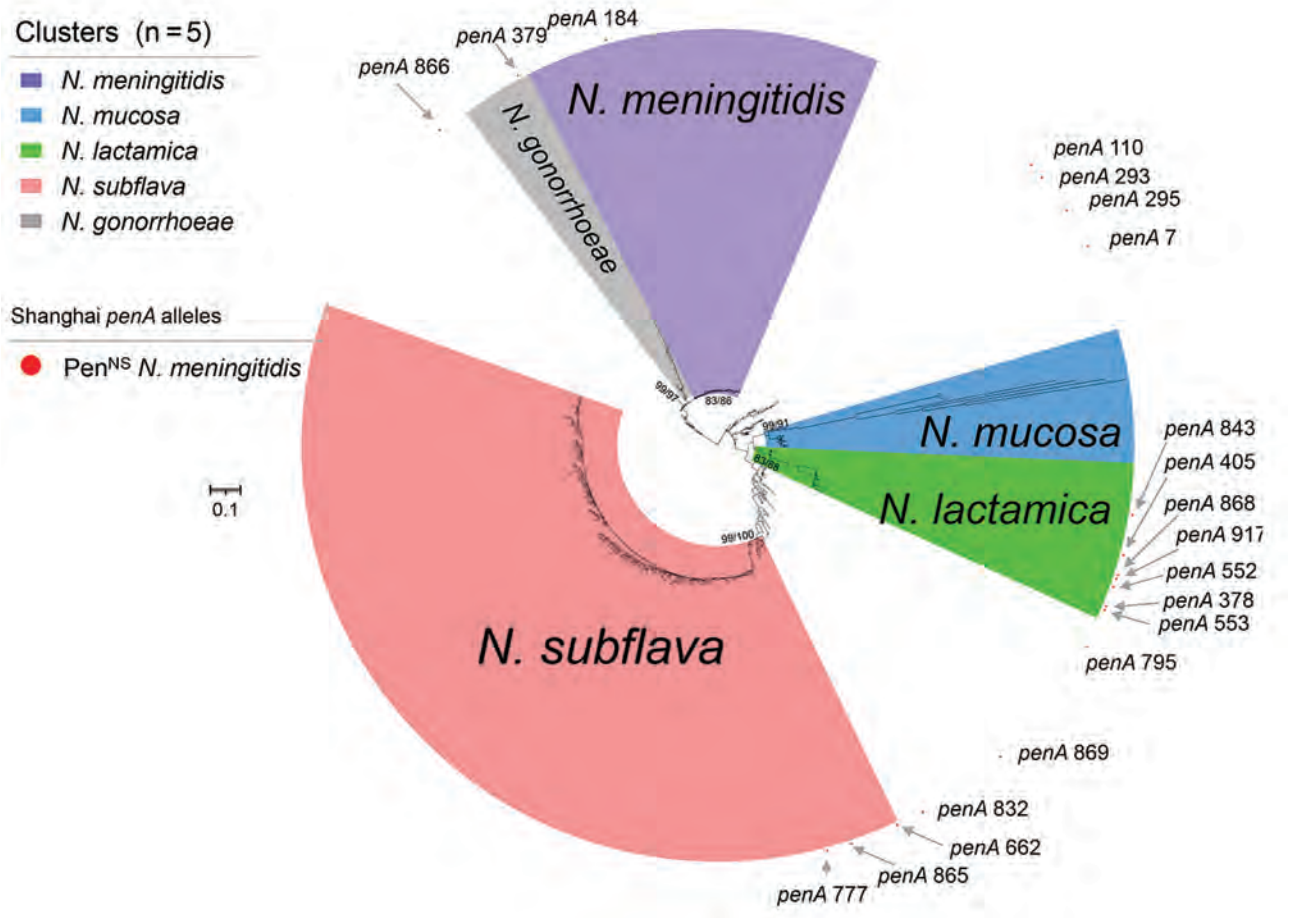

Figure 3. Phylogenetic analysis of *penA* alleles of *Neisseria* isolates and genomes, Shanghai, China, 1965–2020, and reference isolates. Phylogenetic analysis of the nucleotide sequences of 580 *penA* alleles (nucleotides 1321–1722) from *N. meningitidis* (n = 21,582), *N. gonorrhoeae* (n = 7,605), *N. lactamica* (n = 683), *N. subflava* (n = 431), *N. cinerea* (n = 65) , *N. polysaccharea* (n = 52), *N. mucosa* (n = 33), and other commensal *Neisseria* (n = 73) isolates and genomes collected in this study and from the *Neisseria* PubMLST database was constructed by using IQ-TREE version 2.2.0 (*23*), with both SH-aLRT test and UFboot set as 1,000. The values of SH-aLRT and ultrafast bootstrap (Ufboot) are shown on the node of each clade as SH-aLRT/Ufboot. Clusters were determined by using SH-aLRT values of 80% from the SH-aLRT tests with 1,000 replicates and ultrafast bootstrap (UFBoot) values of 85% from bootstrap tests with 1,000 replicates (IQ-TREE). Alleles *penA378*, *penA405*, *penA552*, *penA553*, *penA843*, *penA868*, and *penA917* were within in the *N. lactamica* cluster; *penA662*, *penA777*, and *penA865* were within the *N. subflava* cluster; *penA379* was within the *N. gonorrhoeae* cluster; and the other 8 *penA* alleles were located outside the 5 clusters. Scale bar indicates substitutions per site. Pen^{NS}, penicillin-nonsusceptible meningococci.

1), which is also supported by data from the China CDC and the Zhejiang CDC (*15*–*17*). This trend is similar to trends in other parts of the world, such as North America (≈30%), Europe (≈40%), and Australia (≈90%) (*27*–*29*). The nonsusceptibility was mostly associated with the 5 mutations of PBP2, which were found in widespread Pen^{NS} isolates globally (*14*). Of note, we found 3 isolates with resistance to both penicillin and cefotaxime, together with reduced susceptibility to ceftriaxone, which is rare in *N. meningitidis* worldwide (*30*).

Ceftriaxone is structurally similar to cefotaxime, sharing an exact R1 side chain and similar molecular mechanisms of action. We identified several mutations in the C-terminal or transpeptidase domain of the mosaic PBP2 that were associated with reduced cephalosporin susceptibility (e.g., I312M, V316T, F504L, N512Y, and G545S) (*31*); mutations A311V and T483S were associated with conferring ceftriaxone-resistance to *N. gonorrhoeae*. The cefotaxime-resistant meningococci from China (that contained mutations A311V and T483S in PBP2) differed from the cefotaxime-resistant isolate from the United Kingdom (with PBP2 mutations A501T and D511V) (*12*) but were consistent with the internationally disseminated ceftriaxone-resistant *N. gonorrhoeae* FC428 clone (*25*).

Both *penA795*-bearing isolates Nm507 and FC428 had identical transpeptidase domains of PBP2 (Appendix 2 Figure 3), whereas FC428 displayed a 4-fold higher ceftriaxone MIC than Nm507, possibly resulting from the alterations in *penB* and the promoter region of *mtrR* in FC428 (*32*). We discovered that *penA795* was predominant in commensal *Neisseria* isolates in Shanghai, disseminated among *N. lactamica*, *N. cinerea*, *N. polysaccherae*, *N. subflava*, and *N. gonorrhoeae*. Phylogenetic analysis and genetic transformation suggest that the meningococcal cefotaxime resistance probably originates from *N. subflava* (*penA777* and *penA865*) and another unknown *Neisseria* (*penA795*).

As a hyperinvasive lineage first identified in the NmC meningococcal outbreaks in Anhui, China, during 2003–2005 (*3*), CC4821 has been challenging the preventive strategy of IMD in China for the past 2 decades. After the Anhui outbreaks, the national predominant serogroup shifted from NmA (>95%) before 2000 to NmC (43.3%) and NmA (36.8%) during 2005–2010; in response, in 2008, bivalent NmA and NmC meningococcal polysaccharide vaccine (MPV-AC) was introduced into the Expanded Programme for Immunization in China (*3*,*33*). In 2015, a total of 79% of CC4821 isolates were reported to possess quinolone resistance, and it was recommended that ciprofloxacin not be used as chemoprophylaxis for IMD in 2021 (*5*,*16*). In our study, we observed an increasing trend for acquisition of penicillin nonsusceptibility and cefotaxime resistance in quinolone-resistant CC4821 isolates, which further narrowed the choices for antimicrobial treatment and prophylaxis; safe and effective alternatives such as ceftriaxone, rifampin, and azithromycin could be considered to deal with this hyperinvasive lineage. Another concern is that NmB has become dominant in penicillin- and quinolone-resistant strains, accompanied by increasing nongroupable or rare serogroups (such as NmY and NmW), which could not be protected at present by vaccines in the Expanded Programme for Immunization in China (*33*).

Widespread resistance to either penicillin or ciprofloxacin, which is often associated with emergence of new resistant clones, has challenged the local strategies for treating and preventing IMD. After 2016, a new penicillin-resistant clade of W:P1.5,2:F1-1 (CC11) expanded from Australia to Europe and North America (*13*,*34*). In 2021, a bla_{ROB-1}–containing Y:P1.5-2,10-2:F4-1:ST-3587(CC23) clone, which showed dual resistance to penicillin and ciprofloxacin, was identified in the United States and El Salvador (*35*,*36*). Among global CC4821 isolates, 2 antimicrobial-resistant clones were discovered: one is China$^{CC4821\text{-}R1\text{-}C/B}$ (quinolone-resistant, *gyrA71*, NmC and NmB), expanding from China to other countries, and the other is the Europe-USA CC4821 cluster (Pen^{NS}, *penA9*, NmB), which was restricted to countries outside of China (*7*). In our study, we observed rapid increases of the Pen^{NS} meningococcal strains with diversified Pen^{NS} alleles, which should be attributable to the selective pressure of penicillin after the increased consumption of broad-spectrum penicillin as indicated by the genetic diversity of these strains. Of note, 42.3% of the Pen^{NS} isolates and 2/3 of the cefotaxime-resistant isolates were assigned to the CC4821 cluster (Figure 2). Among the 11 Pen^{NS} isolates in the CC4821 cluster, 7 isolates were assigned to the same sublineage, L44.2. Among the L44.1 sublineage (identical to the hyperinvasive epidemic clone, China$^{CC4821\text{-}R1\text{-}C/B}$), penicillin-, cefotaxime-, and quinolone-resistant ST-4821 strains have caused IMD, which should raise more concerns for public health.

Most (25/26) of the Pen^{NS} isolates in our study (Appendix 1 Table 2) are not covered by the scheduled meningococcal vaccines (MPV-A and MPV-AC) in China (*33*). All 3 cefotaxime-resistant isolates were from toddlers, who were unable to obtain protection from the corresponding vaccines (NmC or NmB) according to scheduled vaccination in China (*33*). MPV-AC is used only for children >3 years of age, and no NmB vaccines are available nationwide. To protect young children from cefotaxime-resistant isolates, on one hand, serogroup A and C meningococcal polysaccharide conjugate vaccine could be a good choice because it can cover populations >3 months of age (*37*); on the other hand, it is necessary to introduce or develop NmB vaccines for CC4821 strains from China.

In our study, 18/20 *penA* alleles identified in the Pen^{NS} isolates harbored the 5 penicillin-resistance-associated mutations in PBP2, and no prevalent alleles were found. In Europe and the United States, *penA12* (8%), *penA14* (6%), and *penA9* (5%) were the most prevalent alleles in Pen^{NS} isolates (*14*), but none of them were observed in isolates from China.

Phylogenetic analysis showed that most of the altered *penA* fragments of the Pen^{NS} isolates from China were acquired by horizontal gene transfer and most likely from *N. lactamica*, *N. subflava*, and *N. gonorrhoeae*. Analysis of >700 local commensal *Neisseria* isolates showed that their PBP2 all harbored the 5 common mutations, which could provide *N. meningitidis* isolates with various mutation-harboring *penA* alleles. On the basis of 6 *penA* alleles shared by *N. meningitidis* and commensal *Neisseria* isolates, those potential horizontal gene transfer events were

validated by sequence analysis and genetic transformation (Appendix 2 Tables 2, 3).

One limitation of this study is the limited number of IMD isolates, which is mainly attributable to the recent low and decreasing incidence of IMD in China, from 0.18 cases (2005) to 0.0078 cases (2015–2019) per 100,000 population (*33*,*38*). Nevertheless, the isolates were phylogenetically related to the invasive meningococci in China, possessing representative features as demonstrated previously (*5*,*7*,*39*,*40*). The trend of increasing Pen^{NS} meningococci in China provided additional evidence for this study (*15*–*17*). Another limitation is that the *penA184* and *penA866* alleles were represented by only 1 penicillin-intermediate isolate each, which did not meet the requirements for the definition of Pen^{NS} *penA* alleles (*14*), although genetic transformations supported the contributions to the phenotype.

In summary, our study detected an ongoing shift in the penicillin susceptibility of meningococcal isolates in Shanghai. Pen^{NS} meningococcal isolates have increased in recent years, and Pen^{NS} CC4821 isolates have become predominant. Resistant *penA* alleles have been captured by quinolone-resistant CC4821 hyperinvasive epidemic clone with serogroup B or C. Because we do not yet have NmB vaccines with high coverage for NmB isolates of China$^{CC4821\text{-}R1\text{-}C/B}$, the concern is that the triple-resistant CC4821 clone has the potential to cause an epidemic. The altered *penA* of Pen^{NS} isolates originated mainly from commensal *Neisseria* isolates, including *N. lactamica* and *N. subflava*. As part of the increasing trend of penicillin nonsusceptibility among *N. meningitidis* isolates in China during 1965–2020, quinolone-resistant CC4821 has acquired penicillin and cefotaxime resistance closely related to the internationally disseminated ceftriaxone-resistant gonococcal FC428 clone.

Acknowledgments

We appreciate the establishment of the *penA* typing database, which was mainly created by Muhamed-Kheir Taha, Julio A. Vázquez, and several peers from the European Monitoring Group for Meningococci. We thank Eva Hong for her work as the curator of the *penA* database and for assigning the numerous new alleles identified in this study. We thank Zhujun Shao and. Li Xu for checking the MIC values of the cefotaxime-resistant isolates.

This study uses *Neisseria* genomic data deposited in the *Neisseria* MLST Database (https://pubmlst.org/neisseria) at the University of Oxford (*21*). Database development has been funded by the Wellcome Trust and European Union.

This work was supported by the National Natural Science Foundation of China (82272381 and 81872909), Natural Science Foundation of Shanghai (21ZR1459800), Youth Medical Talents – Public Health Leadership Program of Shanghai "Rising Stars of Medical Talents" Youth Development Program (2020), and Three-Year Action Plan of Shanghai Public Health System Construction - Key Discipline Construction (2020-2022; no. GWV-10.1-XK03). The funders had no role in the study design, data collection and interpretation, or the decision to submit the work for publication.

About the Author

Dr. Mingliang Chen is a professor in the Department of Microbiology, Shanghai Municipal Center for Disease Control and Prevention. His research interests include mechanisms of antimicrobial resistance in clinical isolates responsible for respiratory tract infections.

References

1. Pollard AJ. Global epidemiology of meningococcal disease and vaccine efficacy. Pediatr Infect Dis J. 2004;23(Suppl): S274–9. https://doi.org/10.1097/01.inf.0000147642.85129.05
2. Maiden MC, Bygraves JA, Feil E, Morelli G, Russell JE, Urwin R, et al. Multilocus sequence typing: a portable approach to the identification of clones within populations of pathogenic microorganisms. Proc Natl Acad Sci U S A. 1998;95:3140–5. https://doi.org/10.1073/pnas.95.6.3140
3. Shao Z, Li W, Ren J, Liang X, Xu L, Diao B, et al. Identification of a new *Neisseria meningitidis* serogroup C clone from Anhui Province, China. Lancet. 2006;367:419–23. https://doi.org/10.1016/S0140-6736(06)68141-5
4. Zhou H, Shan X, Sun X, Xu L, Gao Y, Li M, et al. Clonal characteristics of invasive *Neisseria meningitidis* following initiation of an A + C vaccination program in China, 2005-2012. J Infect. 2015;70:37–43. https://doi.org/10.1016/j.jinf.2014.07.022
5. Chen M, Guo Q, Wang Y, Zou Y, Wang G, Zhang X, et al. Shifts in the antibiotic susceptibility, serogroups, and clonal complexes of *Neisseria meningitidis* in Shanghai, China: a time trend analysis of the pre-quinolone and quinolone eras. PLoS Med. 2015;12:e1001838. https://doi.org/10.1371/journal.pmed.1001838
6. Lucidarme J, Zhu B, Xu L, Bai X, Gao Y, González-López JJ, et al. Genomic analysis of the meningococcal ST-4821 complex-Western clade, potential sexual transmission and predicted antibiotic susceptibility and vaccine coverage. PLoS One. 2020;15:e0243426. https://doi.org/10.1371/journal.pone.0243426
7. Chen M, Harrison OB, Bratcher HB, Bo Z, Jolley KA, Rodrigues CMC, et al. Evolution of sequence type 4821 clonal complex hyperinvasive and quinolone-resistant meningococci. Emerg Infect Dis. 2021;27:1110–22. https://doi.org/10.3201/eid2704.203612
8. Harrison OB, Cole K, Peters J, Cresswell F, Dean G, Eyre DW, et al. Genomic analysis of urogenital and rectal *Neisseria meningitidis* isolates reveals encapsulated hyperinvasive meningococci and coincident multidrug-resistant gonococci. Sex Transm Infect. 2017;93:445–51. https://doi.org/10.1136/sextrans-2016-052781

9. Nadel S, Kroll JS. Diagnosis and management of meningococcal disease: the need for centralized care. FEMS Microbiol Rev. 2007;31:71–83. https://doi.org/10.1111/j.1574-6976.2006.00059.x
10. Bozio CH, Isenhour C, McNamara LA. Characteristics of and meningococcal disease prevention strategies for commercially insured persons receiving eculizumab in the United States. PLoS One. 2020;15:e0241989. https://doi.org/10.1371/journal.pone.0241989
11 Rosenstein NE, Perkins BA, Stephens DS, Popovic T, Hughes JM. Meningococcal disease. N Engl J Med. 2001;344:1378–88. https://doi.org/10.1056/NEJM200105033441807
12. Willerton L, Lucidarme J, Walker A, Lekshmi A, Clark SA, Walsh L, et al. Antibiotic resistance among invasive *Neisseria meningitidis* isolates in England, Wales and Northern Ireland (2010/11 to 2018/19). PLoS One. 2021;16:e0260677. https://doi.org/10.1371/journal.pone.0260677
13. Willerton L, Lucidarme J, Walker A, Lekshmi A, Clark SA, Gray SJ, et al. Increase in penicillin-resistant invasive meningococcal serogroup W ST-11 complex isolates in England. Vaccine. 2021;39:2719–29. https://doi.org/10.1016/j.vaccine.2021.03.002
14. Taha MK, Vázquez JA, Hong E, Bennett DE, Bertrand S, Bukovski S, et al. Target gene sequencing to characterize the penicillin G susceptibility of *Neisseria meningitidis.* Antimicrob Agents Chemother. 2007;51:2784–92. https://doi.org/10.1128/AAC.00412-07
15. Xu L, Zhu B, Xu Z, Gao Y, Shao Z. Analysis on antibiotic susceptibility of Neisseria meningitidis isolates in China, 2003–2012 [in Chinese]. Disease Surveillence. 2015;30:316–20.
16. Xu L, Han F, Wu D, Zhu B, Gao W, Gao Y, et al. Analysis on antimicrobial sensitivity of Neisseria meningitidis in China from 2005 to 2019 [in Chinese]. Zhonghua Yu Fang Yi Xue Za Zhi. 2021;55:207–11.
17. Zhang Y, Deng X, Jiang Y, Zhang J, Zhan L, Mei L, et al. The epidemiology of meningococcal disease and carriage, genotypic characteristics and antibiotic resistance of *Neisseria meningitidis* isolates in Zhejiang Province, China, 2011–2021. Front Microbiol. 2022;12:801196. https://doi.org/10.3389/fmicb.2021.801196
18. Chen M, Zhang C, Zhang X, Chen M. Meningococcal quinolone resistance originated from several commensal *Neisseria* species. Antimicrob Agents Chemother. 2020;64:e01494-19. https://doi.org/10.1128/AAC.01494-19
19. Clinical and Laboratory Standards Institute. Performance standards for antimicrobial susceptibility testing. 32nd ed. Supplement M100. Wayne (PA): The Institute; 2022.
20. Bratcher HB, Corton C, Jolley KA, Parkhill J, Maiden MC. A gene-by-gene population genomics platform: de novo assembly, annotation and genealogical analysis of 108 representative *Neisseria meningitidis* genomes. BMC Genomics. 2014;15:1138. https://doi.org/10.1186/1471-2164-15-1138
21. Jolley KA, Bray JE, Maiden MCJ. Open-access bacterial population genomics: BIGSdb software, the PubMLST.org website and their applications. Wellcome Open Res. 2018;3:124. https://doi.org/10.12688/wellcomeopenres.14826.1
22 Demczuk W, Sidhu S, Unemo M, Whiley DM, Allen VG, Dillon JR, et al. *Neisseria gonorrhoeae* sequence typing for antimicrobial resistance, a novel antimicrobial resistance multilocus typing scheme for tracking global dissemination of *N. gonorrhoeae* strains. J Clin Microbiol. 2017;55:1454–68. https://doi.org/10.1128/JCM.00100-17
23. Nguyen LT, Schmidt HA, von Haeseler A, Minh BQ. IQ-TREE: a fast and effective stochastic algorithm for estimating maximum-likelihood phylogenies. Mol Biol Evol. 2015;32:268–74. https://doi.org/10.1093/molbev/msu300
24. Martin DP, Murrell B, Golden M, Khoosal A, Muhire B. RDP4: detection and analysis of recombination patterns in virus genomes. Virus Evol. 2015;1:vev003. https://doi.org/10.1093/ve/vev003
25. Lee K, Nakayama SI, Osawa K, Yoshida H, Arakawa S, Furubayashi KI, et al. Clonal expansion and spread of the ceftriaxone-resistant *Neisseria gonorrhoeae* strain FC428, identified in Japan in 2015, and closely related isolates. J Antimicrob Chemother. 2019;74:1812–9. https://doi.org/10.1093/jac/dkz129
26. Van Esso D, Fontanals D, Uriz S, Morera MA, Juncosa T, Latorre C, et al. *Neisseria meningitidis* strains with decreased susceptibility to penicillin. Pediatr Infect Dis J. 1987;6:438–9. https://doi.org/10.1097/00006454-198705000-00003
27. Richter SS, Gordon KA, Rhomberg PR, Pfaller MA, Jones RN. *Neisseria meningitidis* with decreased susceptibility to penicillin: report from the SENTRY antimicrobial surveillance program, North America, 1998–99. Diagn Microbiol Infect Dis. 2001;41:83–8. https://doi.org/10.1016/S0732-8893(01)00289-9
28. Bijlsma MW, Bekker V, Brouwer MC, Spanjaard L, van de Beek D, van der Ende A. Epidemiology of invasive meningococcal disease in the Netherlands, 1960–2012: an analysis of national surveillance data. Lancet Infect Dis. 2014;14:805–12. https://doi.org/10.1016/S1473-3099(14)70806-0
29. Lahra MM, George CRR, Shoushtari M, Hogan TR. Australian Meningococcal Surveillance Programme Annual Report, 2020. Communicable Diseases Intelligence. 2021 Aug 30;45. https://doi.org/10.33321/cdi.2021.45.46 *PMID: 34496732*
30. Deghmane AE, Hong E, Taha MK. Emergence of meningococci with reduced susceptibility to third-generation cephalosporins. J Antimicrob Chemother. 2017;72:95–8. https://doi.org/10.1093/jac/dkw400
31. Tomberg J, Unemo M, Davies C, Nicholas RA. Molecular and structural analysis of mosaic variants of penicillin-binding protein 2 conferring decreased susceptibility to expanded-spectrum cephalosporins in *Neisseria gonorrhoeae*: role of epistatic mutations. Biochemistry. 2010;49:8062–70. https://doi.org/10.1021/bi101167x
32. Nakayama S, Shimuta K, Furubayashi K, Kawahata T, Unemo M, Ohnishi M. New ceftriaxone- and multidrug-resistant *Neisseria gonorrhoeae* strain with a novel mosaic *penA* gene isolated in Japan. Antimicrob Agents Chemother. 2016;60:4339–41. https://doi.org/10.1128/AAC.00504-16
33. Li J, Li Y, Shao Z, Li L, Yin Z, Ning G, et al. Prevalence of meningococcal meningitis in China from 2005 to 2010. Vaccine. 2015;33:1092–7. https://doi.org/10.1016/j.vaccine.2014.10.072
34. Mowlaboccus S, Jolley KA, Bray JE, Pang S, Lee YT, Bew JD, et al. Clonal expansion of new penicillin-resistant clade of *Neisseria meningitidis* serogroup W clonal complex 11, Australia. Emerg Infect Dis. 2017;23:1364–7. https://doi.org/10.3201/eid2308.170259
35. Potts CC, Retchless AC, McNamara LA, Marasini D, Reese N, Swint S, et al.; Antimicrobial-Resistant Neisseria meningitidis Team. Acquisition of ciprofloxacin resistance among an expanding clade of beta-lactamase positive, serogroup Y *Neisseria meningitidis* in the United States. Clin Infect Dis. 2021;73:1185–93. https://doi.org/10.1093/cid/ciab358
36. Marín JEO, Villatoro E, Luna MJ, Barrientos AM, Mendoza E, Lemos APS, et al. Emergence of MDR invasive *Neisseria*

meningitidis in El Salvador, 2017–19. J Antimicrob Chemother. 2021;76:1155–9. https://doi.org/10.1093/jac/dkab010
37. Chinese Preventive Medicine. Experts' consensus on immunization with meningococcal vaccines in China [in Chinese]. Zhonghua Liu Xing Bing Xue Za Zhi. 2019;40:123–8.
38. Xu J, Chen Y, Yue M, Yu J, Han F, Xu L, et al. Prevalence of *Neisseria meningitidis* serogroups in invasive meningococcal disease in China, 2010–2020: a systematic review and meta-analysis. Hum Vaccin Immunother. 2022;18:2071077. https://doi.org/10.1080/21645515.2022.2071077
39. Li J, Shao Z, Liu G, Bai X, Borrow R, Chen M, et al. Meningococcal disease and control in China: findings and updates from the Global Meningococcal Initiative (GMI). J Infect. 2018;76:429–37. https://doi.org/10.1016/j.jinf.2018.01.007
40. Chen M, Rodrigues CMC, Harrison OB, Zhang C, Tan T, Chen J, et al. Invasive meningococcal disease in Shanghai, China from 1950 to 2016: implications for serogroup B vaccine implementation. Sci Rep. 2018;8:12334. https://doi.org/10.1038/s41598-018-30048-x

Address for correspondence: Qinglan Guo and Minggui Wang, Huashan Hospital, Fudan University, 12 Middle Wulumuqi Rd, Shanghai 200040, China; email: qinglanguo@fudan.edu.cn and mgwang@fudan.edu.cn; and Min Chen, Shanghai Municipal Center for Disease Control and Prevention, 1380 West Zhongshan Rd, Shanghai 200336, China; email: chenmin@scdc.sh.cn

Combined Phylogeographic Analyses and Epidemiologic Contact Tracing to Characterize Atypically Pathogenic Avian Influenza (H3N1) Epidemic, Belgium, 2019

Steven Van Borm,[1] Géraldine Boseret,[1] Simon Dellicour,[1] Mieke Steensels, Virginie Roupie, Frank Vandenbussche, Elisabeth Mathijs, Aline Vilain, Michèle Driesen, Marc Dispas, Andy W. Delcloo, Philippe Lemey, Ingeborg Mertens, Marius Gilbert, Bénédicte Lambrecht, Thierry van den Berg

The high economic impact and zoonotic potential of avian influenza call for detailed investigations of dispersal dynamics of epidemics. We integrated phylogeographic and epidemiologic analyses to investigate the dynamics of a low pathogenicity avian influenza (H3N1) epidemic that occurred in Belgium during 2019. Virus genomes from 104 clinical samples originating from 85% of affected farms were sequenced. A spatially explicit phylogeographic analysis confirmed a dominating northeast to southwest dispersal direction and a long-distance dispersal event linked to direct live animal transportation between farms. Spatiotemporal clustering, transport, and social contacts strongly correlated with the phylogeographic pattern of the epidemic. We detected only a limited association between wind direction and direction of viral lineage dispersal. Our results highlight the multifactorial nature of avian influenza epidemics and illustrate the use of genomic analyses of virus dispersal to complement epidemiologic and environmental data, improve knowledge of avian influenza epidemiologic dynamics, and enhance control strategies.

Wild birds in the orders Anseriformes and Charadriiformes are considered natural reservoirs of avian influenza viruses (AIVs; family Orthomyxoviridae), maintaining the 16 hemagglutinin (H1–16) and 9 neuraminidase (N1–9) viral subtypes circulating in bird populations (*1*). This reservoir promotes virus evolution, long-range spread, and frequent spillover events to other animal species, including poultry (*2*,*3*). Most AIVs have low pathogenicity, which is defined by intravenous inoculation of chickens 4–8 weeks of age. In contrast, some H5 and H7 subtype strains have high pathogenicity, causing systemic infection and high mortality in chickens (*4*). A polybasic motif within the endoproteolytic cleavage site of the H5 or H7 hemagglutinin precursor protein was recognized as a major determinant of high pathogenicity (*5*,*6*).

Complete sequences of AIV are increasingly used to model and trace avian influenza epidemics both locally (*7*–*12*) and globally (*13*). Moreover, analysis of genomic sequences can be integrated with epidemiologic and environmental data to improve outbreak investigations (*14*–*16*), estimate importance of different epidemiologic parameters (*17*), investigate the effects of external factors on virus dispersal (*13*), or assess the effect of implemented control measures (*18*).

In 2019, Belgium experienced an epidemic of low pathogenicity AIV of subtype H3N1 with unexpectedly high mortality and severe clinical signs in breeder and laying hens (*19*). After the initial outbreak in January and a voluntary partial depopulation of hens in the index farm, a closely related low-pathogenicity AIV was detected in April in the same index farm; a

Author affiliations: Sciensano, Brussels, Belgium (S. Van Borm, G. Boseret, M. Steensels, V. Roupie, F. Vandenbussche, E. Mathijs, A. Vilain, M. Driesen, M. Dispas, B. Lambrecht, T. van den Berg); Rega Institute KU Leuven, Leuven, Belgium (S. Dellicour, P. Lemey); Université Libre de Bruxelles, Brussels (S. Dellicour, M. Gilbert); Royal Meteorological Institute of Belgium, Uccle, Belgium (A.W. Delcloo); Federal Agency for the Safety of the Food Chain, Brussels (I. Mertens)

DOI: https://doi.org/10.3201/eid2902.220765

[1]These first authors contributed equally to this article.

neuraminidase stalk deletion was detected in the virus, indicating viral adaptation to poultry (*19*). Subsequently, the virus spread to 81 additional farms in Belgium and 3 epidemiologically linked farms in France (*19*).

The overall goal of this study was to characterize and explain the epidemiologic dynamics of the 2019 AIV H3N1 epidemic by analyzing epidemiologic, viral genomic, geographic, and environmental data covering most affected farms. Specifically, we aimed to reconstruct the spread of the virus and test hypotheses regarding potential drivers of virus dispersal.

Methods

Case Definition and Epidemiologic Data Collection

A case or outbreak was defined as a farm with animals infected by AIV subtype H3N1, confirmed by molecular testing (Appendix, https://wwwnc.cdc.gov/EID/article/29/2/22-0765-App1.pdf). We collected data on 62 of 82 affected farms by using individual semistructured questionnaires, encoding farmer's documents (production data, deliveries, and visitor registries), and tracing cadaver transport. We encoded all data in a harmonized format to include contact tracing, zootechnical and clinical information, and geographic location (Appendix). The extracted data enabled the assignment of samples to different production units within a farm. We analyzed contacts between farms (feed/manure/cadaver trucks, veterinarians, hatcheries, slaughterhouses, technicians, visitors) and networks between operators (Appendix Table 1). We considered the infectious period to be ≤7 days before and after the onset of symptoms (reported by the farmer) as validation of a probable transmission event. We separated transmission networks into transport contact networks, comprising farms connected through commercial movement of a vehicle (1 specific time on 1 specific day), and social contact networks, comprising farms linked through social connections occurring several times during the infectious period, such as family or neighbor visits. We obtained hourly and daily records of wind directions and speeds from August 1, 2018, to July 31, 2019, from 2 synoptic weather stations situated in Beitem and Melle, Belgium, that were close to the initial outbreak area (Figure 1). We detected spatiotemporal case clusters by using SaTScan version 9.6 (https://www.SaTScan.org). We used time-associated settings according to incubation and clinical periods reported by farmers that were estimated to last a total of 14 days, from infection (day –7) to recovery (day +7), and according to the entire epidemic period (15 weeks). To align to zones defined in surveillance recommendations (Directive EU/2005/94 for AI surveillance), we defined circular clusters of a 3 or 10 km radius. We mapped the identified clusters by using QGIS version 3.18 (https://qgis.org).

AIV Whole-Genome Sequencing

We extracted viral RNA from clinical samples or virus isolates and amplified influenza A segments by reverse transcription PCR using universal primers (*20*). We performed Illumina-based (https://www.illumina.com) sequencing, aiming for a minimum of 0.5 million read pairs per sample. We performed reference-based (GenBank accession nos. MN006980–7) AIV genome assembly (Appendix). We concatenated virus genomes by joining size-sorted segment sequences (S1 through S8) without inclusion of a spacer sequence. The resulting sequenced consensus genomes (n = 103) were added to the GISAID EpiFlu database (https://www.gisaid.org), where the genome from the epidemic index case was previously submitted (*19*) (Appendix Table 2). We verified the monophyletic, single introduction nature of the outbreak by using exploratory maximum likelihood phylogenetic analysis (Appendix).

Spatially Explicit Phylogeographic Reconstruction

We aligned the 104 concatenated H3N1 genomes (representing 70 of 82 affected farms) by using MAFFT version 7.310 (*21*) and masked regions without coverage during pairwise comparisons of genomes. For each concatenated genome, we included the geographic coordinates of the affected farm, farm and production unit identification, and sampling date of the original clinical sample in the metadata. We performed a regression of root-to-tip genetic distances against sequence sampling times to assess the phylogenetic temporal signal by using the program TempEst (*22*) (yielding a coefficient of determination R^2 = 0.32) on the basis of a maximum likelihood tree generated with SeaView version 5.0.5 (*23*). We assessed the absence of a recombination signal by using the Φ-test (*24*) implemented in the program SplitsTree 4 (*25*).

For spatially explicit phylogeographic reconstruction of H3N1 lineage dispersal history during the epidemic, we used the relaxed random walk diffusion model (*13*,*26*,*27*) implemented in the software package BEAST 1.10 (*28*). This model enables a joint inference of time-calibrated phylogenetic trees and continuous character mapping of longitude and latitude at internal tree nodes (Appendix). We used 1,000 trees sampled from the posterior distribution for different post hoc analyses.

Potential Drivers of Virus Spread

To investigate the effect of wind direction on H3N1 lineage dispersal, we compared wind direction data with dispersal directions of lineages inferred through our phylogeographic analysis and with dispersal directions of the same lineages in a null dispersal model (*29*). For each phylogenetic branch, for which position was inferred or randomized in the study area, we then computed the angle between dispersal direction and wind direction at the time of the dispersal event. We used a Bayesian approach (Appendix) to test the hypothesis that wind direction was correlated more with inferred than randomized dispersal direction for viral lineages (*30*,*31*). We interpreted Bayes factors (BFs) as previously described (*32*), where 3<BF<20 corresponded to positive support and BF>20 corresponded to strong support. We performed this test during different time periods (Figure 1) and with different geographic distance cutoff values (1, 2, 5, and 10 km) to select phylogenetic branches for inclusion in the analysis. The 4 time periods were delineated by key events and decisions made during the epidemic, such as key dates in human activity and behavior toward avian influenza biosecurity measures (Appendix).

We used a Bayesian approach (*29*) to assess the phylogenetic signal associated with 3 categorical epidemiologic covariates attributed to virus source

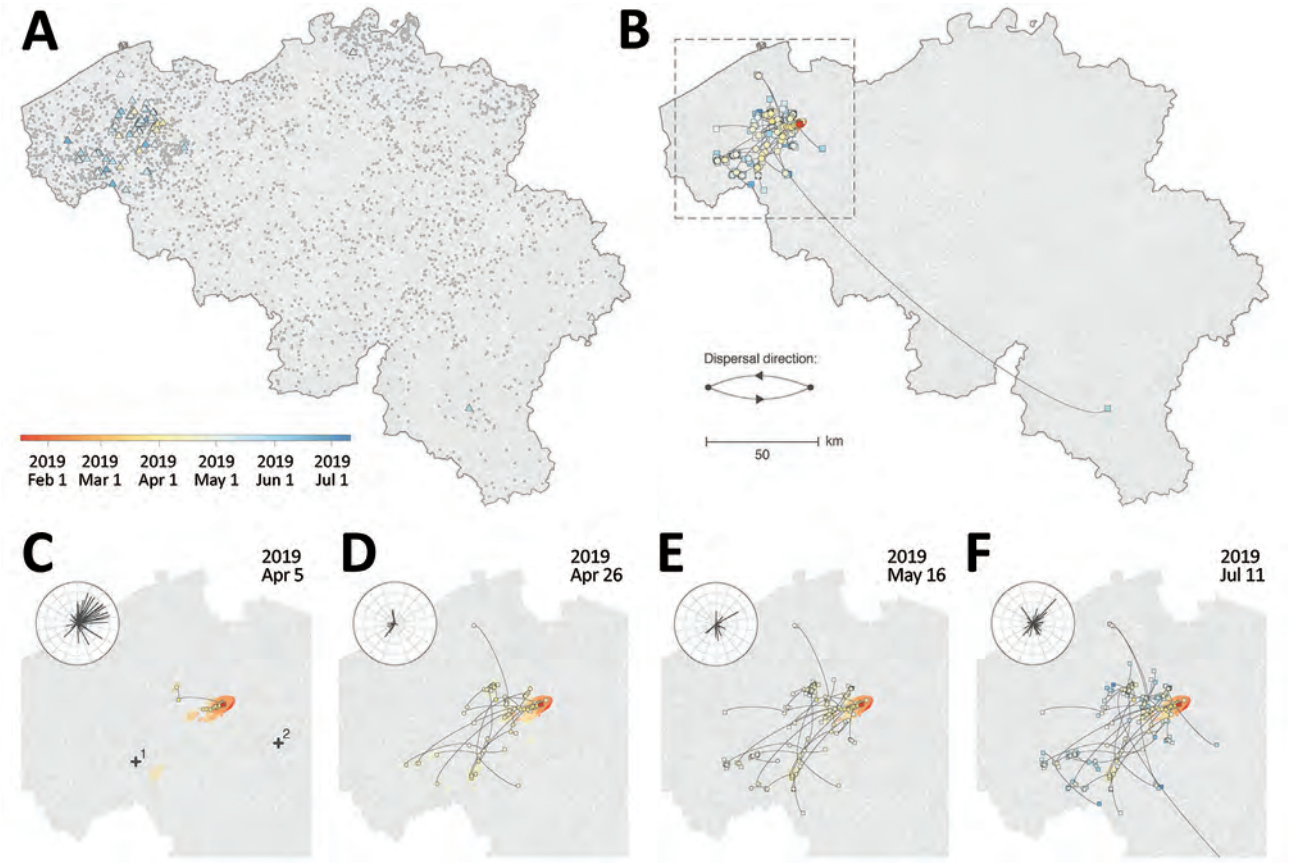

Figure 1. Spatiotemporal dispersal history of H3N1 lineages in study combining phylogeographic analyses and epidemiologic contact tracing to characterize the atypically pathogenic avian influenza (H3N1) epidemic in Belgium during 2019. A, B) We mapped the spatiotemporal distribution of H3N1 outbreaks (triangles) among the distribution of Belgian poultry farms (gray dots) (A) and the maximum clade credibility tree obtained by continuous phylogeographic inference on the basis of 1,000 posterior trees (B). The tree is superimposed on 80% highest posterior density polygons reflecting phylogeographic uncertainty associated with inferred positions of internal nodes. Tip (squares) and internal (circles) nodes are displayed, and dispersal direction of viral lineages is indicated by the edge curvature (anticlockwise). Outbreaks, tree nodes, and highest posterior density regions are all colored according to their date of occurrence. C–F) Four snapshots of the area shown in the box in panel B, which display the dispersal history of H3N1 lineages through time and on which we coplotted the wind direction and intensity (length of line, not used for hypothesis testing) recorded for the days in each period. The period was defined as the time between the date of the previous snapshot and the date of the snapshot under consideration. Wind direction and intensity were averaged measurements taken at 2 meteorological stations (1, Beitum; 2, Melle). A visual comparison between the time-scaled tree and the phylogeographic reconstruction is provided in Appendix Figure 4 (https://wwwnc.cdc.gov/EID/article/29/2/22-0765-App1.pdf).

farms: spatiotemporal SaTScan clusters, transport contact networks (including feed delivery, manure and cadaver collection, and live animal transport), and social networks (same veterinarian, family, or neighbors) during the epidemic. We used the same 1,000 trees sampled from the posterior distribution and the R package phytools (http://www.phytools.org) to estimate the Blomberg *K* statistic. The *K* statistic measures the phylogenetic signal of a covariate by comparing the observed signal with the signal under a Brownian motion model of trait evolution (*30*,*31*). The statistical support (BF) associated with the inferred distribution of *K* for a given covariate was evaluated by comparing with its corresponding null distribution (Appendix) (*28*,*33*). BF support levels were interpreted as previously described (*32*,*34*).

Results

Epidemiologic Findings

Most affected poultry farms (91.5%) were situated in a single area of dense poultry farming (Figure 1, panel A) and mainly involved laying hens (mean age at onset of symptoms was 45 weeks). All the identified spatiotemporal clusters were located in the area of dense poultry farming, including 4 clusters with a 3 km radius (Appendix Figure 1) and 3 clusters with a 10 km radius. Of the 4 clusters with a 3 km radius, cluster 1 included the index case, clusters 2 and 3 represented short distance dispersal in a westerly direction, and cluster 4 represented a medium distance (<50 km) dispersal in a southwesterly direction (Appendix Figure 1). A long-distance dispersal event (>100 km) in the southeasterly direction into the province of Luxemburg was linked with the transport of live animals from cluster 2. A potential long-distance dispersal event in the northeasterly direction consisted of 2 weak PCR-positive asymptomatic farms in the province of Antwerp; no data were obtained, excluding those farms from the phylogenetic analysis. Contact tracing data from outbreak investigation efforts covered 62 (75%) of 82 affected farms. Documented anthropogenic transmission routes (Appendix Table 1) showed potential connectivity between affected farms, involving transport (live animals, eggs, feed, manure, or cadavers) and human movements between farms. We identified 6 transport contact networks and 9 social contact networks.

Whole-Genome Sequencing

Of the 104 virus sequences (representing 85% of the affected farms during the epidemic), 73 were complete genomic sequences (all segments had ≥95% coverage), 5 were near complete sequences (some segments had only partial coverage), and 26 were partial sequences (some segment sequences were missing) (Appendix Table 3). A preliminary phylogenetic investigation confirmed that all sequences corresponding to the 2019 epidemic in Belgium were clustered together within a monophyletic clade (Appendix Figure 2). A reasonable temporal signal was highlighted by our root-to-tip regression analysis ($R^2 = 0.35$; Appendix Figure 3). We did not find statistical support for a recombination signal ($p = 0.442$).

Phylogeographic Reconstruction

Spatially explicit phylogeographic reconstruction (Figure 1, panel B; Appendix Figure 4) confirmed that the spread of the virus began within an area near the index case. Local circulation during the initial epidemic phase was suggested by the presence of multiple internal nodes dating before the reoccurrence of clinical signs in chickens on April 5, 2019, in the same index farm (Figure 1, panel C). A relatively fast initial spread of the virus occurred in an area of dense poultry farming toward the southwest (Figure 1, panel D), followed by local short distance dispersal events in the affected area and medium-to-long distance dispersal events without a clear directional trend. In addition, we observed secondary dispersal clusters and a further extension of the affected geographic area (Figure 1, panels E, F). Our phylogeographic reconstruction also confirmed a link between the isolated long-distance (>100 km) (Figure 1, panel B) dispersal event in the province of Luxemburg and the area corresponding to spatiotemporal cluster 2 (Appendix Figure 1).

Potential Drivers of AIV Spread

Moderate support for an association between virus dispersal direction and wind direction was only found for lineage dispersal events >5 km (BF = 3.08) and >10 km (BF = 3.76). When we analyzed different time periods (Figure 1, panels C–F; Appendix), we found positive but weak support for an association between virus dispersal and wind direction during the second time period (April 6–26, 2019) and, again, only for lineage dispersal events >5 km (BF = 3.33) and >10 km (BF = 4.05).

We analyzed evolutionary relationships among viruses from affected farms and potential covariates: SaTScan spatiotemporal clustering, transport-related contact networks, and social contact networks. We used a Bayesian approach to assess the phylogenetic signal associated with each of these covariates (*30*) (i.e., the tendency for farms sharing genetically similar viruses to share the same covariate value).

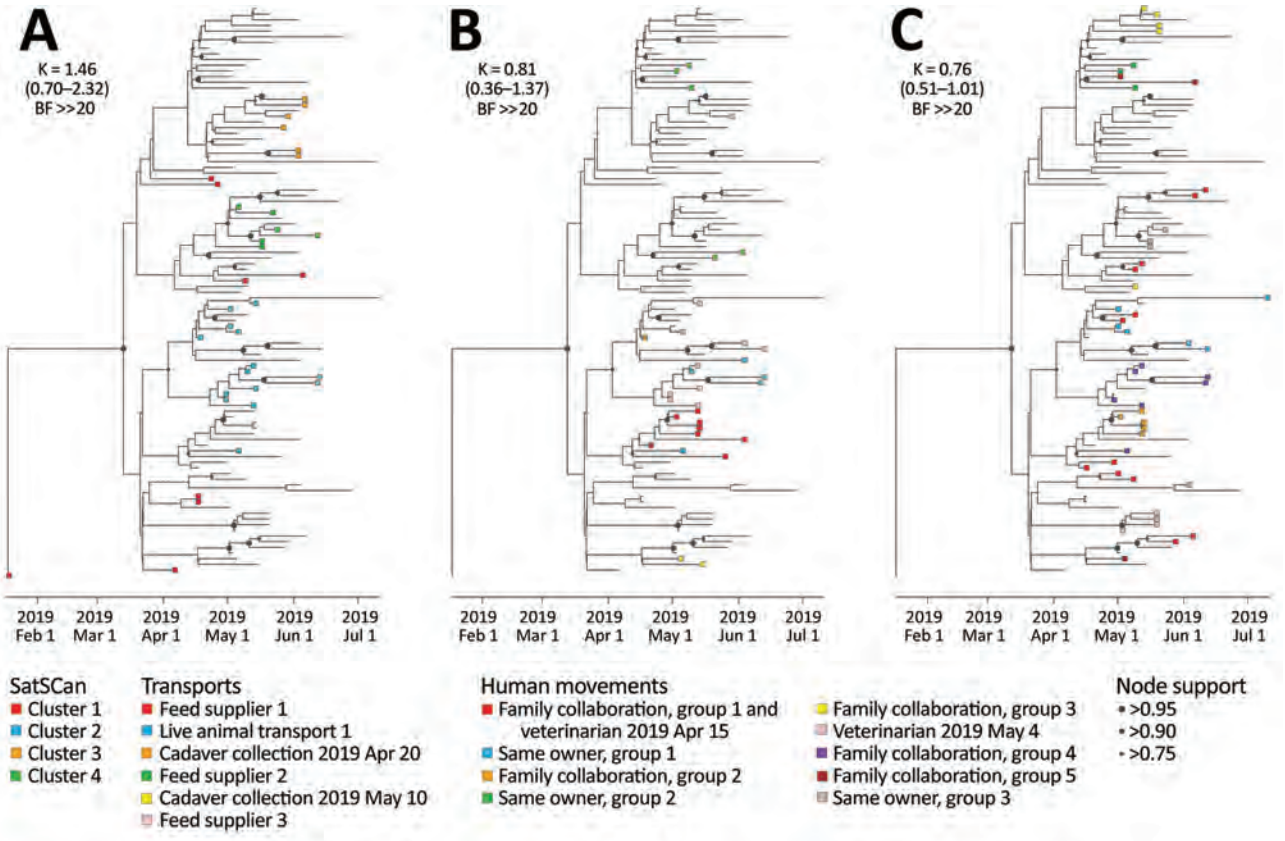

Figure 2. Analysis of the phylogenetic signal associated with 3 covariates in study combining phylogeographic analyses and epidemiologic contact tracing to characterize the atypically pathogenic avian influenza (H3N1) epidemic, Belgium, 2019. We assessed the phylogenetic signal associated with 3 covariates: A) Spatiotemporal SaTScan clusters (https://www.SaTScan.org); B) transport contact networks; C) social contact networks. Tree tip nodes are colored on the basis of the cluster or network to which they belong. For each covariate, we also report the estimated Blomberg *K* statistic and associated 95% highest posterior density interval (in parentheses) and BF support. BF, Bayes factor; ≫, much greater than.

We observed strong statistical support (BF ≫ [much greater than] 20) for the phylogenetic signal associated with each tested covariate (Figure 2). In particular, the strong association between the 3 km geographic clusters identified in the SaTScan analysis and the phylogenetic reconstruction (Figure 2) illustrated the importance of geographic proximity as a main driver of H3N1 dispersal. Cases from SaTScan cluster 1 (Figure 2), which appeared first during the epidemic, were spread over the entire phylogenetic tree, while the other spatiotemporal clusters formed distinct clades within the tree, indicative of secondary spread and diversification. Both transport (including feed delivery, manure and cadaver collection, and live animal transport) and social contact (same veterinarian, family, or neighbors) networks identified through epidemiologic investigations also had strong phylogenetic signals (BF >>20 for both covariates) (Figure 2). However, contact variable mapping to the tree did not perfectly fit into unique clades, leaving several traced contacts invalidated by the phylogenetic analysis (Figure 2).

Discussion

The atypical pathogenicity, high and prolonged viral excretory titers, and the swift dispersal observed for the low-pathogenicity H3N1 virus (*19*,*35*) affecting poultry in Belgium during 2019 merited an in depth investigation of its dispersal dynamics. For this purpose, spatially explicit phylogeographic reconstruction on the basis of AIV whole-genome sequence analysis was used to supplement and validate the available descriptive contact tracing data collected during and after the epidemic. This approach had 3 main advantages. First, sufficiently diverse genetic data enabled the reconstruction of a high resolution and objective spatiotemporal dispersal history of viral lineages. Second, available samples from routine diagnostics during the epidemic permitted high coverage of affected farms, although not necessarily

of asymptomatic farms because of surveillance and methodological biases. Third, the reconstructed dispersal history of viral lineages could be used to test the validity of hypotheses formulated from epidemiologic data, thereby upgrading the contact investigation from a descriptive to qualitative assessment of potential drivers of the epidemic.

AIV whole-genome sequences provide high resolution data that permitted detailed reconstruction of the dispersal history of viral lineages (*11*,*36*). Moreover, phylogeographic analyses of whole genomes were previously used to verify or supplement epidemiologic tracing (*14*–*16*), predict AIV wildlife to poultry jumps (*10*), and associate eco-climatic host density predictors (*15*) or environmental factors (*17*) with AIV outbreak patterns.

Our spatially explicit phylogeographic reconstruction confirmed the origin of the epidemic was near the index farm. The first infection with a low-pathogenicity AIV (H3N1) occurred in outdoor laying hens at a farm in January 2019, where the farmer depopulated only the affected flocks on a voluntary basis, maintaining the healthy flocks in other production units. A closely related virus was detected on April 5, 2019 (date of official notification of an AIV H3N1 outbreak) and contained a neuraminidase stalk deletion indicative of adaptation to poultry and an alternative hemagglutinin precursor protein activation mechanism (*19*,*35*). Several internal nodes of our phylogeographic reconstruction dated before the reemergence of the adapted virus in the index farm, suggesting continued local circulation accompanied by virus diversification in or near the index farm. In the second phase, the virus spread into an area with a high density of poultry farms. Secondary spread included both short and medium distance transmission events and a single long-distance transmission event caused by direct transportation of live animals from a subclinically affected farm.

The windborne virus spread hypothesis was frequently suggested by farmers. We only found weak statistical support for effects of wind direction on virus spread during the early phase of the epidemic when uncontrolled viral spread occurred before the poultry sector increased biosecurity awareness (starting around April 26, 2019). Effects were limited to long distance (>5 km) spread. The absence of correlation between virus dispersal direction and wind direction for shorter distances seems counter-intuitive, especially when considering the dense poultry farming area where the outbreak occurred in combination with the strong correlation between spatiotemporal clustering (at distances <3 km) and genetic relatedness of viral genomes. Wind-based AIV dispersal remains a much debated topic. Strain specific excretion patterns (duration, respiratory versus intestinal, concentration), outbreak specific farm biosecurity and farm organization (number of animals, ventilation, disinfection of vehicles and fomites), and meteorological conditions have a major effect on virus survival, aerosolization, and dispersal. Some studies predicted a wind contribution of up to 20% of dispersal events for a highly pathogenic AIV epidemic (*12*,*37*,*38*), whereas other studies predicted an effect limited to very short distances of <1 km for highly pathogenic AIV (*39*) and no effect of wind dispersal for low-pathogenicity AIV (*40*). These studies illustrate the importance of additional factors such as poultry type and density, housing type, biosecurity protocols and of other anthropogenic dispersal mechanisms in the particular context of a given AIV epidemic (*41*,*42*).

Farms in epidemiologically defined contact networks had a marked tendency to host viruses more closely related within the phylogenetic tree. Those contact networks promoted efficient virus transmission. The initial spatiotemporal cluster in the epidemic source region corresponded to relatively widespread taxa within the phylogenetic tree, which highlights a pronounced genetic diversification in the index farm. Although we cannot formally exclude diversification in the surrounding source area following multiple introductions in the index farm, we believe this process is highly unlikely because all but the first virus sample contained a neuraminidase stalk deletion marker for poultry adaptation. Of note, the 3 categorical epidemiologic variables, spatiotemporal clustering, transport networks, and social contact networks, are not entirely independent. Spatial proximity or social links might, for instance, have an influence on documented transport links between farms, which was illustrated by social networks such as family group 2 that was represented as part of larger transport network, including feed supplier 1 (Figure 2). In some instances, contact networks identified through tracing efforts host various phylogenetic clades, such as family collaboration group 3, which experienced 2 independent virus introductions. Another example was family collaboration group 5, where only 2 of 3 farms contained genetically similar viruses. In addition, suspected contact networks are sometimes invalidated by the phylogenetic analysis. For instance, the feed supplier 3 contact network did not correspond to taxa directly connected within the maximum clade credibility tree. Although the association between spatiotemporal and epidemiologic contact networks and genetic reconstruction is highly supported, the examples of

imperfect associations between epidemiologic and genetic reconstructions indicate that farms in those contact networks were affected by genetically diverse viruses.

Whole-genome analysis of AIV dispersal provides additional insights that can be used to evaluate control policies and enhances information obtained from descriptive epidemiologic investigations. For example, our phylogeographic reconstruction suggests unnoticed virus circulation and diversification before H3N1 reemergence in the index farm. In addition, our phylogenetic signal analyses invalidated several epidemiologically identified contact networks that did not contain genetically related viruses. Finally, our hypothesis testing confirmed that, in addition to spatiotemporal proximity, transport and social contact variables were likely the main factors involved in virus spread during both the initial phase and secondary cluster establishment.

Beyond showing the highly complementary nature of epidemiologic contact tracing and genomic dissemination reconstruction, our findings highlight the importance of surveillance and swift implementation of biosecurity measures. Enhanced surveillance could improve the likelihood of detecting cryptic virus circulation, diversification, and adaptation, and would also enable more rapid implementation of outbreak intervention measures. In addition, enhanced surveillance could improve the coverage of both epidemiologic and genetic data, ultimately improving our understanding of epidemic dispersal dynamics and providing novel insights for surveillance design and outbreak management strategies.

Acknowledgments

We thank Lison Dejouy for excellent technical assistance and Griet Cocquyt and Sofie Van Lancker for compiling outbreak investigation data.

Raw sequencing data were professionally generated by the VIB Neuromics Support Facility, Antwerp, Belgium. R scripts and related files needed to run the phylogenetic and phylogeographic analyses are available at https://github.com/sdellicour/h3n1_belgian_outbreak. Influenza A virus genomic sequences are available in the GISAID EpiFlu database under the accession numbers specified in Appendix Table 2.

The Federal Agency for the Safety of the Food Chain, Belgium, provided detailed outbreak investigation interview data and funding for the whole-genome sequencing. S.D. was supported by the Fonds National de la Recherche Scientifique (FNRS, Belgium, grant no. F.4515.22) and the Research Foundation-Flanders (Fonds voor Wetenschappelijk Onderzoek-Vlaanderen, grant no. G098321N). S.D. and P.L. were supported by the European Union Horizon 2020 project MOOD (grant agreement no. 874850). P.L. was supported by the European Research Council under the European Union's Horizon 2020 research and innovation programme (grant agreement no. 725422-ReservoirDOCS). Computational resources were provided by the Consortium des Équipements de Calcul Intensif (CÉCI) and funded by the Fonds de la Recherche Scientifique de Belgique (grant no. 2.5020.11) and by the Walloon Region.

About the Author

Dr. Van Borm is a senior scientist in the avian virology and immunology unit of Sciensano in Brussels. His research interests focus on molecular diagnostics, characterization, and evolution of livestock viruses, including avian influenza and Newcastle disease.

References

1. Fouchier RAM, Munster V, Wallensten A, Bestebroer TM, Herfst S, Smith D, et al. Characterization of a novel influenza A virus hemagglutinin subtype (H16) obtained from black-headed gulls. J Virol. 2005;79:2814–22. https://doi.org/10.1128/JVI.79.5.2814-2822.2005
2. Venkatesh D, Poen MJ, Bestebroer TM, Scheuer RD, Vuong O, Chkhaidze M, et al. Avian influenza viruses in wild birds: virus evolution in a multihost ecosystem. J Virol. 2018;92:e00433-18. https://doi.org/10.1128/JVI.00433-18
3. Webster RG, Bean WJ, Gorman OT, Chambers TM, Kawaoka Y. Evolution and ecology of influenza A viruses. Microbiol Rev. 1992;56:152–79. https://doi.org/10.1128/mr.56.1.152-179.1992
4. World Organisation for Animal Health. Manual of diagnostic tests and vaccines for terrestrial animals. Avian influenza (including infection with high pathogenicity avian influenza viruses). 2021 [cited 2022 Mar 15]. https://www.oie.int/en/what-we-do/standards/codes-and-manuals/terrestrial-manual-online-access
5. Steinhauer DA. Role of hemagglutinin cleavage for the pathogenicity of influenza virus. Virology. 1999;258:1–20. https://doi.org/10.1006/viro.1999.9716
6. Horimoto T, Kawaoka Y. Reverse genetics provides direct evidence for a correlation of hemagglutinin cleavability and virulence of an avian influenza A virus. J Virol. 1994;68:3120–8. https://doi.org/10.1128/jvi.68.5.3120-3128.1994
7. Bergervoet SA, Heutink R, Bouwstra R, Fouchier RAM, Beerens N. Genetic analysis identifies potential transmission of low pathogenic avian influenza viruses between poultry farms. Transbound Emerg Dis. 2019;66:1653–64. https://doi.org/10.1111/tbed.13199
8. Fusaro A, Tassoni L, Hughes J, Milani A, Salviato A, Schivo A, et al. Evolutionary trajectories of two distinct avian influenza epidemics: parallelisms and divergences. Infect Genet Evol. 2015;34:457–66. https://doi.org/10.1016/j.meegid.2015.05.020
9. Hall M, Woolhouse M, Rambaut A. Epidemic reconstruction in a phylogenetics framework: transmission trees as partitions of the node set. PLOS Comput Biol. 2015;11:e1004613. https://doi.org/10.1371/journal.pcbi.1004613

10. Harvey WT, Mulatti P, Fusaro A, Scolamacchia F, Zecchin B, Monne I, et al. Spatiotemporal reconstruction and transmission dynamics during the 2016–17 H5N8 highly pathogenic avian influenza epidemic in Italy. Transbound Emerg Dis. 2021;68:37–50. https://doi.org/10.1111/tbed.13420
11. Van Borm S, Jonges M, Lambrecht B, Koch G, Houdart P, van den Berg T. Molecular epidemiological analysis of the transboundary transmission of 2003 highly pathogenic avian influenza H7N7 outbreaks between the Netherlands and Belgium. Transbound Emerg Dis. 2014;61:86–90. https://doi.org/10.1111/tbed.12009
12. Ypma RJF, Jonges M, Bataille A, Stegeman A, Koch G, van Boven M, et al. Genetic data provide evidence for wind-mediated transmission of highly pathogenic avian influenza. J Infect Dis. 2013;207:730–5. https://doi.org/10.1093/infdis/jis757
13. Dellicour S, Lemey P, Artois J, Lam TT, Fusaro A, Monne I, et al. Incorporating heterogeneous sampling probabilities in continuous phylogeographic inference—application to H5N1 spread in the Mekong region. Bioinformatics. 2020;36:2098–104. https://doi.org/10.1093/bioinformatics/btz882
14. Mulatti P, Fusaro A, Scolamacchia F, Zecchin B, Azzolini A, Zamperin G, et al. Integration of genetic and epidemiological data to infer H5N8 HPAI virus transmission dynamics during the 2016–2017 epidemic in Italy. Sci Rep. 2018;8:18037. https://doi.org/10.1038/s41598-018-36892-1
15. Scolamacchia F, Mulatti P, Mazzucato M, Barbujani M, Harvey WT, Fusaro A, et al. Different environmental gradients associated to the spatiotemporal and genetic pattern of the H5N8 highly pathogenic avian influenza outbreaks in poultry in Italy. Transbound Emerg Dis. 2021;68:152–67. https://doi.org/10.1111/tbed.13661
16. Ypma RJF, Bataille AMA, Stegeman A, Koch G, Wallinga J, van Ballegooijen WM. Unravelling transmission trees of infectious diseases by combining genetic and epidemiological data. Proc Biol Sci. 2012;279:444–50. https://doi.org/10.1098/rspb.2011.0913
17. Magee D, Beard R, Suchard MA, Lemey P, Scotch M. Combining phylogeography and spatial epidemiology to uncover predictors of H5N1 influenza A virus diffusion. Arch Virol. 2015;160:215–24. https://doi.org/10.1007/s00705-014-2262-5
18. Chakraborty D, Guinat C, Müller NF, Briand F-X, Andraud M, Scoizec A, et al. Phylodynamic analysis of the highly pathogenic avian influenza H5N8 epidemic in France, 2016–2017. Transbound Emerg Dis. 2022;69:e1574–83. PubMed https://doi.org/10.1111/tbed.14490
19. Steensels M, Gelaude P, Van Borm S, Van Den Berg T, Cargnel M, Roupie V, et al. Atypical pathogenicity of avian influenza (H3N1) virus involved in outbreak, Belgium, 2019. Emerg Infect Dis. 2020;26:1899–903. https://doi.org/10.3201/eid2608.191338
20. Hoffmann E, Stech J, Guan Y, Webster RG, Perez DR. Universal primer set for the full-length amplification of all influenza A viruses. Arch Virol. 2001;146:2275–89. https://doi.org/10.1007/s007050170002
21. Katoh K, Standley DM. MAFFT multiple sequence alignment software version 7: improvements in performance and usability. Mol Biol Evol. 2013;30:772–80. https://doi.org/10.1093/molbev/mst010
22. Rambaut A, Lam TT, Max Carvalho L, Pybus OG. Exploring the temporal structure of heterochronous sequences using TempEst (formerly Path-O-Gen). Virus Evol. 2016;2:vew007. https://doi.org/10.1093/ve/vew007
23. Gouy M, Guindon S, Gascuel O. SeaView version 4: a multiplatform graphical user interface for sequence alignment and phylogenetic tree building. Mol Biol Evol. 2010;27:221–4. https://doi.org/10.1093/molbev/msp259
24. Bruen TC, Philippe H, Bryant D. A simple and robust statistical test for detecting the presence of recombination. Genetics. 2006;172:2665–81. https://doi.org/10.1534/genetics.105.048975
25. Huson DH. SplitsTree: analyzing and visualizing evolutionary data. Bioinformatics. 1998;14:68–73. https://doi.org/10.1093/bioinformatics/14.1.68
26. Lemey P, Rambaut A, Welch JJ, Suchard MA. Phylogeography takes a relaxed random walk in continuous space and time. Mol Biol Evol. 2010;27:1877–85. https://doi.org/10.1093/molbev/msq067
27. Pybus OG, Suchard MA, Lemey P, Bernardin FJ, Rambaut A, Crawford FW, et al. Unifying the spatial epidemiology and molecular evolution of emerging epidemics. Proc Natl Acad Sci USA. 2012;109:15066–71. https://doi.org/10.1073/pnas.1206598109
28. Suchard MA, Lemey P, Baele G, Ayres DL, Drummond AJ, Rambaut A. Bayesian phylogenetic and phylodynamic data integration using BEAST 1.10. Virus Evol. 2018;4:vey016. https://doi.org/10.1093/ve/vey016
29. Martinet B, Dellicour S, Ghisbain G, Przybyla K, Zambra E, Lecocq T, et al. Global effects of extreme temperatures on wild bumblebees. Conserv Biol. 2021;35:1507–18. https://doi.org/10.1111/cobi.13685
30. Blomberg SP, Garland T Jr, Ives AR. Testing for phylogenetic signal in comparative data: behavioral traits are more labile. Evolution. 2003;57:717–45. https://doi.org/10.1111/j.0014-3820.2003.tb00285.x
31. Revell LJ. A comment on the use of stochastic character maps to estimate evolutionary rate variation in a continuously valued trait. Syst Biol. 2013;62:339–45. https://doi.org/10.1093/sysbio/sys084
32. Kass RE, Raftery AE. Bayes Factors. J Am Stat Assoc. 1995;90:773–95. https://doi.org/10.1080/01621459.1995.10476572
33. Dellicour S, Rose R, Faria NR, Vieira LFP, Bourhy H, Gilbert M, et al. Using viral gene sequences to compare and explain the heterogeneous spatial dynamics of virus epidemics. Mol Biol Evol. 2017;34:2563–71. https://doi.org/10.1093/molbev/msx176
34. Lee MD, Wagenmakers E-J. Bayesian cognitive modeling: a practical course. Cambridge: Cambridge University Press; 2014.
35. Schön J, Breithaupt A, Höper D, King J, Pohlmann A, Parvin R, et al. Neuraminidase-associated plasminogen recruitment enables systemic spread of natural avian influenza viruses H3N1. PLoS Pathog. 2021;17:e1009490. https://doi.org/10.1371/journal.ppat.1009490
36. Bataille A, van der Meer F, Stegeman A, Koch G. Evolutionary analysis of inter-farm transmission dynamics in a highly pathogenic avian influenza epidemic. PLoS Pathog. 2011;7:e1002094. https://doi.org/10.1371/journal.ppat.1002094
37. Ssematimba A, Hagenaars TJ, de Jong MCM. Modelling the wind-borne spread of highly pathogenic avian influenza virus between farms. PLoS One. 2012;7:e31114. https://doi.org/10.1371/journal.pone.0031114
38. Zhao Y, Richardson B, Takle E, Chai L, Schmitt D, Xin H. Airborne transmission may have played a role in the spread of 2015 highly pathogenic avian influenza outbreaks in the United States. Sci Rep. 2019;9:11755. https://doi.org/10.1038/s41598-019-47788-z
39. Jonges M, van Leuken J, Wouters I, Koch G, Meijer A, Koopmans M. Wind-mediated spread of low-pathogenic

avian influenza virus into the environment during outbreaks at commercial poultry farms. PLoS One. 2015;10:e0125401. https://doi.org/10.1371/journal.pone.0125401

40. Guinat C, Rouchy N, Camy F, Guérin JL, Paul MC. Exploring the wind-borne spread of highly patho- genic avian influenza H5N8 during the 2016–2017 epizootic in France. Avian Dis. 2019;63:246–8. https://doi.org/10.1637/11881-042718-ResNote.1
41. Guinat C, Comin A, Kratzer G, Durand B, Delesalle L, Delpont M, et al. Biosecurity risk factors for highly pathogenic avian influenza (H5N8) virus infection in duck farms, France. Transbound Emerg Dis. 2020;67:2961–70. https://doi.org/10.1111/tbed.13672
42. Guinat C, Durand B, Vergne T, Corre T, Rautureau S, Scoizec A, et al. Role of live-duck movement networks in transmission of avian influenza, France, 2016–2017. Emerg Infect Dis. 2020;26:472–80. https://doi.org/10.3201/eid2603.190412

Address for correspondence: Steven Van Borm, Sciensano, Avian Virology and Immunology Service, Groeselenberg 99, B1180 Ukkel Brussels, Belgium; email: Steven.VanBorm@sciensano.be

Age-Stratified Model to Assess Health Outcomes of COVID-19 Vaccination Strategies, Ghana

Sylvia K. Ofori, Jessica S. Schwind, Kelly L. Sullivan, Gerardo Chowell, Benjamin J. Cowling, Isaac Chun-Hai Fung

We assessed the effect of various COVID-19 vaccination strategies on health outcomes in Ghana by using an age-stratified compartmental model. We stratified the population into 3 age groups: <25 years, 25–64 years, and ≥65 years. We explored 5 vaccination optimization scenarios using 2 contact matrices, assuming that 1 million persons could be vaccinated in either 3 or 6 months. We assessed these vaccine optimization strategies for the initial strain, followed by a sensitivity analysis for the Delta variant. We found that vaccinating persons <25 years of age was associated with the lowest cumulative infections for the main matrix, for both the initial strain and the Delta variant. Prioritizing the elderly (≥65 years of age) was associated with the lowest cumulative deaths for both strains in all scenarios. The consensus between the findings of both contact matrices depended on the vaccine rollout period and the objective of the vaccination program.

Ghana reported its first case of COVID-19 on March 12, 2020, and 171,065 cases and 1,445 deaths had been recorded as of December 31, 2022 (*1*). The country introduced various public health measures when the pandemic first emerged, including school closures, travel bans, mask mandates, and, later, vaccination, all of which were associated with a decline in transmission (*2*). Ghana was the first country to receive 600,000 doses of the Oxford-AstraZeneca COVID-19 AZD1222 vaccine (https://www.astrazeneca.com) on February 24, 2021, through the COVAX program (*3*). The vaccination program was deployed in March 2021; politicians and civil society leaders publicly received vaccines to boost nationwide trust in the program (*4*). The first batch of vaccines was delivered to regions and populations with the highest burden of COVID-19: the Greater Accra and Ashanti regions, frontline healthcare workers, the elderly, and persons with comorbidities. In addition to the initially dispersed vaccine doses, the Ministry of Health received an additional supply of the AZD1222 vaccine and the Pfizer-BioNTech BNT162b2 vaccine (https://www.pfizer.com) from several high-income countries (*5*).

Given the limited availability of doses and vaccine hesitancy, only 9.2% of the Ghana population of 30,800,000 was fully vaccinated as of December 2021 (*6*). Hence, the government's goal to reach widespread vaccine coverage by October 2021 was not met (*3*). Studies of COVID-19 vaccine hesitancy among residents of Ghana reported that >35% of study participants said they would not receive the vaccine because of concerns about vaccine efficacy and conspiracy theories (*4*,*7*). Moreover, a seroprevalence study in August 2020 found that only 19% of Ghana residents tested positive for SARS-CoV-2 IgM, IgG, or both (*8*). Such studies suggest that most of the population in Ghana remains susceptible to SARS-CoV-2, and mitigating the pandemic might best be achieved through effectively prioritizing the dispensation of limited vaccines. To optimize Ghana's vaccination strategy, provide evidence of the benefits of vaccination, and increase uptake in the population, research is required to quantify the vaccine's effect on the magnitude of the epidemic peak, cumulative infections,

Author affiliations: Harvard T.H. Chan School of Public Health, Boston, Massachusetts, USA (S.K. Ofori); Georgia Southern University Jiann-Ping Hsu College of Public Health, Statesboro, Georgia, USA (S.K. Ofori, K.L. Sullivan, I.C.-H. Fung); Georgia Southern University Institute for Health Logistics and Analytics, Statesboro (J.S. Schwind); Georgia State University School of Public Health, Atlanta, Georgia, USA (G. Chowell); WHO Collaborating Centre for Infectious Disease Epidemiology and Control, The University of Hong Kong School of Public Health, Pokfulam, Hong Kong (B.J. Cowling)

DOI: http://doi.org/10.3201/eid2902.221098

and deaths in the context of limited vaccine supplies and logistical barriers.

Several mathematical modeling studies of COVID-19 vaccination strategies in other countries and jurisdictions were published in 2020 and 2021 (*9*–*13*). Alagoz et al. used an agent-based model to simulate the transmission dynamics of COVID-19, accounting for the proportion of the population vaccinated, vaccine capacity, and adherence to nonpharmaceutical interventions (*9*). Moghadas et al. used an agent-based model to evaluate the effect of vaccination campaigns on reducing incidence, hospitalizations, and deaths (*10*). Aside from agent-based models, homogenous-mixing and age-stratified compartmental models also have been used. Matrajt et al. used an age-stratified deterministic model, paired with optimization algorithms, for 16 age groups by varying vaccination efficacy and coverages in the population (*11*). Mumtaz et al. used an age-stratified model to assess the vaccination rollout under different vaccination coverages accounting for the decline in transmission and age-mixing matrix (*12*). Bubar et al. expanded their work further to account for contact structure, seroprevalence, and age-specific vaccine efficacy (*13*). The outcomes explored in these studies included symptomatic infections, cumulative infections and deaths, and hospitalizations, focusing mainly on high-income countries outside Africa. Thus, determining who to vaccinate first when vaccines are available and analyzing the sensitivity of modeling outputs to the choice of contact matrices are underexplored in the Africa context and in Ghana specifically.

We employed an age-stratified model to assess the effect of vaccinating 1 million persons in 3 versus 6 months using 2 Africa contact matrices. We retrospectively assessed the counterfactual effect of various age-targeted vaccine optimization strategies against the initial and Delta strains of SARS-CoV-2 when vaccines first became available. Our aim was to inform future vaccination programs by identifying factors critical to achieving optimal outcomes. The Georgia Southern University Institutional Review Board determined that this project (H20364) was exempt from full review under the nonhuman subjects determination (G8) according to the Code of Federal Regulations Title 45 Part 46.

Methods

Model Formulation

We proposed an age-stratified Susceptible-Exposed-Presymptomatic-Symptomatic-Asymptomatic-Recovered-Dead-Vaccinated (SEPIARD-V) model to simulate SARS-CoV-2 transmission dynamics and the effect of various vaccination scenarios (Appendix 1 Figure) (*14*). The SEPIARD-V model acknowledges that persons who are initially asymptomatic and later develop symptoms transmit the virus while in the presymptomatic phase. A 2020 study of presymptomatic transmission of SARS-CoV-2 in Singapore provided evidence of COVID-19 transmission 1–3 days before symptom onset (*15*). The model was suitable for studying the transmission dynamics of COVID-19 in Ghana because of the growing evidence that both symptomatic and asymptomatic patients transmit the infection, regardless of their symptomatic status (*16*,*17*). Our model, therefore, assumed that presymptomatic, asymptomatic, and symptomatic persons contributed to transmission. Our model also assumed that immunity from both natural infection and vaccination waned over time, making reinfection possible (Table 1; Appendix 1). An effective reproduction number (R_t) of 3.13 was assumed for the virus in the main analysis to represent the virus strain that first hit Ghana in the spring of 2020, referred to as the initial strain in this study (Armachie et al., unpub. data, https://doi.org/10.20944/preprints202104.0125.v1). A higher R_t of 5.35 was assumed for the Delta variant in the scenario analyses, with a reduced vaccine efficacy of 67% for the AZD1222 vaccine (*32*; Pearson et al., unpub. data, https://doi.org/10.1101/2021.12.19.21268038). Our model was run for 500 days to allow enough time for the first wave of the epidemic to subside and to include observations relevant to when the second wave began to emerge.

Age Groups and Contact Matrices

Because of the strong evidence of assortative mixing between age groups in sub-Saharan Africa (*33*,*34*), we incorporated a contact matrix between age groups into the model. We stratified the population was stratified into 3 groups: <25 years, 25–64 years, and ≥65 years of age. Two contact matrices were adapted from studies in Uganda (main matrix) and Ethiopia (second matrix) (*33*,*35*). The main matrix suggested that, on average, the within-group contact rate among persons <25 years of age was 23.58 per day; for persons 25–64 years of age, that contact rate was 15.05 per day; and for persons ≥65 years of age, the contact rate was 0.54 per day (*33*). For the second matrix, on average, the within-group daily contact rate was 8.2 among persons <25 years of age, 7.8 for persons 25–64 years of age, and 1.6 for persons ≥65 years of age (*35*). The population breakdown for Ghana was 56.08% <25 years of age (n = 17,272,640), 39.48% 25–64 years of age (n = 12,159,840), and 4.44% ≥65 years of age (n = 1,367,520) (*36*) (Appendix 1).

Scenario Analyses

Our analysis aimed to determine which age group should be prioritized in the case of limited vaccine supply under different rollout speeds. We analyzed multiple scenarios, looking at a percentage of each subpopulation vaccinated when prioritizing different age groups, with coverage calculated for 1 million people using the 2021 population (*37*). The primary scenarios, by percentage of persons vaccinated in each age group, were as follows: (i) 73.1% of persons ≥65 years of age; (ii) 8.2% of persons 25–64 years of age; (iii) 5.8% of persons <25 years of age; and (iv) 3.4% of persons <65 years of age. We also assessed projected outcomes of vaccinating each age group at the same rate without prioritization (v). We used 2 rollout speeds (daily vaccination rates) in each scenario, assuming 2 million doses can be exhausted in 3 months and 6 months (Appendix 1 Tables 1–3). Finally, we performed analyses for 2 additional scenarios by changing the assumptions on vaccine supplies. First, the number of people to be vaccinated was either halved or doubled. Hence, we assumed enough vaccines were available for 500,000 persons (1 million doses) and 2,000,000 persons (4 million doses). We repeated our age-specific scenario analysis using the second contact matrix, adapted from Trentini et al. (*35*).

Analysis

We solved our model's system of ordinary differential equations according to the Runge-Kutta 4 method in the deSolve package in R version 4.1.1 (The R Foundation for Statistical Computing, https://www.r-project.org). We estimated the number of infections and deaths averted in the general population and compared them across all study scenarios. We assessed the percent of the population who were symptomatic at the peak, those who were ever infected (cumulative infections), and those who died (cumulative deaths) (Appendix 1; Appendix 2).

Results

Symptomatic Infections at the Peak under the Main Scenario of Vaccinating 1 Million Persons

The following results of our main analysis assumed an R_t of 3.13 for the initial strain. We demonstrated that vaccinating 1 million persons <25 years of age in 3 months was associated with the lowest percentage (6.75%) of symptomatic persons in the population at the peak. However, prioritizing the elderly (≥65 years of age) resulted in the highest percentage of symptomatic persons (7.19%) at the peak, given a 3-month rollout using the main matrix. If the rollout period was increased to 6 months, prioritizing persons <25 years of age also resulted in the lowest symptomatic percentages (7.01%) using the main matrix. The second matrix suggested that focusing vaccination initiatives on persons 25–64 years of age was associated with the lowest percentage of symptomatic infections (6.96%) (Tables 2, 3; Figure 1).

Table 1. Parameter values for age-stratified SEPIARD-V COVID-19 model to assess health outcomes of COVID-19 vaccination strategies, Ghana*

Parameter	Symbol	Value	References
Mean latency period which is the period from exposure to infectiousness	1/k	1.85 d	Abbasi et al. (*18*), Liu et al. (*19*)
Mean duration of being infectious and symptomatic	1/f	15.7 d	Cai et al. (*20*), Xing et al. (*21*)
Mean duration of being infectious and asymptomatic	1/q	7.25 d	Ma et al. (*22*), Byrne et al. (*23*)
Mean duration of being infectious and presymptomatic	1/c	2.9 d	Tindale et al. (*24*), Byrne et al. (*23*)
Reproduction number for the initial strain	R	3.13	Armachie et al., unpub. data, https://doi.org/10.20944/preprints202104.0125.v1
Reproduction number for the Delta strain	R	5.35	Pearson et al., unpub. data, https://doi.org/10.1101/2021.12.19.21268038
Probability of exposed person becoming presymptomatically infected	δ	0.30	Chen et al. (*25*), Buitrago-Garcia et al. (*26*)
Vaccine efficacy against infection	σ	0.745	Knoll et al. (*27*)
Relative transmissibility of asymptomatic persons	u	0.75	CDC (*28*)
Relative transmissibility of presymptomatic persons	r	0.75	CDC (*28*)
Mean duration of immunity after vaccination	χ	182 d	Iacobucci (*29*)
Mean duration of immunity after natural infection	w	365 d	Good and Hawkes (*30*)
Age-specific case-fatality ratio	z	0.002 for <25 y, 0.005 for 25–64 y, 0.048 for ≥65 y	Our World in Data (January 26, 2021–November 12, 2021; *22*), Lawal (*31*)
Daily vaccination rate	v	Varied by 0.00009–0.0163977 d^{-1} per person	Estimated

*CDC, Centers for Disease Control and Prevention; SEPIARD-V, Susceptible-Exposed-Presymptomatic-Symptomatic-Asymptomatic-Recovered-Dead-Vaccinated.

Table 2. Scenario analysis of outcomes in the total population under various vaccination scenarios, using the main matrix method for the initial strain, Ghana

Vaccine prioritization by age group, y	Scenario, % infections					
	500,000 vaccinated in 3 mo	500,000 vaccinated in 6 mo	1 million vaccinated in 3 mo	1 million vaccinated in 6 mo	2 million vaccinated in 3 mo	2 million vaccinated in 6 mo
Symptomatic infections at peak						
Only ≥65	7.22	7.24	7.19	7.22	7.16	7.19
25–64	7.09	7.17	6.92	7.09	6.61	6.92
<25	7.01	7.13	6.75	7.01	6.26	6.75
<65	7.03	7.15	6.81	7.03	6.37	6.81
Same rate across age groups	7.04	7.15	6.83	7.04	6.40	6.83
Cumulative infections						
Only ≥65	172.88	173.50	172.09	172.88	171.33	172.09
25 –64	170.80	172.57	167.44	170.80	161.00	167.44
<25	170.04	172.20	165.76	170.04	157.17	165.76
<65	170.28	172.43	166.19	170.28	158.20	166.19
Same rate across age groups	170.41	172.39	166.44	170.41	158.51	166.44
Deaths						
Only ≥65	0.18	0.19	0.17	0.18	0.17	0.17
25–64	0.19	0.19	0.19	0.19	0.18	0.19
<25	0.19	0.19	0.19	0.19	0.18	0.19
<65	0.19	0.19	0.19	0.19	0.18	0.19
Same rate across age groups	0.19	0.19	0.19	0.19	0.18	0.19

Cumulative Infections under the Main Scenario of Vaccinating 1 Million Persons

Our results suggest that vaccinating persons <25 years of age was associated with the largest number of cumulative infections averted in Ghana under the assumption of vaccinating 1 million people in 3 months (2,653,676 cases), whereas vaccinating persons ≥65 years of age was associated with the smallest number averted (702,432 cases) (Figure 2). We also found that vaccinating persons <25 years of age should be prioritized when the population was vaccinated at a slower rate (over 6 months) or when the vaccine supply doubled or halved (Table 2). The results were sensitive to a change in the contact matrix (Table 3).

Cumulative Deaths Averted under the Main Scenario of Vaccination of 1 Million Persons

Vaccinating the elderly (≥65 years of age) could avert >7,000 deaths if 1 million people were vaccinated over 3 months, assuming the main contact matrix, and >4,000 deaths would be averted if the elderly population was vaccinated over 6 months. The number of deaths prevented was the lowest when persons <25 years of age were prioritized in both vaccination time frames (2,317 in 3 months vs. 1,157 in 6 months),

Table 3. Scenario analysis of outcomes in the total population under various vaccination scenarios using the second matrix method for the initial strain, Ghana

Vaccine prioritization by age group, y	Scenario, % infections					
	500,000 vaccinated in 3 mo	500,000 vaccinated in 6 mo	1 million vaccinated in 3 mo	1 million vaccinated in 6 mo	2 million vaccinated in 3 mo	2 million vaccinated in 6 mo
Symptomatic infections at peak						
Only ≥65	7.02	7.10	6.92	7.02	6.82	6.92
25–64	6.96	7.07	6.75	6.96	6.35	6.75
<25	6.99	7.09	6.79	6.99	6.42	6.79
<65	6.97	7.08	6.76	6.97	6.35	6.76
Same rate across age groups	6.98	7.08	6.76	6.98	6.35	6.76
Cumulative infections						
Only ≥65	177.71	179.61	175.36	177.71	173.19	175.36
25–64	178.22	180.28	174.26	178.22	166.42	174.26
<25	178.62	180.48	174.95	178.62	167.74	174.95
<65	178.39	180.48	174.42	178.39	166.69	174.42
Same rate across age groups	178.30	180.33	174.25	178.30	166.13	174.25
Deaths						
Only ≥65	0.19	0.20	0.18	0.19	0.17	0.18
25–64	0.21	0.22	0.21	0.21	0.19	0.21
<25	0.22	0.22	0.22	0.22	0.21	0.21
<65	0.22	0.22	0.21	0.22	0.20	0.21
Same rate across age groups	0.21	0.22	0.21	0.21	0.20	0.21

assuming the main contact matrix (Figure 2). Vaccinating the elderly (≥65 years of age) remained the best option to reduce deaths, regardless of the mixing patterns (Tables 2, 3; Figures 1, 2).

Varying Vaccine Supply to Vaccinate 500,000 or 2 Million Persons

Similar to the base case scenarios of vaccinating 1 million persons, prioritizing persons <25 years of age was associated with the lowest percentage of cumulative infections if 500,000 or 2 million persons were vaccinated in 3 or 6 months (Table 2). However, simulations using the second matrix reported mixed results. For example, prioritizing the elderly seemed to be the best strategy for lowering cumulative infections when vaccine supplies were only enough for 500,000 people (177.71% for 3 months and 179.61% for 6 months). In contrast, vaccinating each age group at the same rate was preferred when the supply was enough to vaccinate 2 million persons (166.13% for 3 months and 174.25% for 6 months) (Table 3). Prioritizing the elderly (≥65 years of age) remained the strategy of choice to specifically lower COVID-19 mortality for both matrices (Tables 2, 3).

Comparing Outcomes for the Initial and Delta Variants in the Absence of Vaccination

In the absence of vaccination, the scenario analysis for the Delta variant using the main matrix suggested 10.29% of symptomatic persons at the peak, 231.24% of persons having cumulative incidence of COVID-19, and 0.28% deaths in the population (Appendix 1 Table

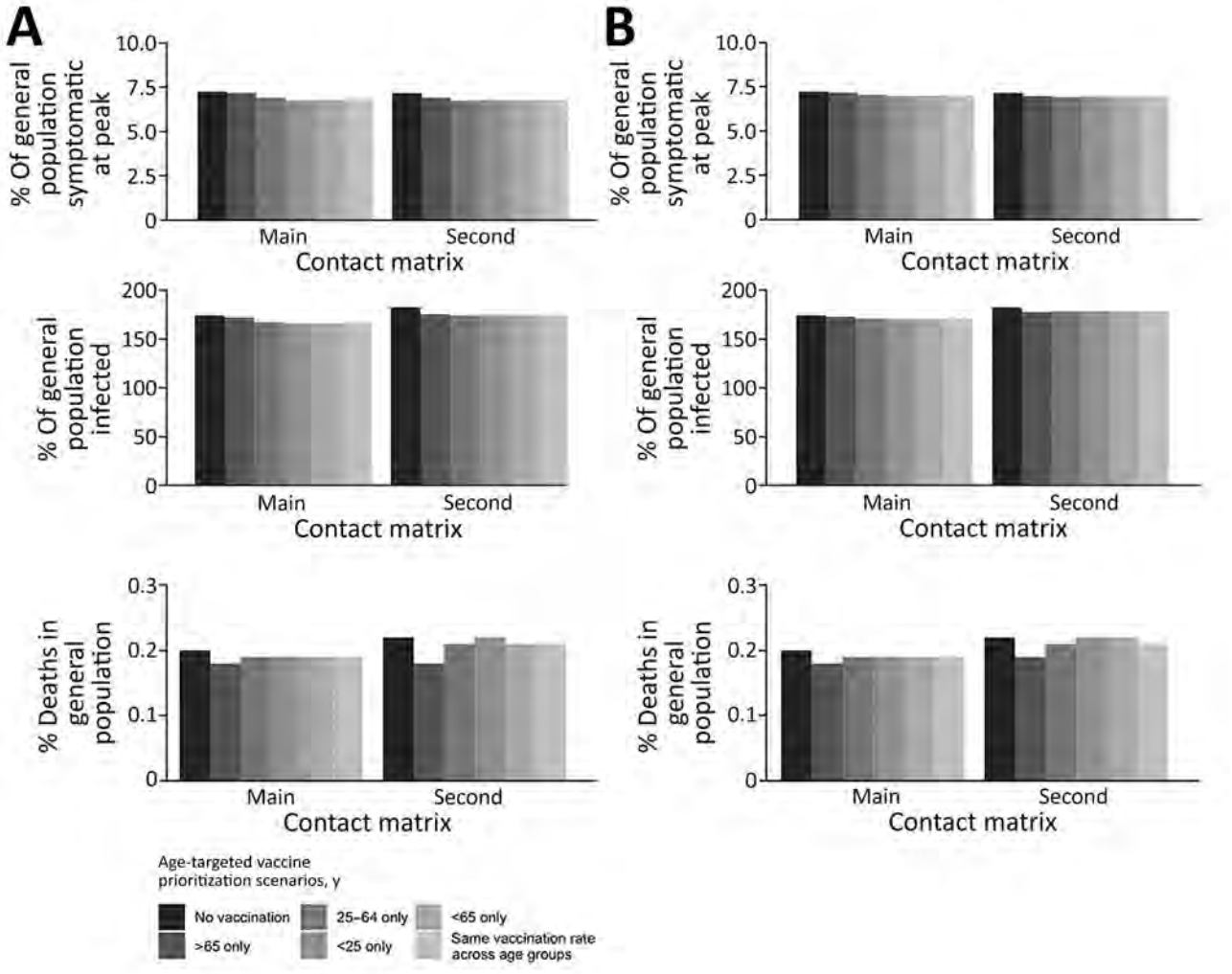

Figure 1. Effects of various vaccination scenarios on symptomatic infections at peak (upper panels), cumulative infections (middle panels), and deaths (lower panels) as a percentage of the general population, Ghana. The assessment used 2 different contact matrices in the main analysis and an effective reproductive number of 3.13 for the initial strain. A) Results assuming 1 million persons were vaccinated in 3 months. B) Results assuming 1 million persons were vaccinated in 6 months. Percentage of cumulative infections is >100% because of waning immunity from natural infection and vaccination.

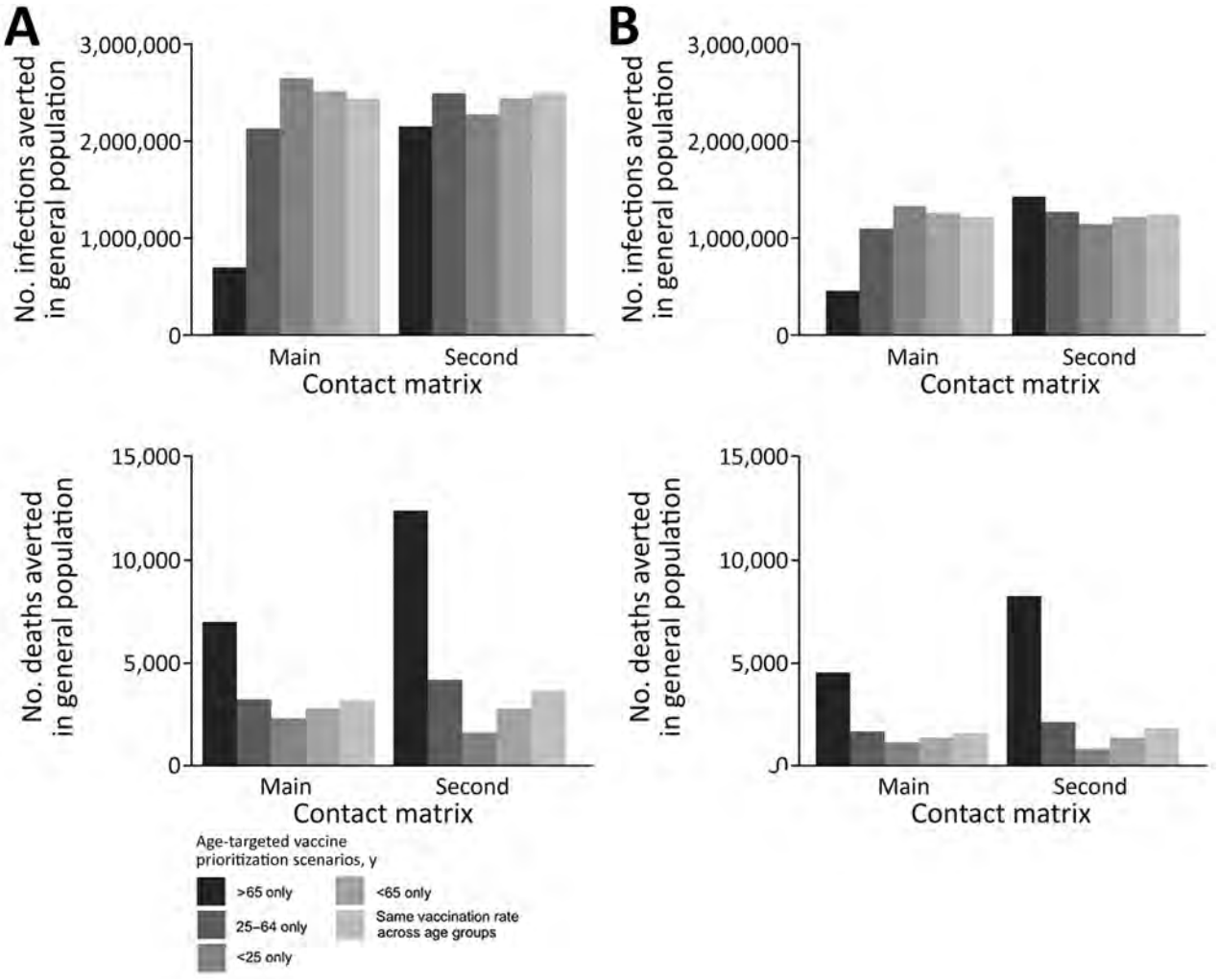

Figure 2. Effects of various vaccination scenarios on the number of cumulative infections averted (upper panels) and the number of deaths averted (lower panels) in the general population, Ghana. The assessment used 2 different contact matrices in the main analysis and an effective reproductive number of 3.13 for the initial strain. A) Results assuming 1 million persons were vaccinated in 3 months. B) Results assuming 1 million persons were vaccinated in 6 months.

4). Those percentages were higher than those for the initial strain, which were calculated as 7.26% of symptomatic persons at peak, 174.37% of persons having cumulative incidence of COVID-19, and 0.20% deaths in the population (Figure 1). Those findings were consistent with the results from the second matrix (Appendix 1 Table 5). In the Delta variant scenario, the percentage of symptomatic persons at the peak was slightly lower with the second matrix (10.14%) than with the main matrix (10.29%). However, cumulative infections (238.73%) and deaths (0.31%) were higher with the second matrix in the Delta variant scenario (Appendix 1 Tables 4, 5).

Impact of Vaccination Strategies on Symptomatic Infections at the Peak Due to the Delta Variant

In analyzing vaccine prioritization for the Delta variant scenario, we found that prioritizing persons <25 years of age was associated with the lowest percentage of symptomatic infections at the peak, regardless of the available vaccine doses and rollout speed, using the main matrix (Table 4). As for the initial strain scenario, prioritizing persons <65 years of age was associated with the lowest percentage of symptomatic infections at the peak (9.89%) under the assumption of vaccinating 1 million persons over 3 months using the second matrix for the Delta variant (Table 5).

Impact of Vaccination Strategies on Cumulative Infections and Deaths Caused by Delta Variant

The scenario where 1 million people were vaccinated over 3 months suggested that focusing on persons <25 years of age had the lowest value of cumulative infections (226.32%) for the Delta variant,

Table 4. Comparing outcomes for the Delta variant if 1 million persons were vaccinated under the various vaccination strategies using the main matrix method, Ghana

Vaccine prioritization by age group, y	Scenario, % infections			
	Initial strain, 3 mo	Delta variant, 3 mo	Initial strain, 6 mo	Delta variant, 6 mo
Symptomatic infections at peak				
Only ≥65	7.19	10.22	7.22	10.25
25–64	6.92	10.08	7.09	10.18
<25	6.75	9.99	7.01	10.14
<65	6.81	10.02	7.03	10.15
Same rate across age groups	6.83	10.03	7.04	10.16
Cumulative infections				
Only ≥65	172.09	228.43	172.88	229.50
25–64	167.44	227.00	170.80	229.07
<25	165.76	226.32	170.04	228.77
<65	166.19	226.50	170.28	228.87
Same rate across age groups	166.44	226.55	170.41	228.89
Deaths				
Only ≥65	0.17	0.25	0.18	0.26
25–64	0.19	0.27	0.19	0.28
<25	0.19	0.28	0.19	0.28
<65	0.19	0.27	0.19	0.28
Same rate across age groups	0.19	0.27	0.19	0.28

findings that paralleled our analysis of the initial strain (165.76%). Prioritizing persons <25 years of age was the best option to minimize cumulative infections in the population with a 6-month rollout for the Delta variant (228.77%) (Table 4). Importantly, the results on cumulative infections of the second matrix suggested the elderly (235.15%) should be prioritized for vaccination first for the Delta variant with a 6-month rollout (Table 5). Prioritizing the elderly remained the best strategy for lowering deaths in the population for the initial strain and the Delta variant in all the scenarios (Tables 4, 5; Appendix 1 Tables 4, 5).

Discussion

Vaccination is the best tool to control the spread of SARS-CoV-2 and minimize the burden of COVID-19 globally. Because Ghana primarily relies on multilateral donations for their COVID-19 vaccine supply, there is a need to determine the best vaccine optimization strategies to minimize deaths, cumulative case counts, and epidemic peaks over a relatively short period. Using 2 contact matrices, we used an age-stratified mathematic model to answer the question of who should get vaccinated first when the vaccine supply is limited and when supplies are exhausted over 3 and 6 months. Our findings suggest that, for both the initial strain and the Delta variant, prioritizing persons <25 years of age for vaccination would avert the most cumulative infections and prioritizing the elderly (≥65 years of age) would result in the lowest death counts.

Optimization of vaccine prioritization strategy is sensitive to the population structure. Prioritizing younger persons to avert cumulative infections is a finding that has been reported in other studies (*13*,*38*,*39*). Bubar et al. concluded in their multicountry research that the cumulative incidence of COVID-19 was lowest when adults 20–49 years of age were prioritized, especially with a highly effective transmission-blocking vaccine (*13*). In Senegal, Diarra et al. used an age-structured dynamic mathematical model to explore various vaccination strategies and reported that prioritizing persons <60 years of age was associated with the lowest case burden (*40*). Those authors argued that countries with younger populations, such as Ghana, should prioritize vaccinating younger persons to minimize hospital costs and productivity loss.

As was the case for our team, most research teams conducting previous studies concluded that prioritizing the elderly was associated with the lowest mortality. However, Bubar et al. reported that persons 20–49 years of age should be prioritized to minimize mortality when transmission is low, when vaccine efficacy is lower in older adults, and when the vaccine is highly effective in blocking transmission. Buckner et al. reported results similar to those in our study and found that, to control deaths directly, the elderly should be vaccinated first, after stratifying young adults by essential worker status (*41*). Although the conclusions in that study and our study were similar, Buckner et al. used a dynamic approach in modeling vaccine allocation strategies that accounted for changes in the epidemiologic status of the population (shares of the population in different disease states) over 6 months using stochastic nonlinear programming techniques. In a vaccine optimization modeling study in India, Foy et al. concluded that prioritizing older adults (≥60 years of age) was associated with the most significant reduction in deaths, regardless of vaccine efficacy, control

measures, and rollout speed (*38*). Another modeling study by Chapman et al., using COVID-19 data from California, reported similar results (*42*); however, that study focused on identifying the groups to prioritize after healthcare workers and long-term facility residents received initial vaccine doses.

The differences in outcomes between the contact matrices in our study might be due to the much lower reported contact rates among the younger population in the matrix adapted from Trentini et al. (i.e., second matrix) (*35*). The study by Bubar et al. on vaccine optimization strategies across multiple countries, including South Africa, concluded the best vaccination strategy depended on the extent of mixing patterns (*13*). The use of 2 contact matrices reflects the degree to which decision makers should consider social interactions in the population before optimizing vaccination strategies when vaccine supplies are limited. Our findings demonstrate that the mixing pattern is relevant when the goal of the vaccination program is to minimize infection burden and the vaccine rollout takes place over an extended period. Thus, a population with lower contact rates among the older population would need to prioritize younger persons. However, contact patterns in the population may not be relevant if the goal of the vaccination program is to minimize deaths and vaccine uptake is high. Future studies might consider exploring differences observed using matrices of different settings; for example, rural versus urban and household versus community mixing.

As reported by Ko et al., the question of who should receive vaccinations first depends also on the objective for vaccination (minimizing cumulative infections or deaths) and the effective reproduction number (*39*). Thus, policymakers might need to consider compromises in deciding the best vaccine allocation strategies. For example, prioritizing the elderly may lead to fewer deaths but higher case numbers, which could exacerbate economic loss due to a high case count in a younger population. The transmissibility of the circulating variant also might inform a vaccine optimization strategy. We did not see evidence of this effect in our study because the priority group remained the same for the Delta variant, which carried a higher reproduction number. Another study concluded vaccine optimization depended on the vaccine supply (*42*).

Although our study demonstrates the need to prioritize certain age groups to minimize the burden of COVID-19 in Ghana, depending on the objective of the program, other factors need to be considered to ensure people receive vaccinations when they become eligible. Employing targeted vaccine campaigns to minimize hesitancy among the prioritized group might be a necessary part of the program. Acheampong et al. reported the level of reluctance among older adults was lower than that for younger adults in Ghana (*43*). Likewise, a survey among persons >65 years of age in the United States found that 91% of the elderly were willing to get vaccinated (*44*). This reported vaccine hesitancy across different age groups suggests a need for campaigns to create an enabling environment and engage younger populations about their role in mitigating the pandemic.

The first limitation of our study is that our model was age-stratified only. Other demographic variables (e.g., occupation and comorbidity) might change a person's COVID-19 infection risk and clinical prognosis (*45*). Second, our model did not include a hospitalization compartment. Thus, we

Table 5. Comparing outcomes for the Delta variant if 1 million persons were vaccinated under the various vaccination strategies using the second matrix methods, Ghana

Vaccine prioritization by age group, y	Scenario, % infections			
	Initial strain, 3 mo	Delta variant, 3 mo	Initial strain, 6 mo	Delta variant, 6 mo
Symptomatic infections at peak				
Only ≥65	6.92	9.96	7.02	10.04
25–64	6.75	9.90	6.96	10.01
<25	6.79	9.90	6.99	10.01
<65	6.76	9.89	6.97	10.01
Same rate across age groups	6.76	9.89	6.98	10.01
Cumulative infections				
Only ≥65	175.36	232.82	177.71	235.15
25–64	174.26	234.30	178.22	236.48
<25	174.95	234.44	178.62	236.57
<65	174.42	232.29	178.39	236.50
Same rate across age groups	174.25	234.13	178.30	236.43
Deaths				
Only ≥65	0.18	0.26	0.19	0.28
25–64	0.21	0.31	0.21	0.31
<25	0.22	0.31	0.22	0.31
<65	0.21	0.31	0.22	0.31
Same rate across age groups	0.21	0.31	0.21	0.31

could not evaluate the effects of the Omicron variant, for which vaccines demonstrated effectiveness against severe infections but modest effectiveness against infection. Third, the contact matrices we used were adapted from other countries in Africa. Those countries had similar demographic distributions as Ghana, and we assumed that the frequency of contact in the population would be similar. Fourth, we did not have data to represent the rural and urban differences in contact matrices in Ghana. Fifth, our model design specified the symptomatic period to be the same for persons who recovered from COVID-19 and those who died from it. Sixth, the highly transmissible Omicron variant was not included in our study because of limited evidence of the effectiveness of vaccines against infection from that variant (*46*). Last, our model accounted for vaccine effectiveness against infection but did not account for the reduction of the case-fatality ratio if a person was vaccinated and still became infected.

In conclusion, we used an age-stratified compartmental model to assess the impact of various COVID-19 vaccine allocation strategies in Ghana. Our study reiterates the need to increase vaccination rates by ensuring increased vaccine supplies and faster rollout speed. Vaccinating persons <25 years of age was associated with the highest numbers of cumulative infections averted for the initial strain and the Delta variant. Prioritizing persons ≥65 years of age was associated with the lowest deaths in the population. Our findings indicate that vaccine prioritization strategies in Ghana, or in any country, depend on the country's policy objectives, population structure, mixing patterns, and vaccine supply.

S.K.O. and I.C.H.F. conceptualized the study; S.K.O. programmed the model in R and ran the simulations and drafted the manuscript under I.C.H.F.'s supervision. J.S.S., K.L.S., G.C., and B.J.C. provided consultation to S.K.O. and I.C.H.F. All authors edited, reviewed, and approved the manuscript.

S.K.O. is a paid intern at Ionis Pharmaceuticals; the financial relationship does not affect the content of the article. B.J.C. was a consultant for Roche and Sanofi Pasteur. All other co-authors declare no competing interest.

About the Author

Dr. Ofori is a postdoctoral curriculum and research fellow in the Center for Communicable Disease Dynamics at the Harvard T.H. Chan School of Public Health. Her research interests are infectious disease epidemiology and mathematical modeling.

References

1. Ghana Health Service. COVID-19 Ghana's outbreak response management updates. 2022 [cited 2023 Jan 06]. https://ghanahealthservice.org/covid19/archive.php
2. Ofori SK, Schwind JS, Sullivan KL, Cowling BJ, Chowell G, Fung IC-H. Transmission dynamics of COVID-19 in Ghana and the impact of public health interventions. Am J Trop Med Hyg. 2022;107:175–9. https://doi.org/10.4269/ajtmh.21-0718
3. Quakyi NK, Agyemang Asante NA, Nartey YA, Bediako Y, Sam-Agudu NA. Ghana's COVID-19 response: the Black Star can do even better. BMJ Glob Health. 2021;6:e005569. https://doi.org/10.1136/bmjgh-2021-005569
4. Alhassan RK, Aberese-Ako M, Doegah PT, Immurana M, Dalaba MA, Manyeh AK, et al. COVID-19 vaccine hesitancy among the adult population in Ghana: evidence from a pre-vaccination rollout survey. Trop Med Health. 2021;49:96. https://doi.org/10.1186/s41182-021-00357-5
5. World Health Organization Africa. More COVID-19 vaccines arrive in Ghana. 2021. [cited 2022 Dec 6]. https://www.afro.who.int/news/more-covid-19-vaccines-arrive-ghana
6. Ghana Health Service. COVID-19 Ghana's outbreak response management updates. 2020 [cited 2022 Feb 21]. https://ghanahealthservice.org/covid19/archive.php
7. Botwe BO, Antwi WK, Adusei JA, Mayeden RN, Akudjedu TN, Sule SD. COVID-19 vaccine hesitancy concerns: Findings from a Ghana clinical radiography workforce survey. Radiography (Lond). 2022;28:537–44. https://doi.org/10.1016/j.radi.2021.09.015
8. Quashie PK, Mutungi JK, Dzabeng F, Oduro-Mensah D, Opurum PC, Tapela K, et al. Trends of SARS-CoV-2 antibody prevalence in selected regions across Ghana. Wellcome Open Res. 2021;6:173. https://doi.org/10.12688/wellcomeopenres.16890.1
9. Alagoz O, Sethi AK, Patterson BW, Churpek M, Alhanaee G, Scaria E, et al. The impact of vaccination to control COVID-19 burden in the United States: a simulation modeling approach. PLoS One. 2021;16:e0254456. https://doi.org/10.1371/journal.pone.0254456
10. Moghadas SM, Vilches TN, Zhang K, Wells CR, Shoukat A, Singer BH, et al. The impact of vaccination on coronavirus disease 2019 (COVID-19) outbreaks in the United States. Clin Infect Dis. 2021;73:2257–64. https://doi.org/10.1093/cid/ciab079
11. Matrajt L, Eaton J, Leung T, Brown ER. Vaccine optimization for COVID-19: who to vaccinate first? Sci Adv. 2021;7:eabf1374. https://doi.org/10.1126/sciadv.abf1374
12. Mumtaz GR, El-Jardali F, Jabbour M, Harb A, Abu-Raddad LJ, Makhoul M. Modeling the impact of COVID-19 vaccination in Lebanon: a call to speed-up vaccine roll out. Vaccines (Basel). 2021;9:697. https://doi.org/10.3390/vaccines9070697
13. Bubar KM, Reinholt K, Kissler SM, Lipsitch M, Cobey S, Grad YH, et al. Model-informed COVID-19 vaccine prioritization strategies by age and serostatus. Science. 2021;371:916–21. https://doi.org/10.1126/science.abe6959
14. University of British Columbia Department of Zoology. COVID-19 models lecture. 2020 [cited 2020 Nov 15]. https://www.zoology.ubc.ca/~bio301/Bio301/Lectures/Lecture1/COVID_Models.pdf
15. Wei WE, Li Z, Chiew CJ, Yong SE, Toh MP, Lee VJ. Presymptomatic Transmission of SARS-CoV-2 - Singapore, January 23-March 16, 2020. MMWR Morb Mortal Wkly Rep. 2020;69:411–5. https://doi.org/10.15585/mmwr.mm6914e1
16. Li Y, Shi J, Xia J, Duan J, Chen L, Yu X, et al. Asymptomatic

and symptomatic patients with non-severe coronavirus disease (COVID-19) have similar clinical features and virological courses: a retrospective single center study. Front Microbiol. 2020;11:1570. https://doi.org/10.3389/fmicb.2020.01570
17. Zhao H, Lu X, Deng Y, Tang Y, Lu J. COVID-19: asymptomatic carrier transmission is an underestimated problem. Epidemiol Infect. 2020;148:e116-e. https://doi.org/10.1017/S0950268820001235
18. Abbasi Z, Zamani I, Mehra AHA, Shafieirad M, Ibeas A. Optimal control design of impulsive SQEIAR epidemic models with application to COVID-19. Chaos Solitons Fractals. 2020;139:110054. https://doi.org/10.1016/j.chaos.2020.110054
19. Liu Z, Magal P, Seydi O, Webb GA. COVID-19 epidemic model with latency period. Infect Dis Model. 2020;5:323–37. https://doi.org/10.1016/j.idm.2020.03.003
20. Cai Q, Huang D, Ou P, Yu H, Zhu Z, Xia Z, et al. COVID-19 in a designated infectious diseases hospital outside Hubei Province, China. Allergy. 2020;75:1742–52. https://doi.org/10.1111/all.14309
21. Xing YH, Ni W, Wu Q, Li WJ, Li GJ, Wang WD, et al. Prolonged viral shedding in feces of pediatric patients with coronavirus disease 2019. J Microbiol Immunol Infect. 2020;53:473–80. https://doi.org/10.1016/j.jmii.2020.03.021
22. Ma S, Zhang J, Zeng M, Yun Q, Guo W, Zheng Y, et al. Epidemiological parameters of COVID-19: cases series study. J Med Internet Res. 2020;22:e19994. https://doi.org/10.2196/19994
23. Byrne AW, McEvoy D, Collins AB, Hunt K, Casey M, Barber A, et al. Inferred duration of infectious period of SARS-CoV-2: rapid scoping review and analysis of available evidence for asymptomatic and symptomatic COVID-19 cases. BMJ Open. 2020;10:e039856. https://doi.org/10.1136/bmjopen-2020-039856
24. Tindale LC, Stockdale JE, Coombe M, Garlock ES, Lau WYV, Saraswat M, et al. Evidence for transmission of COVID-19 prior to symptom onset. eLife. 2020;9:e57149. https://doi.org/10.7554/eLife.57149
25. Chen M, Li M, Hao Y, Liu Z, Hu L, Wang L. The introduction of population migration to SEIAR for COVID-19 epidemic modeling with an efficient intervention strategy. Inf Fusion. 2020;64:252–8. https://doi.org/10.1016/j.inffus.2020.08.002
26. Buitrago-Garcia D, Egli-Gany D, Counotte MJ, Hossmann S, Imeri H, Ipekci AM, et al. Occurrence and transmission potential of asymptomatic and presymptomatic SARS-CoV-2 infections: a living systematic review and meta-analysis. PLoS Med. 2020;17:e1003346-e.
27. Knoll MD, Wonodi C. Oxford-AstraZeneca COVID-19 vaccine efficacy. Lancet. 2021;397:72–4. https://doi.org/10.1016/S0140-6736(20)32623-4
28. Centers for Disease Control and Prevention. Pandemic planning scenarios. 2020 [cited 2020 Nov 12]. https://www.cdc.gov/coronavirus/2019-ncov/hcp/planning-scenarios.html
29. Iacobucci G. Covid-19: Protection from two doses of vaccine wanes within six months, data suggest. BMJ. 2021;374:n2113. https://doi.org/10.1136/bmj.n2113
30. Good MF, Hawkes MT. The interaction of natural and vaccine-induced immunity with social distancing predicts the evolution of the COVID-19 Pandemic. MBio. 2020;11:e02617–20. https://doi.org/10.1128/mBio.02617-20
31. Lawal Y. Africa's low COVID-19 mortality rate: A paradox? Int J Infect Dis. 2021;102:118–22. https://doi.org/10.1016/j.ijid.2020.10.038
32. Lopez Bernal J, Andrews N, Gower C, Gallagher E, Simmons R, Thelwall S, et al. Effectiveness of Covid-19 vaccines against the B. 1.617. 2 (Delta) variant. N Engl J Med. 2021;385:585–94. https://doi.org/10.1056/NEJMoa2108891
33. le Polain de Waroux O, Cohuet S, Ndazima D, Kucharski AJ, Juan-Giner A, Flasche S, et al. Characteristics of human encounters and social mixing patterns relevant to infectious diseases spread by close contact: a survey in Southwest Uganda. BMC Infect Dis. 2018;18:172. https://doi.org/10.1186/s12879-018-3073-1
34. Kiti MC, Kinyanjui TM, Koech DC, Munywoki PK, Medley GF, Nokes DJ. Quantifying age-related rates of social contact using diaries in a rural coastal population of Kenya. PLoS One. 2014;9:e104786. https://doi.org/10.1371/journal.pone.0104786
35. Trentini F, Guzzetta G, Galli M, Zardini A, Manenti F, Putoto G, et al. Modeling the interplay between demography, social contact patterns, and SARS-CoV-2 transmission in the South West Shewa Zone of Oromia Region, Ethiopia. BMC Med. 2021;19:89. https://doi.org/10.1186/s12916-021-01967-w
36. Central Intelligence Agency. The world factbook. 2020 [cited 2022 Jan 15]. https://www.cia.gov/the-world-factbook
37. Anaadem P. Ghana: population hits 30.8 million—Greater Accra most populous region—GSS. Ghana Today. 2021 Sep 22 [cited 2022 Dec 6]. https://ghanatoday.gov.gh/news/ghanas-population-hits-30-8-million-greater-accra-most-populous-region-gss/
38. Foy BH, Wahl B, Mehta K, Shet A, Menon GI, Britto C. Comparing COVID-19 vaccine allocation strategies in India: a mathematical modelling study. Int J Infect Dis. 2021;103:431–8. https://doi.org/10.1016/j.ijid.2020.12.075
39. Ko Y, Lee J, Kim Y, Kwon D, Jung E. COVID-19 vaccine priority strategy using a heterogenous transmission model based on maximum likelihood estimation in the Republic of Korea. Int J Environ Res Public Health. 2021;18:6469. https://doi.org/10.3390/ijerph18126469
40. Diarra M, Kebir A, Talla C, Barry A, Faye J, Louati D, et al.; REPAIR consortium. Non-pharmaceutical interventions and COVID-19 vaccination strategies in Senegal: a modelling study. BMJ Glob Health. 2022;7:e007236. https://doi.org/10.1136/bmjgh-2021-007236
41. Buckner JH, Chowell G, Springborn MR. Dynamic prioritization of COVID-19 vaccines when social distancing is limited for essential workers. Proc Natl Acad Sci U S A. 2021;118:e2025786118. https://doi.org/10.1073/pnas.2025786118
42. Chapman LAC, Shukla P, Rodríguez-Barraquer I, Shete PB, León TM, Bibbins-Domingo K, et al. Risk factor targeting for vaccine prioritization during the COVID-19 pandemic. Sci Rep. 2022;12:3055. https://doi.org/10.1038/s41598-022-06971-5
43. Acheampong T, Akorsikumah EA, Osae-Kwapong J, Khalid M, Appiah A, Amuasi JH. Examining vaccine hesitancy in sub-saharan Africa: a survey of the knowledge and attitudes among adults to receive COVID-19 vaccines in Ghana. Vaccines (Basel). 2021;9:814. https://doi.org/10.3390/vaccines9080814
44. Nikolovski J, Koldijk M, Weverling GJ, Spertus J, Turakhia M, Saxon L, et al. Factors indicating intention to vaccinate with a COVID-19 vaccine among older U.S. adults. PloS one. 2021;16:e0251963-e. PubMed https://doi.org/ 10.1371/journal.pone.0251963
45. Dembek ZF, Schwartz-Watjen KT, Swiatecka AL, Broadway KM,Hadeed SJ, Mothershead JL, et al. Coronavirus disease 2019 on the heels of Ebola virus disease

in West Africa. Pathogens. 2021;10:1266. https://doi.org/10.3390/pathogens10101266
46. Andrews N, Stowe J, Kirsebom F, Toffa S, Rickeard T, Gallagher E, et al. Covid-19 vaccine effectiveness against the Omicron (B.1.1.529) variant. N Engl J Med. 2022;386:1532–46. https://doi.org/10.1056/NEJMoa2119451

Address for correspondence: Isaac Chun-Hai Fung, PO Box 7989, Department of Biostatistics, Epidemiology and Environmental Health Sciences, Jiann-Ping Hsu College of Public Health, Georgia Southern University, Statesboro, GA 30458-7989, USA; email: cfung@georgiasouthern.edu

Early Introduction and Community Transmission of SARS-CoV-2 Omicron Variant, New York, New York, USA

Dakai Liu,[1] Yexiao Cheng,[1] Hangyu Zhou, Lulan Wang, Roberto Hurtado Fiel, Yehudah Gruenstein, Jean Jingzi Luo, Vishnu Singh, Eric Konadu, Keither James, Calvin Lui, Pengcheng Gao, Carl Urban, Nishant Prasad, Sorana Segal-Maurer, Esther Wurzberger, Genhong Cheng, Aiping Wu, William Harry Rodgers

The Omicron variant of SARS-CoV-2 has become dominant in most countries and has raised significant global health concerns. As a global commerce center, New York, New York, USA, constantly faces the risk for multiple variant introductions of SARS-CoV-2. To elucidate the introduction and transmission of the Omicron variant in the city of New York, we created a comprehensive genomic and epidemiologic analysis of 392 Omicron virus specimens collected during November 25–December 11, 2021. We found evidence of 4 independent introductions of Omicron subclades, including the Omicron subclade BA.1.1 with defining substitution of R346K in the spike protein. The continuous genetic divergence within each Omicron subclade revealed their local community transmission and co-circulation in New York, including both household and workplace transmissions supported by epidemiologic evidence. Our study highlights the urgent need for enhanced genomic surveillance and effective response planning for better prevention and management of emerging SARS-CoV-2 variants.

During the global pandemic of SARS-CoV-2, novel variants have continuously emerged (*1*). Some variants constitute an increased risk to global public health and are being monitored as variants of concern by the World Health Organization (WHO). The Omicron variant was detected from patients in Botswana and South Africa in November 2021 (*2*); it was designated as the fifth variant of concern. Since its detection, it rapidly spread across the world and became the predominant variant in several countries (*3*). Omicron has a higher number of mutations than previously detected variants. Of note, some mutations located in the receptor-binding domain (RBD) of the spike (S) protein altered the immune escape ability of Omicron (*4*–*6*). The 69–70 deletion in the S gene of Omicron can be characterized by the failure to detect the S gene using certain diagnostic tests (*7*), known as the S gene target failure (SGTF). In the context of the global dominance of Delta and Omicron, some studies defined the Omicron case as the presence of SGTF and the Delta case as the absence of SGTF in the test samples (*8*–*10*). Three studies reported the genomic, epidemiologic, and clinical analysis of early Omicron introductions (*10*–*12*); combining viral genome analysis with epidemiologic evidence supports the study of introduction and community transmission patterns of emerging viruses.

As a major cosmopolitan city, New York, New York, USA (NYC), has been at risk for multiple variant introductions of SARS-CoV-2 during the COVID-19 pandemic (*13*–*15*). Studies have shown that a patient infected with the Omicron variant attended a

Author affiliations: NewYork-Presbyterian Queens Hospital, Flushing, New York, USA (D. Liu, J.J. Luo, V. Singh, E. Konadu, K. James, C. Lui, P. Gao, C. Urban, N. Prasad, S. Segal-Maurer, W.H. Rodgers); Chinese Academy of Medical Sciences & Peking Union Medical College, Beijing, China (Y. Cheng, H. Zhou, A. Wu); Suzhou Institute of Systems Medicine, Suzhou, China (Y. Cheng, H. Zhou, A. Wu); University of California, Los Angeles, California, USA (L. Wang, G. Cheng); Kaiser Permanente Health, North Valley, California, USA (R.H. Fiel); LabQ Diagnostics, Brooklyn, New York, USA (Y. Gruenstein, E. Wurzberger); Weill Cornell Medical College, New York (J.J. Luo, C. Urban, N. Prasad, S. Segal-Maurer, W.H. Rodgers)

DOI: https://doi.org/10.3201/eid2902.220817

[1]These authors contributed equally to this article.

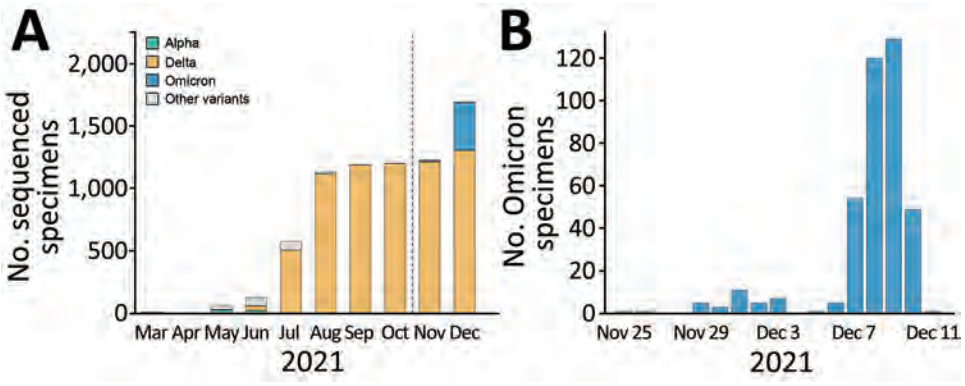

Figure 1. Distribution of SARS-CoV-2 viruses in New York, New York, USA. A) Temporal distribution of 7,237 sequenced viruses, March–December 2021. B) Temporal distribution of 392 Omicron viruses, November 25–December 11, 2021.

large indoor convention with attendees from 52 US jurisdictions and 30 foreign countries during November 19–November 21, 2021, in NYC; a total of 119 event-associated cases were identified after the investigation (*16*,*17*). In addition, some Omicron-associated mutations were detected in wastewater in NYC on November 21, 2021 (*18*). This evidence indicates that the Omicron variant was introduced to NYC early in its outbreak. Shortly after its introduction, Omicron replaced Delta as the dominant variant in NYC (https://www1.nyc.gov/site/doh/covid/covid-19-data-variants.page), suggesting potential community transmission.

In this study, we performed whole-genome sequencing for 392 Omicron viruses obtained from persons in NYC during November 25–December 11, 2021. These dates encompass the expected early Omicron introduction into the city. Using the epidemiologic and genetic data of these sequencing samples, we determined the introduction and community transmission pattern of early Omicron in NYC. This study was reviewed and approved by the NewYork-Presbyterian Queens Hospital Institutional Review Board (IRB no. 13740321).

Methods

Sample Collection

Being in the epicenter of the COVID-19 pandemic, NewYork-Presbyterian Queens Hospital has received 185,870 specimens for SARS-CoV-2 RNA testing by diagnostic multiplex real-time PCR since the COVID-19 pandemic started in March 2020. In addition to those specimens, we analyzed specimens collected by mobile service vans from residential communities and workplaces. We used demographics, including residential and business addresses associated with collection sites, for the epidemiology analysis. We considered households as persons at the same residential address, identical business addresses as workplace, and family members as family. We determined traveler status by the home address and traveling inquiry performed during sampling. We advised all patients testing positive or exposed patients to follow the Centers for Disease Control and Prevention (CDC) quarantine guidelines.

Viral Genomic Next-Generation Sequencing and Bioinformatics Processing

To investigate SARS-CoV-2 mutations and variant epidemiology, we performed next-generation sequencing (NGS) on the positive specimens with real-time PCR cycle threshold (Ct) value <33 cycles and analyzed virus mutations among the specimens from our laboratory and LabQ Diagnostics (New York, New York, USA). We performed NGS by using the Illumina COVID-Seq test kit (https://www.illumina.com). We extracted viral RNA from a viral transport medium containing a nasopharyngeal swab specimen, then performed cDNA synthesis through reverse transcription using random hexamer primers. We amplified the cDNA of the viral genome by 2 separate PCR reactions and pooled the products together. The fragments underwent bead-based tagmentation to the adaptor sequences. Subsequently, the adaptor-tagged fragments underwent another round of PCR amplification. Using the purification beads, we pooled and cleaned the indexed tagged libraries. We clustered pooled libraries onto a flow cell and then sequenced on the NovaSeq 6000 sequencing system (Illumina). We used VarSeq version 2.2.2 (Golden Helix, https://www.goldenhelix.com) for sequence analysis; we used consensus sequences of these viruses as input to Nextclade version 1.10.1 (*19*) for quality control, mutation calling, and Nextstrain clade assignment. Viruses <29,000 nt in length or with Nextclade-assessed QC.overallStatus below good were considered low quality and removed.

Phylogenetic Analysis

To investigate the genetic relationship between Omicron viruses in NYC, we constructed a genotype network of all sequenced Omicron viruses; nodes represented nucleotide genotypes of viruses and edges between nodes represented pairs of nucleotide genotypes with the highest genetic similarity. We visualized this network using Gephi version 0.9.2 (*20*). We also constructed a phylogenetic tree of those Omicron viruses in NYC using Nextstrain SARS-CoV-2 workflow version 3.0.6 (*21*) and visualized it as timescaled using Auspice version 2.33.0 (https://auspice.us), which is part of the Nextstrain workflow. We then identified different clades of Omicron viruses based on the genotype network and the phylogenetic tree.

To investigate the introductions of the Omicron variant in NYC, we downloaded all global Omicron sequences collected before December 11, 2021 and their metadata from GISAID (https://www.gisaid.org) (*22*). We removed sequences with incomplete information such as collection date or location. We performed mutation calling of these contextual sequences using Nextclade version 1.10.1 (*19*). We applied the same quality control standards for our sequenced samples as we did for GISAID sequences. Sequences that were <29,000 nt long or had Nextclade-assessed QC.overallStatus value below good were considered low quality and removed. To identify the genetic relationship between viruses clustered into different clades from NYC and the rest of the world, we constructed a phylogenetic tree using local viruses and global contextual viruses. We defined the viruses in NYC clustered into these clades as local viruses. For each clade, global viruses detected before the time at which we detected the virus within the clade in NYC were selected as contextual viruses. We used Nextstrain SARS-CoV-2 workflow version 3.0.6 (*21*) to construct this phylogenetic tree and Auspice to visualize it as divergence-scaled.

To investigate the genetic relationship between viruses from travelers and locals, we reanalyzed the same phylogenetic tree that was used to investigate the genetic relationship between Omicron viruses in NYC and highlighted travelers. To reveal the detailed transmission pattern of Omicron in NYC, we

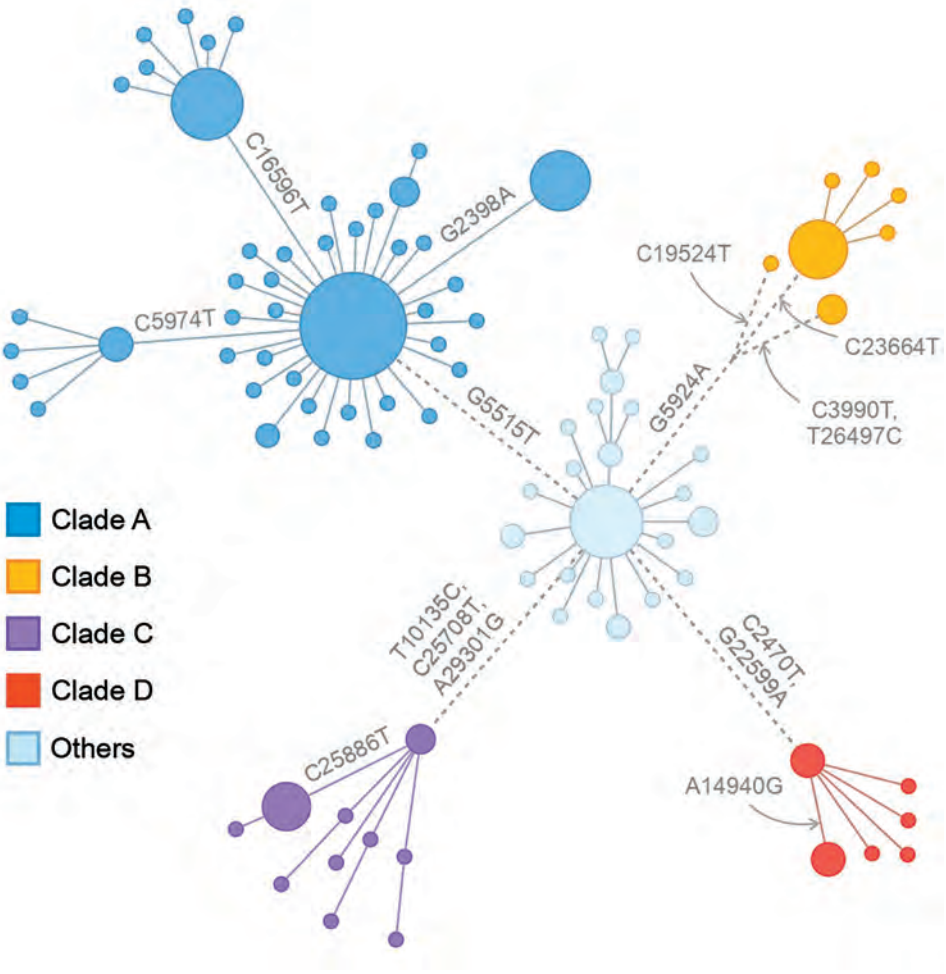

Figure 2. Genotype network of 392 Omicron viruses from New York, New York, USA, November 25–December 11, 2021. In this network, nodes represent nucleotide genotypes by clade, and lines between nodes represent pairs of nucleotide genotypes with the highest genetic similarity. Node size is scaled to $\log_2$ of the number of viruses with the corresponding genotype. Dashed lines indicate pairs of similar genotypes of different clades.

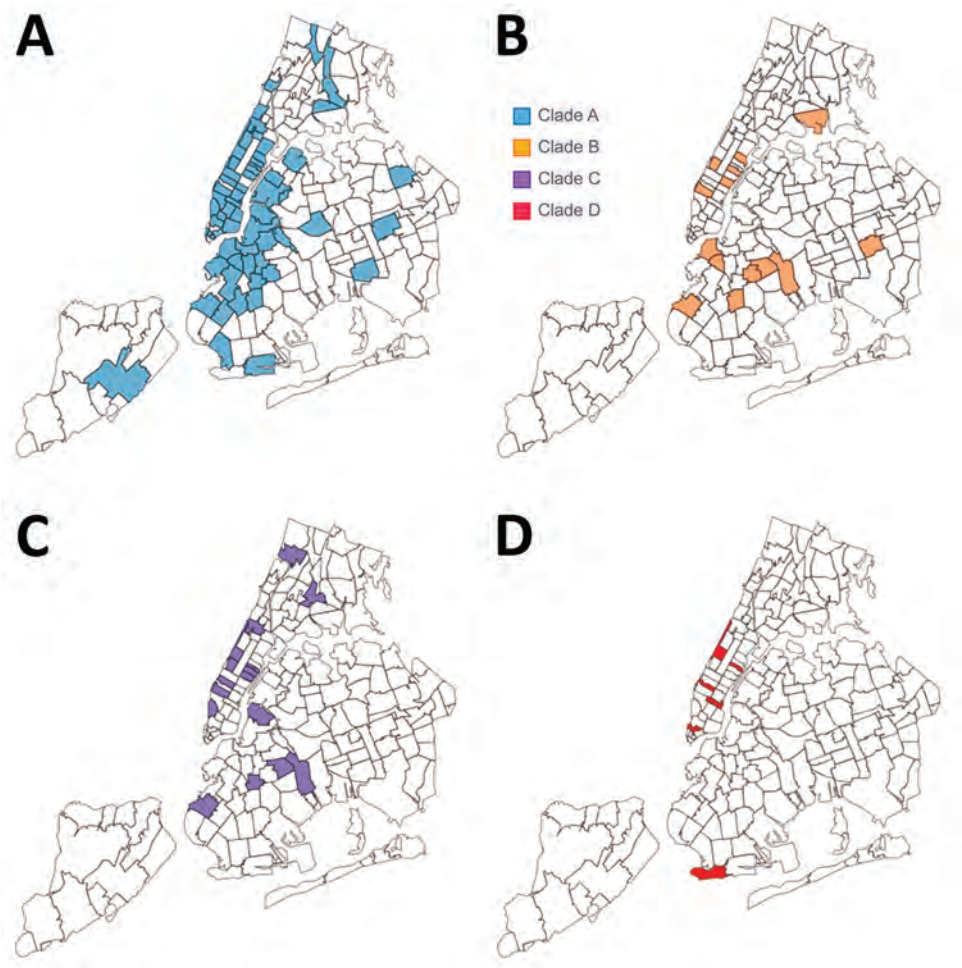

Figure 3. Geographic distributions of 4 main clades of SARS-CoV-2 Omicron variant virus from New York, New York, USA, November 25–December 11, 2021. A) Clade A. B) Clade B. C) Clade C. D) Clade D. Map source: New York City Department of Health and Mental Hygiene (https://github.com/nychealth/coronavirus-data/blob/master/Geography-resources/MODZCTA_2010_WGS1984.geo.json).

analyzed the mutational profiles of Omicron viruses in 2 local districts. In the mutational profiles, we presented only the substitutions that were not Omicron-defining substitutions.

Data and Code Availability

We have provided GISAID accession numbers and metadata of Omicron sequences generated in this study (Appendix Table 1, https://wwwnc.cdc.gov/EID/article/29/2/22-0817-App1.xlsx) and the GISAID global Omicron sequences used in this study (Appendix Table 2). The source code used to generate the figures has been released at GitHub (https://github.com/wuaipinglab/sarscov2-omicron-nyc).

Results

Spatiotemporal Distribution of Omicron Variant in NYC

Since the COVID-19 pandemic started in March 2020, we tested 185,870 specimens for SARS-CoV-2 RNA by diagnostic multiplex RT-PCR. A total of 17,058 (9.18%) specimens were positive. These specimens were collected from 87,616 unique persons who were tested once or multiple times. Of those persons, 12,858 had SARS-CoV-2 infection; average incidence rate was 14.68%.

A total of 9,516 specimens were run through NGS; 7,237 specimens passed our quality control, of which 392 specimens were identified as Omicron (Figure 1, panel A). Those Omicron viruses were collected during November 25–December 11, 2021 (Figure 1, panel B); they were widespread throughout NYC, and densities were higher in the boroughs of Manhattan and Brooklyn.

Epidemiologic and Genomic Evidence for Multiple Introductions of Omicron Subclades

We performed a phylogenetic analysis of these 392 Omicron isolates. We found that these isolates could be divided into 4 main clades based on the genotype network, phylogenetic tree, and nucleotide substitutions (Figures 2–4). Most (n = 262; 67%) of these isolates clustered into clade A; those isolates shared a G5515T nucleotide substitution. A total of 65

isolates clustered into 3 smaller clades: clade B (n = 26; 7%), with clade-defining substitution G5924A; clade C (n = 25; 6%), with 3 clade-defining substitutions T10135C, C25708T, and A29301G; and clade D (n = 14; 4%), with 2 clade-defining substitutions C2470T and G22599A. Of note, clade D was consistent with the Omicron subclade BA.1.1 because of its G22599A nucleotide substitution (spike, R346K).

We also noted that some Omicron viruses in regions other than NYC had the same substitutions as those 4 clades (Figure 5). To investigate the origins of these 4 clades, we clustered 14,817 global Omicron viruses downloaded from GISAID (*22*) into the 4 clades based on their clade-defining substitutions. Among the global Omicron viruses, 861 (6%) clustered into clade A, 3,563 (24%) clustered into clade B, 1,716 (12%) clustered into clade C, and 1,686 (11%) clustered into clade D.

We subsequently investigated the spatiotemporal distribution and phylogenetic relationship of global and NYC viruses within these 4 clades (Figures 5, 6). Clade A and its corresponding substitutions were initially detected in NYC on November 29, 2021; clade B on November 25, clade C on December 6, and clade D on December 1. Of note, we found viruses from other regions clustered into these 4 clades that had been collected earlier than our sequenced viruses in NYC (Figure 5): a total of 12 clade A viruses, 71 clade B viruses, 233 clade C viruses, and 83 clade D viruses. The earlier detection of these viruses in other regions suggests independent introductions into NYC.

To further identify the potential introductions, we constructed a phylogenetic tree using viruses clustered into clades A, B, C, and D, including 327 viruses from NYC and 399 viruses from around the world (Figure 6). We found that the early viruses clustered into clade A were detected in North America, Africa, and Europe. Of note, 3 of them (GISAID accession nos. EPI_ISL_7129868, EPI_ISL_7782594, and EPI_ISL_7908023) were detected in other laboratories in New York state. In the phylogenetic tree, early global clade A viruses were located near the base of clade A, and some viruses in NYC were distributed along main branches. Combining the phylogenetic and spatiotemporal distribution of all clade A viruses, we inferred that this clade was introduced into NYC and then spread through local transmission.

Most clade B early viruses were detected mainly in Africa, with sporadic detection in Europe, North America, and Asia. The viruses in NYC clustered closely with those viruses in the early stage of the wave. Clade B viruses were detected only in Africa before November 21, 2021, suggesting that clade B had spread outside of Africa after early local transmission. Thus, we believe that clade B viruses in NYC were the result of another independent introduction. Similarly, clade C and clade D were distributed in regions including Europe, North America, and Africa before our detections in NYC. The close genetic relationship within these 2 clades suggests 2 additional independent introduction events.

Potential Importation Risk for Omicron Variant from Travelers

Our phylogenetic analysis shows that the Omicron variant outbreak in NYC likely resulted from multiple independent introductions. We found that, among the 392 sequenced Omicron viruses in NYC, 13 of them were obtained from domestic travelers from

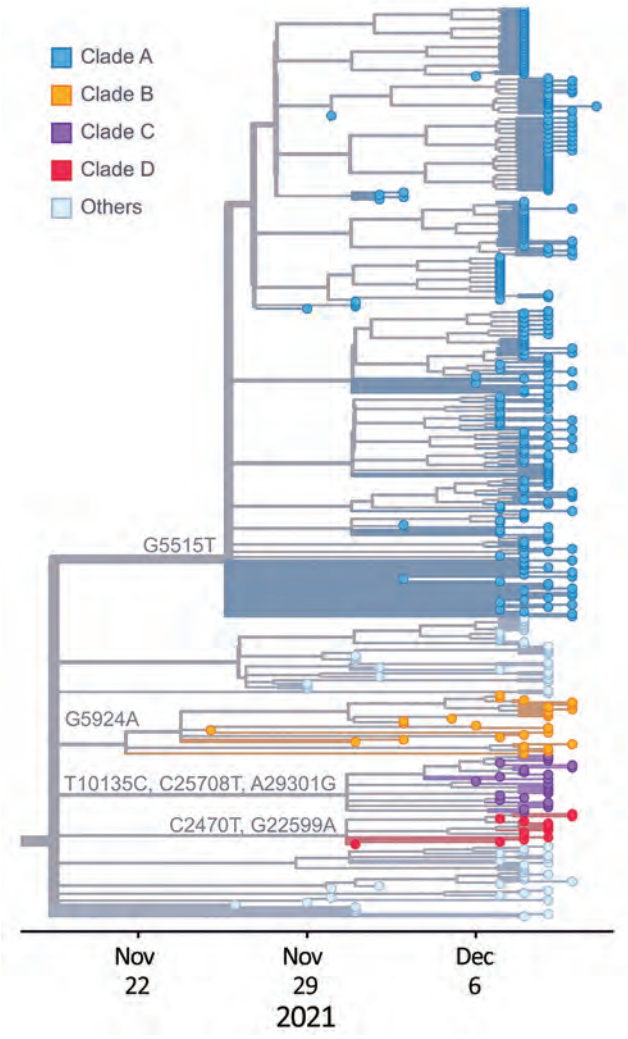

Figure 4. Phylogeny of 392 SARS-CoV-2 Omicron variant virus isolates from New York, New York, USA, November 25–December 11, 2021. Colored dots represent isolates from this study by clade. Substitution locations are indicated.

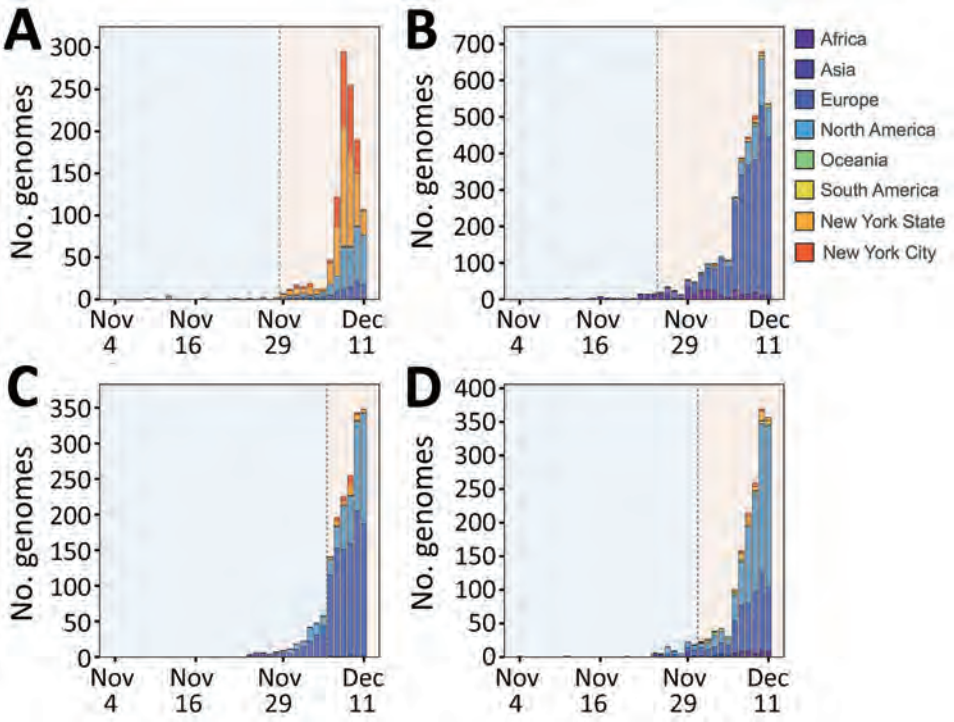

Figure 5. Distribution of SARS-CoV-2 Omicron variant virus isolates clustered into 4 main clades, including viruses identified in this study from New York, New York, USA, November 25–December 11, 2021, and viruses from various regions as obtained from GISAID (https://www.gisaid.org). A) Clade A. B) Clade B. C) Clade C. D) Clade D. For viruses from GISAID, regions were divided into Africa, Asia, Europe, North America (excluding New York state), Oceania, South America, and New York State. Vertical gray dashed lines are to the left of the time at which viruses within the indicated clade were detected in the city of New York during this study. Light blue shading represents the time before our detection of viruses within the indicated clade; light red shading represents the time after we detected the viruses.

the following states: California (2), Florida (2), Georgia (1), Maryland (1), Maine (1), North Carolina (2), Oregon (1), Rhode Island (1), Texas (1), and Utah (1) (Figure 7). To investigate the genetic relationship between viruses from travelers and locals, we analyzed the 392 Omicron viruses in a timescaled phylogenetic tree, which we constructed using Nextstrain workflow and visualized as timescaled using Auspice (*21*) (Figure 7). The viruses from travelers were distributed across the phylogeny: 8 of them fell into clade A and 1 into clade C; the remaining 4 did not fall into any of the 4 main clades being discussed. Considering the collection time and genetic similarity, we did not find irrefutable evidence that the sequenced viruses from domestic travelers were the origin of the Omicron variant in NYC.

Community Transmission and Co-circulation of Omicron Subclades in NYC

The Omicron variants were distributed in various areas in NYC (Figure 3). To investigate if introductions from outside NYC led to local transmission, we constructed the genotype network and timescaled phylogenetic tree of these 392 viruses (Figures 2, 4). We

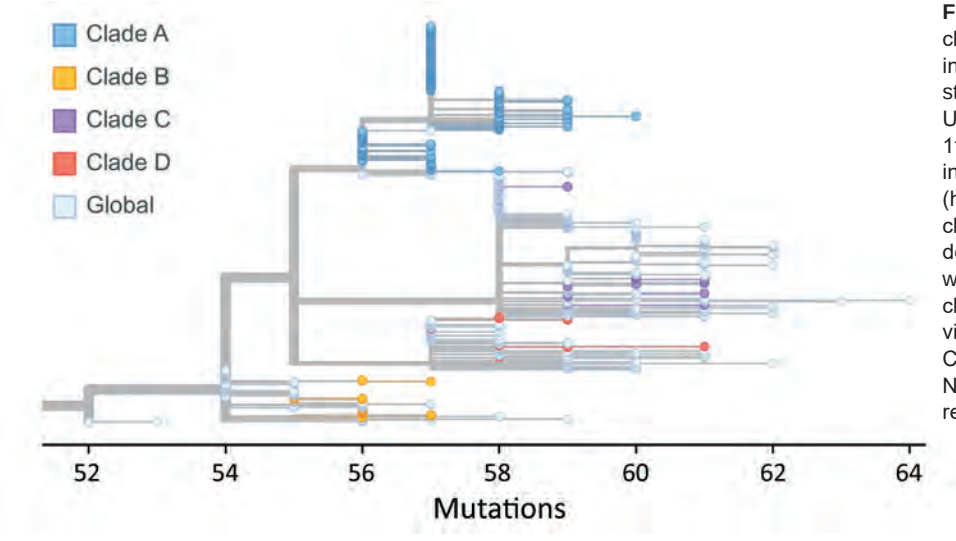

Figure 6. Phylogeny of viruses clustered into 4 main clades, including viruses identified in this study from New York, New York, USA, November 25–December 11, 2021, and contextual viruses in various regions from GISAID (https://www.gisaid.org). For each clade, we designated global viruses detected before the time at which we detected the virus within the clade in New York as contextual viruses for phylogeny construction. Colored dots represent viruses from New York by clade; light blue dots represent global contextual viruses.

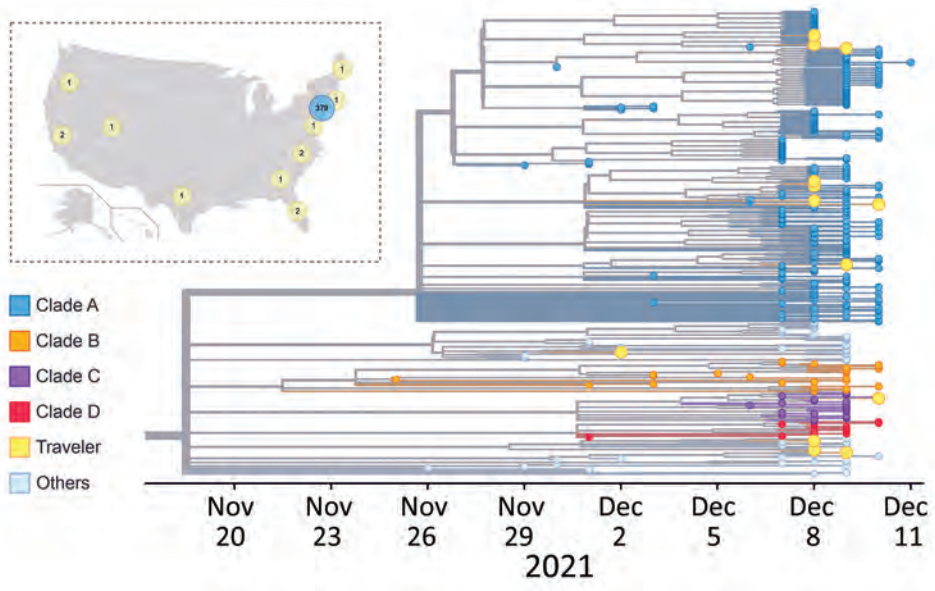

Figure 7. Phylogeny of SARS-CoV-2 Omicron viruses identified from travelers and locals in this study, New York, New York, USA, November 25–December 11, 2021. In the phylogenetic tree, colored dots represent viruses from New York residents by clade. Yellow dots represent viruses from travelers. The inset map shows the states and number of patients with isolated viruses. Yellow circles represent travelers' home states; blue circle represents local New York residents. Map source: Wikimedia Commons (https://commons.wikimedia.org/wiki/File:Blank_US_Map_(states_only).svg).

constructed this phylogenetic tree using Nextstrain workflow and visualized it as timescaled using Auspice (*21*). In addition to clade-defining substitutions, we found many novel heritable substitutions added to the subsequent progenies. The close genetic relationship within different clades showed that multiple clades spread in NYC with a co-circulation pattern after introductions.

We also discovered several instances of Omicron community transmission in NYC. We noted the viral distribution in 2 postal (ZIP) codes that had the highest detected number of viruses (Figure 8). In the 11201 ZIP code, we found the 2 viruses (nyomi222 and nyomi335) shared the G2398A substitution that belonged to 2 patients from the same family (family 1). Two viruses (nyomi200 and nyomi352) from patients living in the same household shared the C16596T substitution (household 4). These viruses with shared genome sequences from patients within the same family or the same household address suggest local household transmission (Figure 8, panel A; Figure 9). In the 11220 ZIP code, 8 viruses were from patients working in the same building (workplace 1), and 4 of them (nyomi198, nyomi228, nyomi337 and nyomi358) shared identical genetic substitutions. This epidemiologic evidence suggests community transmission in the workplace (Figure 8, panel B; Figure 9). We also found that even viruses isolated from patients at the same working address might fall into different clades, implying complex and possibly cryptic transmission.

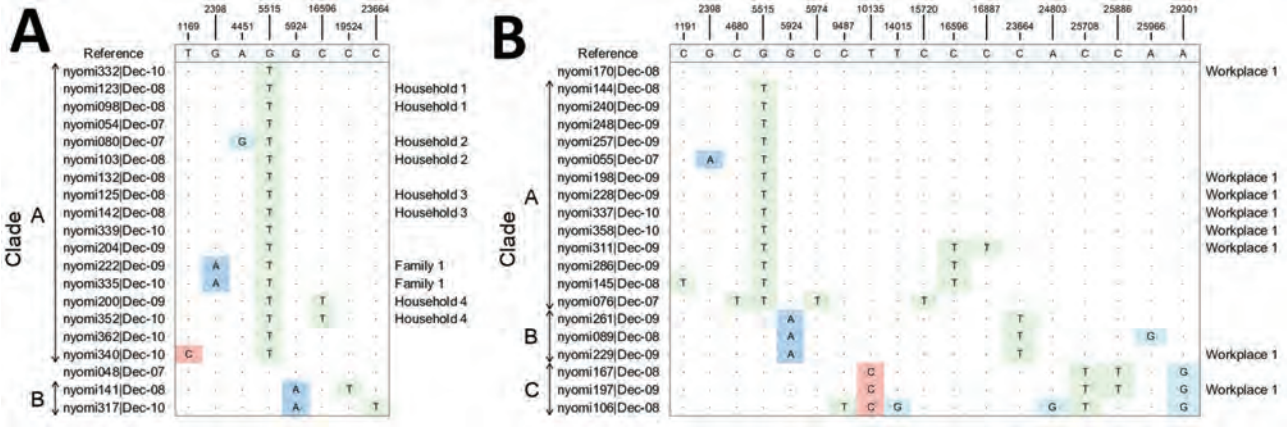

Figure 8. Mutational profiles of SARS-CoV-2 Omicron variant viruses in 2 local districts, New York, New York, USA, November 25–December 11, 2021. A) District of postal (ZIP) code 11201. Viruses isolated from patients within the same living address or the same family are labeled on the right. B) District of ZIP code 11220. Viruses isolated from patients working at the same building are labeled on the right. Column labels at top indicate substitution locations; shading indicates substitution from any nucleotide to a nucleic acid: dark blue indicates substitution to adenine; red, substitution to cytosine; green, substitution to thymine; and light blue, substitution to guanine.

Discussion

Since the first detections in November 2021, the Omicron variant has gained global attention for its increased transmissibility and immune escape (*23*). It was identified in 87 countries within 3 weeks (*2*) and established itself as the global dominant variant within a few months (*3*). Although several measures were implemented to reduce the introduction and spread of SARS-CoV-2 into the United States, 22 states reported ≥1 case of Omicron as of December 8, 2021 (*24*). As a major cosmopolitan city, NYC has been challenged with multiple introductions of different variants of SARS-CoV-2 during the pandemic (*13*–*15*). The high contact rates observed in densely populated cities may promote community transmissions of the virus (*25*).

Our analyses suggest that there have been 4 main independent introductions of different Omicron subclades into NYC from regions including Africa, Europe, and North America during the early outbreak of Omicron. Those introductions were followed by subsequent community transmission across NYC. Similarly, the rapid local spread after early Omicron introductions was observed in Finland (*10*), Denmark (*11*), and Mexico City (*12*). In addition, through the combination of genome sequencing analysis and epidemiologic studies of SARS-CoV-2 patients in individual districts of NYC, we discovered evidence of both household and workplace transmission patterns. Our observation of multiple Omicron introductions followed by onward transmission during a 17-day period highlights the potential for introductions of emerging variants to spread locally. Therefore, after emerging variant outbreaks, timely enhanced tracking and monitoring of travelers and subsequent transmission reduction interventions are urgently needed to ensure that those introductions do not result in widespread community transmission.

Given the limited sequencing coverage and surveillance, we were unable to determine the first case of the introduction for each of 4 clades in our study and its subsequent transmission chain. Differences in sampling and sequencing may bias results and make accurate estimation of introduction times difficult. In addition, the possible convergent evolution of viruses within immunocompromised or immunocompetent hosts in NYC could complicate interpretation.

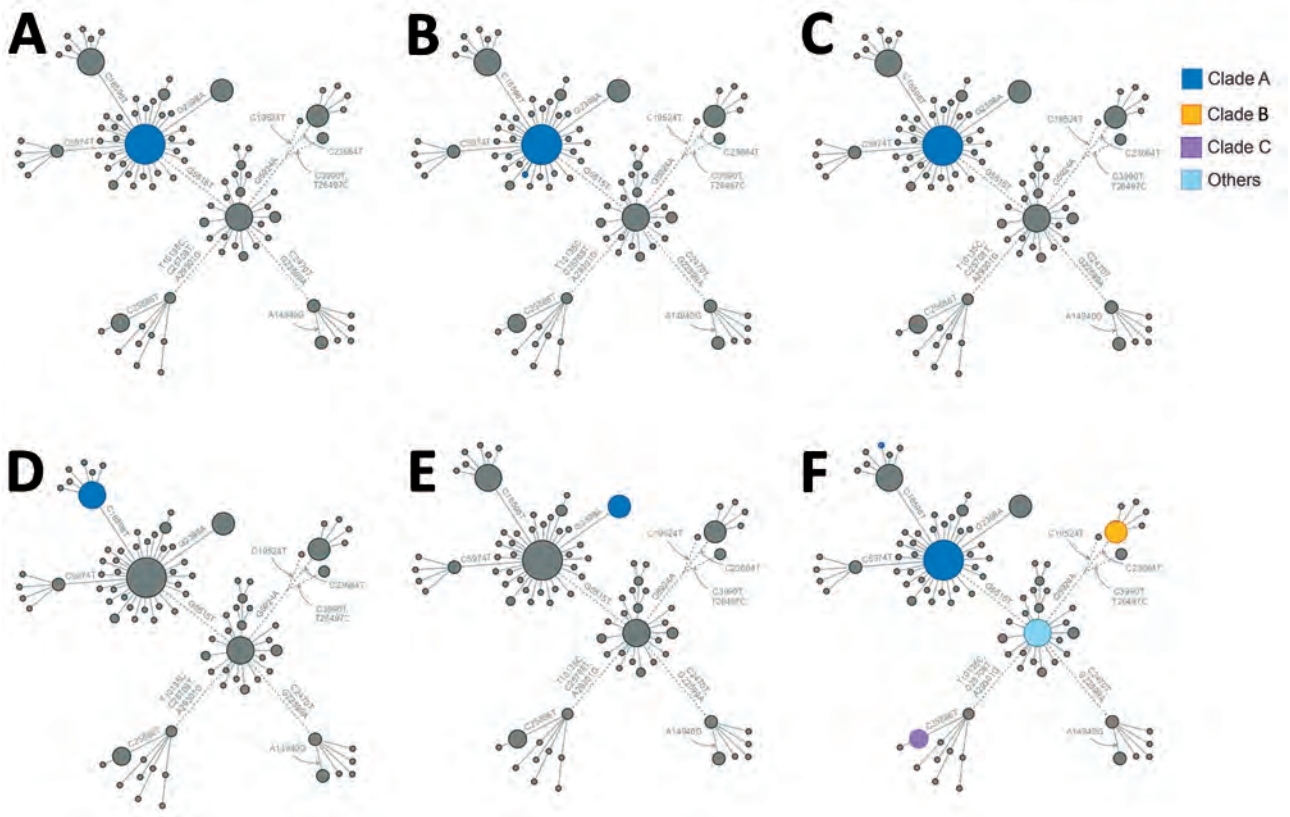

Figure 9. Genotype network mapping of transmission events of SARS-CoV-2 Omicron variant in specific groups, New York, New York, USA, November 25–December 11, 2021. Colored dots indicate genotypes of viruses within each transmission event by clade, if known. A) Household 1. B) Household 2. C) Household 3. D) Household 4. E) Family 1. F) Workplace 1.

As more genomes of Omicron viruses are being sequenced, we expect to be able to further elucidate the origins of Omicron introductions and chain of the community transmission.

Our analysis also highlights the importance of timely genomic surveillance, which can reduce the effects of emerging variants (*26*). Through genomic surveillance, we can make an initial assessment of the risk for the emerging variant by its mutation profile and growth advantage (*2*). Analysis of sequenced data can augment testing strategies to monitor the variant in real-time without whole-genome sequencing. For example, SGTF can be used as a proxy for Omicron during the early days of an outbreak (*8*–*10*). In addition, the introduction and transmission pattern of the emerging variants can be elucidated using viral sequences. Early identification of the emerging variant outbreak provided by genomic surveillance could aid us in making timely and appropriate policy responses, including enhanced tracking and monitoring of travelers and social control measures. Therefore, combining real-time genomic and epidemiologic surveillance is critical for effective responses for tracking, understanding, and controlling infectious disease outbreaks.

Acknowledgments

We thank all data contributors: the authors and their originating laboratories for obtaining the specimens and their submitting laboratories for generating the genetic sequences and metadata and sharing via the GISAID Initiative, on which this research is based. We thank Anupamjit Ahluwalia, Nasrin Azad, Mishauna Baptise, Gaitrie Balkaran, Jun Young Choi, Elizabeth Deguzman, David Kim, Sandy Lin, Hui Li, Edgar Magnayon, Daphnee Remy, Hoda Shafik-Seddik, Shahida Sultana, Prajna Tamang, Florian Vlad, and Huimin Wu for their technical assistance. We appreciate the scientific discussions with George Rodriguez and thank Grace Chen and Yvonne Chen for review and suggestions.

A.W. was supported by the National Key Research and Development Program (grant no. 2021YFC2301300, China); the CAMS Innovation Fund for Medical Sciences (2021-I2M-1-061, China); the National Natural Science Foundation of China (92169106, China); and Non-profit Central Research Institute Fund of Chinese Academy of Medical Sciences (2021-PT180-001, China). G.C. was supported by US National Institutes of Health (NIH) grant no. 5 R01AI58154 and NIH 5 R01AI160120. L.W. was supported by NIH grant no. 5T32AI007323.

About the Authors

Dr. Liu is the laboratory director of microbiology, immunology and molecular diagnostics, Department of Pathology and Clinical Laboratories, NewYork-Presbyterian Queens Hospital. His research focus is to develop rapid molecular assays for pathogen diagnosis. Mr. Cheng is a master's degree candidate at the China Pharmaceutical University and the Institute of Systems Medicine, Chinese Academy of Medical Sciences & Peking Union Medical College. His research interest is the molecular evolution of viruses.

References

1. Rambaut A, Holmes EC, O'Toole Á, Hill V, McCrone JT, Ruis C, et al. A dynamic nomenclature proposal for SARS-CoV-2 lineages to assist genomic epidemiology. Nat Microbiol. 2020;5:1403–7. https://doi.org/10.1038/s41564-020-0770-5
2. Viana R, Moyo S, Amoako DG, Tegally H, Scheepers C, Althaus CL, et al. Rapid epidemic expansion of the SARS-CoV-2 Omicron variant in southern Africa. Nature. 2022;603:679–86. https://doi.org/10.1038/s41586-022-04411-y
3. Chen C, Nadeau S, Yared M, Voinov P, Xie N, Roemer C, et al. CoV-Spectrum: analysis of globally shared SARS-CoV-2 data to identify and characterize new variants. Bioinformatics. 2022;38:1735–7. https://doi.org/10.1093/bioinformatics/btab856
4. Carreño JM, Alshammary H, Tcheou J, Singh G, Raskin AJ, Kawabata H, et al. Activity of convalescent and vaccine serum against SARS-CoV-2 Omicron. Nature. 2022;602:682–8.
5. Cao Y, Wang J, Jian F, Xiao T, Song W, Yisimayi A, et al. Omicron escapes the majority of existing SARS-CoV-2 neutralizing antibodies. Nature. 20221;602:657–63.
6. Hu J, Peng P, Cao X, Wu K, Chen J, Wang K, et al. Increased immune escape of the new SARS-CoV-2 variant of concern Omicron. Cell Mol Immunol. 2022;19:293–5. https://doi.org/10.1038/s41423-021-00836-z
7. Bal A, Destras G, Gaymard A, Stefic K, Marlet J, Eymieux S, et al.; COVID-Diagnosis HCL Study Group. Two-step strategy for the identification of SARS-CoV-2 variant of concern 202012/01 and other variants with spike deletion H69-V70, France, August to December 2020. Euro Surveill. 2021;26:2100008. https://doi.org/10.2807/1560-7917.ES.2021.26.3.2100008
8. Accorsi EK, Britton A, Fleming-Dutra KE, Smith ZR, Shang N, Derado G, et al. Association between 3 doses of mRNA COVID-19 vaccine and symptomatic infection caused by the SARS-CoV-2 Omicron and Delta variants. JAMA. 2022;327:639–51. https://doi.org/10.1001/jama.2022.0470
9. Wolter N, Jassat W, Walaza S, Welch R, Moultrie H, Groome M, et al. Early assessment of the clinical severity of the SARS-CoV-2 omicron variant in South Africa: a data linkage study. Lancet. 2022;399:437–46. https://doi.org/10.1016/S0140-6736(22)00017-4
10. Vauhkonen H, Nguyen PT, Kant R, Plyusnin I, Erdin M, Kurkela S, et al. Introduction and rapid spread of SARS-CoV-2 Omicron variant and dynamics of BA. 1 and BA. 1.1 sublineages, Finland, December 2021. Emerg Infect Dis. 2022;28:1229–32. https://doi.org/10.3201/eid2806.220515
11. Espenhain L, Funk T, Overvad M, Edslev SM, Fonager J, Ingham AC, et al. Epidemiological characterisation of the

first 785 SARS-CoV-2 Omicron variant cases in Denmark, December 2021. Euro Surveill. 2021;26:2101146. https://doi.org/10.2807/1560-7917.ES.2021.26.50.2101146
12. Cedro-Tanda A, Gómez-Romero L, de Anda-Jauregui G, Garnica-López D, Alfaro-Mora Y, Sánchez-Xochipa S, et al. Early genomic, epidemiological, and clinical description of the SARS-CoV-2 omicron variant in Mexico City. Viruses. 2022;14:545. https://doi.org/10.3390/v14030545
13. Gonzalez-Reiche AS, Hernandez MM, Sullivan MJ, Ciferri B, Alshammary H, Obla A, et al. Introductions and early spread of SARS-CoV-2 in the New York City area. Science. 2020;369:297–301. https://doi.org/10.1126/science.abc1917
14. Maurano MT, Ramaswami S, Zappile P, Dimartino D, Boytard L, Ribeiro-Dos-Santos AM, et al. Sequencing identifies multiple early introductions of SARS-CoV-2 to the New York City region. Genome Res. 2020;30:1781–8. https://doi.org/10.1101/gr.266676.120
15. Bushman D, Alroy KA, Greene SK, Keating P, Wahnich A, Weiss D, et al.; CDC COVID-19 Surge Laboratory Group. Detection and genetic characterization of community-based SARS-CoV-2 infections—New York City, March 2020. MMWR Morb Mortal Wkly Rep. 2020;69:918–22. https://doi.org/10.15585/mmwr.mm6928a5
16. Sami S, Horter L, Valencia D, Thomas I, Pomeroy M, Walker B, et al. Investigation of SARS-CoV-2 transmission associated with a large indoor convention—New York City, November–December 2021. MMWR Morb Mortal Wkly Rep. 2022;71:243–8. https://doi.org/10.15585/mmwr.mm7107a4
17. Smith-Jeffcoat SE. Multistate outbreak of SARS-CoV-2 B. 1.1. 529 (Omicron) variant infections among persons in a social network attending a convention—New York City, November 18–December 20, 2021. MMWR Morb Mortal Wkly Rep. 2022;71.
18. Kirby AE, Welsh RM, Marsh ZA, Yu AT, Vugia DJ, Boehm AB, et al.; New York City Department of Environmental Protection. Notes from the field: early evidence of the SARS-CoV-2 B.1.1.529 (Omicron) variant in community wastewater—United States, November–December 2021. MMWR Morb Mortal Wkly Rep. 2022;71:103–5. https://doi.org/10.15585/mmwr.mm7103a5
19. Aksamentov I, Roemer C, Hodcroft EB, Neher RA. Nextclade: clade assignment, mutation calling and quality control for viral genomes. J Open Source Softw. 2021;6:3773. https://doi.org/10.21105/joss.03773
20. Bastian M, Heymann S, Jacomy M. Gephi: an open source software for exploring and manipulating networks. In: Adar E, Hurst M, Finin T, Glance N, Nicolov N, Tseng B, editors. Proceedings of the Third International AAAI Conference on Weblogs and Social Media. Menlo Park (CA): The AAAI Press; 2009. p. 361–2.
21. Hadfield J, Megill C, Bell SM, Huddleston J, Potter B, Callender C, et al. Nextstrain: real-time tracking of pathogen evolution. Bioinformatics. 2018;34:4121–3. https://doi.org/10.1093/bioinformatics/bty407
22. Shu Y, McCauley J. GISAID: Global initiative on sharing all influenza data—from vision to reality. Euro Surveill. 2017;22:30494. https://doi.org/10.2807/1560-7917.ES.2017.22.13.30494
23. Karim SSA, Karim QA. Omicron SARS-CoV-2 variant: a new chapter in the COVID-19 pandemic. Lancet. 2021;398:2126–8. https://doi.org/10.1016/S0140-6736(21)02758-6
24. CDC COVID-19 Response Team. SARS-CoV-2 B.1.1.529 (Omicron) variant—United States, December 1–8, 2021. MMWR Morb Mortal Wkly Rep. 2021;70:1731–4. https://doi.org/10.15585/mmwr.mm7050e1
25. Sy KTL, White LF, Nichols BE. Population density and basic reproductive number of COVID-19 across United States counties. PLoS One. 2021;16:e0249271. https://doi.org/10.1371/journal.pone.0249271
26. Grubaugh ND, Hodcroft EB, Fauver JR, Phelan AL, Cevik M. Public health actions to control new SARS-CoV-2 variants. Cell. 2021;184:1127–32. https://doi.org/10.1016/j.cell.2021.01.044

Address for correspondence: Genhong Cheng, Department of Microbiology, Immunology, & Molecular Genetics, University of California, Los Angeles, 615 Charles Young Dr S, Los Angeles, CA 90095, USA; email: gcheng@mednet.ucla.edu; Aiping Wu, Suzhou Institute of Systems Medicine, Suzhou 215123, China; email: wap@ism.cams.cn; William H. Rodgers, Department of Pathology and Clinical Laboratories, NewYork-Presbyterian Queens Hospital, 56-45 Main St, Flushing, NY 11355, USA; email: whr9001@nyp.org

Correlates of Protection, Thresholds of Protection, and Immunobridging among Persons with SARS-CoV-2 Infection

David S. Khoury, Timothy E. Schlub, Deborah Cromer, Megan Steain, Youyi Fong, Peter B. Gilbert, Kanta Subbarao, James A. Triccas, Stephen J. Kent, Miles P. Davenport

Several studies have shown that neutralizing antibody levels correlate with immune protection from COVID-19 and have estimated the relationship between neutralizing antibodies and protection. However, results of these studies vary in terms of estimates of the level of neutralizing antibodies required for protection. By normalizing antibody titers, we found that study results converge on a consistent relationship between antibody levels and protection from COVID-19. This finding can be useful for planning future vaccine use, determining population immunity, and reducing the global effects of the COVID-19 pandemic

Determining the relationship between immune response and protection from symptomatic SARS-CoV-2 infection (i.e., COVID-19) is useful for predicting the future effectiveness of vaccines. That relationship should enable immunobridging (i.e., predicting the efficacy of candidate vaccines) that can help with approval of new or updated vaccines based on immunogenicity data, without the need for large phase 3 trials (*1*). Immunobridging is used for approval of seasonal influenza vaccines in the European Union and the United States and reduces the costs and time required to develop vaccines. In addition, defining levels of immunity required for protection from novel SARS-CoV-2 variants will be useful for predicting population-level immunity to infection and guiding public health policy on vaccination and boosting.

Author affiliations: The University of New South Wales, Sydney, New South Wales, Australia (D.S. Khoury, D. Cromer, M.P. Davenport); University of Sydney, Sydney (T.E. Schlub, M. Steain, J.A. Triccas); Fred Hutchinson Cancer Research Center, Seattle, Washington, USA (Y. Fong, P.B. Gilbert); The University of Melbourne at the Peter Doherty Institute for Infection and Immunity, Melbourne, Victoria, Australia (K. Subbarao, S.J. Kent); Monash University, Melbourne (S.J. Kent)

DOI: https://doi.org/10.3201/eid2902.221422

Several studies have shown that higher levels of neutralizing antibody are associated with immune protection from symptomatic SARS-CoV-2 infection during short-term follow-up after vaccination (*2*–*6*). Three of those studies also tried to estimate the level of protection associated with particular antibody levels by using 2 approaches to estimate the relationship between neutralizing antibody levels and vaccine efficacy (*2*–*4*) (protection curve; Table; Figure 1). Although those studies reported threshold antibody levels required for 50% or 70% protection, all found that protection changes gradually with neutralization titer and, thus, there is not a strict threshold below which persons are not protected or above which protection is achieved.

The study of immune correlates by Khoury et al. used a vaccine-comparison approach, which estimated the relationship between mean neutralizing antibody levels (in phase 1/2 trials) and vaccine efficacy (in phase 3 trials) across 7 vaccines and convalescing persons (after first normalizing neutralization titers to convalescing persons in each study) (*2*) (Table; Figure 1, panels A–C). That study estimated that the neutralizing antibody level associated with 50% protection from COVID-19 was ≈20% of the mean titer for persons in the convalescent phase (or 54 IU/mL) (*2*). More recently, 2 studies compared neutralizing antibody titers from persons vaccinated with mRNA 1273 (Moderna, https://www.modernatx.com) or ChAdOx1 (AstraZeneca, https://www.astrazeneca.com) with or without symptomatic breakthrough infection (Figure 1, panels D–F). Those studies reported 70% protective thresholds ranging from 4 to 33 IU/mL (Table), depending on the assay used, suggesting a potential role of assay differences in the discrepancies (Appendix, https://wwwnc.cdc.gov/EID/article/29/2/22-1422-App1.pdf) (*3*,*4*). The apparent discrepancies between studies pose a challenge to the use of protection curves in guiding public health

decisions. Therefore, we studied whether those results can be reconciled by accounting for the different methods used. This work was approved under the University of New South Wales Sydney Human Research Ethics Committee (approval HC200242). All data and codes are available from GitHub (https://github.com/InfectionAnalytics/ReconcilingCorrelatesOfProtection).

Reconciling the Studies on Thresholds of Protection

A major limitation for reconciling thresholds of protection (Table) is lack of a standardized assay for measuring in vitro neutralization titers. Although an international standard has been established (*7*), reported titers seem affected by the assay used, as would be expected from differences in cells, virus, and outcomes measured (*8*). For example, even when neutralization titers are measure against the same stocks of pooled convalescent-phase plasma (e.g., the World Health Organization [WHO] 20/130 standard), different assays produced geometric mean neutralization titers (GMT) that varied from 120 to >12,000 (*7*). Even after standardizing measurements from different assays into international units (Table), standardized neutralization titers across the assays still differed by up to 50-fold (*7*). This difference in neutralization titers across different assays is also evident when comparing the 3 studies quantifying the threshold of protection (Table) (*2*–*4*). For example, Gilbert et al. reported the GMT for mRNA-1273 as ≈247 IU/mL (*4*), compared with 1,057 IU/mL reported by Khoury et al. (*2*) (Appendix). A quick survey of the literature reveals 6 reported estimates of the GMT for mRNA-1273 vaccinees, ranging from 247 IU/mL (95% CI 231–264) to 1,404 (95% CI 795–2,484) IU/mL, depending on the study (Appendix Table 1). Similarly, estimates of the GMT for ChAdOx1 vaccinees ranged from 23 IU/mL (*3*) to 144 IU/mL (*2*). When the same neutralization assay is run across different laboratories, then international standards are probably a very effective mechanism for adjusting for interlaboratory variability. However, it is clear from those discrepancies that expression of titers in international units is insufficient for normalizing between different assays and comparing the thresholds of protection reported in these studies (Appendix), which most likely results from differences in the assays themselves (*8*).

Table. Glossary of terms used in study of correlates of protection for SARS-CoV-2 infection

Term	Definition
Protection curve	The relationship between the measured immune response of a vaccine in a subgroup of persons and the level of protection from symptomatic infection provided by the vaccine in that subgroup compared with placebo group (protection = vaccine efficacy).
Threshold of protection	The level of immune response required to provide a specified level of protection (vaccine efficacy) from COVID-19. The 50% protective threshold is commonly reported.
Fold-of-convalescent scale	An attempt to compare different assays by normalizing titers to that of convalescing persons in the same assay. Accurate comparison requires convalescing persons to have similar infection histories.
IU/mL	A neutralization titer (or mean neutralization titer) calibrated to a World Health Organization international standard and reported in IU/mL.

An alternative approach for normalizing neutralization titers between studies is to assume that similar groups of vaccinees should have similar titers. For example, rather than relying on conversion to the WHO international units, we can assume that the mean neutralization for the mRNA-1273 vaccinees is similar in the phase 1/2 trials (as analyzed by Khoury et al. [*2*,*10*]) and in the phase 3 trial (as analyzed by Gilbert et al. [*4*,*11*]) (Appendix). Normalization is limited because it does not account for differences in baseline characteristics of the cohort vaccinated in each study (e.g., age), which may influence neutralization titers. However, because immunobridging studies also rely on comparing vaccine titers among different groups, this approach is pragmatic for overcoming the limitations of comparing different assays.

Applying this normalization approach enabled us to compare the protection curves across different immune correlate studies (Appendix). We aligned the data by assuming that the mean titer for mRNA-1273- or ChAdOx1-vaccinated persons is the same between the phase 1/2 trials and the phase 3 trials for each vaccine (Figure 2; Appendix). Although this normalization is independent of the x-axis scale used, we plotted both curves onto a fold-of-convalescent level scale (Table) developed by Khoury et al. (*2*) for illustration. This transformation enabled a more direct comparison of the protection curve across the 3 studies. Considering the mRNA-1273 breakthrough-infection model (*4*) (Figure 2, panel A), for example, we saw good agreement with the Khoury et al. model (*2*) at the higher neutralization levels achieved with mRNA-1273 vaccination (albeit a seemingly slightly lower maximum protection level predicted in the breakthrough-infection model) but very poor agreement at low neutralization levels. This finding is easily

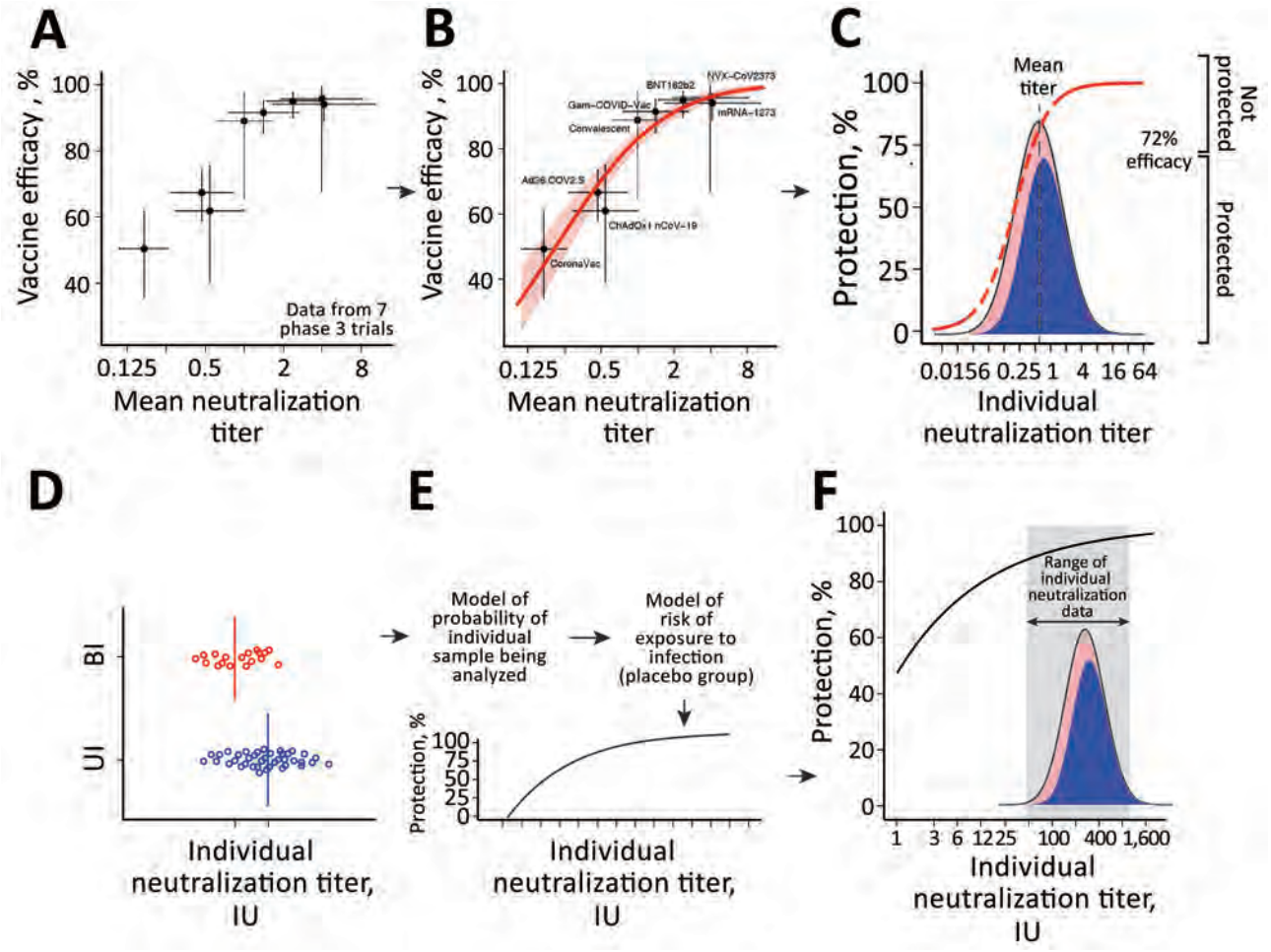

Figure 1. Predicting protection from symptomatic SARS-CoV-2 infection by using approaches to elucidate the relationship between neutralizing antibody titers and protection from COVID-19 (the protection curve): the vaccine-comparison (A–C) and breakthrough-infection (D–F) approaches. The 2 approaches are illustrated schematically: data used (A, D); model fit to data (B, E); and estimated protection (C, F) The vaccine-comparison approach used data on mean neutralization titer from phase 1/2 vaccine trials (normalized to convalescing persons in the same study; x-axis) and observed vaccine efficacy against symptomatic SARS-CoV-2 infection in phase 3 trials (y-axis; n = 7 vaccine trials plus 1 study of infection risk in convalescing persons) (A, B). Using the observed distribution in neutralization titers for a given vaccine and the protection curve, we sum over the whole population to predict the proportion of susceptible (red) or protected (blue) persons for a given vaccine and to estimate protective efficacy for different neutralizing antibody levels (C). Fitting across all vaccines and convalescent persons simultaneously derives the protection curve that best fits the neutralization and protection data (B). The breakthrough-infection model uses neutralization titers of persons with symptomatic breakthrough infections (n = 36 for mRNA-1273 [Moderna, https://www.modernatx.com] and n = 47 for ChAdOx1 [AstraZeneca, https://www.astrazeneca.com]) and uninfected persons (n = 1,005 for mRNA-1273 and n = 828 for ChAdOx1) (*3*,*4*). This method's underlying risk model adjusts for demographic risk factors and for the probability of being sampled in the study to remove these potential sources of bias (E). The protection curve reflects an estimate of the vaccine efficacy in subgroups of persons with specific neutralization titers after the 2-phase sampling design was adjusted for (F). Data and model relationship in panels A and B are from (*2*).

understandable considering the distribution of individual neutralization titers in the mRNA-1273 breakthrough-infection study, in which only ≈10% of participants had a neutralization titer less than the mean titer of early convalescent-phase participants (Figure 2, panel A). Thus, neutralization data with which to estimate protection at lower neutralization levels are sparse (hence, the wide confidence intervals in this region of the curve). Similarly, the ChAdOx1 protection curve (Figure 2, panel B) shows good agreement with the Khoury et al. analysis (2) in the region in which neutralization data are available in the breakthrough-infection study (Figure 2, panel B).

The broad CIs and divergence of the models for which neutralization data are sparse suggests the need for caution when extrapolating the relationship

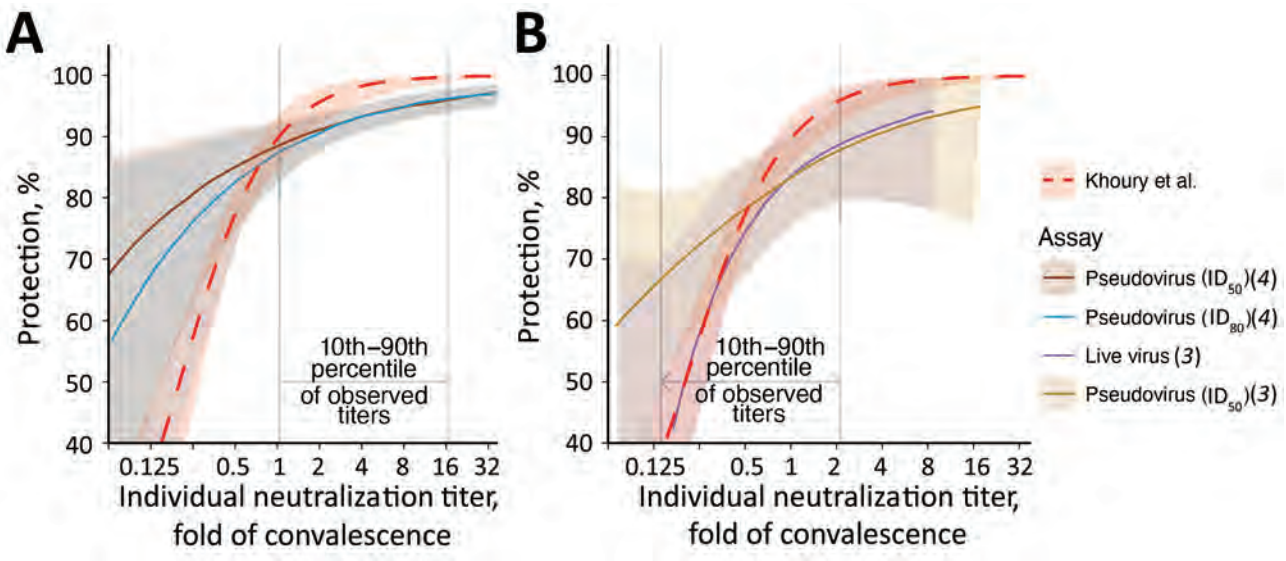

Figure 2. Comparisons of the estimated curves for protection from SARS-CoV-2 infection from 2 vaccines: A) mRNA-1273 (Moderna, https://www.modernatx.com) (*4*); B) ChAdOx1 (AstraZeneca, https://www.astrazeneca.com) (*3*). The relationships between vaccine efficacy against COVID-19 infection (y-axis) and neutralization titers (protection curve) that were estimated in each study (*2*–*4*) are shown. The protection curve derived from the vaccine-comparison model (red dashed line) is compared with the modeled protection curves estimated from breakthrough-infection studies by Gilbert et al. (*4*) (dark brown for the results from the ID_{50} and teal lines for the results from the ID_{80} neutralization titer in in vitro pseudovirus neutralization assays) (A) and Feng et al. (*3*) (purple for the results from in vitro native (live) SARS-CoV-2 virus and light brown for the pseudovirus neutralization assays) (B). Shaded areas indicate 95% CIs from each model. These curves were extracted from the cited studies (Appendix, https://wwwnc.cdc.gov/EID/article/29/2/22-1422-App1.pdf), and differences between assays were controlled for by normalizing the curve from each study by the mean neutralization titer of the uninfected vaccinees in each study. The normalized curves were then represented on a fold-of-convalescent scale by multiplying by the mean neutralization titer of vaccinees compared with convalescing persons as reported in the phase 1/2 trials (*9*,*10*). The vaccine-comparison model agrees closely with the breakthrough-infection models in the neutralization titer ranges where data were most abundant (vertical gray lines indicate 10th to 90th percentiles of the data available in each study). ID_{50}, 50% infectious dose; ID_{80}, 80% infectious dose.

between neutralization and protection beyond the ranges of data available in each study. The vaccine comparison approach has the advantage of fitting to a large span of neutralization titers (a 20-fold range in GMT between the 7 vaccines) (*2*), enabling prediction of the vaccine efficacy over a wide range of neutralization titers. Because none of the reported phase 3 studies of ancestral SARS-CoV-2 infection reported efficacy <50% or >95%, the vaccine-comparison analysis also extrapolates efficacy above and below these levels. However, studies of vaccine efficacy and effectiveness against SARS-CoV-2 variants suggests that the curve remains predictive against the Alpha, Beta, Delta, and Omicron variants, for which lower neutralization titers are observed (*12*; D.S. Khoury et al., unpub. data, https://www.medrxiv.org/content/10.1101/2021.12.13.21267748v2).

The analysis above does not allow direct visualization or comparison of the fit of the data from breakthrough infection to the data from the vaccine-comparison study. We developed a method for estimating unadjusted protection at different neutralization levels from the breakthrough-infection data (Appendix), which also enables inclusion of data from a third breakthrough-infection study of BNT162b2 (Pfizer-BioNTech, https://www.pfizer.com) vaccinees (*5*). We show data from the 3 breakthrough-infection studies compared with the vaccine-comparison approach (normalized for the mean vaccinee titer in each study) (Figure 3). Data from the breakthrough-infection studies show remarkable agreement with the vaccine-comparison model (within the neutralization ranges for which sufficient data were available for each breakthrough-infection study), despite the fundamentally different data, assays, and approaches used to estimate protection curves in each study. Furthermore, after alignment to the GMT of each vaccine group, we can use the underlying distribution in neutralizing antibody titers along with the protection curves from each of these studies to predict the overall vaccine efficacy for existing vaccines (as has been done for the Khoury et al. model [*2*]) (Appendix Methods). That approach reveals good agreement between all models and the observed data, at least in the ranges where data were available to parameterize the models (Appendix Figure 1). This approach provides cross-validation of the protection curves but also provides a lesson that all

models should be used cautiously outside the ranges of the data over which they were developed.

Using the Protection Curve

Immunobridging to Predict Vaccine Efficacy

For vaccine development, an immune correlate to predict the efficacy of a novel vaccine without the need for large and expensive phase 3 efficacy trials would greatly accelerate the approval of novel vaccines (*13*). Similarly, for incorporating novel SARS-CoV-2 variant immunogens, being able to use surrogate measures to predict vaccine efficacy would be helpful. On a public health level, information about neutralization of new variants as they arise and predicting likely population immunity to them would help with predicting future infection risk. In addition, predicting changes in vaccine efficacy with immunity waning and in cohorts with lower neutralization titers after vaccination (e.g., in elderly or immunocompromised persons) could provide information about the need for boosting and other immune protective strategies (*12*).

If a standardized neutralization assay were widely used, it would, in principle, be possible to offer a globally applicable GMT neutralization titer (threshold) associated with a given level of protection, which regulators and vaccine developers could use as a target when assessing and approving vaccines (e.g., as the hemagglutination inhibition titer provides for influenza infection). However, the lack of assay standardization means that no such threshold in international units can be determined that is broadly applicable across different neutralizing antibody assays. Alternatively, regulators have signaled that immunobridging studies, which compare the immunogenicity of new vaccines with that of existing vaccines (for which efficacy has previously

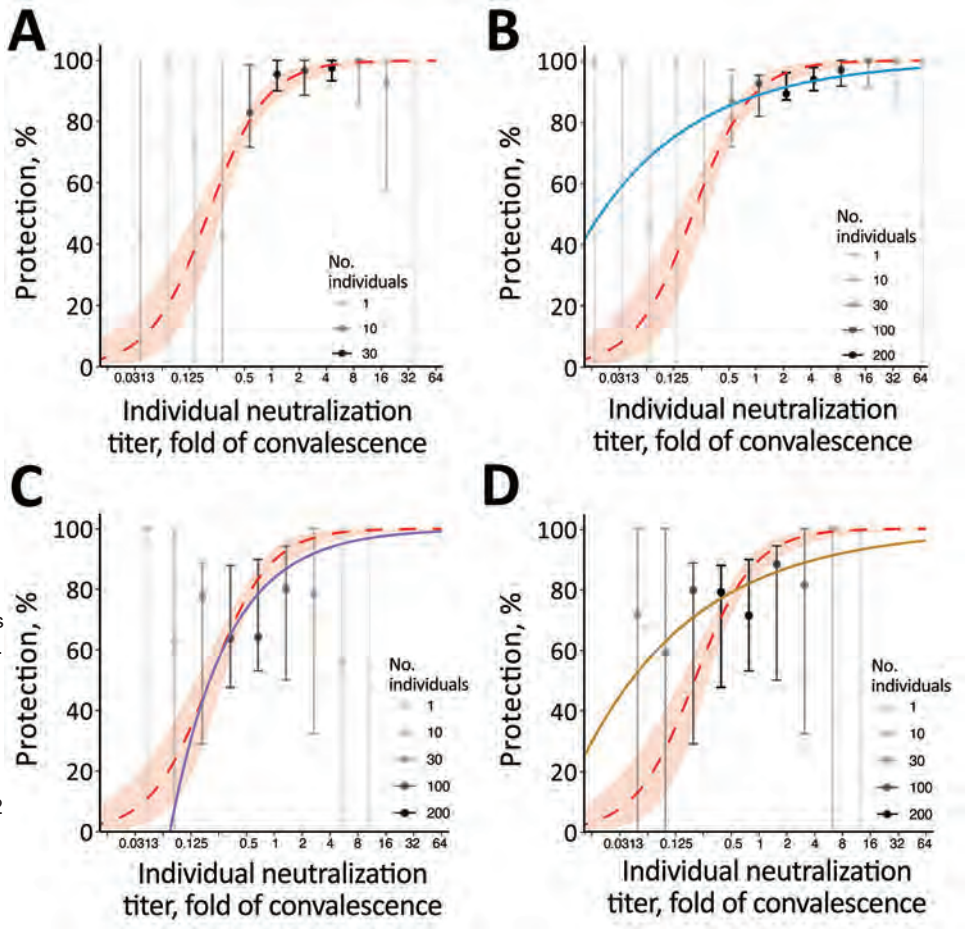

Figure 3. Breakthrough-infection data and protection from SARS-CoV-2 infection showing the association between neutralizing antibody titer and protection from symptomatic SARS-CoV-2 infection for an individual person. A) BNT162b2 (Pfizer-BioNTech, https://www.pfizer.com) (*5*); B) mRNA-1273 (Moderna, https://www.modernatx.com), pseudovirus ID_{50} (*4*); C) ChAdOx1 (AstraZeneca, https://www.astrazeneca.com), live virus (*3*); D) ChAdOx 1, pseudovirus ID_{50} (*3*). The protection curve derived from the vaccine-comparison model (red dashed line and shading 95% CIs) is compared with the observed normalized frequencies of neutralization level (calculations in Appendix, https://wwwnc.cdc.gov/EID/article/29/2/22-1422-App1.pdf) of breakthrough infections reported in 3 studies (gray/black dots). Data from 2 mRNA vaccine studies of mRNA-1273 (A) and BNT162b2 (B), and the adenoviral vector vaccine ChAdOx1 nCoV19 (C, D) are shown. Lower opacity dots indicate fewer persons with neutralization titers in that range. Also shown in each panel are modelled protection curves showing the relationship between individual neutralizing antibodies and protection estimated in each breakthrough-infection study. Note: Breakthrough-infection data of BNT162b2 vaccinees were generously supplied by the authors of reference (*5*). The data were unavailable for the other 2 studies and were extracted from the original manuscripts; extraction of data from Gilbert et al. (*4*) was conducted manually and may be less reliable than that of the other studies (Appendix). ID_{50}, 50% infectious dose; ID_{80}, 80% infectious dose.

been determined) should be conducted (*14*,*15*). That is, vaccine developers need to identify a suitable existing vaccine for comparison and determine the noninferiority or superiority margins relative to these vaccines in a randomized controlled trial (i.e., how much higher neutralization titers are required to be or how much lower titers are permitted to be compared with existing vaccines). The protection curves reported so far (*2*–*4*) can be used to define the parameters of these noninferiority or superiority trials. For example, using the vaccine-comparison model derived by Khoury et al. (*2*) (Figure 1, panel C), we can estimate the noninferiority or superiority margins to existing vaccines that would provide ≥80% efficacy against ancestral virus (Appendix Table 2, Figure 2). If mRNA-1273 or BNT162b2 are used as comparator vaccines, finding a noninferiority margin of 0.44-fold of the GMT observed in mRNA-1273 vaccinees or 0.54-fold of the GMT observed in BNT162b2 vaccinees would provide high confidence that the candidate vaccine has ≥80% efficacy (against ancestral virus). Using ChAdOx1 (with 4-week spacing of doses) as a comparator, we found that a superiority margin of 2.6-fold of GMT compared with ChAdOx1 vaccinees would provide similarly high confidence of ≥80% vaccine efficacy. Of note, those margins are in strong agreement with the lower 95% CIs predicted in the breakthrough-infection studies (Figure 2), which would predict that a candidate vaccine that induced 0.44-fold of the GMT for mRNA-1273 vaccinees would be expected to have an efficacy of ≥85% (either of the 2 neutralization assays reported in that study, on the basis of the reported lower 95% CI) and that a margin of 2.6-fold of the mean ChAdOx1 titer would predict an efficacy of ≥76% (the lower 95% CI of Feng et al. models do not reach 80% in all cases (Figure 2; Appendix) (*3*,*4*). The consensus of these 3 studies provides strong support for using noninferiority or superiority margins in future immunobridging studies.

Identifying Protective Thresholds for Individual Persons

A second goal for the study of protective thresholds is to identify a protective titer for clinical use, that is, a simple blood test for clinically relevant antibody level to indicate if a person is likely to have good protection from COVID-19. The studies that have defined the relationship between neutralization titer and vaccine efficacy have not been designed for, and are not primarily concerned with, defining such a threshold because they deal only with estimates of vaccine efficacy at a population level. Furthermore, individual predictions from population statistics can be fraught with difficulty. Unfortunately, the term "threshold" gives the impression that there might be an antibody level above which one is fully protected (and below which one is susceptible). However, the shapes of the protection curves (Figure 2) make it clear that there is a gradient of risk at different neutralization titers. Moreover, the between-run variability of assays is typically large enough that the uncertainty in the neutralization titer estimated for an individual serum sample is sufficient to lead to wide confidence intervals for the predicted protection for that person (Appendix). For example, when typical duplicate-well and 2-fold serum dilution neutralizing assay designs are used (*16*,*17*), a person with a neutralizing antibody titer at exactly the level associated with 50% protection would have 95% CIs on the estimated protection, ranging from 15% to 85% protection (Appendix), although that range will depend on the precision of a particular assay. It is worth noting that these are estimates of protection from symptomatic SARS-CoV-2 infection (the primary outcome of the studies analyzed), and protection against severe outcomes is achieved at lower neutralization titers (*2*). Together, the wide CIs when estimating individual neutralization titers and the standardization between different serologic assays are major limitations for ability to accurately assess individual neutralizing antibody titers and predict individual protection.

Discussion

Predicting vaccine efficacy or a clinically useful threshold of protection against COVID-19 would be a major advance. The in vitro neutralization titer has been demonstrated by multiple studies to be well correlated with vaccine efficacy and with a person's protection from symptomatic SARS-CoV-2 infection (*2*–*6*,*12*; D.H. Khoury et al., unpub. data). The 4 studies that found significant relationships between neutralization titers and vaccine efficacy used different methods (*2*–*5*), and data from different clinical trials with neutralization data assessed across a range of neutralization assays. Those factors may all contribute to apparent discrepancies between the relationships reported in each study. However, we show that after centering the data from each study on the GMT of the vaccine used in each study, the 4 studies converge on a common prediction of the relationship between neutralization and protection against infection (within the bounds of data available within each study). The agreement of these studies strongly supports the use of neutralizing antibody titers to predict the efficacy of new vaccines or vaccine efficacy against new variants (assuming the fold drop in neutralization titer for the variant can be estimated). Although neutralizing antibody levels are a clear correlate of protection, identifying a protective threshold applicable to a serologic test is more challenging, in part because no such threshold exists, but instead, there is a

gradient of vaccine efficacy that increases with neutralization. Furthermore, significant challenges to defining a particular threshold at which a person's neutralization titer might be deemed to provide high protection from COVID-19 include the diversity of assays used to measure neutralization, the difficulty in translating neutralization levels between assays, the constant emergence of new and more escaped variants, and the uncertainties of estimating individual neutralization titers.

An additional major challenge is adapting assays (and protection curves) to deal with neutralization of current and future SARS-CoV-2 variants. The studies discussed in this analysis primarily deal with neutralization of and protection from the ancestral SARS-CoV-2 strain because the breakthrough-infection data and vaccine efficacy data in most studies was from phase 3 clinical trials (*2*–*4*), which studied infection within the first few months after vaccination and which were mainly conducted before variants of concern had a major foothold, except for the Bergwerk et al. study (*5*), which was conducted during in the Alpha-dominant period. It would be ideal to be able to adapt each model of immune correlates to test its ability to predict protection against variants of concern. However, until recently, only the vaccine-comparison model has been extended to analyze protection against SARS-CoV-2 variants (*12*,*18*,*19*; D. Cromer et al., unpub. data, https://www.medrxiv.org/content/10.1101/2022.06.09.22275942v1), although a recent study has begun to explore this question by using a breakthrough-infection approach (*20*). The work on the vaccine-comparison model approach has so far shown that this model, which was originally calibrated on data for ancestral SARS-CoV-2 infections, can also be used to predict vaccine effectiveness against SARS-CoV-2 variants and after boosting, as long as one adjusts for the drop in neutralization titers to the variants and rise in neutralization after boosting (*12*,*18*,*19*; D. Cromer et al., unpub. data). However, the need to standardize neutralization assays for SARS-CoV-2 variants presents an ongoing challenge.

In vitro neutralizing antibody titers against SARS-CoV-2 present a clear correlate of protection from symptomatic SARS-CoV-2 infection. Studies of passive administration of neutralizing monoclonal antibodies in animals and humans support that neutralizing antibody titers are a mechanistic correlate of protection (*21*–*23*). Indeed, a recent study comparing protective titers in prophylactic and therapeutic studies suggests that the protective titers may be very similar (E. Stadler et al., unpub. data, https://www.medrxiv.org/content/10.1101/2022.03.21.22272672v2). Neutralizing antibody levels are also correlated with protection from severe SARS-CoV-2 infection (*2*).

In conclusion, our findings show that the different COVID-19 correlate of protection studies, which seemingly report different thresholds of protection, have strong agreement. However, other immune responses may also play a substantial role in protection against progression from symptomatic to severe SARS-CoV-2 infection. The agreement across multiple studies of the relationship between neutralizing antibodies and efficacy against COVID-19 can be useful for planning future vaccine use, determining population immunity, and reducing the global effects of the COVID-19 pandemic.

Acknowledgments

We thank Moriah Bergwerk, Tal Gonen, Gili Regev-Yoshay, and colleagues for supplying the raw data from their study of neutralization titers in BNT162b2-vaccinated healthcare workers (*5*).

This work is supported by Australian government Medical Research Future Fund awards GNT2002073 (M.P.D. and S.J.K.), MRF2005544 (S.J.K. and M.P.D.), MRF2005760 (M.P.D.), and MRF2007221 (J.A.T. and M.S.); a National Health and Medical Research Council (NHMRC) program grant GNT1149990 (S.J.K. and M.P.D.); and the Victorian Government (S.J.K.). D.S.K. and S.J.K. are supported by NHMRC fellowships. D.C. and M.P.D. are supported by NHMRC Investigator grants. The Melbourne WHO Collaborating Centre for Reference and Research on Influenza is supported by the Australian Government Department of Health.

The funding sources had no role in the writing of the manuscript or the decision to submit it for publication or in data collection, analysis, or interpretation or in any aspect pertinent to the study. Authors were not precluded from accessing data in the study, and they accept responsibility to submit for publication

D.S.K., D.C., M.S., K.S., S.J.K., J.A.T., and M.P.D. contributed to the conceptual development and data collection. D.S.K., T.E.S., D.C., Y.F., P.B.G., and M.P.D. contributed to the methods, formal analysis, and visualization. All authors contributed to the writing and reviewed and approved the final report. All authors had full access to all the data in the study and had final responsibility for the decision to submit for publication.

About the Author

Dr. Khoury is an interdisciplinary researcher and group leader at the Kirby Institute, University of New South Wales. He originally trained in applied mathematics and has conducted research on infectious disease drug treatment and immunity since 2012, with a focus on malaria, HIV, and COVID-19.

References

1. Huddleston J, Barnes JR, Rowe T, Xu X, Kondor R, Wentworth DE, et al. Integrating genotypes and phenotypes improves long-term forecasts of seasonal influenza A/H3N2 evolution. eLife. 2020;9:e60067. https://doi.org/10.7554/eLife.60067
2. Khoury DS, Cromer D, Reynaldi A, Schlub TE, Wheatley AK, Juno JA, et al. Neutralizing antibody levels are highly predictive of immune protection from symptomatic SARS-CoV-2 infection. Nat Med. 2021;27:1205–11. https://doi.org/10.1038/s41591-021-01377-8
3. Feng S, Phillips DJ, White T, Sayal H, Aley PK, Bibi S, et al.; Oxford COVID Vaccine Trial Group. Correlates of protection against symptomatic and asymptomatic SARS-CoV-2 infection. Nat Med. 2021;27:2032–40. https://doi.org/10.1038/s41591-021-01540-1
4. Gilbert PB, Montefiori DC, McDermott AB, Fong Y, Benkeser D, Deng W, et al.; Immune Assays Team; Moderna, Inc. Team; Coronavirus Vaccine Prevention Network (CoVPN)/Coronavirus Efficacy (COVE) Team; United States Government (USG)/CoVPN Biostatistics Team. Immune correlates analysis of the mRNA-1273 COVID-19 vaccine efficacy clinical trial. Science. 2022;375:43–50. https://doi.org/10.1126/science.abm3425
5. Bergwerk M, Gonen T, Lustig Y, Amit S, Lipsitch M, Cohen C, et al. Covid-19 breakthrough infections in vaccinated health care workers. N Engl J Med. 2021;385:1474–84. https://doi.org/10.1056/NEJMoa2109072
6. Earle KA, Ambrosino DM, Fiore-Gartland A, Goldblatt D, Gilbert PB, Siber GR, et al. Evidence for antibody as a protective correlate for COVID-19 vaccines. Vaccine. 2021;39:4423–8. https://doi.org/10.1016/j.vaccine.2021.05.063
7. World Health Organization. Establishment of the WHO International Standard and Reference Panel for anti-SARS-CoV-2 antibody. Geneva: Expert Committee on Biological Standardization; 2020. p. 9–10.
8. Khoury DS, Wheatley AK, Ramuta MD, Reynaldi A, Cromer D, Subbarao K, et al. Measuring immunity to SARS-CoV-2 infection: comparing assays and animal models. Nat Rev Immunol. 2020;20:727–38. https://doi.org/10.1038/s41577-020-00471-1
9. Folegatti PM, Ewer KJ, Aley PK, Angus B, Becker S, Belij-Rammerstorfer S, et al.; Oxford COVID Vaccine Trial Group. Safety and immunogenicity of the ChAdOx1 nCoV-19 vaccine against SARS-CoV-2: a preliminary report of a phase 1/2, single-blind, randomised controlled trial. Lancet. 2020;396:467–78. https://doi.org/10.1016/S0140-6736(20)31604-4
10. Jackson LA, Anderson EJ, Rouphael NG, Roberts PC, Makhene M, Coler RN, et al.; mRNA-1273 Study Group. An mRNA vaccine against SARS-CoV-2—preliminary report. N Engl J Med. 2020;383:1920–31. https://doi.org/10.1056/NEJMoa2022483
11. Baden LR, El Sahly HM, Essink B, Kotloff K, Frey S, Novak R, et al.; COVE Study Group. Efficacy and safety of themRNA-1273 SARS-CoV-2 vaccine. N Engl J Med. 2021;384:403–16. https://doi.org/10.1056/NEJMoa2035389
12. Cromer D, Steain M, Reynaldi A, Schlub TE, Wheatley AK, Juno JA, et al. Neutralising antibody titres as predictors of protection against SARS-CoV-2 variants and the impact of boosting: a meta-analysis. Lancet Microbe. 2022;3:e52–61. https://doi.org/10.1016/S2666-5247(21)00267-6
13. Walter EB, Talaat KR, Sabharwal C, Gurtman A, Lockhart S, Paulsen GC, et al.; C4591007 Clinical Trial Group. Evaluation of the BNT162b2 Covid-19 vaccine in children 5 to 11 years of age. N Engl J Med. 2022;386:35–46. https://doi.org/10.1056/NEJMoa2116298
14. Medicines & Healthcare Products Regulatory Agency. Access Consortium: alignment with ICMRA consensus on immunobridging for authorising new COVID-19 vaccines [cited 2022 Apr 8]. https://www.gov.uk/government/publications/access-consortium-alignment-with-icmra-consensus-on-immunobridging-for-authorising-new-covid-19-vaccines/access-consortium-alignment-with-icmra-consensus-on-immunobridging-for-authorising-new-covid-19-vaccines
15. Medicines & Healthcare Products Regulatory Agency. Guidance on strain changes in authorised COVID-19 vaccines [cited 2022 Apr 8]. https://www.gov.uk/government/publications/access-consortium-guidance-on-strain-changes-in-authorised-covid-19-vaccines/guidance-on-strain-changes-in-authorised-covid-19-vaccines
16. Juno JA, Tan HX, Lee WS, Reynaldi A, Kelly HG, Wragg K, et al. Humoral and circulating follicular helper T cell responses in recovered patients with COVID-19. Nat Med. 2020;26:1428–34. https://doi.org/10.1038/s41591-020-0995-0
17. Wheatley AK, Juno JA, Wang JJ, Selva KJ, Reynaldi A, Tan HX, et al. Evolution of immune responses to SARS-Co V-2 in mild-moderate COVID-19. Nat Commun. 2021;12:1162. https://doi.org/10.1038/s41467-021-21444-5
18. Cele S, Jackson L, Khoury DS, Khan K, Moyo-Gwete T, Tegally H, et al. Omicron extensively but incompletely escapes Pfizer BNT162b2 neutralization. Nature. 2022;602:654–6. https://doi.org/10.1038/s41586-021-04387-1
19. Cromer D, Reynaldi A, Steain M, Triccas JA, Davenport MP, Khoury DS. Relating in vitro neutralisation level and protection in the CVnCoV (CUREVAC) trial. Clin Infect Dis. 2022;75:e878–9. https://doi.org/10.1093/cid/ciac075
20. Fong Y, McDermott AB, Benkeser D, Roels S, Stieh DJ, Vandebosch A, et al.; Immune Assays Team; the Coronavirus Vaccine Prevention Network (CoVPN)/ENSEMBLE Team; and the United States Government (USG)/CoVPN Biostatistics Team. Immune correlates analysis of the ENSEMBLE single Ad26.COV2.S dose vaccine efficacy clinical trial. Nat Microbiol. 2022;7:1996–2010. https://doi.org/10.1038/s41564-022-01262-1
21. Plotkin SA. Vaccines: correlates of vaccine-induced immunity. Clin Infect Dis. 2008;47:401–9. https://doi.org/10.1086/589862
22. O'Brien MP, Forleo-Neto E, Musser BJ, Isa F, Chan KC, Sarkar N, et al.; Covid-19 Phase 3 Prevention Trial Team. Subcutaneous REGEN-COV antibody combination to prevent Covid-19. N Engl J Med. 2021;385:1184–95. https://doi.org/10.1056/NEJMoa2109682
23. Cohen MS, Nirula A, Mulligan MJ, Novak RM, Marovich M, Yen C, et al.; BLAZE-2 Investigators. Effect of bamlanivimab vs placebo on incidence of COVID-19 among residents and staff of skilled nursing and assisted living facilities: a randomized clinical trial. JAMA. 2021;326:46–55. https://doi.org/10.1001/jama.2021.8828

Addresses for correspondence: David Khoury and Miles Davenport, L6 Wallace Wurth Building, Kirby Institute, UNSW Sydney, Kensington, NSW 2052, Australia; email: dkhoury@kirby.unsw.edu.au and m.davenport@unsw.edu.au

Longitudinal Analysis of Electronic Health Information to Identify Possible COVID-19 Sequelae

Eleanor S. Click,[1] Donald Malec,[1] Jennifer R. Chevinsky, Guoyu Tao, Michael Melgar, Jennifer E. Giovanni, Adi V. Gundlapalli, S. Deblina Datta, Karen K. Wong

Ongoing symptoms might follow acute COVID-19. Using electronic health information, we compared pre– and post–COVID-19 diagnostic codes to identify symptoms that had higher encounter incidence in the post–COVID-19 period as sequelae. This method can be used for hypothesis generation and ongoing monitoring of sequelae of COVID-19 and future emerging diseases.

SARS-CoV-2 causes acute COVID-19 and may cause post–COVID-19 conditions, which include a range of long-term sequelae (*1*,*2*). Review of multiple studies describes ongoing symptoms after acute COVID-19 (*3*). Post–COVID-19 conditions might include symptoms of nonspecific chest pain, fatigue, and malaise, as well as cardiomyopathy, renal failure, lung disease, and venous thromboembolism. Identifying possible sequelae of an emerging disease has traditionally required aggregating clinical experiences; this approach might miss sequelae that are rare or where the increase above baseline is not obvious (*4*).

Large electronic health information databases might aid in detecting these early signals, especially when potential sequelae events are temporally and geographically dispersed. The International Classification of Diseases, 10th revision (ICD-10), code for post–COVID-19 conditions was not available for use in the United States until October 2021; thus, examining other diagnosis codes is needed to infer potential sequelae (*5*). We evaluated feasibility of a method comparing pre– and post–COVID-19 diagnosis healthcare codes to identify possible sequelae from a large national database of healthcare encounters.

Author affiliations: Centers for Disease Control and Prevention, Atlanta, Georgia, USA (E.S. Click, J.R. Chevinsky, G. Tao, M. Melgar, J.E. Giovanni, A.V. Gundlapalli, S.D. Datta, K.K. Wong); Centers for Disease Control and Prevention, Hyattsville, Maryland, USA (D. Malec)

DOI: https://doi.org/10.3201/eid2902.220712

The Study

The Premier Healthcare Database, Special COVID-19 Release (PHD-SR) is a large, hospital-based, service-level, all-payer database with >900 contributing hospitals and healthcare systems. The database includes diagnostic codes from the International Classification of Diseases, 10th Revision, Clinical Modification (ICD-10-CM), for inpatient and selected outpatient encounters with representation in all US census regions (*6*–*8*) (Appendix, https://wwwnc.cdc.gov/EID/article/29/2/22-0712-App1.pdf).

Using PHD-SR (release date February 4, 2021), we analyzed variables for encounter type (inpatient, outpatient including emergency), encounter date sequence variables (length of stay, admission and discharge month, and days between encounters), and discharge ICD-10-CM codes. We included patients with a first COVID-19 inpatient or outpatient encounter (i.e., a COVID-19 discharge ICD-10-CM code). COVID-19 index date was the first day of the first COVID-19 encounter. Pre–COVID-19 encounters were any encounters within 365 days before the patient's first COVID-19 encounter. Post–COVID-19 encounters were the first COVID-19 encounter and all subsequent encounters.

We included encounters with discharge dates during January 1, 2019–December 31, 2020. We calculated relative rates (RRs) of post– to pre–COVID-19 diagnoses in the post–COVID-19 intervals of 60–89, 90–119, and 120–149 days, where day 0 is the COVID-19 index date. Rates were total number of encounters with a particular ICD-10-CM code observed in the specified time interval divided by total number of days in that interval that patients were also in the database (some patients might have died or been no longer observed in the database (i.e., right-censored). Pre–COVID-19 rates were calculated similarly for the whole interval, accounting for when they were first observed in the dataset (i.e., left-censored).

[1]These authors contributed equally to this article.

Because the day of reported diagnosis is only known to have occurred sometime between day of admission and day of discharge, we assigned a specific day (assigned randomly over the encounter duration) as the day of diagnosis for analysis. We generated 5 versions of the dataset with imputed diagnosis dates to capture this uncertainty. To compare diagnosis rates for the pre– and post–COVID-19 intervals, we used 1-sided t-tests of the equality of rates performed on a log RR scale (*9*). We limited analyses to ICD-10-CM codes that occurred in ≥5 encounters during ≥1 post–COVID-19 interval because of difficulty in interpreting RR for rare events (Appendix).

We evaluated whether RR was >1 in the post– versus pre–COVID-19 intervals by using a t-test that includes variability due to multiple imputations (*10*). We report results significant at $p<0.05$ after performing the Benjamini-Hochberg adjustment procedure that excludes marginally significant results that could have occurred by chance because of performing a large number of significance tests. We performed analyses in R 3.6.0 (The R Foundation for Statistical Computing, https://cran.r-project.org/bin/windows/base/old/3.6.0). We defined diagnoses with significantly increased encounter rates ≥60 days after COVID-19 index date relative to pre–COVID-19 as possible post-acute sequelae.

We identified 385,067 patients with a COVID-19 discharge date January–December 2020 and ≥1 visit within the previous 365 days. Median encounters per patient was 4 (interquartile range [IQR] 3–7; pre–COVID-19, 2 [IQR 1–5]; post–COVID-19, 1 [IQR 1–2]); 87% were outpatient encounters. The cohort was 59% female. Median age was 54 (IQR 35–69) years; 5.1% were <18 years of age. Median length of stay for inpatient encounters was 4 (IQR 2–8) days.

Encounters for sequelae of specified infectious and parasitic diseases were increased at least through 149 days after the index date (RR 11.6 at 120–149 days) (Table). Encounters were increased for several months after acute illness for postviral fatigue syndrome, headache, and certain respiratory diseases, including pneumonia and acute respiratory distress syndrome. We identified general sequelae of treatment in intensive care, including polyneuropathy (RR 9.1 at 90–119 days) and myopathy (RR 5.0 at 60–89 days), nonscarring hair loss (RR 2.3–3.5 in multiple intervals beyond 60 days), and pressure ulcers (stage 3 and 4, RR 1.6–1.7 at 60–89 days).

Viral cardiomyopathy (RR 9.8 at 60–89 days) and sepsis codes were only increased in the first 90 days after index date. Rates of nonfollicular diffuse lymphomas were increased in the 60–119 day periods (RR 272.6–411), but most encounters were for 1 patient. Encounters for stage 3 chronic kidney disease (RR 2.5–6.4 beyond 60 days) and for increased liver aminotransferase levels (RR 4.8–6.5 beyond 60 days) were higher for several months after the index date; infective myocarditis (RR 12.6) was increased for 90–119 days.

The possible cardiac, respiratory, kidney, and liver sequelae identified through this method are consistent with those of previous studies (*11*–*13*). For kidney injury, new diagnoses of stage 3 kidney illness (glomerular filtration rate 30–59 mL/min/1.73 m^2) were higher than pre–COVID-19. Stage 3 kidney injury might occur when there is more permanent damage requiring repeated healthcare encounters. This method might generate useful hypotheses about the duration of possible sequelae because we found that encounters for increased aminotransferase levels remain increased at least through the 120–149-day interval after acute illness.

The first limitation of our study is that increased encounter rates might be caused by health-seeking behavior. Encounters for new diagnoses are not equivalent to new disease entities, and rates of encounter diagnosis codes might not represent the rates of disease. For long hospitalizations, diagnosis timing might be mischaracterized because actual diagnosis date is uncertain; however, we used imputation to account for this uncertainty. Counting the initial COVID-19 visit as part of the post–COVID-19 period might identify complications of acute illness as sequelae; however, we focused on sequelae with increased rates ≥60 days after the COVID-19 index date to mitigate that factor. This analysis does not capture exacerbations of underlying conditions, such as worsening heart failure or reactive airway disease, unless disease exacerbation is captured by a different diagnosis code.

The data in this analysis are more representative of adults than children. We excluded pregnancy-related conditions from the analysis. Our findings might not be generalizable to patients with asymptomatic or mild COVID-19 who might not seek healthcare, and we did not control for factors such as aging and changes in societal behavior, so we cannot attribute increased rates of new diagnoses solely to COVID-19. Advantages of our method include rapid application to large longitudinal healthcare datasets and extension over time to identify possible sequelae occurring long after acute illness.

Conclusions

Our findings are consistent with those of other studies using different methods to identify sequelae, including

Table. Diagnostic codes reported during post–COVID-19 interval with increased rate ≥60 d after acute illness relative to pre–COVID-19 baseline rate, by interval from index date, from large administrative all-payer database, United States, January 2019–December 2020*

	Rate increase relative to pre–COVID-19 rate (SE)†			Post–COVID-19 rate, encounters/1,000 person-months		
Diseases and codes	60–89 d	90–119 d	120–149 d	60–89 d	90–119 d	120–149 d
Certain infectious and parasitic diseases						
B97.21: SARS-associated coronavirus as the cause of diseases classified elsewhere	28.7 (12.8)	31.9 (15.6)	82.2 (39.5)	0.22	0.24	0.63
B94.8: Sequelae of other specified infectious and parasitic diseases	15.4 (4.5)	17 (5.1)	11.6 (4.2)	0.26	0.29	0.20
A41.53: Sepsis due to *Serratia*	6 (3.9)	NS	NS	0.60	NS	NS
A41.89: Other specified sepsis	2.8 (0.5)	NS	NS	0.69	NS	NS
B34.2: Coronavirus infection, unspecified	2 (0.6)	2.4 (0.7)	NS	0.24	0.29	NS
R65.21: Severe sepsis with septic shock	1.5 (0.2)	NS	NS	1.29	NS	NS
Diseases of blood and blood-forming organs and certain disorders involving the immune mechanism						
D84.821: Immunodeficiency due to drugs	7.9 (6.0)	NS	NS	0.30	NS	NS
Diseases of the circulatory system						
B33.24: Viral cardiomyopathy	9.8 (8.8)	NS	NS	0.30	NS	NS
I46.8: Cardiac arrest due to other underlying condition	4.8 (2.3)	3.5 (1.9)	NS	0.70	0.50	NS
I46.9: Cardiac arrest, cause unspecified	4.6 (0.9)	3.7 (0.9)	4.5 (1.1)	0.40	0.32	0.38
I40.0: Infective myocarditis	NS	12.6 (10.6)	NS	NS	0.40	NS
Diseases of the digestive system						
K20.91: Esophagitis, unspecified with bleeding	19.8 (18.4)	NS	NS	0.30	NS	NS
K21.00: Gastro-esophageal reflux disease with esophagitis, without bleeding	5.7 (1.3)	6.1 (1.5)	5.7 (1.7)	0.29	0.31	0.29
K20.90: Esophagitis, unspecified without bleeding	3.1 (1.4)	5.8 (2.3)	NS	0.70	0.13	NS
K00.7: Teething syndrome	NS	4 (2.3)	NS	NS	0.50	NS
Diseases of the genitourinary system						
N18.31: Chronic kidney disease, stage 3a	4 (1.4)	5.1 (1.9)	6.4 (2.2)	0.14	0.18	0.22
N18.30: Chronic kidney disease, stage 3 unspecified	3.6 (0.3)	3.8 (0.4)	4.2 (0.5)	1.83	1.91	2.13
N18.32: Chronic kidney disease, stage 3b	2.5 (1.0)	3.2 (1.2)	5.1 (1.9)	0.90	0.12	0.19
Diseases of the musculoskeletal system and connective tissue						
M62.59: Muscle wasting and atrophy, not elsewhere classified, multiple sites	NS	4.1 (2.1)	NS	NS	0.10	NS
M65.071: Abscess of tendon sheath, right ankle and foot	NS	NS	280.3 (550.3)	NS	NS	0.10
Diseases of the nervous system						
G62.81: Critical illness polyneuropathy	11.8 (6.8)	9.1 (6.8)	NS	0.70	0.50	NS
G93.3: Postviral fatigue syndrome	6.8 (2.5)	4.2 (2.1)	NS	0.12	0.70	NS
G72.81: Critical illness myopathy	5 (1.5)	NS	NS	0.30	NS	NS
R51.9: Headache, unspecified	2.6 (0.3)	3.9 (0.3)	3.9 (0.4)	1.47	2.23	2.23
Diseases of the respiratory system						
J12.81: Pneumonia due to SARS-associated coronavirus	8.5 (3.6)	NS	NS	0.90	NS	NS
J80: Acute respiratory distress syndrome	7.4 (2.9)	3.9 (1.7)	NS	0.32	0.17	NS
J95.851: Ventilator associated pneumonia	5.2 (2.4)	4 (2.1)	NS	0.90	0.70	NS
J12.89: Other viral pneumonia	NS	16.1 (2.6)	11 (2.0)	NS	1.33	0.91
Diseases of skin and subcutaneous tissue						
L65.9: Nonscarring hair loss, unspecified	2.4 (0.5)	3.5 (0.7)	2.3 (0.6)	0.36	0.54	0.35
L89.153: Pressure ulcer of sacral region, stage 3	1.7 (0.4)	NS	NS	0.42	NS	NS
L89.154: Pressure ulcer of sacral region, stage 4	1.6 (0.3)	NS	NS	0.68	NS	NS
Endocrine, nutritional, and metabolic diseases						
E87.71: Transfusion associated circulatory overload	4.9 (3.0)	NS	NS	0.40	NS	NS
Mental, behavioral, and neurodevelopmental disorders						
F10.139: Alcohol abuse with withdrawal, unspecified	8.8 (7.6)	NS	NS	0.30	NS	NS
Neoplasms						
C83.90: Non-follicular (diffuse) lymphoma, unspecified, unspecified site	411 (807)	272.6 (535.2)	NS	0.14	0.90	NS
Symptoms, signs, and abnormal clinical and laboratory findings, not elsewhere classified						
R74.01: Elevation of liver transaminase levels	4.8 (1.2)	5 (1.4)	6.5 (1.9)	0.21	0.21	0.28

*Results are significant at p<0.05. Diagnoses are limited to those with RRs significantly increased at >60 d. Clinical Classification Software Refined categories were taken from Agency for Healthcare Research and Quality Clinical Classifications Software Refined (https://www.hcup-us.ahrq.gov/toolssoftware/ccsr/ccs_refined.jsp). NS, not significant; RR, relative rate.

†A specific diagnosis is counted for each patient encounter so that 1 patient might contribute >1 diagnosis if they were admitted for that diagnosis more than once during time period of interest.

a matched cohort analysis of PHD-SR during the same period and a direct survey of persons with and without previous SARS-CoV-2 test results (*14*,*15*). This hypothesis-generating method can provide early signals of possible sequelae for novel diseases and inform additional studies to identify, characterize, and refine potential sequelae for COVID-19 or other emerging diseases.

Acknowledgments

We thank Sean Browning for providing indispensable work in extracting, organizing, and maintaining the Premier data needed for this study.

About the Author

Dr. Click is the lead for Extramural Innovation, Office of Advanced Molecular Detection, National Center for Emerging and Zoonotic Infectious Diseases, Centers for Disease Control and Prevention, Atlanta, GA. Her primary research interests are infectious diseases and molecular epidemiology.

References

1. Al-Aly Z, Xie Y, Bowe B. High-dimensional characterization of post-acute sequelae of COVID-19. Nature. 2021;594:259–64. https://doi.org/10.1038/s41586-021-03553-9
2. Datta SD, Talwar A, Lee JT. A proposed framework and timeline of the spectrum of disease due to SARS-CoV-2 infection: illness beyond acute infection and public health implications. JAMA. 2020;324:2251–2. https://doi.org/10.1001/jama.2020.22717
3. Nalbandian A, Sehgal K, Gupta A, Madhavan MV, McGroder C, Stevens JS, et al. Post-acute COVID-19 syndrome. Nat Med. 2021;27:601–15. https://doi.org/10.1038/s41591-021-01283-z
4. Carfì A, Bernabei R, Landi F, Gemelli Against C-P-ACSG; Gemelli Against COVID-19 Post-Acute Care Study Group. Persistent symptoms in patients after acute COVID-19. JAMA. 2020;324:603–5. https://doi.org/10.1001/jama.2020.12603
5. Centers for Disease Control and Prevention. Public health recommendations: evaluating and caring for patients with post-COVID conditions: interim guidance [cited 2022 Aug 22]. https://www.cdc.gov/coronavirus/2019-ncov/hcp/clinical-care/post-covid-public-health-recs.html
6. PINC. AI™ healthcare data - special release: COVID-19. October 2021. PINC AI™ Applied Sciences, 2021 [cited 2022 Mar 24]. https://offers.premierinc.com/rs/381-NBB-525/images/PHD_COVID19_White_Paper.pdf
7. Rosenthal N, Cao Z, Gundrum J, Sianis J, Safo S. Risk factors associated with in-hospital mortality in a US national sample of patients with COVID-19. JAMA Netw Open. 2020;3:e2029058. https://doi.org/10.1001/jamanetworkopen.2020.29058
8. World Health Organization. ICD-10: international statistical classification of diseases and related health problems, 10th revision. 2nd edition. 2004 [cited 2022 Nov 18]. https://apps.who.int/iris/handle/10665/42980
9. Lachin J. Biostatistical methods: the assessment of relative risks. Hoboken (NJ): John Wiley & Sons; 2009.
10. Rubin D, Little RJ. Statistical analysis with missing data. New York: John Wiley & Sons; 1987.
11. Peleg Y, Kudose S, D'Agati V, Siddall E, Ahmad S, Nickolas T, et al. Acute kidney injury due to collapsing glomerulopathy following COVID-19 infection. Kidney Int Rep. 2020;5:940–5. https://doi.org/10.1016/j.ekir.2020.04.017
12. Puntmann VO, Carerj ML, Wieters I, Fahim M, Arendt C, Hoffmann J, et al. Outcomes of cardiovascular magnetic resonance imaging in patients recently recovered from coronavirus disease 2019 (COVID-19). JAMA Cardiol. 2020;5:1265–73. https://doi.org/10.1001/jamacardio.2020.3557
13. Zhang C, Shi L, Wang FS. Liver injury in COVID-19: management and challenges. Lancet Gastroenterol Hepatol. 2020;5:428–30. https://doi.org/10.1016/S2468-1253(20)30057-1
14. Chevinsky JR, Tao G, Lavery AM, Kukielka EA, Click ES, Malec D, et al. Late conditions diagnosed 1-4 months following an initial coronavirus disease 2019 (COVID-19) encounter: a matched-cohort study using inpatient and outpatient administrative data—United States, 1 March–30 June 2020. Clin Infect Dis. 2021;73(Suppl 1):S5–16. https://doi.org/10.1093/cid/ciab338
15. Wanga V, Chevinsky JR, Dimitrov LV, Gerdes ME, Whitfield GP, Bonacci RA, et al. Long-term symptoms among adults tested for SARS-CoV-2—United States, January 2020–April 2021. MMWR Morb Mortal Wkly Rep. 2021;70:1235–41. https://doi.org/10.15585/mmwr.mm7036a1

Address for correspondence: Eleanor S. Click, Centers for Disease Control and Prevention, 1600 Clifton Rd NE, Mailstop H16-5, Atlanta, GA 30329-4027, USA; email: eoc9@cdc.gov

Nipah Virus Exposure in Domestic and Peridomestic Animals Living in Human Outbreak Sites, Bangladesh, 2013–2015

Ausraful Islam, Deborah L. Cannon, Mohammed Ziaur Rahman, Salah Uddin Khan, Jonathan H. Epstein, Peter Daszak, Stephen P. Luby, Joel M. Montgomery, John D. Klena, Emily S. Gurley

Spillovers of Nipah virus (NiV) from *Pteropus* bats to humans occurs frequently in Bangladesh, but the risk for spillover into other animals is poorly understood. We detected NiV antibodies in cattle, dogs, and cats from 6 sites where spillover human NiV infection cases occurred during 2013–2015.

Henipaviruses are batborne zoonoses that have caused fatal neurologic and respiratory disease outbreaks in humans, horses, and pigs. In Bangladesh, the Indian flying fox (*Pteropus medius*) is the known natural reservoir for Nipah virus (NiV). NiV causes annual outbreaks in humans in Bangladesh, where the primary mode of spillover is through consumption of date palm sap contaminated by *P. medius* bats (*1*); NiV infection is a particular concern for public health because of the high case-fatality ratio and the risk for person-to-person transmission (*2*).

Domestic and peridomestic animals have been important intermediate hosts for zoonotic henipavirus transmission in outbreaks occurring in Australia, Malaysia, and the Philippines (*3*,*4*). One cross-sectional study suggested possible exposure of livestock to henipaviruses in Bangladesh (*5*). Three instances in which animal contact was associated with human NiV infections in Bangladesh have been reported (*1*,*6*,*7*), although little is known about the transmission mechanisms of henipaviruses into livestock and peridomestic animals in Bangladesh. Our study aimed to detect prior NiV infection among livestock and peridomestic animals living in proximity to humans with spillover cases and identify possible exposure pathways in Bangladesh.

Author affiliations: icddr,b, Dhaka, Bangladesh (A. Islam, M.Z. Rahman, E.S. Gurley); Centers for Disease Control and Prevention, Atlanta, Georgia, USA (D.L. Cannon, J.M. Montgomery, J.D. Klena); Public Health Agency of Canada, Ottawa, Ontario, Canada (S.U. Khan); EcoHealth Alliance, New York, New York, USA (J.H. Epstein, P. Daszak); Stanford University, Stanford, California, USA (S.P. Luby); Johns Hopkins Bloomberg School of Public Health, Baltimore, Maryland, USA (E.S. Gurley)

DOI: https://doi.org/10.3201/eid2902.221379

The Study

During January 2013–January 2015, a total of 6 confirmed human Nipah outbreaks were identified through the Nipah surveillance system in Bangladesh (Figure) (*8*). Once an index case-patient was identified, we identified the closest bat roosts to the case-patient's household and collected urine from underneath the roosts by using plastic tarps. We aliquoted roost urine in cryovials containing lysis buffer, stored them at cryogenic temperatures, and tested them for evidence of NiV RNA. We used extracted RNA from bat roost urine for detecting NiV by using a probe-based real-time reverse transcription PCR assay (*9*). Roosts were located from 150 m to 2 km from the human spillover index case-patient's household for all 6 outbreaks (Table 1). Ultimately, we sampled only 5 of the 6 roosts; 1 roost could not be sampled because of political unrest. We identified evidence of NiV RNA shedding in urine collected from 4 roosts. We defined a positive sample as one having ≥1 aliquot with a cycle threshold value ≤39.

During October 2013–October 2015, at 4–9 months after onset in human case-patients, we revisited the villages surrounding each bat roost to test for evidence of infection among domestic animals (e.g., cattle and goats) and peridomestic animals (e.g., dogs, cats, rodents, and house shrews) living near the bat roosts; none of the villages had

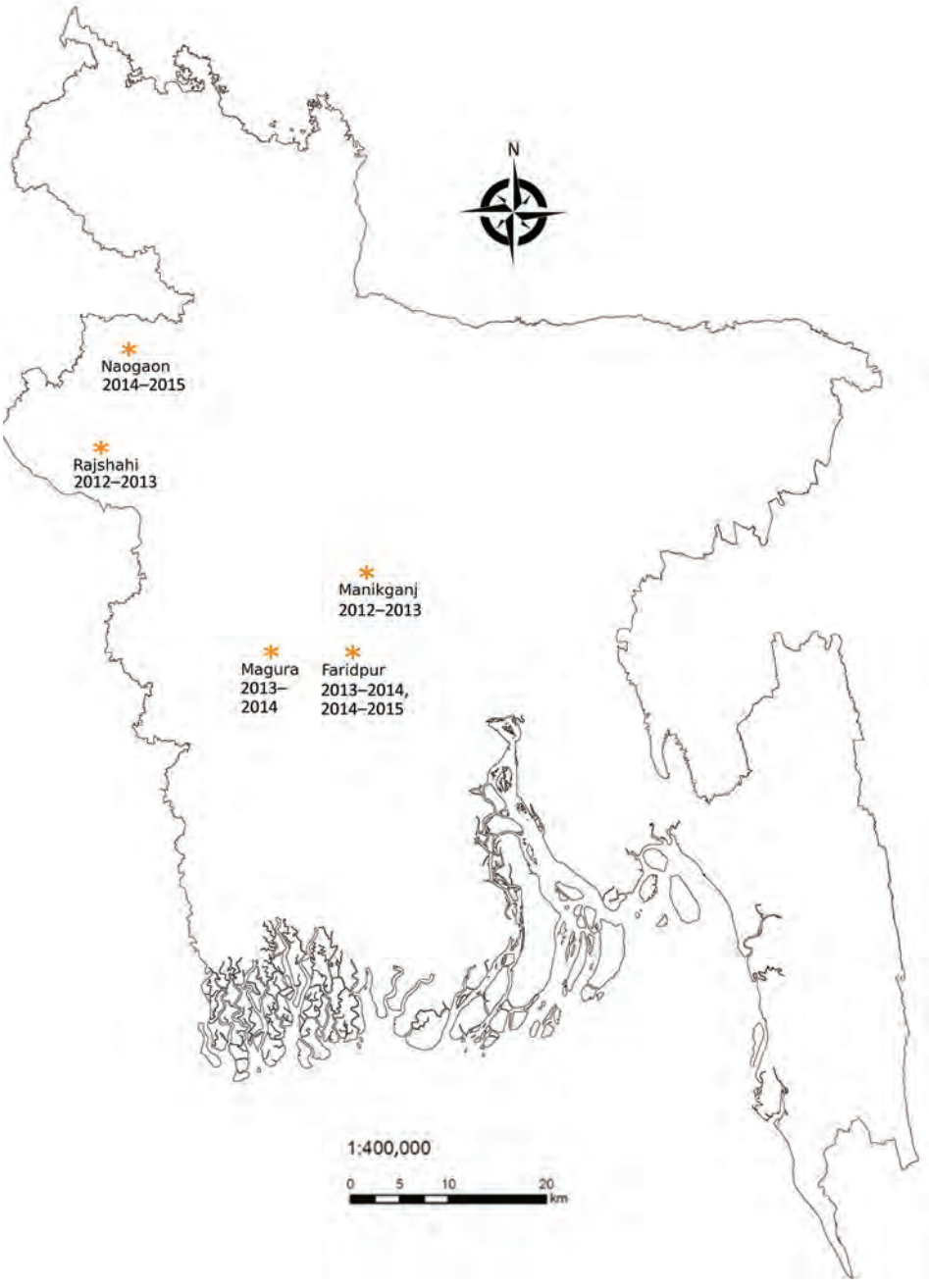

Figure. Sites where spillover human Nipah virus infection cases were detected and domestic and peridomestic animals were sampled, Bangladesh, 2013–2015. In Faridpur District, we sampled twice, once during 2013–2014 and once during 2014–2015.

animal cases during outbreaks. Starting from the household closest to each bat roost, we approached each nearby household to determine whether they owned cattle, goats, cats, or dogs that had resided there for the previous month; households owning any of these animals were asked to participate in the study. We continued this process until we reached the target sample size of 100 domestic animals (0.1% prevalence, 3% null, 80% power, 95% CI, and design effect of 2) and 90 peridomestic animals (1.0% prevalence, 3% null, 80% power, 95% CI, and design effect of 2) in each village. In the first 2 sites we could not sample the targeted number of domestic animals because of unavailability according to our inclusion criteria.

We asked each animal owner about rearing practices, the health status of animals during the month before the human Nipah outbreak, and whether the animal was fed date palm sap or fruit found on the ground or was ever observed to scavenge bat carcasses or bat placentas. For blood collection, we manually restrained cattle, goats, dogs, and cats and

Table 1. Spillover human Nipah virus infection cases and bat roost and animal sampling, 6 sites, Bangladesh, 2013–2015*

Characteristic	Outbreak site						
	1	2	3	4	5	6	All sites
Date of outbreak	2013 Jan	2013 Mar	2014 Jan	2014 Jan	2015 Jan	2015 Jan	
No. human cases	2	7	4	4	7	5	
District	Rajshah	Manikgonj	Faridpur	Magura	Faridpur	Naogaon	
Bat roost sampled, Y/N	Y	Y	Y	Y	N	Y	
Ct value, median (IQR)	38.62 (38.50–38.72)	29.94 (29.60–33.90)	37.5	N/A	N/A	37.25	
Nipah virus RNA in urine underneath roost	Pos	Pos	Pos	Neg	N/A	Pos	
Distance from households to bat roosts, m, median (IQR)	609 (367–1,200)	770 (400–1,970)	583 (499–812)	325 (152–1,040)	359 (162–520)	1,065 (224–1,190)	
Months from outbreak to sampling animals (sampling date)	9 mo (2013 Oct)	8 mo (2013 Nov)	4 mo (2014 May)	6 mo (2014 Jul)	5 mo (2015 Jun)	8 mo (2015 Sep)	
Domestic animals sampled and tested, no. (%)							
Cattle	0/43	0/47	0/50	0/50	1/45 (2)	2/39 (5)	3/274 (1)
Goat	0/49	0/51	0/50	0/50	0/69	0/61	0/330
Total	0/92	0/98	0/100	0/100	1/114 (1)	2/100 (2)	3/604 (1)
Peridomestic animals sampled and tested, no. (%)							
Dog	1/36 (3)	0/28	1/27 (4)	1/35 (3)	0/44	2/19 (11)	5/189 (3)
Cat	0/14	1/22 (5)	3/15 (20)	0/8	0/6	0/20	4/85 (5)
Rat	0/28	0/23	0/36	0/17	0/17	0/21	0/142
House shrew	0/12	0/25	0/13	0/33	0/23	0/30	0/136
Total	1/90 (1)	1/98 (1)	4/91 (4)	1/93 (1)	0/90	2/90 (2)	9/552 (2)

*Ct, cycle threshold; IQR, interquartile range; NA, data not available; neg, negative; pos, positive.

captured rats (*Rattus rattus*, *Bandicota bengalensis*, *B. indica*) and shrews (*Suncas murinus*) by using baited traps in and around the houses of the study participants. We sent serum samples to the US Centers for Disease Control and Prevention (Atlanta, GA, USA), where a human IgG ELISA (*10*) was adapted and optimized to test animal serum by using alternative positive and negative control serum and horseradish peroxidase–conjugated Pierce Recombinant Protein A/G (ThermoFisher Scientific, https://www.thermofisher.com). The ELISA was developed by infecting Vero-E6 cells with whole NiV. The study protocol was reviewed and approved by Research Review Committee and Animal Experimentation Ethics Committee of icddr,b.

We sampled 1,156 animals from 369 households at 6 locations (Table 1). No sick animals were reported by animal owners around the time of the human outbreak or during sampling. Previous studies indicate that, except for cats, NiV does not cause severe infection among the animals that we sampled (*11*). Each study site had ≥1 animal with evidence of IgG against NiV. Serum samples from 1% of cattle (3/274), 3% of dogs (5/189), and 5% of cats (4/85) had evidence of NiV antibodies (Table 1). Thirteen cattle (5%) and 3 goats (1%) were fed date palm sap, but none had evidence of NiV antibodies. One third of cattle (91/274) and goats (110/330) were fed dropped fruit, including 2 cattle with NiV antibodies (Table 2). No owner of either dogs or cats reported observing their animal feeding on bat carcasses or bat placentas.

Conclusions

No animal owners reported sick animals at the time of the human Nipah outbreak. However, the long gap between the outbreak and the survey may have led to underreporting of clinical signs by owners. Pteropid bats forage on fruit trees near human residences in Bangladesh and drop partially eaten fruits on the ground (*12*). Those partially eaten fruits could act as a source of infection with NiV (or related henipaviruses) for cattle and goats (*13*). Serologic evidence of NiV infection in goats was reported from Malaysia during the human Nipah outbreak during 1998–1999 (*14*). Cattle and goats were very rarely fed date palm sap but frequently fed dropped fruit, and nearly all livestock with NiV antibodies were fed dropped fruit. A previous study from Bangladesh detected NiV antibodies among cattle, goats, and pigs using a Luminex assay (biotechne, https://www.bio-techne.com), but none of the animals with antibodies detected in that study had antibodies detected by CDC's in-house ELISA used in our study (*5*). A conjugate that is more

Table 2. Domestic animals fed with dropped fruit and date palm sap by households in 6 sites where spillover human NiV infection cases were detected, Bangladesh, 2013–2015*

Parameters	Value	p value†
Domestic animals fed with dropped fruit	201 (100)	
NiV antibody–positive cattle	2/91 (2)	0.21
NiV antibody–positive goats	0/110	
Domestic animals fed with date palm sap	16 (100)	
NiV antibody–positive cattle	0/13	
NiV antibody–positive goats	0/3	

*Values are no. (%) or no. positive/no. tested (%). NiV, Nipah virus.
†By χ^2 test; p<0.05 considered significant.

general to catching all species was used because controls for each of the species tested, except for pigs, were not available. CDC's in-house ELISA was previously used to test for Hendra virus and NiV antibodies and showed cross-reaction for Hendra virus IgG (*6*). The positive animals in the earlier study could have been exposed to NiV or a related henipavirus, given that *P. medius* bats carry genetically diverse genotypes that might be antigenically similar.

Our study found that a small proportion of domestic animals (e.g., cattle and goats) had evidence of NiV antibodies, whereas evidence of antibodies were more common in peridomestic animals (e.g., cats and dogs). Because peridomestic dogs and cats roam around freely, they may have scavenged bat carcasses or placentas underneath the roost without knowledge of the owners. Previous studies have described henipavirus infection among dogs and cats in other countries (*4*,*11*,*15*). Characterizing the risk factors for infection and the potential role of domestic animals as intermediate or amplifying hosts in Bangladesh would provide a more complete understanding of the ecology of NiV in Bangladesh. In addition, to avoid potential spillover, owners of domestic animals could be advised to not feed them dropped fruit.

This research study was funded by the National Academy of Sciences. The Centers for Disease Control and Prevention conducted the sample testing using their resources. This manuscript was developed with funding from the Defense Advanced Research Projects Agency (administered through cooperative agreement no. D18AC00031-PREEMPT) and from the National Institutes of Health's National Institute for Allergy and Infectious Diseases (grant no. U01AI15320). icddr,b acknowledges with gratitude the commitment of the National Academy of Sciences, the Centers for Disease Control and Prevention, and the Defense Advanced Research Projects Agency to its research efforts. icddr,b is also grateful to the governments of Bangladesh, Canada, Sweden, and the United Kingdom for providing core and unrestricted support.

About the Author

Dr. Islam is a veterinarian at icddr,b (formerly known as the International Centre for Diarrhoeal Disease Research, Bangladesh). His primary research interests include zoonotic pathogens.

References

1. Luby SP, Gurley ES, Hossain MJ. Transmission of human infection with Nipah virus. Clin Infect Dis. 2009;49:1743–8. https://doi.org/10.1086/647951
2. Gurley ES, Montgomery JM, Hossain MJ, Bell M, Azad AK, Islam MR, et al. Person-to-person transmission of Nipah virus in a Bangladeshi community. Emerg Infect Dis. 2007;13:1031–7. https://doi.org/10.3201/eid1307.061128
3. Looi LM, Chua KB. Lessons from the Nipah virus outbreak in Malaysia. Malays J Pathol. 2007;29:63–7.
4. Ching PK, de los Reyes VC, Sucaldito MN, Tayag E, Columna-Vingno AB, Malbas FF Jr, et al. Outbreak of henipavirus infection, Philippines, 2014. Emerg Infect Dis. 2015;21:328–31. https://doi.org/10.3201/eid2102.141433
5. Chowdhury S, Khan SU, Crameri G, Epstein JH, Broder CC, Islam A, et al. Serological evidence of henipavirus exposure in cattle, goats and pigs in Bangladesh. PLoS Negl Trop Dis. 2014;8:e3302. https://doi.org/10.1371/journal.pntd.0003302
6. Hsu VP, Hossain MJ, Parashar UD, Ali MM, Ksiazek TG, Kuzmin I, et al. Nipah virus encephalitis reemergence, Bangladesh. Emerg Infect Dis. 2004;10:2082–7. https://doi.org/10.3201/eid1012.040701
7. icddr,b. Outbreaks of encephalitis due to Nipah/Hendra-like viruses, western Bangladesh. Health Sci Bull. 2003;1:1–6.
8. Rahman M, Chakraborty A. Nipah virus outbreaks in Bangladesh: a deadly infectious disease. WHO South-East Asia J Public Health. 2012;1:208–12. https://doi.org/10.4103/2224-3151.206933
9. Lo MK, Lowe L, Hummel KB, Sazzad HMS, Gurley ES, Hossain MJ, et al. Characterization of Nipah virus from outbreaks in Bangladesh, 2008–2010. Emerg Infect Dis. 2012;18:248–55. https://doi.org/10.3201/eid1802.111492
10. Daniels P, Ksiazek T, Eaton BT. Laboratory diagnosis of Nipah and Hendra virus infections. Microbes Infect. 2001;3:289–95. https://doi.org/10.1016/S1286-4579(01)01382-X
11. Middleton DJ, Westbury HA, Morrissy CJ, van der Heide BM, Russell GM, Braun MA, et al. Experimental Nipah virus infection in pigs and cats. J Comp Pathol. 2002;126:124–36. https://doi.org/10.1053/jcpa.2001.0532
12. Sudhakaran MR, Doss PS. Food and foraging preferences of three pteropodid bats in southern India. J Threat Taxa. 2012;4:2295–303. https://doi.org/10.11609/JoTT.o2227.2295-303
13. Chua KB, Koh CL, Hooi PS, Wee KF, Khong JH, Chua BH, et al. Isolation of Nipah virus from Malaysian Island flying-foxes. Microbes Infect. 2002;4:145–51. https://doi.org/10.1016/S1286-4579(01)01522-2
14. Chua KB. Nipah virus outbreak in Malaysia. J Clin Virol. 2003;26:265–75. https://doi.org/10.1016/S1386-6532(02)00268-8
15. Field H, Young P, Yob JM, Mills J, Hall L, Mackenzie J. The natural history of Hendra and Nipah viruses. Microbes Infect. 2001;3:307–14. https://doi.org/10.1016/S1286-4579(01)01384-3

Address for correspondence: Ausraful Islam, icddr,b, 68 Shaheed Tajuddin Ahmed Sarani, Mohakhali, Dhaka-1212, Bangladesh; email: islam_ausraf@icddrb.org.

(Mis)perception and Use of Unsterile Water in Home Medical Devices, PN View 360+ Survey, United States, August 2021[1]

Shanna Miko, Sarah A. Collier, Claire E. Burns-Lynch, Ashley A. Andújar, Katharine M. Benedict, Julia C. Haston, Catherine O. Hough, Jennifer R. Cope

Tap water is not sterile, and its use in home medical devices can result in infections from waterborne pathogens. However, many participants in a recent survey in the United States said tap water could safely be used for home medical devices. These results can inform communication materials to reduce the high consequence of infections.

Tap water in the United States is treated to meet safe drinking standards; however, low levels of microorganisms remain in drinking water distribution systems, wells, and premise plumbing (*1*,*2*). Although most of these microorganisms are harmless and the water is safe for drinking and cooking, it might not always be safe for other uses, such as aerosolized inhalation and ocular or nasal irrigation (*2*–*4*). Microorganisms that can be found in water systems include *Pseudomonas aeruginosa*, nontuberculous mycobacteria (NTM), *Legionella* spp., *Acanthamoeba* spp., and *Naegleria fowleri* (*1*,*2*). In the United States, biofilm-associated pathogens such as *Pseudomonas* spp., NTM, and *Legionella* spp. are responsible for a large portion of the 120,000 hospitalizations, 7,000 deaths, and billions in direct healthcare costs annually related to waterborne diseases (*5*).

Persons who are at a higher risk for acquiring high-consequence opportunistic infections include the elderly, infants and young children, and persons who have weakened immune systems and other concurrent conditions (*2*,*6*). Some persons who have weakened immune systems might want to take precautions and use water free from microbes. Sterile water does not contain organic microbes but might contain inorganic materials, such as minerals; distilled water does not contain organic and inorganic materials (*7*).

At home, water is used for various health activities, including filling nasal rinsing devices and respiratory devices such as continuous positive airway pressure (CPAP) machines, vaporizers, and portable humidifiers. We hypothesize that people might not understand that tap water is not sterile, leading to its use for specific purposes, such as nasal rinsing, inhalation, and contact lens rinsing that are not recommended.

One study reported demographic data on household water use for home medical devices (*8*). Few data sources describe the understanding of sterile water sources by the population of the United States. This study aimed to quantify perceptions of sterile water, water sources, and actual use of water for home medical purposes among US adults and identify differences among demographic groups regarding perceptions and use of water. These findings can help focus educational efforts to increase awareness of safe water use practices for home medical activities, supporting healthcare providers and public health practitioners in advising their patients and communities about safe water practices for home medical activities.

Author affiliations: Centers for Disease Control and Prevention, Atlanta, Georgia, USA (S. Miko, S.A. Collier, C.E. Burns-Lynch, A.A. Andújar, K.M. Benedict, J.C. Haston, C.O. Hough, J.R. Cope); Oak Ridge Institute for Science and Education, Oak Ridge, Tennessee, USA (C.E. Burns-Lynch); Chenega Enterprise System & Solutions, Chesapeake, Virginia, USA (C.O. Hough)

DOI: https://doi.org/10.3201/eid2902.221205

[1]Preliminary results from this study were presented at the 2022 Epidemic Intelligence Service (EIS) Conference, May 2–5, 2022, Atlanta, Georgia, USA.

The Study

For this cross-sectional study, we used data from Porter Novelli Public Services and the ENGINE Insights' PN View 360+ survey (https://styles.porternovelli.com), delivered August 16–18, 2021 (Appendix, https://wwwnc.cdc.gov/EID/article/29/2/22-1205-App1.pdf). Porter Novelli used quota sampling and statistical weighting to make the panel representative of the US population by sex, age, region, race/ethnicity, and education. All analyses were performed using SAS software version 9.4 (SAS Institute Inc., https://www.sas.com), and $p<0.05$ indicated significance. Survey procedures were used to assess the proportions of response variables by demographics. χ^2 tests were conducted to test the association of each response variable with each demographic variable. Post hoc Wald F tests from contrast statements and the SurveyReg procedure in SAS

Table 1. Demographic characteristics of 1,004 respondents to question about potential uses for tap water, by response, in survey of knowledge about uses for tap water, PN 360 View 2021, United States*

	Do you agree or disagree with the following statements about US tap water?				
Characteristic	Can be used for drinking	Can be used for rinsing contact lenses	Can be used for nasal rinsing	Can be used in respiratory devices†	Bacteria and other living things are not present in US tap water
I don't know	38	140	157	194	119
General population	81 (78–83)	50 (47–54)	62 (59–66)	42 (38–45)	33 (30–36)
Sex					
F	77 (73–81)	43 (38–48)	58 (52–63)	37 (32–42)	24 (20–28)
M	84 (81–88)	57 (52–62)	67 (62,72)	46 (41–51)	42 (37–47)
p value	**0.0090**	**0.0002**	**0.0073**	**0.0153**	**<0.0001**
Race					
White	84 (81–86)	51 (47–55)	64 (60–68)	42 (38–46)	32 (28–35)
Black or African American	76 (68–84)	47 (37–57)	58 (48–68)	48 (37–58)	48 (38–58)
Other‡	69 (59–78)	46 (35–57)	57 (46–68)	35 (24–45)	26 (17–35)
p value	**0.0013**§	0.5781	0.2917	0.2145	**0.0039**¶#
Ethnicity					
Hispanic**	67 (58–76)	48 (38–58)	60 (51–70)	38 (28–48)	31 (22–40)
Non-Hispanic	83 (81–86)	50 (47–54)	63 (59–66)	42 (38–46)	33 (30–37)
p value	**<0.0001**	0.7034	0.6528	0.4189	0.6011
Age, y					
18–34	73 (68–79)	50 (44–56)	65 (59–71)	45 (38–52)	38 (31–44)
35–54	80 (75–85)	52 (46–58)	58 (52–64)	37 (31–43)	35 (29–40)
≥55	86 (82–90)	49 (43–55)	64 (58–70)	43 (36–49)	28 (23–33)
p value	**0.0008**††	0.7743	0.2784	0.1910	**0.0378**††
Region					
Northeast	80 (74–87)	59 (51–67)	66 (57–74)	49 (41–58)	34 (26–41)
Midwest	85 (80–90)	46 (38–54)	60 (53–68)	41 (33–49)	33 (26–41)
South	82 (78–86)	48 (42–54)	63 (58–69)	40 (34–45	34 (29–39)
West	75 (68–81)	51 (44–58)	61 (54–68)	39 (32–47)	30 (24–37)
p value	0.0663	0.1199	0.7756	0.2810	0.8283
Metro status					
Urban	81 (76–86)	59 (52–65)	66 (60–72)	49 (43–56)	44 (38–50)
Suburban	79 (75–83)	46 (40–51)	59 (54–64)	38 (32–43)	28 (24–33)
Rural	83 (78–88)	47 (40–55)	64 (57–72)	39 (31–46)	28 (21–34)
p value	0.5218	**0.0052**‡‡	0.1933	**0.0163**‡‡	**<0.001**‡‡
Household income					
<$59,999	79 (76–83)	48 (43–53)	62 (57–66)	39 (35–44)	31 (26–35)
≥$60,000	82 (78–86)	53 (47–58)	63 (58–68)	44 (39–50)	36 (31–41)
p value	0.2638	0.2013	0.6294	0.1722	0.0978
Water source, n = 932					
Private well	90 (85–96)	63 (54–72)	71 (63–79)	55 (46–65)	48 (39–57)
Municipal	81 (78–84)	48 (44–52)	61 (57–65)	39 (35–43)	30 (26–34)
p value	**0.0101**	**0.0046**	0.0540	**0.0009**	**0.0002**

*Values are percentages agreeing (95% CIs) unless otherwise indicated. Boldface indicates significance ($p<0.05$ by χ^2 or by Wald F-tests where there are ≥3 categories; specific comparisons are footnoted). "I don't know" was not included in analysis; "Agree" and "Strongly Agree" were analyzed as "Agree"; "Disagree" and "Strongly Disagree" were not included in analysis. PN 360 View, Porter Novelli Public Services and the ENGINE Insights' PN View 360+ Survey.
†Respiratory devices include vaporizers, humidifiers, and continuous positive airway pressure machines.
‡Other race grouped persons who identified as >1 race, Asian, Native American, Alaska Native, or other because of small sample size.
§For comparison between White and other race categories.
¶For comparison between Black or African American and other race categories.
#For comparison between White and Black or African American.
**Hispanic, Spanish, or Latino.
††For comparison between 18–34-y and ≥55-y age groups.
‡‡For comparisons between urban and suburban and between urban and rural.

Table 2. Demographic characteristics of 1,004 respondents to question about how they use tap water, by response, in survey of knowledge about tap water, PN 360 View 2021, United States*

	How do you use your household tap water?					
Characteristic	Consumption†	Bathing/ showering	Washing hands	Rinsing contact lenses	Nasal rinsing	Filling respiratory devices‡
General population	66 (63–69)	84 (82–86.4)	88 (86–90)	9 (7–11)	13 (11–15)	24 (21–27)
Sex						
F	64 (59–68)	83 (80–87)	87 (84–90)	8 (5–10)	12 (9–15)	24 (21–28)
M	68 (63–72)	85 (81–88)	89 (86–92)	10 (7–13)	14 (11–17)	23 (20–27)
p value	0.2140	0.6004	0.3666	0.3034	0.3902	0.7322
Race						
White	71 (68–74)	87 (84–89)	89 (87–92)	9 (7–11)	13 (11–16)	24 (21–27)
Black or African American	53 (44–62)	77 (70–85)	85 (78–91)	10 (5–16)	10 (5–,15)	22 (15–30)
Other§	52 (42–62)	77 (69–86)	83 (75–91)	8 (3–14)	14 (7–20)	24 (15–32)
p value	**<0.0001**¶	**0.0078**¶	0.0814	0.8320	0.5920	0.9130
Ethnicity						
Hispanic#	51 (42–61)	71 (63–79)	78 (70–86)	13 (7–19)	21 (14–29)	25 (17–33)
Non-Hispanic	69 (65–72)	87 (84–89)	90 (88–92)	8 (6–10)	11 (9–13)	24 (21–27)
p value	**0.0003**	**<0.0001**	**0.0003**	0.0813	**0.0012**	0.7937
Age, y						
18–34	57 (51–63)	73 (67–78)	81 (76–86)	14 (10–18)	19 (14–24)	25 (20–30)
35–54	64 (58–69)	83 (79–88)	87 (83–91)	10 (7–14)	13 (10–17)	25 (20–30)
≥55	74 (70–79)	93 (90–96)	94 (9–97)	4 (2–5)	8 (5–11)	22 (18–26)
p value	**<0.0001****	**<0.0001**††	**<0.0001****	**<0.0001****	**0.0002****	0.5591
Region						
Northeast	70 (63–77)	82 (76–88)	89 (84–94)	10 (5–14)	12 (7–16)	31 (24–38)
Midwest	69 (63–76)	84 (78–89)	85 (80–91)	8 (4–12)	12 (8–17)	27 (21–34)
South	66 (61–71)	87 (84–91)	89 (86–93)	8 (5–11)	12 (8–15)	18 (14–22)
West	58 (52–65)	81 (75–86)	87 (82–91)	10 (6–15)	15 (11–20)	25 (19–31)
p value	0.0601	0.2120	0.5344	0.7265	0.5647	**0.0054**‡‡
Community setting						
Urban	62 (56–67)	82 (78–87)	88 (84–2)	13 (9–17)	16 (12–20)	24 (19–28)
Suburban	65 (60–69)	83 (79–87)	86 (83–90)	8 (5–10)	13 (10–16)	24 (20–28)
Rural	74 (68–80)	89 (85–93)	91 (86–95)	6 (3–9)	7 (4–11)	24 (18–30)
p value	**0.0189**§§	0.1004	0.3463	**0.0115**¶¶	**0.0147**§§	0.9797
Household income						
<$59,999	63 (59–67)	83 (80–87)	86 (83–89)	7 (5–10)	9 (7–12)	20 (17–24)
≥$60,000	69 (65–74)	85 (82–89)	90 (87–93)	11 (8–14)	17 (14–21)	29 (25–34)
p value	0.0608	0.4593	0.0837	**0.0355**	**0.0003**	**0.0024**
Water source, n = 932						
Private well	68 (61–76)	76 (69–83)	82 (75–88)	14 (8–19)	18 (12–24)	38 (29–46)
Municipal	67 (63–70)	87 (84–89)	90 (87–92)	8 (6–10)	12 (10–14)	22 (19–25)
p value	0.6712	**0.0016**	**0.0102**	**0.0179**	**0.0388**	**0.0001**

*Values are percentages (95% CIs) unless otherwise indicated. Boldface indicates significance ($p<0.05$ by χ^2 or by Wald F-tests where there are ≥3 categories; specific comparisons are footnoted). PN360 View, Porter Novelli Public Services and the ENGINE Insights' PN View 360+ Survey.
†Includes drinking, rinsing produce, or making ice.
‡Respiratory devices include vaporizers, humidifiers, and continuous positive airway pressure machines.
§Other race grouped persons who identified as >1 race, Asian, Native American, or Alaska Native, or other because of small sample size.
¶For comparison between White and Black or African American and between White and other race categories.
#Hispanic, Spanish, or Latino.
**For comparisons between 18–34-y and ≥55-y age groups and between 35–54-y and ≥55-y age groups.
††For comparisons between 18–34-y and 35–54-y age groups, between 18–34-y and ≥55-y age groups, and between 35–54-y and ≥55-y age groups.
‡‡For comparisons between Northeast and South, between Midwest and South, and between South and West.
§§For comparisons between urban and rural and between suburban and rural.
¶¶For comparisons between urban and suburban and between urban and rural.

were used to compare subgroups for demographic variables with >2 levels.

The survey defined tap water as water from faucets and asked participants if they agreed or disagreed with a series of statements (Table 1). One-third (33%, 95% CI 30%–36%) of respondents incorrectly answered that tap water does not have bacteria or living things present. Men, African American or Black persons, and urban residents were more likely to answer incorrectly. More than half (62%, 95% CI 59%–66%) of participants said that tap water could be used for rinsing sinuses, 50% (95% CI 47%–54%) for rinsing contact lenses, and 42% (95% CI 38%–45%) for respiratory devices. Men and urban residents were more likely to choose ≥1 of these incorrect answers.

Respondents were asked how they used their household tap water (Table 2). Most persons reported using tap water for drinking, cooking, bathing, and handwashing. Approximately one quarter (24%, 95% CI 21%–27%) of persons reported filling humidifiers

or CPAP machines with tap water, 13% (95% CI 11%–15%) reported using tap water for nasal rinsing, and 9% (95% CI 7%–11%) reported using tap water for rinsing contact lenses.

Conclusions

The results of this survey highlight opportunities to reinforce messaging regarding appropriate uses of tap water and recommendations for using water in medical devices at home. Although most persons understand what sterile water is and acknowledge that tap water is not sterile, a large proportion of persons responded that tap water can be used for nasal rinsing devices, contact lens rinsing, and filling respiratory devices. These findings represent an opportunity for public health practitioners and water utilities to continue communicating the value of US tap water and its appropriate use.

Although waterborne opportunistic infections can occur through multiple routes and can depend on a person's health status, most NTM and *Legionella* infections are acquired through inhalation (*9*). In this study, 24% of respondents reported filling respiratory devices with tap water, consistent with a recent study in which 20% of respondents reported filling respiratory devices with tap water (*8*). Studies have demonstrated measurable concentrations of NTM (*9*), concentrated minerals (*10*), and other contaminants in aerosols from humidifiers (*11*). Water quality affects the quality of aerosolized air emitted from humidifiers, CPAP machines, and vaporizers, underlying the need for sterilized or distilled water to be used in those devices. Healthcare providers and pharmacists are uniquely positioned to share additional recommendations on appropriate waters (i.e., sterile, distilled, or boiled and cooled) for respiratory devices when they are sold or prescribed. Persons should be informed that they can reduce their exposure to waterborne pathogens by using distilled water or water that has been appropriately boiled and cooled and by regularly cleaning and disinfecting all respiratory devices that use water.

Water can be sterilized at home for safe medical use for respiratory devices and neti pots (containers designed to rinse debris or mucus from the nasal cavity). Ordemann et al. tested water treatment options of UV light treatment, granular activated carbon filtration, and boiling to eliminate *Staphylococcus aureus*, *Pseudomonas aeruginosa*, *Moraxella catarrhalis*, *Acinetobacter baumannii*, *Klebsiella pneumoniae*, *Legionella pneumophila*, and *N. fowleri.* They reported that sterilization could be achieved by boiling water for 5 minutes then cooling, or by UV treatment (e.g., SteriPEN, https://www.katadyngroup.com) for 45 seconds or following the manufacturer's instructions (*12*). The Centers for Disease Control and Prevention also has recommendations for preparing safer water for nasal rinsing, which includes boiling for 1 minute (3 minutes at elevations >6,500 feet) and cooling (*13*). Focused public health messaging and communications from health departments, pharmacists, and healthcare providers should increase awareness of how best to achieve sterile water at home for those who need it, reducing the number of biofilm-associated waterborne pathogens persons are exposed to when performing home medical activities.

Biofilm-associated waterborne pathogens make up a substantial portion of waterborne disease-related illnesses and deaths in the United States. Our results indicate demographic groups to which future public health and provider efforts should be directed to promote appropriate household tap water management practices when using home medical devices that aerosolize water or irrigate the eyes and nose. Public health messaging and healthcare provider guidance that incorporates risk factors for these device users and aligns with recommendations of the Centers for Disease Control and Prevention (*2*) are effective risk communication strategies that can influence population behavior change.

Acknowledgments

We thank Fred Fridinger, Deanne Weber, and Amanda Garcia-Williams for providing assistance.

About the Author

Dr. Miko is a nurse and Epidemic Intelligence Service Officer in the Department of Food, Water, and Environmental Diseases, National Center for Emerging and Zoonotic Infectious Diseases, Centers for Disease Control and Prevention, Atlanta, GA. Her primary research interest is improving public health nationally and internationally through preventing and controlling disease, disability, and death caused by waterborne and environmental incidents and building capacity for better health outcomes.

References

1. Ingerson-Mahar M, Reid A. Microbes in pipes (MIP): the microbiology of the water distribution system, 2013. Washington (DC): American Society for Microbiology [cited 2022 Dec 6], https://www.ncbi.nlm.nih.gov/books/NBK560449/#!po=98.8636
2. Centers for Disease Control and Prevention. Drinking water: preventing waterborne germs at home, 2021 [cited 2022 Jul 1]. https://www.cdc.gov/healthywater/drinking/preventing-waterborne-germs-at-home.html

3. Centers for Disease Control and Prevention. Sinus rinsing for health or religious practice, 2021 [cited 2022 Jun 10]. https://www.cdc.gov/parasites/naegleria/sinus-rinsing.html
4. Food and Drug Administration. Is rinsing your sinuses with neti pots safe? 2021 [cited 2022 May10]. https://www.fda.gov/consumers/consumer-updates/rinsing-your-sinuses-neti-pots-safe
5. Collier SA, Stockman LJ, Hicks LA, Garrison LE, Zhou FJ, Beach MJ. Direct healthcare costs of selected diseases primarily or partially transmitted by water. Epidemiol Infect. 2012;140:2003–13. https://doi.org/10.1017/S0950268811002858
6. Cope J, Roy S, Ali I. *Acanthamoeba disease* associated with the practice of nasal rinsing in immunocompromised patients. Open Forum Infect Dis. 2018;5(Suppl 1):S22. https://doi.org/10.1093/ofid/ofy209.050
7. Environmental Protection Agency. Bottled water basics, 2005 [cited 2022 Dec 6]. https://www.epa.gov/sites/default/files/2015-11/documents/2005_09_14_faq_fs_healthseries_bottledwater.pdf
8. Vanden Esschert K, Barrett CE, Collier SA, Garcia-Williams AG, Hannapel E, Yoder JS, et al. Demographic differences in use of household tap water in a representative sample of US adults, FallStyles 2019. J Water Health. 2021;19:1014–20. https://doi.org/10.2166/wh.2021.118
9. Dowdell K, Haig SJ, Caverly LJ, Shen Y, LiPuma JJ, Raskin L. Nontuberculous mycobacteria in drinking water systems: the challenges of characterization and risk mitigation. Curr Opin Biotechnol. 2019;57:127–36. https://doi.org/10.1016/j.copbio.2019.03.010
10. Yao W, Dal Porto R, Gallagher DL, Dietrich AM. Human exposure to particles at the air-water interface: influence of water quality on indoor air quality from use of ultrasonic humidifiers. Environ Int. 2020;143:105902. https://doi.org/10.1016/j.envint.2020.105902
11. Davis MJ, Janke R, Taxon TN. Assessing inhalation exposures associated with contamination events in water distribution systems. PLoS One. 2016;11:e0168051. https://doi.org/10.1371/journal.pone.0168051
12. Ordemann AG, Stanford JK II, Sullivan DC, Reed JM. Can contaminated water be rendered safe for nasal saline irrigations? Laryngoscope. 2017;127:1513–9. https://doi.org/10.1002/lary.26538
13. Centers for Disease Control and Prevention. Parasites—*Naegleria fowleri*—primary amebic meningoencephalitis (PAM)—amebic encephalitis, 2021 [cited 2022 Jun 15]. https://www.cdc.gov/parasites/naegleria/general.html

Address for correspondence: Shanna Miko, Centers for Disease Control and Prevention, 1600 Clifton Rd NE, Mailstop H24-9, Atlanta, GA 30329-4027, USA; email: rhu6@cdc.gov

etymologia revisited

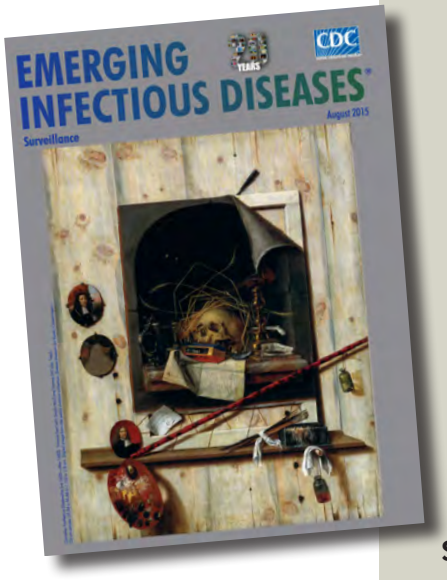

Originally published in August 2015

Escherichia coli

[esh″ə-rik′e-ə co′lī]

A gram-negative, facultatively anaerobic rod, *Escherichia coli* was named for Theodor Escherich, a German-Austrian pediatrician. Escherich isolated a variety of bacteria from infant fecal samples by using his own anaerobic culture methods and Hans Christian Gram's new staining technique. Escherich originally named the common colon bacillus *Bacterium coli commune*. Castellani and Chalmers proposed the name *E. coli* in 1919, but it was not officially recognized until 1958.

Sources:

1. Oberbauer BA. Theodor Escherich—Leben und Werk. Munich: Futuramed-Verlag; 1992.
2. Shulman ST, Friedmann HC, Sims RH. Theodor Escherich: the first pediatric infectious diseases physician? Clin Infect Dis. 2007;45:1025–9 .

https://wwwnc.cdc.gov/eid/article/21/8/et-2108_article

Molecular Detection of *Candidatus* Orientia chuto in Wildlife, Saudi Arabia

Hadil A. Alkathiry, Samia Q. Alghamdi, Holly E.J. Morgan, Madeleine E. Noll, Jing J. Khoo, Abdulaziz N. Alagaili, Benjamin L. Makepeace

Scrub typhus is a zoonosis caused by 3 species of *Orientia* bacteria, including *Candidatus* Orientia chuto. This species is known only from a human case in Dubai and infections in wildlife in Kenya. We report molecular detection of *Candidatus* O. chuto in 2 wild rodent species from Saudi Arabia.

Scrub typhus is a zoonotic bacterial disease caused by 3 intracellular species of bacteria in the genus *Orientia* (Rickettsiales: Rickettsiaceae). The disease is widespread in the Asia-Pacific Region and is associated with fever, as well as pneumonitis, encephalitis, and myocarditis if not promptly treated. The median case fatality rate is ≈6% (*1*), and one third of infections during pregnancy result in adverse outcomes (*2*).

Orientia spp. are transmitted to humans through the bite of infected trombiculid mite larva (chiggers), which feed primarily on small mammals or birds and only incidentally attack humans. *Orientia* spp. are maintained by vertical transmission in trombiculid mites, but wild vertebrate hosts can become infected. However, whether host species are epidemiologically meaningful *Orientia* reservoirs is controversial because horizontal transmission of *Orientia* spp. to chiggers during feeding rarely translates into successful transstadial transfer and transovarial transmission into the next generation (*3*). At minimum, wild hosts contribute to scrub typhus risk by amplifying trombiculid populations; individual hosts can potentially be infested with thousands of chiggers simultaneously (*4*).

Author affiliations: Al Imam Mohammad Ibn Saudi Islamic University, Riyadh, Saudi Arabia (H.A. Alkathiry); University of Liverpool, Liverpool, England, UK (H.A. Alkathiry, H.E.J. Morgan, M.E. Noll, J.J. Khoo, B.L. Makepeace); Al-Bahah University, Al-Bahah, Saudi Arabia (S.Q. Alghamdi); King Saud University, Riyadh (A.N. Alagaili)

DOI: https://doi.org/10.3201/eid2902.221131

Until the early 21st Century, only 1 species of *Orientia* was known: *Orientia tsutsugamushi*, which is restricted to the tsutsugamushi triangle across the Asia-Pacific region. The precise western limit of *O. tsutsugamushi* endemicity is unclear, but reports beyond the Hindu Kush region, where Afghanistan, Tajikistan, and Pakistan converge, are very rare. However, in 2006, a woman contracted scrub typhus while visiting Dubai (*5*). The pathogen was isolated in culture, and molecular characterization established that it was sufficiently distinct from *O. tsutsugamushi* to be classified as a new species, *Candidatus* Orientia chuto. Since that report, *Candidatus* O. chuto–like sequences rarely have been detected, but 1 report describes detection from chiggers infesting a Natal multimammate mouse (*Mastomys natalensis*) in Baringo County, Kenya (*6*). A third species of scrub typhus pathogen, *Candidatus* O. chiloensis, was recently described from patients in Chile (*7*). We investigated whether *Orientia* spp. are circulating in small mammals and chiggers in Saudi Arabia.

The Study

We trapped rodents in southwestern Saudi Arabia, as previously described (*8*) (Figure 1). We humanely euthanized rodents by inhaled anesthetic overdose and preserved any attached chiggers in 70% ethanol. The fieldwork was approved by the Saudi Wildlife Authority (approval no. 288/33/A) and the University of Liverpool's Animal Welfare and Ethics Review Board.

We dissected rodents and fixed the internal organs (lungs, spleen, liver, and kidney) in 70% ethanol. To identify chiggers, we cleared a 10% subsample from each rodent in Berlese fluid and mounted these for microscopic examination (*8*). We pooled the remaining chiggers by species (10–30 specimens per pool) from each rodent. We crushed chigger pools

with a pellet-pestle, then extracted DNA by using the DNeasy Blood & Tissue Kit (QIAGEN, https://www.qiagen.com) according to the manufacturer's instructions and eluted DNA in 30 µL ultrapure water.

We purified genomic DNA from individual mammal host organs (10 mg spleen or 25 mg for other organs) by using the DNeasy Blood & Tissue Kit (QIAGEN) and eluting DNA in 50 µL ultrapure water. We identified rodents by amplifying a cytochrome B gene fragment and performing BLAST analysis (https://blast.ncbi.nlm.nih.gov).

To detect *Orientia* DNA, we screened rodent and chigger extracts by using a quantitative PCR targeting the multicopy *traD* gene (*9*). We subjected positive

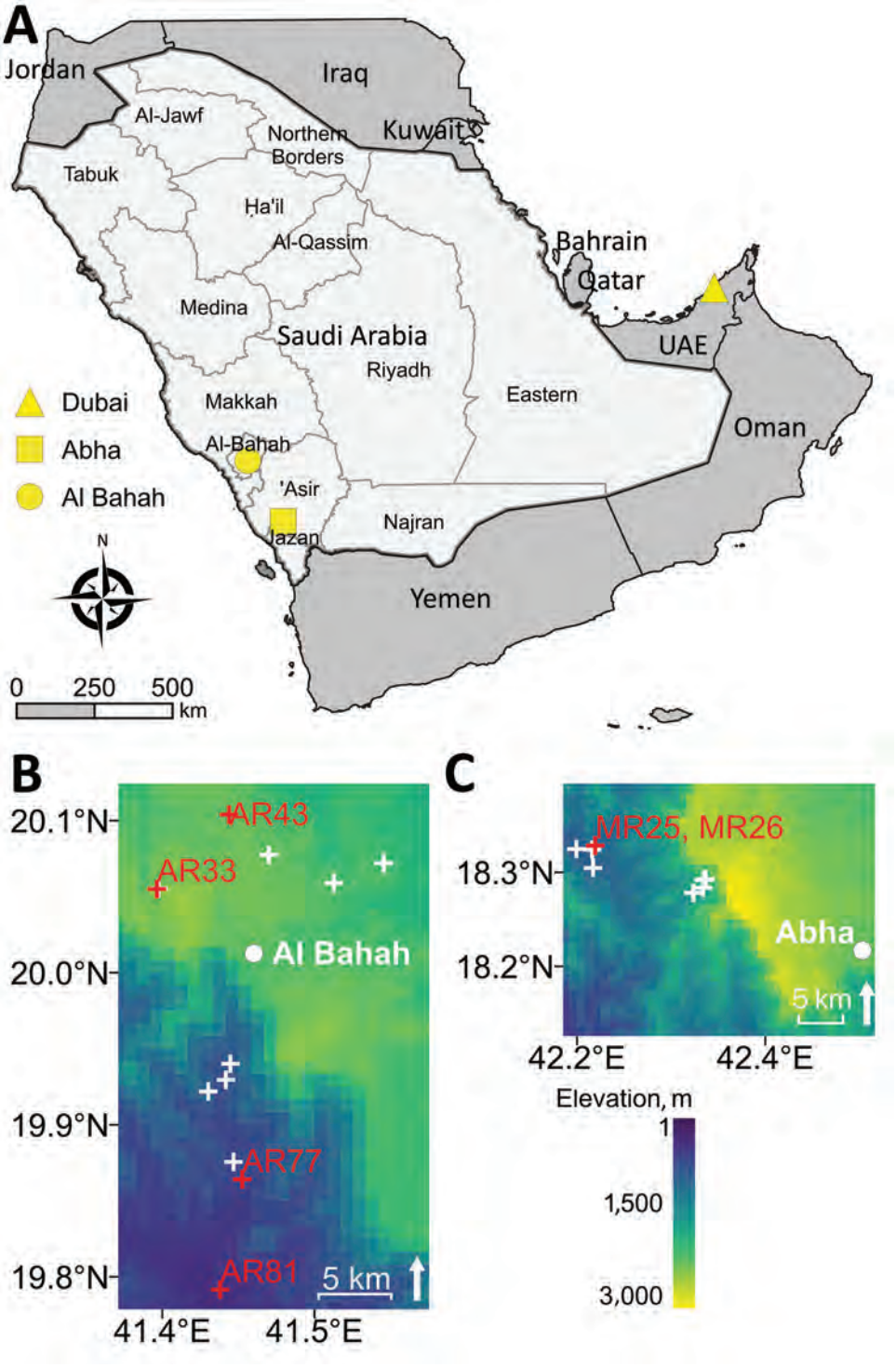

Figure 1. Sampling sites and elevation from which rodents were collected for molecular detection of *Candidatus* Orientia chuto in wildlife, Saudi Arabia. A) Study region on the Arabian Peninsula, including Dubai (yellow triangle), where a clinical case of scrub typhus caused by *Candidatus* O. chuto was reported in a previous study (*5*). Light gray area indicates Saudi Arabia; dark gray area indicates bordering countries on the Arabian Peninsula. Rodents were trapped in the Hijaz Mountains and surrounding towns of Al-Bahah Province (yellow circle indicates Al-Bahah, the capital city) and in the Asir Mountains of Asir Province (yellow square indicates Abha, the capital city). B, C) Heat maps detailing elevation above sea level of trapping locations in Al-Bahah Province (B) and Asir Province (C). Red crosses and sample labels indicate where *Orientia*-positive rodents were found; white crosses indicate areas in which rodents showed no evidence of infection. UAE, United Arab Emirates.

Table 1. Wild rodents screened during molecular detection of *Candidatus* Orientia chuto in wildlife, Saudi Arabia*

Common name	Latin name	Province	
		Asir	Al-Bahah
Eastern spiny mouse	*Acomys dimidiatus*	27	48
Wagner's gerbil	*Dipodillus dasyurus*	0	4
House mouse	*Mus musculus*	0	3
Total		27	55

*Rodents were identified by amplification of a fragment of the cytochrome B gene and sequences were uploaded to the Barcode of Life Data System version 4 (https://boldsystems.org), under project code HAK.

samples to nested PCRs designed to amplify the 47 kDa high-temperature requirement A (*htrA*) gene, also known as TSA47, from *O. tsutsugamushi* or *Candidatus* O. chuto (*6*). We sent amplicons from the second round of the nested PCR to Eurofins Genomics (https://www.eurofins.com) for Sanger sequencing in both directions, then trimmed results to 698 bp, and aligned with reference sequences from GenBank. We used MrBayes (*10*) to construct a phylogenetic tree by using MUSCLE alignment in the Phylogeny.fr web service (*11*). We estimated the best-fit model of nucleotide substitution by using Akaike information criterion in jModelTest 2.1.7 (*12*) and selected the general time-reversible plus gamma distribution plus invariable site model as the best fit. We calculated pairwise distances between sequences by using MEGA 11 (https://www.megasoftware.net).

We trapped 27 rodents in Asir Province, all of which we identified as Eastern spiny mice (*Acomys dimidiatus*). We trapped 55 rodents of 3 different species in Al-Bahah Province (Table 1). Using *htrA* primers for *Candidatus* O. chuto, we identified 7 sequence-confirmed positive organs from 6 individual animals, 2 (7.4%) from Asir Province and 4 (7.3%) from Al-Bahah Province (Table 2). We found infected *A. dimidiatus* in both provinces, and a single infected Wagner's gerbil (*Dipodillus dasyurus*) in Al-Bahah. Positive rodents were widely distributed both in terms of habitat type and elevation (388–2,477 meters above sea level) at the trap location (Table 2; Figure 1). One *A. dimidiatus* from Asir had 2 organs that tested positive for *Candidatus* O. chuto, but all other rodents had a single PCR-positive organ (Table 2). Only 2 rodents were infested with chiggers, and we identified a total of 5 chigger species. None of the chigger samples were PCR-positive for *Orientia* spp. DNA.

Phylogenetic analysis of publicly available *htrA* gene sequences revealed 3 well-supported clades representing *O. tsutsugamushi*, *Candidatus* O. chiloensis, and *Candidatus* O. chuto (Figure 2). The *Candidatus* O. chuto lineage was split into 2 main clades comprising isolates from the Arabian Peninsula, including isolates from this study and the clinical isolate from Dubai in 1 clade and the isolate from Kenya in the other clade. The *Candidatus* O. chuto sequences from this study were distinct from the Dubai isolate (pairwise distance of 0.7%–1.3%) and comprised 2 genotypes exhibiting a pairwise distance of 0.9% (Appendix Table, https://wwwnc.cdc.gov/EID/article/29/2/22-1131-App1.xlsx), which was linked to geographic origin from Al-Bahah or Asir Province (Figure 2).

Conclusions

Only 2 published records of *Candidatus* O. chuto have been available worldwide, 1 from Dubai (*5*) and 1 from Baringo, Kenya (*6*), and only the Dubai isolate has been cultured in vitro and fully sequenced. We identified 2 *Orientia* genotypes from Saudi Arabia, neither of which was identical to previously described

Table 2. Positive rodent specimens, chigger infestations, and collection sites used for molecular detection of *Candidatus* Orientia chuto in wildlife, Saudi Arabia

Province, sample ID	Host species	Tissue, *htrA* accession no.	No. chiggers per species*	Nearest settlement or feature	GPS coordinates	Elevation†	Collection date
Asir							Oct 2020
MR25	*Acomys dimidiatus*	Liver, ON844109	12 *E. caucasicum*; 16 *E. kazeruni*; 1 *S. saudi*; 1 *S. zarudnyi*	Wosanib village	N18.328347, E42.219233	917	
MR26	*A. dimidiatus*	Liver, ON84411; kidney, ON844111	None	Wosanib village	N18.328347, E42.219233	917	
Al-Bahah							Aug 2021
AR33	*Dipodillus dasyurus*	Spleen, ON844112	1 *M. hoogstraali*	Khairah Forest Park	N20.054973, E41.396330	2,477	
AR43	*A. dimidiatus*	Spleen, ON844113	None	Bani Sar town	N20.103946, E41.443762	2,218	
AR77	*A. dimidiatus*	Spleen, ON844114	None	King Fahd Road, Al Makhwah	N19.864027, E41.452468	545	
AR81	*A. dimidiatus*	Spleen, ON844115	None	King Fahd Road, Al Makhwah	N19.791421, E41.437912	388	

*Full genus names: *Ericotrombidium*, *Schoutedenichia*, *Microtrombicula*.
†Meters above sea level.

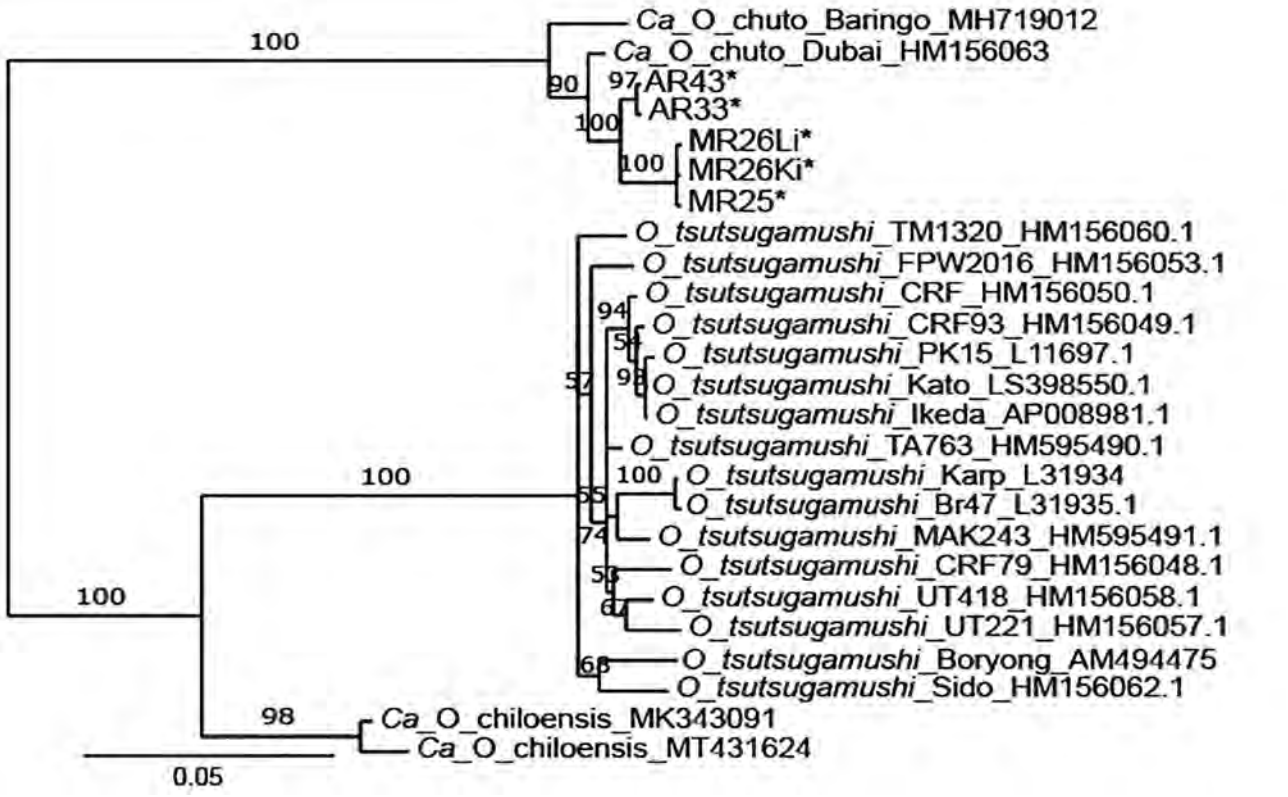

Figure 2. Bayesian inference phylogenetic tree of *Orientia htrA* gene sequences detected in wildlife, Saudi Arabia. Tree represents 698 nt positions of *hrtA*. Asterisks (*) indicate samples from this study; identification numbers are listed in Table 2. Only sequences confirmed by 2 independent PCR amplifications of the same tissue are included. Numbers at nodes represent Bayesian posterior probabilities (%). Accession numbers are given for reference sequences from GenBank. Ki, kidney; Li, liver.

isolates. Separation between *Orientia* spp. at the *htrA* locus is ≈11%–14%, whereas within *O. tsutsugamushi*, *htrA* attains a maximum separation of 1.5%. The maximum separation between the sequences from the Arabian Peninsula and Kenya was 2.5% (Appendix Table), indicating that whole-genome sequencing studies are needed to resolve relationships between *Candidatus* O. chuto–like organisms.

The potential range of *Candidatus* O. chuto is vast, and the bacterium is suspected of causing scrub typhus on the continent of Africa, which is indicated by serologic and clinical evidence, albeit without confirmation by sequencing or culture to date. The *Orientia*-infected rodents detected in this study were found in locations >2,000 km northeast of Baringo County, Kenya, and >1,500 km southwest of Dubai. Thus, the endemic zone of *Candidatus* O. chuto clearly includes northeastern Africa and the Arabian Peninsula, at least, but also could potentially extend eastwards to the western extremity of the tsutsugamushi triangle. Of note, *Orientia* spp. detected by 16S amplicon sequencing in house mice (*Mus musculus domesticus*) in West Africa resembled *Candidatus* O. chuto, although sequences obtained from rodents in France formed a clade that was distinct from known *Orientia* spp. (*13*).

Scrub typhus has not been reported from Saudi Arabia, but our findings highlight the need for vigilance. Moreover, further investigations of the diverse chigger fauna of Saudi Arabia are required to identify the local vectors of *Orientia* spp. Because other agents of febrile illness are endemic in the southwest of the country, including *Plasmodium vivax* (*14*) and dengue virus (*15*), and the region is popular with tourists because of its relatively cool climate, we recommend scrub typhus be included in the differential diagnosis for fever in Saudi Arabia.

Acknowledgments

We are grateful to Al-Bahah University for access to research facilities during fieldwork.

This work was funded by a doctoral scholarship from Imam Muhammad Ibn Saud Islamic University to H.A.A. The Vice Deanship of Research Chairs, Deanship of Scientific Research of the King Saud University, Kingdom of Saudi Arabia, provided support to A.N.A.

H.A.A., S.Q.A. and B.L.M. designed the study; H.A.A., S.Q.A. and A.N.A. selected field sites and trapped rodents; H.A.A. identified rodents and mites; H.A.A. and H.E.J.M. performed DNA extractions, PCR assays and sequence analysis; M.E.N. produced Figure 1; J.J.K. conducted the phylogenetics; B.L.M. supervised the study and wrote the first manuscript draft. All authors read and approved the manuscript. The authors declare no conflict of interest.

About the author

Mrs. Alkathiry is a biologist and PhD student of parasitology in the Institute of Infection, Veterinary & Ecological Sciences at the University of Liverpool, Liverpool, England, UK. Her primary research interests include rodents, vector-borne diseases, and microbiomes.

References

1. Bonell A, Lubell Y, Newton PN, Crump JA, Paris DH. Estimating the burden of scrub typhus: a systematic review. PLoS Negl Trop Dis. 2017;11:e0005838. https://doi.org/10.1371/journal.pntd.0005838
2. McGready R, Prakash JAJ, Benjamin SJ, Watthanaworawit W, Anantatat T, Tanganuchitcharnchai A, et al. Pregnancy outcome in relation to treatment of murine typhus and scrub typhus infection: a fever cohort and a case series analysis. PLoS Negl Trop Dis. 2014;8:e3327. https://doi.org/10.1371/journal.pntd.0003327
3. Traub R, Wisseman CL Jr, Jones MR, O'Keefe JJ. The acquisition of *Rickettsia tsutsugamushi* by chiggers (trombiculid mites) during the feeding process. Ann N Y Acad Sci. 1975;266(1 Pathobiology):91–114. https://doi.org/10.1111/j.1749-6632.1975.tb35091.x
4. Elliott I, Pearson I, Dahal P, Thomas NV, Roberts T, Newton PN. Scrub typhus ecology: a systematic review of *Orientia* in vectors and hosts. Parasit Vectors. 2019;12:513. https://doi.org/10.1186/s13071-019-3751-x
5. Izzard L, Fuller A, Blacksell SD, Paris DH, Richards AL, Aukkanit N, et al. Isolation of a novel *Orientia* species (*O. chuto* sp. nov.) from a patient infected in Dubai. J Clin Microbiol. 2010;48:4404–9. https://doi.org/10.1128/JCM.01526-10
6. Masakhwe C, Linsuwanon P, Kimita G, Mutai B, Leepitakrat S, Yalwala S, et al. Identification and characterization of *Orientia chuto* in trombiculid chigger mites collected from wild rodents in Kenya. J Clin Microbiol. 2018;56:e01124-18. https://doi.org/10.1128/JCM.01124-18
7. Abarca K, Martínez-Valdebenito C, Angulo J, Jiang J, Farris CM, Richards AL, et al. Molecular description of a novel *Orientia* species causing scrub typhus in Chile. Emerg Infect Dis. 2020;26:2148–56. https://doi.org/10.3201/eid2609.200918
8. Stekolnikov AA, Al-Ghamdi SQ, Alagaili AN, Makepeace BL. First data on chigger mites (Acariformes: Trombiculidae) of Saudi Arabia, with a description of four new species. Syst Appl Acarol. 2019;24:1937–63. https://doi.org/10.11158/saa.24.10.12
9. Chao C-C, Belinskaya T, Zhang Z, Jiang L, Ching W-M. Assessment of a sensitive qPCR assay targeting a multiple-copy gene to detect *Orientia tsutsugamushi* DNA. Trop Med Infect Dis. 2019;4:113. https://doi.org/10.3390/tropicalmed4030113
10. Ronquist F, Teslenko M, van der Mark P, Ayres DL, Darling A, Höhna S, et al. MrBayes 3.2: efficient Bayesian phylogenetic inference and model choice across a large model space. Syst Biol. 2012;61:539–42. https://doi.org/10.1093/sysbio/sys029
11. Dereeper A, Guignon V, Blanc G, Audic S, Buffet S, Chevenet F, et al. Phylogeny.fr: robust phylogenetic analysis for the non-specialist. Nucleic Acids Res. 2008;36(Suppl 2):W465–9. https://doi.org/10.1093/nar/gkn180
12. Posada D. jModelTest: phylogenetic model averaging. Mol Biol Evol. 2008;25:1253–6. https://doi.org/10.1093/molbev/msn083
13. Cosson JF, Galan M, Bard E, Razzauti M, Bernard M, Morand S, et al. Detection of *Orientia* sp. DNA in rodents from Asia, West Africa and Europe. Parasit Vectors. 2015;8:172. https://doi.org/10.1186/s13071-015-0784-7
14. Al-Mekhlafi HM, Madkhali AM, Ghailan KY, Abdulhaq AA, Ghzwani AH, Zain KA, et al. Residual malaria in Jazan region, southwestern Saudi Arabia: the situation, challenges and climatic drivers of autochthonous malaria. Malar J. 2021;20:315. https://doi.org/10.1186/s12936-021-03846-4
15. Alhaeli A, Bahkali S, Ali A, Househ MS, El-Metwally AA. The epidemiology of dengue fever in Saudi Arabia: a systematic review. J Infect Public Health. 2016;9:117–24. https://doi.org/10.1016/j.jiph.2015.05.006

Address for correspondence: Benjamin Makepeace, Institute of Infection, Veterinary & Ecological Sciences, University of Liverpool, Liverpool Science Park IC2, Liverpool L3 5RF, UK; email: blm1@liverpool.ac.uk

Neoehrlichiosis in Symptomatic Immunocompetent Child, South Africa

Colleen Bamford,[1] Lucille H. Blumberg, Michelle Bosman, John Frean, Kim G.P. Hoek, Janet Miles, Charlotte Sriruttan, Ilse Vorster, Marinda C. Oosthuizen[1]

We describe a case of neoehrlichiosis in an immunocompetent child with acute febrile illness in South Africa. Neoehrlichiosis was diagnosed by PCR on 16S rDNA from bone marrow aspirate. Phylogenetic analysis indicated an organism closely related to *Candidatus* Neoehrlichia. Clinicians should be aware of possible ehrlichiosis even in immunocompetent patients.

Ehrlichia species and related organisms are obligate intracellular membrane-bound bacteria transmitted via ticks between a range of mammalian animal hosts, including humans. In recent years, taxonomy and phylogeny of these bacterial species has been revised. The family Anaplasmataceae comprises 5 genera: *Ehrlichia*, *Anaplasma*, *Neorickettsia*, *Neoehrlichia*, and *Wolbachia*. However, the number of recognized species and candidate species has substantially increased in recent years. We describe a case of neoehrlichiosis in an immunocompetent child in South Africa.

The Study

A previously healthy 9-year-old boy from Eastern Cape Province, South Africa, was admitted to the hospital with a 3-week history of fever, back pain, and myalgia. Symptoms failed to respond to a course of azithromycin prescribed by his general practitioner for suspected tickbite fever. The child lived on a farm and was exposed to a variety of domestic companion and farm animals, but he had no history of recent tick bites or travel.

At admission, results of a physical examination were unremarkable, except for a temperature of >40°C. The patient had no rash, skin lesions, lymphadenopathy, or clinically detectable hepatosplenomegaly. Laboratory investigation results were unremarkable (Table). The patient received empiric treatment with ceftriaxone for 5 days, but symptoms did not improve.

Clinicians considered brucellosis because of initial equivocal *Brucella* serologic test results, despite absence of definite exposure history, and began treatment with doxycycline, rifampin, and gentamicin. The patient gradually experienced partial improvement over the next week.

Clinicians performed bone marrow aspirate and trephine to exclude malignancy and investigate possible brucellosis; results showed a reactive inflammatory background. PCR for *Brucella* spp. was negative, and cultures yielded no growth. However, PCR and sequencing of a 598-bp section of the hypervariable 5 to 8 regions of the 16S rRNA gene (*1*), revealed probable *Ehrlichia* species.

Clinicians discontinued rifampin and gentamicin but continued doxycycline for a total of 14 days, and the symptoms completely resolved. The child remained well at follow-up 12 months later. The child's mother gave written informed consent for publication, and approval was granted by the Human Research Ethics Committee of the University of Cape Town (reference no. 551/2022).

We subjected the bone marrow samples to a reverse line blot hybridization assay for simultaneous

Author affiliations: Pathcare, East London, South Africa (C. Bamford); University of Cape Town, Cape Town, South Africa (C. Bamford); National Institute for Communicable Diseases, Johannesburg, South Africa (L.H. Blumberg, J. Frean, C. Sriruttan); University of Pretoria, Onderstepoort, South Africa (L.H. Blumberg, J. Frean, I. Vorster, M.C. Oosthuizen); University of Stellenbosch, Tygerberg, South Africa (L.H. Blumberg, K.G.P. Hoek); Ampath, East London, South Africa (M. Bosman); University of the Witwatersrand, Johannesburg, South Africa (J. Frean); PathCare Reference Laboratory, Cape Town (K.G.P. Hoek); East London, South Africa (J. Miles)

DOI: https://doi.org/10.3201/eid2902.221451

[1]These authors contributed equally to this article.

Table. Laboratory and imaging investigations in a case of neoehrlichiosis in a symptomatic immunocompetent child, South Africa

Investigation	Patient result	Reference value or range
C-reactive protein, mg/L	17.2	<5
Leukocytes, × 10^9 cells/L	15.8	4.5–13.5
Neutrophils, × 10^9 cells/L	10.98	1.50–8.5
Lymphocytes, × 10^9 cells/L	2.99	1.0–6.5
Monocytes, × 10^9 cells/L	1.50	0–0.8
Platelets, × 10^9 cells /L	219	140–420
Hemoglobin, g/dL	12.7	11.5–15.5
Blood cultures	No growth	NA
Urine culture	No growth	NA
Rickettsia conorii/R. africae serology and PCR on blood	Negative	NA
SARS-CoV-2 PCR, nasopharyngeal swab and serology	Negative	NA
Cytomegalovirus PCR and serology	Negative	NA
Epstein-Barr serology	Negative	NA
Widal test	Negative	NA
Mastazyme *Brucella* ELISA	IgM and IgG equivocal	NA
Multiplex PCR for atypical and viral respiratory pathogens*	Negative	NA
QuantiFERON Gold test for tuberculosis†	Negative	NA
Imaging		
Ultrasound of the abdomen	15 cm spleen	10–11 cm at this age
Chest radiograph	No abnormalities detected	NA
Cervical and thoracic spine radiograph	No abnormalities detected	NA
Transthoracic echocardiography	No abnormalities detected	NA
Magnetic resonance imaging spine	No abnormalities detected	NA

*FilmArray RP2.1plus (BioFire Diagnostics, https://www.biofiredx.com).
†QuantiFERON, https://www.quantiferon.com.

detection and differentiation of the most common *Ehrlichia* and *Anaplasma* spp. by using a PCR targeting the 16S rRNA gene (*2*,*3*). PCR product hybridized with the *Ehrlichia/Anaplasma* genus-specific probe but not with any species-specific probes, suggesting a novel species or variant of a known species.

We PCR amplified the near full-length 16S rRNA gene (1,467 bp) using primers fD1 and rP2 (*4*), cloned and sequenced the resultant amplicons. We assembled and edited the generated sequences using the Staden Package (https://staden.sourceforge.net). The consensus sequence was deposited

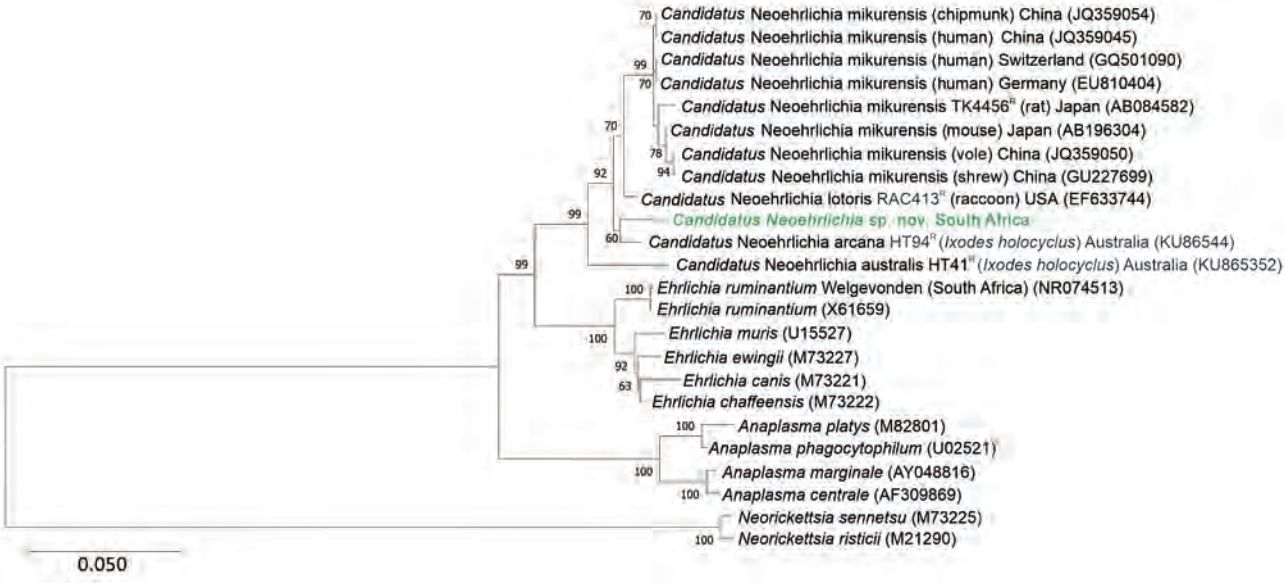

Figure. Phylogenetic tree of *Candidatus* Neoehrlichia species detected in a case of neoehrlichiosis in a symptomatic immunocompetent child, South Africa. We used Kimura 2-parameter plus gamma plus invariable site substitution model in MEGA X (https://www.megasoftware.net) to infer a maximum-likelihood phylogenetic tree in combination with the bootstrap method using 1,000 replicates. Green bold text indicates *Candidatus* Neoehrlichia species detected from the patient in this case-study; we compared this isolate to other Anaplasmataceae species detected from ticks, humans, and mammals available in GenBank (indicated by species name and GenBank accession number; host species and country are given for other *Candidatus* Neoehrlichia species). Scale bar indicates nucleotide substitutions per site.

in Genbank (accession no. OP208838). BLASTn (https://blast.ncbi.nlm.nih.gov) homology search results revealed no identical sequences in the public databases. The most closely related sequences, at 96%–98% identity, were various *Candidatus* Neoehrlichia 16S rDNA sequences, including *Candidatus* N. mikurensis (strain TK4456^{R}), *Candidatus* N. lotoris (strain RAC413^{R}), and *Candidatus* N. arcana (strain HT94^{R}) (Figure).

We aligned the consensus sequence with closely related 16S rDNA sequences from Genbank by using ClustalX (http://www.clustal.org). We manually examined the alignments and truncated to smallest sequence size, a 1,264-bp *Candidatus* N. australis sequence, by using BioEdit 7.2.5 (https://bioedit.software.informer.com). We used MEGA X (https://www.megasoftware.net) to determine Kimura 2-parameter plus gamma plus invariable site substitution as the best-fit model. We used it in combination with the bootstrap method using 1,000 replicates to infer a maximum-likelihood phylogenetic tree, which indicated that our obtained sequence clustered with *Candidatus* N. arcana, although with low bootstrap support (60%) (Figure). The sequence was closely related to, but distinct from, *Candidatus* N. lotoris and *Candidatus* N. mikurensis. As previously shown (*5*,*6*), *Candidatus* Neoehrlichia mikurensis, *Candidatus* N. lotoris, and *Candidatus* N. arcana are distinct from other genera in the Anaplasmataceae family and form a well-supported sister clade to the genus *Ehrlichia*. On the basis of whole-genome sequencing, *Candidatus* N. mikurensis appears to be more closely related to *Ehrlichia chaffeensis* than to *E. ruminantium*, suggesting that establishing the genus *Neoehrlichia* might have been premature (*7*).

We calculated estimated evolutionary divergence by determining the number of nucleotide differences between similar sequences. We removed all ambiguous positions for each sequence pair (pairwise deletion option), which left a total of 1,264 positions in the final dataset. Our obtained sequence differed from GenBank reference strains by 23 bp for *Candidatus* N. lotoris, 24 bp for *Candidatus* N. arcana, and 34 bp for *Candidatus* N. mikurensis. These reference species differ by 46–50 bp from each other. Our findings confirmed that the ehrlichial organism we identified is a member of the family Anaplasmataceae and most closely related to, but distinct from, *Candidatus* N. lotoris and *Candidatus* N. arcana. Until appropriate type-material can be deposited and the species is formally described, we will refer to this novel organism as *Candidatus* Neoehrlichia sp. South Africa (OP208838).

Conclusions

We report a novel ehrlichial organism, most closely related to the genus *Candidatus* Neoehrlichia, a sister genus to *Anaplasma* and *Ehrlichia*, detected in the bone marrow aspirate of an acutely febrile immunocompetent child from South Africa. *Candidatus* N. lotoris has been described from raccoons in Georgia, USA, and an associated tick species (*7*), but it has not been detected in humans or any other wild vertebrate species. *Candidatus* N. arcana has been described from *Ixodes holocyclus* ticks in Australia (*8*), but its pathogenic significance has not yet been determined (*6*). *Candidatus* N. mikurensis was described in 2004 (*5*), and a human case was reported in 2010 (*9*). *Candidatus* N. mikurensis appears to be widely distributed in Europe (*10*), especially in central Europe and Scandinavia, as well as in Asia (*11*). Data from Africa are limited, but *Candidatus* N. mikurensis has been isolated from dog ticks in Nigeria (*12*). The host reservoir of *Candidatus* N. mikurensis is small mammals, and its vectors include *Ixodes* and *Haemaphysalis* tick species (*10*).

Most human neoehrlichia infections described to date have been caused by *Candidatus* N. mikurensis, and clinical findings are usually nonspecific, including fever, headache, and myalgia; however, vasculitis and thrombo-embolic events can occur (*13*). Infections are more commonly recognized in immunocompromised patients; infections in immunocompetent patients can be mild or asymptomatic (*14*).

Another probable clinical neoehrlichia case from Africa was reported in 2013 in a traveler who returned to Denmark from Tanzania (*15*). The researchers described a potentially novel neoehrlichia species isolated from the patient's blood. Based on analysis of short, 300–345-bp fragments, the species was closely related to both *Candidatus* N. lotoris and *Candidatus* N. mikurensis (*15*).

Ehrlichiae and related organisms are usually detected via molecular methods, including PCR of 16S rRNA, or *groEL/groESL* and *gltA* genes. Application of new molecular methods is leading to an explosion in discovery of related novel species or variants, as noted in Australia (*6*) and elsewhere. Recognition of associated human disease is increasing, especially in immunocompetent patients. Further elucidation of the taxonomic status of the novel ehrlichial organism identified in this case study would require whole-genome sequencing or multilocus sequence analysis targeting genes for which *Neoehrlichia* gene sequences are available, including 16S rRNA or *ftsZ*, *gatB*, *groEL*, and *lipA*.

Although tickborne rickettsial infections are common in South Africa, Anaplasmataceae infections

likely are undiagnosed because of lack of awareness among clinicians and unavailability of laboratory tests. Of note, *Ehrlichia* spp. are not susceptible to macrolides and our case would not have been recognized if the patient had initially been treated with doxycycline.

In conclusion, our case represents an expansion of the known range of neoehrlichiosis. Clinicians should be aware of neoehrlichia as a possible tickborne cause of acute febrile illness in Africa.

Acknowledgments

We thank Emma Hooijberg for reviewing some of the microscopic images of the bone marrow aspirate preparation.

About the Author

Dr. Bamford is a clinical microbiologist with Pathcare and the University of Cape Town, East London, South Africa. Her primary research interests include antimicrobial resistance and stewardship as well as the appropriate use of laboratory diagnostic tests.

References

1. Xu J, Smyth CL, Buchanan JA, Dolan A, Rooney PJ, Millar BC, et al. Employment of 16 S rDNA gene sequencing techniques to identify culturable environmental eubacteria in a tertiary referral hospital. J Hosp Infect. 2004;57:52–8. https://doi.org/10.1016/j.jhin.2004.01.011
2. Bekker CP, de Vos S, Taoufik A, Sparagano OA, Jongejan F. Simultaneous detection of *Anaplasma* and *Ehrlichia* species in ruminants and detection of *Ehrlichia ruminantium* in *Amblyomma variegatum* ticks by reverse line blot hybridization. Vet Microbiol. 2002;89:223–38. https://doi.org/10.1016/S0378-1135(02)00179-7
3. Schouls LM, Van De Pol I, Rijpkema SG, Schot CS. Detection and identification of *Ehrlichia, Borrelia burgdorferi* sensu lato, and *Bartonella* species in Dutch *Ixodes ricinus* ticks. J Clin Microbiol. 1999;37:2215–22. https://doi.org/10.1128/JCM.37.7.2215-2222.1999
4. Weisburg WG, Barns SM, Pelletier DA, Lane DJ. 16S ribosomal DNA amplification for phylogenetic study. J Bacteriol. 1991;173:697–703. https://doi.org/10.1128/jb.173.2.697-703.1991
5. Kawahara M, Rikihisa Y, Isogai E, Takahashi M, Misumi H, Suto C, et al. Ultrastructure and phylogenetic analysis of '*Candidatus* Neoehrlichia mikurensis' in the family Anaplasmataceae, isolated from wild rats and found in *Ixodes ovatus* ticks. Int J Syst Evol Microbiol. 2004;54:1837–43. https://doi.org/10.1099/ijs.0.63260-0
6. Gofton AW, Doggett S, Ratchford A, Ryan U, Irwin P. Phylogenetic characterisation of two novel Anaplasmataceae from Australian *Ixodes holocyclus* ticks: '*Candidatus* Neoehrlichia australis' and '*Candidatus* Neoehrlichia arcana'. Int J Syst Evol Microbiol. 2016;66:4256–61. https://doi.org/10.1099/ijsem.0.001344
7. Grankvist A, Jaén-Luchoro D, Wass L, Sikora P, Wennerås C. Comparative genomics of clinical isolates of the emerging tick-borne pathogen *Neoehrlichia mikurensis*. Microorganisms. 2021;9:1488. https://doi.org/10.3390/microorganisms9071488
8. Gofton AW, Doggett S, Ratchford A, Oskam CL, Paparini A, Ryan U, et al. Bacterial profiling reveals novel "*Ca.* Neoehrlichia", *Ehrlichia*, and *Anaplasma* species in Australian human-biting ticks. PLoS One. 2015;10:e0145449. https://doi.org/10.1371/journal.pone.0145449
9. Welinder-Olsson C, Kjellin E, Vaht K, Jacobsson S, Wennerås C. First case of human "*Candidatus* Neoehrlichia mikurensis" infection in a febrile patient with chronic lymphocytic leukemia. J Clin Microbiol. 2010;48:1956–9. https://doi.org/10.1128/JCM.02423-09
10. Portillo A, Santibáñez P, Palomar AM, Santibáñez S, Oteo JA. '*Candidatus* Neoehrlichia mikurensis' in Europe. New Microbes New Infect. 2018;22:30–6. https://doi.org/10.1016/j.nmni.2017.12.011
11. Jha P, Kim CM, Kim DM, Yoon NR, Jha B, Park JW, et al. First detection and identification of *Candidatus* Neoehrlichia mikurensis in South Korea. PLoS One. 2018;13:e0209685. https://doi.org/10.1371/journal.pone.0209685
12. Kamani J, Baneth G, Mumcuoglu KY, Waziri NE, Eyal O, Guthmann Y, et al. Molecular detection and characterization of tick-borne pathogens in dogs and ticks from Nigeria. PLoS Negl Trop Dis. 2013;7:e2108. https://doi.org/10.1371/journal.pntd.0002108
13. Höper L, Skoog E, Stenson M, Grankvist A, Wass L, Olsen B, et al. Vasculitis due to *Candidatus* Neoehrlichia mikurensis: a cohort study of 40 Swedish patients. Clin Infect Dis. 2021;73:e2372–8. https://doi.org/10.1093/cid/ciaa1217
14. Welc-Falęciak R, Siński E, Kowalec M, Zajkowska J, Pancewicz SA. Asymptomatic "*Candidatus* Neoehrlichia mikurensis" infections in immunocompetent humans. J Clin Microbiol. 2014;52:3072–4. https://doi.org/10.1128/JCM.00741-14
15. Schwameis M, Auer J, Mitteregger D, Simonitsch-Klupp I, Ramharter M, Burgmann H, et al. Anaplasmataceae-specific PCR for diagnosis and therapeutic guidance for symptomatic neoehrlichiosis in immunocompetent host. Emerg Infect Dis. 2016;22:281–4. https://doi.org/10.3201/eid2202.141762

Address for correspondence: Colleen Bamford, Pathcare Business Centre, Private Bag X107, N1 City, 7463, South Africa; email: colleen.bamford@pathcare.org

Successful Drug-Mediated Host Clearance of *Batrachochytrium salamandrivorans*

Amadeus Plewnia, Stefan Lötters, Michael Veith, Martin Peters, Philipp Böning

Skin fungi are among the most dangerous drivers of global amphibian declines, and few mitigation strategies are known. For *Batrachochytrium salamandrivorans* (Chytridiomycota), available treatments rely on temperature, partially combined with antifungal drugs. We report the clearance of *B. salamandrivorans* in 2 urodelan species using a solely drug-based approach.

Various emerging infectious diseases have been invoked in global amphibian declines and extinctions, bringing the class Amphibia as a whole to the brink of extinction (*1*). The skin-invading chytrid fungi *Batrachochytrium dendrobatidis* and *B. salamandrivorans*, both originating from Asia, are among the most noteworthy pathogens in the amphibian crisis (*1*–*3*). The few strategies that have proven to be effective in mitigating those fungi usually involve ex situ conservation breeding, which requires successful treatment protocols. Several treatments against *B. dendrobatidis* exist (*4*), based either on the pathogen's susceptibility to high temperatures or antifungal drugs. However, antifungal drugs have been considered ineffective in mitigating the effects of *B. salamandrivorans* on its salamander hosts. Therefore, temperature-based strategies (*5*) or combinations of drug-based and temperature-based approaches seem to be the only treatment protocols for clearing *B. salamandrivorans* (*6*). Because many salamanders from temperate zones prefer low temperatures, successful treatment might be impeded by their upper thermal limit in some taxa (*7*). Moreover, those protocols require laboratory settings, which some ex situ facilities and private keepers might not have available. In addition, heat treatments are not always successful and can require repeated and prolonged application (*8*). Therefore, drug-mediated treatments can be critical in certain hosts. Furthermore, drug-based treatment protocols have been applied as viable mitigation strategies in wild amphibian populations (*9*,*10*).

We report the successful clearance of *B. salamandrivorans* in 2 salamander species by using the antifungal drug itraconazole, commonly used in amphibian medicine (*4*,*11*,*12*). However, we stress that the potential application of our protocol requires further testing with a robust experimental setting far beyond this case.

The Study

In early 2022, we collected 7 specimens (6 fire salamanders [*Salamandra salamandra*], specimens FS1–FS6; and 1 Alpine newt [*Ichthyosaura alpestris*], specimen AN, in terrestrial phase) demonstrating clinical symptoms of *B. salamandrivorans*–induced chytridiomycosis (circular skin lesions) at a formerly unknown outbreak site in Densborn, Eifel Mountains, Germany. Specimens were transported under strict biosecurity standards to the facilities of Trier University for subsequent *B. salamandrivorans* testing and treatment. We confirmed the presence of *B. salamandrivorans* through skin swab specimens and subsequent DNA extraction using the QIAGEN Blood and Tissue kit (QIAGEN, https://www.qiagen.com) and quantitative PCR on a StepOnePlus (ThermoFisher Scientific, https://www.thermofisher.com) following previously described protocols (*8*,*13*). Individual infection loads are expressed as DNA copies (internal transcribed spacer 1 region). We ran all samples in duplicate and set the limit of detection to 100 DNA copies (*8*). Because controlled thermal treatment could not be performed, we applied an adaptation of a previously described protocol (*4*), which has proven to be effective against *B. dendrobatidis* at our facilities. We bathed specimens in a 0.01% solution of itraconazole (Sempera Liquid 10mg/mL diluted in distilled water 1:100 to a final

Author affiliations: Trier University, Trier, Germany (A. Plewnia, S. Lötters, M. Veith, P. Böning); Chemisches und Veterinäruntersuchungsamt Westfalen, Arnsberg, Germany (M. Peters)

DOI: https://doi.org/10.3201/eid2902.221162

concentration of 100 µg/mL) for 10 minutes daily for ≥11 consecutive days. Individual treatment ended when the specimen tested negative. During treatment, specimens were housed individually in 20 cm × 35 cm plastic containers on moist paper towels in a climate chamber at a constant temperature of 15°C and 80% humidity; they were transferred daily after treatment to containers disinfected with Virkon S at 5g/L (https://virkon.us) and thoroughly rinsed. Animals were handled with nitrile gloves and fed crickets ad libitum. We collected skin swab specimens daily before bathing and on individual schemes for ≥8 weeks after treatment to check for reinfection with or regrowth of *B. salamandrivorans* (Appendix Table, https://wwwnc.cdc.gov/EID/article/29/2/22-1162-App1.pdf).

In total, 4 specimens (AN, FS2, FS5, and FS6) demonstrated initial infection loads of 10,000–1 million DNA copies; 1 (FS4) had loads of >1 million and 2 (FS1, FS3) had loads of <100,000 (Figure 1; Appendix Table). After an initial decrease in infection loads, FS4 died on treatment day 6. We preserved FS4 in 4% buffered formalin and conducted a complete necropsy and histologic examination of skin and internal organs with regard to potential effects of treatment and severity of *B. salamandrivorans* infection and to exclude comorbidities (Appendix). In all other specimens except FS6, the infection load decreased over time. In FS6, the number of DNA copies increased over 4 days (23,972 DNA copies) and decreased thereafter (Figure 1; Appendix Table). However, we did not observe any visible progression of clinical symptoms (i.e., skin lesions) (Figure 2). After day 11, all animals except FS2 tested negative through the end of the treatment; FS2 only tested negative on day 23 (Figure 1; Appendix Table). In FS2, the infection load varied throughout treatment, ranging from 0 to 1,411,911 DNA copies (Figure 1; Appendix Table). Infection loads remained high for the first 9 days of treatment in this specimen but then steadily decreased. Initial infection loads and severe macroscopic lesions in FS2 resembled those reported in dying salamanders (*8*), suggesting an advanced stage of infection (Figure 1; Appendix Table). We observed intense skin shedding and complete healing of skin lesions throughout treatment in all specimens (Figure 2). Histopathologic examination of FS4 revealed multifocal extensive necrotic and ulcerative lesions with

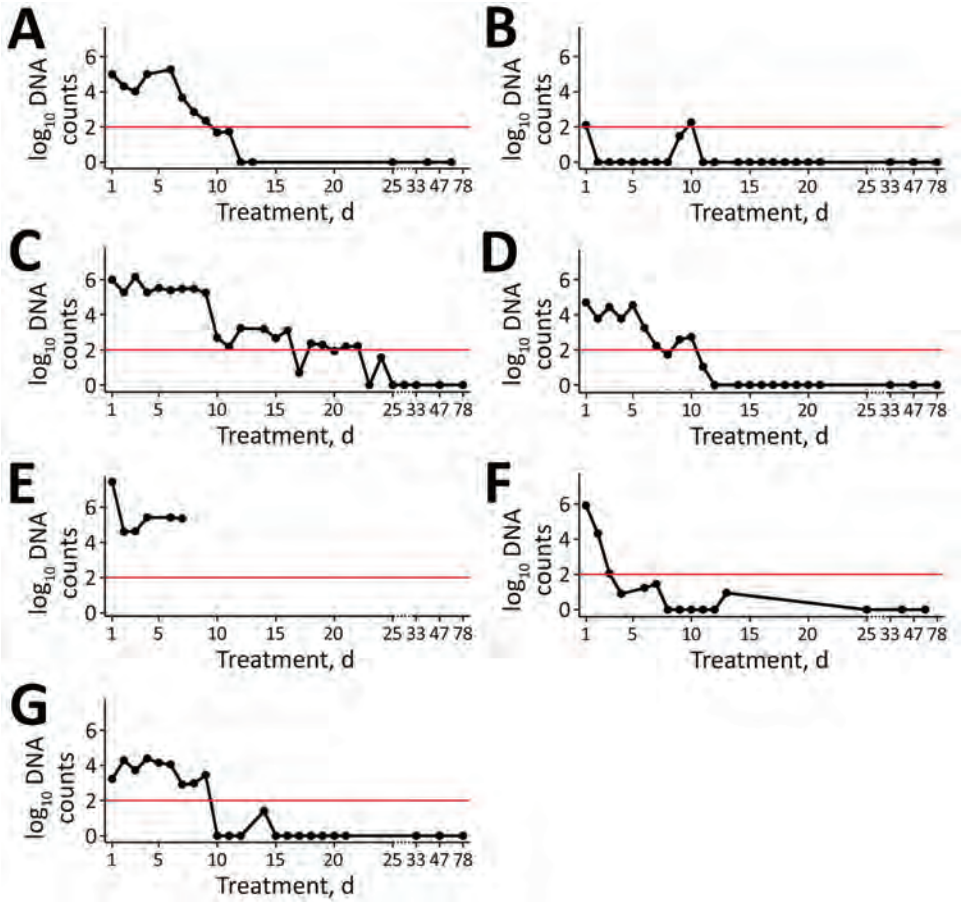

Figure 1. Infection loads of *Batrachochytrium salamandrivorans* in 2 urodelan species during treatment with the antifungal drug itraconazole over time. $\log_{10}$ DNA counts indicate logarithmic scale for the amount of copies of the rRNA internal spacer 1. A) Alpine newt (*Ichthyosaura alpestris*) specimen; B–G) fire salamander (*Salamandra salamandra*): B) specimen FS1; C) specimen FS2; D) specimen FS3; E) specimen FS4; F) specimen FS5; G) specimen FS6. Red line indicates limit of detection.

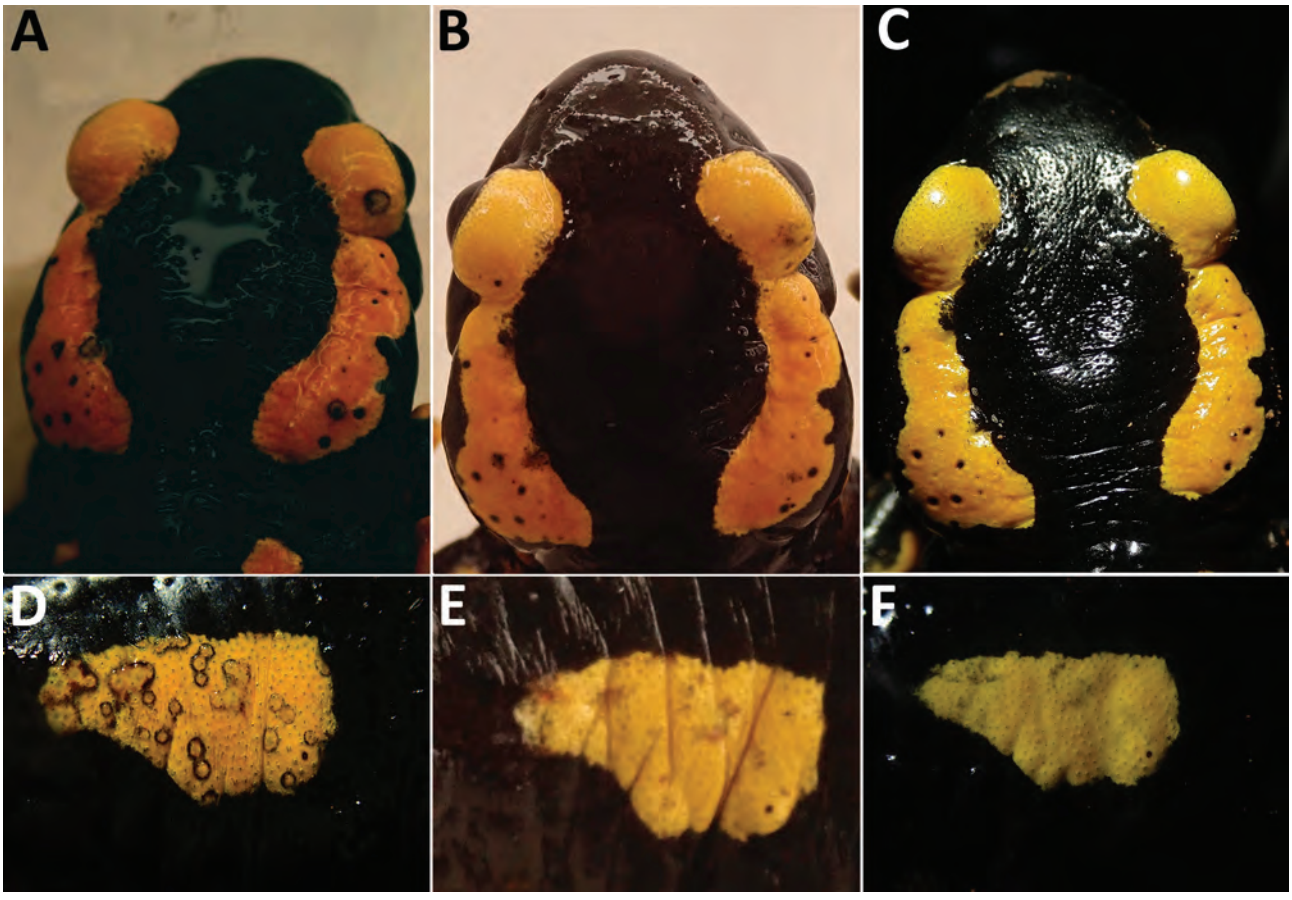

Figure 2. Clearing of skin lesions during the treatment of *Batrachochytrium salamandrivorans* in 2 fire salamanders (*Salamandra salamandra*) specimens, FS6 (A–C) and FS2 (D–F), on day 1 (A, D), day 16 (B, E) and day 87 (C, F).

intralesional chytrid thalli (Appendix Figure, panel A). Furthermore, we identified multifocal secondary epidermal invasion with other unidentified fungal hyphae and bacteria (Appendix Figure, panels B, C). Neither in the epidermis nor the liver (Appendix Figure, panel D) or other organs (not shown) were lesions present that clearly indicate toxic effects of the treatment.

Conclusions

Blooi et al. (*5*) demonstrated a lower MIC of itraconazole for *B. salamandrivorans* than for *B. dendrobatidis*. However, they were unsuccessful in clearing *B. salamandrivorans* infections with itraconazole. Their protocol differed from ours in concentration (0.6 μg/mL), mode of application (spraying), duration (application 2×/d for 10 d) and husbandry conditions (no daily transfer to disinfected cages). Itraconazole has also been used for in situ mitigation of *B. dendrobatidis*, which increased population survival in the midterm (*9*,*10*,*12*). The exceptionally high levels of DNA copies we detected in some specimens along with severe skin lesions during the first days of treatment demonstrate that itraconazole is capable of effectively clearing even high infection loads of chytridiomycosis caused by *B. salamandrivorans* in *S. salamandra* salamanders (*2*, *8*) (Figures 1, 2). The high variation in infection intensity over consecutive days might be because of excessive skin shedding, a common response of amphibians to chytrid fungi (*14*). Moreover, we cannot rule out the possibility that handling specimens with nitrile gloves affected our results, because their runoff impairs the viability of *B. salamandrivorans* zoospores (*15*). However, whether nitrile glove runoff contributes to *B. salamandrivorans* clearance on live specimens is unknown. Furthermore, our applied husbandry conditions could have positively affected the rapid clearance of the salamander fungus. In other studies (*4*–*6*,*8*), only moist tissues were changed, possibly leaving zoospores in the enclosure that could promote reinfection. During and after treatment, we observed no negative side effects such as those discussed in other studies using itraconazole in amphibians (*4*,*11*). The death of specimen FS4 was most likely

caused by the severity of multifocal necroulcerative skin lesions with intralesional *B. salamandrivorans* and secondary fungal and bacterial infection and not as a direct result of itraconazole toxicity (Appendix Figure, panels A–C). The successful healing of multiple and severe skin lesions in the other specimens is consistent with the findings and observations of Schulz et al. (*8*), suggesting itraconazole could be an effective future addition to currently available treatments. However, our treatment primarily intended on-hand curation of infected urodelans and therefore lacks a thorough experimental design, such as negative and positive controls. Therefore, this study must be seen as a case report, strictly requiring additional investigation before applying our protocol as a regular treatment option. Nevertheless, our preliminary findings contribute to mitigating the salamander plague and promote future studies with more robust experimental settings and in other species.

Acknowledgments

We thank Sabine Naber and Karin Fischer for support in the laboratory.

Permits were granted by the Struktur- und Genehmigungsdirektion Nord Rheinland-Pfalz (permit no. 425-104-778-0007/2022).

About the Author

Mr. Plewnia is a MSc student in the department of biogeography, Trier University. His research interests focus on disease-mediated amphibian declines, as well as on biogeography, ecology, and evolution of Neotropical herpetofauna.

References

1. Martel A, Blooi M, Adriaensen C, Van Rooij P, Beukema W, Fisher MC, et al. Wildlife disease. Recent introduction of a chytrid fungus endangers Western Palearctic salamanders. Science. 2014;346:630–1. https://doi.org/10.1126/science.1258268
2. Scheele BC, Pasmans F, Skerratt LF, Berger L, Martel A, Beukema W, et al. Amphibian fungal panzootic causes catastrophic and ongoing loss of biodiversity. Science. 2019;363:1459–63. https://doi.org/10.1126/science.aav0379
3. Stegen G, Pasmans F, Schmidt BR, Rouffaer LO, Van Praet S, Schaub M, et al. Drivers of salamander extirpation mediated by *Batrachochytrium salamandrivorans*. Nature. 2017;544:353–6. https://doi.org/10.1038/nature22059
4. Brannelly LA, Richards-Zawacki CL, Pessier AP. Clinical trials with itraconazole as a treatment for chytrid fungal infections in amphibians. Dis Aquat Organ. 2012;101:95–104. https://doi.org/10.3354/dao02521
5. Blooi M, Martel A, Haesebrouck F, Vercammen F, Bonte D, Pasmans F. Treatment of urodelans based on temperature dependent infection dynamics of *Batrachochytrium salamandrivorans*. Sci Rep. 2015;5:8037. https://doi.org/10.1038/srep08037
6. Blooi M, Pasmans F, Rouffaer L, Haesebrouck F, Vercammen F, Martel A. Successful treatment of *Batrachochytrium salamandrivorans* infections in salamanders requires synergy between voriconazole, polymyxin E and temperature. Sci Rep. 2015;5:11788. https://doi.org/10.1038/srep11788
7. Li Z, Martel A, Bogaerts S, Göçmen B, Pafilis P, Lymberakis P, et al. Landscape connectivity limits the predicted impact of fungal pathogen invasion. J Fungi (Basel). 2020;6:205. https://doi.org/10.3390/jof6040205
8. Schulz V, Schulz A, Klamke M, Preissler K, Sabino-Pinto J, Müsken M, et al. *Batrachochytrium salamandrivorans* in the Ruhr District, Germany: history, distribution, decline dynamics and disease symptoms of the salamander plague. Salamandra (Frankf). 2020;56:189–214.
9. Bosch J, Sanchez-Tomé E, Fernández-Loras A, Oliver JA, Fisher MC, Garner TW. Successful elimination of a lethal wildlife infectious disease in nature. Biol Lett. 2015;11:20150874. https://doi.org/10.1098/rsbl.2015.0874
10. Cook K, Pope K, Cummings A, Piovia-Scott J. *In situ* treatment of juvenile frogs for disease can reverse population declines. Conserv Sci Pract. 2022;4:e12762. https://doi.org/10.1111/csp2.12762
11. Woodhams DC, Geiger CC, Reinert LK, Rollins-Smith LA, Lam B, Harris RN, et al. Treatment of amphibians infected with chytrid fungus: learning from failed trials with itraconazole, antimicrobial peptides, bacteria, and heat therapy. Dis Aquat Organ. 2012;98:11–25. https://doi.org/10.3354/dao02429
12. Knapp RA, Joseph MB, Smith TC, Hegeman EE, Vredenburg VT, Erdman JE Jr, et al. Effectiveness of antifungal treatments during chytridiomycosis epizootics in populations of an endangered frog. PeerJ. 2022;10:e12712. https://doi.org/10.7717/peerj.12712
13. Standish I, Leis E, Schmitz N, Credico J, Erickson S, Bailey J, et al. Optimizing, validating, and field testing a multiplex qPCR for the detection of amphibian pathogens. Dis Aquat Organ. 2018;129:1–13. https://doi.org/10.3354/dao03230
14. Ohmer MEB, Cramp RLC, White CR, Franklin CE. Skin sloughing rate increases with chytrid fungus infection load in a susceptible amphibian. Funct Ecol. 2015;29:674–82. https://doi.org/10.1111/1365-2435.12370
15. Thomas V, Van Rooij P, Meerpoel C, Stegen G, Wauters J, Vanhaecke L, et al. Instant killing of pathogenic chytrid fungi by disposable nitrile gloves prevents disease transmission between amphibians. PLoS One. 2020;15:e0241048. https://doi.org/10.1371/journal.pone.0241048

Address for correspondence: Philipp Böning, Trier University, Biogeography Department, Universitätsring 15, 54296 Trier, Germany; email: boening@uni-trier.de

Powassan Virus Lineage I in Field-Collected *Dermacentor variabilis* Ticks, New York, USA

Charles Hart,[1] Erin Hassett,[1] Chantal B.F. Vogels, Daniel Shapley, Nathan D. Grubaugh, Saravanan Thangamani

Powassan virus is a tickborne flavivirus that can cause lethal or debilitating neurologic illness. It is canonically transmitted by *Ixodes* spp. ticks but might spill over to sympatric *Dermacentor* species. We detected Powassan virus lineage I from a pool of field-collected *D. variabilis* ticks in New York, USA.

Powassan virus (POWV) is a neurotropic, tickborne flavivirus first identified as a human pathogen in 1958, when it was isolated from the brain of a patient who had died of encephalitis (*1*). POWV infection results in febrile illness that can progress to encephalitis, meningitis, and, rarely, meningoencephalitis (*2*), which is associated with head pain, confusion, paralysis, coma, and death in up to 15% of cases. In addition, >50% of survivors experience long-term neurosequelae, including motor deficiency and cognitive deficits (*3*).

POWV was initially associated with the woodchuck tick, *Ixodes cookei* (*4*), although a second lineage was discovered in deer ticks (*I. scapularis*) (*5*). That genotype was termed POWV lineage II, or deer tick virus (DTV). Because of the frequency with which *I. scapularis* tick bites occur in humans compared to *I. cookei* tick bites, DTV is likely the most common etiologic source of Powassan encephalitis in the United States. However, the source is difficult to discern because of serologic homology between the virus lineages and the lack of viral genotyping in most clinical settings.

Recently, interest has grown in the vector competency of other sympatric tick species. *Dermacentor* spp. ticks have been of particular interest because of their common occurrence in POWV- and DTV-endemic areas and because of their tendency to bite humans. POWV has been isolated from *D. andersoni* ticks in Colorado, USA (*6*); genetic analysis suggests that strain, called POWV 791A-52, is most likely a form of DTV (*7*). However, it remains unclear whether the tick in question was infected by spillover from another sylvatic cycle featuring *Ixodes* ticks or constitutes its own sylvatic system. Neither *I. scapularis* nor *I. cookei* ticks are native to Colorado, although several rodent-specific *Ixodes* species are present (*8*) that might be involved in such a system.

The competency of *D. andersoni* ticks for POWV has been confirmed under laboratory conditions when fed from artificially inoculated nonnative species (*9*). Recent analysis has also indicated that *D. variabilis* ticks are capable of acquiring and transmitting DTV under laboratory conditions, including maintaining replicating virus transstadially (*10*). Although that capability has been confirmed in experimentally infected ticks, it remains unclear whether wild populations of *D. variabilis* ticks can maintain and transmit POWV or DTV under natural circumstances. Considering that *D. variabilis* ticks are the second most common human-biting species in New York, USA, (*11*), the ability for the species to transmit POWV in nature represents a critical component of potential human exposure. We detected POWV lineage I from *D. variabilis* ticks collected in New York in 2021.

The Study

As a part of ongoing efforts to track the emergence of POWV in New York, we performed tick surveillance in areas known to contain circulating POWV as identified from a community-engaged tick testing program

Author affiliations: Upstate Medical University, Syracuse, New York, USA (C. Hart, E. Hassett, S. Thangamani); Yale School of Public Health, New Haven, Connecticut, USA (C.B.F. Vogels, N.D. Grubaugh); Upstate Tick Testing Program, Syracuse (D. Shapley); Yale University, New Haven (N.D. Grubaugh)

DOI: https://doi.org/10.3201/eid2902.220410

[1]These first authors contributed equally to this article.

(*11*). From 1 area of interest in Dutchess County, New York, we collected 5 female and 3 male *D. variabilis* ticks, in addition to 68 *I. scapularis* ticks, in the second half of April 2021. We visually speciated the ticks and assessed them for feeding status. The female *D. variabilis* ticks were unfed; we pooled, homogenized, and tested them for POWV by quantitative reverse transcription PCR as described (*11*). In brief, we initially detected POWV with a primer sensitive to both POWV lineage I and DTV. Then, we used a differentiation quantitative reverse transcription PCR to confirm POWV lineage I with a titer of 3.88 $\log_{10}$ FFU/µg RNA. In contrast, none of the *I. scapularis* ticks collected from the same site tested positive for POWV lineage I and DTV.

We used our highly multiplexed PCR amplicon approach to sequence POWV detected from the tick homogenate (*12*). We prepared libraries with the Illumina COVIDSeq Test (RUO version; Illumina, https://www.illumina.com), replacing the SARS-CoV-2 primers with POWV (*13*), and sequenced on the Illumina NovaSeq at the Yale Center for Genome Analysis (New Haven, CT, USA). Consensus genomes were generated at a minimum nucleotide frequency threshold of 0.75 and minimum depth of 10 reads using iVar version 1.3.1 (https://github.com/andersen-lab/ivar).

We reconstructed a maximum-likelihood phylogenetic tree of 29 aligned POWV genomes trimmed to the coding sequence (genome positions 108–10,352) (Figure) using IQ-TREE version 1.6.12 (http://www.iqtree.org) with ultrafast bootstrap approximation (1,000 replicates) (*14*). Our phylogenetic analysis revealed that the virus (deposited in GenBank under accession no. OM681505) belongs to the POWV lineage I clade and is closely related to a POWV lineage I virus that we sequenced from *I. cookei* ticks (GenBank accession no. OM681504) from New York in 2020 (Figure). In addition, we used Sanger sequencing of tick ribosomal RNA to confirm that the sample was derived from *D. variabilis* ticks and not another potential vector species. The resulting sequence (GenBank accession no. ON922563) had 100% homology to *D. variabilis* large subunit ribosomal RNA (GenBank accession no. L34300.1).

Our results confirm POWV in *D. variabilis* ticks in southern New York, suggesting that POWV can exist in this tick species, either because of incidental exposure or because of its own sylvatic cycle. In this study, the POWV we identified groups with lineage I; this

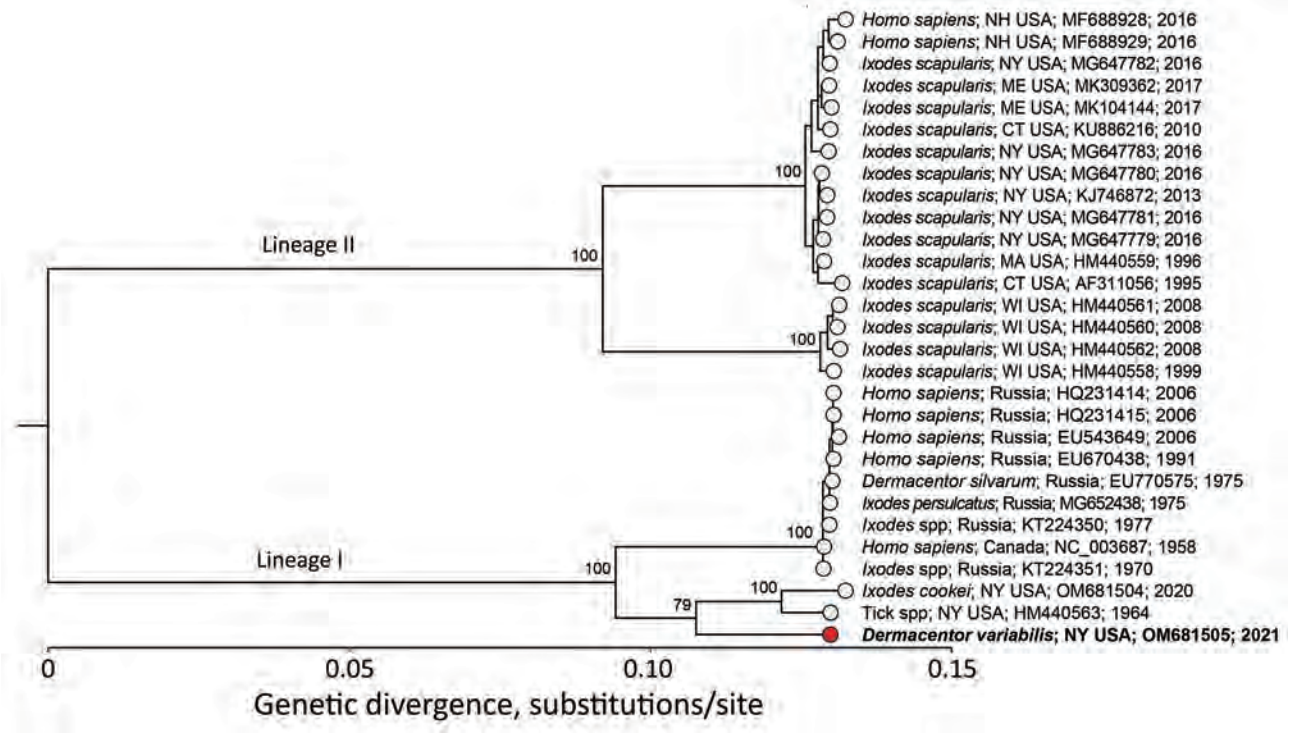

Figure. Maximum-likelihood phylogenetic tree of Powassan virus lineage I and II from *Dermacentor variabilis* ticks collected in New York, USA, and reference sequences. Phylogenetic analysis of the coding sequence (genome positions 108–10,352) of 29 publicly available Powassan lineage I and II genomes. Red circle and bold text indicate the virus sequenced in this study from the *D. variabilis* ticks; the virus is most closely related to other lineage I sequences from ticks in New York. Sequence names consist of host; location; GenBank accession number; year.

lineage is normally associated with *I. cookei* ticks and woodchucks (*Marmota monax*), instead of with *I. scapularis* ticks and *Peromyscus leucopus* mice (*15*). This link suggests either spillover from that sylvatic cycle, a unique *D. variabilis* species-dependent sylvatic cycle for POWV lineage I, or a unique subtype of the virus specific to *D. variabilis* ticks with an unknown sylvatic cycle. Regardless of its source, our data indicate that some *D. variabilis* ticks in POWV-endemic areas could be capable of acquiring a genotype of POWV similar to lineage I.

Conclusions

POWV is a medically noteworthy flavivirus understood to be primarily transmitted by *Ixodes* spp. ticks in North America. The sympatric tick species *D. variabilis*, however, has been recently demonstrated to be a competent vector for POWV under laboratory conditions (*10*). We report the detection of POWV lineage I in *D. variabilis* ticks collected from the wild, suggesting that the species might play a direct role in POWV transmission in nature. The ability of POWV to infect humans and the nature of the disease it causes remain unclear, and further research is needed to understand the role of *D. variabilis* ticks in the ecology of POWV. However, considering that *D. variabilis* ticks are a primary species of human-biting ticks in New York, this finding demonstrates a new potential source of human exposure to POWV.

The study described in this manuscript was funded by Departmental Start-up funds, Upstate Foundation (Fund ID: 23709) and SUNY Empire Innovation Professorship funds to S.T. The funders had no role in study design, data collection and analysis, decision to publish, or preparation of the manuscript.

About the Author

Dr. Hart is a postdoctoral researcher at Upstate Medical University in Syracuse, New York, USA. His primary research focus is on the interaction between vector-borne pathogens, arthropod vectors, and vector-host interactions.

References

1. McLean DM, Donohue WL. Powassan virus: isolation of virus from a fatal case of encephalitis. Can Med Assoc J. 1959;80:708–11.
2. Gholam BI, Puksa S, Provias JP. Powassan encephalitis: a case report with neuropathology and literature review. CMAJ. 1999;161:1419–22.
3. Ebel GD. Update on Powassan virus: emergence of a North American tick-borne flavivirus. Annu Rev Entomol. 2010;55:95–110. https://doi.org/10.1146/annurev-ento-112408-085446
4. McLean DM, Best JM, Mahalingam S, Chernesky MA, Wilson WE. Powassan virus: summer infection cycle, 1964. Can Med Assoc J. 1964;91:1360–2.
5. Telford SR III, Armstrong PM, Katavolos P, Foppa I, Garcia AS, Wilson ML, et al. A new tick-borne encephalitis-like virus infecting New England deer ticks, *Ixodes dammini*. Emerg Infect Dis. 1997;3:165–70. https://doi.org/10.3201/eid0302.970209
6. Thomas LA, Kennedy RC, Eklund CM. Isolation of a virus closely related to Powassan virus from *Dermacentor andersoni* collected along North Cache la Poudre River, Colo. Proc Soc Exp Biol Med. 1960;104:355–9. https://doi.org/10.3181/00379727-104-25836
7. Robich RM, Cosenza DS, Elias SP, Henderson EF, Lubelczyk CB, Welch M, et al. Prevalence and genetic characterization of deer tick virus (Powassan virus, lineage II) in *Ixodes scapularis* ticks collected in Maine. Am J Trop Med Hyg. 2019;101:467–71. https://doi.org/10.4269/ajtmh.19-0281
8. Hutcheson HJ, Mertins JW, Kondratieff BC, White MM. Ticks and tick-borne diseases of Colorado, including new state records for *Argas radiatus* (Ixodida: Argasidae) and *Ixodes brunneus* (Ixodida: Ixodidae). J Med Entomol. 2021;58:505–17. https://doi.org/10.1093/jme/tjaa232
9. Chernesky MA. Powassan virus transmission by ixodid ticks infected after feeding on viremic rabbits injected intravenously. Can J Microbiol. 1969;15:521–6. https://doi.org/10.1139/m69-090
10. Sharma R, Cozens DW, Armstrong PM, Brackney DE. Vector competence of human-biting ticks *Ixodes scapularis*, *Amblyomma americanum*, and *Dermacentor variabilis* for Powassan virus. Parasit Vectors. 2021;14:466. https://doi.org/10.1186/s13071-021-04974-1
11. Hart CE, Bhaskar JR, Reynolds E, Hermance M, Earl M, Mahoney M, et al. Community engaged tick surveillance and *tick*MAP as a public health tool to track the emergence of ticks and tick-borne diseases in New York. PLOS Glob Public Health. 2022;2:e0000215. https://doi.org/10.1371/journal.pgph.0000215
12. Grubaugh ND, Gangavarapu K, Quick J, Matteson NL, De Jesus JG, Main BJ, et al. An amplicon-based sequencing framework for accurately measuring intrahost virus diversity using PrimalSeq and iVar. Genome Biol. 2019;20:8. https://doi.org/10.1186/s13059-018-1618-7
13. Vogels CBF, Brito A, Grubaugh ND. powassan-genomics. 2022 July [cited 2022 Jun 06] https://github.com/grubaughlab/powassan-genomics
14. Nguyen LT, Schmidt HA, von Haeseler A, Minh BQ. IQ-TREE: a fast and effective stochastic algorithm for estimating maximum-likelihood phylogenies. Mol Biol Evol. 2015;32:268–74. https://doi.org/10.1093/molbev/msu300
15. Pesko KN, Torres-Perez F, Hjelle BL, Ebel GD. Molecular epidemiology of Powassan virus in North America. J Gen Virol. 2010;91:2698–705. https://doi.org/10.1099/vir.0.024232-0

Address for correspondence: Saravanan Thangamani, Upstate Medical University, 505 Irving Ave, Syracuse NY 13210, USA; email: thangams@upstate.edu

Bartonella spp. and Typhus Group Rickettsiae among Persons Experiencing Homelessness, São Paulo, Brazil

Álvaro A. Faccini-Martínez, Louise Bach Kmetiuk, Lucas S. Blanton, Laís Giuliane Felipetto, Mara Lúcia Gravinatti, Jorge Timenetsky, Luiz Ricardo Gonçalves, Rosangela Zacarias Machado, Marcos Rogério André, Fabiano Borges Figueiredo, Andrea Pires dos Santos, Marcelo B. Labruna, Gustavo Monti, Alexander Welker Biondo, David H. Walker

Persons experiencing homelessness in São Paulo, Brazil, were seropositive for *Bartonella* spp. (79/109, 72.5%) and typhus group rickettsiae (40/109, 36.7%). *Bartonella quintana* DNA was detected in 17.1% (14/82) body louse pools and 0.9% (1/114) blood samples. Clinicians should consider vectorborne agents as potential causes of febrile syndromes in this population.

Persons experiencing homelessness might be predisposed to vectorborne infections because of increased exposure to ectoparasites (*1*). Members of the genera *Bartonella* and *Rickettsia*, particularly the louseborne pathogens *B. quintana* and *R. prowazekii*, are agents of emerging illnesses among persons who are marginalized or experiencing homelessness (*1*). Studies on *Bartonella* and *Rickettsia* spp. infections in homeless populations within Latin America are scarce (*2*,*3*). Infestations with *Pediculus humanus humanus* body lice were reported in persons experiencing homelessness in Curitiba and São Paulo, 2 major cities in Brazil (*4*). We report results of molecular testing of lice and blood from persons experiencing homelessness in the city of São Paulo in southeastern Brazil. We evaluated their possible exposure to *Bartonella* spp. and typhus group rickettsiae (TGR) by using indirect immunofluorescence assays (IFAs). In addition, we assessed risk factors related to serologic status.

Author affiliations: Fundación Universitaria de Ciencias de la Salud, Servicios y Asesorías en Infectología, Hospital Militar Central, Bogotá, Colombia (Á.A. Faccini-Martínez); University of Texas Medical Branch, Galveston, Texas, USA (Á.A. Faccini-Martínez, L.S. Blanton, D.H. Walker); Oswaldo Cruz Foundation, Curitiba, Brazil (L.B. Kmetiuk, F.B. Figueiredo); Federal University of Paraná, Curitiba (L.G. Felipetto, A.W. Biondo); Central Paulista University Center, São Carlos, Brazil (M.L. Gravinatti); University of São Paulo, São Paulo, Brazil (M.L. Gravinatti, J. Timenetsky, M.B. Labruna); São Paulo State University, Jaboticabal, Brazil (L.R. Gonçalves, R Z. Machado, M.R. André); Purdue University, West Lafayette, Indiana, USA (A.P. dos Santos), Wageningen University and Research, Wageningen, the Netherlands (G. Monti)

DOI: https://doi.org/10.3201/eid2902.221050

The Study

During June–August 2018, a total of 114 persons experiencing homelessness (101 men, 13 women; average age 42.5 ±13.4 years) from a day-shelter in the city of São Paulo signed written informed consent forms and participated in this study, which was approved by the National Ethics Committee in Human Research (protocol no. 80099017.3.0000.0102). Persons responded to a questionnaire that, combined with medical and demographic records (Appendix, https://wwwnc.cdc.gov/EID/article/29/2/22-1050-App1.pdf), we used to assess risk factors. We carefully examined personal clothing and found lice in 14.9% (17/114, 95% CI 6.9%–19.7%) of persons; the lice were taxonomically identified as *P. humanus humanus* (*5*).

We analyzed 109 serum samples from study participants by using IFA to detect IgG against *Bartonella* spp. and TGR. We used commercial slides for *B. quintana* (12-well IFA Substrate Slides; Fuller Laboratories, http://www.fullerlaboratories.com) and in-house slides for *B. henselae* sequence type 9, *B. machadoae* 56A, *R. typhi* Galveston, and *R. prowazekii* Breinl strains. We found 79/109 (72.5%, 95% CI 63.1%–80.1%) persons were seropositive for *Bartonella* spp. and 40/109 (36.7%, 95% CI 27.7%–46.5%) were sero-

positive for TGR (titers ≥64). All antibody titers were ≥128 (Appendix Table 1), except for 2 *B. quintana*–positive and 8 TGR-positive samples. An endpoint titer ≥4-fold higher for a particular *Bartonella*/*Rickettsia* spp. antigen than that observed for other *Bartonella*/*Rickettsia* spp. antigens was considered the possible antigen involved in a homologous reaction (PAIHR) (*6*). Thus, *B. quintana* was the PAIHR in 75/79 (95.0%, 95% CI 87.5%–98.6%) persons, *R. typhi* was the PAIHR in 13/40 (32.5%, 95% CI 18.6%–49.1%) persons, and *R. prowazekii* was the PAIHR in 3/40 (7.5%, 95% CI 1.6%–20.4%) persons (Appendix Table 1).

We extracted DNA by using the Blood/Tissue DNA Kit (MEBEP Bio Science, https://www.mebep.com) for 114 blood samples and guanidine isothiocyanate and phenol/chloroform technique (*7*) for 638 lice (82 pools). We confirmed successful extractions by PCR of glyceraldehyde-3-phosphate dehydrogenase (blood) and invertebrate mitochondrial cytochrome c oxidase subunit I (lice) genes (*8*,*9*). We screened DNA samples for *Bartonella* spp. by PCR of citrate synthase (*gltA*) and β subunit of RNA polymerase (*rpoB*) genes and for *Rickettsia* spp. by PCR of rickettsial 17-kDa antigen gene, as previously described (*10*–*12*). We used ultrapure water as a negative control and genomic DNA from *B. henselae* and *R. sibirica* as positive controls. A total of 14/82 (17.0%, 95% CI 9.7%–27.0%) louse pools and 1/114 (0.9%, 95% CI 0.02%–4.8%) blood samples were positive for *gltA* and *rpoB* but negative for *Rickettsia* spp. (Appendix Table 2).

Amplicons were purified and sequenced at the University of Texas Medical Branch (Galveston, TX, USA). The *gltA* and *rpoB* sequences showed 100% identity to *B. quintana* strain NCTC12899 (GenBank accession no. LS483373.1) by BLASTn analysis (https://blast.ncbi.nlm.nih.gov). *B. quintana* sequences generated in this study were deposited in GenBank (accession nos. ON808843 and ON808844). The person whose blood was PCR-positive for *B. quintana* was not infested with body lice but demonstrated high levels of IgG against *B. quintana* (titer ≥1,024) and TGR (titers were 1,024 for *R. typhi* and 512 for *R. prowazekii*).

We chose risk factor variables by using unconditional logistic regression models ($p<0.25$) and conditional logistic regression to determine relationships between putative risk factors and serologic status. We used Bayesian information criteria to assess the goodness-of-fit for the models. We used R software version 4.1.2 (The R Project for Statistical Computing, https://www.r-project.org) for all statistical analyses and summarized the final conditional logistic regression model (Table). Although the final model for *Bartonella* spp. revealed 3 variables, only 1 was statistically significant and showed an association between body louse infestation and higher risk for *Bartonella* spp. seropositivity (OR [odds ratio] 2.9, 90% CI 1.1–8.1). The final TGR model contained 5 variables of which 3 were associated with higher seropositivity risk, including self-identifying as white (OR 3.9, 90% CI 1.6–10.7), syphilis seropositivity (OR 3.6, 90% CI 1.5–9.4), and homelessness because of unemployment (OR 2.3, 90% CI 1.02–5.5). We detected 5 variables for combined *Bartonella* spp. and TGR of which 4 variables were associated with seropositivity, including self-identifying as white (OR 5.6, 90% CI 2.2–15.5), monthly change of clothes (OR 0.08, 90% CI 0.07–0.4), homelessness because of family conflicts (OR 0.4, 90% CI 0.2–0.8), and higher total plasma protein (OR 2.0, 90% CI 1.1–4.0).

Conclusions

Our study revealed *Bartonella* spp. and TGR exposure, associated risk factors related to serologic status, and *B. quintana* detection in lice and one blood sample among persons experiencing homelessness in São Paulo, Brazil. Seroprevalence of *Bartonella* spp. (72.5%) was higher in our study than previous reports for persons experiencing homelessness (1.8%–65%) (*13*), and *B. quintana* was the dominant antigen involved in homologous reactions. The highest *B. quintana* seroprevalence was previously found in France (65%, antibody titers ≥100) and Japan (57%, titers ≥128) (*13*); those titers were considered indicative of previous exposure. In our study, the antibody titer cutoff was ≥64, explaining our high seroprevalence results, although all but 2 titers were ≥128. TGR seropositivity in our study (36.7%) was within the range observed in the United States, Europe, and Colombia (0.54%–56.2%) (*1*,*3*).

Persons experiencing homelessness in São Paulo had *P. humanus humanus* body louse infestation and seropositivity for *B. quintana* and TGR similar to that reported previously (*1*). Body louse infestation (14.9%) was within the range of other reports (7%–22%) (*14*), highlighting global vulnerability to louse infestation and louseborne diseases in persons experiencing homelessness (*1*).

Through logistic regression, we showed seropositivity for *Bartonella* spp. was associated with louse infestation. Because the association of white ethnicity and TRG seropositivity (alone and in combination with *Bartonella* spp.) might be from a skewed population sampling, our findings should be further investigated. Nonetheless, higher TGR seropositivity was associated with homelessness because of unemployment, duration of homelessness, and syphilis seropositivity,

Table. Conditional logistic regression model results showing factors associated with exposure to *Bartonella* spp. and TGR among persons experiencing homelessness in São Paulo, Brazil, June–August 2018*

Model variables	Odds ratio (90% CI)	p value
Bartonella spp.†		
Intercept	1.72 (0.86–3.56)	0.20
Ethnicity		
Not white	Referent	NA
White	1.03 (0.30–5.40)	0.97
Body lice infestation		
No	Referent	NA
Yes	2.86 (1.06–8.06)	0.08
Have cats		
No	Referent	NA
Yes	0.24 (0.04–1.10)	0.13
TGR‡		
Intercept	0.47 (0.21–1.02)	0.11
Ethniicity		
Not white	Referent	NA
White	3.94 (1.56–10.67)	0.02
Cause of homelessness: unemployment		
No	Referent	NA
Yes	2.33 (1.02–5.46)	0.09
Frequency of changing clothes		
>Monthly	Referent	NA
Monthly	0.01 (0.001–99.53)	0.99
Syphilis infection		
No	Referent	NA
Yes	3.64 (1.50–9.37)	0.02
Duration of homelessness		
<1 y	Referent	NA
>1 y	0.65 (0.28–1.51)	0.40
Combined *Bartonella* spp.and TGR§		
Intercept	0.001 (0.0001–0.03)	0.02
Ethnicity		
Not white	Referent	NA
White	5.56 (2.18–15.50)	0.004
Total plasma protein	2.01 (1.04–4.00)	0.086
Packed cell volume	1.09 (0.99–1.21)	0.127
Cause of homelessness: family conflicts		
No	Referent	NA
Yes	0.36 (0.16–0.80)	0.038
Frequency of changing clothes		
>Monthly	Referent	NA
Monthly	0.08 (0.07–0.42)	0.03

*Bayesian information criteria (BICs) were used to assess the goodness-of-fit for each model. NA, not applicable; TGR, typhus group rickettsiae.
†Model BIC = 100.1.
‡Model BIC = 139.6.
§Model BIC = 140.5.

which represent risk factors that reflect vulnerability and socioeconomic conditions. In addition, seropositivity for both *Bartonella* and TGR was associated with infrequent changes of clothing.

The first limitation of our study is that the small sample size and power for the examined variables might have weakened associations of *Bartonella* seroreactivity with other variables included in our questionnaire, such as alcoholism, tobacco or intravenous drug use, and homelessness as previously reported (*15*), and variables that were significant in univariate analysis. In addition, IgG seropositivity reflects past *Bartonella* and TGR infections (*6*,*13*). IFA cross-reactivity should be addressed with future studies by using cross-adsorption techniques.

Our results should alert public health professionals in the city of São Paulo to initiate preemptive measures and active vector control among persons experiencing homelessness and confirm circulation of *Bartonella* and TGR species. Clinicians should also consider these vectorborne agents as probable etiologic agents of febrile syndromes in this vulnerable population.

Acknowledgments

We thank Sandro Ricardo Ruys and the Community Center of São Martinho de Lima for help with collection, sampling, and follow-up information and Nicole Mendell and Donald H. Bouyer for providing genomic DNA of *Bartonella henselae* and *Rickettsia sibirica* that was used as positive controls for PCR.

During this study, Á.A.F.-M. was supported by the Fogarty International Center and National Institute of Allergy and Infectious Diseases of the US National Institutes of Health (award no. D43 TW010331). The content is solely the authors' responsibility and does not necessarily represent the official views of the National Institutes of Health.

About the Author

Dr. Faccini-Martínez is a researcher and physician. His primary research interests focus on zoonotic and vector-borne diseases.

References

1. Leibler JH, Zakhour CM, Gadhoke P, Gaeta JM. Zoonotic and vector-borne infections among urban homeless and marginalized people in the United States and Europe, 1990–2014. Vector Borne Zoonotic Dis. 2016;16:435–44. https://doi.org/10.1089/vbz.2015.1863
2. Alcantara V, Rolain JM, Eduardo AG, Raul MJ, Raoult D. Molecular detection of *Bartonella quintana* in human body lice from Mexico City. Clin Microbiol Infect. 2009;15:93–4. https://doi.org/10.1111/j.1469-0691.2008.02176.x
3. Faccini-Martínez ÁA, Márquez AC, Bravo-Estupiñan DM, Calixto O-J, López-Castillo CA, Botero-García CA, et al. *Bartonella quintana* and typhus group rickettsiae exposure among homeless persons, Bogotá, Colombia. Emerg Infect Dis. 2017;23:1876–9. https://doi.org/10.3201/eid2311.170341
4. Gravinatti ML, Faccini-Martínez ÁA, Ruys SR, Timenetsky J, Biondo AW. Preliminary report of body lice infesting homeless people in Brazil. Rev Inst Med Trop Sao Paulo. 2018;60:e9. https://doi.org/10.1590/s1678-9946201860009
5. Centers for Disease Control and Prevention. Anoplura: pictorial key to some common genera of sucking lice [cited 2022 Oct 21]. https://www.cdc.gov/nceh/ehs/docs/pictorial_keys/lice-anoplura.pdf
6. Portillo A, de Sousa R, Santibáñez S, Duarte A, Edouard S, Fonseca IP, et al. Guidelines for the detection of *Rickettsia* spp. Vector Borne Zoonotic Dis. 2017;17:23–32. https://doi.org/10.1089/vbz.2016.1966
7. Sangioni LA, Horta MC, Vianna MCB, Gennari SM, Soares RM, Galvão MAM, et al. Rickettsial infection in animals and Brazilian spotted fever endemicity. Emerg Infect Dis. 2005;11:265–70. https://doi.org/10.3201/eid1102.040656
8. Folmer O, Black M, Hoeh W, Lutz R, Vrijenhoek R. DNA primers for amplification of mitochondrial cytochrome c oxidase subunit I from diverse metazoan invertebrates. Mol Mar Biol Biotechnol. 1994;3:294–9.
9. Tan B, Li Y, Zhao Q, Fan L, Liu Y, Wang D, et al. Inhibition of Vav3 could reverse the drug resistance of gastric cancer cells by downregulating JNK signaling pathway. Cancer Gene Ther. 2014;21:526–31. https://doi.org/10.1038/cgt.2014.59
10 Logan JMJ, Hall JL, Chalker VJ, O'Connell B, Birtles RJ. *Bartonella clarridgeiae* infection in a patient with aortic root abscess and endocarditis. Access Microbiol. 2019;1:e000064. PubMed https://doi.org/10.1099/acmi.0.000064
11. Renesto P, Gouvernet J, Drancourt M, Roux V, Raoult D. Use of *rpoB* gene analysis for detection and identification of *Bartonella* species. J Clin Microbiol. 2001;39:430–7. https://doi.org/10.1128/JCM.39.2.430-437.2001
12. Webb L, Carl M, Malloy DC, Dasch GA, Azad AF. Detection of murine typhus infection in fleas by using the polymerase chain reaction. J Clin Microbiol. 1990;28:530–4. https://doi.org/10.1128/jcm.28.3.530-534.1990
13. Mai BH. Seroprevalence of *Bartonella quintana* infection: a systematic review. J Glob Infect Dis. 2022;14:50–6. https://doi.org/10.4103/jgid.jgid_220_21
14. Badiaga S, Raoult D, Brouqui P. Preventing and controlling emerging and reemerging transmissible diseases in the homeless. Emerg Infect Dis. 2008;14:1353–9. https://doi.org/10.3201/eid1409.080204
15. Jackson LA, Spach DH, Kippen DA, Sugg NK, Regnery RL, Sayers MH, et al. Seroprevalence to *Bartonella quintana* among patients at a community clinic in downtown Seattle. J Infect Dis. 1996;173:1023–6. https://doi.org/10.1093/infdis/173.4.1023

Address for correspondence: David H. Walker, University of Texas Medical Branch, Galveston, TX 77555-0609, USA; email: dwalker@utmb.edu

Candida auris Discovery through Community Wastewater Surveillance during Healthcare Outbreak, Nevada, USA, 2022

Alessandro Rossi, Jorge Chavez, Thomas Iverson, John Hergert, Kelly Oakeson, Nathan LaCross, Chidinma Njoku, Andrew Gorzalski, Daniel Gerrity

Candida auris transmission is steadily increasing across the United States. We report culture-based detection of *C. auris* in wastewater and the epidemiologic link between isolated strains and southern Nevada, USA, hospitals within the sampled sewershed. Our results illustrate the potential of wastewater surveillance for containing *C. auris*.

The COVID-19 pandemic has showcased wastewater surveillance as an effective and economical tool for monitoring disease transmission levels and guiding public health interventions (*1*–*2*). Wastewater surveillance could also conceivably contribute to early detection of drug-resistant organisms of high relevance, such as carbapenem-resistant Enterobacterales and the yeast *Candida auris* (*3*). Carbapenem-resistant Enterobacterales have been recovered from influent of wastewater treatment plants (WWTPs), as well as from effluent from healthcare facilities (*4*–*5*). Various fungi and yeast species have also been cultured from wastewater (*6*).

C. auris was first described at the species level in 2009 and quickly became a notable nosocomial pathogen, displaying high levels of resistance to azoles and, to a lesser extent, polyenes and echinocandins (*7*). Limited treatment options, substantial pathogenicity, and environmental persistence in healthcare settings define *C. auris* as one of the most formidable public health threats in the world (*7*). Epidemiologically, *C. auris* isolates are assigned to 5 distinct genomic clades describing their original endemicity patterns: I (southern Asia), II (eastern Asia), III (Africa), IV (South America), and V (Iran) (*7*,*8*). We illustrate the potential utility of community-level wastewater surveillance for *C. auris* through culture-based monitoring at 2 WWTPs in southern Nevada, USA, while they were receiving sewage from healthcare facilities experiencing an outbreak.

Author affiliations: Utah Department of Health and Human Services, Salt Lake City, Utah, USA (A. Rossi, J. Chavez, T. Iverson, J. Hergert, K. Oakeson, N. LaCross); Nevada Department of Health and Human Services, Las Vegas, Nevada, USA (C. Njoku); University of Nevada, Reno, Nevada, USA (A. Gorzalski); Southern Nevada Water Authority, Las Vegas (D. Gerrity).

DOI: https://doi.org/10.3201/eid2902.221523

The Study

In Nevada, the first clinical case of *C. auris* was identified in August 2021. As of June 2022, a total of 300 cases had been reported and 22 healthcare facilities affected, including 10 acute care hospitals, 8 skilled nursing facilities, and 4 long-term acute care facilities. Clade III *C. auris* comprises most cases in Nevada, but clades I, II, and IV have also been identified. This sustained pathogen transmission represented an ideal scenario to explore the potential of wastewater surveillance for *C. auris*.

We collected wastewater influent samples (i.e., raw sewage) from 2 WWTPs (WWTP1 and WWTP2) in southern Nevada. WWTP1 treats an average daily flow of ≈100 million gallons/day; it serves a local population of nearly 1 million people, in addition to ≈800,000 weekly visitors. WWTP2 treats an average daily flow of ≈5 million gallons/day and serves a primarily residential sewershed with ≈90,000 people. We collected 50 mL aliquots of wastewater influent grab samples from each facility on the mornings of May 23 and 31 and June 6 and 13, 2022. We shipped samples on ice overnight to the Utah Public Health Laboratory, Utah Department of Health and Human Services (Taylorsville, UT, USA), where they were processed immediately upon receipt. We centrifuged each 50 mL sample at

5,000 × *g* for 10 minutes and resuspended the resulting pellet in 1 mL of 0.9% saline. We used 100 µL of this suspension to inoculate 2 mL of S² Media salt Sabouraud dulcitol broth (SSDB; Thomas Scientific, https://www.thomassci.com) (*9*) containing fluconazole (SSDBF) at a final concentration of 8 µg/mL. We incubated inoculated SSDBF tubes at 42°C for up to 7 d with vigorous agitation at 250 rpm. After incubation, we plated 100 µL of the inoculated SSDBF broth on HardyCHROM Candida medium (Hardy Diagnostics, https://hardydiagnostics.com) or BBL CHROMagar Candida medium (Becton, Dickinson and Company, https://www.bd.com). Alternatively, we used a 1 µL loop for quadrant streaking. We used matrix-assisted laser desorption/ionization time-of-flight mass spectrometry (Bruker, https://www.bruker.com) to identify species of growing colonies. We performed whole-genome sequencing on NextSeq 2000 or NovaSeq platforms (Illumina, https://www.illumina.com), and performed genome assembly as described elsewhere (*10*). We mapped reads to a reference *C. auris* genome and performed single-nucleotide polymorphism (SNP) and phylogenetic tree analyses using the MycoSNP pipeline (https://github.com/CDCgov/mycosnp-nf) (*10*).

Culture-based recovery of *C. auris* from marine environmental samples has been recently reported (*11*), but isolation from wastewater has not been documented. Following the protocol developed to detect *C. auris* in human specimens, use of SSDB as an enrichment medium was first explored (*9*). However, the selection criteria used for clinical samples in that study proved not stringent enough because fast-growing filamentous fungi and halo- and stress-tolerant *Candida* spp. could easily overgrow during the enrichment step (*12*). Inhibition of competing filamentous fungi, such as *Mucor* spp. and *Geotrichum* spp. (*6*), was mitigated by increasing the incubation temperature of the enrichment broth from 40°C (suggested temperature for patient colonization screening) to 42°C (Figure 1, panels A, B). Suppressing halo- and stress-tolerant *Candida* spp. required adding other selective agents to SSDB. Given that modal MIC for fluconazole

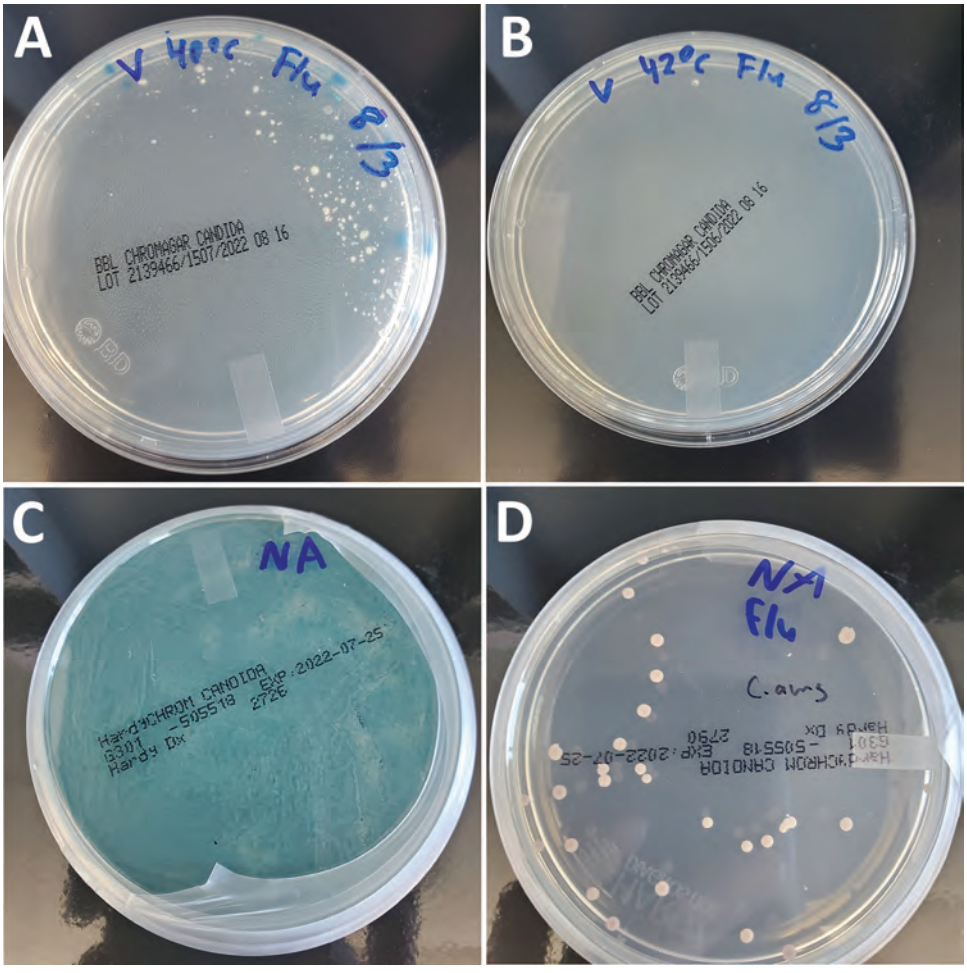

Figure 1. Culture-based isolation of *Candida auris* from wastewater, southern Nevada, USA, 2022, showing the effects of incubation temperature and fluconazole selection on competing organisms. A, B) Incubating the enrichment broth at 42°C (B) instead of 40°C (A) mitigated growth of competing filamentous fungi present in wastewater. C, D) Adding fluconazole to the salt Sabouraud dulcitol broth (SSDB) enrichment broth was essential for recovering *C. auris* from the southern Nevada wastewater samples. We plated 100 µL aliquots of inoculated enrichment broths incubated at 42°C after 2 days on HardyCHROM Candida medium (Hardy Diagnostics, https://hardydiagnostics.com) or BBL CHROMagar Candida medium (Becton, Dickinson, and Co., https://www.bd.com). Inoculation in SSDB without fluconazole resulted in overgrowth of an unidentified competing yeast (C), whereas inoculation in SSDB with fluconazole enabled isolation of *C. auris* colonies (D).

for *C. auris* isolates is significantly higher than for other *Candida* spp. (*13*), we pursued an azole-based selection strategy.

Preliminary experiments using samples from wastewater spiked with a fluconazole-resistant clinical strain of *C. auris* confirmed that adding fluconazole at a final concentration of 8 μg/mL suppressed growth of nontarget *Candida* spp. while ensuring recovery of *C. auris* (data not shown). We then prospectively validated this approach using wastewater samples collected in southern Nevada, which was experiencing an intense *C. auris* outbreak. Of the 8 samples we collected and analyzed during May 23–June 13, we recovered well-isolated *C. auris* colonies from a single WWTP1 sample from May 23 using SSDB broth enriched in the presence of fluconazole (Figure 1, panel D). Without azole selection, the target organism was overgrown by an unidentified yeast species (Figure 1, panel C). Of note, genomic analysis of 2 separate wastewater-derived *C. auris* isolates revealed phylogenetic relatedness to clade III isolates identified in 3 acute care hospitals within the WWTP1 sewershed (Figure 2). The 2 wastewater isolate genomes differed by 4 SNPs from each other and by 13–20 SNPs from the outbreak-associated isolates from the acute care hospitals (Figure 2).

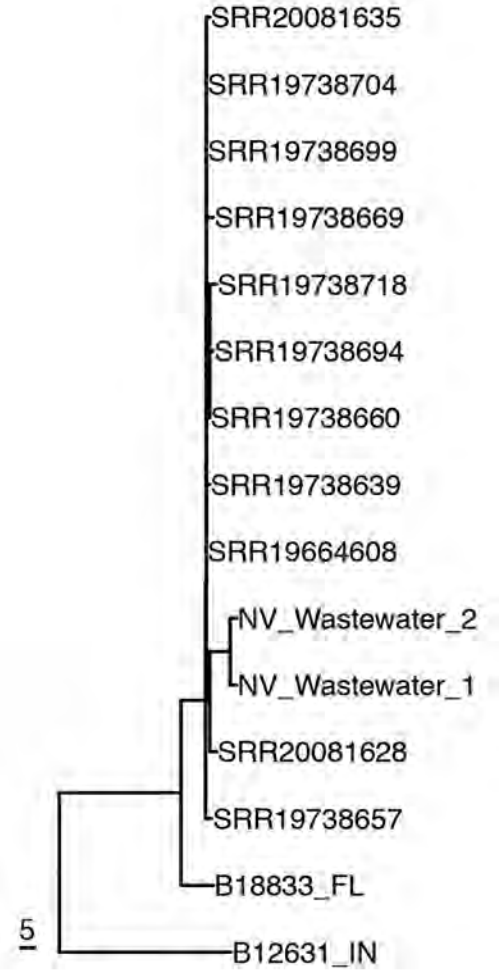

Figure 2. Genetic relatedness of clinical and wastewater isolates identified in the southern Nevada, USA, 2022, to reference clinical isolates. Neighbor-joining phylogenetic tree shows clade III *C. auris* isolates recovered from 3 southern Nevada acute care hospitals (identified by National Center for Biotechnology Information Sequence Read Archive [SRA] accession number) and from the wastewater treatment plants to which they were connected (NV_Wastewater_1 [SRA accession no. SRR21758525] and NV_Wastewater_2[SRA accession no. SRR21758524]). Two unrelated isolates from Florida and Indiana are included in the tree: B188833_FL (SRA accession no. SRR12526241) and B12631_IN (SRA accession no. SRR7909359). Scale bar indicates single-nucleotide polymorphisms.

Conclusions

We report recovery of *C. auris* isolates from wastewater that demonstrated an epidemiologic link to healthcare facilities within the WWTP sewershed in southern Nevada. Although our findings highlight the potential utility of community-level wastewater surveillance for *C. auris*, the methods and the data presented here represent only early-stage implementation. More recent prospective testing of samples in Nevada using both culture and quantitative PCR monitoring (D. Gerrity, unpub. data) has shown considerable variability between samples for the presence of competing organisms, which required increased selection stringency. Indeed, in August 2022, we could repeat isolation of *C. auris* from Nevada samples only by increasing the fluconazole concentration to 32 μg/mL (data not shown). This experience illustrates one limitation of the culture-based approach we used in this study: *C. auris* strains with a fluconazole MIC lower than the concentration of the drug in the broth might not be detected. In addition, the actual sensitivity of this surveillance approach is still unknown, because it can be influenced by the degree of competition between organisms during the enrichment step. PCR-based quantification of *C. auris* genome equivalents in Nevada wastewater indicates that culture-based isolation has occurred at organism concentrations as low as ≈100 CFU/mL (D. Gerrity, unpub. data). In addition, the full extent of *C. auris* colonization, transmission within sewersheds, and organism shedding have not been sufficiently studied. Therefore, it remains to be determined whether *C. auris* could be detected in geographic areas by wastewater surveillance before being recognized in clinical settings. Regardless, wastewater surveillance of pooled samples

at the community level might effectively complement clinical surveillance of individual patients for detecting and characterizing *C. auris* outbreaks.

Acknowledgments

We greatly appreciate the support of personnel of the collaborating wastewater agencies in Utah and Nevada without whom our work would have not been possible.

J.C. was supported by an APHL Fellowship in Antibiotic Resistance. Southern Nevada wastewater sample collection was supported by CDC grant NH75OT000057-01-00.

About the Author

Dr. Rossi is the Clinical Laboratory Improvement Amendments director and infectious diseases chief scientist of the Utah Public Health Laboratory, Utah Department of Health and Human Services, Taylorsville, Utah, USA. His research interests include the description of novel bacterial species relevant to clinical microbiology, drug resistant organisms, and infection control.

References

1. Kitajima M, Ahmed W, Bibby K, Carducci A, Gerba CP, Hamilton KA, et al. SARS-CoV-2 in wastewater: state of the knowledge and research needs. Sci Total Environ. 2020;739:139076. https://doi.org/10.1016/j.scitotenv.2020.139076
2. Vo V, Tillett RL, Papp K, Shen S, Gu R, Gorzalski A, et al. Use of wastewater surveillance for early detection of Alpha and Epsilon SARS-CoV-2 variants of concern and estimation of overall COVID-19 infection burden. Sci Total Environ. 2022;835:155410. https://doi.org/10.1016/j.scitotenv.2022.155410
3. Lainhart W, Yarbrough ML, Jean S, Burnham CD. New bugs and new drugs: updates in clinical microbiology. J Appl Lab Med. 2018;2:925–40. https://doi.org/10.1373/jalm.2017.023101
4. Hoelle J, Johnson JR, Johnston BD, Kinkle B, Boczek L, Ryu H, et al. Survey of US wastewater for carbapenem-resistant *Enterobacteriaceae*. J Water Health. 2019;17:219–26. https://doi.org/10.2166/wh.2019.165
5. Cahill N, O'Connor L, Mahon B, Varley Á, McGrath E, Ryan P, et al. Hospital effluent: a reservoir for carbapenemase-producing *Enterobacterales*? Sci Total Environ. 2019;672:618–24. https://doi.org/10.1016/j.scitotenv.2019.03.428
6. Cooke WB. The enumeration of yeast populations in a sewage treatment plant. Mycologia. 1965;57:696–703. https://doi.org/10.1080/00275514.1965.12018257
7. Osei Sekyere J. *Candida auris*: a systematic review and meta-analysis of current updates on an emerging multidrug-resistant pathogen. Microbiologyopen. 2018;7:e00578. https://doi.org/10.1002/mbo3.578
8. Chow NA, de Groot T, Badali H, Abastabar M, Chiller TM, Meis JF. Potential fifth clade of *Candida auris*, Iran, 2018. Emerg Infect Dis. 2019;25:1780–1. https://doi.org/10.3201/eid2509.190686
9. Welsh RM, Bentz ML, Shams A, Houston H, Lyons A, Rose LJ, et al. Survival, persistence, and isolation of the emerging multidrug-resistant pathogenic yeast *Candida auris* on a plastic health care surface. J Clin Microbiol. 2017;55:2996–3005. https://doi.org/10.1128/JCM.00921-17
10. Bagal UR, Phan J, Welsh RM, Misas E, Wagner D, Gade L, et al. MycoSNP: a portable workflow for performing whole-genome sequencing analysis of *Candida auris*. Methods Mol Biol. 2022;2517:215–28. https://doi.org/10.1007/978-1-0716-2417-3_17
11. Arora P, Singh P, Wang Y, Yadav A, Pawar K, Singh A, et al. Environmental isolation of *Candida auris* from the coastal wetlands of Andaman Islands, India. MBio. 2021;12:e03181-20. https://doi.org/10.1128/mBio.03181-20
12. Lahav R, Fareleira P, Nejidat A, Abeliovich A. The identification and characterization of osmotolerant yeast isolates from chemical wastewater evaporation ponds. Microb Ecol. 2002;43:388–96. https://doi.org/10.1007/s00248-002-2001-4
13. Arendrup MC, Chowdhary A, Astvad KMT, Jørgensen KM. APX001A *in vitro* activity against contemporary blood isolates and *Candida auris* determined by the EUCAST reference method. Antimicrob Agents Chemother. 2018;62:e01225–18. https://doi.org/10.1128/AAC.01225-18

Address for correspondence: Alessandro Rossi, Utah Public Health Laboratory, 4431 S 2700 W, Taylorsville, UT 84129, USA; email: arossi@utah.gov

Estimated Cases Averted by COVID-19 Digital Exposure Notification, Pennsylvania, USA, November 8, 2020–January 2, 2021

Seonghye Jeon, Gabriel Rainisch, A-Mac Harris, Jared Shinabery, Muneeza Iqbal, Amar Pallavaram, Stacy Hilton, Saugat Karki, Patrick K. Moonan, John E. Oeltmann, Martin I. Meltzer

We combined field-based data with mathematical modeling to estimate the effectiveness of smartphone-enabled COVID-19 exposure notification in Pennsylvania, USA. We estimated that digital notifications potentially averted 7–69 cases/1,000 notifications during November 8, 2020–January 2, 2021. Greater use and increased compliance could increase the effectiveness of digital notifications.

Case investigation and contact tracing (CICT) was a pillar among COVID-19 prevention strategies, especially before vaccine availability (*1*,*2*). However, standard CICT relies on staff to reach cases and close contacts, which is labor intensive, and CICT programs often become overwhelmed when caseloads surge (*3*–*5*). Standard CICT also relies on case investigation interviews to identify contacts; thus, it is prone to recall and participation bias and might not identify all potential exposures, such as interactions between strangers in public spaces.

COVID-19 exposure notification smartphone applications (apps) can alleviate those challenges by automatically notifying app users when they have been near other users who reported positive SARS-CoV-2 results (herein referred to as cases). Pennsylvania, USA, and 26 other states implemented digital exposure notifications to complement their standard CICT programs (*6*). However, few studies have evaluated the effectiveness of digital notifications in the United States (*6*,*7*).

Author affiliations: Centers for Disease Control and Prevention, Atlanta, Georgia, USA (S. Jeon, G. Rainisch, S. Karki, P.K. Moonan, J.E Oeltmann, M.I. Meltzer); Pennsylvania Department of Health, Harrisburg, Pennsylvania, USA (A.-M. Harris, J. Shinabery, M. Iqbal, A. Pallavaram, S. Hilton)

DOI: https://doi.org/10.3201/eid2902.220959

We estimated the number of cases and hospitalizations averted by Pennsylvania's digital notification system, COVID Alert PA app. We also investigated strategies to increase the system's efficiency and its effects on the estimated number of cases and hospitalizations.

The Study

During case investigation interviews in Pennsylvania, digital notification app users were identified and given a validation code to enter into their app. The app then automatically sent anonymous notifications to other users identified through smartphone Bluetooth technology as potentially exposed to the person testing positive for COVID-19 (Appendix, https://wwwnc.cdc.gov/EID/article/29/2/22-0959.App1.pdf).

The Pennsylvania Department of Health (PA DoH) collected data on the performance of standard CICT and digital notification apps (Table). We aggregated those data across all counties, excluding Philadelphia County (Appendix), for 8 weeks, November 8, 2020–January 2, 2021 (Table). We extracted the daily number of COVID-19 cases from the Centers for Disease Control and Prevention (CDC) COVID Data Tracker (*8*).

We used CDC's COVIDTracer modeling tool to estimate cases and hospitalizations averted by digital notifications during the 8-week study period (*1*,*2*,*9*). COVIDTracer uses an epidemiologic model to illustrate the spread of COVID-19 and effects of CICT and other nonpharmaceutical interventions (NPIs). We calculated a summary effectiveness measure for CICT and digital notification apps from the various data PA DoH collected and input this measure to the model (Table). We defined this summary effectiveness measure as the proportion of cases that entered isolation and contacts that quarantined in response to CICT

Table. Reported and estimated program metrics in a study of estimated cases averted by COVID-19 digital exposure notification, Pennsylvania, USA, November 8, 2020–January 2, 2021*

Program	Reported metrics
Standard case investigation and contact tracing	
Cases interviewed, no. (% total cases)	77,477 (20)
Cases named ≥1 contact, no. (% interviewed cases)	32,648 (42)
No. contacts named	48,615
Contacts notified and monitored, no. (% identified contacts)	26,203 (54)
Contacts notified but not monitored, no. (% identified contacts)	418 (1)
Timing of case interview, d†	5
Timing of contact notification, d‡	6
Digital exposure notification	
Median no. active daily users (% total population)§	356,835 (3.2)
Cases interviewed and identified as app user, no. (% total cases)	786 (0.2)
No. validation codes generated (% cases that had the app installed)	579 (74)
No. validation codes claimed and certified (% cases that had the app installed)	390 (50)
Timing of digital notification, d‡	6
Estimated program effectiveness#	
Cases and contacts isolated or quarantined, %**	7–11.7
Days from infection to isolation or quarantine	10

*Data excludes Philadelphia County. CICT, case investigation and contact tracing.
†Reported average number of days from specimen collection to case interview.
‡Reported average number of days from specimen collection to contact notification.
§For Android users, the total number of devices that were turned on ≥1 time in the past 30 d. For iOS users, the total number of devices with ≥1 session within 30 d of the selected day. During the study period, only persons ≥18 years of age were eligible to download and activate the digital notification application on their smartphone devices; thus, data provided is equivalent to 4.0% of the eligible population.
#Calculations provided in the Appendix (https://wwwnc.cdc.gov/EID/article/29/2/22-0959-App1.pdf).
**Includes contacts that later become cases. The range reflects the lowest and highest values across 18 studied scenarios of compliance with quarantine guidelines and the degree of overlap between notifications received via the COVID Alert PA app and by Pennsylvania Department of Health staff members (Appendix Tables 4, 5). The low-value results from a scenario assuming 50% of digital notifications were sent to contacts that were already notified by Department of Health staff members and 10% of notified contacts followed quarantine guidance. The high-value results from a scenario assuming all digital notifications were sent to contacts that were not notified via standard CICT and 50% of notified contacts followed quarantine guidance.

and digital notification apps, and the number of days required to do so (i.e., number of days from exposure to isolation or quarantine). We further assumed 60%–100% of interviewed cases and monitored contacts fully adhered to isolation and quarantine guidelines, and that 10%–50% of notified but not monitored contacts complied with quarantine guidance (*10*–*12*). To calculate the number of days from exposure to isolation or quarantine, we averaged the number of days between case interviews (triggering case isolation) and contact notifications (triggering contact quarantine). We performed 2 sensitivity analyses by varying the estimated number of days from infection to isolation by ±1 day and the weight used to estimate the overall proportion of cases isolated and contacts quarantined (Appendix).

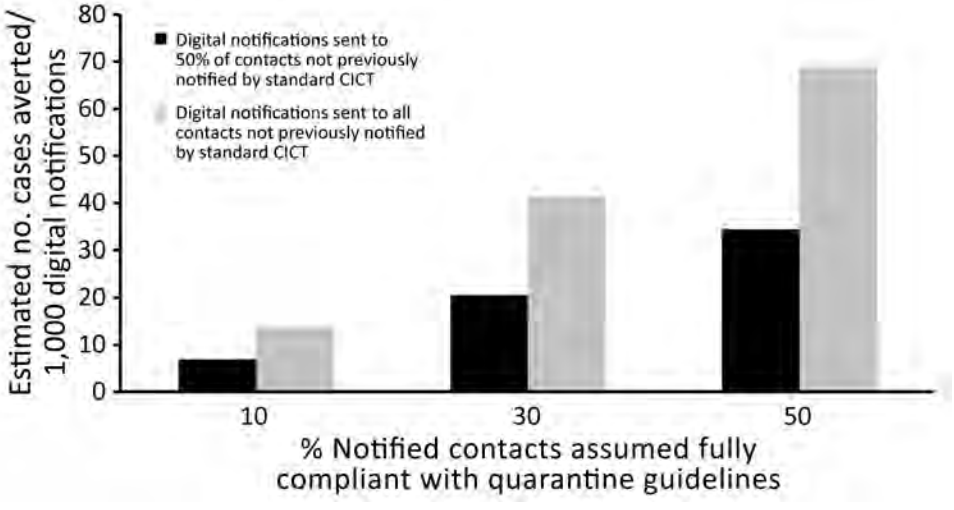

Figure 1. Estimated number of cases averted per 1,000 COVID-19 digital notifications, Pennsylvania, USA, November 8, 2020–January 2, 2021. Estimates show selected scenarios of isolation or quarantine compliance and the digital notification application's ability to identify previously unknown contacts. Data from Philadelphia County are excluded. The figure represents a scenario in which 80% of interviewed cases and monitored contacts comply with isolation and quarantine guidance. We also modeled 60% and 100% compliance scenarios (Appendix Tables 4, 5, https://wwwnc.cdc.gov/EID/article/29/2/22-0959-App1.pdf). At just 10% compliance among notified contacts, digital notifications averted 7 cases/1,000 notifications (or 2 cases); at 50% compliance among notified contacts, digital notifications averted 69 cases/1,000 notifications (or 16 cases). CICT, case investigation and contact tracing.

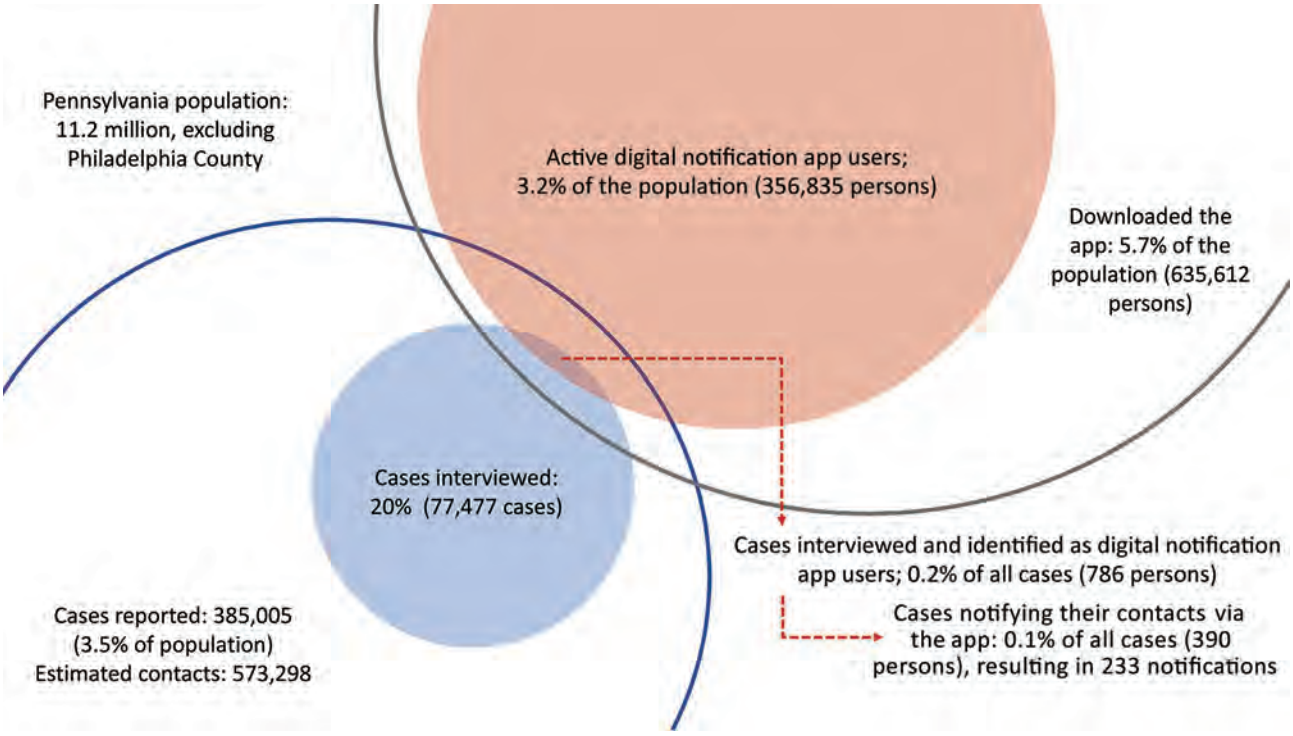

Figure 2. Overlap between standard CICT and digital notifications in a study of estimated cases averted by COVID-19 digital exposure notification, Pennsylvania, USA, November 8, 2020–January 2, 2021. During the study period, standard CICT resulted in interviews and contact elicitation from 20% of the reported cases (blue, shaded circle) and 3.2% of the population actively used the digital notification app (red, shaded circle). During case interviews, app users were provided validation codes for initiating contact notifications via their digital notification app (overlap of red and blue shaded circles; 0.2% of all cases). The effectiveness will be greater in the following scenarios. First, any case in the overlap of shaded red and unshaded blue circle (including persons who used at-home testing) can generate notifications via the app. Second, a larger shaded red circle reflects a higher proportion of the population actively using the digital notification app. Last, a larger unshaded black circle reflects a situation where more individuals can generate validation codes and receive exposure notifications. CICT, case investigation and contact tracing.

We derived CICT program effectiveness from reported data, but data were not available to estimate effectiveness of other NPIs, such as social distancing and mask-wearing. Therefore, we used the tool to estimate the effectiveness of other NPIs by fitting the model-generated curve to observed case curve (Appendix). Finally, to show what might have happen without the digital notifications, we simulated a hypothetical case curve by replacing the CICT effectiveness input with a value excluding contributions of the digital notifications. We considered the difference between cases in the simulated curve and reported cases as the estimated cases averted by the digital notifications. We generated a range of 18 results by varying public compliance with isolation and quarantine guidance and the degree to which recipients of digital notifications were also notified by the PA DoH staff members. First, we assumed no overlap (i.e., all digital notifications were sent to contacts who were not notified by the DoH staff); then, we assumed a 50% overlap (Appendix Tables 4, 5). We also calculated the number of hospitalizations averted by multiplying the estimated number of averted cases by age-stratified infection-to-hospitalization rates (*9*). We did not account for vaccination because only 0.1% of Pennsylvania's population was fully vaccinated during the study period.

Between its launch in late September and the end of the study period, Pennsylvania's digital notification app was downloaded 638,797 times, accounting for ≈5.7% of the population; 56% (n = 356,835) of downloaded apps were actively used, accounting for 3.2% of the population. In all, 786 interviewed case-patients (0.2% of all cases) had the digital notification app installed on their smartphones, among whom <50% (n = 390) used the app to notify others of potential exposure, totaling 233 digital notifications during the 8-week period (Table).

We estimated those digital notifications averted 2–16 additional cases (7–69 cases/1,000 notifications) and <1 hospitalization (Figure 1; Appendix Tables 4, 5). That range reflects uncertainties in both public

compliance and the degree of overlap between notifications received via the digital notification app and DoH staff. In comparison, we estimated standard CICT averted 10,168–17,151 cases and 250–421 hospitalizations during the same period.

Conclusions

Although just 3.2% of the state's population used the COVID Alert PA app, we estimated that 7–69 cases were averted for every 1,000 digital notifications sent during the 8-week study. Those estimates represent a single locality and should not be generalized to other jurisdictions. However, the methods, and the publicly accessible modeling tool, could be used to adjust for differences in uptake, compliance, and epidemic curve to estimate the effect of digital notifications in other jurisdictions.

Greater use, increased compliance, or changes to digital notification system operations might increase its effectiveness (Figure 2). UK researchers assessing a similar app estimated that 167–349 cases were averted for every 1,000 notifications with a 28% adoption rate (*13*). Greater use appears achievable based on multiple reports indicating >17% of the population activated digital notification apps in 11 states and participation approached 50% in states where adoption was greatest (*6*,*7*). When we examined hypothetical scenarios in which 50% of the population actively used the app in Pennsylvania, all else remaining equal, we found that up to 3,995 cases could have been averted by digital notifications during the study period (Appendix).

The potential increase in cases averted by digital notifications requires additional research and should consider other factors, such as alternative digital notification system operations. For example, effectiveness might be improved with automatic digital notification versus relying on case-patients to initiate contact notification after being interviewed. Some jurisdictions also started permitting users to self-report as COVID-19–positive and initiate digital notifications on the basis of at-home testing, which could improve both the number and timeliness of digital notifications (*14*). Although such gains are promising, they are moderated by the public's compliance with digital notifications and technological limitations of Bluetooth signaling, leading to missed exposures and potentially false notifications.

Our findings suggest that the use of digital notification apps helped avert COVID-19 cases in Pennsylvania, although its effectiveness was limited by numerous factors, most notably limited use. The results also suggest opportunities exist to further examine and improve digital notification systems and their use during future outbreaks (Figure 2). Public health practitioners should explore ways to increase public participation in digital notification apps and to improve system efficiency by increasing the timeliness, coverage, and accuracy of digital notifications.

About the Author

Dr. Jeon is a senior statistician in the Health Economics and Modeling Unit, Division of Preparedness and Emerging Infections, National Center for Zoonotic and Emerging Infectious Diseases, Centers for Disease Control and Prevention. Her research interest includes leveraging statistical and mathematical models to estimate impact of public health interventions.

References

1. Jeon S, Rainisch G, Lash RR, Moonan PK, Oeltmann JE Jr, Greening B Jr, et al.; Contact Tracing Impact Group. Estimates of cases and hospitalizations averted by COVID-19 case investigation and contact tracing in 14 health jurisdictions in the United States. J Public Health Manag Pract. 2022;28:16–24. https://doi.org/10.1097/PHH.0000000000001420
2. Rainisch G, Jeon S, Pappas D, Spencer KD, Fischer LS, Adhikari BB, et al. Estimated COVID-19 cases and hospitalizations averted by case investigation and contact tracing in the US. JAMA Netw Open. 2022;5:e224042. https://doi.org/10.1001/jamanetworkopen.2022.4042
3. Spencer KD, Chung CL, Stargel A, Shultz A, Thorpe PG, Carter MW, et al. COVID-19 case investigation and contact tracing efforts from health departments—United States, June 25–July 24, 2020. MMWR Morb Mortal Wkly Rep. 2021;70:83–7. https://doi.org/10.15585/mmwr.mm7003a3
4. Lash RR, Moonan PK, Byers BL, Bonacci RA, Bonner KE, Donahue M, et al. COVID-19 case investigation and contact tracing in the US, 2020. JAMA Netw Open. 2021;4:e2115850. https://doi.org/10.1001/jamanetworkopen.2021.15850
5. Bengio Y, Janda R, Yu YW, Ippolito D, Jarvie M, Pilat D, et al. The need for privacy with public digital contact tracing during the COVID-19 pandemic. Lancet Digit Health. 2020;2:e342–4. https://doi.org/10.1016/S2589-7500(20)30133-3
6. US Government Accountability Office. Report to Congressional Addressees. Exposure notification: benefits and challenges of smartphone applications to augment contact tracing; GAO-21-104622. Washington: The Office; 2021 [cited 2022 May 1]. https://www.gao.gov/assets/gao-21-104622.pdf
7. MIT Technology Review. We investigated whether digital contact tracing actually worked in the US [cited 2022 May 1]. https://www.technologyreview.com/2021/06/16/1026255/us-digital-contact-tracing-exposure-notification-analysis
8. US Centers for Disease Control and Prevention. COVID data tracker [cited 2022 May 1]. https://covid.cdc.gov/covid-data-tracker
9. Adhikari BB, Arifkhanova A, Coronado F, Fischer LS, Greening B, Jeon S, et al. COVIDTracer Advanced: a planning tool to illustrate the resources needed to conduct contact tracing and monitoring of coronavirus disease 2019 (COVID-19) cases and the potential impact of community

interventions and contact tracing efforts on the spread of COVID-19 [cited 2022 May 1]. https://www.cdc.gov/coronavirus/2019-ncov/downloads/php/contact-tracing/AdvancedCOVIDTracerManual.pdf
10. Smith LE, Potts HWW, Amlôt R, Fear NT, Michie S, Rubin GJ. Adherence to the test, trace, and isolate system in the UK: results from 37 nationally representative surveys. BMJ. 2021;372:n608. https://doi.org/10.1136/bmj.n608
11. Park CL, Russell BS, Fendrich M, Finkelstein-Fox L, Hutchison M, Becker J. Americans' COVID-19 stress, coping, and adherence to CDC guidelines. J Gen Intern Med. 2020;35:2296–303. https://doi.org/10.1007/s11606-020-05898-9
12. Pew Research Center. The challenges of contact tracing as U.S. battles COVID-19 [cited 2022 May 1]. https://www.pewresearch.org/internet/2020/10/30/the-challenges-of-contact-tracing-as-u-s-battles-covid-19
13. Wymant C, Ferretti L, Tsallis D, Charalambides M, Abeler-Dörner L, Bonsall D, et al. The epidemiological impact of the NHS COVID-19 app. Nature. 2021;594:408–12. https://doi.org/10.1038/s41586-021-03606-z
14. US Centers for Disease Control and Prevention. Guidelines for the implementation and use of digital tools to augment traditional contact tracing [cited 2022 May 1]. https://www.cdc.gov/coronavirus/2019-ncov/php/contact-tracing/contact-tracing-plan/digital-contact-tracing-tools.html

Address for correspondence: Seonghye Jeon, Centers for Disease Control and Prevention, 1600 Clifton Rd NE, Mailstop H24-11, Atlanta, GA 30329-4029, USA; email: iqc1@cdc.gov

etymologia revisited

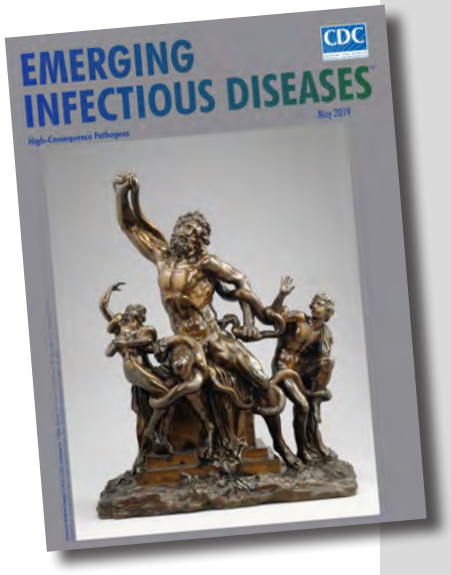

Originally published in May 2019

Nipah Virus

[ne´-pə vī´-rəs]

In 1994, a newly described virus, initially called equine morbillivirus, killed 13 horses and a trainer in Hendra, a suburb of Brisbane, Australia. The reservoir was subsequently identified as flying foxes, bats of the genus *Pteropus* (Greek pteron ["wing"] + *pous* ["foot"]). In 1999, scientists investigated reports of febrile encephalitis and respiratory illness among workers exposed to pigs in Malaysia and Singapore. (The pigs were believed to have consumed partially eaten fruit discarded by bats.)

The causative agent was determined to be closely related to Hendra virus and was later named for the Malaysian village of Kampung Sungai Nipah. The 2 viruses were combined into the genus *Henipavirus*, in the family *Paramyxoviridae*. Three additional species of *Henipavirus*—Cedar virus, Ghanaian bat virus, and Mojiang virus—have since been described, but none is known to cause human disease. Outbreaks of Nipah virus occur almost annually in India and Bangladesh, but *Pteropus* bats can be found throughout the tropics and subtropics, and henipaviruses have been isolated from them in Central and South America, Asia, Oceania, and East Africa.

Sources:

1. Centers for Disease Control and Prevention. Outbreak of Hendra-like virus—Malaysia and Singapore, 1998–1999. MMWR Morb Mortal Wkly Rep. 1999;48:265–9.
2. Selvey LA, Wells RM, McCormack JG, Ansford AJ, Murray K, Rogers RJ, et al. Infection of humans and horses by a newly described morbillivirus. Med J Aust. 1995;162:642–5.

https://wwwnc.cdc.gov/eid/article/25/5/et-2505_article

Next-Generation Sequencing for Identifying Unknown Pathogens in Sentinel Immunocompromised Hosts

Jay A. Fishman

The importance of obtaining a specific microbiologic diagnosis to guide antimicrobial therapy takes on greater urgency in persons immunocompromised after organ or stem cell transplantation or chemotherapy, or with other immune deficits (*1*). These patients tolerate invasive infection poorly, sometimes caused by organisms not previously known to be pathogenic. Incompletely treated or persistent infections in such persons serve as substrates for developing antimicrobial resistance and the evolution of viral mutants unresponsive to natural or vaccine-induced immunity (*2*). Specific diagnoses of infectious syndromes, such as febrile illnesses, pneumonitis, hepatitis, meningitis, and gastroenteritis, despite their relative frequency, are often elusive in immunocompromised hosts. Identifying pathogens using traditional culture systems for bacteria and fungi, even when supplemented by use of organism-specific protein or molecular diagnostics, is limited by requiring comparison with known human pathogens stored in datasets. Identifying viral pathogens in the absence of specific nucleic acid tests might require cell-based culture systems, which are labor-intensive, costly, and inefficient.

Clinical microbiology laboratories are increasingly adopting agnostic metagenomic analysis of clinical samples based on next-generation sequencing (NGS) to identify unexpected or novel pathogenic microorganisms (*3*). NGS platforms, which vary in sensitivity and specificity, enable high-throughput parallel sequencing of nucleic acid fragments in blood and tissues without need for specific targets (*3*). Bioinformatics software is used to reassemble sequenced fragments into a microbial genome, an approach that can be applied to all microbial groups if comparator sequences exist, as well as to identify mutations, resistance markers, and virulence factors.

In this issue, Philippe Pérot et al. report a novel circovirus causing hepatitis in an immunosuppressed heart-lung recipient who had no clear exposures to common sources of infection (*4*). The virus, tentatively called human circovirus type 1 (HCirV-1), was associated with hepatic injury in this case. Identified using NGS and specific primers with the reassembled sequence, HCirV-1 was detected at high levels in blood and by hybridization in ≈2% of hepatocytes examined. Infection resolved after doctors reduced immunosuppression medications.

The source of HCirV-1 remains uncertain, as is common for infections in immunocompromised hosts. Demonstrating the microbial etiology of infection in this case enabled healthcare providers to appropriately manage treatment by reducing immune suppression medication and avoid unnecessary use of antimicrobial therapies. Among the challenges of NGS have been costs (although they have been decreasing), detection of sequences of unknown clinical significance, and gaps in databank records for many viral and other species for comparison with detected sequences, notably among nonhuman species. Thus, new zoonotic exposures or recombinant species may be unrecognized or masked by any of numerous unknown nucleic acids.

The case described by Pérot et al. is unusual because no other contaminating nucleic acids were detected. Related porcine circoviruses (PCV) 1–4 are heterogeneous and thought to be largely species-specific (*5*). Two strains, PCV2 and PCV3, cause liver infection with prolonged viremia, which is exacerbated by immunosuppression in baboon recipients of

Author affiliation: Massachusetts General Hospital Transplant Infectious Disease and Compromised Host Program and Harvard Medical School Transplant Center, Boston, Massachusetts, USA.

DOI: https://doi.org/10.3201/eid2902.221829

porcine cardiac xenografts (*6*–*9*). Human circoviruses have been identified in human feces samples, suggesting that human exposure and infections might be ongoing (*10*). In such circumstances, infection might be missed by routine microbiologic techniques and identified by NGS if the sequence data are included in reference databanks.

In settings such as human xenotransplantation from pigs, where concerns about unrecognized donor-derived infections exist, NGS may serve to bridge gaps in standard clinical microbiology (*11*). Comparisons with closely related known viral sequences, including from zoonotic species, will be required to detect unexpected, novel, or emerging pathogens. Routinely applying NGS tools to uncover pathogenesis in cases of clinical syndromes without an etiologic diagnosis may be costly but might enhance recognition of novel pathogens. Interpreting vast amounts of sequence data, including host sequences, remains daunting for clinical application. The availability of baseline serum samples, such as in the case described by Pérot et al., enables identification of novel sequences; prospective research will require such archived specimens for comparison. Although the prospect is exciting, optimal use of NGS in the clinical care of immunocompromised patients remains to be elucidated.

About the Author

Dr. Fishman is professor of medicine at Harvard Medical School, director of the Transplant Infectious Diseases and Compromised Host Program at Massachusetts General Hospital (MGH), and associate director of the MGH Transplant Center. He has defined paradigms for the care of immunocompromised hosts and the deployment of novel diagnostic tools in their clinical care.

References

1. Fishman JA. Infection in organ transplantation. Am J Transplant. 2017;17:856–79. https://doi.org/10.1111/ajt.14208
2. Fung M, Babik JM. COVID-19 in immunocompromised hosts: what we know so far. Clin Infect Dis. 2021;72:340–50. https://doi.org/10.1093/cid/ciaa863
3. Casto AM, Fredricks DN, Hill JA. Diagnosis of infectious diseases in immunocompromised hosts using metagenomic next generation sequencing-based diagnostics. Blood Rev. 2022;53:100906. https://doi.org/10.1016/j.blre.2021.100906
4. Pérot P, Fourgeaud J, Rouzaud C, Regnault B, Da Rocha N, Fontaine H, et al. Circovirus hepatitis infection in heart-lung transplant patient. Emerg Infect Dis. 2023 Jan XX [Epub ahead of print]. https://doi.org/10.3201/eid2902.221468.
5. Zhai SL, Lu SS, Wei WK, Lv DH, Wen XH, Zhai Q, et al. Reservoirs of porcine circoviruses: a mini review. Front Vet Sci. 2019;6:319. https://doi.org/10.3389/fvets.2019.00319
6. Krüger L, Längin M, Reichart B, Fiebig U, Kristiansen Y, Prinz C, et al. Transmission of porcine circovirus 3 (PCV3) by xenotransplantation of pig hearts into baboons. Viruses. 2019;11:650. https://doi.org/10.3390/v11070650
7. Klaumann F, Dias-Alves A, Cabezón O, Mentaberre G, Castillo-Contreras R, López-Béjar M, et al. Porcine circovirus 3 is highly prevalent in serum and tissues and may persistently infect wild boar (*Sus scrofa scrofa*). Transbound Emerg Dis. 2019;66:91–101. https://doi.org/10.1111/tbed.12988
8. Denner J, Mankertz A. Porcine circoviruses and xenotransplantation. Viruses. 2017;9:83. https://doi.org/10.3390/v9040083
9. Phan TG, Giannitti F, Rossow S, Marthaler D, Knutson TP, Li L, et al. Detection of a novel circovirus PCV3 in pigs with cardiac and multi-systemic inflammation. Virol J. 2016; 13:184. [Erratum in Virol J. 2017;14:87] https://doi.org/10.1186/s12985-016-0642-z
10. Li L, Kapoor A, Slikas B, Bamidele OS, Wang C, Shaukat S, et al. Multiple diverse circoviruses infect farm animals and are commonly found in human and chimpanzee feces. J Virol. 2010;84:1674–82. https://doi.org/10.1128/JVI.02109-09
11. Fishman JA. Infectious disease risks in xenotransplantation. Am J Transplant. 2018;18:1857–64. https://doi.org/10.1111/ajt.14725

Address for correspondence: Jay A. Fishman, MGH Transplant Center, WH510A, 55 Fruit St, Boston, MA 02114, USA; email: fishman.jay@mgh.harvard.edu

Orthopoxvirus Infections in Rodents, Nigeria, 2018–2019

Clement Meseko, Adeyinka Adedeji, Ismaila Shittu, Emmanuel Obishakin, Maurice Nanven, Ladan Suleiman, Daniel Okomah, Visa Tyakaray, Damilola Kolade, Adesola Yinka-Ogunleye, Saleh Muhammad, Clint N. Morgan, Audrey Matheny, Yoshinori Nakazawa, Andrea McCollum, Jeffrey B. Doty

Author affiliations: National Veterinary Research Institute, Vom, Nigeria (C. Meseko, A. Adedeji, I. Shittu, E. Obishakin, M. Nanven); Federal Ministry of Agriculture and Rural Development, Abuja, Nigeria (L. Suleiman, D. Okomah); African Field Epidemiology Network, Abuja (V. Tyakaray); Nigeria Centre for Diseases Control, Abuja (D. Kolade, A. Yinka-Ogunleye); US Centers for Disease Control and Prevention, Abuja (S. Muhammad); US Centers for Disease Control and Prevention, Atlanta, Georgia, USA (C.N. Morgan, A. Matheny, Y. Nakazawa, A. McCollum, J.B. Doty)

DOI: https://doi.org/10.3201/eid2902.221411

To investigate animal reservoirs of monkeypox virus in Nigeria, we sampled 240 rodents during 2018–2019. Molecular (real-time PCR) and serologic (IgM) evidence indicated orthopoxvirus infections, but presence of monkeypox virus was not confirmed. These results can be used to develop public health interventions to reduce human infection with orthopoxviruses.

Resurgence of zoonotic agent monkeypox virus (MPXV); genus *Orthopoxvirus*) in Nigeria since 2017 calls attention to the need to identify the source of primary transmission at the human–animal interface. Results of previous ecologic investigations of the animal reservoir of MPXV have been inconclusive (*1*,*2*). However, molecular and serologic evidence suggest that potential reservoirs are rope squirrels (*Funisciurus*), sun squirrels (*Heliosciurus*), African pouched rats (*Cricetomys*), and dormice (*Graphiurus*) (*3*–*5*). In Nigeria, investigations into the ecology and natural history of MPXV and its reservoir are limited (*4*). Cases of mpox in humans (formerly monkeypox) in Nigeria were reported in 1971 and 1978 but not again until 2017. During 2017–August 2022, a total of 503 cases of MPXV were confirmed, and evidence of exportation from Nigeria is a public health concern (*6*,*7*). In addition to vaccinating humans, another feasible public health intervention would be identifying and avoiding spillover from animals (*8*).

As a preliminary step in identifying the putative MPXV animal reservoir in Nigeria, we sampled 240 rodents during 2018–2019. Humane capture and sampling followed protocols approved by the National Veterinary Research Institute and the Centers for Disease Control and Prevention Animal Care and Use Committees (AEC/03/53/18).

We captured and sampled 240 rodents by using a mixture of Tomahawk (https://www.livetrap.com), Sherman (https://www.shermantraps.com), and snap traps in 4 locations: Afi Mountain rain forest, Cross-River state (n = 56); Okomu National Park, Edo state (n = 61); Yenagoa Forest, Bayelsa state (n = 44); and urban and periurban locations associated with recent human cases in Port Harcourt, River state (n = 79). Before collecting blood and euthanizing the rodents, we anesthetized them with inhalant halothane and examined them visually for the presence of poxlike lesions or other signs of illness. If lesions were observed, as seen in animal N198 (Figure), we collected samples from the lesion site. After euthanizing the rodents, we performed necropsies and collected internal organs (e.g., lung, heart, liver, kidney, spleen, skin). For animals not euthanized (as determined for conservation reasons by park officers), we collected only blood and oral and anal swab samples. We extracted DNA by using a MagMAX magnetic processor (ThermoFisher Scientific, https://www.thermofisher.com) and conducted real-time PCR on all available samples by using OPXV-generic and MPXV-specific assays (*9*). We used ELISA to analyze serum and dried blood spots (*5*) and considered samples that were reactive at 1:100 and 1:200 dilutions to be positive.

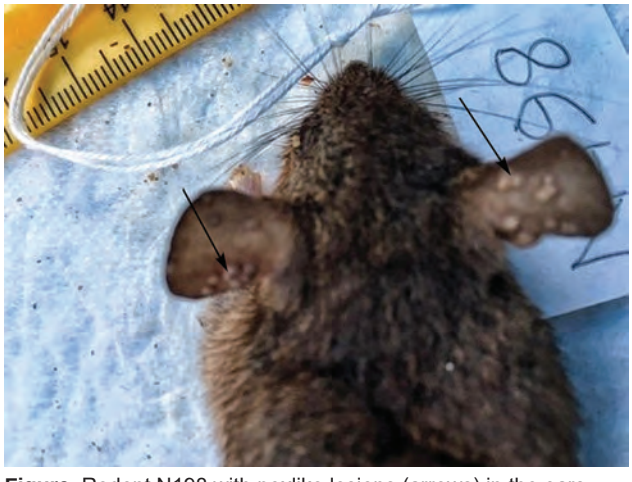

Figure. Rodent N198 with poxlike lesions (arrows) in the ears but negative for orthopoxvirus by quantitative PCR and ELISA, sampled in study of orthopoxvirus infections in rodents, Nigeria, 2018–2019.

Table. Samples positive for OPXV in study of OPXV infections in rodents, Nigeria, 2018–2019*

Rodent species	Animal no.	Sample type	OPXV DNA	OPXV IgG
Mus baoulei	NG114	Skin biopsy	+	Not applicable
M. baoulei	NG114	Spleen and kidney	+	Not applicable
M. baoulei	NG114	Dried blood spots	+	–
Praomys	NG112	Tissues, dried blood spots	–	+
Rattus rattus	NG173	Tissues, dried blood spots	–	+

*By quantitative PCR and ELISA. OPXV, orthopoxvirus.

Animal NG114 (*Mus baoulei*), collected from Okomu National Park, Edo, was positive by generic OPXV PCR of skin, spleen, kidney and by dried blood spot but negative for OPXV antibodies by ELISA**.** All samples from that animal were negative by MPXV-specific assay. Samples from all other animals were negative by PCR (OPXV-generic and MPXV-specific). Samples from 2 rodents, NG112 (*Praomys sp.*) and NG173 (*Rattus rattus*), collected in Okomu National Park on December 12, 2018, and from Port Harcourt, River state (prison environment) on July 5, 2019, were positive by ELISA (OPXV IgG). Khodakevich et al. (*4*) detected OPXV antibodies or "MPXV–specific" antibodies in rodents (including *Praomys*) and nonhuman primates in areas where human cases had been reported. A similar investigation in the Democratic Republic of the Congo, conducted in 2012, 2013, and 2015, detected OPXV IgG in 6 rodents, but no rodent was positive by PCR (*9*). Identifying an unknown OPXV via molecular diagnostics (PCR) from a *M. baoulei* mouse (NG114) in Okomu and confirmation of ELISA-positive rodents from both urban and rural sites (Port Harcourt and Okomu) indicate the potential role of these animals in the circulation and transmission of OPXVs. The IgG-positive *R. rattus* rat captured at a prison in Port Harcourt indicates potential OPXV exposure of prisoners and of the local population in urban areas through inconspicuous contact with peridomestic rodents.

Our laboratory analyses showed molecular and serologic evidence of OPXV infections (Table); however, they did not confirm presence of MPXV in the animal samples. Because the ELISA cannot distinguish between different species of OPXVs, we could not determine if the 2 animals with OPXV IgG (NG112 and NG173) were exposed to MPXV or another OPXV circulating in small mammals in Nigeria. Detection of diverse OPXVs in rodents in Nigeria can be used to develop public health interventions to reduce human infection with orthopoxviruses, including MPXV.

Acknowledgment

We thank the Federal and State Ministries of Agriculture, Health and the Environment for their administrative support.

The US Centers for Disease Control and Prevention funded the Monkeypox Animal Reservoir study in Nigeria. The field team (One Health) includes members from the National Veterinary Research Institute, Nigeria Centre for Disease Control, Federal Ministry of Agriculture and Rural Development, and African Field Epidemiology Network.

About the Author

Dr. Meseko is a veterinarian and virologist with the National Veterinary Research Institute, Vom, Nigeria. He coordinates the One Health team for field and laboratory investigation of animal reservoirs of MPXV in Nigeria.

Reference

1. Khodakevich L, Jezek Z, Messinger D. Monkeypox virus: ecology and public health significance. Bull World Health Organ. 1988;66:747–52.
2. Damon IK. Status of human monkeypox: clinical disease, epidemiology and research. Vaccine. 2011;29(Suppl 4):D54–9. https://doi.org/10.1016/j.vaccine.2011.04.014
3. Reynolds MG, Doty JB, McCollum AM, Olson VA, Nakazawa Y. Monkeypox re-emergence in Africa: a call to expand the concept and practice of One Health. Expert Rev Anti Infect Ther. 2019;17:129–39. https://doi.org/10.1080/14787210.2019.1567330
4. Khodakevich L, Jezek Z, Kinzanzka K. Isolation of monkeypox virus from wild squirrel infected in nature. Lancet. 1986;1:98–9. https://doi.org/10.1016/S0140-6736(86)90748-8
5. Doty JB, Malekani JM, Kalemba LN, Stanley WT, Monroe BP, Nakazawa YU, et al. Assessing monkeypox virus prevalence in small mammals at the human-animal interface in the Democratic Republic of the Congo. Viruses. 2017;9:283. https://doi.org/10.3390/v9100283
6. Alakunle E, Moens U, Nchinda G, Okeke MI. Monkeypox virus in Nigeria: infection biology, epidemiology, and evolution. Viruses. 2020;12:1257. https://doi.org/10.3390/v12111257
7. Mauldin MR, McCollum AM, Nakazawa YJ, Mandra A, Whitehouse ER, Davidson W, et al. Exportation of monkeypox virus from the African continent. J Infect Dis. 2022;225:1367–76. https://doi.org/10.1093/infdis/jiaa559
8. Nolen LD, Osadebe L, Katomba J, Likofata J, Mukadi D, Monroe B, et al. Introduction of monkeypox into a community and household: risk factors and zoonotic reservoirs in the Democratic Republic of the Congo. Am J Trop Med Hyg. 2015;93:410–5. https://doi.org/10.4269/ajtmh.15-0168
9. Li Y, Olson VA, Laue T, Laker MT, Damon IK. Detection of monkeypox virus with real-time PCR assays. J Clin Virol. 2006;36:194–203. https://doi.org/10.1016/j.jcv.2006.03.012

Address for correspondence: Clement Meseko, National Veterinary Research Institute, P.B.M. 01 Vom Plateau, Nigeria; email: cameseko@yahoo.com, clement.meseko@nvri.gov.ng

Occupational Monkeypox Virus Transmission to Healthcare Worker, California, USA, 2022

Jemma Alarcón, Moon Kim, Nora Balanji, Anissa Davis, Francisca Mata, Abraar Karan, Lauren E. Finn, Annette Guerrero, McKailey Walters, Dawn Terashita, Sharon E. Balter

Author affiliations: Centers for Disease Control and Prevention, Atlanta, Georgia, USA (J. Alarcón); Los Angeles County Department of Public Health, Los Angeles, California, USA (J. Alarcón, M. Kim, A. Karan, L.E. Finn, A. Guererro, D. Terashita, S.E. Balter); Long Beach Department of Health and Human Services, Long Beach, California, USA (N. Balanji, A. Davis, M. Walters); APLA Health, Los Angeles (F. Mata)

DOI: https://doi.org/10.3201/eid2902.221750

Risk for transmission of monkeypox virus (MPXV) (clade IIb) to healthcare workers (HCWs) is low. Although many cases have been reported among HCW, only a few have been occupationally acquired. We report a case of non–needle stick MPXV transmission to an HCW in the United States.

Risk for transmission of monkeypox virus (MPXV) (clade IIb), the causative agent of mpox (formerly monkeypox), to healthcare workers (HCWs) is considered to be low, and although many cases have been reported among HCW, only a few have been occupationally acquired (*1*,*2*). We report a case of non–needle stick MPXV transmission to an HCW in California, USA.

The HCW was a 40-year-old female physician with a medical history significant for rheumatoid arthritis (treated with etanercept). In August 2022, she experienced a prodrome of myalgia and fatigue, followed by a mild headache. Two days later, she noticed a small, raised skin lesion on her left middle finger (Figure 1). The skin lesion progressed to a blister and developed umbilication; it grew to 1.5–2 cm, and a swab sample for MPXV was collected on day 6 of illness. On days 9 and 10 after symptom onset, the HCW experienced fever for 48 hours, followed by a cough and sore throat. A total of 10 skin lesions developed throughout her body, including her right arm, ankles, lateral breast, back of neck, and upper back. She received a 2-week course of oral tecovirimat, experienced no complications, and completely recovered (Figure 2).

The Los Angeles County Department of Public Health and the Long Beach Department of Health and Human Services conducted a contact investigation. This activity was reviewed by the Centers for Disease Control and Prevention (CDC) and was conducted in accordance with applicable federal law and CDC policy.

The HCW works as a physician at 2 clinics that primarily serve LGBTQ+ and HIV-positive patients. She sees 15 patients/day and regularly sees patients with mpox, during which she wears full personal protective equipment (PPE) (N95 respirator, a gown, and eye protection). During the presumed incubation period, the HCW interacted with 2 patients

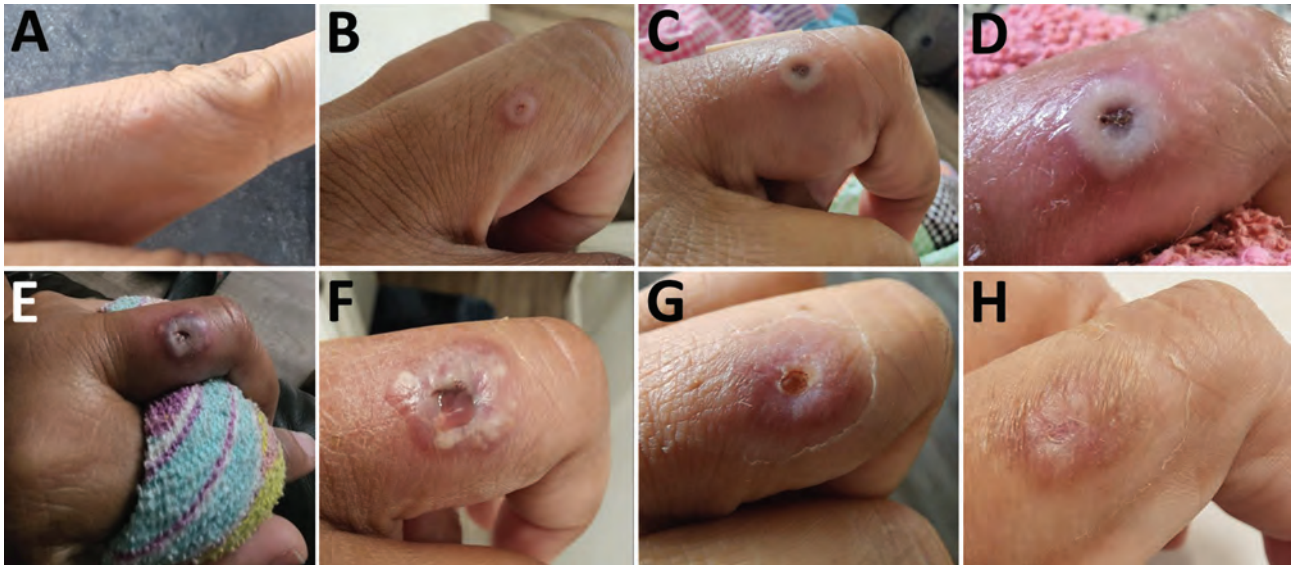

Figure 1. Evolution of finger skin lesions in healthcare worker occupationally exposed to monkeypox virus, California, USA, 2022. A) August 29; B) August 31; C) September 4; D) September 5; E) September 6; F) September 7; G) September 24; H) September 28.

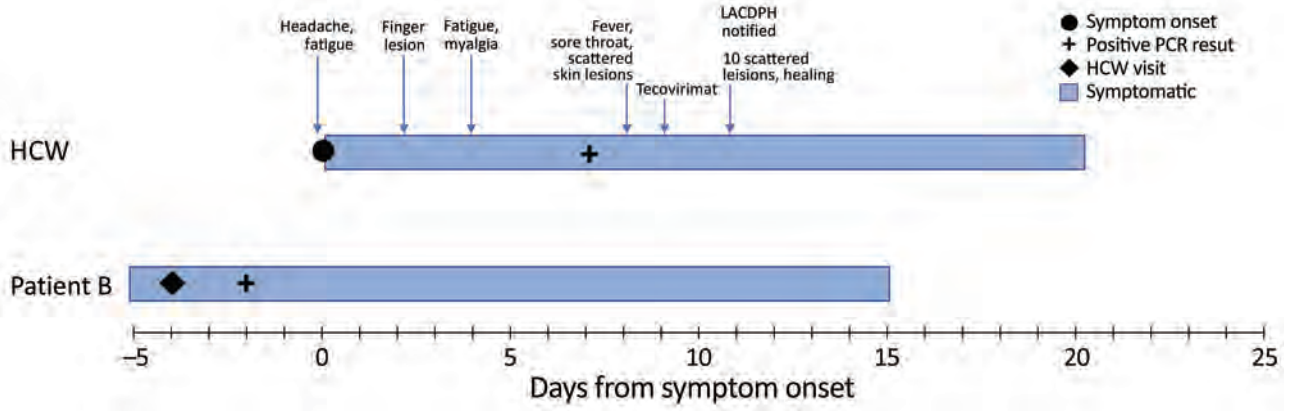

Figure 2. Timeline of symptom onset, testing, treatment, and public health interventions in response to a case of occupationally acquired mpox in an HCW, California, USA, 2022. Patients A and B were treated by the HCW during the presumed incubation period of her infection; however, course of illness for patient A is not shown because the HCW's contact with patient A was >21 days before symptom onset. HCW, healthcare worker; LACDPH, Los Angeles County (California) Department of Public Health.

(patients A and B) who did not undergo triage per clinic protocols for suspected infection with MPXV but, according to the HCW's interview, had symptoms concerning for MPXV infection. The HCW saw patient A 29 days before her own symptom onset. She spent 15 minutes with the patient while wearing a surgical mask and gloves. When the patient disclosed symptoms concerning for mpox, the HCW left the examination room and donned PPE before swabbing the patient's lesions. Samples from patient A tested positive for MPXV. The HCW saw patient B 4 days before her symptom onset. She spent 5 minutes with the patient while wearing a surgical mask and gloves. When the patient disclosed mpox symptoms, the HCW left the room and donned PPE before swabbing the patient's lesions. Samples from patient B tested positive for MPXV.

Of 159 other patients seen by the HCW during the 21 days before her symptom onset, only 3 had been tested for MPXV per database cross-reference, of which 2 tested negative. The patient that tested positive had been seen by the HCW 4 days before the HCW's symptom onset, and all lesions had healed by the visit date. Outside the workplace, investigation of the HCW's contacts identified 1 high-risk (household) contact, 1 intermediate-risk contact, and 1 low-risk contact. High-risk and intermediate-risk contacts were offered postexposure prophylaxis.

A site visit to the outpatient visit indicated that it has 6 examination rooms, including 1 isolation room. No sharps injuries were documented while the HCW was at clinic. The examination room is sanitized after each patient encounter. The main disinfecting products used are CaviCide disinfectant cleaner wipes and spray (Clorox, https://www.clorox.com; EPA List Q, contact time 3 min). Patients and staff share 2 gender-neutral bathrooms, which along with common areas are cleaned by building maintenance staff in the evenings. We notified 17 patients and 23 clinic staff with low-risk exposure to the HCW via calls and letters. Of the 23 staff members, 5 received postexposure prophylaxis.

Limitations to this report include lack of acquiring phylogenetic match with contacts, no swabbing of surfaces in the clinic bathrooms or patient rooms, and no identification of secondary cases. In a previous report of occupationally acquired MPXV by HCWs in Brazil, transmission might have occurred via fomites or surface contamination during specimen collection in the patient's home (*3*). For the HCW reported here, MPXV infection could have been acquired through inadvertent contamination during specimen collection, contact with contaminated environmental surfaces in the examination room or bathroom, or unrecognized skin contamination during glove doffing.

In Los Angeles County, HCWs who care for patients with suspected or confirmed orthopoxvirus infections, including clinicians and environmental services personnel, are now eligible for vaccination against MPXV. CDC provides guidance for specimen collection and proper PPE (*4*). In 1 study, only 23% of exposed HCWs wore all recommended PPE; but despite low adherence, no HCW had mpox develop during the 21-day incubation period (*2*). Although the risk to HCWs in the United States continues to be very low, it is crucial to continue public health outreach, infection prevention, and training of HCWs to prevent MPXV transmission in healthcare settings, especially during specimen collection (*5*).

About the Author

Dr. Alarcón is an Epidemic Intelligence Service Officer with the CDC, assigned to the Los Angeles County Department of Public Health. She is a family medicine physician working to protect and improve the health of vulnerable populations.

References

1. California Department of Public Health. Healthcare provider advisory: guidance for safe specimen collection from monkeypox (MPX) lesions: reminder to not de-roof lesions and not use sharps [cited 2022 Oct 17]. https://www.cdph.ca.gov/Programs/OPA/Pages/CAHAN/Healthcare-Provider-Advisory-Guidance-for-Safe-Specimen-Collection-From-MPX-Lesions.aspx
2. Marshall KE, Barton M, Nichols J, de Perio MA, Kuhar DT, Spence-Davizon E, et al.; Colorado Healthcare Personnel Monitoring Team. Health care personnel exposures to subsequently laboratory-confirmed monkeypox patients—Colorado, 2022. MMWR Morb Mortal Wkly Rep. 2022;71:1216–9. https://doi.org/10.15585/mmwr.mm7138e2
3. Salvato RS, Rodrigues Ikeda ML, Barcellos RB, Godinho FM, Sesterheim P, Bitencourt LCB, et al. Possible occupational infection of healthcare workers with monkeypox virus, Brazil. Emerg Infect Dis. 2022;28:2520–3. https://doi.org/10.3201/eid2812.221343
4. Centers for Disease Control and Prevention. Guidelines for collecting and handling specimens for monkeypox testing [cited 2022 Oct 18]. https://www.cdc.gov/poxvirus/monkeypox/clinicians/prep-collection-specimens.html
5. Centers for Disease Control and Prevention. Infection prevention and control of monkeypox in healthcare settings [cited 2022 Oct 17]. https://www.cdc.gov/poxvirus/monkeypox/clinicians/infection-control-healthcare.html

Address for correspondence: Gemma Alarcon, County of Los Angeles, Department of Public Health, Acute Communicable Disease Control, 313 No. Figueroa St, #202, Los Angeles, CA 90012, USA; email: vqh4@cdc.gov, jalarcon2@ph.lacounty.gov

Familial Monkeypox Virus Infection Involving 2 Young Children

Pascal Del Giudice, Agnes Fribourg, Laurent Roudiere, Juliette Gillon, Anne Decoppet, Mathieu Reverte

Author affiliations: Centre Hospitalier Intercommunal de Fréjus-Saint-Raphaël, Fréjus, France (P. Del Giudice, A. Fribourg, L. Roudiere, J. Gillon, M. Reverte); Agence Régionale de Santé, Toulon, France (A. Decoppet)

DOI: https://doi.org.10.3201/eid2902.221674

We report intrafamilial transmission of monkeypox virus to all members of a family (father, mother, and 2 children). Case reports in young children have been extremely rare during the 2022 mpox outbreak. Their clinical signs were mild, and clinical diagnosis would be difficult without knowledge of the father's monkeypox virus infection.

Monkeypox virus (MPXV) is a zoonotic orthopox virus. An outbreak of MPXV infections emerged in the spring of 2022 outside Africa, mainly in Europe and the United States, such that on July 23, 2022, the World Health Organization declared the outbreak to be a public health emergency of international concern. During this outbreak, MPXV spread has disproportionately affected gay or bisexual men or other men who have sex with men, which suggests transmission through sexual or intimate contact. However, in August 2022, we observed intrafamilial transmission of the virus to all members of a family (father, mother, and 2 children) in France.

The father, a 30-year-old-man, showed a few papular pustules on his body, including his penis. The pustules began appearing on July 17, 2022. A pustule sample was tested for MPXV and showed a positive PCR result. The wife of the man showed a few pustules on August 2 that were later confirmed to be positive for MPXV by PCR. She had no mucous signs. Both persons were HIV negative.

The couple and their 2 young daughters went on vacation to a campsite in southern France on August 6. Their 4-year-old daughter had a fever (temperature 38°C) and a skin eruption that began on August 5, which consisted of 3 types of lesions: an umbilical pustule (Figure, panel A), papular pustules on an erythematous basis (Figure, panel B), and a disseminated faint erythematous macula (Figure, panels C, D). She also had a bilateral conjunctivitis but no lymphadenopathy or mucosal lesions.

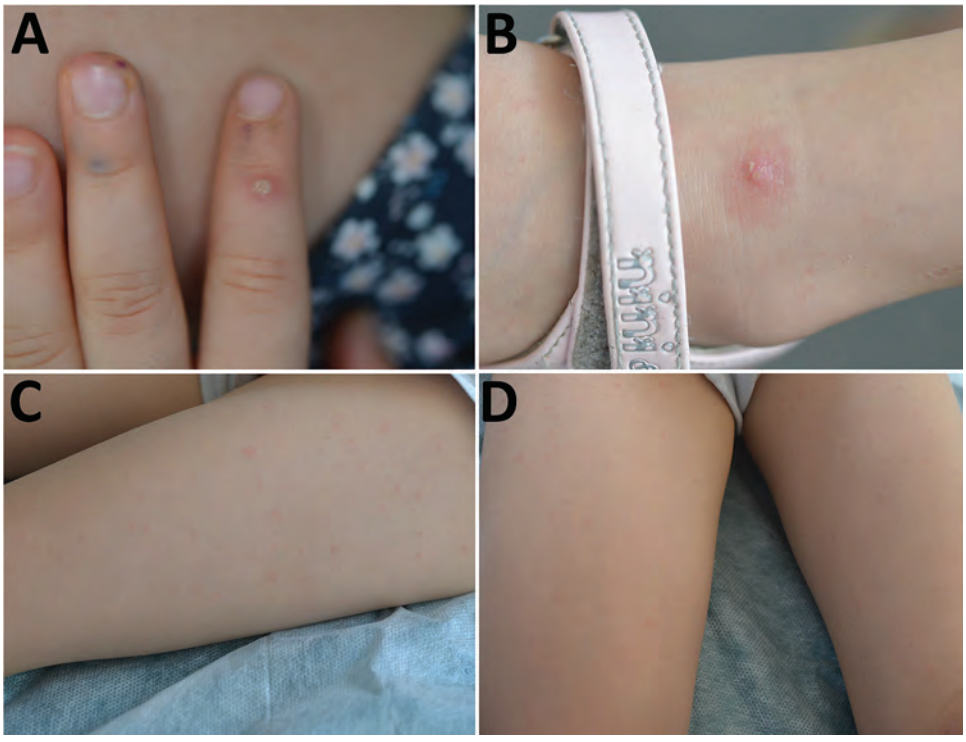

Figure. Monkeypox virus lesions for the 4-year old daughter in a family (father, mother, 2 children) infected with the virus, August 6, 2022. A) Umbilical pustule on pulp of the finger; B) papulopustule on the ankle; C, D) faint erythematous rash on the thighs.

On August 9, her 7-year-old sister showed ≈10 asymptomatic micropapular pustules on a discrete erythematous basis (Appendix Figure 1, https://wwwnc.cdc.gov/EID/article/29/2/22-1674-App1.pdf). She had no fever, mucosal lesion, or lymphadenopathy.

The family was residing at a campsite in southern France, where there is a high burden of *Aedes albopictus* mosquitoes. They were suspected of having either MPXV infection or *Aedes* sp. mosquito bites. A skin scraping from the skin of a micropapular pustule was positive for MPXV by PCR. For all family members, only 1 lesion/person was sampled. Onset symptoms and positive PCR results are shown in the timeline (Appendix Figure 2). The family received isolation instructions and returned home on August 11. The outcome was favorable for all 4 persons. There were no secondary cases at the campsite.

During the ongoing outbreak, cases of MPXV infection in young children have been extremely rare. US data from the Centers for Disease Control and Prevention as of October 7, 2022, reported 26,577 cases in 28 patients (0.1%) <12 years of age (*1*,*2*). Those data were confirmed in Europe. As of August 3, 2022, among 4,663 laboratory-confirmed cases of MPXV infection reported in Spain, only 4 (0.1%) were in children <4 years of age (7, 10, and 13 months, and 3 years) and 12 were in adolescents 13–17 years of age (*3*). As of August 23, 2022, a total of 41 countries in the World Health Organization European Region have reported 21,098 cases, of which 15 (0.07%) were in persons <15 years of age (*4*).

Intrafamilial transmission to all family members including both children, also appears extremely rare in the 2022 outbreak. We assume that the transmission route was through household direct skin-to-skin contact with their parents.

The clinical signs shown by the children were mild, and clinical diagnosis would be extremely difficult in the absence of knowledge of the MPXV infection of the father. Case reports in young children have been extremely rare in this outbreak (*5*–*7*). Thus, a dermatologic description is lacking in this population. The 2 children in this report had mild general signs. Skin lesions consisted of a few umbilical pustules or papulopustules similar to those reported (*8*–*10*). However, the children also had discrete micropapular pustules on an erythematous basis similar to mosquito bites and a faint erythematous rash. Such skin lesions have rarely been reported in children or adults (*8*–*10*).

Acknowledgment

We thank Moussa Hajer for editing the figures, proofreading, and submitting this manuscript.

About the Author

Dr. Del Giudice is a physician in the Infectious Diseases and Dermatology Unit at Bonnet Hospital, Fréjus, France. His primary research interest is skin infections.

References

1. Centers for Disease Control and Prevention. Monkeypox cases by age and gender, race/ethnicity, and symptoms [cited 2022 Dec 1]. https://www.cdc.gov/poxvirus/monkeypox/response/2022/demographics.html
2. Hennessee I, Shelus V, McArdle CE, Wolf M, Schatzman S,Carpenter A, et al.; California Department of Public Health Monkeypox Pediatric Working Group; CDC Monkeypox Pediatric Working Group. Epidemiologic and clinical features of children and adolescents aged <18 years with monkeypox—United States, May 17–September 24, 2022. MMWR Morb Mortal Wkly Rep. 2022;71:1407–11. https://doi.org/10.15585/mmwr.mm7144a4
3. Aguilera-Alonso D, Alonso-Cadenas JA, Roguera-Sopena M, Lorusso N, Miguel LG, Calvo C. Monkeypox virus infections in children in Spain during the first months of the 2022 outbreak. Lancet Child Adolesc Health. 2022;6:e22–3. https://doi.org/10.1016/S2352-4642(22)00250-4
4. Vaughan AM, Cenciarelli O, Colombe S, Alves de Sousa L, Fischer N, Gossner CM, et al. A large multi-country outbreak of monkeypox across 41 countries in the WHO European Region, 7 March to 23 August 2022. Euro Surveill. 2022;27:2200620. https://doi.org/10.2807/1560-7917.ES.2022.27.36.2200620
5. Tutu van Furth AM, van der Kuip M, van Els AL, Fievez LC, van Rijckevorsel GG, van den Ouden A, et al. Paediatric monkeypox patient with unknown source of infection, the Netherlands, June 2022. Euro Surveill. 2022;27:2200552. https://doi.org/10.2807/1560-7917.ES.2022.27.29.2200552
6. Ramnarayan P, Mitting R, Whittaker E, Marcolin M, O'Regan C, Sinha R, et al.; NHS England High Consequence Infectious Diseases (Airborne) Network. Neonatal monkeypox virus infection. N Engl J Med. 2022;387:1618–20. https://doi.org/10.1056/NEJMc2210828
7. Fuente SM, Nava FB, Valerio M, Veintimilla C, Aguilera-Alonso D. A call for attention: pediatric monkeypox case in a context of changing epidemiology. Pediatr Infect Dis J. 2022;41:e548–9. https://doi.org/10.1097/INF.0000000000003695
8. Thornhill JP, Barkati S, Walmsley S, Rockstroh J, Antinori A, Harrison LB, et al.; SHARE-net Clinical Group. Monkeypox virus infection in humans across 16 countries, April–June 2022. N Engl J Med. 2022;387:679–91. https://doi.org/10.1056/NEJMoa2207323
9. Girometti N, Byrne R, Bracchi M, Heskin J, McOwan A, Tittle V, et al. Demographic and clinical characteristics of confirmed human monkeypox virus cases in individuals attending a sexual health centre in London, UK: an observational analysis. Lancet Infect Dis. 2022;22:1321–8. https://doi.org/10.1016/S1473-3099(22)00411-X
10. Tarín-Vicente EJ, Alemany A, Agud-Dios M, Ubals M, Suñer C, Antón A, et al. Clinical presentation and virological assessment of confirmed human monkeypox virus cases in Spain: a prospective observational cohort study. Lancet. 2022;400:661–9. https://doi.org/10.1016/S0140-6736(22)01436-2

Address for correspondence: Pascal Del Giudice, Infectiology and Dermatology Unit, Centre Hospitalier Intercommunal de Fréjus-Saint-Raphaël, Fréjus, France; email: pascal.delgiudice@chi-fsr.fr

Dirofilaria immitis in Dog Imported from Venezuela to Chile

Cristian A. Alvarez Rojas,[1] Beatriz Cancino-Faure,[1] Pablo Lillo, María Luisa Fernández, Alejandro Piñeiro González, Alonso Flores Ramírez

Author affiliations: Escuela de Medicina Veterinaria, Facultad de Agronomía e Ingeniería Forestal, Facultad de Ciencias Biológicas y Facultad de Medicina, Pontificia Universidad Católica de Chile, Santiago, Chile (C.A. Alvarez Rojas, P. Lillo); Laboratorio de Microbiología y Parasitología, Departamento de Ciencias Preclínicas, Facultad de Medicina, Universidad Católica del Maule, Talca, Chile (B. Cancino-Faure, A. Piñeiro González); Hospital Veterinario Mi Mascota, Santiago (M.L. Fernández); Sociedad Chilena de Cardiología Veterinaria, Santiago (A. Flores Ramírez)

DOI: https://doi.org/10.3201/eid2902.221427

We report a case of *Dirofilaria immitis* nematode infection in a dog imported from Venezuela that had been living for 2 years in Santiago, Chile, where this parasite had not been reported before. Our findings warrant surveillance for all dogs imported to Chile, given that suitable conditions exist for establishing this parasite.

Dirofilaria immitis, a species of zoonotic parasitic nematode transmitted by mosquitoes, causes canine dirofilariosis. These nematodes are usually found in countries with temperate and tropical climates and are endemic throughout Europe and in the southeastern regions of Asia and Africa (*1*). In the Americas, *D. immitis* nematodes are present in all countries and territories except Chile and Uruguay (*2*). We report a case of a female dog born in Venezuela and imported to Santiago, Chile, where she lived for 2 years before having *D. immitis* infection diagnosed in January 2022.

The dog was a 5.5-year-old Shar-pei who was brought to 2 veterinary clinics in Santiago during December 2021–January 2022. The initial cause of the consultation was vulvar discharge evolving to vomiting, melena, and general discomfort. Initially, the dog's health improved after treatment with enrofloxacin (5 mg/kg). However, the animal's condition deteriorated after 1 week (in January 2022). Ultrasound examination showed the presence of a fetus for which no heartbeat was detected. Blood work showed severe anemia, kidney failure, and the presence of microfilariae at the blood smear examination. An echocardiogram examination showed signs compatible

[1]These first authors contributed equally to this article.

with tricuspid valve insufficiency, but no nematodes were observed. A blood transfusion was performed before surgery to remove the uterus, which showed maceration of the fetus. The dog was euthanized days after surgery.

We used 1 mL of a blood sample collected with EDTA from the dog to perform the modified Knott's test; we measured microfilariae under microscopic examination by using Leica Application Suite 3.4.0 software (Leica Microsystems, https://www.leica-microsystems.com). The average length of 10 microfilariae was 285.6 µm and average width was 6.5 µm (Table), which agrees with findings by Foreyt (*3*), who reported a length of 270–325 µm and a width of 6.7–7.0 µm for *D. immitis* microfilariae. However, data on the length and width of microfilariae reported in the literature vary considerably (*4*). Amplification and sequencing of DNA from canine microfilariae are required to correctly identify the species causing the infection (*5*,*6*). Therefore, we centrifuged an aliquot (500 µL) of the fresh blood sample with EDTA and isolated DNA from the sediment by using the E.Z.N.A. Tissue DNA Kit (Omega Bio-Tek, https://www.omegabiotek.com) according to the manufacturer's instructions. We used the DNA as a template for PCR with GoTaq DNA Polymerase (Promega, https://www.promega.com) and amplified a section of the mitochondrial cytochrome oxidase I (COI) with the primers COIintF (TGATTGGTGGTTTTGGTAA) and COIintR (ATAAGTACGAGTATCAATATC) (*5*) and a section of the 12S rDNA with the primers 12SF (GTTCCAGAATAATCGGCTA) and 12SR (ATTGACGGATG(AG)TTTGTACC) (*6*). We sequenced PCR products in both directions with the same PCR primers in Macrogen Online Sequencing Order System (https://dna.macrogen.com). We used the acquired sequences as input in BLAST (http://blast.ncbi.nlm.nih.gov) for comparison. The sequence for the *cox1* (OP811228) showed 100% homology with *D. immitis* entries deposited in GenBank from Spain (accession no. LC107816), Slovenia (accession no. OP494255), Hungary (accession no. KM452920), Thailand (accession no. MW577348), and China (accession no. EU159111). Moreover, the sequence acquired from the 12S rDNA (OP819559) showed 100% homology with GenBank entries identified as *D. immitis* from French Guiana (accession nos. MT252014–24), Myanmar (accession nos. OL714336–40), Thailand (accession no. MW512514), Brazil (accession nos. MZ678855–926), France (accession nos. MZ435877–83), and China (accession no. EU182327). Therefore, both sequences confirmed the diagnosis of *D. immitis* infection.

Table. Length and width of 10 microfilariae fixed in formalin and measured using the modified Knott's test, in a dog imported from Venezuela with *Dirofilaria immitis* infection, Chile, January 2022

Microfilariae	Length, µm	Width, µm
1	287.8	6.0
2	295.5	7.2
3	280.2	7.6
4	281.8	6.6
5	277.7	7.3
6	295.7	6.1
7	275.3	5.4
8	284.0	6.2
9	289.7	6.6
10	288.9	6.0
Average	285.6	6.5

The dog was brought into Chile from Venezuela 2 years before the incidental finding of microfilariae in an examination of blood prompted by complications caused by a uterine infection and kidney failure. This finding is relevant because, in recent years, human migration from Venezuela into Chile and other Latin America countries has risen, and the role of pets transported with humans as a reservoir of vector-borne pathogens has not been investigated. More than 6 million people have left Venezuela because of ongoing economic, political, and humanitarian crises (*7*); of those, ≥448,138 live in Chile (*8*). No record exists of how many dogs have entered Chile from Venezuela, and no requirement exists for testing for *D. immitis* infection in dogs arriving in Chile. Little information is available regarding the prevalence of *D. immitis* infection in Venezuela; an older report indicates a 4%–29% prevalence of *D. immitis* infection in hunting dogs in Aragua State based on analysis using the modified Knott´s test (*9*), and a second report indicates a 15.2% prevalence in Sucre State based on analysis using the modified Knott's test and antigen detection (*10*).

Unofficial reports from veterinarians in Santiago have mentioned detecting structures resembling adult specimens of nematodes in echocardiograms of some dogs brought into Chile from Venezuela. Autochthonous cases may occur soon in Chile, where mosquitoes capable of acting as vectors are present and suitable climatic conditions for developing the transmission cycle exist. Furthermore, the sizeable population of free-roaming dogs in Chile can act as a reservoir for the parasite. Since *D. immitis* nematodes are not endemic in Chile, little knowledge of the infection exists among veterinarians. Massive screening of dogs that arrive in Chile from *D. immitis*–endemic countries is urgently needed.

This work was partly funded by the Comisión Nacional de Ciencia y Tecnología of Chile (Fondecyt initiation no. 11180156) and by the Fondos Científicos Purina in Chile.

About the Author

Dr. Alvarez is a veterinarian specializing in parasitology and an assistant professor at the School of Veterinary Medicine, Pontificia Universidad Católica de Chile. His research interests include diagnostic, molecular epidemiology, and control of zoonotic parasites. Dr. Cancino-Faure is an associate professor and researcher at Universidad Católica del Maule. Her research interests include emerging and reemerging vectorborne diseases and transfusion-transmitted infectious diseases.

References

1. McCall JW, Genchi C, Kramer LH, Guerrero J, Venco L. Heartworm disease in animals and humans. Adv Parasitol. 2008; 66:193–285. https://doi.org/10.1016/S0065-308X(08)00204-2
2. Dantas-Torres F, Otranto D. Overview on *Dirofilaria immitis* in the Americas, with notes on other filarial worms infecting dogs. Vet Parasitol. 2020;282:109113. https://doi.org/10.1016/j.vetpar.2020.109113
3. Foreyt WJ. Veterinary parasitology reference manual. 5th edition. New York: John Wiley & Sons; 2013.
4. Magnis J, Lorentz S, Guardone L, Grimm F, Magi M, Naucke TJ, et al. Morphometric analyses of canine blood microfilariae isolated by the Knott's test enables *Dirofilaria immitis* and *D. repens* species-specific and *Acanthocheilonema* (syn. *Dipetalonema*) genus-specific diagnosis. Parasit Vectors. 2013;6:48. https://doi.org/10.1186/1756-3305-6-48
5. Casiraghi M, Anderson TJC, Bandi C, Bazzocchi C, Genchi C. A phylogenetic analysis of filarial nematodes: comparison with the phylogeny of *Wolbachia* endosymbionts. Parasitology. 2001;122:93–103. https://doi.org/10.1017/S0031182000007149
6. Casiraghi M, Bain O, Guerrero R, Martin C, Pocacqua V, Gardner SL, et al. Mapping the presence of *Wolbachia pipientis* on the phylogeny of filarial nematodes: evidence for symbiont loss during evolution. Int J Parasitol. 2004;34:191–203. https://doi.org/10.1016/j.ijpara.2003.10.004
7. UN Refugee Agency and International Organization for Migration. R4V: Regional Interagency Coordination Platform for Refugees and Migrants of Venezuela. 2022 [cited 2022 Jul 27]. https://www.r4v.info
8. Instituto Nacional de Estadísticas (Chile). Estimate of foreigners habitually resident in Chile as of December 31, 2020: methodological report [in Spanish]. 2021 Jul [cited 2022 Jul 27]. https://www.ine.gob.cl/docs/default-source/demografia-y-migracion/publicaciones-y-anuarios/migraci%C3%B3n-internacional/estimaci%C3%B3n-poblaci%C3%B3n-extranjera-en-chile-2018/estimaci%C3%B3n-poblaci%C3%B3n-extranjera-en-chile-2020-metodolog%C3%ADa.pdf
9. D'Alessandro A. Prevalence of *Dirofilaria immitis* (Leidy, 1856) in hunting dogs from Aragua State [in Spanish]. Rev Bras Med Vet. 1971;24:109–30.
10. Guilarte DV, Gómez Martínez E, El Hen F, Guzmán R, Blondell D, Díaz MT, et al. Diagnosis of *Dirofilaria immitis* in Sucre Municipality, Sucre State, Venezuela [in Spanish]. Bol Malariol Salud Ambient. 2011;51:51–8.

Address for correspondence: Cristian A. Alvarez Rojas, Escuela de Medicina Veterinaria, Pontificia Universidad Católica de Chile, Vicuña Mackenna 4860, Macul, Santiago, Chile; email: c.alvarezrojas@uc.cl; Beatriz Cancino-Faure, Laboratorio de Microbiología y Parasitología, Departamento de Ciencias Preclínicas, Facultad de Medicina, Universidad Católica del Maule, Talca, Chile; Avenida San Miguel 3605, Talca, Chile; email: bcancino@ucm.cl.

Relapsing Fever Caused by *Borrelia lonestari* after Tick Bite in Alabama, USA

Laia J. Vazquez Guillamet,[1] Grace E. Marx, William Benjamin, Peter Pappas, Nicole A.P. Lieberman, Kimo Bachiashvili, Sixto Leal, Joshua A. Lieberman

Author affiliations: University of Alabama, Birmingham, Alabama, USA (L.J. Vazquez Guillamet, W. Benjamin, P. Pappas, K. Bachiashvili, S. Leal); Centers for Disease Control and Prevention, Fort Collins, Colorado, USA (G.E. Marx); University of Washington School of Medicine, Seattle, Washington, USA (N.A.P. Lieberman, J.A. Lieberman)

DOI: https://doi.org/10.3201/eid2902.221281

We report an immunocompromised patient in Alabama, USA, 75 years of age, with relapsing fevers and pancytopenia who had spirochetemia after a tick bite. We identified *Borrelia lonestari* by using PCR, sequencing, and phylogenetic analysis. Increasing clinical availability of molecular diagnostics might identify *B. lonestari* as an emerging tickborne pathogen.

Tickborne diseases account for 77% of all vectorborne diseases reported in the United States, and incidence is increasing (*1*). The bacterium *Borrelia lonestari* was first detected in the lone star tick, *Amblyomma americanum,* in 1996 and has since been detected in both ticks and vertebrate hosts in many

[1]Current affiliation: Barcelona Institute for Global Health, Barcelona, Spain.

southeastern states (*2*,*3*). When first discovered, *B. lonestari* was a proposed etiology of southern tick-associated rash illness after *A. americanum* tick bites, but extensive efforts to isolate the bacterium in rash biopsies were unsuccessful (*4*). We report the detection of *B. lonestari* in a patient with febrile illness after a tick bite, demonstrating the potential of this bacterium as a human pathogen.

In late April 2019, a 75-year-old man in Alabama sought care at The Kirklin Clinic of the University of Alabama (Birmingham, AL, USA) for extreme fatigue and relapsing fevers accompanied by chills, sweating, headache, and dizziness that had recurred 1 or 2 times each week for the previous 4 weeks. He had a history of low grade follicular non-Hodgkin lymphoma and was receiving maintenance rituximab therapy. The patient had not traveled out of Alabama for several years but reported that he had removed an attached tick 4 weeks before symptom onset. The patient's symptoms lasted ≈3 months before receiving a diagnosis. During this 3-month period, pancytopenia (lowest hemoglobin 9.3 g/dL; leukocytes, 2×10^9 cells/L; platelets, 120×10^9/L), mildly elevated alkaline phosphatase (216 IU/L), and mild hepatosplenomegaly, noted by computed tomography scan, developed in the patient. Physical examination revealed no skin lesions, lymphadenopathy, or organomegaly. Although the patient was evaluated by the oncology department for suspected recurrent lymphoma, the pathology laboratory reviewed a peripheral blood smear and reported the presence of spirochetes (Appendix Figure, https://wwwnc.cdc.gov/EID/article/29/2/22-1281-App1.pdf). Empirical oral treatment (100 mg doxycycline 2×/d) was initiated immediately. After the first dose, a fever developed in the patient, and he became stuporous. Emergent evaluation for an acute cerebrovascular stroke was negative. The patient returned to his baseline state of health within 24 hours and completed a full 10-day course of doxycycline without additional complications. His pancytopenia resolved in the subsequent months.

A blood sample from the patient was submitted to the University of Washington Medical Center Molecular Microbiology laboratory for broad-range bacterial PCR targeting the V1/V2 domains of the 16S rRNA gene (*5*). PCR yielded a high-quality 497-nt product (GenBank accession no. MN683828) that was sequenced and then classified by using BLAST (https://blast.ncbi.nlm.nih.gov) of sequences from GenBank and the reference laboratory's sequence database. The PCR product had 100% identity to 3 published 16S rRNA gene sequences from *B. lonestari* (GenBank accession nos. AY166715, AAY682921, and U23211) and 99.79% identity to another published 16S rRNA gene sequence from *B. lonestari* (GenBank accession no. AY682920) (Table). Percentage nucleotide identity of the patient sequence to other *Borrelia* spp. with high-confidence identifications was below the laboratory's standard threshold of 99.7% for species-rank classification.

Because the clinical taxonomic classification was determined by a single locus, we retrospectively generated a single-locus phylogeny by using representative V1/V2 16S rRNA gene sequences to evaluate confidence in the clinical result (Figure) (*6*). The V1/V2 16S rRNA phylogenetic analysis appropriately distinguished between *Borrelia* spp. causing Lyme disease and relapsing fever. We observed 2 well-resolved groups, and the bacterial sequence from the patient sample formed a high-confidence clade with *B. lonestari* sequences (bootstrap >0.95) (Figure). The *B. lonestari* clade was well-separated from other homogenous clades of *Borrelia* spp. causing relapsing fever, which had similarly high-confidence bootstrap values. The 2 clades most closely related to *B. lonestari* were *B. miyamotoi* and *B. theileri*, recapitulating published *Borrelia* relapsing fever group phylogeny (*7*).

Table. Summary of BLAST results for 16S rRNA gene sequences used to clinically identify bacteria found in the patient's blood sample in study of relapsing fever caused by *Borrelia lonestari* after tick bite in Alabama, USA*

Species	GenBank accession nos.	% Identity†	Confidence‡
B. lonestari	AY166715, AY682921, U23211	100%	Published
B. lonestari	AY682920	99.79%	Published
B. turicatae	NC_008710, NZ_CP015629	98.38%	RefSeq
B. parkeri	NZ_CP005851	98.38%	RefSeq
B. venezuelensis	MG651649	98.38%	Unpublished
B. coriaceae	NR_114544, NR_121718, NZ_CP005745	98.38%	Type
B. miyamotoi	AB900817, LC164096, LC164108	98.38%	Published
B. hermsii	NC_010673, NR_102957	97.78%	Type

*The V1/V2 hypervariable region of the 16S rRNA bacterial gene was amplified by PCR and BLAST (https://blast.ncbi.nlm.nih.gov) was used to align the patient's sequences with reference sequences in GenBank.
†Percentage identity with the 16S rRNA bacterial sequence from patient blood.
‡Confidence refers to level of curation for each reference sequence identified by using BLAST. Published indicates sequence record associated with peer-reviewed manuscript; RefSeq indicates records from curated GenBank RefSeq database (https://www.ncbi.nlm.nih.gov/refseq); Type indicates sequence from type material; unpublished indicates minimally curated direct submission to GenBank not associated with a peer-reviewed manuscript.

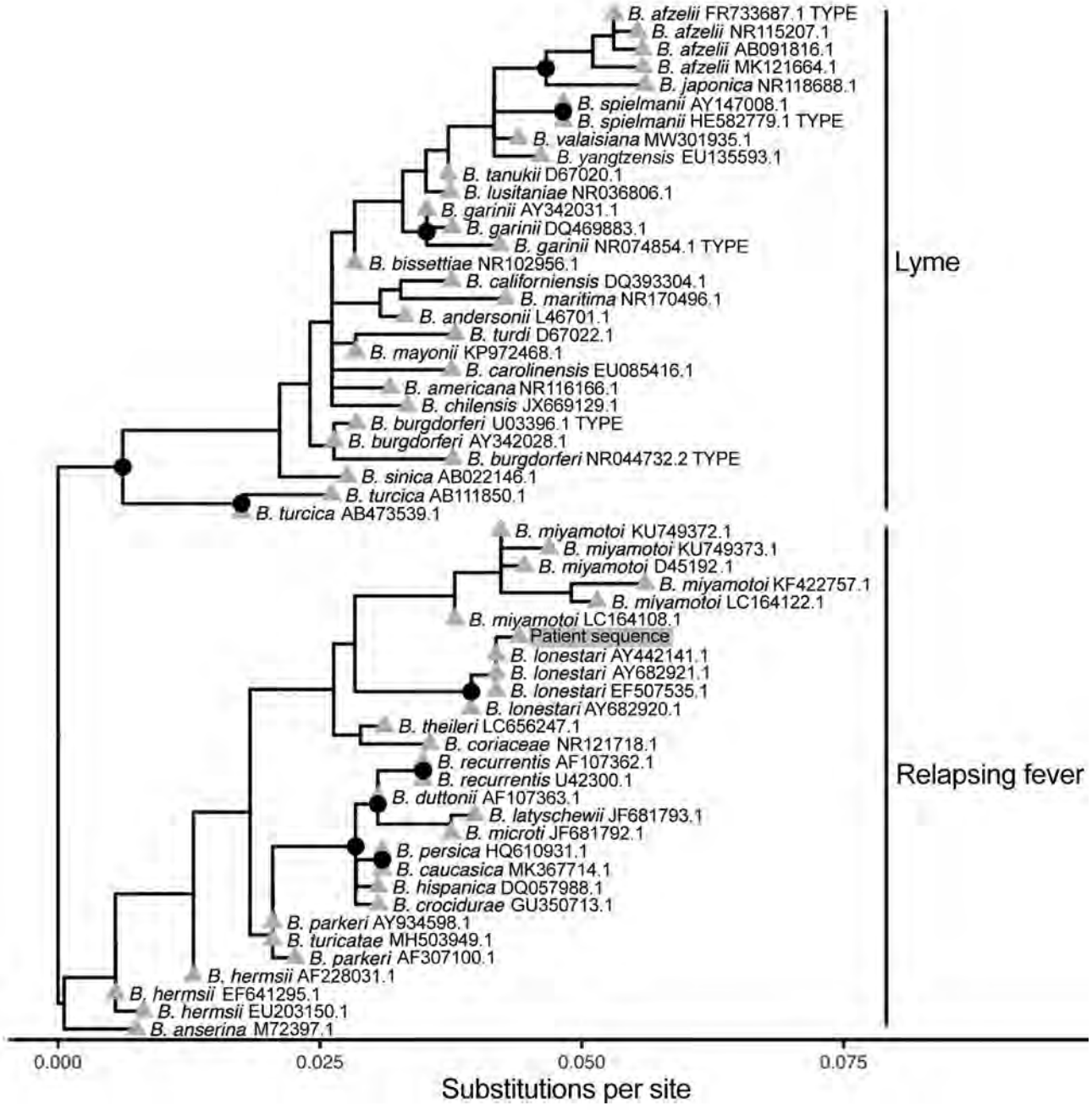

Figure. Phylogenetic analysis of bacterial sequence derived from patient's blood (gray shading) in study of relapsing fever caused by *Borrelia lonestari* after tick bite in Alabama, USA. Phylogenetic tree was constructed from representative V1/V2 regions of 16S rRNA gene sequences from different *Borrelia* spp. known to cause Lyme disease or relapsing fever. GenBank accession numbers are indicated after the species names. The bacterial sequence from the patient sample formed a high-confidence clade with *B. lonestari* sequences and was most closely related to *B. miyamotoi*. Nodes with >95% confidence bootstrap values are labeled with black circles, and branch tips are labeled with gray triangles.

The first reported human case of *B. lonestari* infection was identified in an elderly patient with an erythema migrans-like rash that developed after an *A. americanum* tick bite; PCR identified *B. lonestari* in both a skin biopsy and the removed tick (*8*). In contrast, the patient we report had a longer illness and a pattern of relapsing fevers, absence of erythema migrans, and a possible Jarisch–Herxheimer reaction after initiation of antimicrobial therapy. *B. lonestari* has not been previously reported to cause tickborne relapsing fever, but this manifestation is not unexpected given the close homology to *B. miyamotoi*, the

cause of hard tick relapsing fever (*9*). The patient's immunocompromised condition from CD20 monoclonal antibody therapy might also have affected the patient's clinical manifestations.

The infrequency of reported *B. lonestari* infections despite the frequent isolation of the bacteria from host-seeking *A. americanum* ticks suggests that this species might have a lower pathogenic potential than other *Borrelia* spp. more often associated with human disease. However, this assumption is hindered by the difficult isolation of *B. lonestari* through classic laboratory methods, including culturing (*2*,*10*). This case and associated sequence analysis highlight the clinical utility of molecular diagnostics for patients with suspected tickborne diseases. Increasing availability of molecular diagnostics might enable *B. lonestari* to be identified as an emerging tickborne pathogen, particularly causing opportunistic infections among persons who are immunocompromised.

Acknowledgments

We thank Stefania Carmona for assistance in developing this manuscript.

The opinions expressed by the authors do not necessarily reflect the opinions of the institutions with which the authors are affiliated.

About the Author

Dr. Vazquez Guillamet is an infectious disease specialist and tropical medicine diplomate completing doctoral studies on medicine and translational research at the University of Barcelona and the Barcelona Institute for Global Health.

References

1. Paules CI, Marston HD, Bloom ME, Fauci AS. Tickborne diseases—confronting a growing threat. N Engl J Med. 2018;379:701–3. https://doi.org/10.1056/NEJMp1807870
2. Barbour AG, Maupin GO, Teltow GJ, Carter CJ, Piesman J. Identification of an uncultivable *Borrelia* species in the hard tick *Amblyomma americanum*: possible agent of a Lyme disease-like illness. J Infect Dis. 1996;173:403–9. https://doi.org/10.1093/infdis/173.2.403
3. Burkot TR, Mullen GR, Anderson R, Schneider BS, Happ CM, Zeidner NS. *Borrelia lonestari* DNA in adult *Amblyomma americanum* ticks, Alabama. Emerg Infect Dis. 2001;7:471–3. https://doi.org/10.3201/eid0703.017323
4. Wormser GP, Masters E, Liveris D, Nowakowski J, Nadelman RB, Holmgren D, et al. Microbiologic evaluation of patients from Missouri with erythema migrans. Clin Infect Dis. 2005;40:423–8. https://doi.org/10.1086/427289
5. Lee SA, Plett SK, Luetkemeyer AF, Borgo GM, Ohliger MA, Conrad MB, et al. *Bartonella quintana* aortitis in a man with AIDS, diagnosed by needle biopsy and 16S rRNA gene amplification. J Clin Microbiol. 2015;53:2773–6. https://doi.org/10.1128/JCM.02888-14
6. Katoh K, Standley DM. MAFFT multiple sequence alignment software version 7: improvements in performance and usability. Mol Biol Evol. 2013;30:772–80. https://doi.org/10.1093/molbev/mst010
7. Barbour AG. Phylogeny of a relapsing fever *Borrelia* species transmitted by the hard tick *Ixodes scapularis*. Infect Genet Evol. 2014;27:551–8. https://doi.org/10.1016/j.meegid.2014.04.022
8. James AM, Liveris D, Wormser GP, Schwartz I, Montecalvo MA, Johnson BJ. *Borrelia lonestari* infection after a bite by an *Amblyomma americanum* tick. J Infect Dis. 2001;183:1810–4. https://doi.org/10.1086/320721
9. Krause PJ, Schwab J, Narasimhan S, Brancato J, Xu G, Rich SM. Hard tick relapsing fever caused by *Borrelia miyamotoi* in a child. Pediatr Infect Dis J. 2016;35:1352–4. https://doi.org/10.1097/INF.0000000000001330
10. Varela AS, Luttrell MP, Howerth EW, Moore VA, Davidson WR, Stallknecht DE, et al. First culture isolation of *Borrelia lonestari*, putative agent of southern tick-associated rash illness. J Clin Microbiol. 2004;42:1163–9. https://doi.org/10.1128/JCM.42.3.1163-1169.2004

Address for correspondence: Joshua A. Lieberman, University of Washington, Department of Laboratory Medicine, Box 357110, 1959 NE Pacific St, NW120, Seattle, WA 98195-7110, USA; email: joshuaal@uw.edu

Nocardia neocaledoniensis as Rare Cause of Spondylodiscitis

Emeline Choquet, Veronica Rodriguez-Nava, François Peltier, Rodrigue Wankap-Mogo, Emmanuelle Bergeron, Cédric Joseph, Nadine Lemaitre

Author affiliations: Centre Hospitalier Universitaire, Amiens, France (E. Choquet, F. Peltier, R. Wankap-Mogo, C. Joseph, N. Lemaitre); Université Lyon 1, Lyon, France (V. Rodriguez-Nava, E. Bergeron).

DOI: https://doi.org/10.3201/eid2902.221389

Nocardia neocaledoniensis is a rare species of *Nocardia* bacteria, identified in 2004 in hypermagnesian ultramafic soil of New Caledonia. Culture of this opportunistic pathogen from spinal biopsy samples confirmed *N. neocaledoniensis* spondylodiscitis in an immunocompromised man. Isolation of this unusual species from spinal biopsy samples illustrates its underappreciated ability to cause invasive infection.

Nocardia are aerobic bacteria, order *Corynebacteriales* (*1*), that are ubiquitously found in soil and water. *Nocardia* are typically opportunistic pathogens in immunocompromised patients (*2*). *Nocardia neocaledoniensis* is responsible for skin and soft tissue infections (*3*,*4*); its involvement in invasive infections has been 1 brain abscess and 1 case of bacteremia (*5*,*6*). We report a case of spondylodiscitis caused by *N. neocaledoniensis*.

In December 2021, in Amiens, France, a 68-year-old man with diabetes sought care from a rheumatologist after a 2-month history of persistent low-back pain radiating to his right hip and markedly reducing his ability to walk. He had a medical history of rectal cancer diagnosed 1 year earlier, for which liver metastasis was treated by surgery and 13 cycles of chemotherapy during March–September 2021.

The patient was apyretic, but his general status was deteriorated (asthenia, weight loss, and anorexia). Examination revealed marked tenderness over his mid-lumbar spine at L2–L3 and stiffness of the lumbar spine. Clinically relevant results of blood analysis showed elevated erythrocyte sedimentation rate (94 mm/h) and C-reactive protein (16 mg/L). A computed tomography (CT) scan showed erosion and end-plate deterioration of L2–L3, and a magnetic resonance imaging scan confirmed the diagnosis (Figure). Results of blood cultures were negative, but results of culture of 2 spinal biopsy samples collected during CT were positive in brain–heart infusion broth after 72 h of incubation at 37°C. Direct gram-stained smears showed unexpected branched gram-positive rods. After 48 h of subculture on a blood agar plate under aerobic conditions, the culture showed white opaque and dry *Nocardia*-like colonies. Matrix-assisted laser desorption/ionization time-of-flight (MALDI-TOF) mass spectrometry (Bruker, https://www.bruker.com) identified *N. asteroides*, with a score of 1.87. Sanger sequencing of the 16S rRNA (1,120 bp) gene from the isolate (GenBank accession no. OP028079) did not adequately discriminate between *N. neocaledoniensis* and *N. asteroides*. Therefore, we determined nucleotide sequences of the *secA1* (468 bp) and *sodA* (386 bp) genes and compared them with those from reference strains, as previously described (*7*,*8*). The isolate from the patient showed 99.1% similarity to *secA* and 99.5% to *sodA* sequences of the *N. neocaledoniensis* DSM 44717^T strain compared with ≤97.6% similarity to the *N. asteroides* ATCC 19247^T strain (Appendix Figure, https://wwwnc.cdc.gov/EID/article/29/2/22-1389-App1.pdf).

We performed susceptibility testing according to Clinical and Laboratories Standards Institute 2018 recommendations by using Sensititer RAPMYCO AST Plate (ThermoFisher Scientific, https://www.thermofisher.com). Based on the results of susceptibility testing (Table), treatment was intravenous ceftriaxone (2 g 2×/d) plus oral trimethoprim/sulfamethoxazole (160/800 mg 6×/d) for 1 week, followed by oral tedizolid (200 mg 1×/d). After 3 weeks of antimicrobial chemotherapy, the low-back pain completely regressed and the patient was mobile; after 6 months (antimicrobial therapy completion), the radiologic findings had slowly improved, and the patient was considered cured.

Immunosuppressive therapy, which decreases cellular immunity, is often associated with nocardiosis (*2*). The cancer patient we report had received immunosuppressants for 7 months. Common clinical manifestations are pulmonary infection caused by inhalation of *Nocardia* in aerosols and cutaneous infection after penetrating injuries (*2*). Both primary infection sites could be considered for this patient, who is a gardener. Indeed, the systematic thoracic CT scan performed in September 2021 showed ground-glass opacities with 2 excavations in the left upper lobe, which might be

Figure. Sagittal gadolinium magnetic resonance image of spine of a patient in France with spondylodiscitis caused by *Nocardia neocaledoniensis*. Image shows erosion of the cortical end plate of L2 and L3 (arrows).

Table. Antimicrobial susceptibility of *Nocardia neocalendoniensis* interpreted according to Clinical and Laboratory Standards Institute breakpoints (*7*)*

Antimicrobial	MIC, mg/L	Susceptibility
Amoxicillin/clavulanic acid	>64/32	R
Ceftriaxone	4	S
Imipenem	4	S
Amikacin	<1	S
Tobramycin	<1	S
Linezolid	2	S
Trimethoprim/sulfamethoxazole	0.5/9.5	S
Minocycline	4	I
Doxycycline	8	R
Ciprofloxacin	>4	R
Moxifloxacin	2	I
Clarithromycin	16	R

*I, intermediate; R, resistant; S, susceptible.

interpreted as manifestations of pulmonary nocardiosis, and the patient reported having had hand injuries 4–5 months before the diagnosis. Because the patient was asymptomatic, no microbiological specimens were collected before December 2021; he was twice tested for SARS-CoV-2 by PCR, in October and December, and results were negative. The cause of the pneumonia could not be determined, and the primary infection site of nocardiosis remains unknown for this patient.

Molecular methods based on housekeeping genes (16S rRNA, *hsp65*, *rpoB*, *gyrB*, *sodA*, and *secA1*) DNA sequences have characterized ≈100 species of *Nocardia* (*7*, *8*). For identifying *Nocardia*, MALDI-TOF mass spectrometry is more rapid and cost-effective than molecular methods. Several studies reported correctly identifying *Nocardia* to the species level (≈95%) by using commercial databases with common species (*9*,*10*). We used MALDI-TOF mass spectrometry with the Bruker reference library version 9.0, updated with 8,326 main spectra profiles. This database includes 52 *Nocardia* species but not *N. neocaledoniensis*, unlike the Vitek MD database (bioMérieux, http://www.biomerieux.com). Because *N. neocaledoniensis* is closely related to *N. asteroides* (*7*), the isolate was misidentified (with a low score of 1.87) as *N. asteroides* with the Bruker library. Although sequencing of 16S rRNA is usually adequate for identifying *Nocardia* isolates, in this case, the combined sequence analysis of *secA* and *sodA* genes was required to accurately discriminate between the closely related *N. neocaledoniensis* and *N. asteroides*.

This report of spondylodiscitis caused by *N. neocaledoniensis* provides evidence that *N. neocaledoniensis* is an opportunistic pathogen involved in invasive infection that may be underdiagnosed. Indeed, few commercial MALDI-TOF mass spectrometry databases correctly identify this uncommon species; thus, enlarging of most databases is necessary. Until then, molecular biology-based methods should still be considered the best standard for accurate identification.

About the Author

Dr. Choquet is an assistant in the department of bacteriology at the Amiens University Hospital, Amiens, France. Her primary research interests are diagnosis and treatment of bacterial infections.

References

1. Schoch CL, Ciufo S, Domrachev M, Hotton CL, Kannan S, Khovanskaya R, et al. NCBI taxonomy: a comprehensive update on curation, resources and tools. Database (Oxford). 2020;2020:baaa062. https://doi.org/10.1093/database/baaa062
2. Mehta HH, Shamoo Y. Pathogenic *Nocardia*: a diverse genus of emerging pathogens or just poorly recognized? PLoS Pathog. 2020;16:e1008280. https://doi.org/10.1371/journal.ppat.1008280
3. Saintpierre-Bonaccio D, Maldonado LA, Amir H, Pineau R, Goodfellow M. *Nocardia neocaledoniensis* sp. nov., a novel actinomycete isolated from a New-Caledonian brown hypermagnesian ultramafic soil. Int J Syst Evol Microbiol. 2004;54:599–603. https://doi.org/10.1099/ijs.0.02881-0
4. McGhie T, Fader R, Carpenter J, Brown-Elliott BA, Vasireddy R, Wallace RJ Jr. *Nocardia neocaledoniensis* [corrected] as a cause of skin and soft tissue infection. J Clin Microbiol. 2012;50:3139–40. https://doi.org/10.1128/JCM.00559-12
5. Hazarika K, Sahoo RR, Ekbote D, Dixit AK, Marak RS, Wakhlu A. Multidrug-resistant novel *Nocardia neocaledoniensis* brain abscess in sarcoidosis. BMJ Case Rep. 2021;14:e240123. https://doi.org/10.1136/bcr-2020-240123
6. Regueme A, Vachee A, Duployez C, Petit AE, Coulon P, Wallet F, et al. First case of fatal bacteremia due to *Nocardia neocaledoniensis*. IDCases. 2020;22:e00934. https://doi.org/10.1016/j.idcr.2020.e00934
7. Conville PS, Brown-Elliott BA, Smith T, Zelazny AM. The complexities of *Nocardia* taxonomy and identification. J Clin Microbiol. 2017;56:e01419–17.
8. Sánchez-Herrera K, Sandoval H, Mouniee D, Ramírez-Durán N, Bergeron E, Boiron P, et al. Molecular identification of *Nocardia* species using the *sod*A gene: Identificación molecular de especies de *Nocardia* utilizando el gen *sodA*. New Microbes New Infect. 2017;19:96–116. https://doi.org/10.1016/j.nmni.2017.03.008
9. Marín M, Ruiz A, Iglesias C, Quiroga L, Cercenado E, Martín-Rabadán P, et al. Identification of *Nocardia* species from clinical isolates using MALDI-TOF mass spectrometry. Clin Microbiol Infect. 2018;24:1342.e5–8. https://doi.org/10.1016/j.cmi.2018.06.014
10. Durand T, Vautrin F, Bergeron E, Girard V, Polsinelli S, Monnin V, et al. Assessment of VITEK® MS IVD database V3.0 for identification of *Nocardia* spp. using two culture media and comparing direct smear and protein extraction procedures. Eur J Clin Microbiol Infect Dis. 2020;39:559–67. https://doi.org/10.1007/s10096-019-03758-x

Address for correspondence: Nadine Lemaitre, Service de Bactériologie-Hygiène, CHU Amiens Picardie, 1 Rue du Professeur Christian Cabrol, 80000 Amiens, France; email: lemaitre.nadine@chu-amiens.fr

Cryptococcus tetragattii Meningitis Associated with Travel, Taiwan

Pin-Han Wu, Chih-Hao Chen, Yu-Tzu Lin, Yu Ao, Kuo-Hsi Lin, Wen-Hsin Hsih, Chia-Huei Chou, Chih-Yu Chi, Mao-Wang Ho, Po-Ren Hsueh

Author affiliation: China Medical University Hospital, Taichung, Taiwan (P.-H. Wu, C.-H. Chen, Y.-T. Lin, Y. Ao, W.-H. Hsih, C.-H. Chou, C.-Y. Chi, M.-W. Ho, P.-R. Hsueh); Tungs' Taichung MetroHarbor Hospital, Taichung (K.-H. Lin)

DOI: https://doi.org/10.3201/eid2902.221425

Meningitis caused by *Cryptococcus tetragattii* fungus is rare and has been found in specific geographic regions. We report a case of meningitis caused by *C. tetragattii* (molecular type VGIV) in an immunocompetent patient in Taiwan. The patient had traveled to Egypt and was positive for granulocyte-macrophage colony-stimulating factor autoantibody.

Meningitis caused by members of *Cryptococcus gattii* species complex is found in specific geographic or climatic regions (*1*). The incidence rate of *C. gattii*–caused meningitis is much lower than that caused by *C. neoformans* sensu stricto. We report a case of meningitis caused by *C. tetragattii* in an immunocompetent patient in Taiwan.

A 59-year-old female taxi driver with no systemic diseases sought care at China Medical University Hospital in Taichung, Taiwan, because she had experienced intermittent headache with unsteady gait for 2 months. She had received 1 dose of the ChAdOx1 nCoV-19 vaccine (AstraZeneca, https://www.astrazeneca.com) 4 months before admission. She had no contact history with pets, birds, or other animals. She frequently traveled abroad before the COVID-19 pandemic and had visited Italy, Egypt, and mainland China during 2018–2019.

After she was admitted, brain magnetic resonance imaging revealed mild cortical swelling with narrowing of the cerebral sulci in the bilateral medial frontoparietal lobes, indicating meningitis or leptomeningeal carcinomatosis. We performed lumbar puncture and obtained cerebrospinal fluid (CSF) on the second hospitalization day. Studies on the CSF were positive for yeasts by India ink staining and showed a cryptococcal antigen titer of 1:40× (CrAg LFA; IMMY, https://www.immy.com). We detected *C. neoformans* and *C. gattii* by using a multiplex PCR panel for meningitis (BioFire ME Panel; bioMérieux, https://www.biomerieux.com). Fungal culture of the CSF specimen yielded *Cryptococcus* species. We identified the organism as *C. gattii*; its score value was 1.92 by Bruker Biotyper matrix-assisted laser desorption/ionization time-of-flight mass spectrometry system (Bruker Daltonics GmbH, https://www.bruker.com). We performed multilocus sequence typing (MLST) and phylogenetic analysis MLST for 7 genetic loci, including *CAP59*, *GPD1*, *IGS1*, *LAC1*, *PLB1*, *SOD1*, and the *URA5* region, as previously described (*2*), and detected *C. gattii* ST576. We deposited sequence data of the 7 foci from MLST into GenBank (accession nos. OP828681–87). The URA5 gene restriction fragment length polymorphism of the *C. gattii* isolate performed as previously described (*3*); the results showed that this isolate belonged to the VGIV genotype, *C. tetragattii* (CMU-3028) (*2*).

A serial survey that included autoimmune profiles (antinuclear antibody, rheumatoid factor, anti-neutrophil cytoplasmic antibody, anti–double stranded DNA, complement component 3, and complement component 4), HIV-1/2 antibodies, and free HIV-1 p24 antigen (HIV-1/2 Ag/Ab Comb test; Abbott Laboratories, https://www.abbott.com) all showed negative results, but the result for the anti-granulocyte-macrophage colony-stimulating factor autoantibody (anti-GM-CSF AAb) was positive (titer 0.84), as measured using ELISA as previously described (*4*).

Induction treatment for the cryptococcal meningitis involved liposomal amphotericin B (200 mg/d) plus oral flucytosine (1,250 mg/6 h) for 21 days. A follow-up CSF culture revealed negative growth on hospital day 15. Oral voriconazole (250 mg/12 h) was prescribed as consolidation treatment for 15 days. The patient was discharged in stable condition and followed up at the outpatient department. She received oral fluconazole (400 mg/d) for the subsequent 6 months and remained well.

In this case, the patient is an immunocompetent host who had previously received 1 dose of the ChAdOx1-S vaccine and had a travel history to Egypt 2 years before symptom onset of meningitis. The members of the *C. gattii* species complex has different geographic distribution, and *C. tetragattii* is mostly isolated in Africa (*5*). Approximately 20% of the HIV-infected tested population had cryptococcal meningitis caused by *C. tetragattii* in Zimbabwe (*6*). In addition, anti-GM-CSF AAb has been detected in immunocompetent patients with *C. gattii* infection, as well as those with *C. neoformans* infection (*4*).

Whether COVID-19 vaccines have a trigger effect in unmasking underlying diseases, such as that in our

patient, warrants further study. To our knowledge, no studies demonstrate the relationship between anti-GM-CSF AAb and COVID-19 vaccines. However, research showed that autoantibody such as anti–smooth muscle antibody was triggered by COVID-19 vaccine as autoimmune hepatitis (*7*). In conclusion, clinicians should be aware of possible *C. tetragattii* fungal infection in patients who have traveled to meningitis-endemic regions.

About the Author

Dr. Wu is a clinical physician and specialist in infectious diseases, working at China Medical University Hospital, Taichung, Taiwan. His research interests include central nervous system infection, sepsis, and skin and soft tissue infections.

References

1. Springer DJ, Chaturvedi V. Projecting global occurrence of *Cryptococcus gattii*. Emerg Infect Dis. 2010;16:14–20. https://doi.org/10.3201/eid1601.090369
2. Chen YC, Kuo SF, Lin SY, Lin YS, Lee CH. Epidemiological and clinical characteristics, antifungal susceptibility, and MLST-based genetic analysis of *Cryptococcus* isolates in southern Taiwan in 2013–2020. J Fungi (Basel). 2022;8:287. https://doi.org/10.3390/jof8030287
3. Meyer W, Castañeda A, Jackson S, Huynh M, Castañeda E; IberoAmerican Cryptococcal Study Group. Molecular typing of IberoAmerican *Cryptococcus* neoformans isolates. Emerg Infect Dis. 2003;9:189–95. https://doi.org/10.3201/eid0902.020246
4. Wang SY, Lo YF, Shih HP, Ho MW, Yeh CF, Peng JJ, et al. *Cryptococcus gattii* infection as the major clinical manifestation in patients with autoantibodies against granulocyte–macrophage colony-stimulating factor. J Clin Immunol. 2022;42:1730–41. https://doi.org/10.1007/s10875-022-01341-2
5. Cogliati M. Global molecular epidemiology of Cryptococcus neoformans and *Cryptococcus gattii:* an atlas of the molecular types. Scientifica (Cairo). 2013;2013:1–23. https://doi.org/10.1155/2013/675213
6. Nyazika TK, Hagen F, Meis JF, Robertson VJ. *Cryptococcus tetragattii* as a major cause of cryptococcal meningitis among HIV-infected individuals in Harare, Zimbabwe. J Infect. 2016;72:745–52. https://doi.org/10.1016/j.jinf.2016.02.018
7. Vuille-Lessard É, Montani M, Bosch J, Semmo N. Autoimmune hepatitis triggered by SARS-CoV-2 vaccination. J Autoimmun. 2021;123:102710. https://doi.org/10.1016/j.jaut.2021.102710

Address for correspondence: Po-Ren Hsueh and Mao-Wang Ho, China Medical University Hospital, China Medical University, Taichung, Taiwan; email: hsporen@gmail.com, D7905@mail.cmuh.org.tw

Metagenomic Sequencing of Monkeypox Virus, Northern Mexico

Kame A. Galán-Huerta, Manuel Paz-Infanzon, Laura Nuzzolo-Shihadeh, Alí F. Ruiz-Higareda, Paola Bocanegra-Ibarias, Daniel Z. Villareal-Martínez, Fania Z. Muñoz-Garza, Maria D. Guerrero-Putz, Barbara Sáenz-Ibarra, Oralia Barboza-Quintana, Jorge Ocampo-Candiani, Ana M. Rivas-Estilla, Adrian Camacho-Ortiz

Author affiliation: Universidad Autonónoma de Nuevo León, Monterrey, Mexico

DOI: https://doi.org/10.3201/eid2902.221199

Monkeypox virus (MPXV) has gained interest because of a multicountry outbreak of mpox (formerly monkeypox) cases with no epidemiologic link to MPXV-endemic regions. We sequenced the complete genome of MPXV isolated from a patient in northern Mexico. Phylogenetic analysis grouped the virus with isolates from Germany.

Monkeypox virus (MPXV) is a zoonotic pathogen that causes mpox (formerly monkeypox), a febrile rash disease, in humans. It has caused multiple outbreaks in the past (*1*) but recently acquired international attention because of a multicountry outbreak of mpox cases with no epidemiologic link to MPXV-endemic regions (*2*). During January–June 2022, a total of 3,413 laboratory-confirmed cases and 1 death were reported to the World Health Organization (*3*).

MPXV is a double-stranded DNA virus that belongs to the genus *Orthopoxvirus* within the Poxviridae family. A total of 3 clades have been proposed: clades 1, 2, and 3 (*4*). Genomes belonging to the recent outbreaks gather at clade 3 and create the human MPXV1 subclade.

As of July 4, 2022, Mexico had 27 confirmed mpox infections (*5*). On June 28, 2022, a 34-year-old man with HIV sought care at the Dermatology Service of the Hospital Universitario Dr. José Eleuterio González (Monterrey, Mexico). The patient had multiple 1–2-cm flesh-colored papules with ulcerated centers and elevated borders on the dorsal area of the penis and the groin area and had bilateral inguinal lymphadenopathy. He had engaged in multiple high-risk sexual encounters during the previous several months and had traveled to Mexico City and Guadalajara. We collected skin swab samples from the lesions and extracted DNA by using the High Pure PCR Template Preparation Kit

(Roche, https://www.roche.com) in a biological safety cabinet. We disposed of hazardous biological infectious waste according to NOM-087-ECOL-SSA1–2002 and Centers for Disease Control and Prevention regulations. We used quantitative PCR to detect viral DNA as described in Li et al. (*6*). The study was approved by the ethics committee of the Hospital Universitario Dr. José Eleuterio González (registration no. IF22-00006). Written informed consent was obtained from the patient.

We performed genome sequencing at the Medical Virology Research and Innovation Center (Monterrey, Mexico). We used 700 ng of DNA to prepare the library with the Ligation Sequencing Kit (Oxford Nanopore Technologies, https://nanoporetech.com), by duplicate, following the manufacturer's protocol. We loaded libraries to a FLO-MIN106 R9.4.1. on a MinION device (Oxford Nanopore Technologies). We used high-accuracy basecalling and depleted the human genome by adaptive sampling reference (GRCh38.p14, GCF_000001405.40) in MinKNOW version 22.05.5 (Oxford Nanopore Technologies).

We assembled the genome with Minimap2 version 2.17, using an MPXV reference genome (GenBank accession no. NC_063383.1), and consensus sequence was obtained with Medaka version 1.0.3 (https://pypi.org/project/medaka/1.0.3) and bcftools version 1.10.12 (https://github.com/samtools/bcftools/releases). We deposited the obtained sequence in GISAID (accession no. EPI_ISL_13607904) and GenBank (accession no. ON911481). Furthermore, raw reads were mapped against the human genome and filtered out using Minimap2 and Samtools version 1.16 (http://www.htslib.org). Remaining reads were assembled de novo with Flye version 2.9.1 (https://anaconda.org/bioconda/flye) and subsequently polished using Medaka and homopolish version 0.4 (https://anaconda.org/bioconda/homopolish/files).

We used Nextstrain's mpox bioinformatic processing workflow (*7*) for our initial analysis. Subsequently, we downloaded 399 sequences from GenBank that belonged to clade hMPXV1 from outbreaks in 2017–2019 and 2022 (the available sequences as of July 14, 2022).

We masked and aligned sequences in MAFFT version 7.505 (https://mafft.cbrc.jp/alignment/software). We inferred a maximum-likelihood phylogenetic tree with IQ-TREE version 2.0.3 (http://www.iqtree.org) using the Hasegawa-Kishino-Yano plus base frequencies plus invariant sites substitution model with 1,000 replicates for SH-like approximate likelihood ratio test and 1,000 replicates for ultrafast bootstrap.

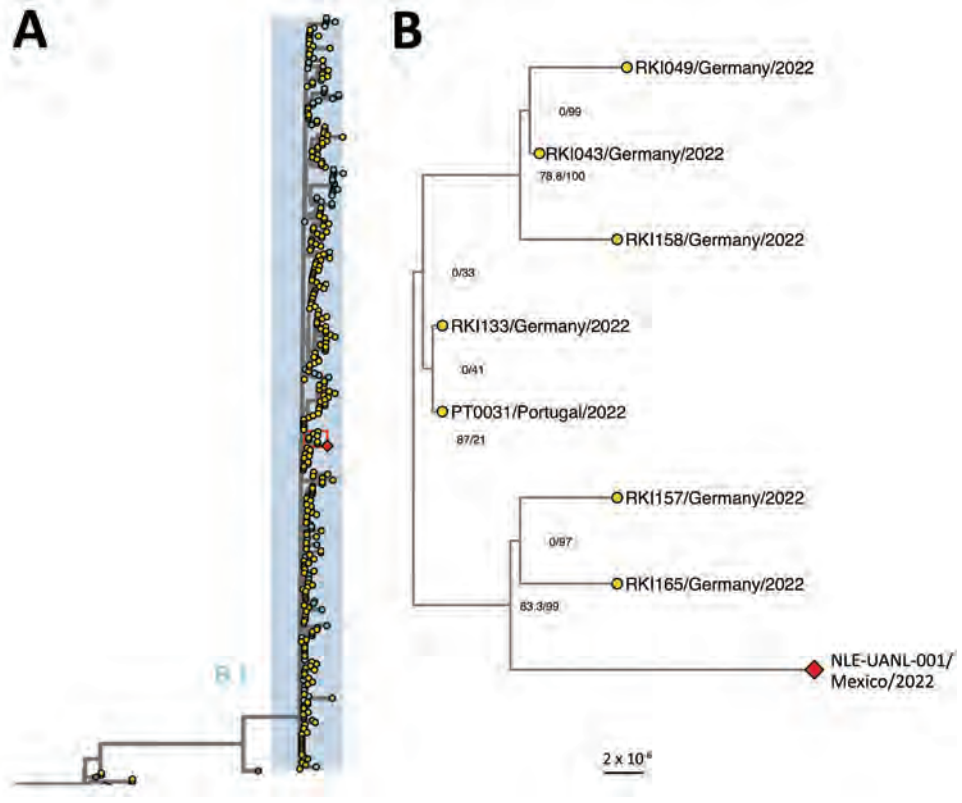

Figure. Phylogenetic relationship of monkeypox virus genomes, 2017–2022. A) Maximum-likelihood phylogenetic tree with 400 whole-genome sequences of monkeypox virus made in IQTree (http://www.iqtree.org). Highlighted genomes in blue belong to the proposed B.1 lineage. B) Magnification of area in red box in panel A showing clade indicating the Mexico isolate and related sequences. Node numbers indicate SH-like approximate likelihood ratio test and ultrafast bootstrap values. The red diamond corresponds to the sequence from this study and yellow circles to sequences from Europe. The list of accession numbers of the sequences is shown in the Appendix Table (https://wwwnc.cdc.gov/EID/article/29/2/22-1199-App1.pdf). The tree was annotated in ggtree (https://bioconductor.org/packages/release/bioc/html/ggtree.html). Scale bar indicates substitutions per site.

Adding both sequencing runs, we obtained 1.77 million reads with an estimated N50 of 17.2 kb after a 20-h run. The MPXV genome sequence obtained by reference assembly was composed of 55,512 mapped reads with a breadth of 197,414 bp, 751× average depth, and 1,212× maximum depth. The sequence obtained by de novo assembly was composed of 58,259 mapped reads with a breadth 197,875 bp, 752× average depth, and 1,215× maximum depth.

Phylogenetic analyses revealed that the obtained sequence clusters within the newly proposed B.1 lineage from clade 3, where sequences from the multicountry mpox outbreak are located (Figure, panel A; Appendix Figure 1, panel A, https://wwwnc.cdc.gov/EID/article/29/2/22-1199-App1.pdf). Sequences from Europe (specifically Portugal and Germany) dominate the tree because they make up most of the available sequences. The Mexico sequence groups in a well-supported clade with sequences from Germany (Figure, panel B; Appendix Figure 1, panel B), although we could not establish an epidemiologic relationship. The sequence is grouped in the same clade in both approaches, independent of the assembly method (Appendix Figure 2). The inferred date of the most recent common ancestor of the clade is May 26, 2022 (95% CI May 26, 2022–June 2, 2022). Sequences from this clade share the mutation G120241A, causing a nonsynonymous substitution in OPG137, D214N. OPG137 encodes for a virion membrane assembly protein, which is involved in the crescent membrane and immature virion formation (*8*). Aspartic acid is an acidic amino acid and asparagine is neutral. The effect of this mutation has yet to be determined.

In conclusion, we sequenced the whole genome of MXPV from a patient with mpox in northern Mexico. Subsequent sequencing will unravel how the virus is transmitting and adapting throughout the population. According to our results, this patient likely had close contact with an infected person who traveled from Europe.

This work was funded by Consejo Nacional de Ciencia y Tecnología (CONACyT) through grants to K.A.G.-H. (grant no. 312328) and A.M.R.-E. (grant no. 315848).

About the Author

Dr. Galán-Huerta is an associate professor in the faculty of medicine and founding member of the Medical Virology Research and Innovation Center at the Autonomous University of Nuevo Leon. His primary research interests are epidemiology and emerging and reemerging viral diseases.

References

1. Yinka-Ogunleye A, Aruna O, Dalhat M, Ogoina D, McCollum A, Disu Y, et al.; CDC Monkeypox Outbreak Team. Outbreak of human monkeypox in Nigeria in 2017–18: a clinical and epidemiological report. Lancet Infect Dis. 2019;19:872–9. https://doi.org/10.1016/S1473-3099(19)30294-4
2. Vivancos R, Anderson C, Blomquist P, Balasegaram S, Bell A, Bishop L, et al.; UKHSA Monkeypox Incident Management team; Monkeypox Incident Management Team. Community transmission of monkeypox in the United Kingdom, April to May 2022. Euro Surveill. 2022;27:2200422. https://doi.org/10.2807/1560-7917.ES.2022.27.22.2200422
3. World Health Organization. Multi-country monkeypox outbreak: situation update Disease Outbreak News. 2022 [cited 2022 Jun 30]. https://www.who.int/emergencies/disease-outbreak-news/item/2022-DON396
4. Happi C, Adetifa I, Mbala P, Njouom R, Nakoune E, Happi A, et al. Urgent need for a non-discriminatory and non-stigmatizing nomenclature for monkeypox virus. Virological.org. 2022 [cited 2022 Jul 4]. https://virological.org/t/urgent-need-for-a-non-discriminatory-and-non-stigmatizing-nomenclature-for-monkeypox-virus/853
5. Panamerican Health Organization, World Health Organization. Monkeypox cases—region of the Americas. 2022 [cited 2022 Jul 5]. https://shiny.pahobra.org/monkeypox/
6. Li Y, Zhao H, Wilkins K, Hughes C, Damon IK. Real-time PCR assays for the specific detection of monkeypox virus West African and Congo Basin strain DNA. J Virol Methods. 2010;169:223–7. https://doi.org/10.1016/j.jviromet.2010.07.012
7. Hadfield J, Megill C, Bell SM, Huddleston J, Potter B, Callender C, et al. Nextstrain: real-time tracking of pathogen evolution. Bioinformatics. 2018;34:4121–3. https://doi.org/10.1093/bioinformatics/bty407
8. Senkevich TG, Yutin N, Wolf YI, Koonin EV, Moss B. Ancient gene capture and recent gene loss shape the evolution of orthopoxvirus-host interaction genes. MBio. 2021;12:e0149521. https://doi.org/10.1128/mBio.01495-21

Address for correspondence: Adrián Camacho-Ortiz, Servicio de Infectología, Hospital Universitario Dr. José Eleuterio González, Facultad de Medicina, Universidad Autónoma de Nuevo León, Avenida Francisco I. Madero S/N, Colonia Mitras Centro, Monterrey, NL, CP: 64460, Mexico; email: acamacho_md@yahoo.com

Monkeypox Virus Evolution before 2022 Outbreak

Eric Dumonteil, Claudia Herrera, Gilberto Sabino-Santos

Author affiliations: Tulane University, New Orleans, Louisiana, USA (E. Dumonteil, C. Herrera, G. Sabino-Santos); University of São Paulo, São Paulo, Brazil (G. Sabino-Santos)

DOI: https://doi.org/10.3201/eid2902.220962

Phylogenetic analysis of monkeypox virus genomes showed statistically significant divergence and nascent subclades during the 2022 mpox outbreak. Frequency of G>A/C>T transitions has increased in recent years, probably resulting from apolipoprotein B mRNA editing enzyme catalytic polypeptide 3G (APOBEC3) deaminase editing. This microevolutionary pattern most likely reflects community spread of the virus and adaptation to humans.

Monkeypox virus (MPXV) is a double-stranded DNA virus mostly associated with rodents and occasionally spilling over to humans, causing outbreaks of mpox (formerly monkeypox) that have been relatively short-lived and self-limiting because of ineffective transmission among humans (*1*). However, this view is challenged by reports that, since the start of the ongoing outbreak, in early April 2022, a total of 49,482 mpox cases in 94 countries had been confirmed (https://ourworldindata.org/monkeypox). Initial epidemiologic studies provided evidence of sustained human-to-human transmission in some non–MPXV-endemic countries in Europe, through close contacts, including in sexual networks (*2*). The first MPXV genome sequences from the outbreak were reported from Portugal on May 19, 2022 (*3*), and multiple additional sequences, which can shed light on virus circulation, are now available. Initial phylogenetic analyses indicated that the virus causing the 2022 outbreak belonged to MPXV clade II (formerly West African clade), which is less severe than clade I (formerly Congo Basin clade) (*4*), suggesting that the current outbreak was caused by the recent introduction of the virus into communities in non–MPXV-endemic countries (*2*). However, further analysis including additional MPXV genome sequences indicates a different scenario.

Indeed, phylogenetic analysis of 105 MPXV genomes (Appendix Table 1, https://wwwnc.cdc.gov/EID/article/29/2/22-0962-App1.pdf) revealed that viruses from 2022 belong to 2 clades that can be traced back to the previous 2017–2018 outbreak (Figure). One of those subclades, so far only identified in the United States (*5*), seems to have limited circulation (only 3 cases). All other 2022 viral genomes form a large monophyletic group, although a substantial level of sequence divergence among strains can already be detected, with several nascent subclades (Figure). Such divergence is not compatible with a recent diversification of the virus during the past few months of the outbreak. Rather, it reflects a continuous microevolution since the previous outbreak in 2017–2018. The most recent common ancestor for the 2022 outbreak can be traced back to around 20 years ago, at a rather similar time as the most recent common ancestor for the 2017–2018 outbreak. Furthermore, MPXVs from the 2022 outbreak are more closely related to strains that had been exported from Africa during the previous outbreak, rather than with strains circulating in Nigeria at that time. A strain from a person who traveled from Nigeria to Maryland, USA, in 2021 (*5*) can also be traced back to the root of the 2022 outbreak. Thus, the most likely scenario is that there has been silent and undetected circulation of MPXV, possibly including multiple non–MPXV-endemic countries outside Africa, since the 2017–2018 outbreak.

Our observations raise the question of potentially increased adaptation of current virus strains to humans. Variations in genomic content may shape the evolution of orthopoxviruses, and gene gain/loss may correlate with pathogenicity and host adaptation (*6*). We found multiple genomic changes in the MPXVs from 2022; at least 51 single-nucleotide polymorphisms (SNPs) differentiated the first 18 viral genomes from the 2022 outbreak from those from 2017–2018 (Appendix Table 2) and a few larger insertions/deletions. Of the 51 SNPs, 26 caused amino acid changes and 21 were synonymous substitutions. Additional SNPs can be detected among genome sequences from 2022, underlying the established divergence within the outbreak (Appendix Table 2). Those changes may be associated with mutational pressure and adaptation (*7*,*8*), and future studies should help assess their phenotypic effects.

Further analysis of the substitutions showed major bias in their distribution in viruses from 2022; 61/70 (87.1%) of all substitutions were G>A/C>T transitions, followed by 6/70 (8.6%) T>C/A>G transitions, and 2/70 (2.8%) were C>A/G>T transversions and 1/70 (1.4%) A>C/T>G transversions. Comparison of these substitution proportions with those observed in clade II up to 2018 and those from the clade I showed a striking pattern (Appendix Figure). Indeed, viruses from both clades had nearly identical proportions of substitution types before 2018, and the proportion of G>A/C>T transitions in clade II

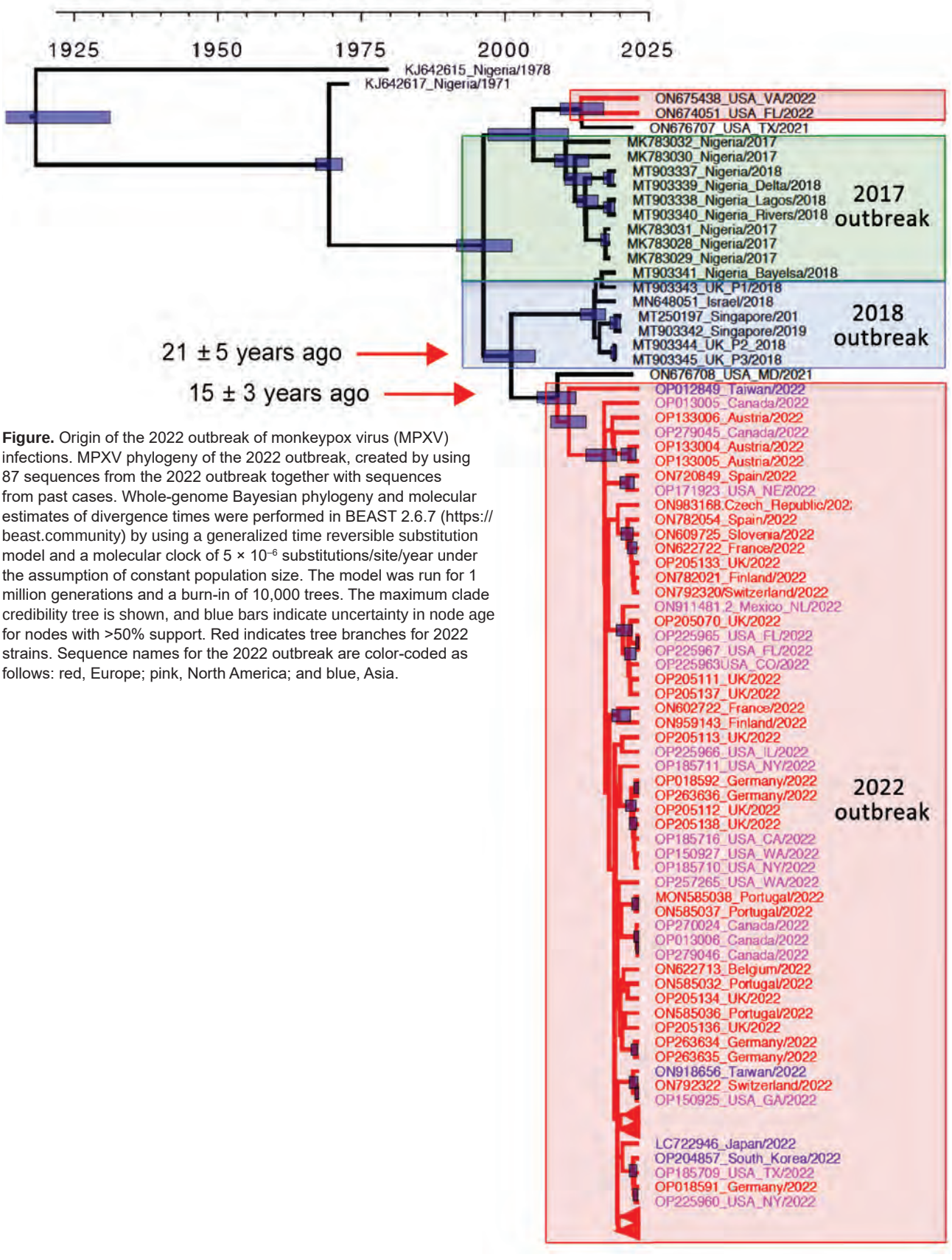

Figure. Origin of the 2022 outbreak of monkeypox virus (MPXV) infections. MPXV phylogeny of the 2022 outbreak, created by using 87 sequences from the 2022 outbreak together with sequences from past cases. Whole-genome Bayesian phylogeny and molecular estimates of divergence times were performed in BEAST 2.6.7 (https://beast.community) by using a generalized time reversible substitution model and a molecular clock of 5×10^{-6} substitutions/site/year under the assumption of constant population size. The model was run for 1 million generations and a burn-in of 10,000 trees. The maximum clade credibility tree is shown, and blue bars indicate uncertainty in node age for nodes with >50% support. Red indicates tree branches for 2022 strains. Sequence names for the 2022 outbreak are color-coded as follows: red, Europe; pink, North America; and blue, Asia.

viruses from 2022 had doubled ($\chi^2 = 55.3$; $p<0.0001$) (Appendix Figure). Those considerable changes in substitutions most likely reflect the editing activity of the human APOBEC3G enzyme (apolipoprotein B mRNA editing enzyme, catalytic subunit 3G), which catalyzes strand-specific C>U deamination, resulting in G>A substitutions in the complementary strand of viral genomes (A. O'Toole, unpub. data, https://virological.org/t/initial-observations-about-putative-apobec3-deaminase-editing-driving-short-term-evolution-of-mpxv-since-2017/830; [*9*]).

In conclusion, our analyses of MPXV genome sequences indicate that the virus has been circulating silently and undetected for about 2 decades, probably in multiple non–MPXV-endemic countries outside of Africa. Also, a clear genomic signature of a recent change in hosts is evidenced by major changes in its nucleotide substitution pattern. Our observations have major public health implications; the changing epidemiology of MPXV infections and human circulation of the virus in non–MPXV-endemic countries call for increased surveillance (*1*). The public health crisis caused by the COVID-19 pandemic may have favored the spread of MPXV under the radar in the past few years; however, the existence of asymptomatic carriers cannot be ruled out and may have contributed to the undetected spread of MPXV.

About the Author

Dr. Dumonteil is an associate professor at the Tulane School of Public Health and Tropical Medicine, New Orleans, LA, USA. His main research interests are neglected infectious diseases and interdisciplinary studies for their surveillance and control.

References

1. Bunge EM, Hoet B, Chen L, Lienert F, Weidenthaler H, Baer LR, et al. The changing epidemiology of human monkeypox—a potential threat? A systematic review. PLoS Negl Trop Dis. 2022;16:e0010141. https://doi.org/10.1371/journal.pntd.0010141
2. Antinori A, Mazzotta V, Vita S, Carletti F, Tacconi D, Lapini LE, et al.; INMI Monkeypox Group. Epidemiological, clinical and virological characteristics of four cases of monkeypox support transmission through sexual contact, Italy, May 2022. Euro Surveill. 2022;27:2200421. https://doi.org/10.2807/1560-7917.ES.2022.27.22.2200421
3. Isidro J, Borges V, Pinto M, Sobral D, Santos JD, Nunes A, et al. Phylogenomic characterization and signs of microevolution in the 2022 multi-country outbreak of monkeypox virus. Nat Med. 2022;28:1569–72. https://doi.org/10.1038/s41591-022-01907-y
4. Saxena SK, Ansari S, Maurya VK, Kumar S, Jain A, Paweska JT, et al. Re-emerging human monkeypox: a major public-health debacle. J Med Virol. 2022;95:e27902. https://doi.org/10.1002/jmv.27902
5. Gigante CM, Korber B, Seabolt MH, Wilkins K, Davidson W, Rao AK, et al. Multiple lineages of monkeypox virus detected in the United States, 2021-2022. Science. 2022:378:560–5. https://doi.org/10.1126/science.add4153 PMID: 36264825
6. Alakunle E, Moens U, Nchinda G, Okeke MI. Monkeypox virus in Nigeria: infection biology, epidemiology, and evolution. Viruses. 2020;12:1257. https://doi.org/10.3390/v12111257
7. Shackelton LA, Parrish CR, Holmes EC. Evolutionary basis of codon usage and nucleotide composition bias in vertebrate DNA viruses. J Mol Evol. 2006;62:551–63. https://doi.org/10.1007/s00239-005-0221-1
8. Bailey SF, Alonso Morales LA, Kassen R. Effects of synonymous mutations beyond codon bias: the evidence for adaptive synonymous substitutions from microbial evolution experiments. Genome Biol Evol. 2021;13:evab141. https://doi.org/10.1093/gbe/evab141
9. Yu Q, König R, Pillai S, Chiles K, Kearney M, Palmer S, et al. Single-strand specificity of APOBEC3G accounts for minus-strand deamination of the HIV genome. Nat Struct Mol Biol. 2004;11:435–42. https://doi.org/10.1038/nsmb758

Address for correspondence: Eric Dumonteil, Department of Tropical Medicine, School of Public Health and Tropical Medicine, and Vector-Borne and Infectious Disease Research Center, Tulane University, 1440 Canal St, New Orleans, LA 70112, USA; e-mail: edumonte@tulane.edu

Epidemiology of SARS-CoV-2 Omicron BA.5 Infections, Macau, June–July 2022

Weijia Xiong, Liping Peng, Tim K. Tsang, Benjamin J. Cowling

Author affiliations: University of Hong Kong, Hong Kong (W. Xiong, L. Peng, T.K. Tsang, B.J. Cowling); Laboratory of Data Discovery for Health Limited, Hong Kong (T.K. Tsang, B.J. Cowling)

DOI: https://doi.org/10.3201/eid2902.221243

A SARS-CoV-2 Omicron BA.5 outbreak occurred in Macau from mid-June through July 2022. Out of >1,800 laboratory-confirmed cases, most were mild or asymptomatic; only 6 deaths were recorded. The outbreak was controlled through stringent public health and social measures, such as repeated universal testing and a stay-at-home order lasting 2 weeks.

The SARS-CoV-2 Omicron subvariant BA.5 has spread rapidly worldwide. A recent outbreak of BA.5 occurred in Macau during June 18–July 31, 2022. The outbreak resulted in 1,821 confirmed cases and 6 deaths but was promptly controlled. We describe the basic epidemiology of this outbreak.

Macau, a special administrative region of China with 683,000 persons, has been applying intensive public health and social measures to reduce SARS-CoV-2 variant importation and prevent community outbreaks as part of China's dynamic zero COVID strategy. In Macau, this strategy has included stringent travel restrictions and up to 28-day on-arrival quarantines (*1*) to avoid infections within communities. As in China, all SARS-CoV-2–infected persons are strictly isolated in special facilities, and contact tracing expedites timely quarantine of close contacts outside the home. Throughout the pandemic before June 2022, only 17 domestic confirmed cases (2.5 cases/100,000 population) and no deaths were reported in Macau. Since early 2021, inactivated virus (Sinopharm, http://www.sinopharm.com) and mRNA (Pfizer-BioNTech, https://www.pfizer.com) vaccines have been available in Macau. By June 19, 2022, vaccine coverage within the entire population was 85.6% for ≥2 doses and 40.5% for 3 doses.

In mid-June 2022, a SARS-CoV-2 Omicron BA.5 outbreak began in Macau (*2*). The first case was detected in a person with symptoms who sought treatment at a hospital on June 18, 2022. The source of infection remains unknown (*3*). Identification of a community outbreak prompted the government of Macau to impose a series of domestic public health and social measures to control local transmission (Appendix Table 1, https://wwwnc.cdc.gov/EID/article/29/2/22-1243-App1.pdf). Macau entered an immediate prevention state at 1:00 AM on June 19, 2022. Multiple rounds of universal PCR testing were

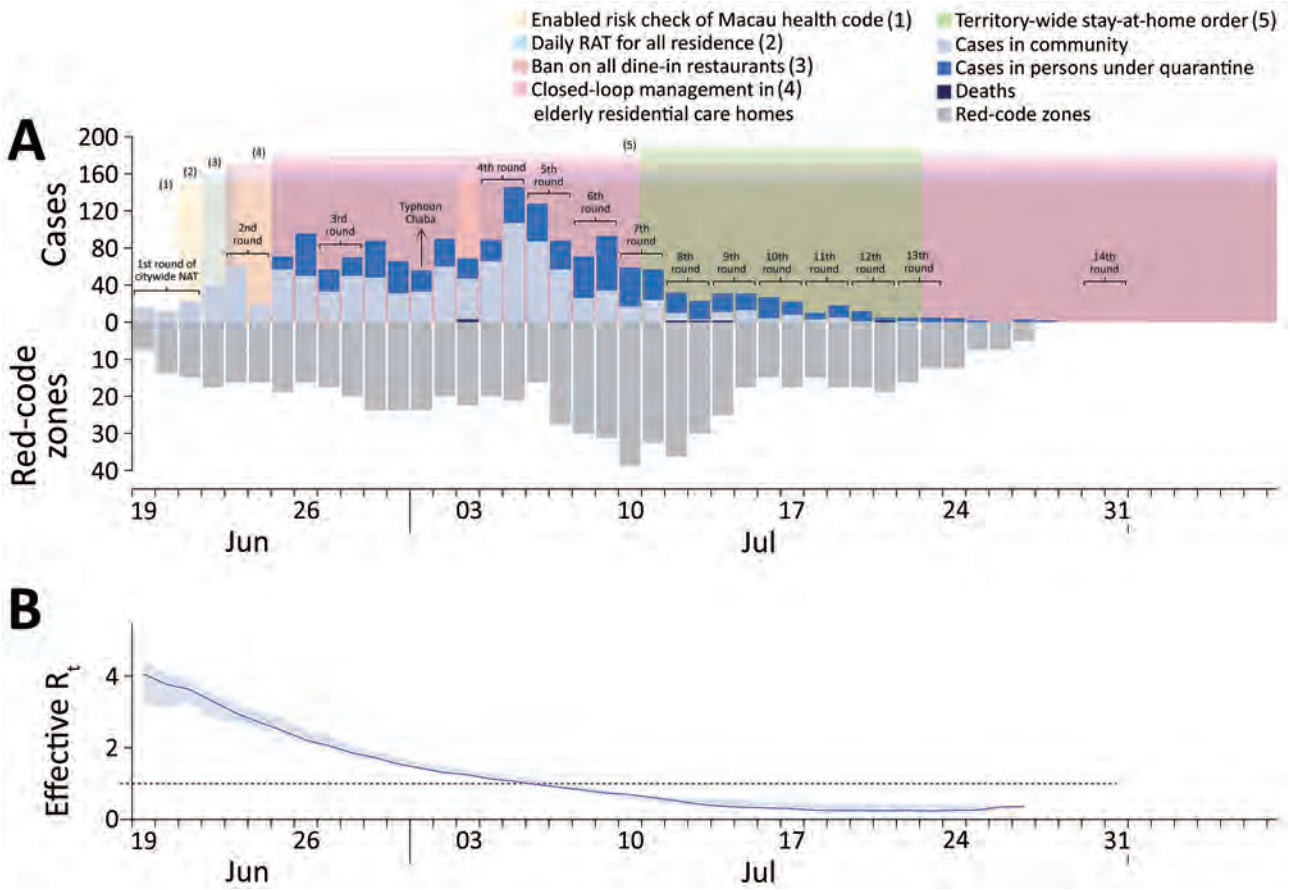

Figure. Number of PCR-positive COVID-19 cases and time-varying reproductive number in study of epidemiology of SARS-CoV-2 Omicron BA.5 infections, Macau, June–July 2022. A) PCR-confirmed COVID-19 cases and deaths in Macau during June and July 2022. Light blue bars indicate daily numbers of COVID-19 cases confirmed by PCR in the community; dark blue bars indicate persons under quarantine; black bars indicate number of reported deaths. Gray bars under the x-axis indicate the number of real-time red-code zones (areas with movement restrictions in place) in Macau. Shaded areas indicate when public health and social measures (indicated by numbers 1–5) were implemented to control COVID-19 transmission. B) Estimates of time-varying R_t to quantify real-time transmissibility of SARS-CoV-2 Omicron BA.5 in Macau. Dotted line indicates R_t of 1. RAT, rapid antigen test; R_t, effective reproductive number

Table. Estimated incubation periods for SARS-CoV-2 Omicron BA.5 variant according to population percentiles using lognormal, gamma, or Weibull probability distributions in study of epidemiology of SARS-CoV-2 Omicron BA.5 infections, Macau, June–July 2022*

Percentile	Incubation, d (95% CI)		
	Lognormal	Gamma	Weibull
Mean	3.27 (3.07–3.45)	3.00 (2.83–3.16)	3.26 (3.07–3.40)
2.5th	1.46 (1.17–1.74)	1.87 (1.74–2.00)	1.10 (0.93–1.25)
5th	1.64 (1.37–1.90)	2.02 (1.89–2.16)	1.38 (1.20–1.52)
50th	3.04 (2.87–3.18)	2.95 (2.79–3.12)	3.23 (3.03–3.38)
95th	5.67 (4.97–6.67)	4.13 (3.94–4.33)	5.24 (4.74–5.52)
97.5th	6.39 (5.49–7.77)	4.39 (4.19–4.59)	5.61 (5.05–5.94)
99th	7.34 (6.16–9.29)	4.70 (4.49–4.91)	6.03 (5.40–6.44)
AIC value†	360.80	377.57	370.45

*Mean number of days was estimated after adjusting for exponential growth. AIC, Akaike information criterion.
†AIC values were calculated to compare the fit of each model.

scheduled; and 14 rounds of citywide PCR testing were conducted for all persons in Macau. To identify infected persons, PCR testing was performed on June 22 and 25 for specific groups that included persons with Myanmar passports and those who sought care at places visited by persons who had SARS-CoV-2–positive tests (*4*,*5*). On June 23, schools, entertainment venues, public dining, and other nonessential businesses were closed, and residents were encouraged to stay at home. Closed-loop management was implemented in residential care homes beginning on June 25. Beginning on June 27, all persons were asked to conduct daily rapid antigen tests and report test results to an online platform (Appendix Tables 1, 2). The government enabled the risk check function of the Macau health code and implemented a district-specific epidemic prevention plan. Yellow- and red-code zones with movement restrictions were announced daily. As the daily case numbers grew, the government issued static management instructions comparable to a complete stay-at-home order beginning after midnight on July 11 and lasting until midnight on July 23; essential workers were excluded.

Among 1,821 cases that included 937 female and 884 male persons (3 months to 100 years of age), a total of 1,116 were classified as asymptomatic. The daily number of new positive cases peaked on July 5, 2022, at 146 PCR-positive cases (Figure 1, panel A). We estimated the time-varying reproductive number (Figure 1, panel B) to quantify real-time transmissibility (Appendix). The estimated time-varying reproductive number was <1 after July 7, 2022. In the final (14th) round of universal PCR testing on July 30–31, SARS-CoV-2 RNA was not found in specimens from persons in the community, confirming that the outbreak was contained.

Using information on 500 case-patients with known exposure and symptom onset reported during the early outbreak phase, we estimated that the mean incubation period for Omicron BA.5 was 3.27 days (SD ±1.05 days), after adjusting for exponential growth (*6*) (Table; Appendix Figure). The BA.5 incubation period was similar to 3.2 days for Omicron BA.1 (*7*) and 4.5 days for BA.2 (*8*) and shorter than that for other SARS-COV-2 variants (*9*).

Among 572 PCR-confirmed cases reported by June 30, a total of 23 case-patients had received 1 SARS-CoV-2 vaccine dose, 216 had received 2 vaccine doses, 224 had received 3 vaccine doses, and 109 were unvaccinated (Appendix Table 3). Although only 10% of the population was unvaccinated, 19% of the SARS-CoV-2–infected persons were unvaccinated.

Among the 1,821 locally infected case-patients, 6 deaths occurred (Appendix Table 4). Therefore, the case-fatality risk for Omicron-infected persons in Macau was 0.33% (95% CI 0.13%–0.76%). Persons who died of COVID-19 were 86–100 (mean 92.5, SD ±5.0) years of age. Among the 6 case-patients who died, 3 had received 2 doses of vaccine, and the other 3 were unvaccinated.

A limitation of our study is that we could not separate the effects of each public health and social measure because they were implemented as a package. High compliance with those stringent measures during the outbreak might have maximized the effectiveness of the interventions (*10*), although those measures might not be easily applicable to other locations outside of China. In conclusion, our study indicates that SARS-CoV-2 outbreaks can be controlled through stringent public health and social measures, such as repeated universal PCR testing and stay-at-home orders lasting at least 2 weeks.

Acknowledgments

We thank Julie Au for technical assistance.

This project was supported by the Collaborative Research Fund from the University Grants Committee of Hong Kong (project no. C7123-20G), Health and Medical Research Fund, Food and Health Bureau, Government of the Hong Kong Special Administrative Region, and Research Grants Council of Hong Kong Special Administrative Region, China (GRF 17110221).

B.J.C. reports honoraria from AstraZeneca, Fosun Pharma, GSK, Moderna, Pfizer, Roche, and Sanofi Pasteur. All other authors report no other potential conflicts of interest.

About the Author

Ms. Xiong is a PhD candidate at the School of Public Health, University of Hong Kong. Her research interests focus on infectious disease epidemiology and modeling and the development of statistical approaches for infectious disease analysis.

References

1. Macao Government. Novel Coronavirus Response and Coordination Center of Macau. New epidemic prevention measures will be implemented from midnight on January 6. 2021 Dec 30 [cited 2022 Nov 14]. https://www.gcs.gov.mo/detail/zh-hans/N21LdGxjb9?8
2. Macau Government. Novel Coronavirus Response and Coordination Center of Macau. The virus in this outbreak is identified as Omicron BA.5. 2022 Jul 8 [cited 2022 Nov 14]. https://www.gcs.gov.mo/detail/zh-hans/N22GHgyjUl?4
3. Macau Government. Novel Coronavirus Response and Coordination Center of Macau. So far (20th) at 4 p.m., there have been 36 nucleic acid positive cases, and the two confirmed groups are related. 2022 Jun 20 [cited 2022 Nov 14]. https://www.gcs.gov.mo/detail/zh-hant/N22FTpK7To?30
4. Macau Government. Novel Coronavirus Response and Coordination Center of Macau. Novel Coronavirus Response and Coordination Centre announces nucleic acid testing arrangements in key areas and for key groups on June 22. 2022 June 22 [cited 2022 Nov 14]. https://www.gcs.gov.mo/detail/en/N22FU62sfT
5. Macau Government. Novel Coronavirus Response and Coordination Center of Macau. The Response and Coordination Centre announces the arrangements of the NAT for key areas tomorrow (25 June). 2022 June 25 [cited 2022 Nov 14]. https://www.gcs.gov.mo/detail/en/N22FYNcgqW
6. Verity R, Okell LC, Dorigatti I, Winskill P, Whittaker C, Imai N, et al. Estimates of the severity of coronavirus disease 2019: a model-based analysis. Lancet Infect Dis. 2020;20:669–77. https://doi.org/10.1016/S1473-3099(20)30243-7
7. Backer JA, Eggink D, Andeweg SP, Veldhuijzen IK, van Maarseveen N, Vermaas K, et al. Shorter serial intervals in SARS-CoV-2 cases with Omicron BA.1 variant compared with Delta variant, the Netherlands, 13 to 26 December 2021. Euro Surveill. 2022;27:2200042. https://doi.org/10.2807/1560-7917.ES.2022.27.6.2200042
8. Mefsin YM, Chen D, Bond HS, Lin Y, Cheung JK, Wong JY, et al. Epidemiology of infections with SARS-CoV-2 Omicron BA.2 variant, Hong Kong, January–March 2022. Emerg Infect Dis. 2022;28:1856–8. https://doi.org/10.3201/eid2809.220613
9. Wu Y, Kang L, Guo Z, Liu J, Liu M, Liang W. Incubation period of COVID-19 caused by unique SARS-CoV-2 strains: a systematic review and meta-analysis. JAMA Netw Open. 2022;5:e2228008. PubMed https://doi.org/10.1001/jamanetworkopen.2022.28008
10. Zhou L, Wu Z, Li Z, Zhang Y, McGoogan JM, Li Q, et al. One hundred days of coronavirus disease 2019 prevention and control in China. Clin Infect Dis. 2021;72:332–9. https://doi.org/10.1093/cid/ciaa725

Address for correspondence: Tim K. Tsang, School of Public Health, Li Ka Shing Faculty of Medicine, University of Hong Kong, 7 Sassoon Road, Pokfulam, Hong Kong; email: timtsang@connect.hku.hk

Serologic Evidence of *Orientia* Infection among Rural Population, Cauca Department, Colombia

Álvaro A. Faccini-Martínez, Carlos Ramiro Silva-Ramos, Lucas S. Blanton, Esteban Arroyave, Heidy-C. Martínez-Diaz, Paola Betancourt-Ruiz, Marylin Hidalgo, David H. Walker

Author affiliations: Fundación Universitaria de Ciencias de la Salud, Bogotá, Colombia (Á.A. Faccini-Martínez); Servicios y Asesorías en Infectología, Bogotá (Á.A. Faccini-Martínez); Hospital Militar Central, Bogotá (Á.A. Faccini-Martínez); Hospital Militar Central, Bogotá (Á.A. Faccini-Martínez) University of Texas Medical Branch, Galveston, Texas, USA (Á.A. Faccini-Martínez, L.S. Blanton, E. Arroyave, D.H. Walker); Pontificia Universidad Javeriana, Bogotá (C.R. Silva-Ramos, H.-C. Martínez-Diaz, P. Betancourt-Ruiz, M. Hidalgo)

DOI: https://doi.org/10.3201/eid2902.221458

We assessed serum samples collected in Cauca Department, Colombia, from 486 persons for *Orientia* seroreactivity. Overall, 13.8% showed reactive IgG by indirect immunofluorescence antibody assay and ELISA. Of those samples, 30% (20/67) were confirmed to be positive by Western blot, showing ≥1 reactive band to *Orientia* 56-kD or 47-kD antigens.

Scrub typhus, caused by species in the genus *Orientia*, is a reemerging mite-borne rickettsiosis and a major cause of acute undifferentiated febrile illness (AUFI) (*1*). Classically, scrub typhus was believed to be strictly endemic to the so-called tsutsugamushi triangle, which ranges from southeastern Siberia in the North to the Kamchatka Peninsula in the East, northern Australia in the South, and Pakistan in the West (*1*). However, scrub typhus outside the tsutsugamushi triangle was suggested 70 years ago because

Table. *Orientia* seropositivity in rural populations of Cauca Department, by testing method, Colombia, 2017*

Municipalities and rural localities	No. samples	No. (%) *Orientia* IgG positive samples		
		IFA	ELISA	Western blot†
Caloto	48	5 (10.4)	2 (4.2)	6 (100)‡
El Credo	35	4 (11.4)	1 (2.9)	4 (100)‡
Huellas	13	1 (1.7)	1 (1.7)	2 (100)
El Tambo	262	0	45 (17.2)	11 (24.4)
Betania	46	0	3 (6.5)	2 (66.7)
Placer	88	0	14 (15.9)	6 (42.9)
Zarzal	128	0	28 (21.9)	3 (7)
La Sierra	30	0	5 (16.7)	1 (20)
Juan Castaña	30	0	5 (16.7)	1 (20)
Santander de Quilichao	146	1 (0.7)	10 (6.8)	2 (18.2)
Lomitas Arriba	65	0	6 (9.2)	0
Lomitas Ajabo	81	1 (1.2)	4 (4.9)	2 (40)
Total	486	6 (1.2)	62 (12.8)	20 (29.9)‡

*IFA, indirect immunofluorescence antibody assay.
†Denominators are IFA-positive or ELISA-positive samples.
‡One sample was positive by both IFA and ELISA.

seropositivity to *O. tsutsugamushi* was found among persons from several countries in Africa (*1*).

In 2006, a confirmed case of scrub typhus outside the classical disease-endemic region was described in a traveler who visited Dubai (United Arab Emirates); the case was caused by a novel species, *Candidatus* Orientia chuto (*2*). More recently,in Latin America, autochthonous cases of scrub typhus have been reported in Chile and attributed to a new *Orientia* species, *Candidatus* Orientia chiloensis, associated with *Herpetacarus*

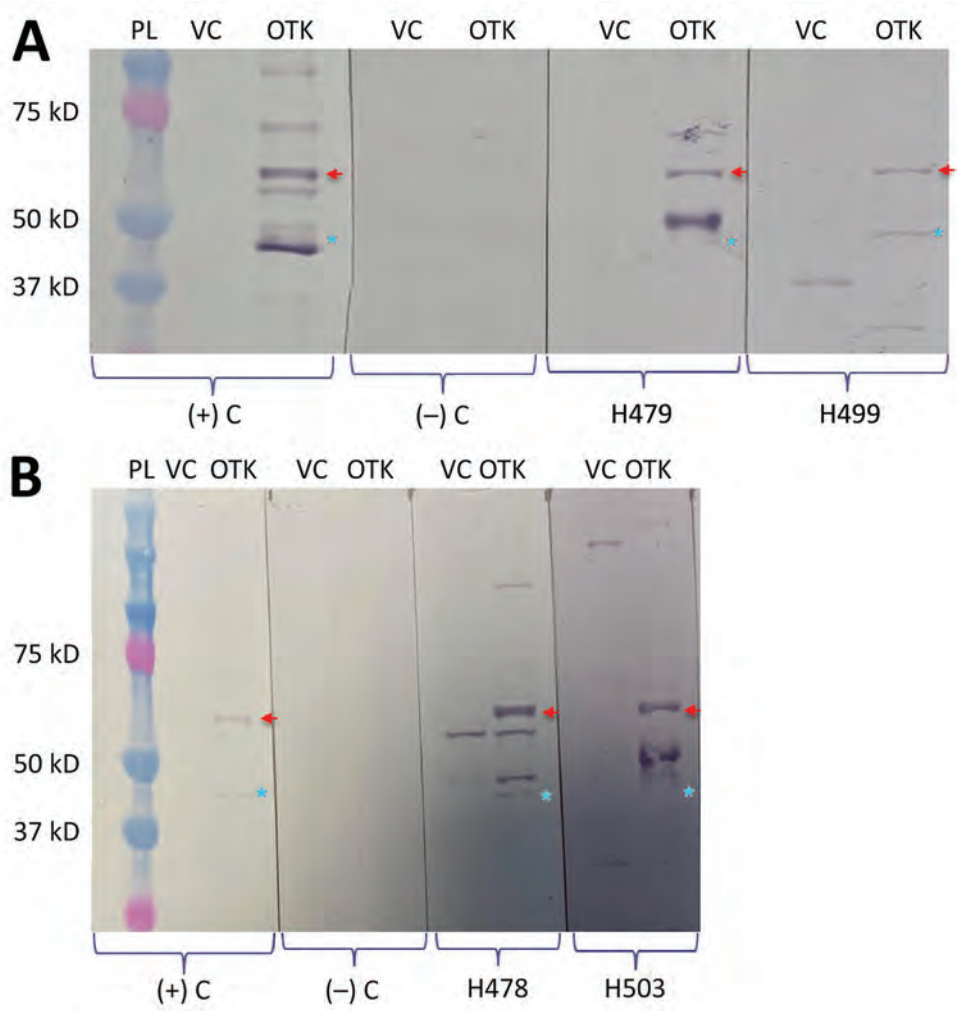

Figure. Serologic evidence of *Orientia* infection among rural population, Cauca Department, Colombia. Western blot analysis was performed using Vero cell extracts and *O. tsutsugamushi* Karp strain whole-cell antigens. Examples of some reactive samples that were applied to probe-migrating *Orientia*-specific antigens (56 kD and 47 kD) are shown: A) samples H479 and H499; B) samples H478 and H503. Red arrows indicate 56-kD protein, and blue stars indicate 47-kD protein. OTK, *O. tsutsugamushi* Karp strain; PL, protein ladder; VC, Vero cell; (–) C, negative control; (+) C, positive control.

spp. mites, which have been recognized as novel vectors of scrub typhus in this newly recognized disease-endemic region (*3*,*4*).

In addition to the aforementioned studies in Chile, serologic surveys have been performed among military personnel stationed in the Peruvian Amazon and Honduras, demonstrating exposure to *Orientia*, as well as a possible role for this bacterium in the etiology of AUFI (*5*,*6*). Thus, to explore new geographic regions that might have *Orientia* circulation, we report serologic evidence of this rickettsial agent in Colombia.

We screened 486 serum samples collected in 4 municipalities in the Cauca Department, Colombia, during 2017 and used in a previous study (*7*) for *Orientia* seroreactivity. Cauca Department is located in southwestern Colombia, mainly in the Andean and Pacific regions plus a tiny part in the Amazonian region. The climate is warm and humid on the western slope; warm and semiarid toward the Patía basin; and temperate humid to semihumid centrally, with cold climates recorded on both sides of the Popayán (capital city) Plateau.

We tested for antibodies reactive to *O. tsutsugamushi* by indirect immunofluorescence antibody (IFA) assay and ELISA (Appendix, https://wwwnc.cdc.gov/EID/article/29/2/22-1458-App1.pdf). To further confirm the specificity of the reactive samples, we performed a Western blot assay (Appendix).

Of 486 serum samples, 6 (1%) were seropositive for *Orientia* by IFA with an endpoint titer of 1:28 to 1:1,024, and 62 (13%) yielded positive results by ELISA (optical density cutoff >0.37). Only 1 sample was positive by both methods. Overall, 67 (13.8%) serum samples were positive by ≥1 screening method. Testing of 67 of the seropositive samples by Western blot showed that 20 (30%) were reactive with ≥1 *O. tsutsugamushi* band. A total of 8 samples were reactive to 56-kD, 5 to 47-kD, and 7 to both (Table; Figure).

Our results show serologic evidence of *Orientia* exposure among the rural population of 4 municipalities from Cauca Department, Colombia. This evidence suggested circulation of this rickettsial agent in this region.

Using 2 serologic techniques (IFA and ELISA), we found different seropositivity rates (1% for IFA and 13% for ELISA) for the same serum samples. Similar discordance has been observed for persons from Sao Tome and Principe (*8*). The difference in seropositivity rates between methods might be caused by the antigens used because our IFA used only antigens of the Karp strain, which could fail to detect antibodies stimulated by organisms of other serotypes and species. Moreover, some autochthonous cases of scrub typhus in Chile have also shown discordant serologic results (reactive IgG by IFA/negative IgG by ELISA, and vice versa) (*9*,*10*).

As briefly mentioned, the use of ELISA to detect IgG reactive against *Orientia* showed reactivity in 5.3% of convalescent-phase serum samples from febrile patients in the region of Iquitos (Peruvian Amazon) (*5*) and in 5.6% of US military personnel stationed at least 6 months in Honduras (*6*). Our study found 13% seropositivity by using the same serologic approach (IgG ELISA), which is greater than results obtained in Perú and Honduras. In addition to ELISA and IFA screening methods, we used a confirmatory test (Western blot), which demonstrated reactivity to ≥1 immunodominant protein (56 kD and 47 kD) of *Orientia* in 30% of the tested samples, which were positive by ≥1 screening method.

In conclusion, we report serologic evidence of *Orientia* in Colombia, supporting that these bacteria are probably widely distributed in Latin America. Our study also supports emerging evidence that *Orientia* spp. is no longer restricted to the tsutsugamushi triangle. Prospective studies to examine acute-phase and convalescent-phase serum samples and isolation of the agent in those with AUFI in Colombia and other countries in Latin America should be undertaken. In addition, scrub typhus should be considered as a potential diagnosis by physicians and public health officials when an eschar-associated rickettsiosis is suspected in this region.

Acknowledgment

We thank Nicole Mendell, Donald H. Bouyer and Patricia Valdes for providing in-house slides coated and fixed with whole-cell antigens of *O. tsutsugamushi* Karp strain, and whole Vero cells extracts and whole-cell antigens of *O. tsutsugamushi* Karp strain for Western blot assay.

This study was supported by COLCIENCIAS (project no. 120374455209, Colombia). At the time of this study, Á.A.F.-M. was supported by the Fogarty International Center and the National Institute of Allergy and Infectious Diseases, National Institutes of Health under grant D43 TW010331.

About the Author

Dr. Faccini-Martínez is a physician–scientist at Fundación Universitaria de Ciencias de la Salud, Bogotá, Colombia. His primary research interests include zoonotic and vector-borne diseases.

References

1. Richards AL, Jiang J. Scrub typhus: historic perspective and current status of the worldwide presence of *Orientia* species. Trop Med Infect Dis. 2020;5:49. https://doi.org/10.3390/tropicalmed5020049
2. Izzard L, Fuller A, Blacksell SD, Paris DH, Richards AL, Aukkanit N, et al. Isolation of a novel *Orientia* species (*O. chuto* sp. nov.) from a patient infected in Dubai. J Clin Microbiol. 2010;48:4404–9. https://doi.org/10.1128/JCM.01526-10
3. Abarca K, Martínez-Valdebenito C, Angulo J, Jiang J, Farris CM, Richards AL, et al. Molecular description of a novel *Orientia* species causing scrub typhus in Chile. Emerg Infect Dis. 2020;26:2148–56. https://doi.org/10.3201/eid2609.200918
4. Weitzel T, Silva-de la Fuente MC, Martínez-Valdebenito C, Stekolnikov AA, Pérez C, Pérez R, et al. Novel vector of scrub typhus in sub-Antarctic Chile: evidence from human exposure. Clin Infect Dis. 2022;74:1862–5. https://doi.org/10.1093/cid/ciab748
5. Kocher C, Jiang J, Morrison AC, Castillo R, Leguia M, Loyola S, et al. Serologic evidence of scrub typhus in the Peruvian Amazon. Emerg Infect Dis. 2017;23:1389–91. https://doi.org/10.3201/eid2308.170050
6. Chao CC, Zhang Z, Belinskaya T, Chen HW, Ching WM. Leptospirosis and rickettsial diseases sero-conversion surveillance among U.S. military personnel in Honduras. Mil Med. 2022;187:802–7. https://doi.org/10.1093/milmed/usab120
7. Forero-Becerra E, Patel J, Martínez-Díaz HC, Betancourt-Ruiz P, Benavides E, Durán S, et al. Seroprevalence and genotypic analysis of *Ehrlichia canis* infection in dogs and humans in Cauca, Colombia. Am J Trop Med Hyg. 2021;104:1771–6. https://doi.org/10.4269/ajtmh.20-0965
8. Yen TY, Zhang Z, Chao CC, Ching WM, Shu PY, Tseng LF, et al. Serologic evidence for *Orientia* exposure in the Democratic Republic of Sao Tome and Principe. Vector Borne Zoonotic Dis. 2019;19:821–7. https://doi.org/10.1089/vbz.2018.2426
9. Weitzel T, Dittrich S, López J, Phuklia W, Martinez-Valdebenito C, Velásquez K, et al. Endemic scrub typhus in South America. N Engl J Med. 2016;375:954–61. https://doi.org/10.1056/NEJMoa1603657
10. Weitzel T, Martínez-Valdebenito C, Acosta-Jamett G, Jiang J, Richards AL, Abarca K. Scrub typhus in continental Chile, 2016–2018. Emerg Infect Dis. 2019;25:1214–7. https://doi.org/10.3201/eid2506.181860

Address for correspondence: David H. Walker, Department of Pathology, University of Texas Medical Branch, Galveston, TX 77555, USA; email: dwalker@utmb.edu

etymologia revisited

Influenza

[in''floo-en'zə]

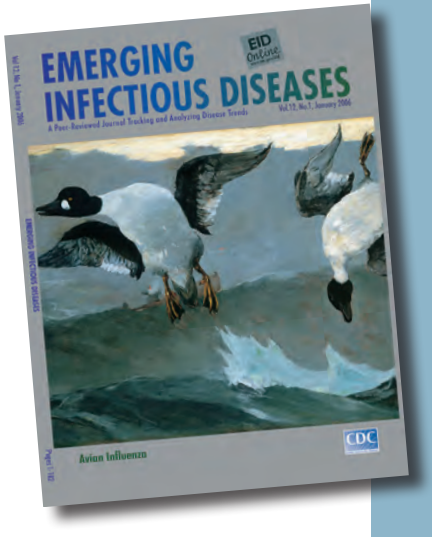

Originally published in January 2006

An acute viral infection of the respiratory tract. From Latin influentia,"to flow into"; in medieval times, intangible fluid given off by stars was believed to affect humans. The Italian influenza referred to any disease outbreak thought to be influenced by stars. In 1743, what Italians called an influenza di catarro ("epidemic of catarrh") spread across Europe, and the disease came to be known in English as simply "influenza."

Source:

Dorland's illustrated medical dictionary. 30th ed. Philadelphia: Saunders; 2003 and Quinion M. World wide words. 1998 Jan 3 [cited 2005 Dec 5]. Available from http://www.worldwidewords.org/topicalwords/tw-inf1.htm

Hepatitis E Virus Outbreak among Tigray War Refugees from Ethopia, Sudan

Andrew S. Azman, Etienne Gignoux, Robin Nesbitt, John Rumunu, Rakesh Aggarwal, Iza Ciglenecki

Author affiliations: Johns Hopkins Bloomberg School of Public Health, Baltimore, Maryland, USA (A.S. Azman); Médecins Sans Frontières, Geneva, Switzerland (A.S. Azman, I. Ciglenecki); Epicentre, Paris, France (E. Gignoux, R. Nesbitt); Ministry of Health South Sudan, Juba, South Sudan (J. Rumunu); Jawaharlal Institute of Postgraduate Medical Education and Research, Puducherry, India (R. Aggarwal)

DOI: https://doi.org/10.3201/eid2901.221495

To the Editor: We read with interest the article by Ahmed et al. on a large hepatitis E virus (HEV) outbreak among refugees from Ethiopia in Sudan, underscoring the challenges in controlling HEV outbreaks (*1*). As part of the rationale for not using HEV vaccine, the authors state that no data on virus genotype were available from cases and "the success of vaccination is dependent on the HEV genotype." We believe that current evidence contradicts this assertion.

Evidence to date suggests that all major HEV genotypes that infect humans (genotypes 1–4) show cross-protection with a single serotype. Several pieces of data indicate that the only available and licensed vaccine (Hecolin; Wantai BioPharm, https://www.ystwt.cn), which contains recombinant partial capsid protein of HEV genotype 1, offers protection against infection with other genotypes. Studies in rhesus macaques have demonstrated protection by this vaccine against infection with genotypes 1 and 4 (*2*). In a large phase 3 trial of Hecolin, of the 23 persons who had HEV infection (1 in vaccine group and 22 in placebo group), viral genotype was identified in 13 placebo group patients. Of those, 12 were genotype 4 and 1 was genotype 1, providing evidence of protection against genotype 4 infection, a heterologous strain to that in the vaccine (*3*). Furthermore, in vitro data also support cross-protection across HEV genotypes (*4*).

A safe and efficacious vaccine is available and has been recommended for use as an outbreak control tool by the World Health Organization Strategic Advisory Group of Experts on Immunization (*5*), and this recommendation does not refer to virus genotype. Because empirical evidence from in vitro studies, nonhuman primate challenge studies, and a phase 3 clinical trial all point to cross-genotype protection, we believe that the lack of genotyping data during an outbreak should not prevent or delay the use of the HEV vaccine.

References

1. Ahmed A, Ali Y, Siddig EE, Hamed J, Mohamed NS, Khairy A, et al. Hepatitis E virus outbreak among Tigray War refugees from Ethiopia, Sudan. Emerg Infect Dis. 2022;28:1722–4. https://doi.org/10.3201/eid2808.220397
2. Li SW, Zhang J, Li YM, Ou SH, Huang GY, He ZQ, et al. A bacterially expressed particulate hepatitis E vaccine: antigenicity, immunogenicity and protectivity on primates. Vaccine. 2005;23:2893–901. https://doi.org/10.1016/j.vaccine.2004.11.064
3. Zhu FC, Zhang J, Zhang XF, Zhou C, Wang ZZ, Huang SJ, et al. Efficacy and safety of a recombinant hepatitis E vaccine in healthy adults: a large-scale, randomised, double-blind placebo-controlled, phase 3 trial. Lancet. 2010;376:895–902. https://doi.org/10.1016/S0140-6736(10)61030-6
4. Gu Y, Tang X, Zhang X, Song C, Zheng M, Wang K, et al. Structural basis for the neutralization of hepatitis E virus by a cross-genotype antibody. Cell Res. 2015;25:604–20. https://doi.org/10.1038/cr.2015.34
5. World Health Organization. Hepatitis E vaccine: WHO position paper, May 2015—recommendations. Vaccine. 2016;34:304–5. https://doi.org/10.1016/j.vaccine.2015.07.056

Address for correspondence: Andrew S. Azman, Department of Epidemiology, Johns Hopkins Bloomberg School of Public Health, 615 N Wolfe St, Baltimore, MD 21205, USA; email: azman@jhu.edu

In Response: We appreciate the insightful comments from Azman et al. on use of licensed hepatitis E virus (HEV) vaccine (Hecolin; Wantai BioPharm, https://www.ystwt.cn) for outbreak control regardless of virus genotype (*1*). We share their concern about the need for timely use of effective outbreak control measures, particularly among those at high risk for illness and death, such as forcibly displaced populations in humanitarian camps. We also agree that vaccines are an effective tool for prevention and control of outbreaks, including HEV (*2*).

When we confirmed an HEV outbreak among refugees from Ethiopia in east Sudan, according to the World Health Organization (WHO) recommendation, the National Immunization Technical Advisory Groups of Sudan convened an emergency meeting to discuss the feasibility of deploying HEV vaccine. After considering the WHO position paper about the use of HEV vaccine (*3*) and careful discussion, they raised several concerns about introducing the vaccine. These concerns included the limited evidence on efficacy and safety data in pregnant women, persons <16 years of age, the elderly (>65 years of age), and persons with underlying diseases (e.g., liver disease) or conditions such as immunosuppression (*3*). Of particular concern were children and pregnant women in humanitarian crisis, who are most at risk during HEV outbreaks (*4*). A major concern was that, according to

the WHO statement on the vaccine, "there are no data on specific protection afforded by the HEV 239 vaccine against genotype 1, 2, or 3 HEV infection." Therefore, the final recommendation was to invest more resources toward improving water, sanitation, and hygiene interventions until further evidence is available. In addition, several diseases prevalent among displaced populations in Sudan are preventable through water, sanitation, and hygiene interventions (*5*). These infections include waterborne diseases such as HEV and cholera (*2*,*6*); vectorborne diseases such as Chikungunya, dengue, and Rift Valley fever (*5*,*7*); and measles, meningitis, and poliomyelitis (*5*).

References

1. Azman AS, Gignoux E, Nesbitt R, Rumunu J, Aggarwal R, Ciglenecki I. Hepatitis E virus outbreak among Tigray War refugees from Ethiopia, Sudan. Emerg Infect Dis. 2023 Feb [*date cited*]. https://doi.org/10.3201/eid2902.221495
2. Ahmed A, Ali Y, Siddig EE, Hamed J, Mohamed NS, Khairy A, et al. Hepatitis E virus outbreak among Tigray War refugees from Ethiopia, Sudan. Emerg Infect Dis. 2022;28:1722–4. https://doi.org/10.3201/eid2808.220397
3. World Health Organization. Hepatitis E vaccine: WHO position paper, May 2015. Wkly Epidemiol Rec. 2015;90:185–200.
4. Desai AN, Mohareb AM, Elkarsany MM, Desalegn H, Madoff LC, Lassmann B. Viral hepatitis E outbreaks in refugees and internally displaced populations, sub-Saharan Africa, 2010–2020. Emerg Infect Dis. 2022;28:1074–6.
5. Ahmed A, Mohamed NS, Siddig EE, Algaily T, Sulaiman S, Ali Y. The impacts of climate change on displaced populations: a call for action. J Clim Chang Health. 2021;3;100057.
6. Mohamed NS, Ali Y, Abdalrahman S, Ahmed A, Siddig EE. The use of cholera oral vaccine for containment of the 2019 disease outbreak in Sudan. Trans R Soc Trop Med Hyg. 2022;116:763–6. https://doi.org/10.1093/trstmh/trac041
7. Ahmed A, Ali Y, Mohamed NS. Arboviral diseases: the emergence of a major yet ignored public health threat in Africa. Lancet Planet Health. 2020;4:e555. https://doi.org/10.1016/S2542-5196(20)30269-2

Address for correspondence: Ayman Ahmed, Human and Animal Health Unit, Department of Epidemiology and Public Health, Swiss Tropical and Public Health Institute, Kreuzstrasse 2, 4123 Allschwil, Switzerland; email: ayman.ame.ahmed@gmail.com

Ayman Ahmed, Yousif Ali, Nouh S. Mohamed, Jakob Zinsstag, Emmanuel Edwar Siddig, Amna Khairy

Author affiliations: Sirius Training and Research Centre, Khartoum, Sudan (A. Ahmed, N.S. Mohamed); Swiss Tropical and Public Health Institute, Allschwil, Switzerland (A. Ahmed, J. Zinsstag); University of Basel, Basel, Switzerland (A. Ahmed, J. Zinsstag); University of Khartoum, Khartoum (A. Ahmed, E.E. Siddig); Sudan Federal Ministry of Health, Khartoum (Y. Ali, A. Khairy); Erasmus MC University Medical Center, Rotterdam, the Netherlands, (E.E. Siddig)

DOI: https://doi.org/10.3201/eid2902.221796

***Jack in the Box* (circa 1890), Father Tuck's Tiny Tots' Series** (detail). Illustrated children's book. Raphael Tuck & Sons, Ltd, London; Paris; New York. Public domain image contributed by University of California Libraries.

Emerging Pathogens Pose Inevitable Surprises

Byron Breedlove

Anthony Fauci, who retired as head of the National Institute of Allergy and Infectious Diseases, National Institutes of Health, at the end of 2022, wrote that "The emergence of new infections and the reemergence of old ones are largely the result of human interactions with and encroachment on nature. As human societies expand in a progressively interconnected world and the human–animal interface is perturbed, opportunities are created, often aided by climate changes, for unstable infectious agents

Author affiliation: Centers for Disease Control and Prevention, Atlanta, Georgia, USA

DOI: https://doi.org/10.3201/eid2902.AC2902

to emerge, jump species, and in some cases adapt to spread among humans."

Factors that can lead to emergence of pathogens also include contaminated food and water, modern agricultural practices, human migration, use and misuse of antimicrobial agents, and lack of public health resources in some areas. In 2013, Morens and Fauci wrote, "The inevitable, but unpredictable, appearance of new infectious diseases has been recognized for millennia, well before the discovery of causative infectious agents. Today, however, despite extraordinary advances in development of countermeasures (diagnostics, therapeutics, and vaccines), the ease of world travel and increased global interdependence have added layers of complexity to containing these infectious diseases that affect not only the health but the economic stability of societies."

A number of emerging diseases confirm the challenge of predicting when and where an outbreak may occur and how severe and widespread it may be. Examples include the first cases of what would be known as AIDS in the early 1980s, multiple outbreaks of Ebola in parts of Africa, Zika in South and North America, severe acute respiratory syndrome, Middle East respiratory syndrome, and COVID-19.

Fauci noted, "Today, there is no reason to believe that the threat of emerging infections will diminish, since their underlying causes are present and most likely increasing." Invariably, public health experts will be surprised by some yet unknown emerging pathogen or disease outbreak. This month's cover art, an image of a jack in the box from the cover of a children's book, speaks to the element of surprise.

Believed to date from the 1500s according to various sources, including the Strong National Museum of Play, this enduring children's toy is essentially a puppet, clown, or caricature of a person mounted on a spring inside a box. After jostling a latched box or cranking a handle to wind the spring, a child is rewarded with a short tune before the "Jack" suddenly pops open the lid, eliciting a laugh or cry. The Victoria and Albert Museum notes, "Despite their frightening qualities such toys were not only cheap and popular, but also helped to provide children with their first awareness of basic scientific principles."

This month's cover image, whose creator is not credited, appeared on the cover of one of the many books from the Father Tuck's Tiny Tots' Series (circa 1895), produced by Raphael Tuck & Sons, Ltd., a company that produced children's books, postcards, greeting cards, puzzles, and various ephemera. The grimacing figure in the image, arms splayed outward, has emerged from its unlatched box and frightened a trio of prowling mice. Rodents, in turn, are known to spread various emerging pathogenic agents and could factor in to the next unexpected disease outbreak. As humans encroach with their machines, the animals run away, but nature will return and perhaps have already left something even more frightening in the animals' wake. It is not surprising, therefore, that the recommendations from the 1992 Institute of Medicine report *Emerging Infections: Microbial Threats to Health in the United States* underscoring the value of public health surveillance, preparedness, and infrastructure remain relevant and applicable.

Bibliography

1. British Museum. Raphael Tuck & Sons [cited 2022 Dec 16]. https://www.britishmuseum.org/collection/term/BIOG77171
2. Fauci AS. It ain't over till it's over … but it's never over—emerging and reemerging infectious diseases. N Engl J Med. 2022;387:2009–11. https://doi.org/10.1056/NEJMp2213814
3. Lederberg J, Shope RE, Oaks SC Jr, editors. Emerging infections: microbial threats to health in the United States. Washington (DC): The National Academies Press; 1992 [cited 2023 Jan 4]. http://www.nap.edu/catalog/2008/emerging-infections-microbial-threats-to-health-in-the-united-states
4. Morens DM, Fauci AS. Emerging infectious diseases: threats to human health and global stability. PLoS Pathog. 2013;9:e1003467. https://doi.org/10.1371/journal.ppat.1003467
5. Strong National Museum of Play. Jack-in-the-box [cited 2022 Dec 16]. https://www.museumofplay.org/toys/jack-in-the-box
6. Victoria and Albert Museum. Jack in the box [cited 2022 Dec 16]. https://collections.vam.ac.uk/item/O93266/jack-in-the-unknown

Address for correspondence: Byron Breedlove, EID Journal, Centers for Disease Control and Prevention, 1600 Clifton Rd NE, Mailstop H16-2, Atlanta, GA 30329-4027, USA; email: wbb1@cdc.gov

EMERGING INFECTIOUS DISEASES®

Upcoming Issue

- Multicenter Retrospective Study on Vascular Infections and Endocarditis Caused by *Campylobacter* spp.
- Yellow Fever Vaccine–Associated Viscerotropic Disease among Siblings, Sao Paulo, Brazil
- *Bartonella* spp. Infections Identified by Molecular Methods, United States
- Prevalence of *Mycobacterium tuberculosis* Complex among Wild Rhesus Macaques and 2 Subspecies of Long-Tailed Macaques, Thailand, 2018–2022
- Postacute Sequelae of SARS-CoV-2 in University Setting
- Increase in Colorado Tick Fever Virus Disease Cases and Impact of COVID-19 Pandemic on Behaviors and Testing Practices, Montana, 2020
- Comparative COVID-19 Vaccines Effectiveness in Preventing Infections and Disease Progression with SARS-CoV-2 BA.5 and BA.2 Omicron, Portugal
- COVID-19 Test Allocation Strategy to Mitigate SARS-CoV-2 Infections across School Districts
- Extended Viral Shedding in MERS-CoV Clade B Virus Compared with African Clade C Strain in Llamas
- Clonal Dissemination of Antifungal-Resistant *Candida haemulonii*, China
- Using Disposable Handkerchiefs to Monitor and Diagnose Viral Respiratory Infections
- Clonal Expansion of Multidrug-Resistant *Streptococcus dysgalactiae* subsp. *equisimilis* Causing Bacteremia, Japan, 2005–2021
- Associations of *Anaplasma phagocytophilum* Bacteria Variants in *Ixodes scapularis* Ticks and Humans, New York, USA
- Risk Factors for Reinfection with SARS-CoV-2 Omicron Variant among Previously Infected Frontline Workers
- Reemergence of Lymphocytic Choriomeningitis Mammarenavirus, Germany
- SARS-CoV-2 Incubation Period during the Omicron BA.5–Dominant Period in Japan
- *Emergomyces pasteurianus* in Patient from Liberia and Review of the Literature
- *Mycobacterium leprae* in Armadillo Tissues from Museum Collections, United States
- Seroprevalence of SARS-CoV-2 Specific Antibodies during Omicron BA.5 Wave, Portugal, April–June 2022
- *Burkholderia thailandensis* Isolated from the Environment, United States
- New Detection of Locally Acquired Japanese Encephalitis Virus using Clinical Metagenomics, New South Wales, Australia
- Correlation of High Seawater Temperature with *Vibrio* and *Shewanella* Infections, Denmark, 2010–2018
- Tuberculosis Preventive Therapy among Persons Living with HIV, Uganda, 2016–2022
- Tick-Borne Encephalitis in Pregnant Woman and Long-Term Sequelae
- *Babesia microti* Causing Intravascular Hemolysis in Immunocompetent Child, China
- Possible Mpox Protection from Smallpox Vaccine–Generated Antibodies among Adult and Elderly Persons
- Sustained Mpox Proctitis with Primary Syphilis and HIV Seroconversion from Single-Source Exposure, Australia
- New Postmortem Perspective on Emerging SARS-CoV-2 Variants of Concern, Germany
- *Inquilinus limosus* Bacteremia in Lung Transplant Recipient, France
- Intrahost Monkeypox Virus Genome Variation in Patient with Early Infection, Finland, 2022
- SARS-CoV-2 Spillback to Wild Coatis in Sylvatic–Urban Hotspot, Brazi

Complete list of articles in the March issue at https://wwwnc.cdc.gov/eid/#issue-296

Earning CME Credit

To obtain credit, you should first read the journal article. After reading the article, you should be able to answer the following, related, multiple-choice questions. To complete the questions (with a minimum 75% passing score) and earn continuing medical education (CME) credit, please go to http://www.medscape.org/journal/eid. Credit cannot be obtained for tests completed on paper, although you may use the worksheet below to keep a record of your answers.

You must be a registered user on http://www.medscape.org. If you are not registered on http://www.medscape.org, please click on the "Register" link on the right hand side of the website.

Only one answer is correct for each question. Once you successfully answer all post-test questions, you will be able to view and/or print your certificate. For questions regarding this activity, contact the accredited provider, CME@medscape.net. For technical assistance, contact CME@medscape.net. American Medical Association's Physician's Recognition Award (AMA PRA) credits are accepted in the US as evidence of participation in CME activities. For further information on this award, please go to https://www.ama-assn.org. The AMA has determined that physicians not licensed in the US who participate in this CME activity are eligible for AMA PRA Category 1 Credits™. Through agreements that the AMA has made with agencies in some countries, AMA PRA credit may be acceptable as evidence of participation in CME activities. If you are not licensed in the US, please complete the questions online, print the AMA PRA CME credit certificate, and present it to your national medical association for review.

Article Title

CME Questions

1. Which one of the following statements regarding the epidemiology and outcomes of infant botulism (IB) is most accurate?

A. Botulinum toxin is fairly benign
B. IB is characterized by a flaccid descending paralysis
C. The mortality rate of IB among hospitalized infants is nearly 15%
D. The distribution of cases of IB is spread fairly evenly throughout the world

2. Which one of the following characteristics was notable in the current series of 8 patients with IB?

A. Nearly all patients did not have significant comorbidities
B. Nearly all patients resided in rural areas
C. Most patients had Bedouin ethnicity
D. Most patients were from families with lower annual incomes

3. Which 1 of the following risk factors was most prominent for IB in the current study?

A. Consumption of honey
B. Age less than 3 months
C. Female sex
D. Infection during spring and summer months

4. Which one of the following statements regarding clinical features of IB in the current study is most accurate?

A. Only 1 of 8 patients had a classical descending paralysis
B. Use of antitoxin reduced the hospital length of stay by half
C. Most cases required intubation
D. No neurologic sequelae or cases of mortality were recorded

Earning CME Credit

To obtain credit, you should first read the journal article. After reading the article, you should be able to answer the following, related, multiple-choice questions. To complete the questions (with a minimum 75% passing score) and earn continuing medical education (CME) credit, please go to http://www.medscape.org/journal/eid. Credit cannot be obtained for tests completed on paper, although you may use the worksheet below to keep a record of your answers.

You must be a registered user on http://www.medscape.org. If you are not registered on http://www.medscape.org, please click on the "Register" link on the right hand side of the website.

Only one answer is correct for each question. Once you successfully answer all post-test questions, you will be able to view and/or print your certificate. For questions regarding this activity, contact the accredited provider, CME@medscape.net. For technical assistance, contact CME@medscape.net. American Medical Association's Physician's Recognition Award (AMA PRA) credits are accepted in the US as evidence of participation in CME activities. For further information on this award, please go to https://www.ama-assn.org. The AMA has determined that physicians not licensed in the US who participate in this CME activity are eligible for AMA PRA Category 1 Credits™. Through agreements that the AMA has made with agencies in some countries, AMA PRA credit may be acceptable as evidence of participation in CME activities. If you are not licensed in the US, please complete the questions online, print the AMA PRA CME credit certificate, and present it to your national medical association for review.

Article Title

Crimean-Congo Hemorrhagic Fever, Spain, 2013–2021

CME Questions

1. Which one of the following statements regarding Crimean-Congo hemorrhagic fever (CCHF) is most accurate?

A. It is caused by a single-stranded RNA virus of the genus Orthonairovirus
B. It invariably causes severe illness
C. It often promotes leukocytosis and thrombocytosis
D. Its distribution is limited to Africa and southern Europe

2. Which one of the following statements regarding the epidemiology of CCHF in the current study is most accurate?

A. The mean age of patients was 17 years
B. All cases occurred in spring and summer
C. 90% of cases occurred in rural areas
D. No patient reported tick bites

3. Which one of the following statements regarding the clinical presentation and outcomes of CCHF in the current study is most accurate?

A. The median duration between tick bites and symptoms was 9 days
B. All patients presented with fever and exanthems
C. Bleeding occurred in 2 patients
D. The mortality rate was 70%

4. Which one of the following genotypes was most common in the current study?

A. I
B. II
C. III
D. IV